

# **Quick intro to magnetic confinement... waiting for next lectures during the week**

**Piero Martin**

Department of Physics and Astronomy, University of Padova, Italy  
Consorzio RFX, Padova, Italy

# 1

## **Modeling magnetic fusion plasmas**

# Fusion plasma

- A fusion plasma is a fully ionized gas
- Behavior dominated by **long-range electric and magnetic fields**
- Very good conductor of electricity
  - $n_e(\text{plasma}) \approx 10^{-8} \times n_e(\text{Cu})$
  - $\sigma(\text{plasma}) \approx 40 \times \sigma(\text{Cu})$
  - Very little collisions at high temperature and low density
- Plasma shielded from DC electric fields
- DC magnetic fields can penetrate

# Self-consistency in magnetized plasma

Sources ( $\rho, \mathbf{J}$ )  $\longleftrightarrow$  fields ( $\mathbf{E}, \mathbf{B}$ )

$$\nabla \cdot \mathbf{E} = \frac{\rho}{\varepsilon_0}$$

$$\nabla \cdot \mathbf{B} = 0$$

$$\nabla \times \mathbf{E} = -\frac{\partial \mathbf{B}}{\partial t}$$

$$\nabla \times \mathbf{B} = \mu_0 \mathbf{J} + \mu_0 \varepsilon_0 \frac{\partial \mathbf{E}}{\partial t}$$

# Models for plasma description

**How magnetic fields confine charged particles ?**

- Single-particle model

$$m \frac{d^2 \vec{r}}{dt^2} = q(\vec{E} + \vec{v} \times \vec{B})$$

- Kinetic theory

$$f_\alpha(\vec{r}, \vec{v}, t) = \frac{dN_\alpha(\vec{r}, \vec{v}, t)}{d^3 r d^3 v}$$

- **Fluid model**

$$\begin{aligned}\frac{\partial \rho}{\partial t} + \nabla \cdot (\rho \underline{v}) &= 0 \\ \rho \left( \frac{\partial \underline{v}}{\partial t} + \underline{v} \cdot \nabla \underline{v} \right) &= \nabla P - \underline{J} \times \underline{B} \\ \frac{\partial P}{\partial t} + \underline{v} \cdot \nabla P &= \gamma P \nabla \cdot \underline{v} \\ \frac{\partial \underline{B}}{\partial t} &= \nabla \times (\underline{v} \times \underline{B})\end{aligned}$$

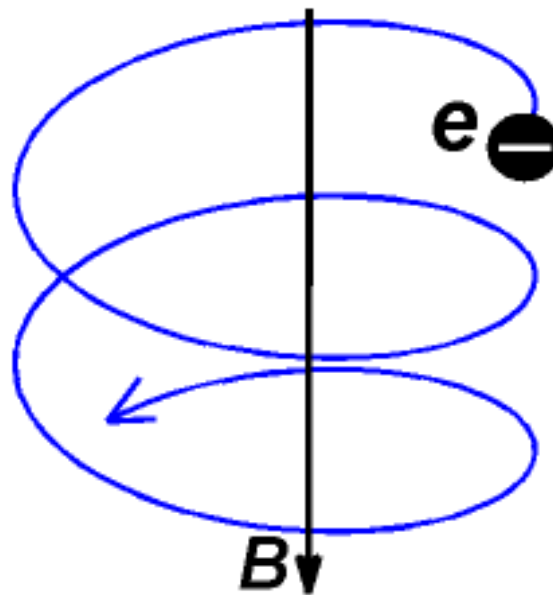
**2**

## **Single-particle motion**

# Single-particle motion

- Motion in **prescribed** magnetic and electric fields

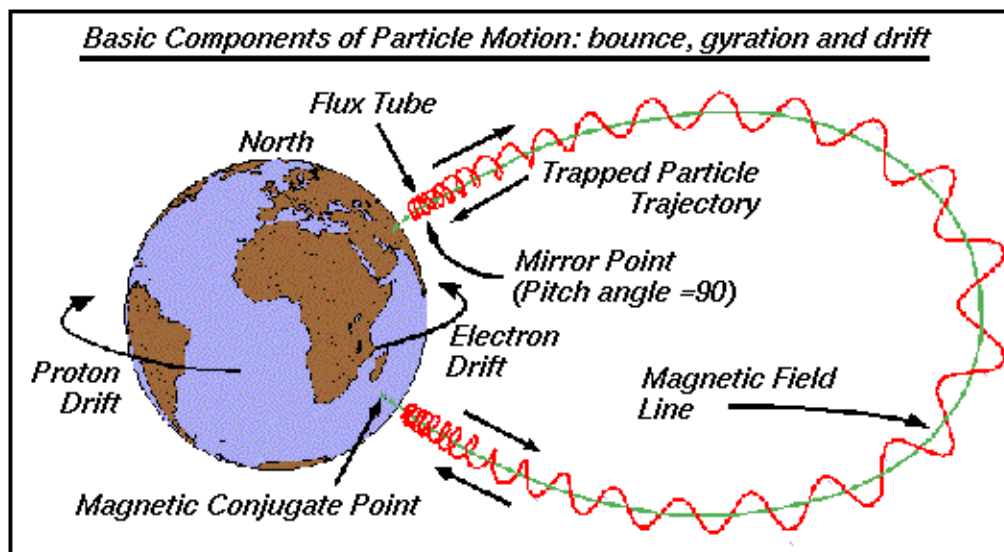
$$m \frac{d^2 \vec{r}}{dt^2} = q(\vec{E} + \vec{v} \times \vec{B})$$



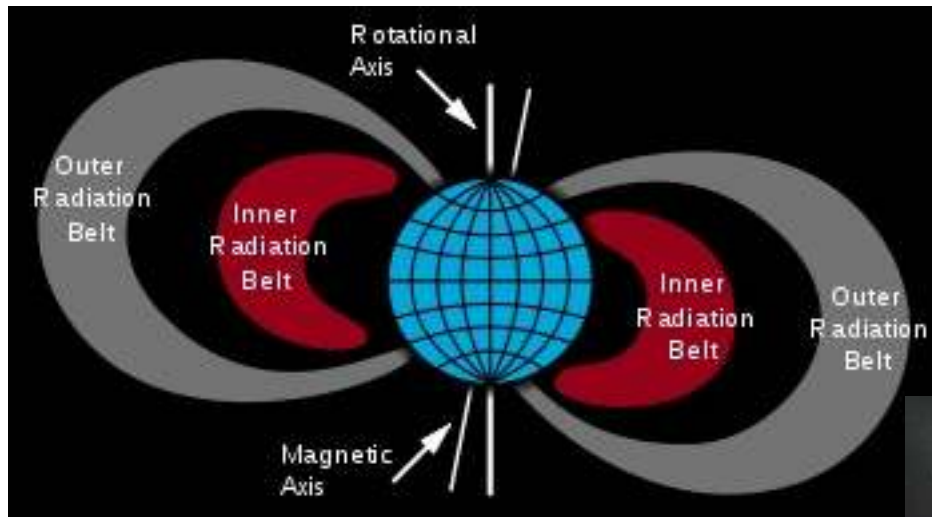
# Single-particle motion

- Motion in **prescribed** magnetic and electric fields

$$m \frac{d^2 \vec{r}}{dt^2} = q(\vec{E} + \vec{v} \times \vec{B})$$



# Particle motion in Earth magnetic field



***Single-particle model describes a variety of physics phenomena***

# 3

**Need for self-consistency:  
the fluid model**

# Need for self-consistency: an example

- Equilibrium: plasma confined by background  $\mathbf{B}$
- This magnetic field is partly produced by the plasma itself

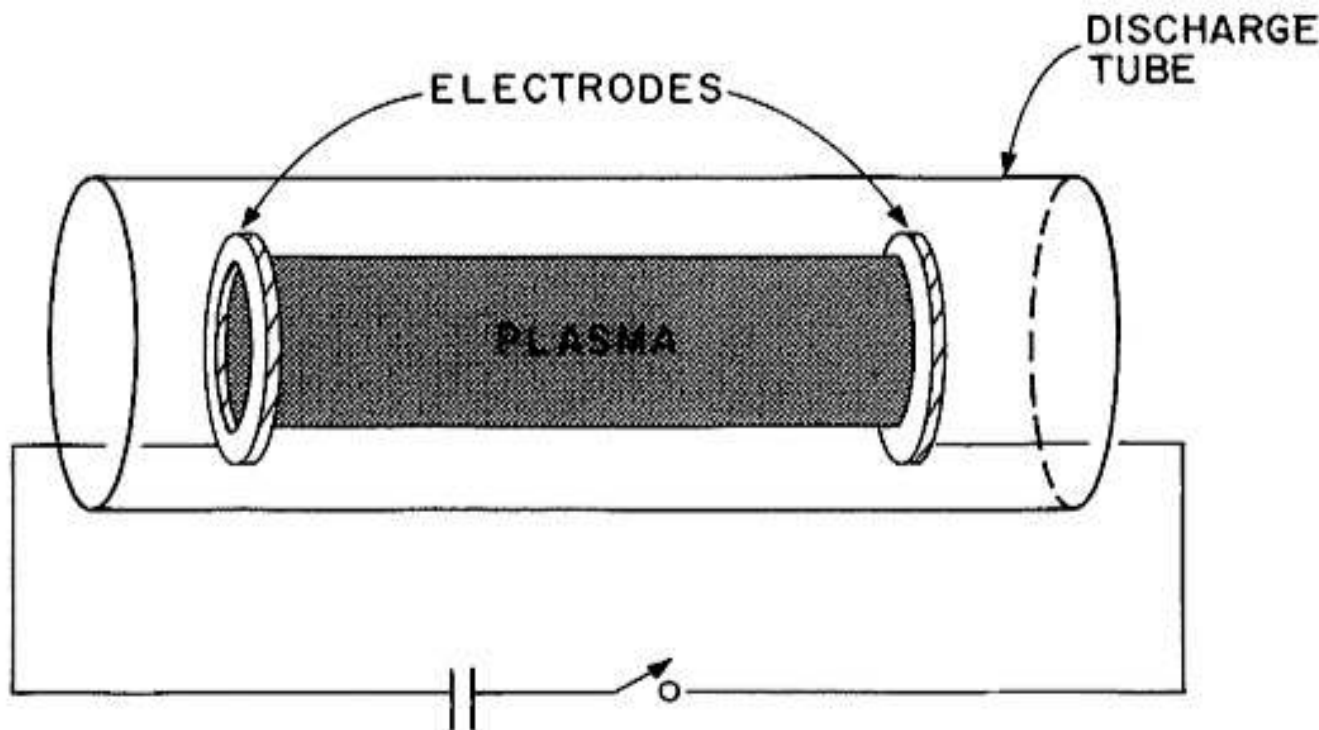
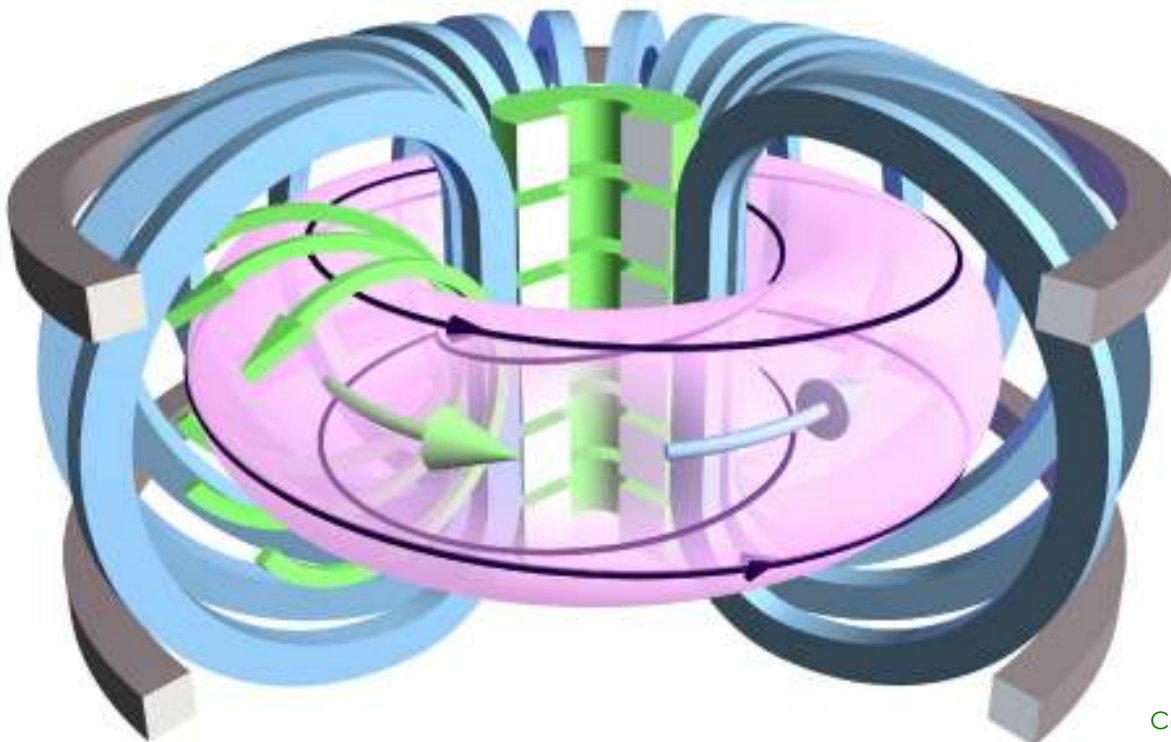


Figure 5.6. Schematic diagram of a linear Z-pinch experiment.

# Magnetic Confinement Fusion

**The goal:** energy production

**The tool:** a toroidal magnetic container, with helical magnetic field



Courtesy of S. Pinches

$$\nabla p = \vec{J} \times \vec{B}$$

force balance between magnetic and pressure forces

# Fluid equations

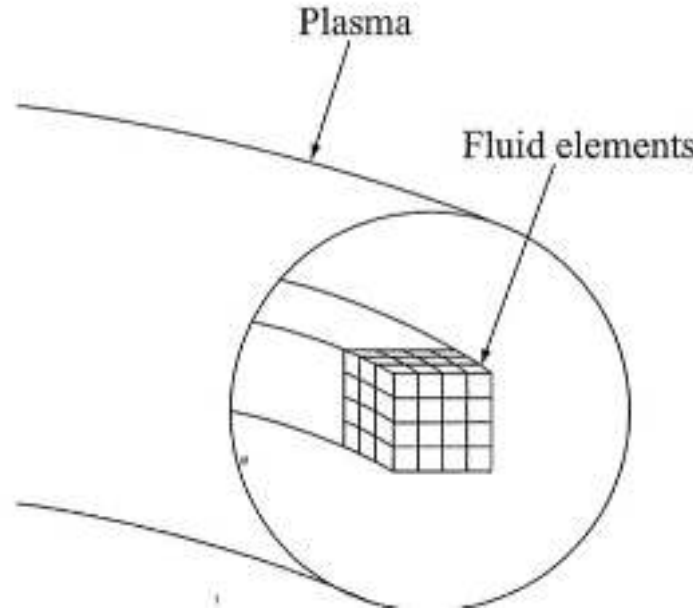
- **Neutral gases and liquids:** fluid equations derived treating the fluid as a continuous medium and considering the dynamics of a small volume of the plasma.

$$\frac{\partial \rho}{\partial t} + \vec{\nabla} \cdot \rho \vec{V} = 0$$

$$\rho \frac{d\vec{V}}{dt} = \rho \vec{g} - \vec{\nabla} p + \mu \nabla^2 \vec{V} + \frac{2}{3} \mu \vec{\nabla} (\vec{\nabla} \cdot \vec{V})$$

# Fluid equations in plasmas

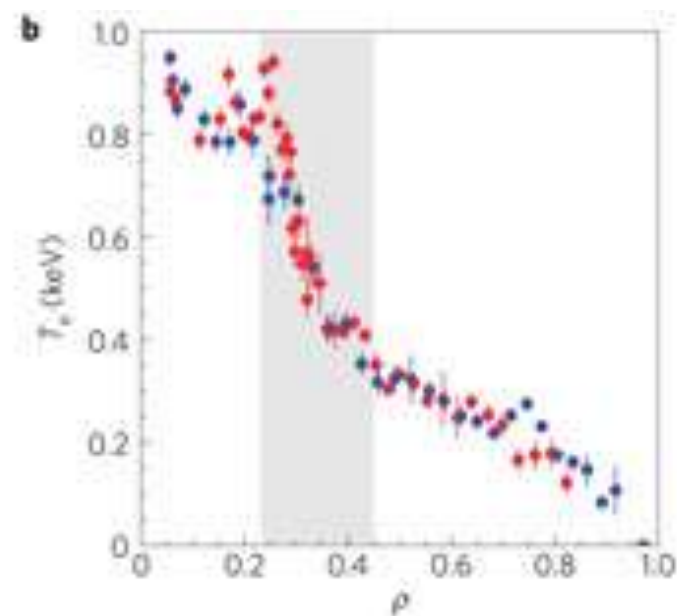
- Subdivide the plasma in a **large number of small and moving fluid elements**
- The behavior of each fluid element is described by **average macroscopic properties** of the particles contained in it



# Macroscopic averages

- **Fluid description** → developing a model describing the evolution of important macroscopic plasma properties

- $n_e(\mathbf{r}, t)$ ,  $n_i(\mathbf{r}, t)$
- $\mathbf{u}_e(\mathbf{r}, t)$ ,  $\mathbf{u}_i(\mathbf{r}, t)$
- $T_e(\mathbf{r}, t)$ ,  $T_i(\mathbf{r}, t)$
- $p_e(\mathbf{r}, t)$ ,  $p_i(\mathbf{r}, t)$



- E.g.: macroscopic velocity  $\mathbf{u}_e$ 
  - Average velocity of all the electrons contained in the fluid element

# Size of a fluid element

- It has to be possible to define a range of sizes for each element that satisfies two conflicting requirements:
  - **The element can not be too small, otherwise too few particles inside and averaging makes little sense**
  - **Not too big, otherwise spatial accuracy lost**
- **Fusion plasma**
  - $N_e = 10^{20} \text{ m}^{-3}$
  - $L = 1 \text{ m}$
  - $\Delta x = 10^{-5}$  good resolution
  - $\Delta V = 10^{-15} \text{ m}^{-3}$
  - $N_e = 10^5 \gg 1$

# Is a fluid model useful for a plasma ?

- Example: **air at atmospheric pressure**
  - Molecules within each fluid element are collision dominated
  - Collisions keep molecules closely confined together
  - A molecule can not move over long distances with respect to its neighbors. It is confined in a region of the size of its mean free path
  - Molecules in each element form a well-defined cluster of particles, whose identity is maintained as the system evolves in time.
- **Coherence due to high collisionality** → fluid model useful for air

**Each fluid element correspond to a super-particle  
with mass  $mn\Delta V$  and velocity  $u$**

# Is a fluid model useful for a plasma ?

Fusion plasma are nearly collisionless....

- ...but magnetic field acts to keep them together in the perpendicular direction.
  - The small size of the gyro-radius keep particles close to one another

**The magnetic field replaces collisions in providing perpendicular coherence to the particles in a fluid element**

- ...but particles move freely along  $\mathbf{B}$ ...
  - Need kinetic treatment
  - But fluid model often incorrect when unimportant..
  - ..not a huge problem

# Two-fluid model

*Conservation of mass*

$$\begin{aligned}\frac{\partial n_e}{\partial t} + \nabla \cdot (n_e \mathbf{u}_e) &= 0, \\ \frac{\partial n_i}{\partial t} + \nabla \cdot (n_i \mathbf{u}_i) &= 0.\end{aligned}\tag{10.50}$$

*Conservation of momentum*

$$\begin{aligned}m_e n_e \left( \frac{\partial}{\partial t} + \mathbf{u}_e \cdot \nabla \right) \mathbf{u}_e &= -en_e(\mathbf{E} + \mathbf{u}_e \times \mathbf{B}) - \nabla p_e - m_e n_e \bar{v}_{ci} (\mathbf{u}_e - \mathbf{u}_i), \\ m_i n_i \left( \frac{\partial}{\partial t} + \mathbf{u}_i \cdot \nabla \right) \mathbf{u}_i &= en_i(\mathbf{E} + \mathbf{u}_i \times \mathbf{B}) - \nabla p_i - m_e n_e \bar{v}_{ei} (\mathbf{u}_i - \mathbf{u}_e).\end{aligned}\tag{10.51}$$

*Conservation of energy*

$$\begin{aligned}\frac{3}{2} n_e \left( \frac{\partial}{\partial t} + \mathbf{u}_e \cdot \nabla \right) T_e + p_e \nabla \cdot \mathbf{u}_e + \nabla \cdot \mathbf{q}_e &= S_e, \\ \frac{3}{2} n_i \left( \frac{\partial}{\partial t} + \mathbf{u}_i \cdot \nabla \right) T_i + p_i \nabla \cdot \mathbf{u}_i + \nabla \cdot \mathbf{q}_i &= S_i,\end{aligned}\tag{10.52}$$

with

$$\begin{aligned}S_e &= \frac{F_e^{(a)}}{4} E_a n_e^2 \langle \sigma v \rangle + F_e^{(a)} S_a + \eta J^2 - C_B n_e^2 T_e^{1/2} - \frac{3}{2} n_e \bar{v}_{eq} (T_e - T_i), \\ S_i &= \frac{1 - F_e^{(a)}}{4} E_a n_e^2 \langle \sigma v \rangle + (1 - F_e^{(a)}) S_a - \frac{3}{2} n_e \bar{v}_{eq} (T_i - T_e).\end{aligned}\tag{10.53}$$

# Two-fluid model

- **Collisional friction force:** result of momentum exchange collisions

*Conservation of momentum*

$$\begin{aligned} m_e n_e \left( \frac{\partial}{\partial t} + \mathbf{u}_e \cdot \nabla \right) \mathbf{u}_e &= -en_e(\mathbf{E} + \mathbf{u}_e \times \mathbf{B}) - \nabla p_e - m_e n_e \bar{v}_{ei} (\mathbf{u}_e - \mathbf{u}_i), \\ m_i n_i \left( \frac{\partial}{\partial t} + \mathbf{u}_i \cdot \nabla \right) \mathbf{u}_i &= en_i(\mathbf{E} + \mathbf{u}_i \times \mathbf{B}) - \nabla p_i - m_e n_e \bar{v}_{ei} (\mathbf{u}_i - \mathbf{u}_e). \end{aligned} \quad (10.51)$$



# Two-fluid model

- Rate of change of internal energy
- Compression work
- Thermal conduction

Conservation of energy

$$\begin{aligned} \frac{3}{2}n_e \left( \frac{\partial}{\partial t} + \mathbf{u}_e \cdot \nabla \right) T_e + p_e \nabla \cdot \mathbf{u}_e + \nabla \cdot \mathbf{q}_e &= S_e, \\ \frac{3}{2}n_i \left( \frac{\partial}{\partial t} + \mathbf{u}_i \cdot \nabla \right) T_i + p_i \nabla \cdot \mathbf{u}_i + \nabla \cdot \mathbf{q}_i &= S_i, \end{aligned} \quad (10.52)$$

with

$$\begin{aligned} S_e &= \frac{F_e^{(\alpha)}}{4} E_\alpha n_e^2 \langle \sigma v \rangle + F_e^{(a)} S_a + \eta J^2 - C_B n_e^2 T_e^{1/2} - \frac{3}{2} n_e \bar{v}_{eq} (T_e - T_i), \\ S_i &= \frac{1 - F_e^{(\alpha)}}{4} E_\alpha n_e^2 \langle \sigma v \rangle + (1 - F_e^{(a)}) S_a - \frac{3}{2} n_e \bar{v}_{eq} (T_i - T_e). \end{aligned} \quad (10.53)$$

# From two-fluid to single fluid assumptions of ideal MHD

- Length scales  $\gg$  Larmor radius
- Frequencies  $\ll$  gyrofrequency
- Fluid velocity  $\ll$  thermal velocity
- No electron inertia
- Quasi-neutrality
- No Hall term in Ohm's law

$$a \gg r_{Li} \gg r_{Le} \approx \lambda_{de}$$

# The single fluid model

○

mass :  $\frac{d\rho}{dt} + \rho \nabla \cdot \mathbf{v} = 0;$

momentum :  $\rho \frac{d\mathbf{v}}{dt} = \mathbf{J} \times \mathbf{B} - \nabla p;$

Ohm's law :  $\mathbf{E} + \mathbf{v} \times \mathbf{B} = 0 \quad \text{ideal MHD},$

$\mathbf{E} + \mathbf{v} \times \mathbf{B} = \eta_{||} \mathbf{J} \quad \text{resistive MHD};$

energy :  $\frac{d}{dt} \left( \frac{p}{\rho^\gamma} \right) = 0;$

Maxwell :  $\nabla \times \mathbf{E} = -\frac{\partial \mathbf{B}}{\partial t},$

$\nabla \times \mathbf{B} = \mu_0 \mathbf{J},$

$\nabla \cdot \mathbf{B} = 0.$

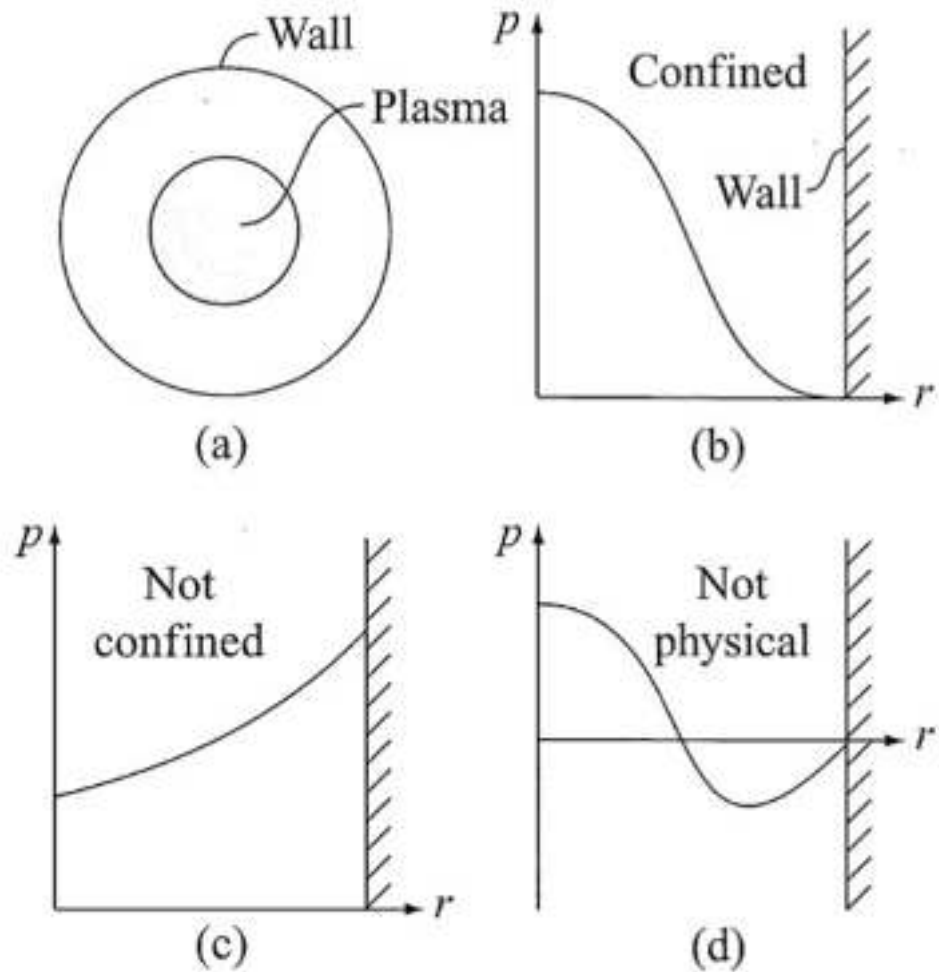
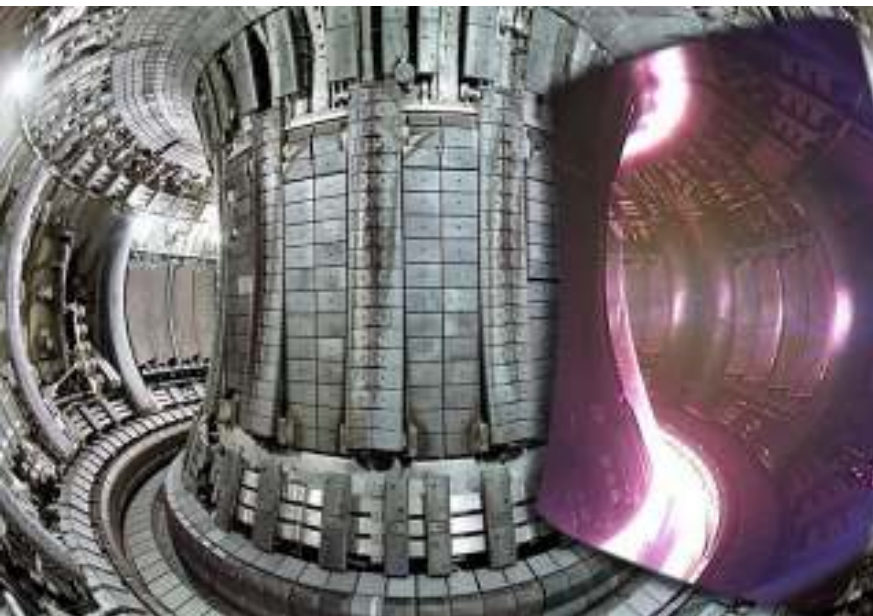
***Plasma can be described as a single magnetized fluid***

**4**

# **MHD equilibrium**

# The problem of MHD equilibrium

JET ([www.efda.org](http://www.efda.org))



# The MHD equilibrium

$$\frac{\partial \rho}{\partial t} + \nabla \cdot (\rho \underline{v}) = 0 \quad (1)$$

$$\rho \left( \frac{\partial \underline{v}}{\partial t} + \underline{v} \cdot \nabla \underline{v} \right) = \nabla P - \underline{J} \times \underline{B} \quad (2)$$

$$\frac{\partial P}{\partial t} + \underline{v} \cdot \nabla P = \gamma P \nabla \cdot \underline{v} \quad (3)$$

$$\frac{\partial \underline{B}}{\partial t} = \nabla \times (\underline{v} \times \underline{B}) \quad (4)$$

- Plasma equilibrium ( $\underline{v}=0$  if flow  $\ll$  sound speed):

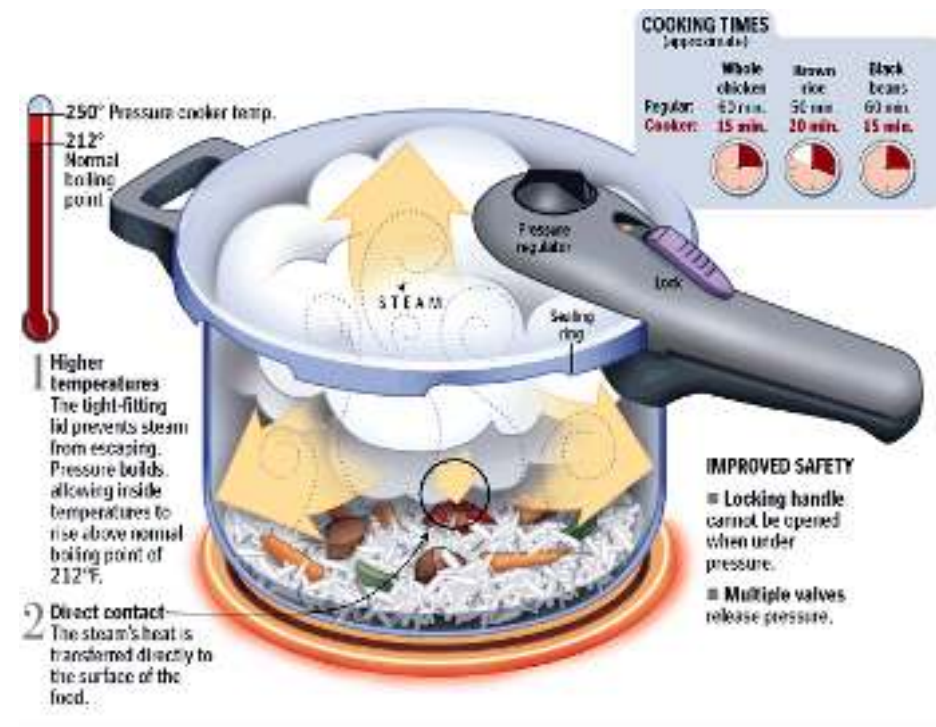
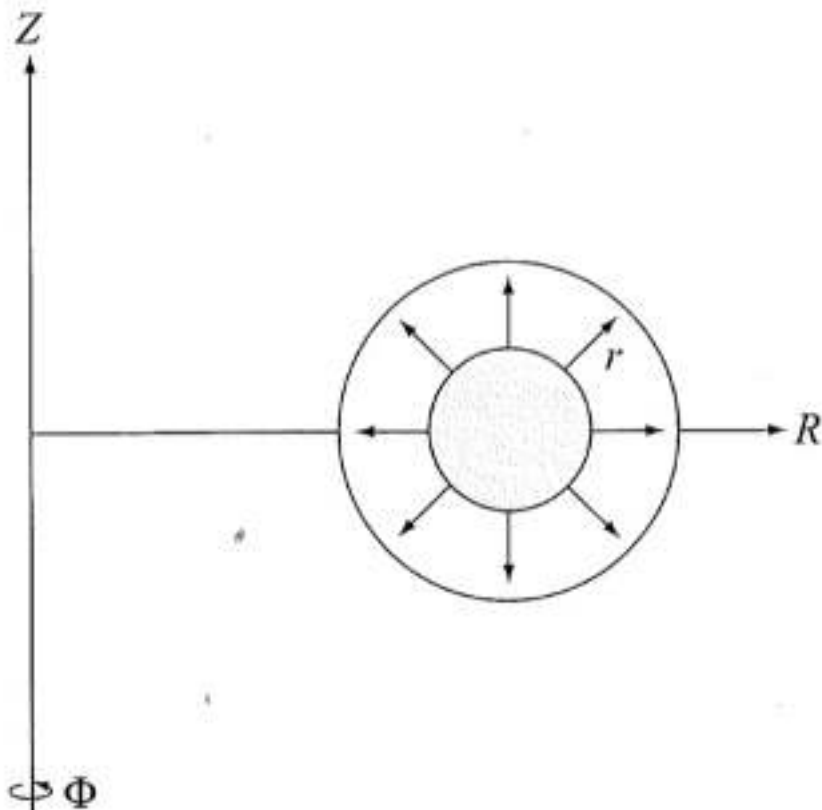
$$\frac{\partial}{\partial t} = 0 \quad \vec{v} = 0$$

# The MHD equilibrium

- MHD equilibrium in toroidal geometry has two parts
  - **RADIAL PRESSURE BALANCE**
  - **TOROIDAL FORCE BALANCE**

# Radial pressure balance

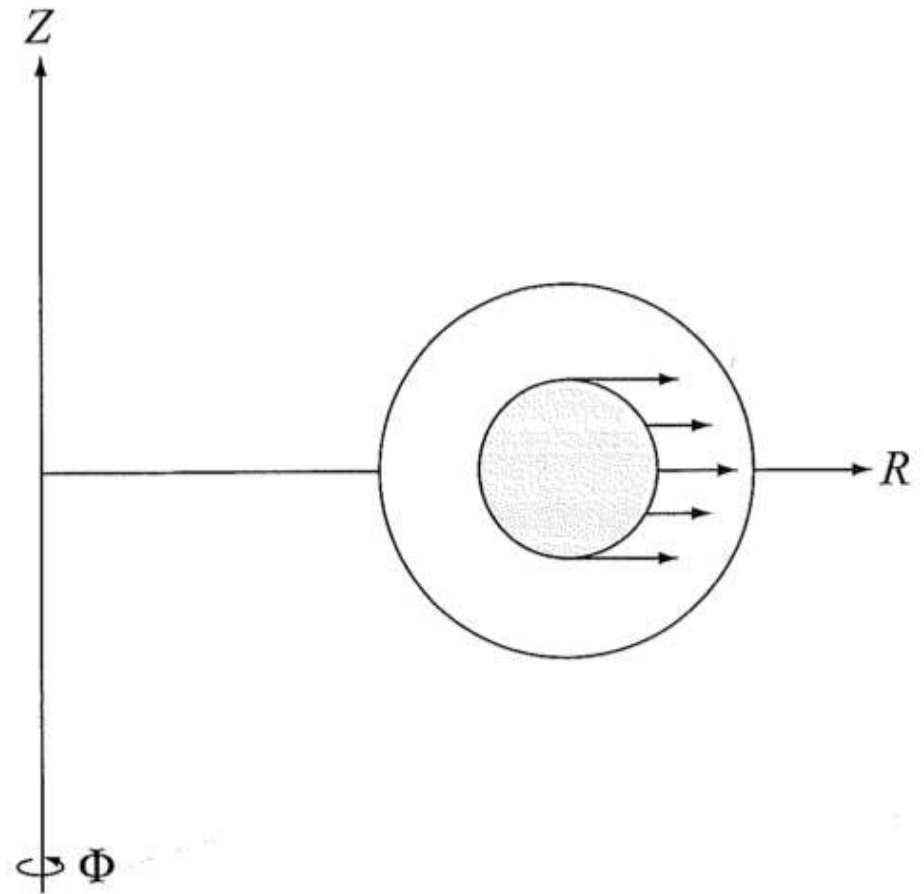
- The plasma is a hot core of gas that tends to expand uniformly along the minor radius  $r$



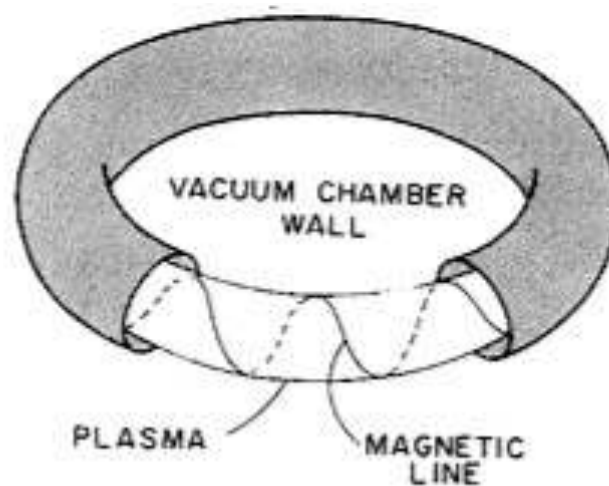
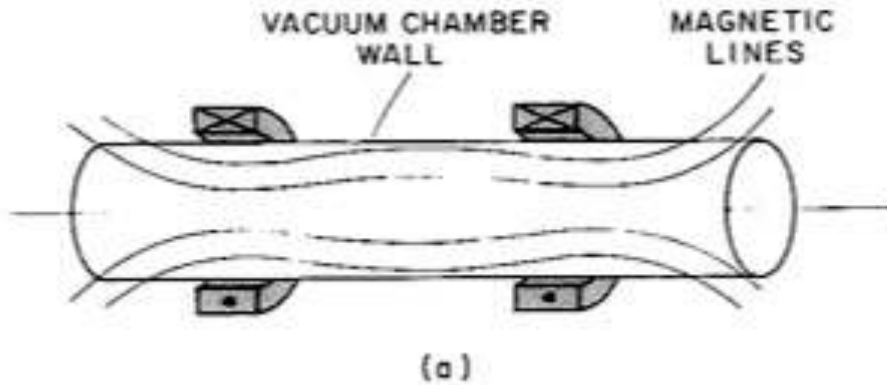
# Toroidal force balance

- Because of the toroidal geometry, unavoidable forces are generated by both the toroidal and poloidal B

- They tend to push the plasma outward.
- Need to be balanced

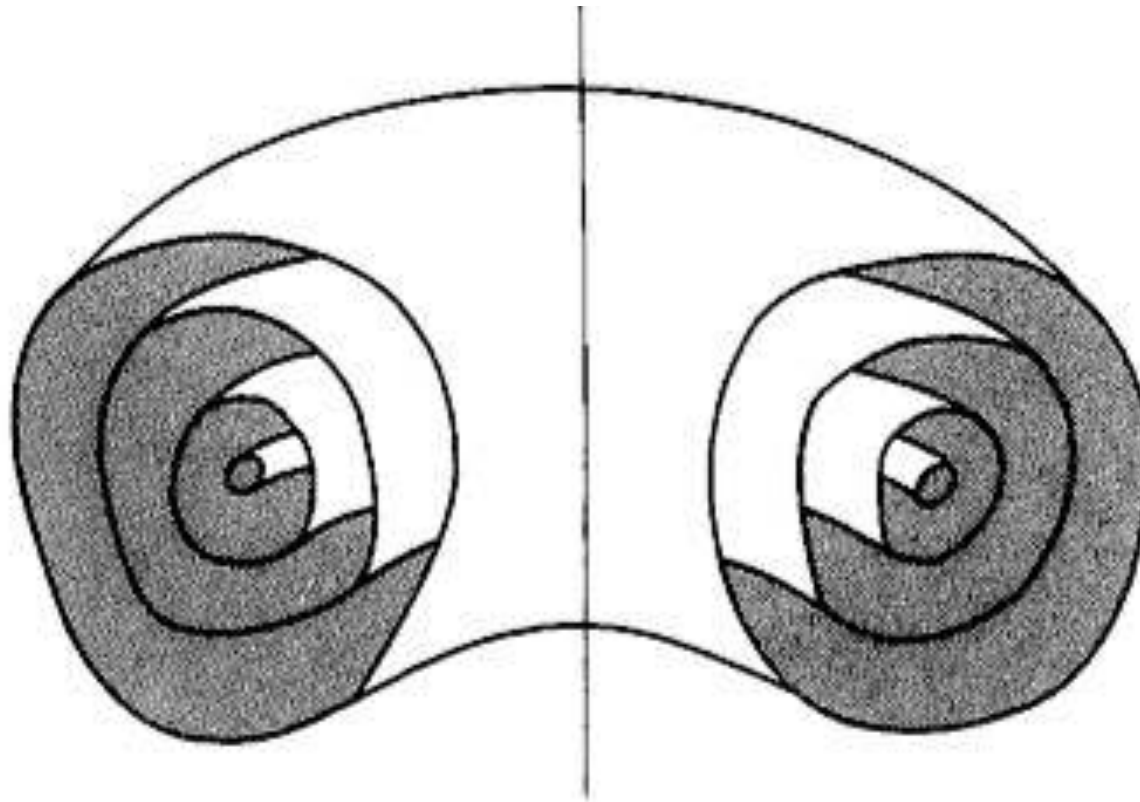


# Linear vs. toroidal configurations



# Magnetic flux surfaces

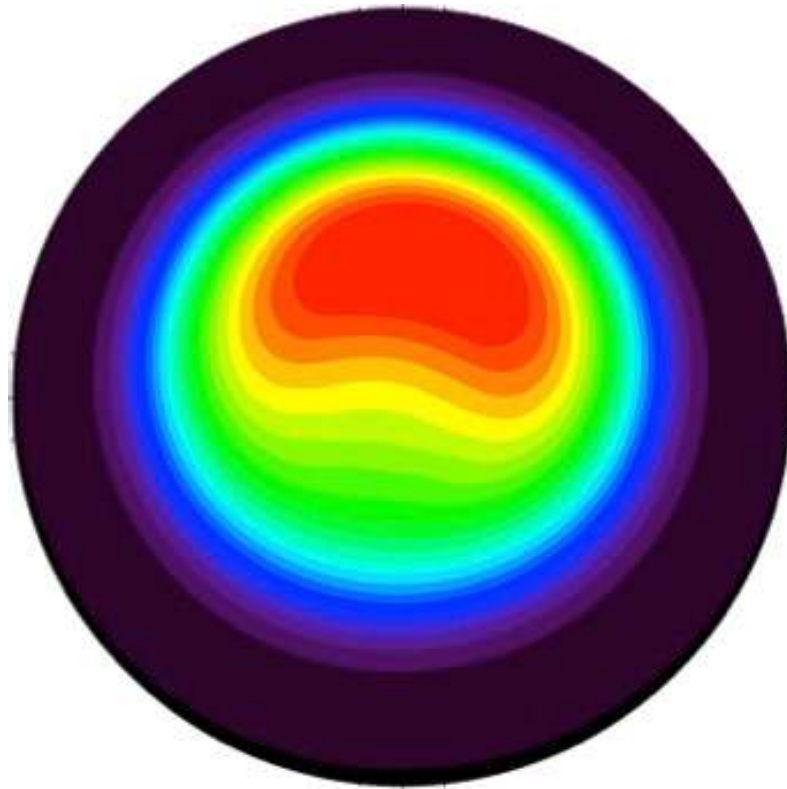
$$\mathbf{B} \cdot \nabla p = 0$$



Magnetic field perpendicular to pressure gradient

# Pressure is constant on magnetic flux surfaces

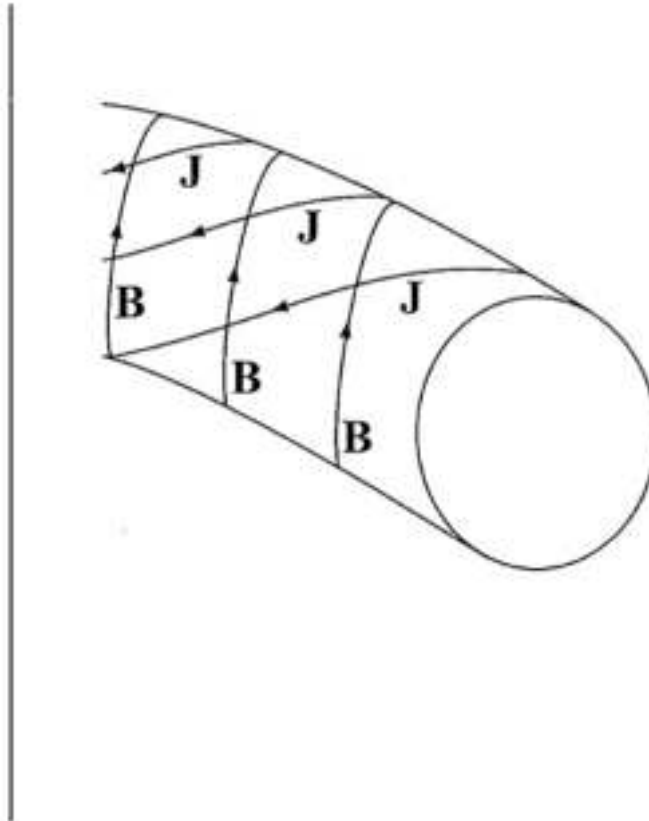
- Important for experimental measurements



***Pressure is constant on magnetic flux surfaces***

# Current, magnetic and pressure surfaces

The angle between  $\mathbf{J}$  and  $\mathbf{B}$  is in general arbitrary



$$\vec{J} \bullet \nabla p = 0$$

Current density perpendicular to pressure gradient

# MHD equilibrium equation

$$\vec{J} \times \vec{B} = \nabla p$$

# MHD equilibrium equation

$$\vec{J} \times \vec{B} = \nabla p$$

$$\nabla \times \vec{B} = \mu_0 \vec{J}$$

$$\frac{1}{\mu_0} (\nabla \times \vec{B}) \times \vec{B} = \nabla p$$

# MHD equilibrium equation

$$\vec{J} \times \vec{B} = \nabla p$$

$$\nabla \times \vec{B} = \mu_0 \vec{J}$$

$$\frac{1}{\mu_0} (\nabla \times \vec{B}) \times \vec{B} = \nabla p$$

$$\vec{B} \times (\nabla \times \vec{B}) = \frac{1}{2} \nabla B^2 - (\vec{B} \cdot \nabla) \vec{B}$$

# MHD equilibrium equation

$$\vec{J} \times \vec{B} = \nabla p$$

$$\nabla \times \vec{B} = \mu_0 \vec{J}$$

$$\frac{1}{\mu_0} (\nabla \times \vec{B}) \times \vec{B} = \nabla p$$

$$\vec{B} \times (\nabla \times \vec{B}) = \frac{1}{2} \nabla B^2 - (\vec{B} \cdot \nabla) \vec{B}$$

$$\nabla \left( p + \frac{B^2}{2\mu_0} \right) - (\vec{B} \cdot \nabla) \vec{B} = 0$$

# Radial pressure balance

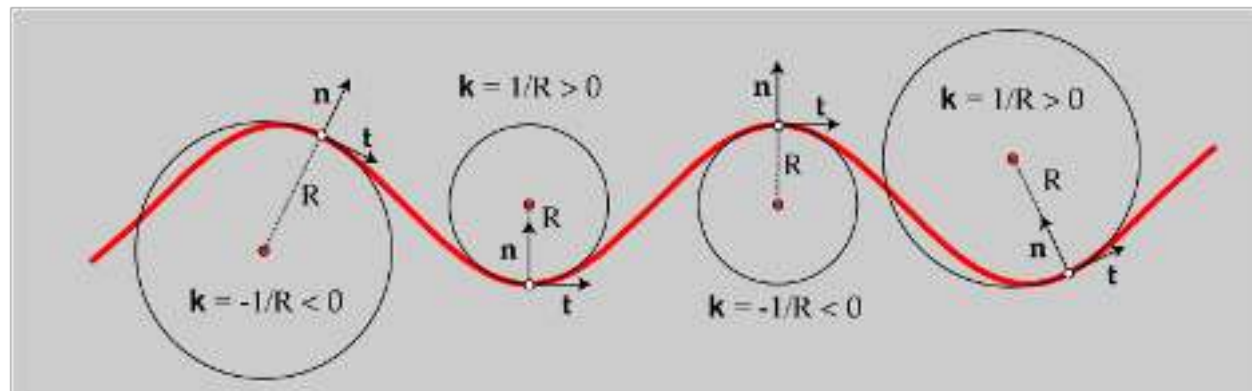
$$\nabla_{\perp} \left( p + \frac{B^2}{2\mu_0} \right) - \frac{B^2}{\mu_0} (\hat{b} \cdot \nabla) \hat{b} = 0$$

$$\hat{b} = \frac{\vec{B}}{B}$$

$$\nabla_{\perp} = \nabla - \hat{b}(\hat{b} \cdot \nabla)$$

Curvature

$$\vec{\kappa} = \hat{b}(\hat{b} \cdot \nabla) = -\frac{\vec{R}_C}{R_C^2}$$



# Radial pressure balance

Magnetic field provide two radial force terms:

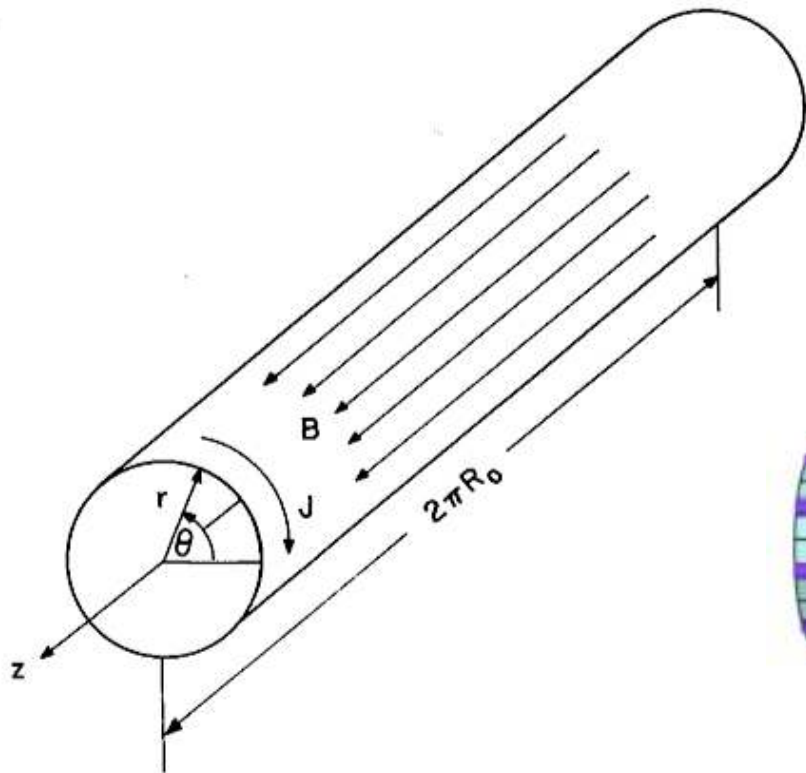
$$\nabla_{\perp} \left( p + \frac{B^2}{2\mu_0} \right) - \frac{B^2}{\mu_0} (\hat{b} \cdot \nabla) \hat{b} = 0$$

**PRESSURE**      **TENSION**

**Magnetic field exerts pressure and tension**

# Magnetic pressure: $\Theta$ -pinch

- Configuration with pure toroidal field



$$\mathbf{J} \times \mathbf{B} = \nabla p$$
$$\nabla \times \mathbf{B} = \mu_0 \mathbf{J}$$
$$\nabla \cdot \mathbf{B} = 0$$

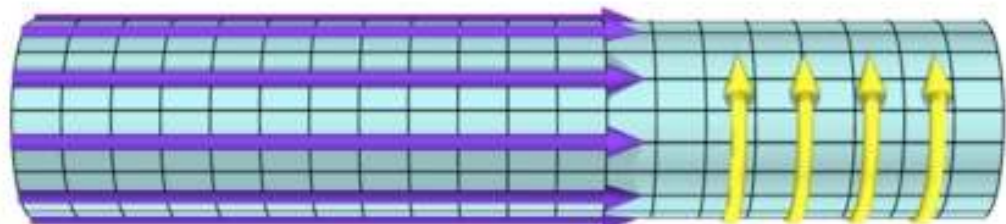


Figure 5.1. Linear  $\Theta$ -pinch geometry.

# A simple example: $\Theta$ -pinch

- **MAGNETIC + KINETIC** pressure = **CONSTANT** in the plasma
- Plasma confined **by the pressure of the applied magnetic field**

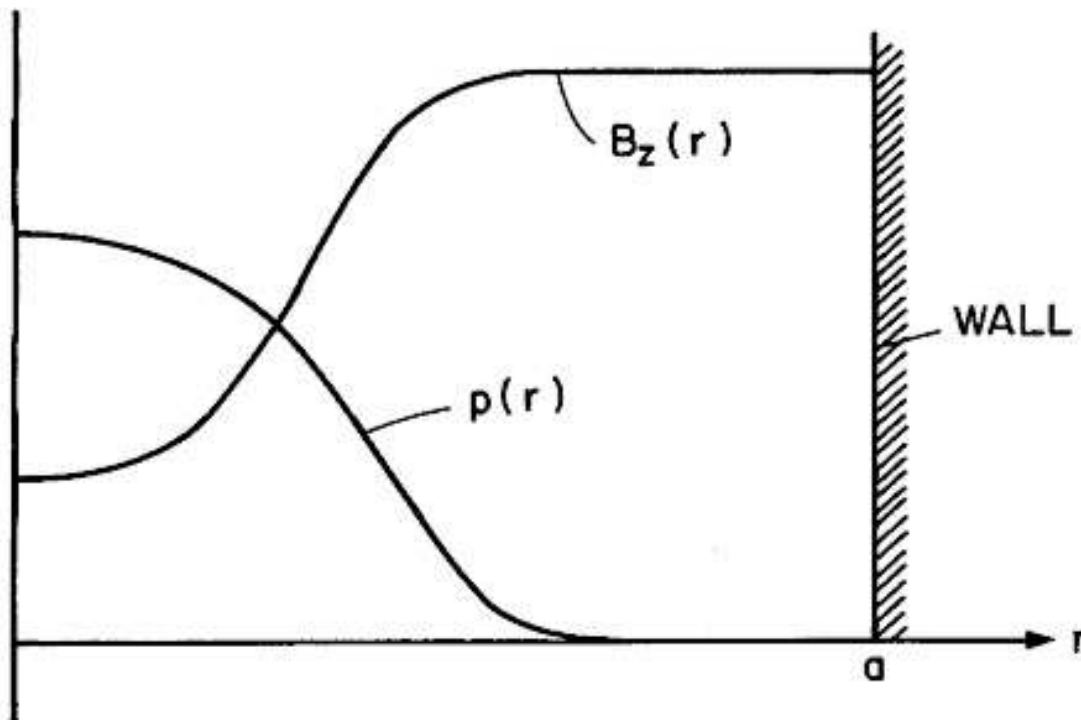
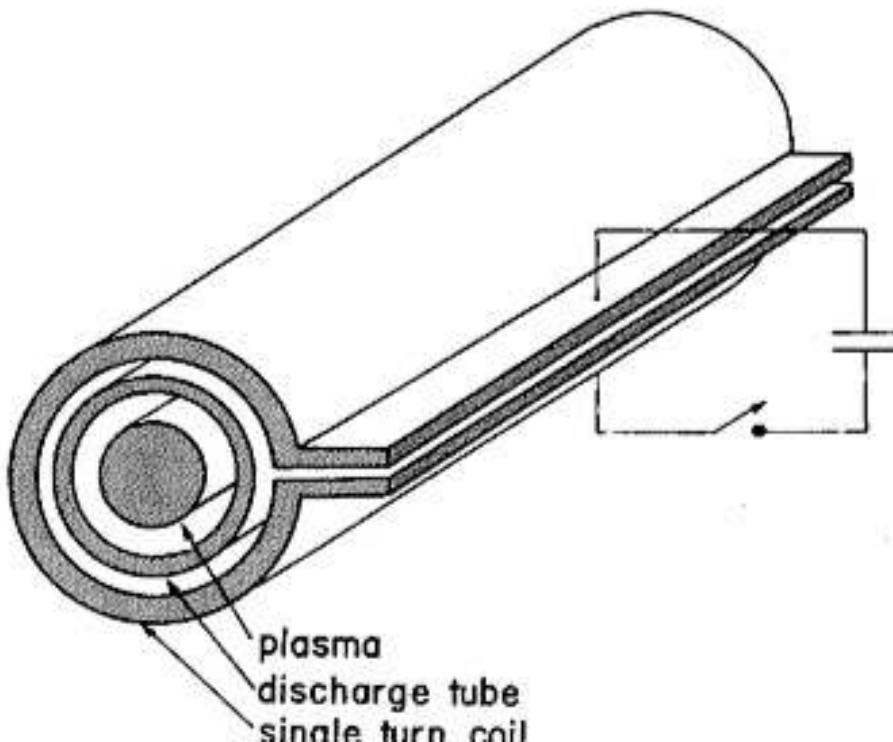
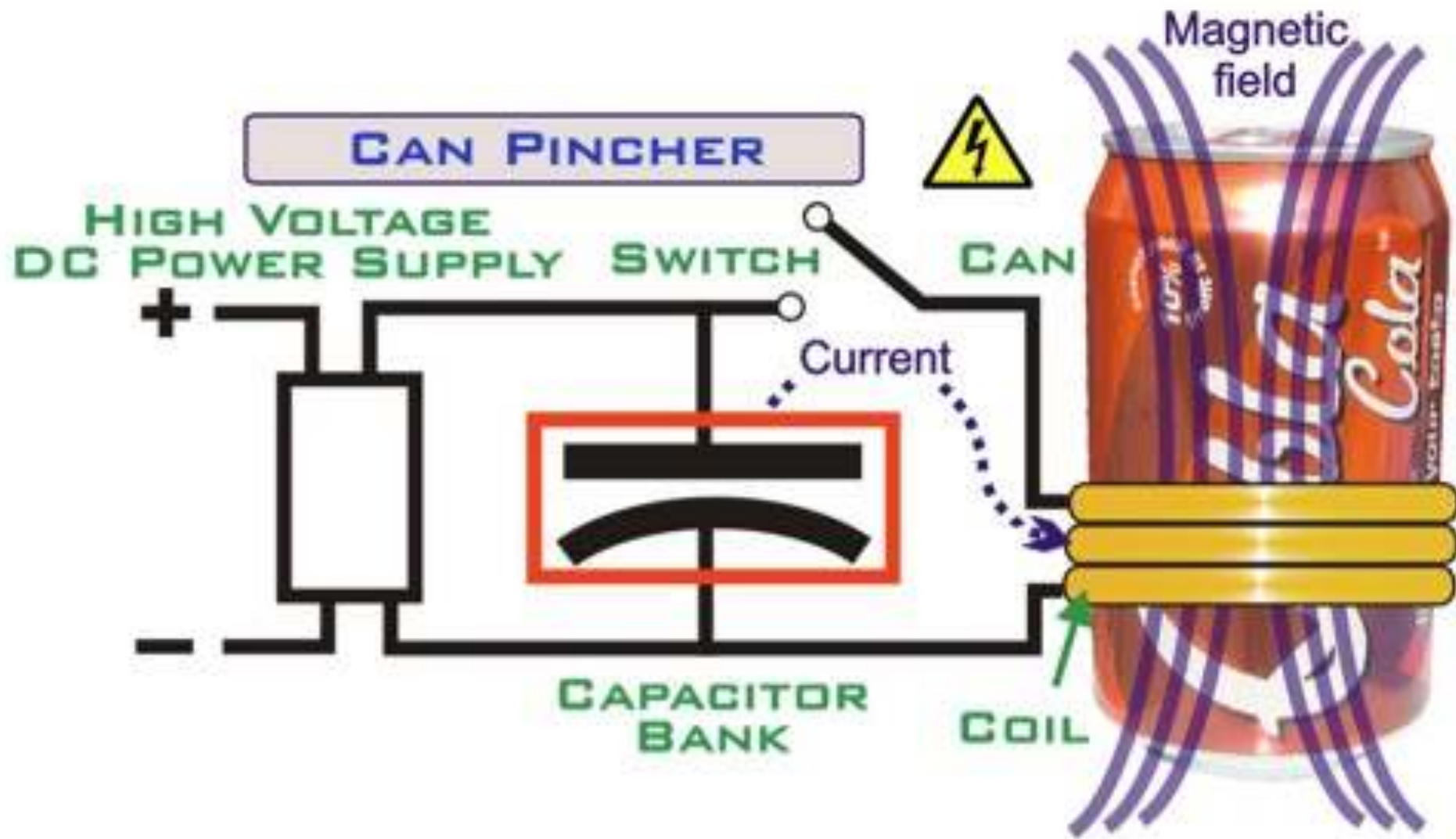


Figure 5.2. Equilibrium profiles for a  $\theta$  pinch.

# Experimental $\Theta$ -pinch

- $\Theta$ -pinch devices **among the first experiments to be realized**
- **End-losses severe problem**
- A  $\Theta$ -pinch can not be bent into a toroidal equilibrium





# Z-pinch

- Purely poloidal field
- All quantities are only functions of  $r$

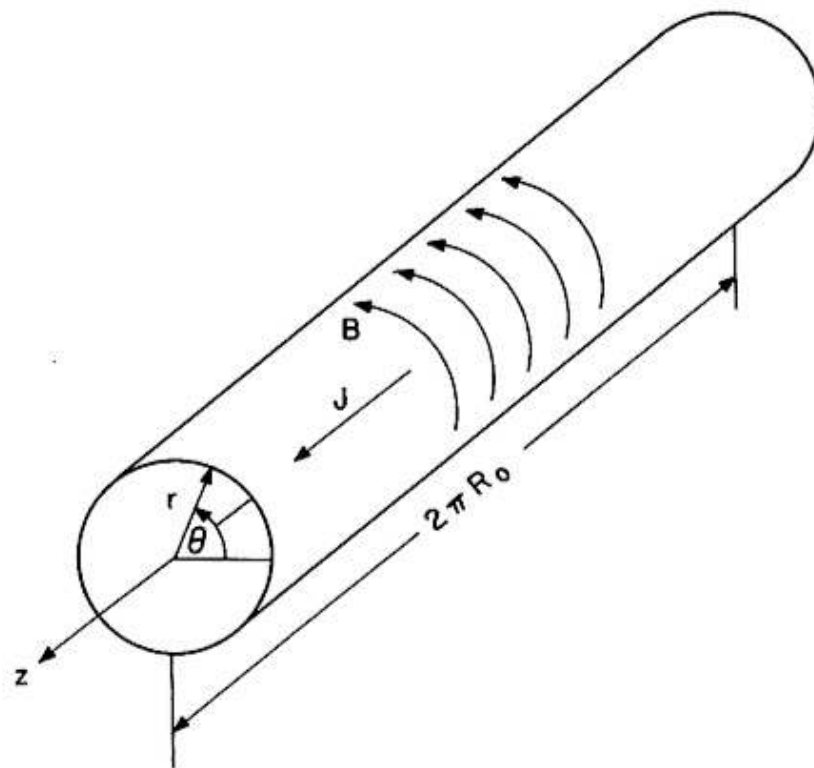


Figure 5.4. Linear Z-pinch geometry.

# Z-pinch

- In contrast to the  $\Theta$ -pinch, for a Z-pinch it is the tension force and not the magnetic pressure gradient that provides radial confinement of the plasma

$$\frac{d}{dr} \left( p + \frac{B_\theta^2}{2\mu_0} \right) + \frac{B_\theta^2}{\mu_0 r} = 0 \quad (5.15)$$

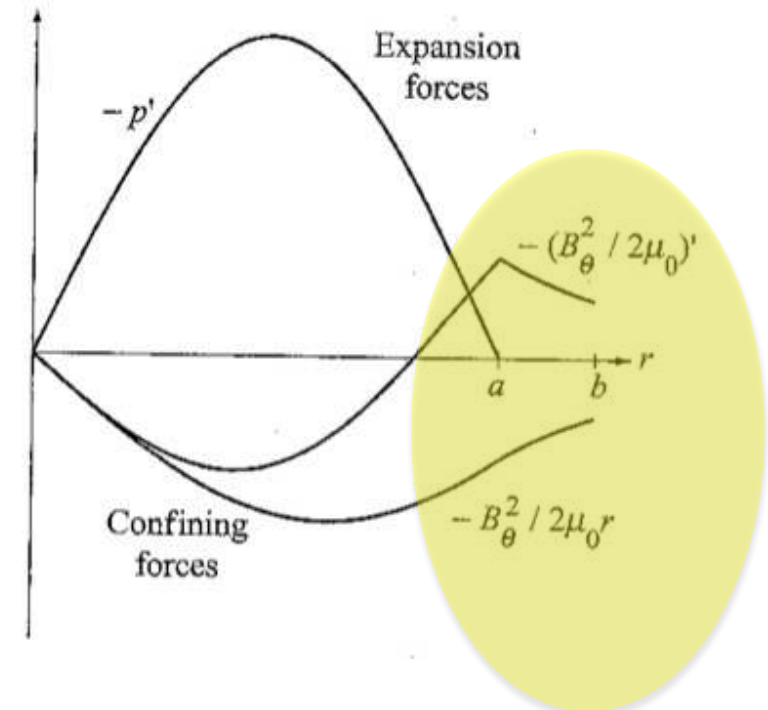
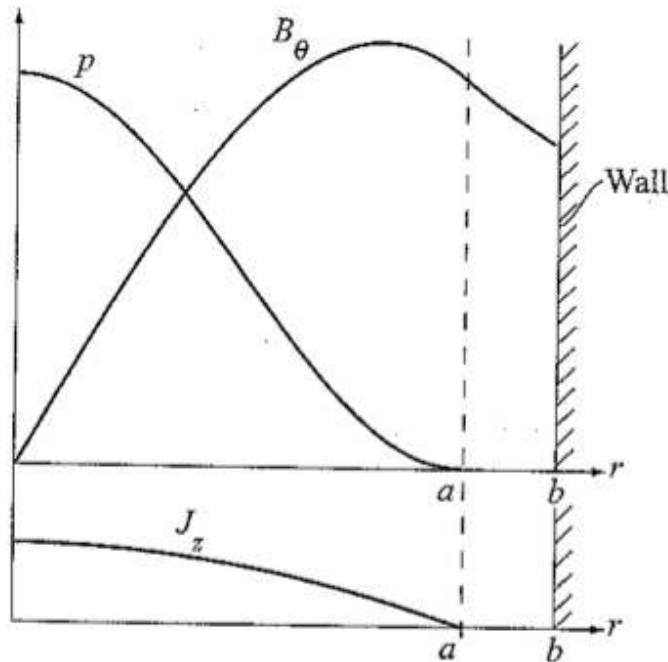
- The Bennet pinch satisfies the Z-pinch equilibrium



Willard Harrison Bennett (far right) with colleagues at the U.S. Naval Research Laboratory, working on the Störmertron tube

$$B_\theta = \frac{\mu_0 I_0}{2\pi} \frac{r}{r^2 + r_0^2}$$
$$J_z = \frac{I_0}{\pi} \frac{r_0^2}{(r^2 + r_0^2)^2}$$
$$p = \frac{\mu_0 I_0^2}{8\pi^2} \frac{r_0^2}{(r^2 + r_0^2)^2}$$

# Z-pinch



Tension force acts inwards at the edge  
providing radial pressure balance.

# Experimental Z-pinch

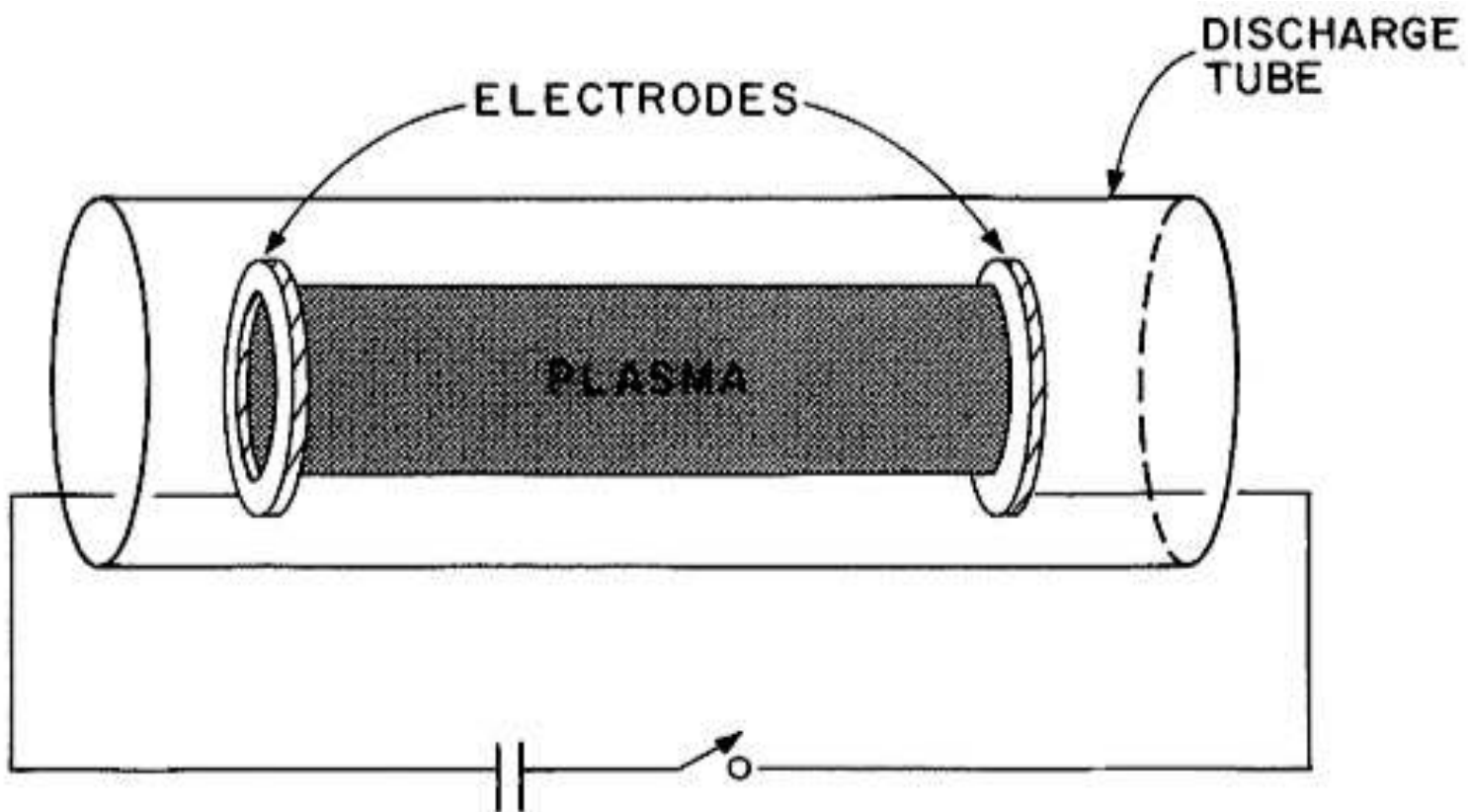


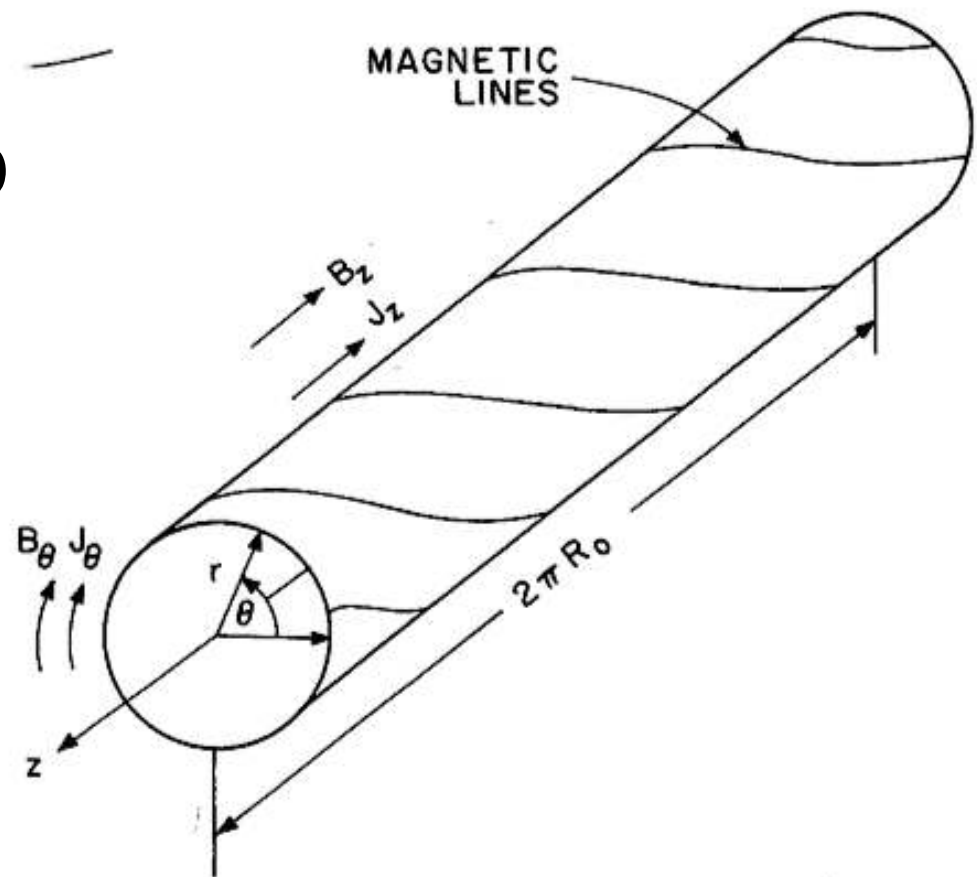
Figure 5.6. Schematic diagram of a linear  $Z$ -pinch experiment.

**Z- and Theta-pinches are at the basis of many toroidal confinement concepts**

# General screw pinch

Though the momentum equation is non-linear, the  $\Theta$ -pinch and Z-pinch forces add as a linear superposition

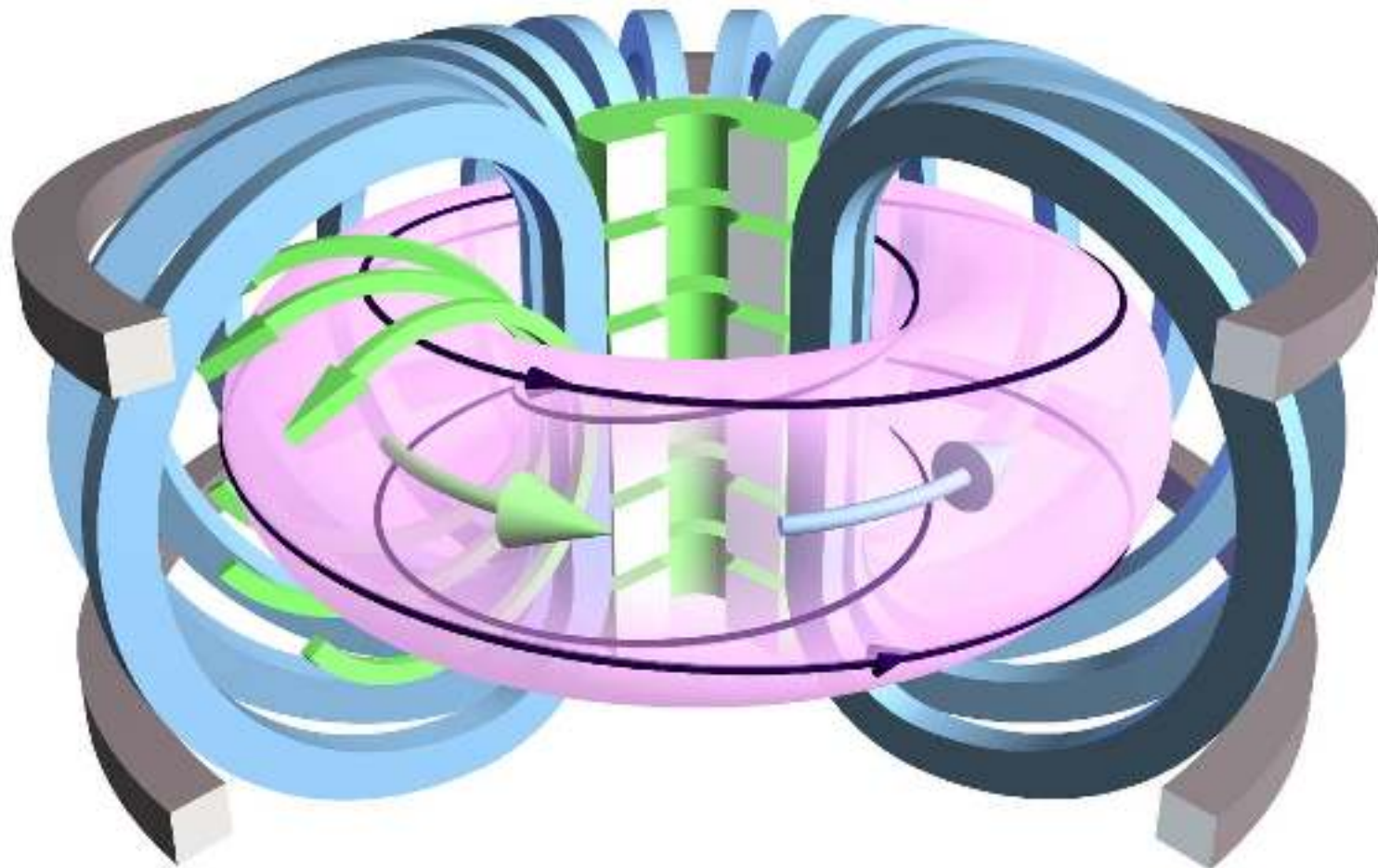
$$\frac{d}{dr} \left( p + \frac{B_p^2}{2\mu_0} + \frac{B_t^2}{2\mu_0} \right) + \frac{B_p^2}{\mu_0 r} = 0$$



One is free to specify two functions, e.g.  $B_p(r)$  and  $B_t(r)$

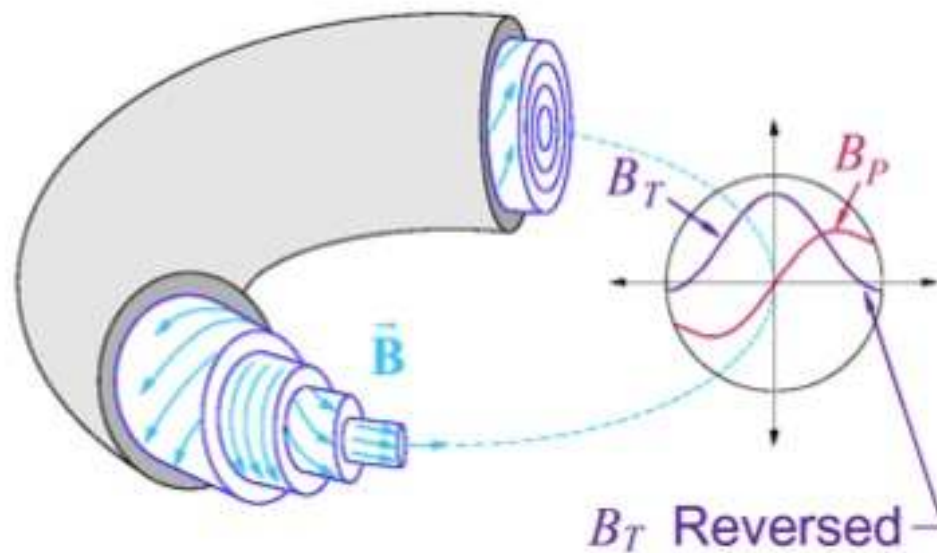
Figure 5.7. General screw-pinch geometry.

# The tokamak



# Reversed Field Pinch: the low field approach

- The RFP configuration is similar to a tokamak:
  - it is toroidal
  - a toroidal electrical current is driven in a plasma embedded in a toroidal magnetic field: pinch effect.
  - ....but the **applied toroidal field is 10x weaker** than in a tokamak

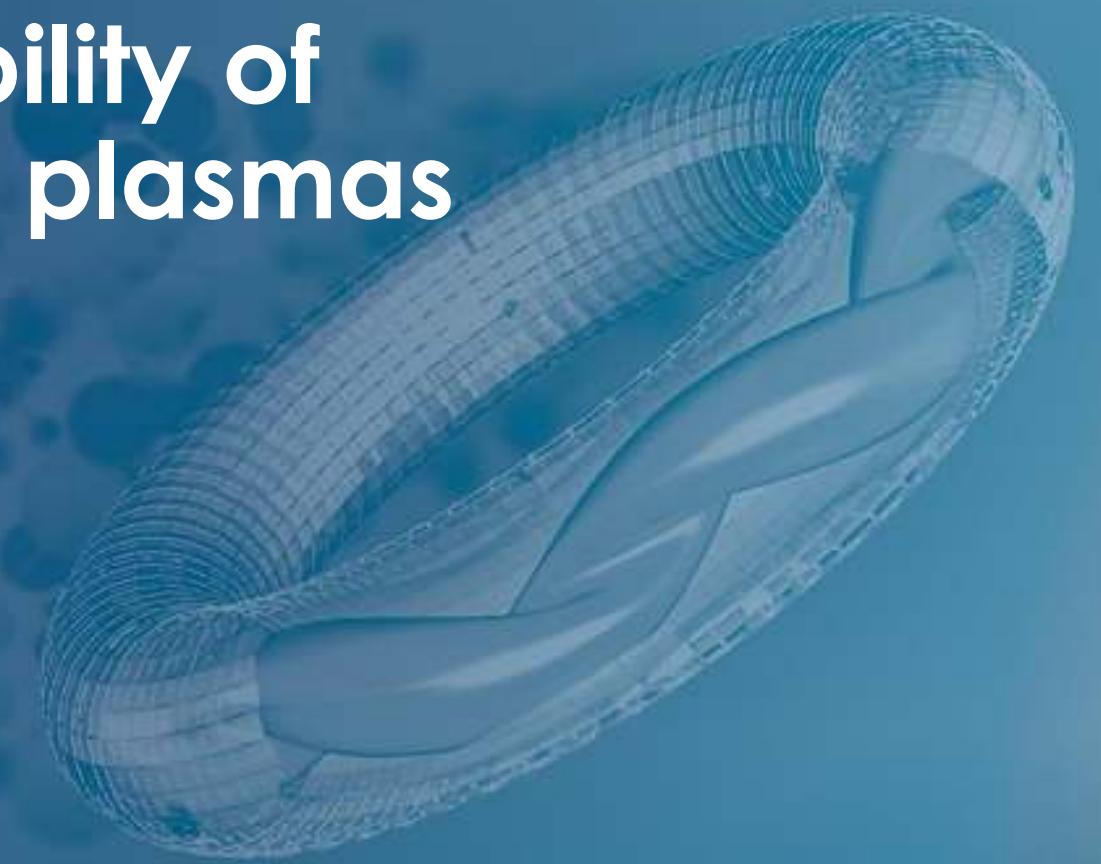




CONSORZIO RFX  
*Ricerca Formazione Innovazione*

# MHD equilibrium & stability of magnetically confined plasmas

Plasma physics & diagnostics (AC1)  
Padova (& zoom), November 26<sup>th</sup> 2024



By Leonardo Pigatto (presented by Tommaso Bolzonella)

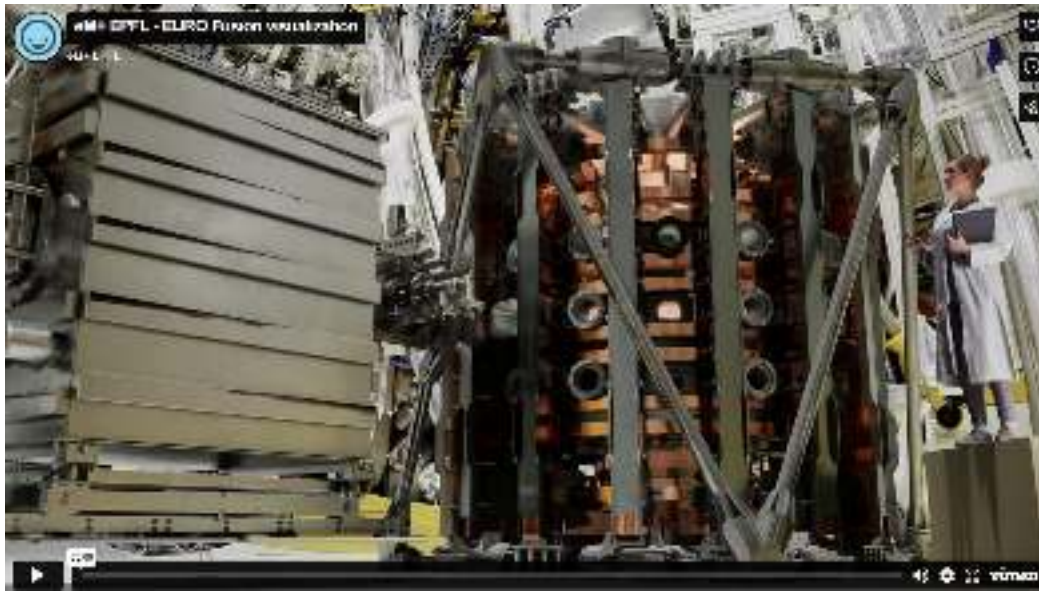
Consortium RFX (CNR, ENEA, INFN, University of Padova, Acciaierie Venete SpA) Corso Stati Uniti, 4 – 35127 Padova (Italy)

[leonardo.pigatto@igi.cnr.it](mailto:leonardo.pigatto@igi.cnr.it) [tommaso.Bolzonella@igi.cnr.it](mailto:tommaso.Bolzonella@igi.cnr.it)

0039 049 829 5606

0039 049 829 5083

# Video: 3D visualization brings nuclear fusion to life



## Acknowledgement:

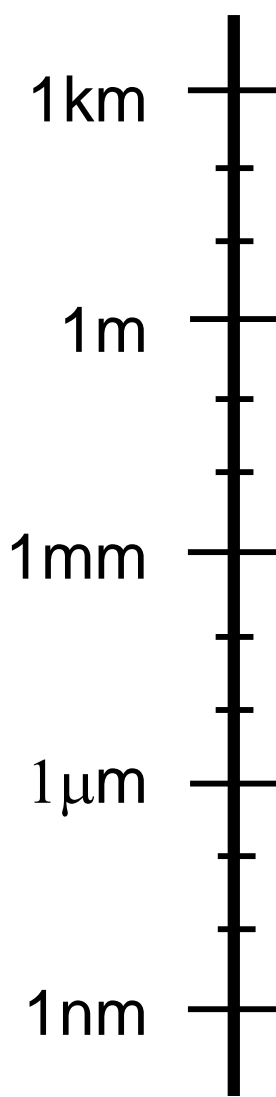
Render from the realtime application developed by the Laboratory for Experimental Museology and the Swiss Plasma Centre as part of EPFL's Advanced Computing Hub of the EUROfusion Consortium, 2023.

Le particelle che hanno una velocità parallela al campo piccola sono le candidate per avere trapped orbits (banana orbits).

- **Video:** <https://player.vimeo.com/video/986450227?share=copy>
- **Description:** <https://www.epfl.ch/labs/emplus/advanced-computing-hub-eurofusion-2021-2025/>
- **EUROfusion news:** <https://euro-fusion.org/member-news/3d-visualization-brings-nuclear-fusion-to-life/>

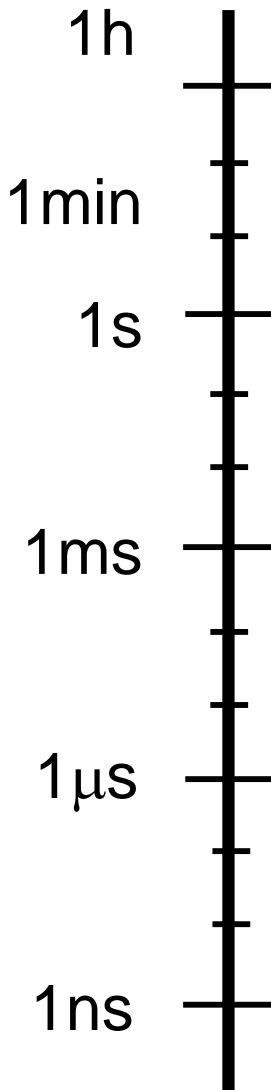


# Scales in plasma physics: lengths



- Mean free path
  - Major radius  $R$ , minor radius  $a$
  - Gradient length of n and T
  - Ion Larmor radius  $\rho_{Li}$
  - Electron Larmor radius  $\rho_{Le}$
  - Debye length  $\lambda_D$
  - Visible light
  - X-ray
- 
- The diagram shows three circular regions representing plasma configurations. The top region contains blue dots representing ions, with a red zigzag line showing a particle's path between them. The middle region is a circle with a central cross and two arrows pointing outwards, labeled  $\rho_{Li}$ . The bottom region is a circle with a central cross and one arrow pointing outwards, labeled  $\rho_{Le}$ . Below these circles is a horizontal double-headed arrow labeled  $\lambda_D$ . To the right of the circles is a double-headed arrow labeled  $B$ .

# Scales in plasma physics: times

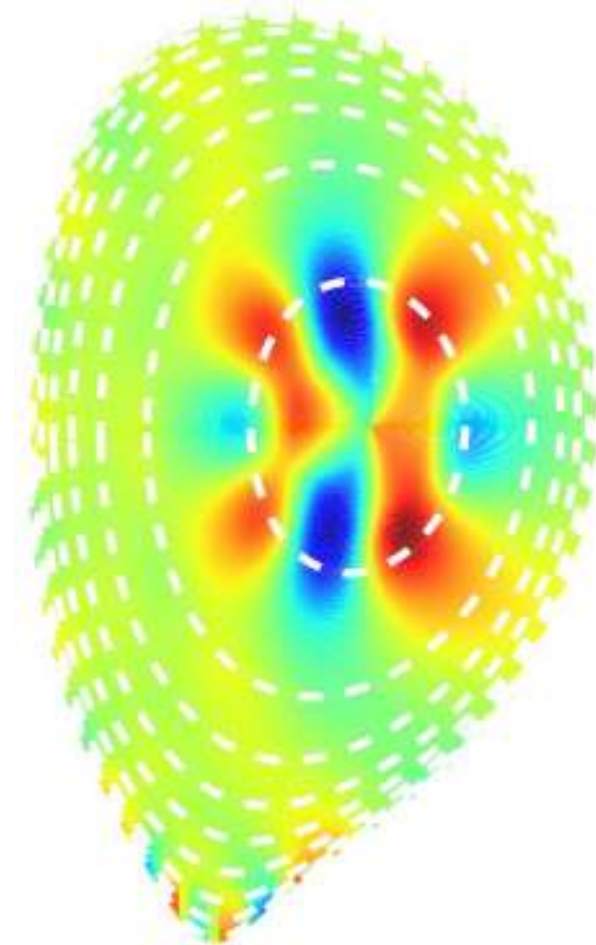


- Current diffusion time
- Plasma discharge time
- Energy confinement time
- Energy exchange time
- Ion collision time
- Electron collision time



# Outline

1. Recap on models for plasma description
2. Magnetohydrodynamic model
  - Basic properties
  - Ideal MHD
  - Equilibrium
3. Toroidal equilibrium: the Grad-Shafranov equation
4. Figures of merit and “straight tokamak” limit
5. Linearized equations and force operator
6. Stability
  - Normal modes
  - Energy principle and intuitive form of  $W$
7. Current driven instabilities
8. Global MHD instabilities in Tokamaks

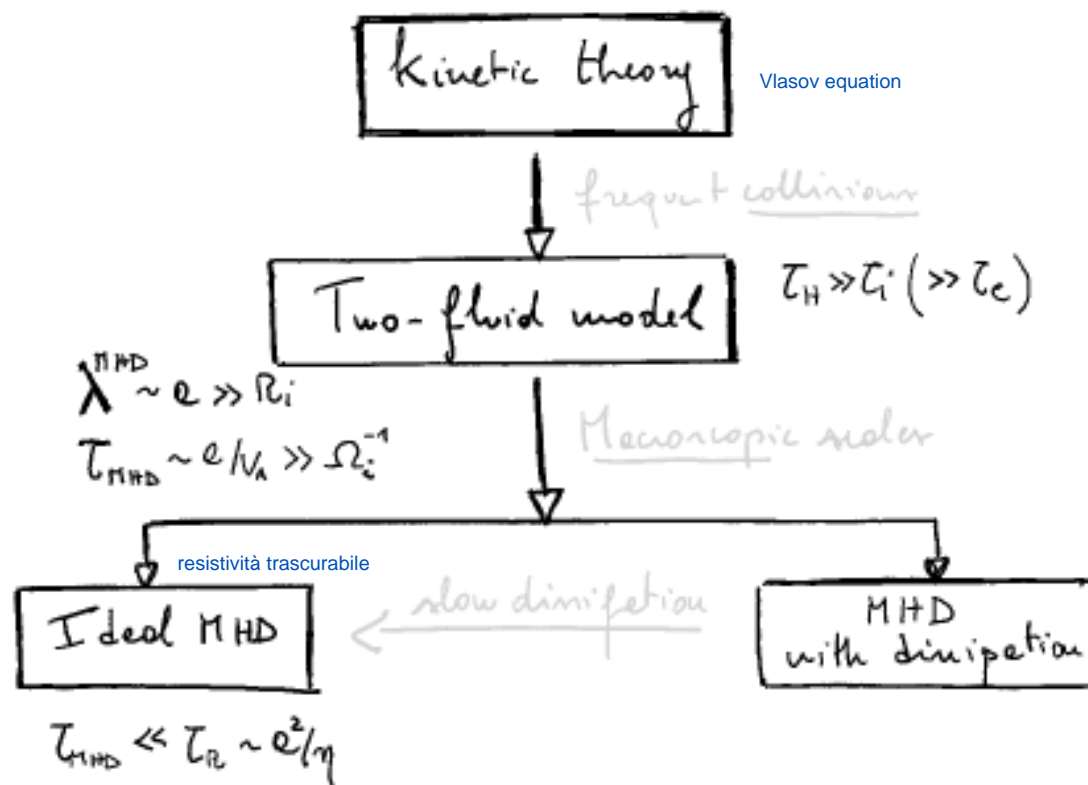


# PART 1: MHD model and equilibrium



# Different ways to describe charged particles in EM field depending on scales & interactions...

- **Single particle** description: equation of motion for a charged particle in EM field
- **Kinetic** plasma theory: a statistical approach describing collective behavior with distribution functions



Frequent collisions for separation of e- & ion fluids

$$\tau_H \gg \tau_i (\gg \tau_e)$$

Macroscopic scales for **single fluid** description of plasma in terms of averaged macroscopic quantities

Slow (no) dissipation: **ideal MHD**



# The MHD model

Covers a wide range of plasma dynamics  
relevant for equilibrium, waves and instabilities  
with  $\tau \sim [10^{-6} \div 10^{-3}]s$

MHD EQUATION - one fluid model

$$\frac{\partial \rho}{\partial t} + \nabla \cdot \rho \mathbf{v} = 0$$

$$\rho \left( \frac{\partial \mathbf{v}}{\partial t} + \mathbf{v} \cdot \nabla \mathbf{v} \right) + \nabla p - \mathbf{j} \times \mathbf{B} = 0$$

$$\frac{\partial p}{\partial t} + \mathbf{v} \cdot \nabla p + \Gamma p \nabla \cdot \mathbf{v} = (\Gamma - 1)\eta |\mathbf{j}|^2$$

$$\frac{\partial \mathbf{B}}{\partial t} + \nabla \times \mathbf{E} = 0$$

$$\nabla \times \mathbf{B} = \mu_0 \mathbf{j}$$

$$\mathbf{E} + \mathbf{v} \times \mathbf{B} = \eta \mathbf{j}$$

$$\nabla \cdot \mathbf{B} = 0$$

(1) continuity

(2) momentum

(3) internal energy

Conservation of energy. Spesso sostituita da casi semplificati (equazioni scalari con la pressione)

(4) Faraday

(5) Ampere

(6) Ohm

(7) No magnetic monopoles



# Assumptions in MHD

Typical system **length** much **larger than single particle orbit** extension (i.e. Larmor radius)

$$r_{Li} = \frac{\sqrt{m_i k T_i}}{eB} \ll L$$

This requirement can be violated when applying the model to some instabilities, and finite Larmor radius effects need to be taken into account.

**Time scales longer than collision time** (i.e. many collisions equilibrate temperature in the MHD characteristic time). This also translates to the mean free path being small w.r.t. characteristic length

$$\tau_{coll} \ll \tau \quad \lambda_{mfp} \ll L$$

Can be violated in fusion plasmas, dynamics parallel to the magnetic field, can have large mfp. Nevertheless, perpendicular macroscopic phenomena are well described by the model



# Remarks on MHD model

- The MHD model **can be rigorously derived from two-fluid equations** or using an intuitive approach involving conservation macroscopic quantities (see Goedbloed & Freidberg in bibliography)
- The MHD equations **involve conservation** of mass, momentum, energy and magnetic flux. Can be written in conservation form (some algebra required, see references)
- The momentum equation (2) only shows the Lorentz force ( $\perp \mathbf{B}$ ) and the pressure gradient. Other forces can be added and contribute to acceleration (or damping)  $\parallel \mathbf{B}$ , e.g. gravity, viscous drag etc.



# Remarks on MHD model

►  $\mathbf{j}$  &  $\mathbf{E}$  can be ruled out by using (5), (6) in Faraday's law (4). This yields the **induction equation**

$$\frac{\partial \mathbf{B}}{\partial t} = \nabla \times (\mathbf{v} \times \mathbf{B}) - \frac{n}{\mu_0} \nabla \times (\nabla \times \mathbf{B}) \quad (8)$$



► **Ideal MHD** case: when the plasma is a perfect conductor (or can be treated as one) a closure of the MHD system is obtained ( $\eta = 0$ ) with the equation of state:

$$\frac{d}{dt} \left( \frac{p}{\rho^\Gamma} \right) = 0 \quad \rightarrow \quad \frac{\partial p}{\partial t} + \mathbf{v} \cdot \nabla p = -\Gamma p \nabla \cdot \mathbf{v} \quad (9)$$

$\eta = 0 \rightarrow$  only convective term  $\rightarrow$  variation of  $\mathbf{B}$  only with fluid  $\rightarrow$  magnetic flux conservation

“In ideal MHD the field lines are frozen in the plasma”



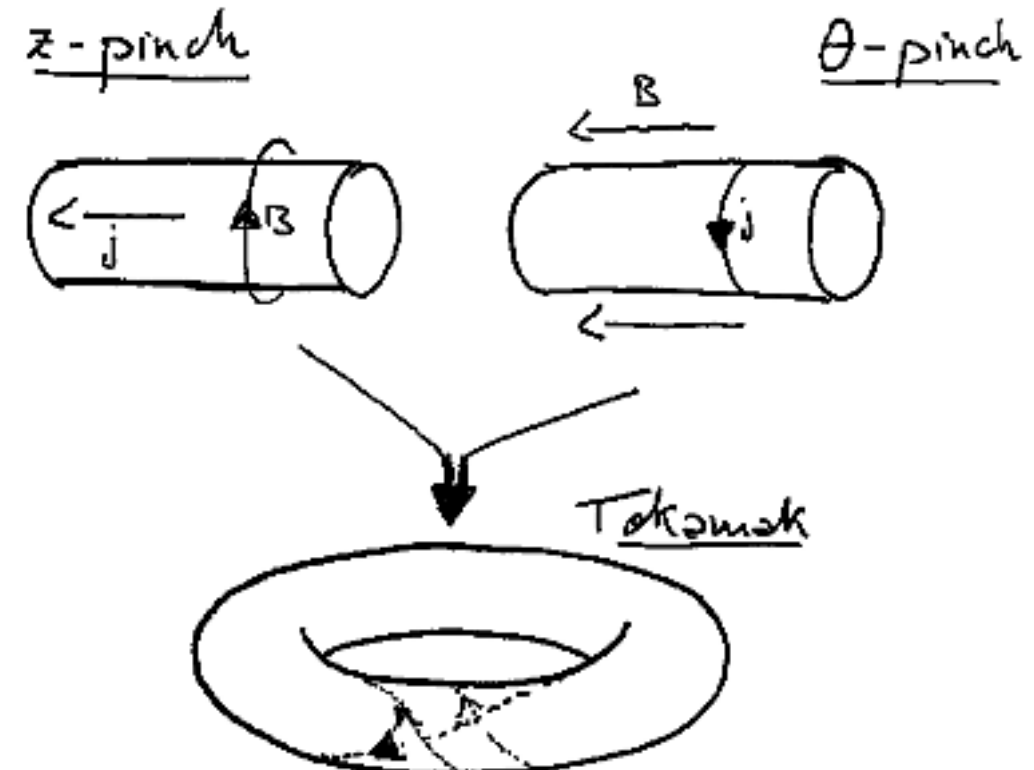
# Plasma equilibrium

## In the beginning there was the cylinder

In cylindrical geometry plasma equilibria are either very **unstable** and/or suffer of **end losses** that are detrimental for confinement

Closing the cylinder into a **torus**:

- ▶ Cures losses  $\parallel B_z$
- ▶ Instabilities can be avoided within certain operational boundaries



Note: although the Tokamak configuration is one of the most advanced, it is not the only toroidal confinement scheme!

e.g. RFP (also pinch-like) or Stellarator



# Equilibrium is balance between confining magnetic field and plasma pressure

Important **assumptions** are often made in studying toroidal equilibrium configurations (mostly fine for Tokamak cases):

1. Take the **static** case as first approx.

- $\mathbf{v} = 0, \frac{\partial}{\partial t}\{\rho, p, \mathbf{B}\} = 0$

2. **Axisymmetry** (used later)

- $\partial/\partial\Phi = 0$



# Static equilibrium for toroidal plasmas

$$\mathbf{v} = 0, \quad \frac{\partial}{\partial t}\{\rho, p, \mathbf{B}\} = 0$$

With these assumptions the ideal MHD equations reduce to:

$$\mathbf{j} \times \mathbf{B} = \nabla p \quad \text{Force balance}$$

$$\nabla \times \mathbf{B} = \mu_0 \mathbf{j} \quad \text{Ampere's law}$$

$$\nabla \cdot \mathbf{B} = 0 \quad \text{Magnetic flux law}$$



# Focus on the pressure balance equation

If the magnetic force perfectly balances the plasma pressure

$$\mathbf{j} \times \mathbf{B} = \nabla p$$

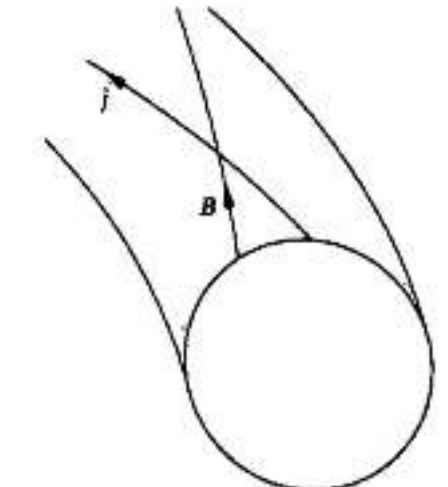
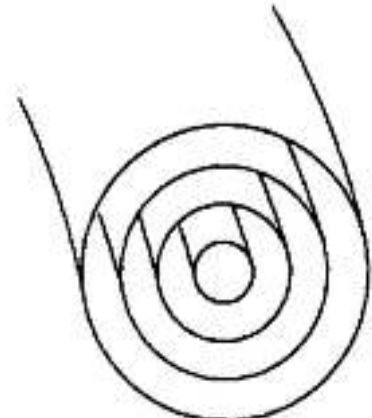
This implies that  $\mathbf{B}$  is perpendicular to both  $\mathbf{j}$  and  $\nabla p$ :

►  $\mathbf{B} \cdot \nabla p = 0$

There is no pressure gradient along the field lines and the magnetic surfaces are surfaces of constant pressure

►  $\mathbf{j} \cdot \nabla p = 0$

Current lines also lie on isobaric surfaces

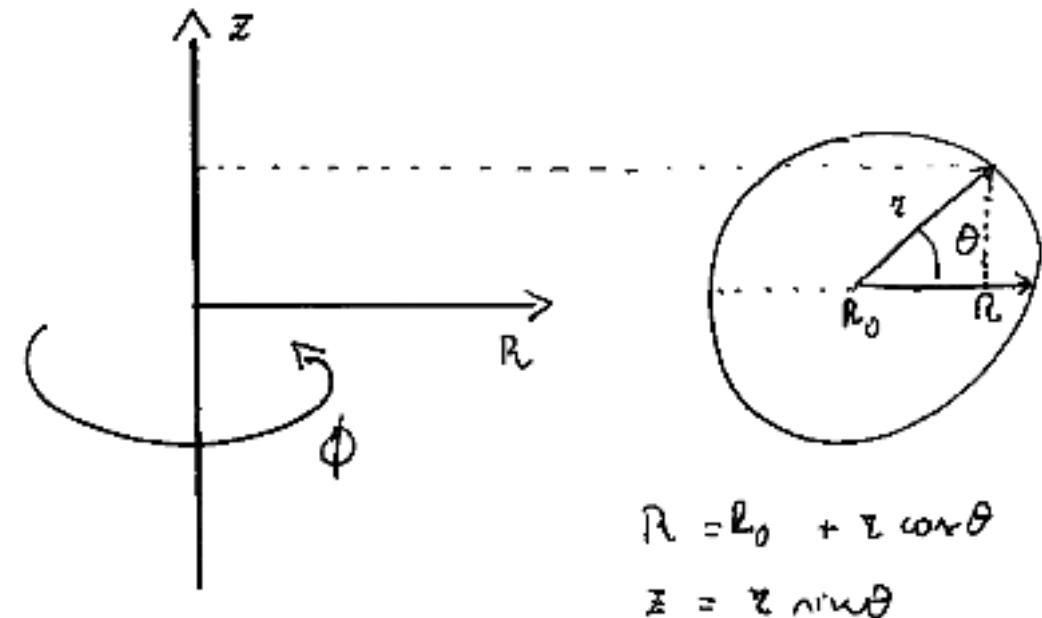


# How can we describe a toroidal equilibrium?

To do so we can work in a cylindrical coordinate system  $(R, \phi, z)$  where we can write the magnetic field as:

$$\mathbf{B} = B_\phi \hat{e}_\phi + \mathbf{B}_p$$

Where the poloidal field lies on  $(R, Z)$



# How can we describe a toroidal equilibrium?

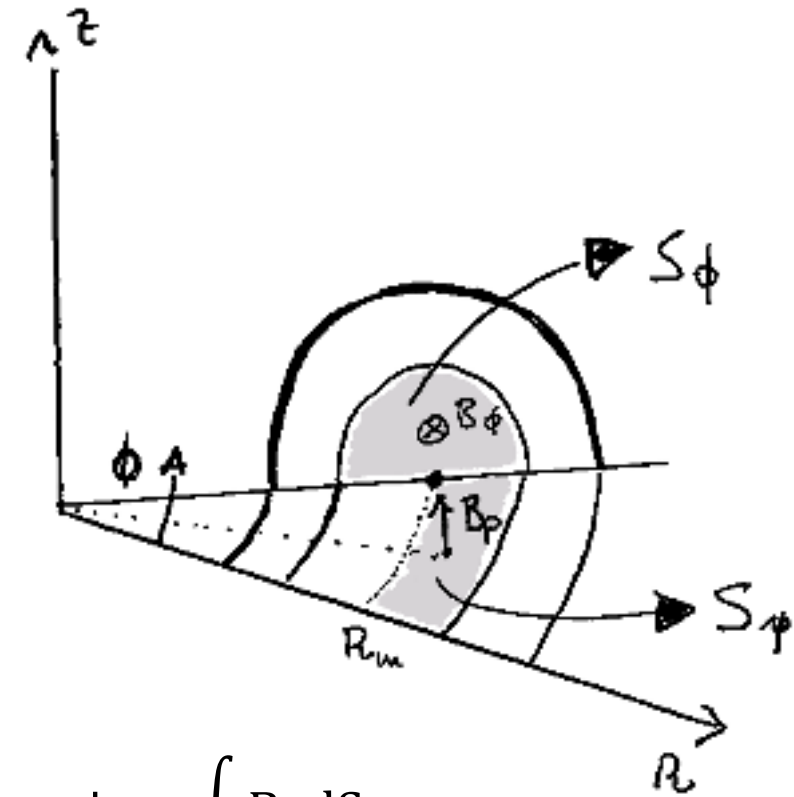
To do so we can work in a cylindrical coordinate system  $(R, \phi, z)$  where we can write the magnetic field as:

$$\mathbf{B} = B_\phi \hat{e}_\phi + \mathbf{B}_p$$

Where the poloidal field lies on  $(R, Z)$

We introduce a function ( $\Psi$ ) defined as the **poloidal flux within each magnetic surface**

And a function  $\Phi$ : the toroidal flux inside a given magnetic surface.



$$\Psi = \int B_p dS_\Psi$$

$$\Phi = \int B_\phi dS_\phi$$

Both are constant on a given surface



# How can we describe a toroidal equilibrium?

We introduce a function ( $\psi$ ) define as the **poloidal flux within each magnetic surface**, therefore this acts as a radial coordinate and is constant on a given surface

$$\begin{cases} B_R = -\frac{1}{R} \frac{\partial \psi}{\partial z} \\ B_z = \frac{1}{R} \frac{\partial \psi}{\partial R} \end{cases}$$

This satisfies the divergence requirement, which in **axisymmetric** assumption becomes:

$$\frac{1}{R} \frac{\partial(RB_R)}{\partial R} + \frac{\partial B_z}{\partial z} = 0$$

The flux ( $\psi$ ) is found to be **constant along the magnetic surfaces**:

$\psi$  can be used to label the surfaces where  $B$  lays, finding these surfaces is equivalent to finding the  $\psi=\text{const}$  surfaces

$$\mathbf{B} \cdot \nabla \psi = B_R \frac{\partial \psi}{\partial R} + B_z \frac{\partial \psi}{\partial z} = RB_R B_z - RB_z B_R = 0$$



# How can we describe a toroidal equilibrium?

The same can be done for the current, defining a **current flux function** (**f**) so that the components of the poloidal current density become:

$$\begin{cases} j_R = -\frac{1}{R} \frac{\partial f}{\partial z} \\ j_z = \frac{1}{R} \frac{\partial f}{\partial R} \end{cases}$$

Using Ampere's law we get an expression for **f**:

$$\nabla \times \mathbf{B} = \mu_0 \mathbf{j} \implies \begin{cases} j_R = -\frac{1}{\mu_0 R} \frac{\partial B_\phi}{\partial z} \\ j_z = \frac{1}{\mu_0 R} \frac{\partial (RB_\phi)}{\partial R} \end{cases} \implies f = \frac{RB_\phi}{\mu_0}$$

Again the flux function (**f**) is constant of the current density surfaces:

$$\mathbf{j} \cdot \nabla f = 0$$



# How can we describe a toroidal equilibrium?

We can now take the force balance equation and write it in the new notation, splitting toroidal and poloidal parts

$$\begin{aligned}\nabla p &= \mathbf{j}_p \times \hat{e}_\phi B_\phi + \hat{e}_\phi j_\phi \times \mathbf{B}_p \\ &= \frac{1}{R} (\nabla f \times \hat{e}_\phi) \times \hat{e}_\phi B_\phi + \hat{e}_\phi j_\phi \times \frac{1}{R} (\nabla \psi \times \hat{e}_\phi) \\ &= -\frac{B_\phi}{R} \nabla f + \frac{j_\phi}{R} \nabla \psi\end{aligned}$$



# How can we describe a toroidal equilibrium?

We can now take the force balance equation and write it in the new notation, splitting toroidal and poloidal parts

$$\begin{aligned}\nabla p &= \mathbf{j}_p \times \hat{e}_\phi B_\phi + \hat{e}_\phi j_\phi \times \mathbf{B}_p \\ &= \frac{1}{R} (\nabla f \times \hat{e}_\phi) \times \hat{e}_\phi B_\phi + \hat{e}_\phi j_\phi \times \frac{1}{R} (\nabla \psi \times \hat{e}_\phi) \\ &= -\frac{B_\phi}{R} \nabla f + \frac{j_\phi}{R} \nabla \psi\end{aligned}$$

$$\mathbf{j}_p = \frac{1}{R} (\nabla f \times \hat{e}_\phi)$$

Poloidal current density

$$\mathbf{B}_p = \frac{1}{R} (\nabla \psi \times \hat{e}_\phi)$$

Poloidal field



# How can we describe a toroidal equilibrium?

The next step is writing pressure (**p**) and current flux function (**f**) in terms of poloidal flux

$$\nabla f(\psi) = \frac{df}{d\psi} \nabla \psi \quad \nabla p(\psi) = \frac{dp}{d\psi} \nabla \psi$$

And by substitution in the force balance we get (recall  $f = RB_\phi / \mu_0$  !!):

$$j_\phi = R \frac{dp}{d\psi} + B_\phi \frac{df}{d\psi} = R \frac{dp}{d\psi} + \frac{\mu_0}{R} f \frac{df}{d\psi}$$

Named p' & f'

Ampere's law gives us the current density in terms of poloidal flux:

$$\begin{aligned}\mu_0 j_\phi &= \frac{dB_R}{dz} - \frac{dB_z}{dR} \\ &= -\frac{1}{R} \frac{\partial^2 \psi}{\partial z^2} - \frac{\partial}{\partial R} \left( \frac{1}{R} \frac{\partial \psi}{\partial R} \right)\end{aligned}$$



# How can we describe a toroidal equilibrium?

Putting everything together we obtain the **Grad-Shafranov** equation

$$R \frac{\partial}{\partial R} \left( \frac{1}{R} \frac{\partial \psi}{\partial R} \right) + \frac{\partial^2 \psi}{\partial z^2} = -\mu_0 R^2 p'(\psi) - \mu_0^2 f(\psi) f'(\psi)$$

Solutions of the G-S equation can be obtained analytically (e.g. Solov'ev equilibria, circular cross section case) or numerically with a variety of equilibrium codes (e.g. CHEASE, HELENA ...)

**p** & **f** are arbitrary flux functions, by specifying which everything else is determined by the solution of the G-S equation !



# Ingredients of toroidal axisymmetric equilibrium: current & pressure

$$R \frac{\partial}{\partial R} \left( \frac{1}{R} \frac{\partial \psi}{\partial R} \right) + \frac{\partial^2 \psi}{\partial z^2} = -\mu_0 R^2 p'(\psi) - \mu_0^2 f(\psi) f'(\psi)$$

Usually written as  $\Delta^* \psi$   
Where  $\Delta^*$  is a Laplacian-like operator with inverted R and 1/R

Flux function linked to **pressure**

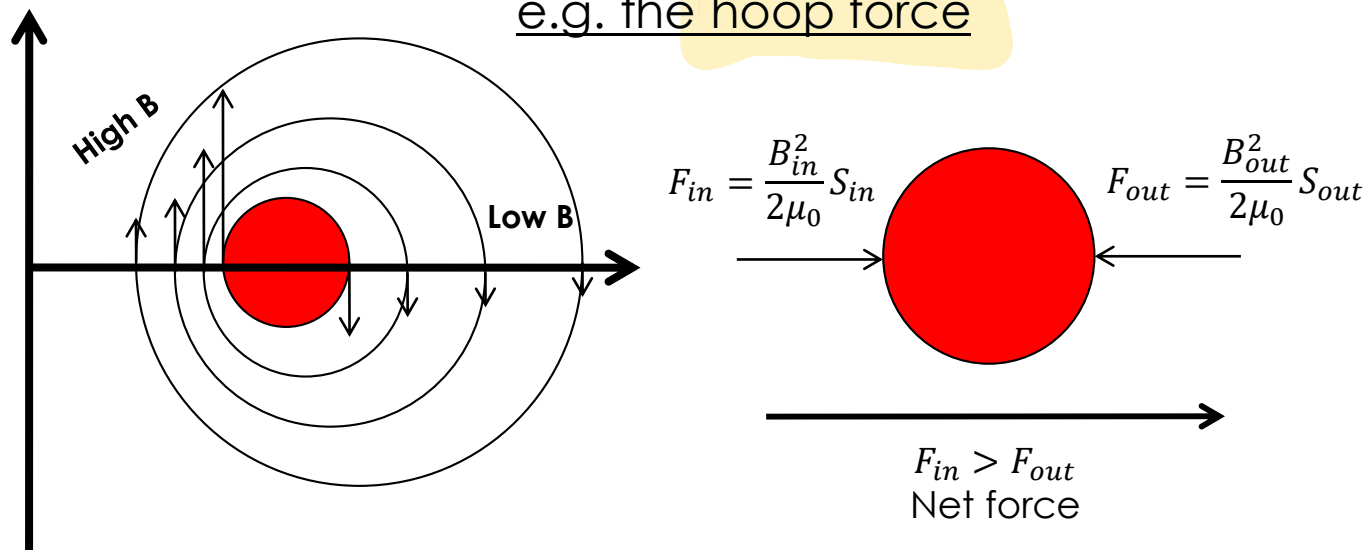
Flux function linked to **current**

**Defining current and pressure (or the source profiles  $p'$  &  $f'$ ) is the starting point to solve the G-S equation**  
**The solution yields  $\psi \rightarrow B \rightarrow$  equilibrium**



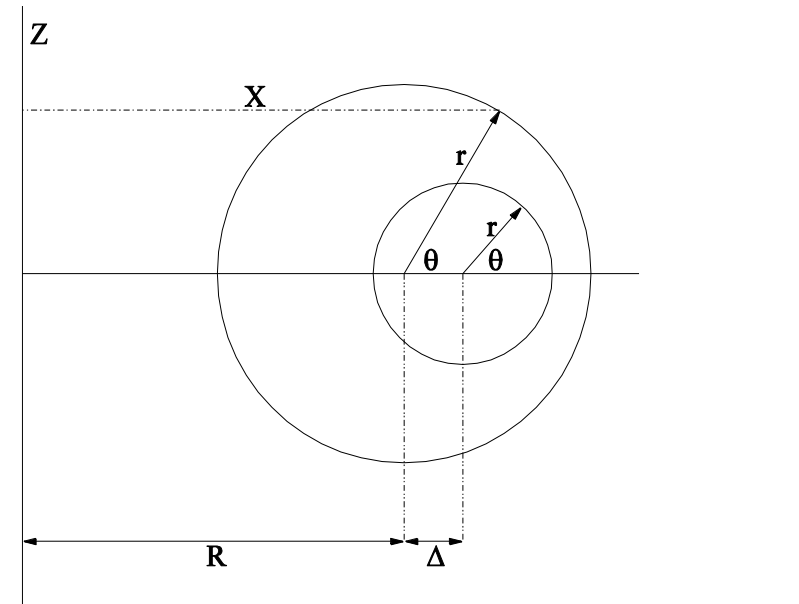
# Remarks on equilibrium for toroidal plasmas

Toroidal geometry introduces **outward directed forces** which cause radial shift of the GS solution: flux surfaces whose centers are no longer concentric but **shifted** outward along R with respect to one another



Same flux inside and outside  
→ inside is squeezed in  
smaller area

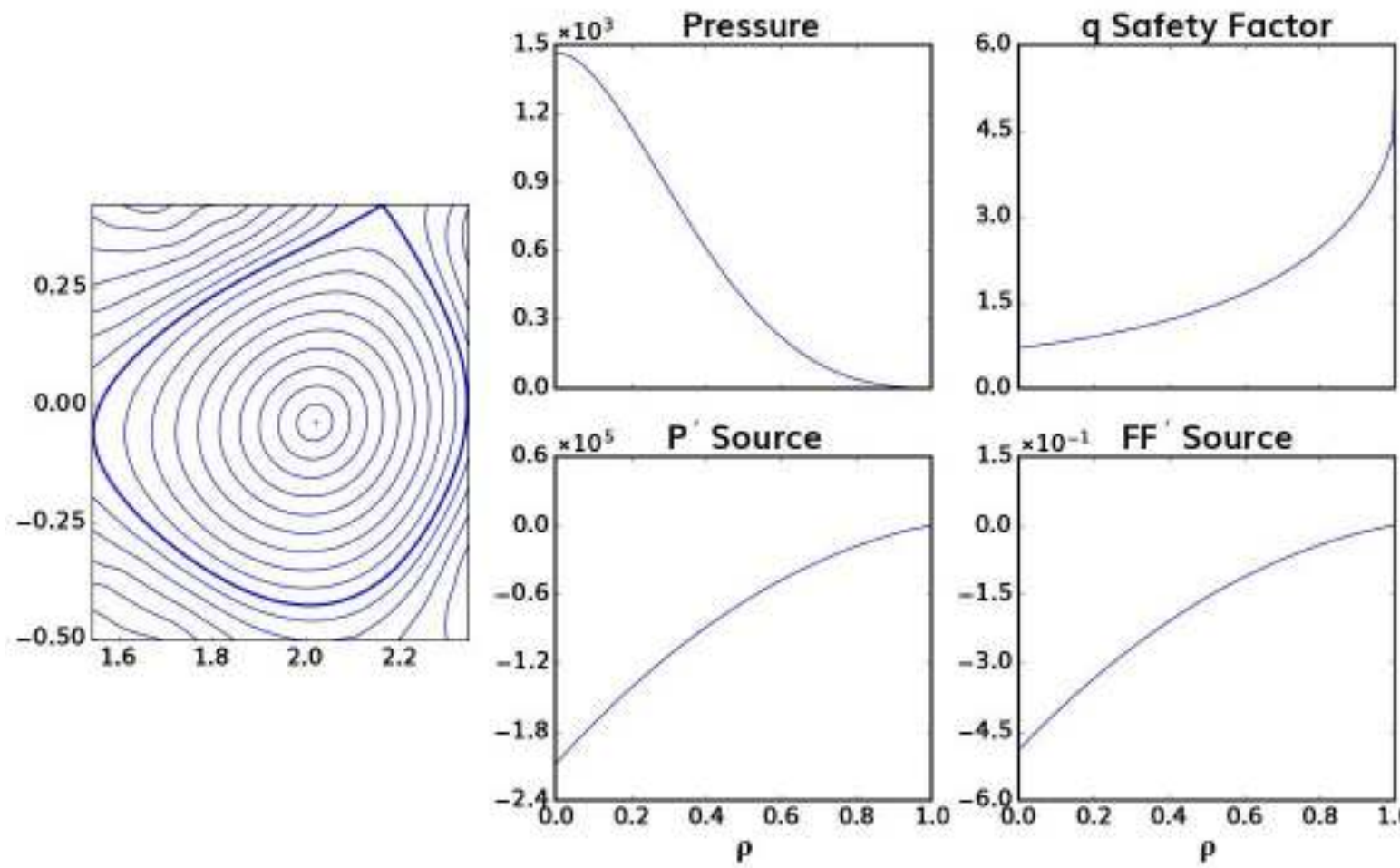
**Net outward forces (like hoop force, from poloidal field, or tyre force, due to plasma pressure) require vertical external field for compensation**



**"Shafranov shift"**



# Numerical solution of the Grad-Shafranov equation with the fixed-boundary code CHEASE



In this example a numerical solution of the G-S equation is shown

The solver takes  $p'$  and  $ff'$  as input profiles and calculates the poloidal flux function ( $\Psi$ ) within a computational boundary defined by the plasma last closed surface



# Figures of merit: safety factor ( $q$ )

Represents the **number of toroidal turns after which the field line returns to a given poloidal position**. In axisymmetric equilibria each field line has a specific value of  $q$ :

$$q = \frac{\Delta\Phi}{2\pi}$$

In infinitesimal terms, the toroidal angle that a field line runs for given poloidal angle, translating into flux we get the definition:

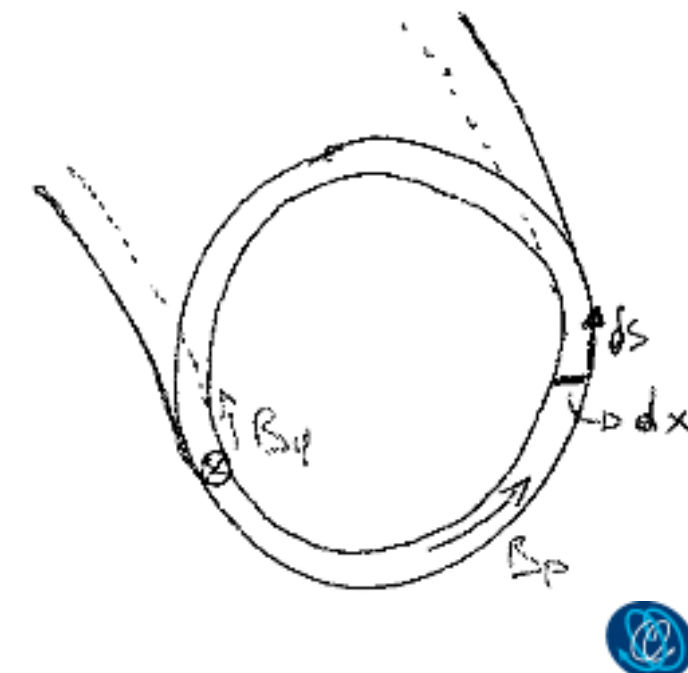
$$q = \frac{d\Phi}{d\Psi}$$

Recalling the definitions of toroidal and poloidal fluxes, **for an infinitesimal ring between two surfaces** the poloidal flux is:

$$d\Psi = 2\pi R B_p dx$$

While the toroidal flux:

$$d\Phi = \oint (B_\phi dx) ds \quad \xrightarrow{\text{yields}} \quad q(\Psi) = \frac{1}{2\pi} \oint_{\Psi} \frac{B_\phi}{RB_p} ds$$



# Figures of merit: $\beta$

The ratio between **kinetic** and **magnetic pressure**: telling us how efficiently the magnetic field is confining plasma pressure

$$\beta = \frac{p}{B^2/2\mu_0}$$

Several forms and definitions of this parameters are used: average  $\beta$ , poloidal  $\beta_p$ , toroidal  $\beta_t$ , normalized  $\beta_N$ ...

$$\langle \beta \rangle = \frac{\int p dV / \int dV}{B_0^2/2\mu_0}, \quad \beta_p = \frac{\langle p \rangle}{B_\theta^2(a)/2\mu_0}, \quad \beta_t = \frac{\langle p \rangle}{B_\phi^2/2\mu_0}, \quad \beta_N = \beta_t \frac{a [m] B_\phi [T]}{I [MA]}$$



# The ‘‘straight tokamak’’ approximation

We define the **inverse aspect ratio** of a torus as:

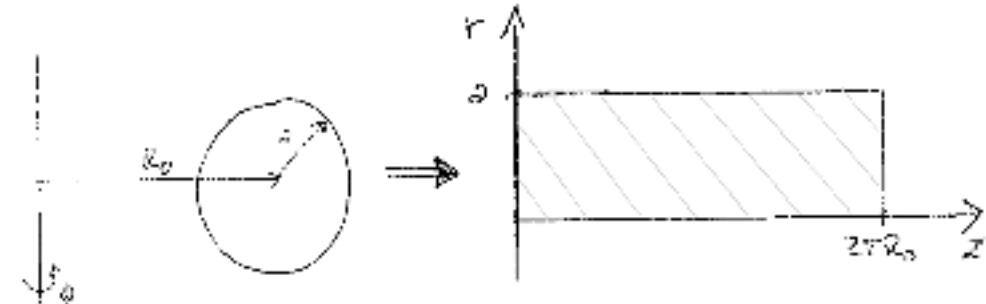
$$a/R_0 = \epsilon$$

In base al valore dell'aspect ratio usiamo uno o l'altra definizione.

When  $\epsilon \ll 1$  (i.e. large aspect ratio) a slender torus can be approximated by a periodic cylinder of length  $L = 2\pi R_0$ . The toroidal angle becomes the ‘z’ axis:  $\phi \rightarrow z$

This is called the **straight tokamak** limit and gives a first approximation of toroidal equilibrium. Leading order expansions can be obtained in  $\epsilon$  for each quantity.

Equilibrium equations are greatly simplified in this limit, and figures of merit can aid understanding physical properties of the system.



Using differential operators expressed in cylindrical coordinates  $(r, \theta, z)$  and with symmetries:  $\partial/\partial\theta = 0$ ,  $\partial/\partial z = 0$

$$\begin{cases} \mathbf{j} \times \mathbf{B} = \nabla p \\ \nabla \times \mathbf{B} = \mu_0 \mathbf{j} \\ \nabla \cdot \mathbf{B} = 0 \end{cases} \Rightarrow \begin{cases} \frac{dp}{dr} = j_\theta B_z - j_z B_\theta \\ j_\theta = -\frac{1}{\mu_0 r} \frac{dB_z}{dr} \\ j_z = \frac{1}{\mu_0 r} \frac{d(rB_\theta)}{dr} \end{cases}$$



# Figures of merit: safety factor ( $q$ ) in straight tokamak limit

$$\frac{1}{\xi} \gg 1 \quad \xi \ll 1$$

In large aspect ratio approx. with circular cross section the flux surfaces become nested cylinders with radius  $r \leq a$

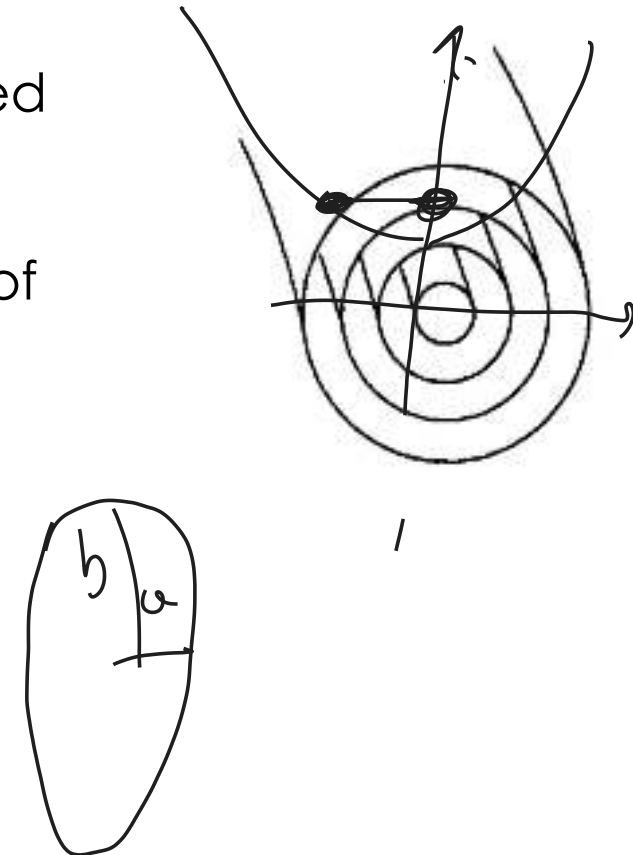
The  $q$ -profile integral can be carried out over a single poloidal circuit of radius  $r$ :

$$q(\psi) = \frac{1}{2\pi} \oint_{\psi} \frac{B_\phi}{RB_p} ds \quad \xrightarrow{\text{yields}} \quad \underline{q(r)} = \frac{rB_\phi}{R_0 B_p}$$

Using Ampère's law we get a useful expression:

$$2\pi r B_p = \mu_0 I(r) \rightarrow q(r) \frac{2\pi r^2 B_\phi}{\mu_0 I(r) R_0}$$

At plasma edge:  $\underline{q_a} = \frac{2\pi a^2 B_\phi}{\mu_0 I_p R_0}$

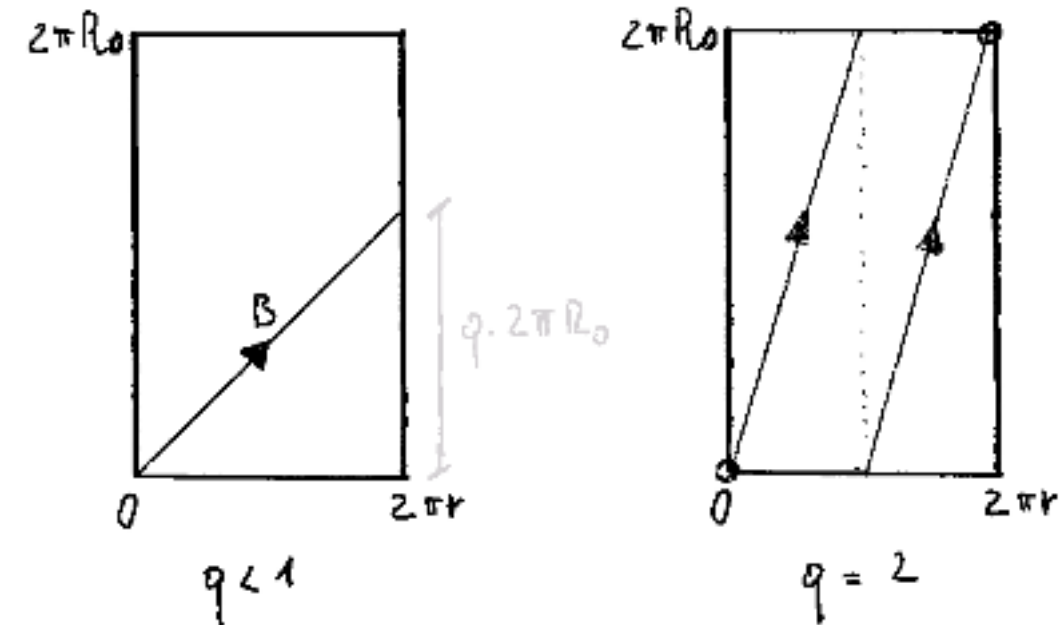


# Figures of merit: safety factor ( $q$ ) in straight tokamak limit

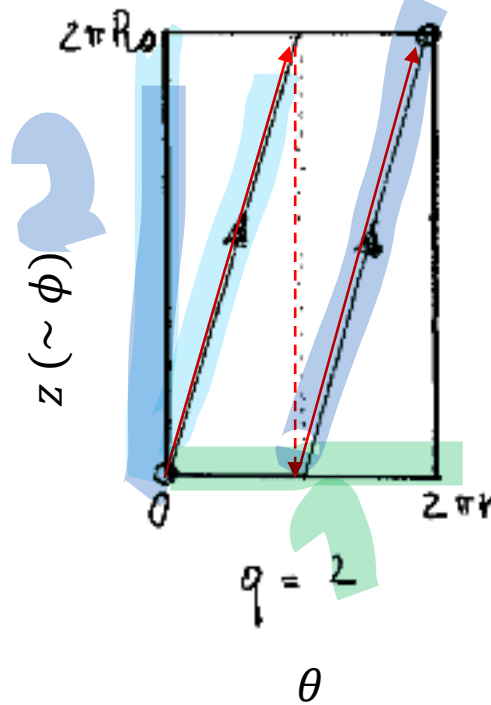
Each magnetic surface has a specific safety factor value (i.e. a specific pitch of magnetic field lines) that can be visualized by **unrolling the cylinder** !

An important concept is that of **rational magnetic surfaces**: those where the field lines close upon themselves after  $M$  poloidal turns and  $N$  toroidal revolutions

$$q_{rat} = \frac{N}{M}$$



# Figures of merit: safety factor ( $q$ ) in straight tokamak limit

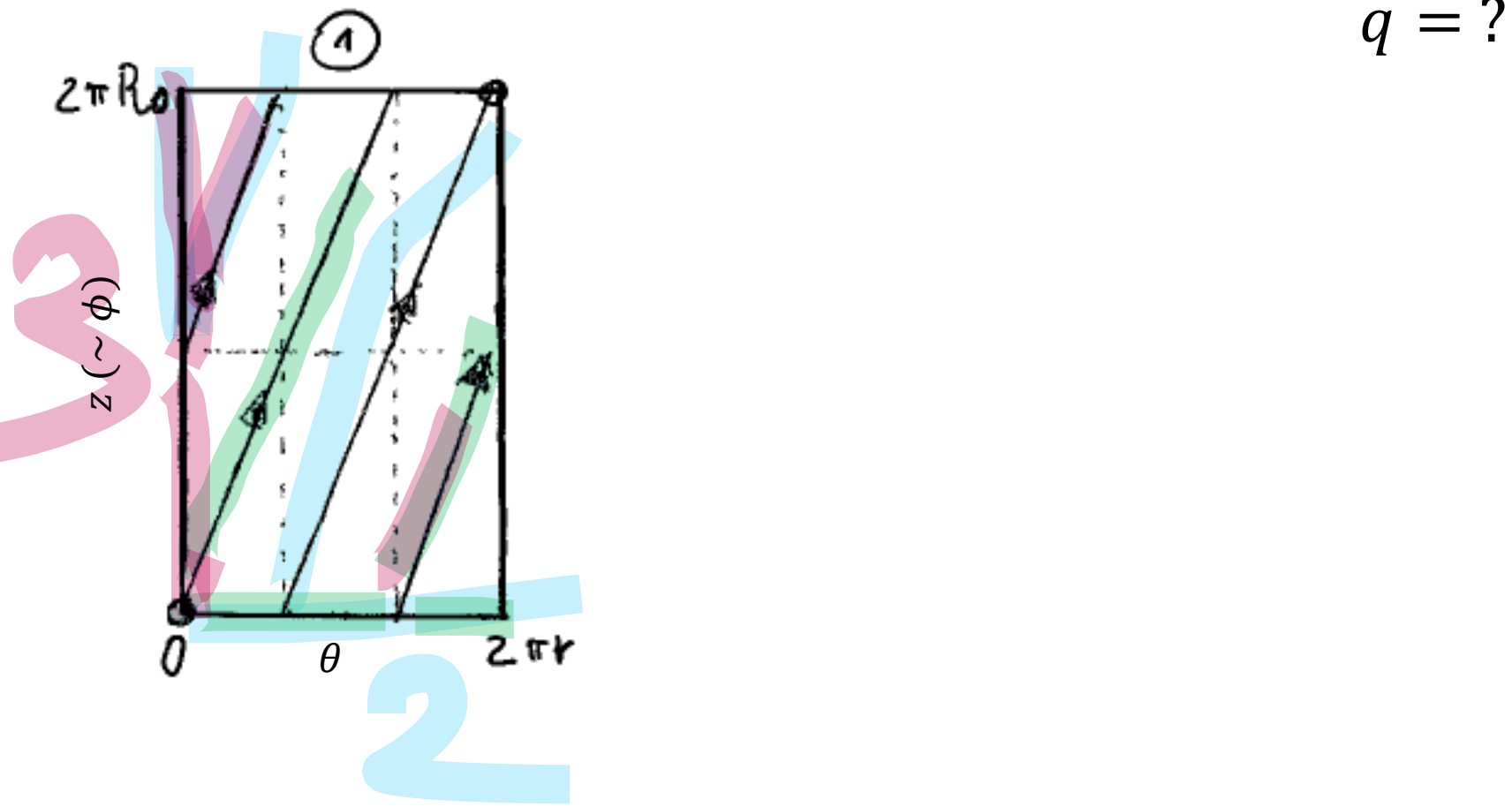


Example: following the field line from the origin (lower left angle) we see that it runs along the 'z' axis twice ( $N=2$ ) in order to make a single complete poloidal turn ( $M=1$ ). Note the periodic boundary conditions needed to properly handle the straight&unrolled tokamak model.

$$\rightarrow q = 2$$



# Figures of merit: safety factor ( $q$ ) in straight tokamak limit



# A useful model for toroidal current density

With **large aspect-ratio** and **circular cross section**, q-profile is determined by toroidal current density  $j(r)$

Useful class of profiles:

$$j = j_0 \left(1 - \frac{r^2}{a^2}\right)^v$$

$$I(r) = 2\pi \int_0^r j(r') r' dr' = j_0 \frac{\pi a^2}{v+1} \left[ 1 - \left(1 - \frac{r^2}{a^2}\right)^{v+1} \right]$$

Use Ampère to get  $B_\theta$ :

$$\mu_0 j = \frac{1}{r} \frac{d(rB_\theta)}{dr}$$

$$B_\theta(r) = \frac{\mu_0 j_0 a^2}{2r(v+1)} \left[ 1 - \left(1 - \frac{r^2}{a^2}\right)^{v+1} \right]$$

For the q-profile we get the expression:

$$q(r) = \frac{2(v+1)}{\mu_0 j_0} \frac{B_\phi}{R} \frac{r^2/a^2}{[1 - (1 - r^2/a^2)^{v+1}]}$$

$$\frac{q(a)}{q(0)} = v + 1$$

Use approximation for q:

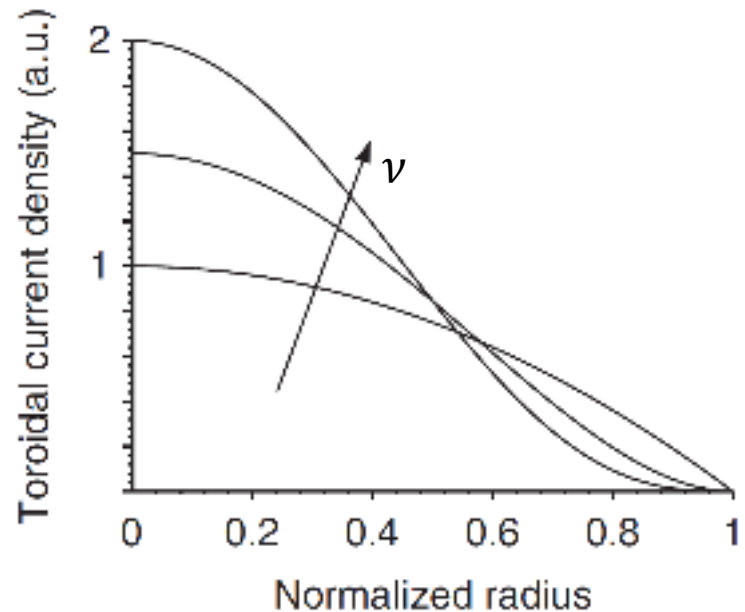
$$q(r) = \frac{rB_\phi}{R_0 B_p}$$



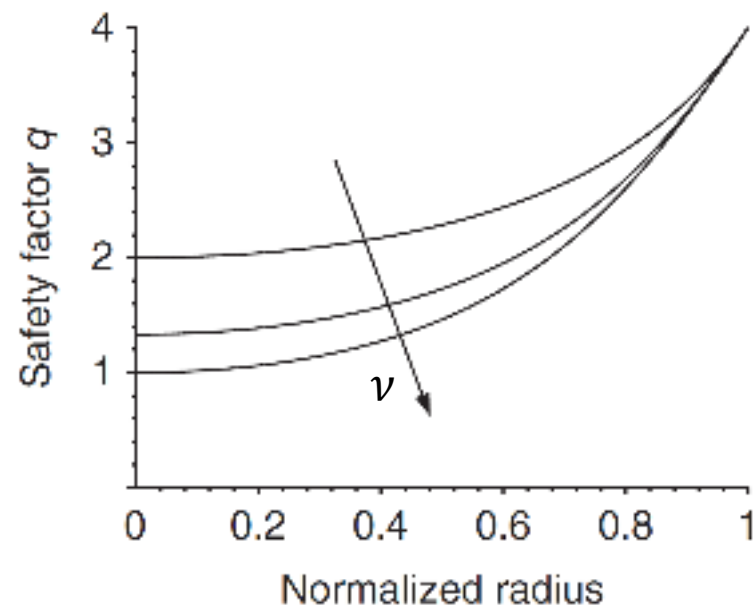
# A useful model for toroidal current density

With large aspect-ratio and circular cross section, q-profile is determined by toroidal current density  $j(r)$

$$j = j_0 \left(1 - \frac{r^2}{a^2}\right)^{\nu}$$



$$q(r)$$



# PART 2: linear MHD stability



# Intuitive stability



$$\begin{array}{c} \longrightarrow \xi \\ \longleftarrow F \end{array}$$

$$w_0 < w_1$$



$$\begin{array}{c} \longleftarrow \xi \\ \longleftarrow F \end{array}$$

$$w_0 > w_1$$

e.g. potential  
energy  $W$  due  
to gravity

} eq. of motion

} energy principle  
(variational  
methods)



# Linear stability concerns the behavior of a dynamical system w.r.t. **small** (infinitesimal) **perturbations**

The original non-linear problem is split into **equilibrium** and **perturbation**, we will start again from time-independent static equilibrium defined by  $\mathbf{B}_0, \mathbf{j}_0, p_0, \rho_0, \mathbf{v}_0$ :

questa suddivisione a prescindere, sia lineare che non-lineare

$$\mathbf{j}_0 \times \mathbf{B}_0 = \nabla p_0$$

$$\nabla \times \mathbf{B}_0 = \mu_0 \mathbf{j}_0$$

$$\nabla \cdot \mathbf{B}_0 = 0$$

$$\mathbf{v}_0 = 0 \rightarrow \text{STATIC EQUILIBRIUM}$$

Time dependence is kept in the perturbed quantities  $X_1$ . The assumption here is that perturbations are small w.r.t equilibrium:  $|X_1| \ll |X_0|$

perchè è linear stability

$$\mathbf{v}(\mathbf{r}, t) = \mathbf{v}_1(\mathbf{r}, t)$$

$$\mathbf{B}(\mathbf{r}, t) = \mathbf{B}_0(\mathbf{r}) + \mathbf{B}_1(\mathbf{r}, t) \quad \rho(\mathbf{r}, t) = \rho_0(\mathbf{r}) + \rho_1(\mathbf{r}, t)$$

$$\mathbf{j}(\mathbf{r}, t) = \mathbf{j}_0(\mathbf{r}) + \mathbf{j}_1(\mathbf{r}, t) \quad p(\mathbf{r}, t) = p_0(\mathbf{r}) + p_1(\mathbf{r}, t)$$



# Perturbed momentum equation

By substitution into the momentum equation, and retaining just the first order terms, we obtain the first piece of linearized (ideal) MHD

$$\rho \left( \frac{\partial \mathbf{v}}{\partial t} + \mathbf{v} \nabla \mathbf{v} \right) = \mathbf{j} \times \vec{B} - \nabla p \quad \text{original}$$
$$(\rho_0 + \rho_1) \left( \frac{\partial \mathbf{v}_1}{\partial t} + \mathbf{v}_1 \nabla \mathbf{v}_1 \right) = (\mathbf{j}_0 + \mathbf{j}_1) \times (\mathbf{B}_0 + \mathbf{B}_1) - \nabla (p_0 + p_1)$$

$$\rho_0 \frac{\partial \mathbf{v}_1}{\partial t} = -\nabla p_1 + \mathbf{j}_1 \times \mathbf{B}_0 + \mathbf{j}_0 \times \mathbf{B}_1$$



# Linearized ideal MHD equations

The same is done for all the MHD equations and with some easy algebra the linearized system is obtained:

$$\left\{ \begin{array}{l} \rho_0 \frac{\partial \mathbf{v}_1}{\partial t} = -\nabla p_1 + \mathbf{j}_1 \times \mathbf{B}_0 + \mathbf{j}_0 \times \mathbf{B}_1 \\ \frac{\partial p_1}{\partial t} = -\mathbf{v}_1 \cdot \nabla p_0 - \Gamma p_0 \nabla \cdot \mathbf{v}_1 \\ \frac{\partial \rho_1}{\partial t} = -\nabla \cdot (\rho_0 \mathbf{v}_1) \end{array} \right. \quad \left\{ \begin{array}{l} \nabla \times \mathbf{B}_1 = \mu_0 \mathbf{j}_1 \\ \frac{\partial \mathbf{B}_1}{\partial t} = \nabla \times (\mathbf{v}_1 \times \mathbf{B}_0) \\ \nabla \cdot \mathbf{B}_1 = 0 \end{array} \right.$$



# Linearized ideal MHD equations: introducing plasma displacement

These can be simplified by introducing the *Lagrangian displacement vector*  $\xi(r, t)$  of a plasma element from its equilibrium state.

SAN210r

The fluid velocity is then the Lagrangian time derivative of this new variable: the variation in time in a coordinate system co-moving with the fluid.

$$\mathbf{v} = \frac{D\xi}{Dt} \equiv \frac{\partial \xi}{\partial t} + \mathbf{v} \cdot \nabla \xi$$

definizione di derivata lagrangiana

NOTE: the displacement  $\xi$  is a first order quantity by definition!

For the first order linearized problem this becomes:

$$\mathbf{v} \approx \mathbf{v}_1 = \frac{\partial \xi}{\partial t}$$



# Using $\xi$ in the linearized equations leads to the **force operator**

The definition of plasma displacement helps with time integration:

$$\begin{cases} \frac{\partial p_1}{\partial t} = -\frac{\partial \xi}{\partial t} \cdot \nabla p_0 - \Gamma p_0 \nabla \cdot \frac{\partial \xi}{\partial t} \\ \frac{\partial \rho_1}{\partial t} = -\nabla \cdot \left( \rho_0 \frac{\partial \xi}{\partial t} \right) \\ \frac{\partial \mathbf{B}_1}{\partial t} = \nabla \times \left( \frac{\partial \xi}{\partial t} \times \mathbf{B}_0 \right) \end{cases} \implies \begin{cases} p_1 = -\xi \cdot \nabla p_0 + \Gamma p_0 \nabla \cdot \xi \\ \rho_1 = -\nabla \cdot (\rho_0 \xi) \\ \mathbf{B}_1 = \nabla \times (\xi \times \mathbf{B}_0) \\ \Rightarrow \mathbf{j}_1 = \frac{1}{\mu_0} \nabla \times (\nabla \times (\xi \times \mathbf{B}_0)) \end{cases}$$

This leads to a very useful expression of the momentum equation, which now depends solely on  $\xi$ !

$$\begin{aligned} \rho_0 \frac{\partial^2 \xi}{\partial t^2} &= -\nabla (-\xi \nabla p_0 - \Gamma p_0 \nabla \xi) + \mathbf{j}_0 \times [\nabla \times (\xi \times \mathbf{B}_0)] + \frac{1}{\mu_0} \nabla \times [\nabla \times (\xi \times \mathbf{B}_0)] \times \mathbf{B}_0 \\ &= \mathbf{F}(\xi) \end{aligned}$$

The right hand side of this expression is called force operator



# Using $\xi$ in the linearized equations leads to the **force operator**

The definition of plasma displacement helps with time integration:

$$\begin{cases} \frac{\partial p_1}{\partial t} = -\frac{\partial \xi}{\partial t} \cdot \nabla p_0 - \Gamma p_0 \nabla \cdot \frac{\partial \xi}{\partial t} \\ \frac{\partial \rho_1}{\partial t} = -\nabla \cdot \left( \rho_0 \frac{\partial \xi}{\partial t} \right) \\ \frac{\partial \mathbf{B}_1}{\partial t} = \nabla \times \left( \frac{\partial \xi}{\partial t} \times \mathbf{B}_0 \right) \end{cases} \implies \begin{cases} p_1 = -\xi \cdot \nabla p_0 + \Gamma p_0 \nabla \cdot \xi \\ \rho_1 = -\nabla \cdot (\rho_0 \xi) \\ \mathbf{B}_1 = \nabla \times (\xi \times \mathbf{B}_0) \\ \Rightarrow \mathbf{j}_1 = \frac{1}{\mu_0} \nabla \times (\nabla \times (\xi \times \mathbf{B}_0)) \end{cases}$$

This leads to a very useful expression of the momentum equation, which now depends solely on  $\xi$ !

$$\begin{aligned} \rho_0 \frac{\partial^2 \xi}{\partial t^2} &= -\nabla (-\xi \nabla p_0 - \Gamma p_0 \nabla \xi) + \mathbf{j}_0 \times [\nabla \times (\xi \times \mathbf{B}_0)] + \frac{1}{\mu_0} \nabla \times [\nabla \times (\xi \times \mathbf{B}_0)] \times \mathbf{B}_0 \\ &= \mathbf{F}(\xi) \end{aligned}$$

perturbed field  $\equiv \mathbf{Q}$       perturbed field  $\equiv \mathbf{Q}$

The right hand side of this expression is called force operator



# Using $\xi$ in the linearized equations leads to the **force operator**

We can rearrange the terms to highlight the physical meaning:

$$\rho_0 \frac{\partial^2 \xi}{\partial t^2} = \mathbf{F}(\xi) = \underbrace{\nabla (\Gamma p_0 \nabla \cdot \xi)}_{\text{Isotropic force due to plasma compressibility}} - \frac{1}{\mu_0} \mathbf{B}_0 \times (\nabla \times \mathbf{Q}) + \underbrace{\nabla (\xi \cdot \nabla p_0)}_{\text{force due to equilibrium pressure gradient}} + \underbrace{\mathbf{j}_0 \times \mathbf{Q}}_{\text{force due to equilibrium current}}$$

$\perp \mathbf{B}$  force due to **field line bending**

Present even in homogeneous plasma, responsible for stable perturbations such as Alfvén waves

For inhomogeneous plasmas (such as fusion relevant ones!) pressure gradients and currents can lead to instability



# Normal modes

Equilibrium quantities are time independent, we can separate variables and write solutions in the form of **normal modes**:

$$\xi(\mathbf{r}, t) = \hat{\xi}(\mathbf{r}) e^{-i\omega t}$$

We can then write the momentum equation as an **eigenvalue problem!**

$$\rho_0 \frac{\partial^2 \xi}{\partial t^2} = -\rho_0 \omega^2 \hat{\xi}(\mathbf{r}) = \mathbf{F}(\hat{\xi})$$

Where  $\mathbf{F}$  is again the linear force operator and  $\omega^2$  its eigenvalues  
-> full picture of system stability!

Aside few analytical solutions, a numerical approach is usually needed.



# These eigenvalues have interesting properties

1. The eigenvalues  $\omega^2$  are **purely real**

→ Consequence of the operator **F** being **self-adjoint** ( for ideal MHD ) in the Hilbert space of displacement vectors (quite lengthy calculation for proof):  
 $\int \boldsymbol{\eta}^* \cdot \mathbf{F}(\boldsymbol{\xi}) dV = \int \boldsymbol{\xi} \cdot \mathbf{F}(\boldsymbol{\eta}^*) dV$

2. Given the form of perturbations  $\boldsymbol{\xi}(\mathbf{r}, t) = \hat{\boldsymbol{\xi}}(\mathbf{r}) e^{-i\omega t}$ , we can have:

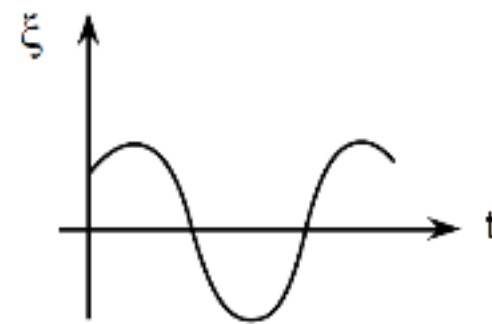
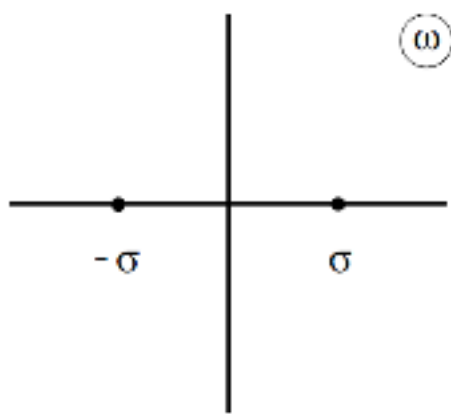
1.  $\omega^2 > 0$  then  $\omega$  is real and the perturbations  $\boldsymbol{\xi}$  are stable oscillations
2.  $\omega^2 < 0$  then  $\omega$  is imaginary and  $\boldsymbol{\xi} \sim e^{+\omega t}$  is exponentially unstable!



# In ideal MHD we only have stable waves or exponential instabilities

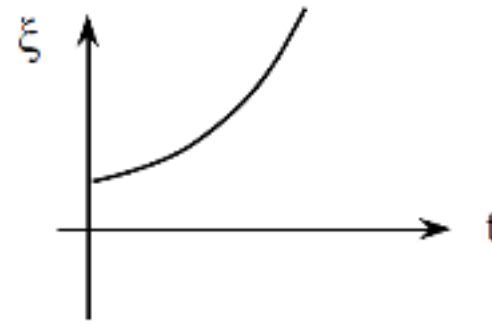
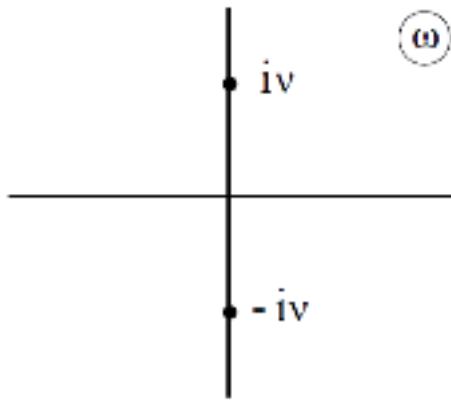
$$\omega = \sigma + i\nu$$

(a)



$$\omega^2 > 0$$

(b)



$$\omega^2 < 0$$



# The meaning of $\text{Re}(\omega)$

Assuming an **m=1 external kink** in a  
**"straight tokamak"** ( $\xi_z = 0$ )

➤ constant eigenfunction  $\xi_r = \xi_a = \text{const.}$

Assuming **incompressibility**:

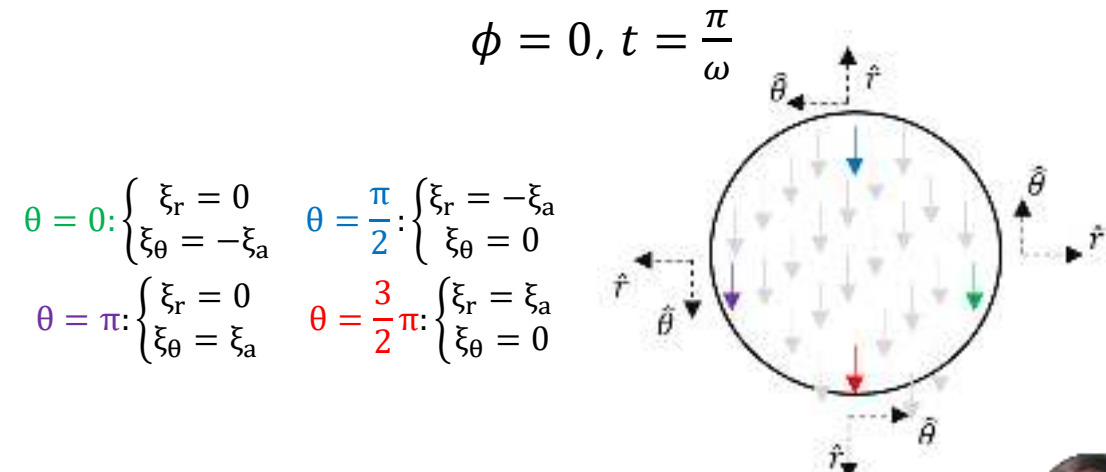
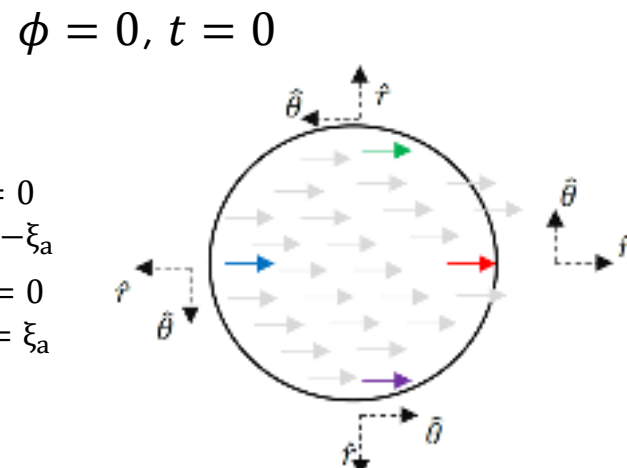
➤  $\nabla \cdot \xi = 0 \rightarrow \xi_\theta = \frac{i}{m} \frac{d(r\xi_r)}{dr} = i\xi_a$

The complete eigenfunction in time is described by:

$$\xi_r(r, \theta, \phi, t) = \text{Re}\{\xi_a e^{i\theta - in\phi - i\omega t}\} = \xi_a \cdot \cos(\theta - n\phi - \omega t)$$

$$\xi_\theta(r, \theta, \phi, t) = \text{Re}\{i\xi_a e^{i\theta - in\phi - i\omega t}\} = -\xi_a \cdot \sin(\theta - n\phi - \omega t)$$

The components evolve coherently with a **rotation** on the poloidal plane



# Energy principle: insight on stability without solving the eigenvalue problem

Task: write an expression for **plasma potential energy** and **minimize** it using plasma displacements  $\xi$  as test functions.

A step back to plasma displacement: it can be used to define a linear expression for plasma **kinetic energy**!

$$K \equiv \frac{1}{2} \int \rho \mathbf{v}^2 dV \approx \frac{1}{2} \int \rho_0 \left( \frac{\partial \xi}{\partial t} \right)^2 dV = \frac{1}{2} \int \rho_0 \dot{\xi}^2 dV$$

The variation in time of the total energy  $H$ , with  $W$  the potential energy, is zero for energy conservation  $H = K + W = \text{const}$

$$\frac{d}{dt} (K + W) = 0$$



# Energy principle: insight on stability without solving the eigenvalue problem

Using the expression for K and the equation of motion:

$$\frac{dK}{dt} = \frac{d}{dt} \left[ \frac{1}{2} \int \rho_0 \dot{\xi}^2 dV \right] = \int \rho_0 \dot{\xi}^* \cdot \ddot{\xi} dV = \int \dot{\xi}^* \cdot \mathbf{F}(\xi) dV$$

Using self-adjointness and energy conservation:

$$\begin{aligned}\frac{dW}{dt} &= -\frac{dK}{dt} = -\int \dot{\xi}^* \cdot \mathbf{F}(\xi) dV \\ &= -\frac{1}{2} \left[ \int \dot{\xi}^* \cdot \mathbf{F}(\xi) dV + \int \xi^* \cdot \mathbf{F}(\dot{\xi}) dV \right] \\ &= \frac{d}{dt} \left[ -\frac{1}{2} \int \xi^* \cdot \mathbf{F}(\xi) dV \right]\end{aligned}$$

$$W = -\frac{1}{2} \int \xi^* \cdot \mathbf{F}(\xi) dV$$

Expression for **linearized potential energy**

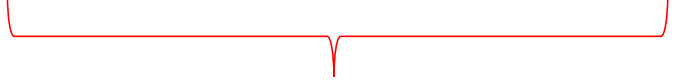
\* Indicates the complex conjugate and integrals are carried out over the plasma volume



# Energy principle: insight on stability without solving the eigenvalue problem

Finally using energy conservation we find:

$$\frac{d}{dt} \left[ K - \frac{1}{2} \int \boldsymbol{\xi}^* \cdot \mathbf{F}(\boldsymbol{\xi}) dV \right] = \frac{d}{dt} (K + \delta W) = 0$$

  
 $= W$

If we only have discrete eigenvalues  $\{\omega_n\}$  with eigenfunctions  $\{\boldsymbol{\xi}_n\}$ :

$$-\rho_0 \omega_n^2 \boldsymbol{\xi}_n = \mathbf{F}(\boldsymbol{\xi}_n) \quad \xrightarrow{\text{yields}} \quad \delta W = -\frac{1}{2} \int \boldsymbol{\xi}_n \cdot \mathbf{F}(\boldsymbol{\xi}_n) dV = \frac{1}{2} \omega_n^2 \int \rho_0 \boldsymbol{\xi}_n^2 dV$$

$$\omega_n^2 = \frac{\delta W}{\frac{1}{2} \int \rho_0 \boldsymbol{\xi}_n^2 dV}$$

The sign if  $\delta W$  defines stability !!



# The meaning of $W$

The perturbed potential energy can be put into the so-called *intuitive form* to highlight the underlying physics

$$W = \frac{1}{2\mu_0} \int_F dV |\mathbf{Q}_\perp|^2$$

$$+ B_0^2 |\nabla \cdot \boldsymbol{\xi}_\perp + 2\boldsymbol{\xi}_\perp \cdot \boldsymbol{\kappa}|^2$$

$$+ \Gamma \mu_0 p_0 |\nabla \cdot \boldsymbol{\xi}|^2$$

$$- 2\mu_0 (\boldsymbol{\xi}_\perp \cdot \nabla p_0) (\boldsymbol{\xi}_\perp^* \cdot \boldsymbol{\kappa})$$

$$- \mu_0 \frac{j_{0\parallel}}{B_0} (\boldsymbol{\xi}_\perp^* \times \mathbf{B}_0) \cdot \mathbf{Q}_\perp$$

Positive terms: stabilizing

Associated with stable waves  
(Alfvén waves, sound waves)

Can be either positive or negative! These terms describe the main sources of instability



# The meaning of $W$ : pressure driven term

$$(\boldsymbol{\xi}_\perp \cdot \nabla p_0) (\boldsymbol{\xi}_\perp^* \cdot \boldsymbol{\kappa})$$

- Depends on pressure gradient ( $\nabla p_0$ ) and magnetic field curvature ( $\boldsymbol{\kappa}$ )
- In a generic configuration the confining magnetic field will have regions with good and bad curvature
- Overall stability depends on both contributions
- In a toroidal system the inner part has good curvature, the outer part bad: pressure driven instabilities will tend to go that way!



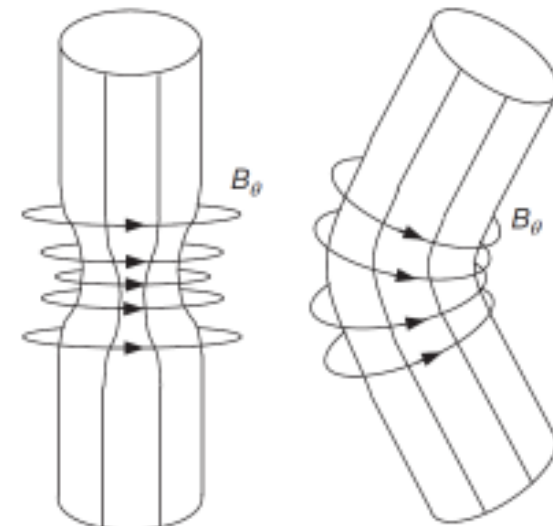
# The meaning of $W$ : current driven term

$$\frac{j_{0\parallel}}{B_0} (\xi_\perp^* \times \mathbf{B}_0) \cdot \mathbf{Q}_\perp$$

- Energy source is current density parallel to the equilibrium field
- Examples can be the sausage instability and the current driven kink

In general a real-life instability will be driven by a mix of both pressure and current

e.g. z-pinch with no axial field



# Current driven kink for large aspect ratio with low $\beta$

Consider the ordering

$$\begin{aligned} W &\sim \varepsilon^2 \\ \beta &\sim \varepsilon^2 \end{aligned}$$

! Use perturbations of the form  
 $\xi \sim e^{i(m\theta - n\phi)}$

$m$  = poloidal mode number  
 $n$  = toroidal mode number

We can describe one of the strongest ideal MHD instabilities. The potential energy can be written as:

$$\begin{aligned} W = & \frac{2\pi^2 B_z^2}{\mu_0 R_0} \int_0^a \left[ \left( r \frac{d\xi}{dr} \right)^2 + (m^2 - 1)\xi^2 \right] \left( \frac{n}{m} - \frac{1}{q} \right)^2 r dr \\ & + \frac{2\pi^2 B_z^2}{\mu_0 R_0} \xi_a^2 a^2 \left( \frac{n^2}{m^2} - \frac{1}{q_a^2} + \Lambda m \left( \frac{1}{q_a} - \frac{n}{m} \right)^2 \right) \end{aligned}$$

$$W = W_P + W_B = \text{plasma} + \text{boundary (with vacuum)}$$



# Current driven kink for large aspect ratio with low $\beta$

Consider the ordering

$$W \sim \varepsilon^2$$
$$\beta \sim \varepsilon^2$$

! Use perturbations of the form  
 $\xi \sim e^{i(m\theta - n\phi)}$

$m$  = poloidal mode number  
 $n$  = toroidal mode number

We can describe one of the strongest ideal MHD instabilities. The potential energy can be written as:

$$W = \frac{2\pi^2 B_z^2}{\mu_0 R_0} \int_0^a \left[ \left( r \frac{d\xi}{dr} \right)^2 + (m^2 - 1)\xi^2 \right] \left( \frac{n}{m} - \frac{1}{q} \right)^2 r dr$$

$$+ \frac{2\pi^2 B_z^2}{\mu_0 R_0} \xi_a^2 a^2 \left( \frac{n^2}{m^2} - \frac{1}{q_a^2} + \Lambda m \left( \frac{1}{q_a} - \frac{n}{m} \right)^2 \right)$$

$\xi_a = \xi(a)$  is the plasma displacement at  $r = a$ , i.e. at the plasma boundary!

$$W = W_P + W_B = \text{plasma} + \text{boundary (with vacuum)}$$



# Current driven kink for large aspect ratio with low $\beta$

Consider the ordering

$$W \sim \varepsilon^2$$
$$\beta \sim \varepsilon^2$$

! Use perturbations of the form  
 $\xi \sim e^{i(m\theta - n\phi)}$

$m$  = poloidal mode number  
 $n$  = toroidal mode number

We can describe one of the strongest ideal MHD instabilities. The potential energy can be written as:

$$W = \frac{2\pi^2 B_z^2}{\mu_0 R_0} \int_0^a \left[ \left( r \frac{d\xi}{dr} \right)^2 + (m^2 - 1)\xi^2 \right] \left( \frac{n}{m} - \frac{1}{q} \right)^2 r dr$$

$$+ \frac{2\pi^2 B_z^2}{\mu_0 R_0} \xi_a^2 a^2 \left( \frac{n^2}{m^2} - \frac{1}{q_a^2} + \Lambda m \left( \frac{1}{q_a} - \frac{n}{m} \right)^2 \right)$$

$\xi_a = \xi(a)$  is the plasma displacement at  $r = a$ , i.e. at the plasma boundary!

Effect of a perfectly conducting (ideal) wall is stabilizing and represented by  $\Lambda$

$$W = W_P + W_B = \text{plasma} + \text{boundary (with vacuum)}$$



# Current driven kink for large aspect ratio with low $\beta$

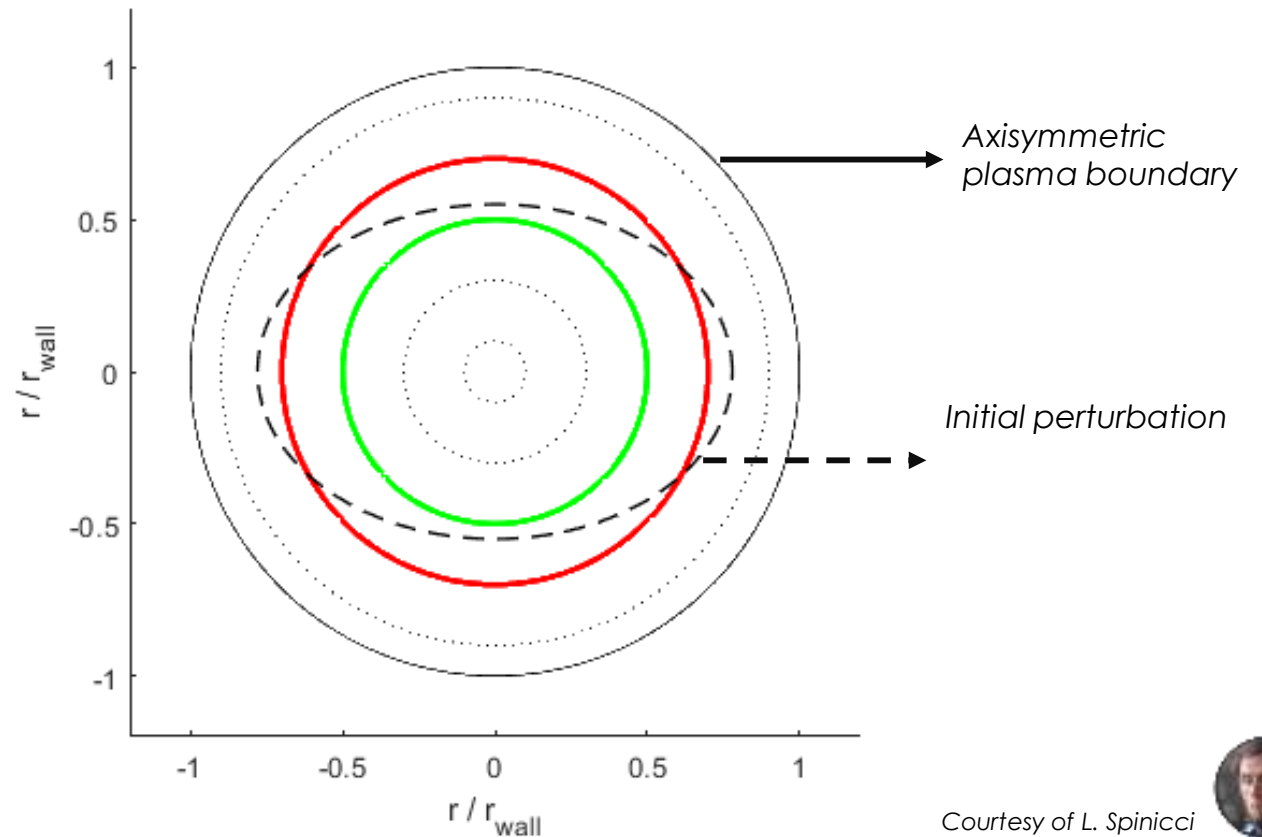
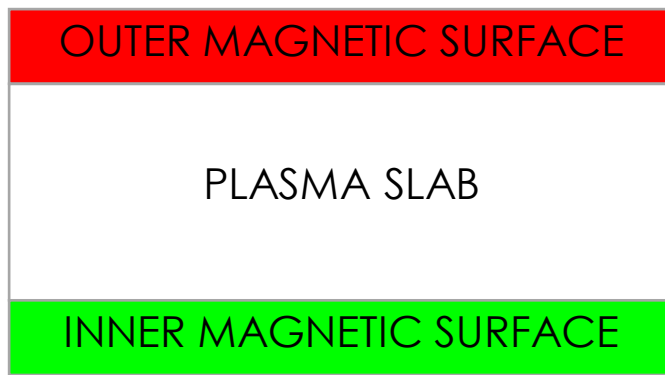
- For  $\xi_a = 0$  the boundary term is zero and the integral is positive: called **internal kink** modes, stable in  $\sim \varepsilon^2$ ! Need expansion to  $\sim \varepsilon^4$
- When  $\xi_a \neq 0$  the perturbation affects the plasma boundary: called **external kink** mode

Let's consider the case  $\xi_a > 0$  and  $\mathbf{m} = \mathbf{1}$ , with wall at infinity ( $\Lambda = 1$ ) -> the integral part of  $W$  is positive, we only need to discuss the boundary term ( $W_B$ )!



# Toy model for current driven kink

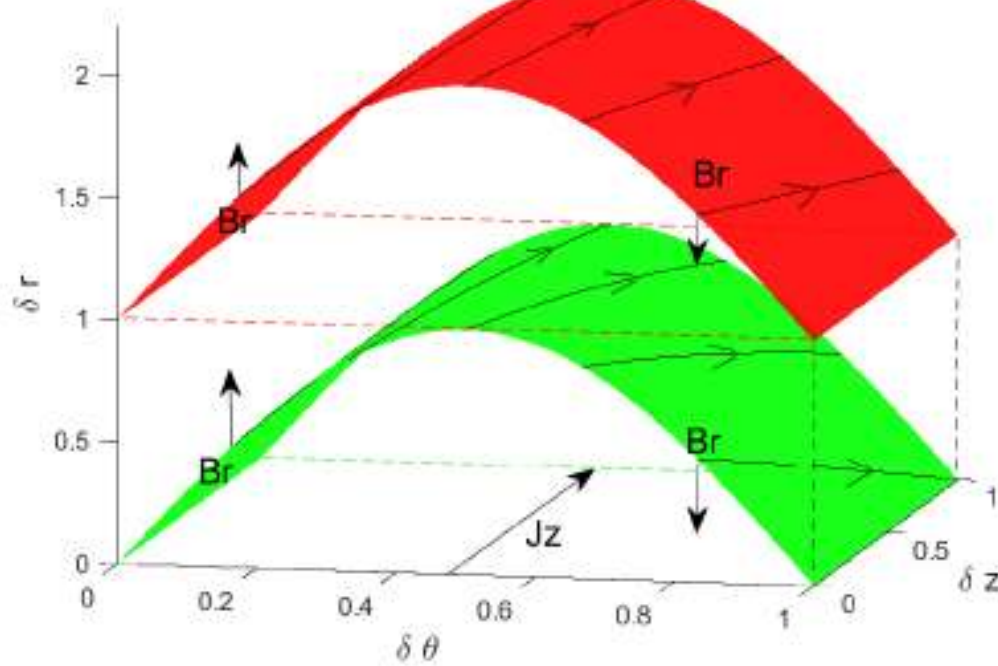
- Large aspect ratio  $R/a \gg 1$
- Monotonically decreasing current density towards edge (e.g. Wesson's parametrization)



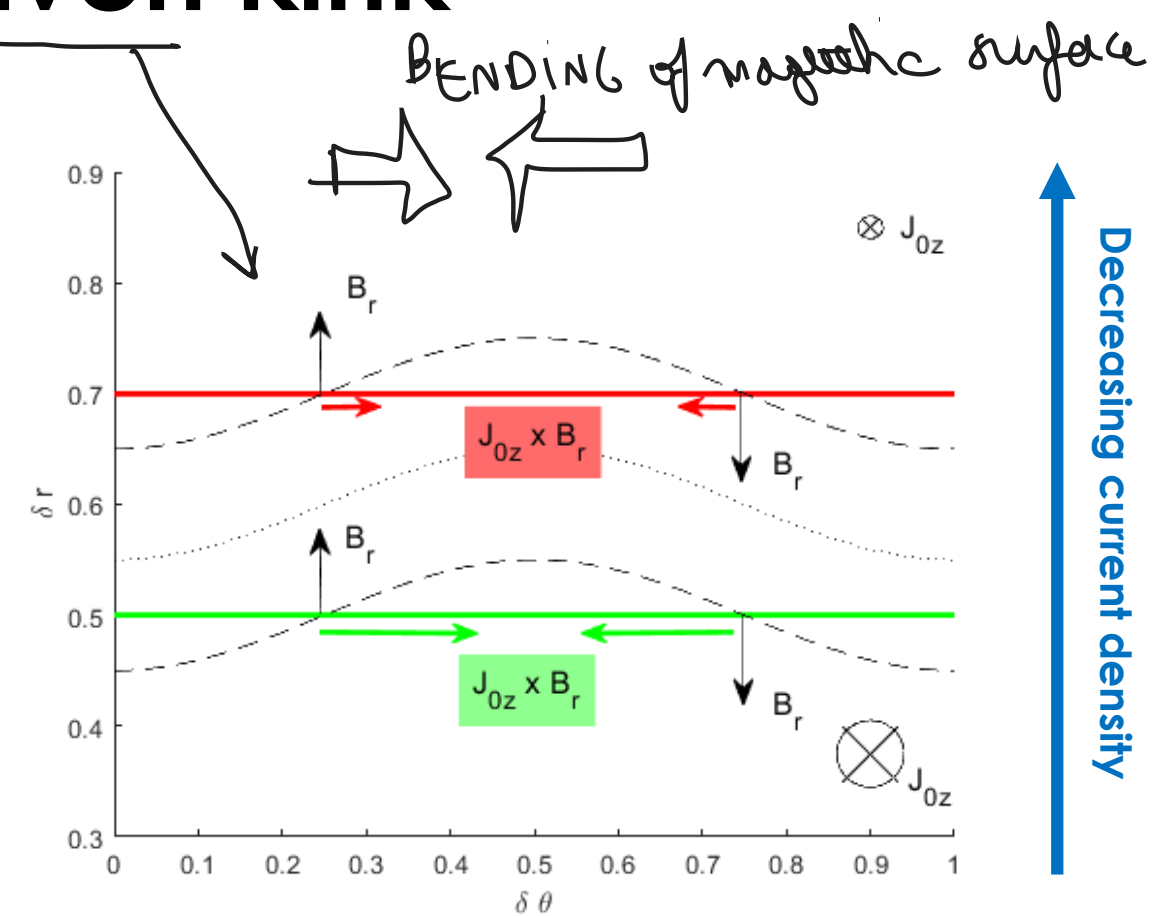
Courtesy of L. Spinicci



# Toy model for current driven kink



On bent surfaces the magnetic field gets a radial dependence:  $B_r$  component



$B_r$  interacts with toroidal current into  $J \times B$  force-couples, **stronger where  $J_z$  is larger**

These forces enhance the initial perturbation → instability



Courtesy of L. Spinicci

# Current driven **external kink**

$$q = \frac{n}{n}$$

$$W_B = \frac{4\pi^2 B_z^2}{\mu_0 R_0} n \left( n - \frac{1}{q_a} \right) a^2 \xi_a^2$$

$q_a < n$

This implies stability if  $W_B$ :

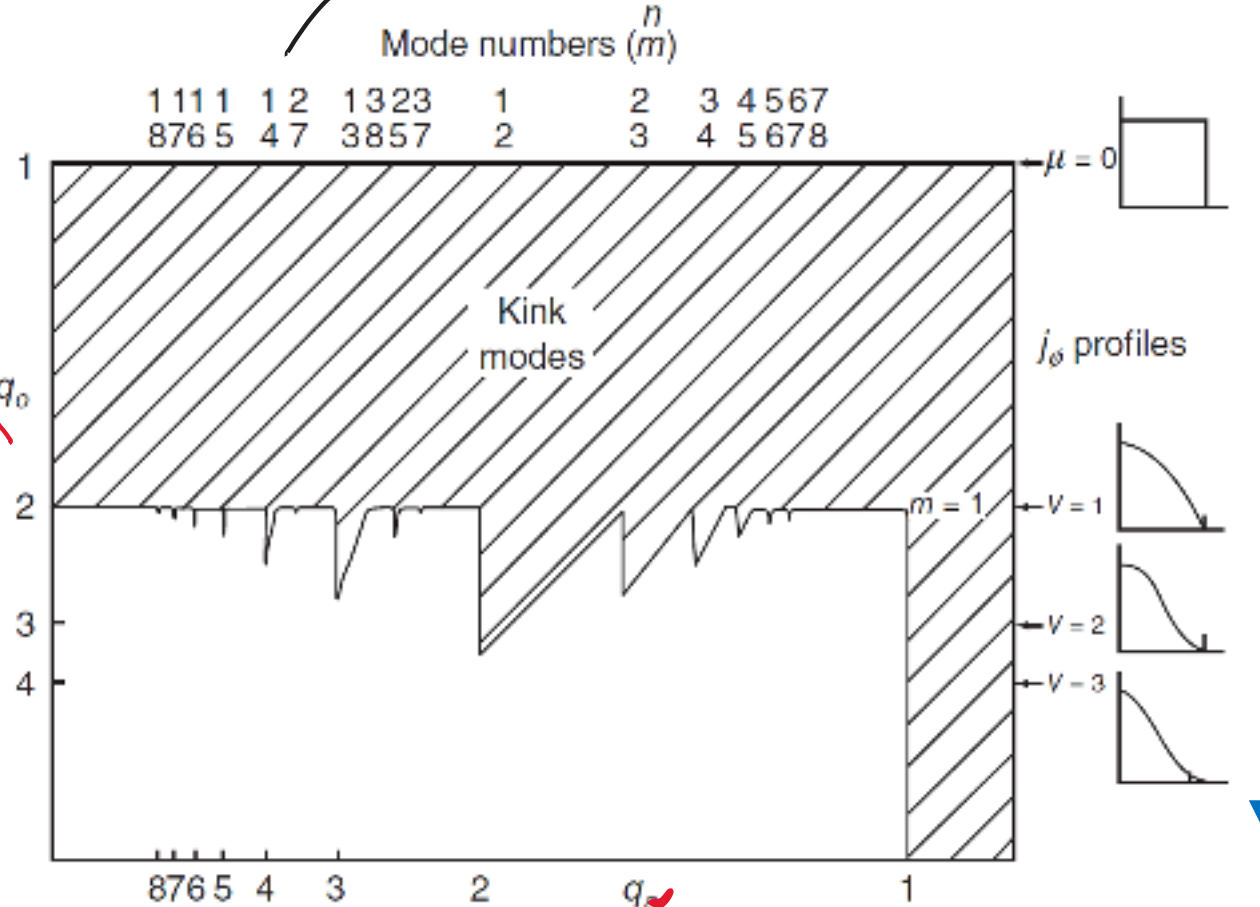
$$q_a < n$$

$$q_a > \frac{1}{n} \xrightarrow{\text{restrictive}} q_a > 1$$

This translates into a limit on the plasma current

$$q_a = \frac{2\pi a^2 B_\phi}{\mu_0 I_p R_0} \xrightarrow{\text{yields}} I_p < \frac{2\pi a^2}{\mu_0 R_0} B_\phi$$

**Kruskal-Shafranov limit**



Stability plot for equilibria with  $j = j_0 \left(1 - \frac{r^2}{a^2}\right)^v$

Remember that  $\frac{q_a}{q_0} = v + 1 !!$



# Comments on the Kruskal-Shafranov limit

- This operational boundary is actually not so limiting in present day machines, other instabilities are triggered first!
  - The ( **$m=2, n=1$** ) external kink (current driven) kicks in when  $q_a \sim 2$
- The presence of a **perfectly conducting wall** also stabilizes the external kink
  - Real world shells are not ideal though -> partial stabilization leads the **Resistive Wall Mode**
- For  $m \geq 2$  stability depends on balance of terms in  $W_B$ . For given  $(m, n)$  the mode can be unstable if  $q_a < m/n$  i.e. if the mode resonant surface lies outside the plasma



# Stability diagram of the current driven kink

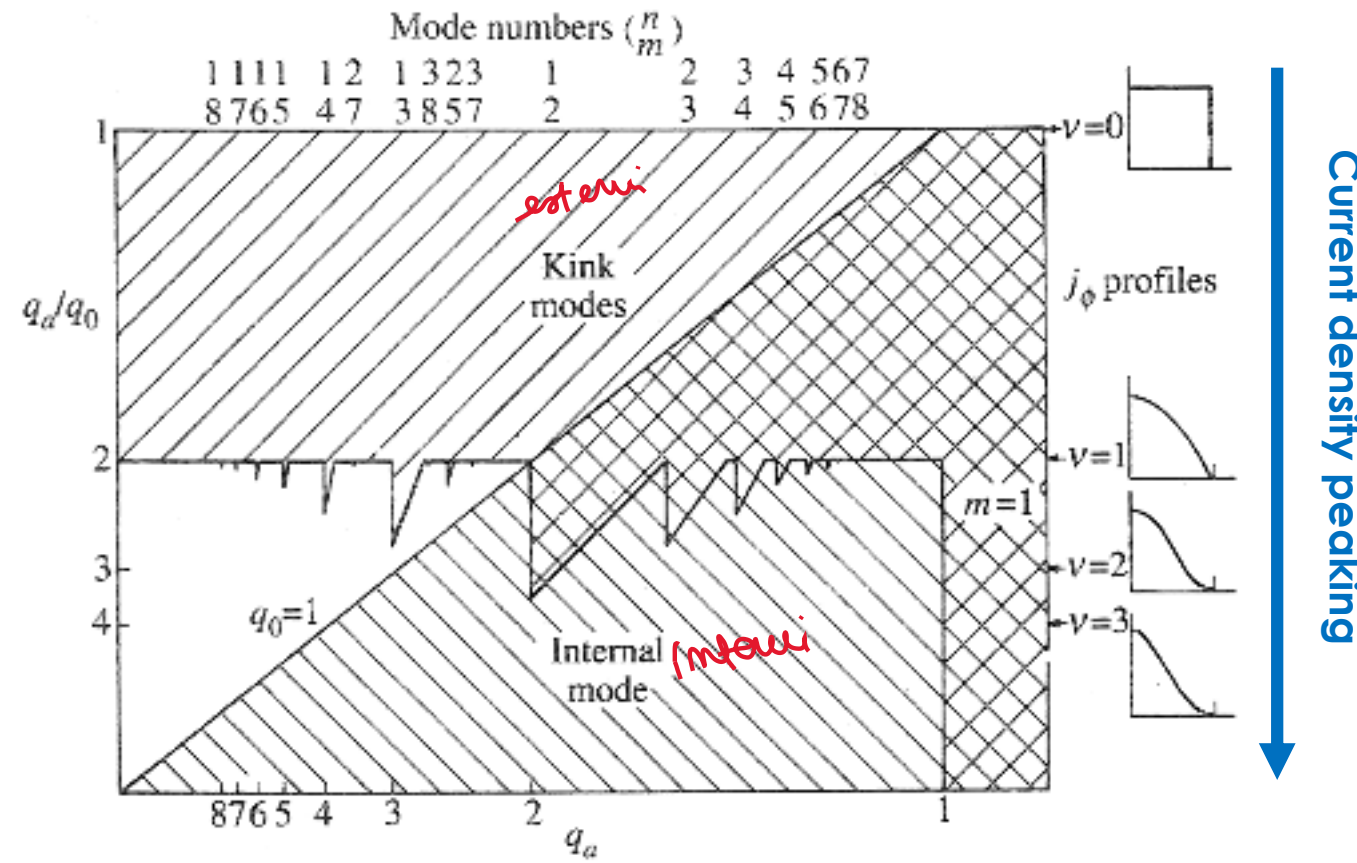
Internal kink stability (for  $m=1$ ) leads to a further requirement\*

$$q_0 > 1$$

An effect of pressure is also possible here (finite  $\beta$  effect): usually destabilizing

Ideal kink modes limit **achievable plasma current**

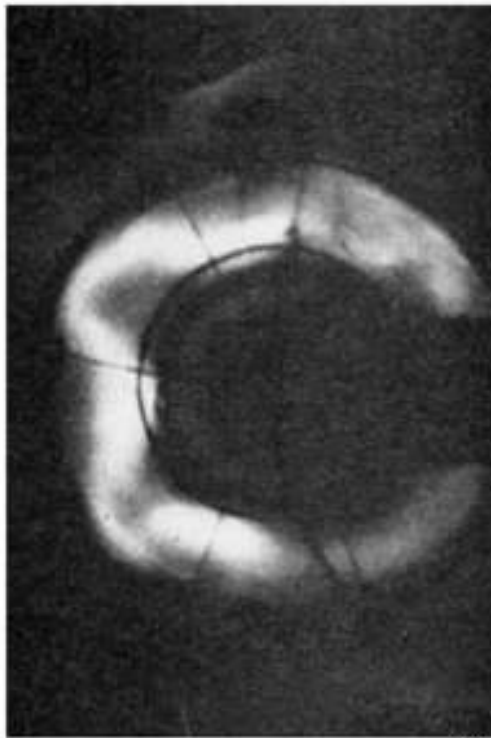
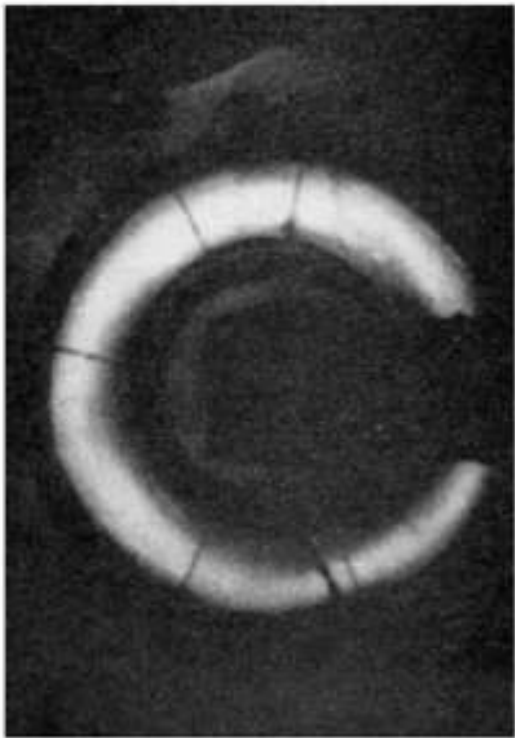
**Current density peaking** important for kink stability (and for other modes as well!)



\*see references: Zohm, Wesson



# Early kinks



Kink instability in an early pinch experiment

From: Carruthers, PhysSoc. London (1957)



# Global MHD instabilities

Instabilities with a global structure causing non-negligible displacement at the plasma surface.

These instabilities are appropriately known as eXternal Kink modes  
**(XK)**.

- Predicted for long time [D. Pfirsh and H. Tasso, Nucl. Fusion **11**, 259 1971]

In **tokamaks** this led to the prediction of the Troyon  $\beta$  limit (i.e. maximum achievable pressure with no conducting wall)

- ▶ Instability linked to **pressure**
- ▶ Strongly depends on shape of plasma radial profiles!

Intrinsic in **Reversed Field Pinch** even at  $\beta \rightarrow 0$

- ▶ Instability linked to **current**



# The Troyon limit

Obtained **numerically** with a combination of all ideal MHD limits, gives an estimate of the **maximum achievable  $\beta$**  for given machine parameters (with no stabilizing wall)

$$\beta < \beta_{t,\max} [\%]$$

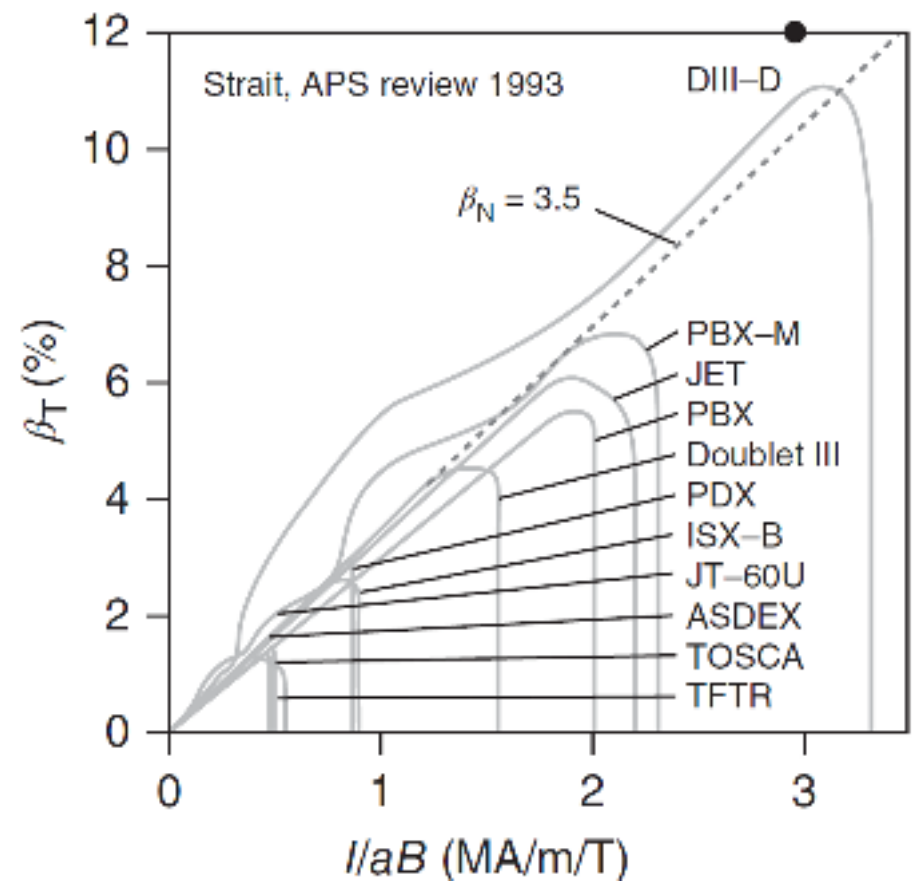
$$\beta_{t,\max} [\%] = [2.8 \div 5.6] \frac{I_p [\text{MA}]}{a [\text{m}] B_t [\text{T}]}$$

*g TROYON FACTOR*

Leads to definition of **normalized  $\beta$**

$$\beta_N = \beta_{t,\max} [\%] \frac{a [\text{m}] B_t [\text{T}]}{I_p [\text{MA}]}$$

There is a full class of instabilities linked to pressure gradients that are called external kink modes, and normally in Tokamaks, where the plasma is surrounded not by an ideal conductor, but by a resistive conductor (so a conductor where magnetic field perturbation



# The Advanced Tokamak (AT) scenario for steady state operation

Gli scenari che massimizzano beta sono gli AT

Steady state achieved through high bootstrap current

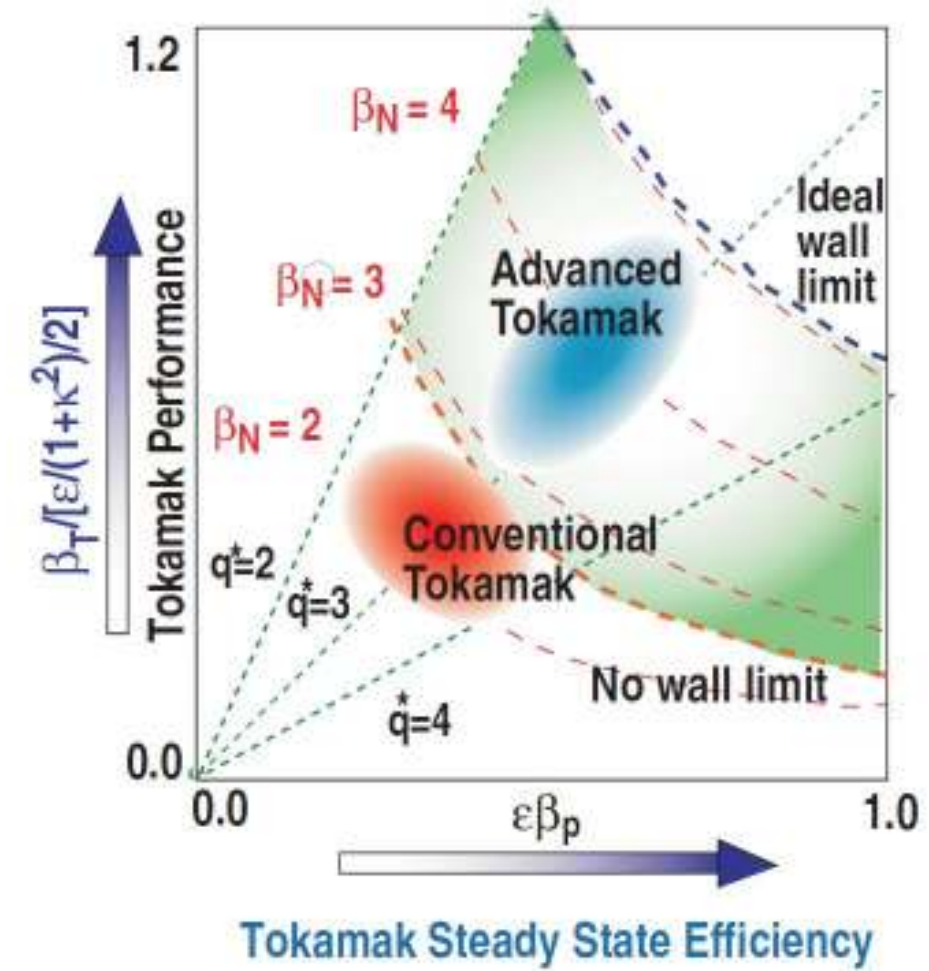
-> proportionality with  $\beta_p = 2\mu_0 \langle p \rangle / \langle B_p^2 \rangle$

Sustained fusion reaction

-> high enough  $\beta_T = 2\mu_0 \langle p \rangle / B_T^2$

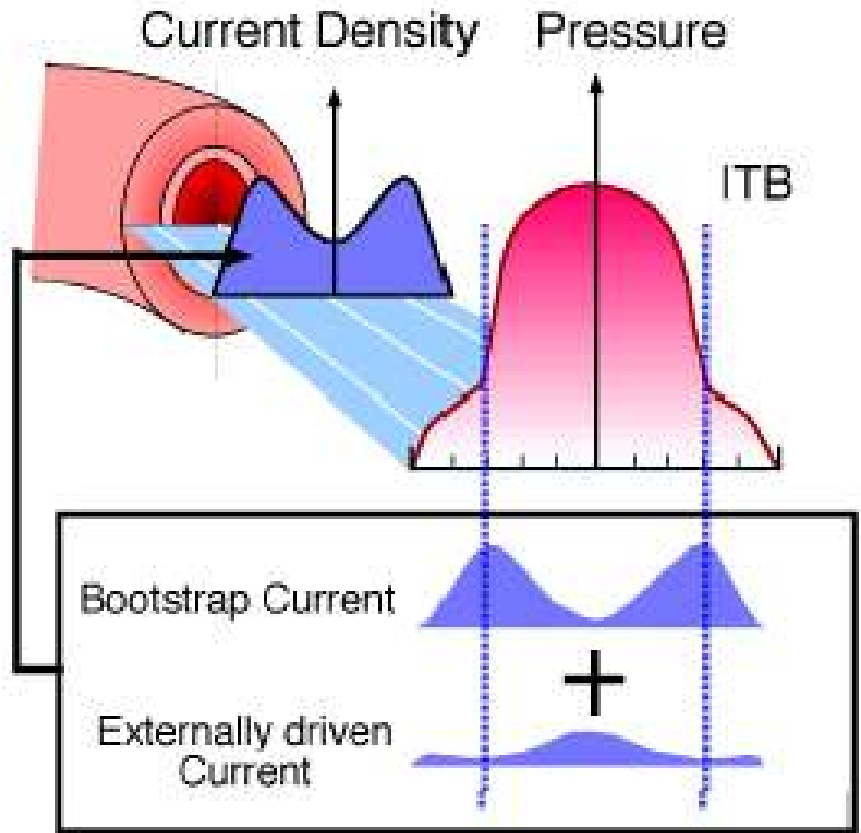
$$\beta_p \beta_T \sim 25 \left[ \frac{1 + E^2}{2} \right] \left( \frac{\beta_N}{100} \right)^2$$

Raising  $\beta_N$  will allow the simultaneous achievement of high **bootstrap current fraction** and high **fusion power density**.



# The many faces of having high bootstrap fraction

Si vuole high bootstrap current raggiungibile ad alto beta --> superato il troyon limit --> XK unstable



High bootstrap current fraction for steady state operation (75-90%)

$$j_b \sim \nabla p$$

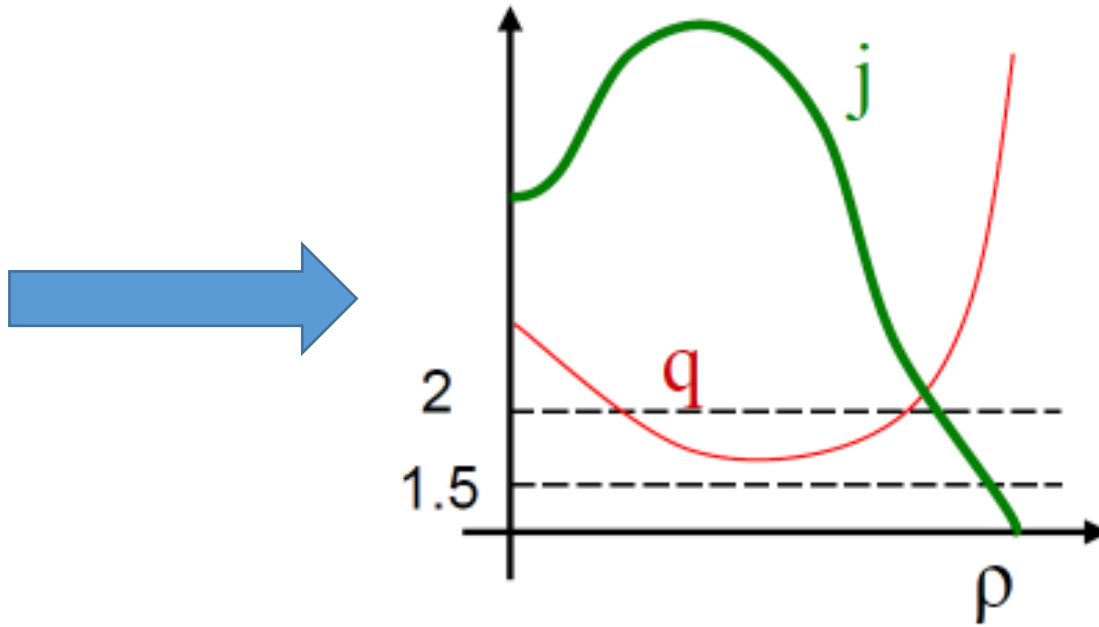
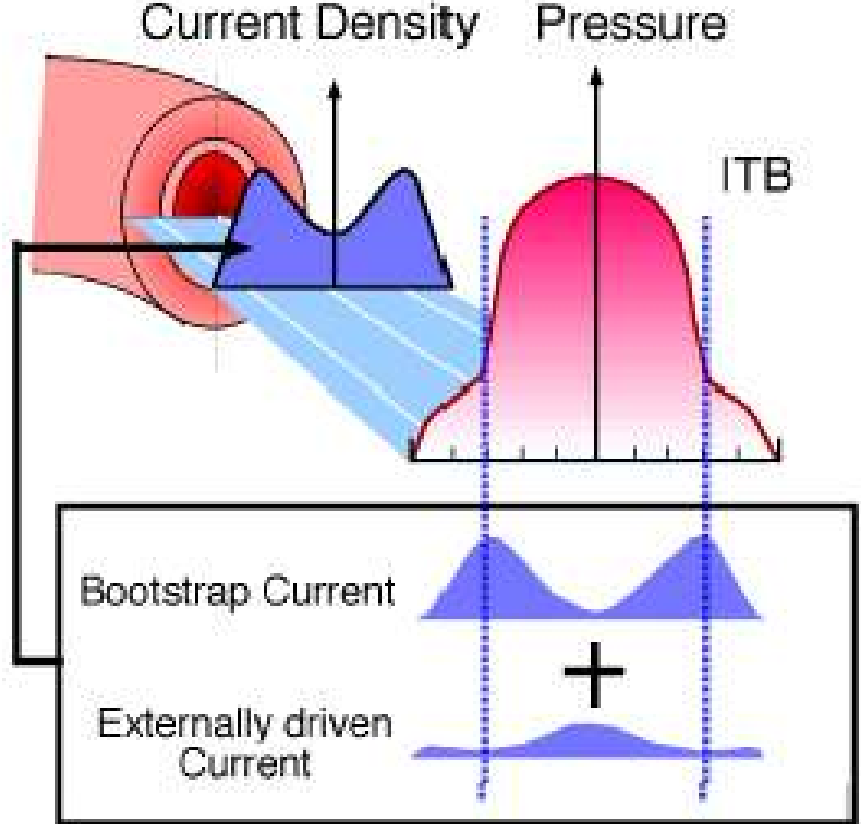
- > high  $\beta_N$  is required to achieve the target bootstrap current
- > usually exceeds Troyon pressure limit: **XK unstable**

Current profiles in AT are usually hollow:

- > Turbulence suppression & Internal Transport Barriers (**ITBs**)
- > Reversed q-profiles: low-shear combined with pressure gradient produces new MHD (Infernal modes)



# The many faces of having high bootstrap fraction



A close fitting conducting wall is required to slow down the XK → Resistive Wall Mode (**RWM**)

RWM stabilization methods are needed for Advanced Tokamak operation



# Current-driven kinks in Reversed Field Pinch devices

The RFP relies on an **ideally conducting wall** to maintain plasma stability with respect to the **current-driven** kink modes.

- A **resistive shell** can reduce the mode growth rates to values comparable to the vertical field penetration time of the wall
- Resistive Wall Modes predicted by theory and found by experiments. The main RWMS in the RFP are intrinsic, non-resonant, current-driven kink modes that are largely unaffected by sub Alfvénic plasma rotation

[C. G. Gimblett, *Nucl. Fusion* **26**, 617 1986]

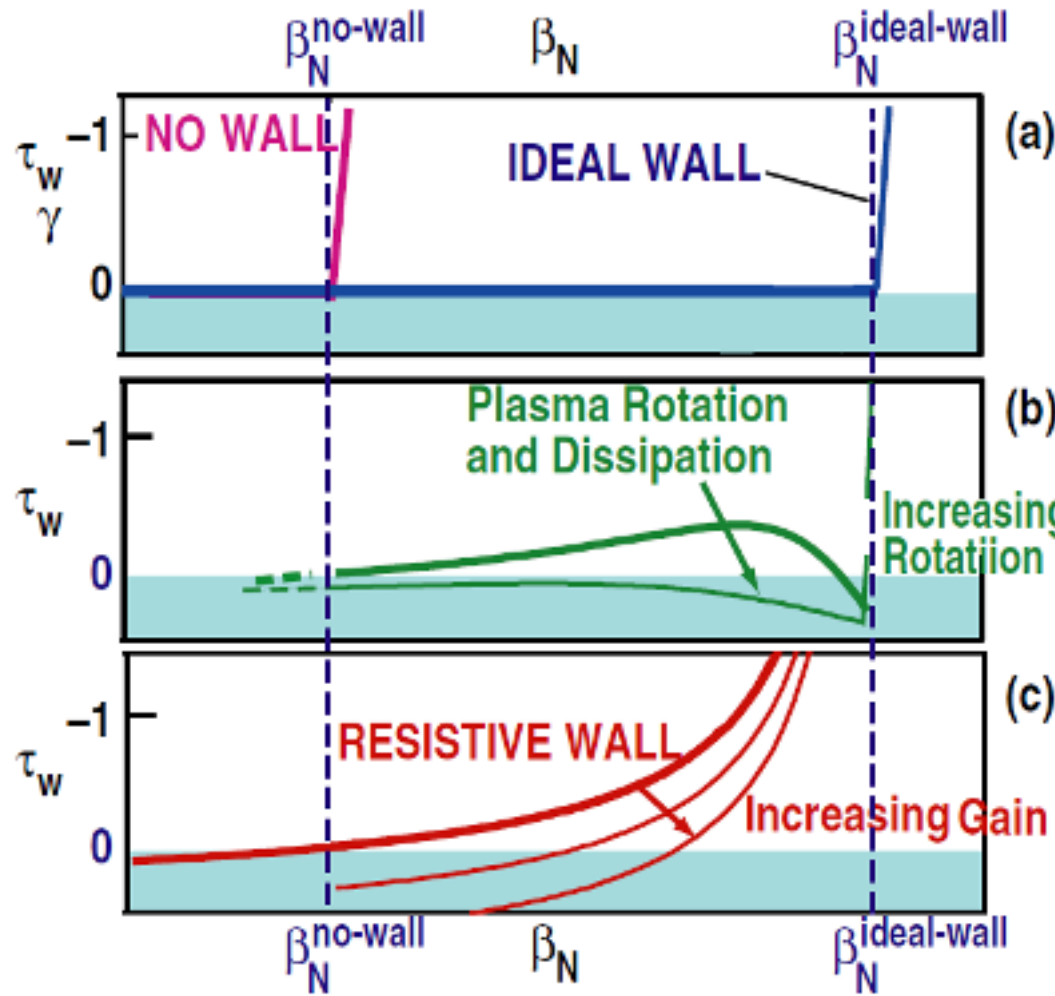
[R. Paccagnella, *Nucl. Fusion* **38**, 1067 1998]

[S.C. Guo, J.P. Freidberg and R. Nachtrieb *Phys. Plasmas* **6** 3868 1999]

- RFPs have different RWM **spectrum** w.r.t tokamaks: a range of modes are unstable. **Simultaneous** stabilization of multiple RWMS is required.



# What is a Resistive Wall Mode?



Focusing on **pressure-driven** instabilities in tokamaks

The Resistive Wall Mode (RWM) is an external kink (**XK**) mode which interacts with external structures having finite conductivity

Schematic diagram of XK and RWM growth rates as a function of normalized  $\beta_N$

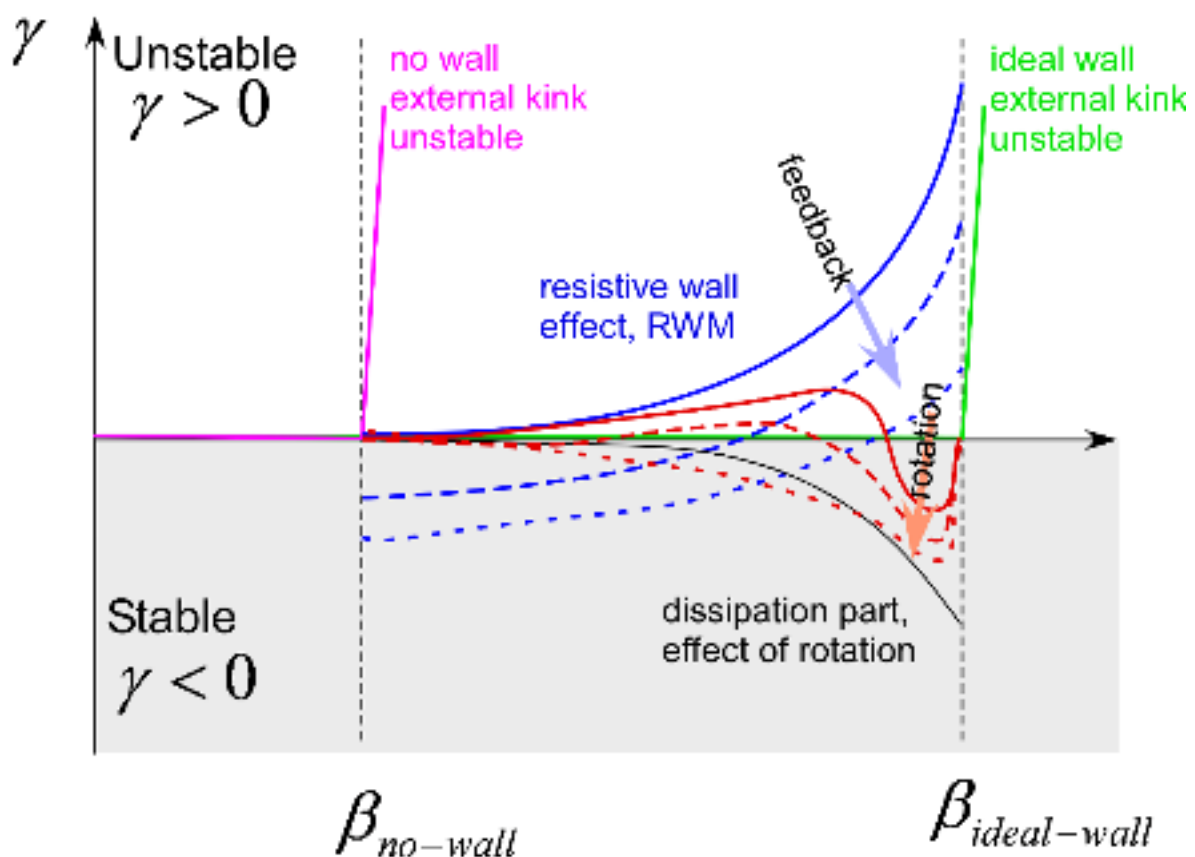
- (a) Stabilization of the XK mode by an ideal wall and of the RWM by a wall with finite conductivity.
- (b) Stabilization of the RWM by increasing plasma rotation and dissipation.
- (c) Stabilization of the RWM with magnetic feedback.



# Effects of resistive wall & plasma rotation on the XK: the Chu et al. dispersion relation

$$(\gamma + i\eta\Omega)D + \delta W_p + \frac{\delta W_{vac}^b \gamma \tau_w + \delta W_{vac}^\infty}{\gamma \tau_w + 1} = 0$$

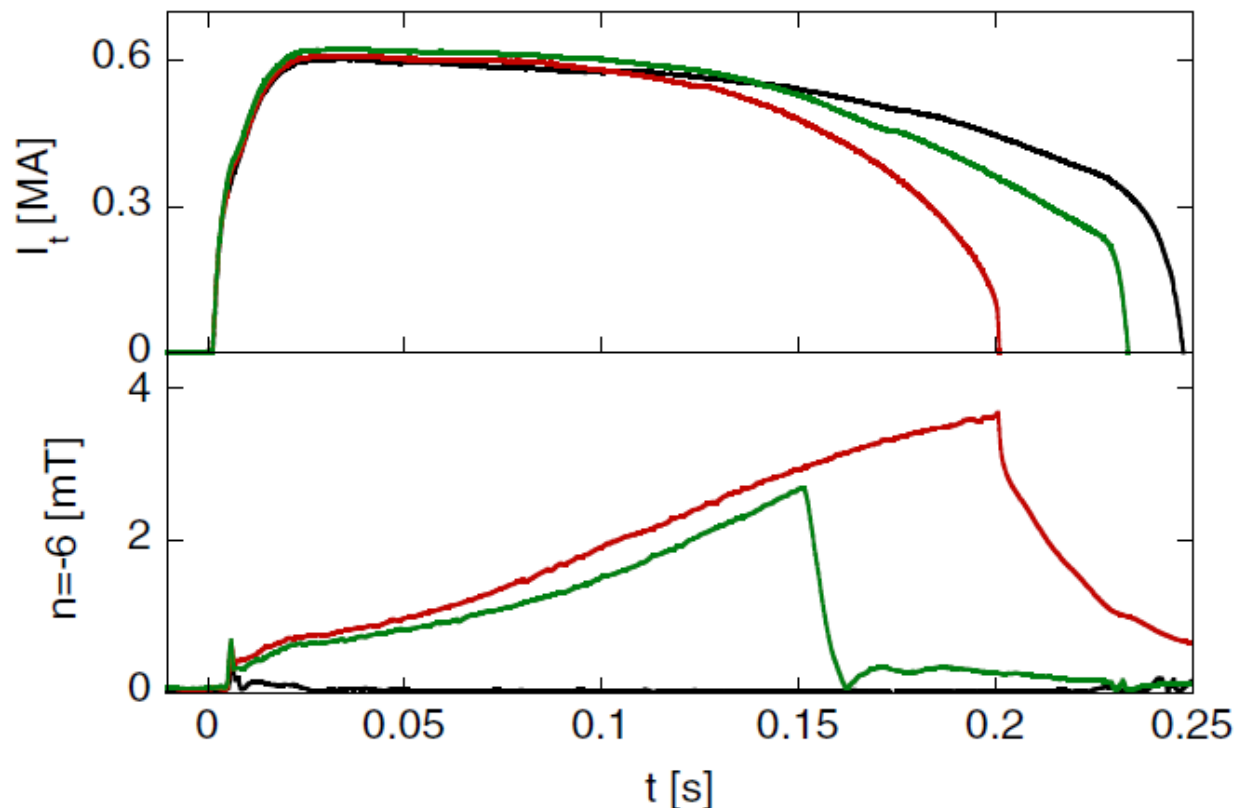
- D : dissipation integral
- $\delta W_p$  : Plasma potential energy integral
- $\delta W_{vac}^b$  : vacuum energy with ideal wall at  $r=b$
- $\delta W_{vac}^\infty$  : vacuum energy with ideal wall at  $r=\infty$



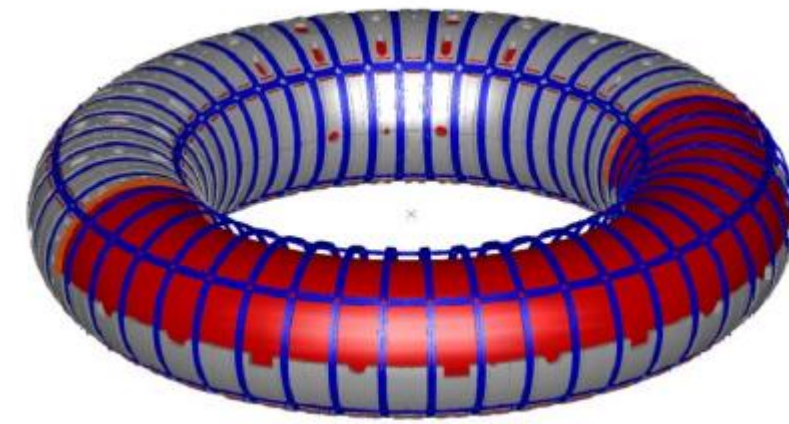
[Chu et al. Phys. Plasmas, 2, 2236 (1995)]



# Active control of the Resistive Wall Mode: RFX-mod



192 independent active coils  
arranged in 4 toroidal arrays  
and 48 poloidal sections



[S. Ortolani and the RFX team 2006 Plasma Phys.  
Control. Fusion **48** B371]

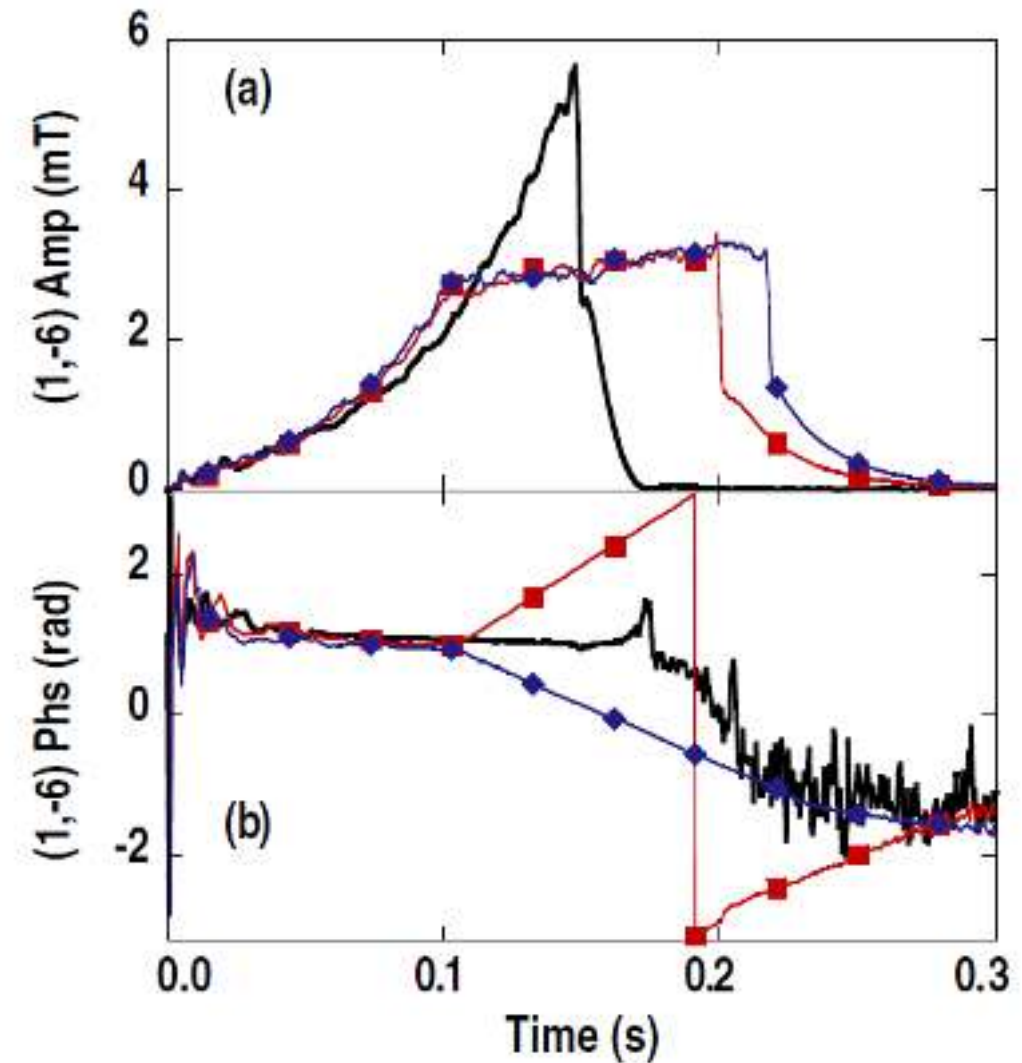
Multi-modal RWM feedback on RFX-mod. **Black** (#17287) full virtual shell. **Red** (#17301)  $m = 1, n = -3$  to  $-6$  are excluded from the control: early pulse termination. **Green** (#17304) the control on the  $m = 1, n = -6$  mode is switched on and rapid stabilization is achieved.



# Active control of the Resistive Wall Mode: RFX-mod

A complex proportional gain can be used to **rotate** a selected RWM in a given direction.

Reversing the phase of feedback rotates the RWM in the opposite direction.



# Useful bibliography

This lecture is based on a number of books treating the subject of MHD at different levels. The following list is by no means intended to be complete, but rather provides a starting point for diving into the subject.

- Wesson, John, and David J. Campbell. *Tokamaks*. Vol. 149. Oxford university press, 2011.
- Zohm, Hartmut. *Magnetohydrodynamic stability of tokamaks*. John Wiley & Sons, 2015.
- Freidberg, Jeffrey P. *Ideal MHD*. Cambridge University Press, 2014.
- Schnack, Dalton D. *Lectures in magnetohydrodynamics: with an appendix on extended MHD*. Vol. 780. Springer, 2009.
- Goedbloed, Hans, Rony Keppens, and Stefaan Poedts. *Magnetohydrodynamics: Of Laboratory and Astrophysical Plasmas*. Cambridge University Press, 2019.



Feedback is welcome !

[leonardo.pigatto@igi.cnr.it](mailto:leonardo.pigatto@igi.cnr.it)

[tommaso.Bolzonella@igi.cnr.it](mailto:tommaso.Bolzonella@igi.cnr.it)



# Nonlinear magnetohydrodynamics theory

&

## HPC physics

Marco Veranda

[marco.veranda@igi.cnr.it](mailto:marco.veranda@igi.cnr.it)

*Consorzio RFX (CNR, ENEA, INFN, Università di Padova, Acciaierie Venete SpA)  
CNR, Istituto per la Scienza e la Tecnologia dei Plasmi*

Padova, Italy

November 26<sup>th</sup> 2024

# OUTLINE of the lesson

- Intro: meaning of nonlinearity, why it is necessary to deal with it;
- Basics: recap of MHD models
- example 1: magnetic reconnection
- example 2: sawtoothing in tokamaks
- HPC physics (and programming techniques)

# why nonlinearity is difficult

- Most nonlinear systems are impossible to solve analytically. Why are nonlinear systems so much harder to analyze than linear ones?
- The essential difference is that linear systems can be broken down into parts. Then each part can be solved separately and finally recombined to get the answer. This idea allows a fantastic simplification of complex problems, and underlies such methods as normal modes, Laplace transforms, Fourier analysis and the superposition principle.
- In this sense, a linear system is precisely equal to the sum of its parts.
- But many things in nature don't act this way. Whenever parts of a system interfere, or cooperate, or compete, there are nonlinear interactions going on.
- Most of everyday life is nonlinear, and the principle of superposition fails spectacularly (try to listen to your two favorite songs at the same time, you won't get double the pleasure!)
- Within the realm of physics, nonlinearity is vital to the operation of a laser, the formation of turbulence in a fluid, and the superconductivity of Josephson junctions, just to write the first phenomena coming to my mind.

quotes from Steven H. Strogatz, Nonlinear dynamics and Chaos, 2015, Westview Press

# speaking with equations

- linear differential equation of order n

$$a_n(x) \frac{d^n y(x)}{dx^n} + a_{n-1}(x) \frac{d^{n-1} y(x)}{dx^{n-1}} + \cdots + a_1(x) \frac{dy(x)}{dx} + a_0(x)y(x) = f(x)$$

- $y(x)$  cannot have powers higher than 1, i.e. no  $y(x)^2$ , and multiplication of derivatives  $\frac{dy}{dx} \cdot \frac{d^3y}{dx^3}$ , or be contained in nonlinear functions (no  $\ln(y)$ ).
- superposition principle: if  $y_1(x)$  and  $y_2(x)$  are solutions, then also  $ay_1(x) + by_2(x)$  is a solution of the differential equation (i.e. it can create a vector space, very useful)
- nonlinear differential equation of order n

$$a_n(x) \color{red}{y(x)} \frac{d^n y(x)}{dx^n} + a_{n-1}(x) \color{red}{\sin(y(x))} \frac{d^{n-1} y(x)}{dx^{n-1}} + a_1(x) \frac{dy(x)}{dx} \color{red}{\frac{dy(x)}{dx}} + a_0(x)y(x) = f(x)$$

# What is and why we need a nonlinear exploration of the MHD model for plasmas

- MHD describes the macroscopic behaviour of electrically conducting fluids, i.e. a plasma;
- Since the first studies in the 1950s, equilibrium and stability have been widely tackled:
  - equilibrium state is separated from small perturbations, linear MHD;

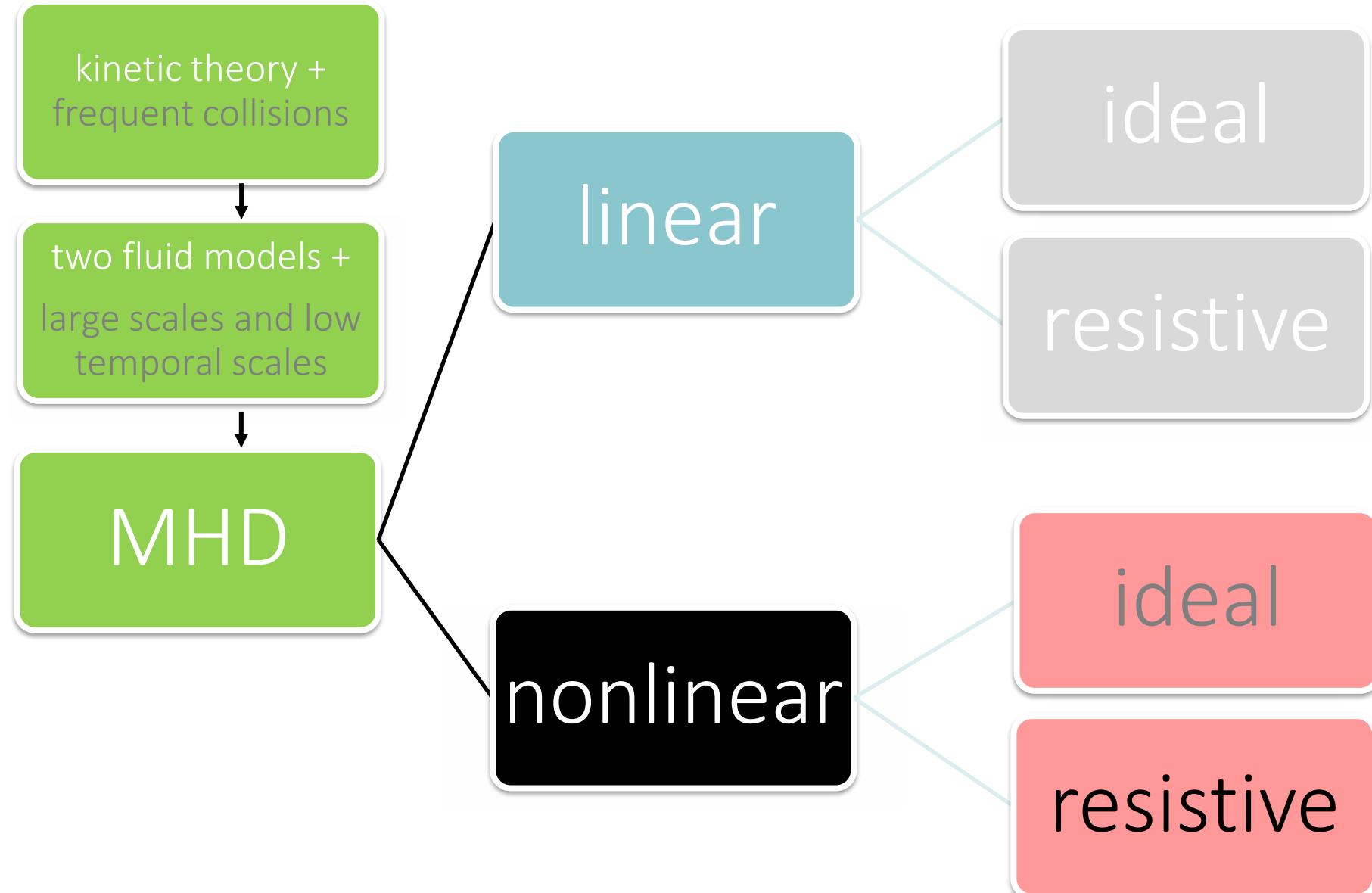
# Linear / quasi linear / nonlinear approaches

- Linear picture: instability would lead to the destruction of the equilibrium configuration and loss of the plasma confinement.
- Linear dynamics is a very important tool, but it is insufficient to predict the final state of unstable dynamics in various types of disrupted processes routinely observed in magnetically confined fusion plasmas
- → necessity to consider nonlinear dynamics
- Plasma discharges in reality exist even if instabilities are present → need to compute nonlinear behaviour or, at least, saturation levels.
- The most privileged approach would be to follow the nonlinear development from an unstable equilibrium;

# Linear / quasi linear / nonlinear approaches

- POSSIBLE APPROACHES:
  - study slowly evolving equilibrium states (ideal kink mode, resistive kink, asymptotic states of system relaxed under some constraints);
  - Fully developed MHD turbulence (averages);
  - numerical computations: problem is considered solved if “scaling laws” can be obtained.
- But also QUASI-LINEAR theory: only take into account the action of the unstable modes on the equilibrium profiles.

# a diagram about possible modelling of hot plasmas



# 3D nonlinear resistive MHD equations

$\frac{\partial \rho}{\partial t} + \nabla \cdot (\rho \mathbf{v}) = 0$	mass continuity equation
$\rho \frac{\partial \mathbf{v}}{\partial t} + \rho \mathbf{v} \cdot \nabla \mathbf{v} = \mathbf{J} \times \mathbf{B} - \nabla p$	momentum equation
$\frac{\partial p}{\partial t} + \mathbf{v} \cdot \nabla p + \gamma p \nabla \cdot \mathbf{v} = (1 - \gamma) \eta J^2$	energy equation
$\frac{\partial \mathbf{B}}{\partial t} = -\nabla \times \mathbf{E}$	Faraday equation
$\mathbf{E} + \mathbf{v} \times \mathbf{B} = \eta \mathbf{J}$	Ohm equation
$\nabla \times \mathbf{B} = \mu_0 \mathbf{J}$	Ampère equation
$\nabla \cdot \mathbf{B} = 0$	Gauss equation

# Model equations: fundamental time scales

- by studying the linearized small-amplitude oscillatory solution of the MHD model (theory of *MHD waves*, it would require a lesson on its own) the fundamental temporal and velocity scales emerge:

$$\text{Alfvén velocity } v_A \equiv \frac{B_0}{\sqrt{\mu_0 \rho_0}}$$

and, by assuming a macroscopic lenght of the system  $L$  one gets the Alfvén time  $\tau_A = \frac{L}{v_A}$

- By rewriting the equations of slide 6 normalizing all quantities to the Alfvén velocity and time and to the macroscopic length one can obtain the

$$\text{resistive time scale } \tau_R = \frac{\mu_0 L^2}{\eta}$$

# resistive MHD: basics / timescales involved

- Faraday equation + Ohm's law for a plasma:

$$\frac{\partial \mathbf{B}}{\partial t} = -\nabla \times \mathbf{E} \quad \text{and} \quad \mathbf{E} + \mathbf{v} \times \mathbf{B} = \eta \mathbf{J} \quad \text{and} \quad \nabla \times \mathbf{B} = \mu_0 \mathbf{J}$$

- interesting fact: Ohm's law is similar to the one valid in electromagnetism, only the electric field is replaced by an effective one  $\mathbf{E} + \mathbf{v} \times \mathbf{B}$ , the effective electric field seen by a fluid element moving with velocity  $\mathbf{v}$  across a magnetic field  $\mathbf{B}$ , taking into account the Lorentz transformation for  $v \ll c$ .

$$\frac{\partial \mathbf{B}}{\partial t} = \nabla \times \left( \mathbf{v} \times \mathbf{B} - \frac{\eta}{\mu_0} \nabla \times \mathbf{B} \right) = \nabla \times (\mathbf{v} \times \mathbf{B}) - \frac{\nabla \eta}{\mu_0} \times \nabla \times \mathbf{B} + \frac{\eta}{\mu_0} \nabla^2 \mathbf{B} \quad \begin{matrix} \text{EQUAZIONE} \\ \text{DI INDUZIONE} \end{matrix}$$

- assume uniform resistivity and compare the two terms:

$$\frac{|\nabla \times (\mathbf{v} \times \mathbf{B})|}{\left| \frac{\eta}{\mu_0} \nabla^2 \mathbf{B} \right|} = \frac{v B \mu_0 L^2}{L \eta B} = \boxed{\frac{\mu_0 L v}{\eta} = Re_M} \quad R \propto L$$

( $Re_M$ : magnetic Reynolds number)

def:  $\tau_R \equiv \frac{\mu_0 L^2}{\eta}$

- upper bound:  $v \sim v_A$ , Lundquist number

$$\boxed{S = \frac{\tau_R}{\tau_A} = \frac{\mu_0 L v_A}{\eta}}$$

# resistive MHD: basics / remind of Spitzer's formula for the resistivity of a plasma

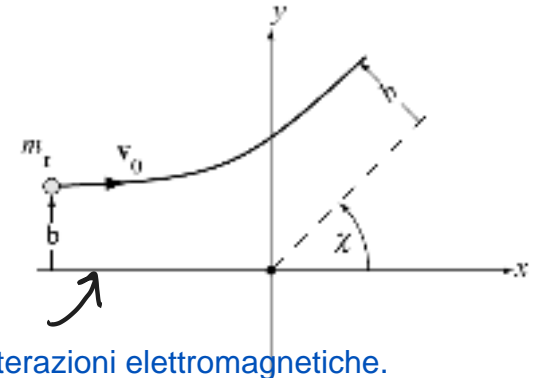
- Lundquist number  $S = \frac{\tau_R}{\tau_A} = \frac{\mu_0 L v_A}{\eta}$
- due to charged particles "collisions" (semantics);
- dependence on the typical time scale of electron-ion collision frequency;

la resistività deriva non dalle collisioni degli elettroni con la struttura cristallina (considerando un plasma) ma dalle interazioni elettromagnetiche.

$$\boxed{\eta = \frac{0.06 e^2 m_e^{1/2}}{\pi^{3/2} \epsilon_0^2} \frac{\ln \Lambda}{T_e^{3/2}}}$$

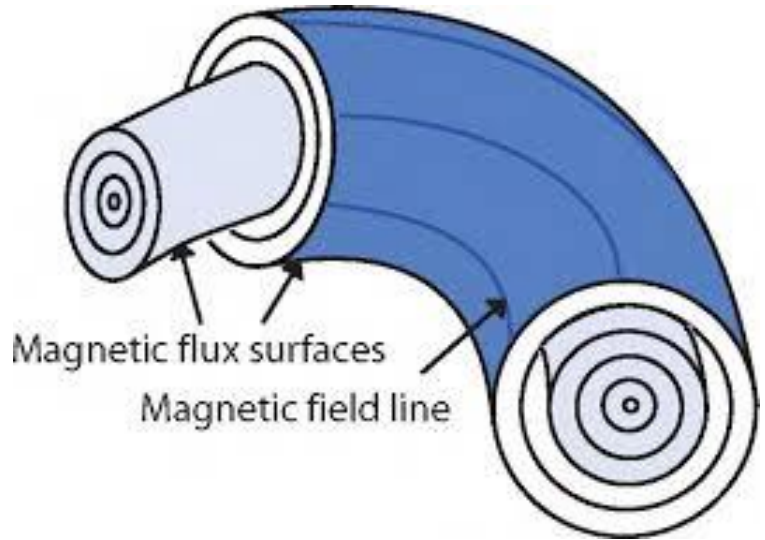
all units in SI, temperature in [J]

- Coulomb logarithm  $\ln \Lambda$  contains details about the close encounters between an electron and an ion, and it is practically constant for fusion plasmas  $\ln \Lambda \sim 15$
- in hot fusion plasmas  $S \sim 10^6 - 10^9$

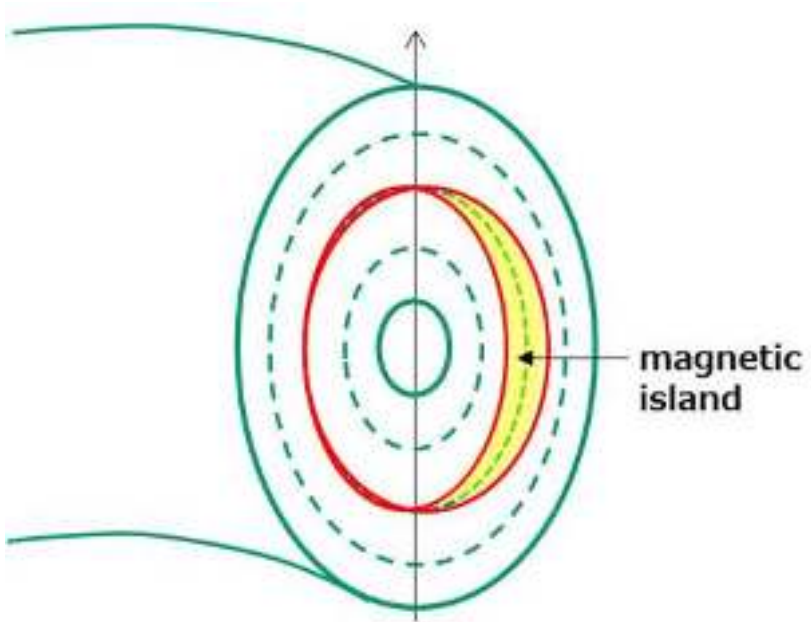


REF: chapter 9 of J. Freidberg, Plasma Physics and Fusion Energy, Cambridge University Press 2007

# ideal vs resistive MHD



**Ideal MHD:**  $\eta = 0$   
**flux conservation inside a**  
**magnetic flux surface\***  
**topology unchanged**

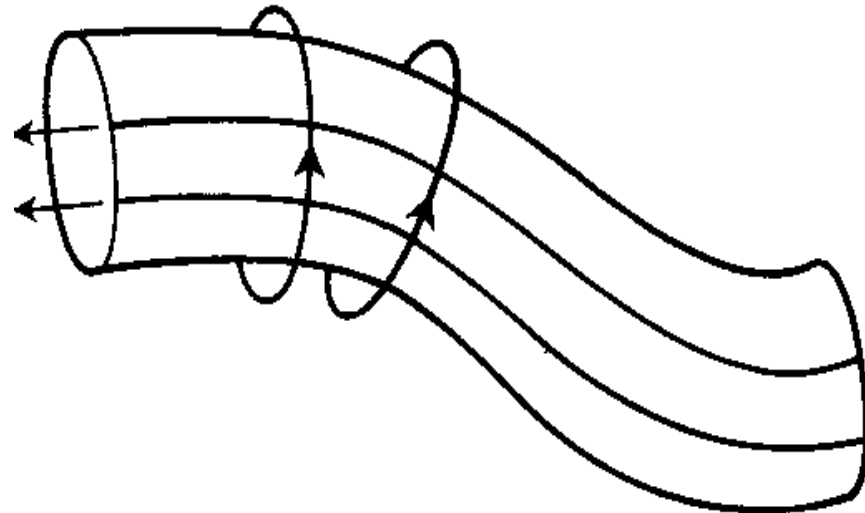


**Resistive MHD:**  $\eta \neq 0$   
**reconnection of field lines**  
**topology changes**

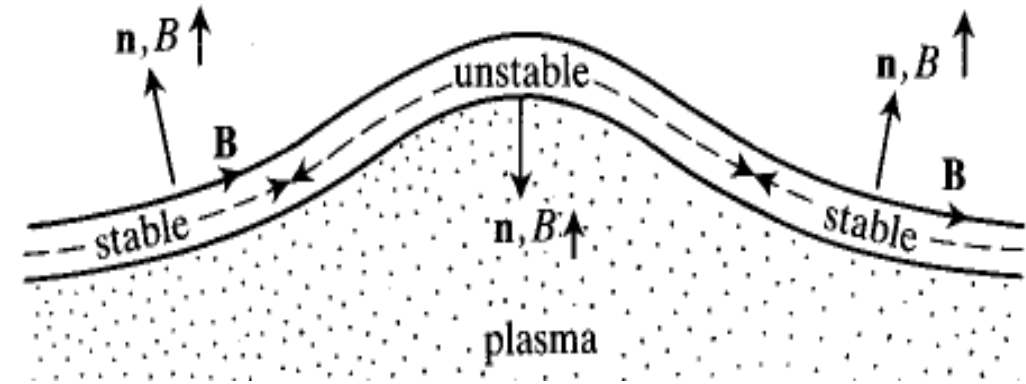
\*the lines of force of the magnetic field are ‘frozen’ in the plasma if ideal MHD holds. Indeed, in ideal MHD (perfect conductivity!), the concept of magnetic field lines obtains more physical reality than it even had in Faraday’s times. cfr. Alfvén theorem.

# Free energies to drive MHD modes

DA QUI CONSIDERIAMO SOLO RESISTIVE MHD



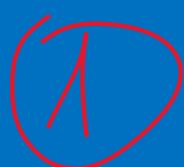
current driven instabilities  
(kink / tearing modes)



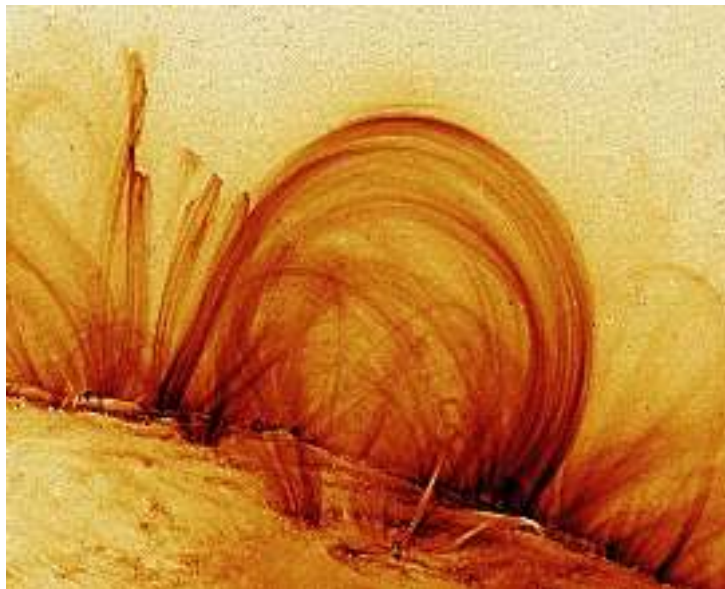
pressure driven instabilities  
(interchange mode)

## two cases (between many, not exhaustive)

- 1) Magnetic reconnection / resistive-kink tearing modes dynamics in resistive MHD
- 2) Sawtoothing in tokamaks / nonlinear cycles



- Magnetic reconnection is a change of connections of magnetic field lines in highly conducting plasmas. A modification of the magnetic field topology results<sup>1</sup>.
- Magnetic reconnection is a common phenomenon in space and laboratory plasmas: it is found in solar flares<sup>2</sup>, jets from active galactic nuclei<sup>3</sup>, strongly magnetized neutron stars<sup>4</sup>, astrophysical dynamos<sup>5</sup>, large-scale magnetic self-organization of toroidal plasmas for magnetic fusion experiments<sup>6</sup>.



[http://soi.stanford.edu/results/SolPhys200/Schrijver/images/loops\\_6nov99b.gif](http://soi.stanford.edu/results/SolPhys200/Schrijver/images/loops_6nov99b.gif)

coronal loops over the eastern limb of the Sun was taken in the TRACE 171Å pass band, characteristic of plasma at 1 MK, on November 6, 1999, at 02:30 UT

## MINIMAL BIBLIOGRAPHY ABOUT MAGNETIC RECONNECTION

1 Yamada M, Kulsrud R, Ji H (2010) Magnetic reconnection. Rev Mod Phys 82:603–664.

2 Innes D, Inhester B, Axford W, Wilhelm K (1997) Bi-directional plasma jets produced by magnetic reconnection on the sun. Nature 368:811

3 Romanova MM, Lovelace RVE (1992) Magnetic field, reconnection and particle acceleration in extragalactic jets. Astron Astrophys 262:26–36

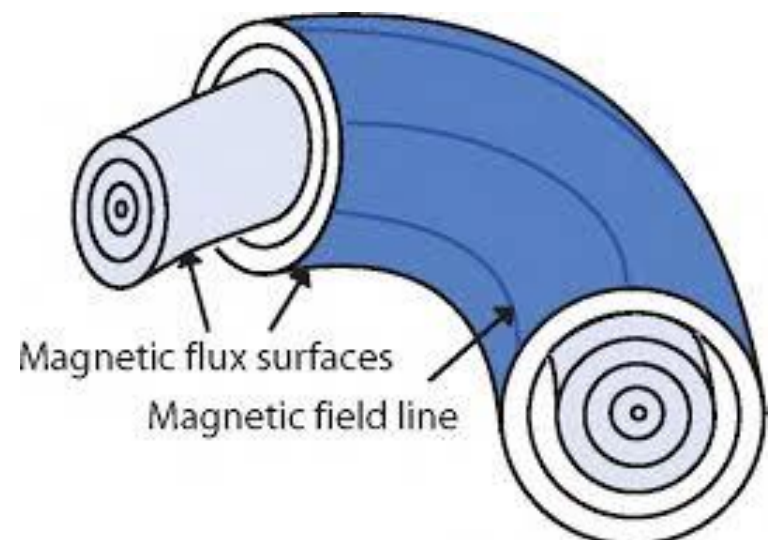
4 Hurley K, Boggs S, An exceptionally bright flare from sgr1806-20 and the origins of short-duration gamma-ray bursts. Nature 434:1098–1103.

5 Plasmas 23(3):032111. <https://doi.org/10.1063/1.4942940> Cowling T (1934) The magnetic field of sunspots. Mon Not R Astron Soc 94:39

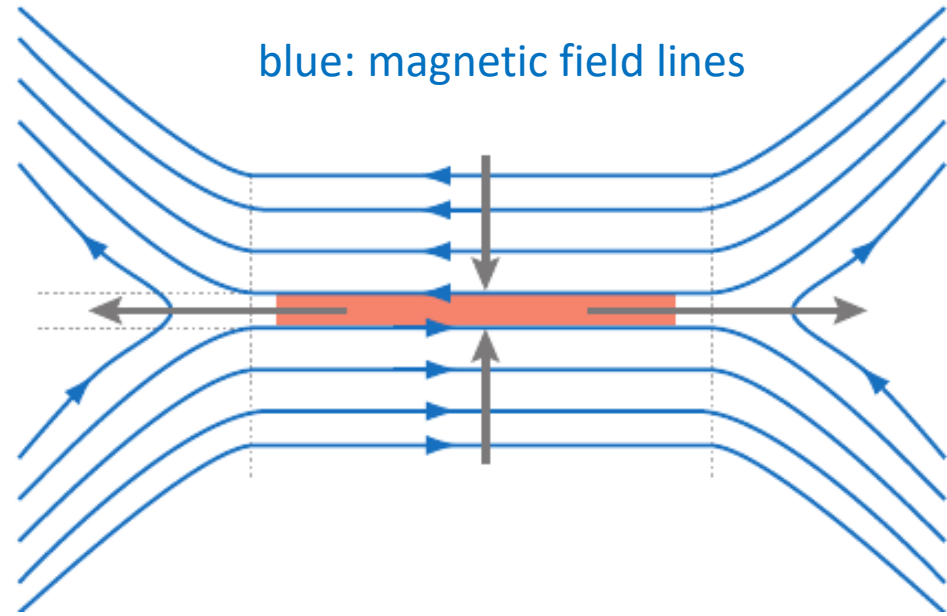
6 Taylor J (1974) Relaxation of toroidal plasma and generation of reversed magnetic fields. Phys Rev Lett 33(19):1139

# magnetic reconnection

- Magnetic reconnection is a change of connections of magnetic field lines in highly conducting plasmas. A modification of the magnetic field topology results<sup>1</sup>.
- Magnetic reconnection is a common phenomenon in space and laboratory plasmas: it is found in solar flares<sup>2</sup>, jets from active galactic nuclei<sup>3</sup> strongly magnetized neutron stars<sup>4</sup> astrophysical dynamos<sup>5</sup> large-scale magnetic self-organization of toroidal plasmas for magnetic fusion experiments<sup>6</sup>.
- A common signature of magnetic reconnection is the release of magnetic energy, converted into kinetic and thermal internal energy of the plasma, and observed as acceleration of particles to non-thermal velocities, and as generation of waves and turbulence. Another signature of reconnection is the presence of so-called current sheets.
- In toroidal experiments for magnetic confinement of fusion plasmas, reconnection is generally linked to the opening of “islands” in the field lines topology. For optimum confinement magnetic field lines should lie on nested magnetic flux surfaces (which means existence of a function  $\chi$  such that  $\mathbf{B} \cdot \nabla \chi = 0$ , with the shape of a topological torus).
- However, such magnetic fields can be unstable in the vicinity of the regions where field lines close on themselves, and a transverse component of the magnetic field opens the magnetic islands, bounded by a so-called separatrix containing a region with “X” topology.

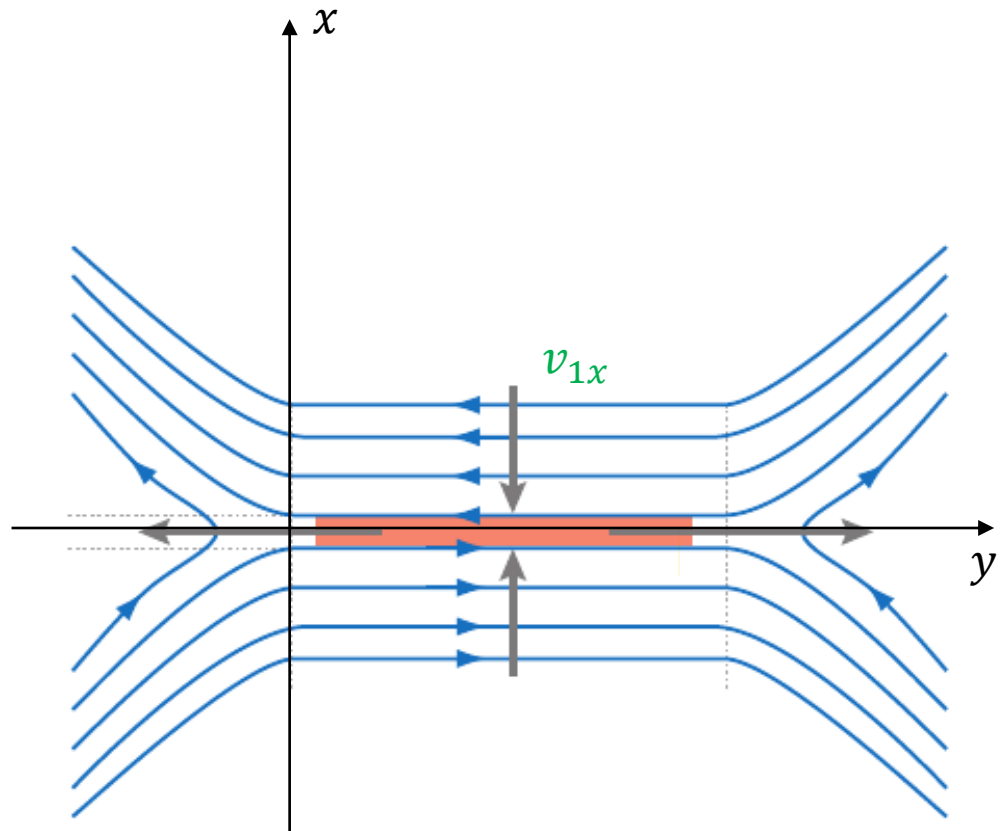


# the basic model of magnetic reconnection



basic picture: two magnetic field lines being carried by the fluid come closer together and by the action of resistivity they are cut and reconnected in a different topology

# simplest model to study reconnection: Sweet - Parker



$$\frac{\partial \mathbf{B}}{\partial t} = \nabla \times (\mathbf{v} \times \mathbf{B} - \eta \mathbf{J})$$

if  $\partial_t \mathbf{B} = 0$  then

$$\mathbf{J} = \frac{1}{\eta} \mathbf{v} \times \mathbf{B}$$

- current sheet at  $x \sim 0$  (because  $\mathbf{B}$  changes direction)
- unstable system, the sheet tends to be levelled by the plasma
- but not in ideal MHD!
- Imagine a force trying to compress the plasma towards  $x = 0$ . Imagine that the plasma moves across magnetic field lines without changing  $\mathbf{B}$  (thus violating ideal MHD) with velocity  $v_{1x}$ : this would create an induced electric field and, using Ohm's law, a current  $J_{1z} = \frac{1}{\eta} v_{1x} B_{0y}$ .
- This would lead to a restoring  $\mathbf{J} \times \mathbf{B}$  force
- $F_x = \frac{1}{\eta} v_{1x} B_{0y}^2$ : infinite if  $\eta \rightarrow 0$  (i.e. frozen-in flux theorem),
- but also  $F_x \sim 0$  at  $x = 0 \rightarrow$  ideal MHD breaks down there

# Sweet Parker: some basic use of continuity equation and Ohm's law

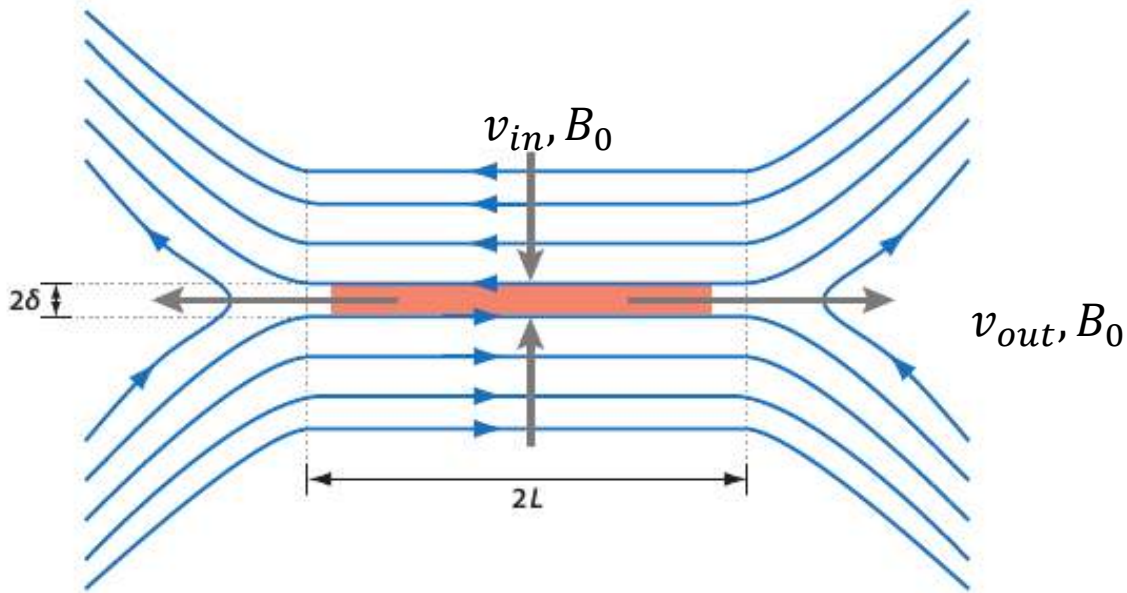


**Figure 1**

Sketch of magnetic field geometry in Sweet-Parker reconnection. Oppositely directed magnetic fields are brought together over a length  $2L$  and reconnect in a diffusion layer of width  $2\delta$ .

- continuity equation:  $v_{in}L = v_{out}\delta$ ;
- consider stationary conditions. Ohm's law:  $E + v_{in}B_0 = \eta J$ : perpendicular to the plane.
- in the **red current sheet** the resistive term dominates,  $E$  negligible:

$$v_{in}B_0 = \eta J = \eta \frac{B_0}{\delta}$$

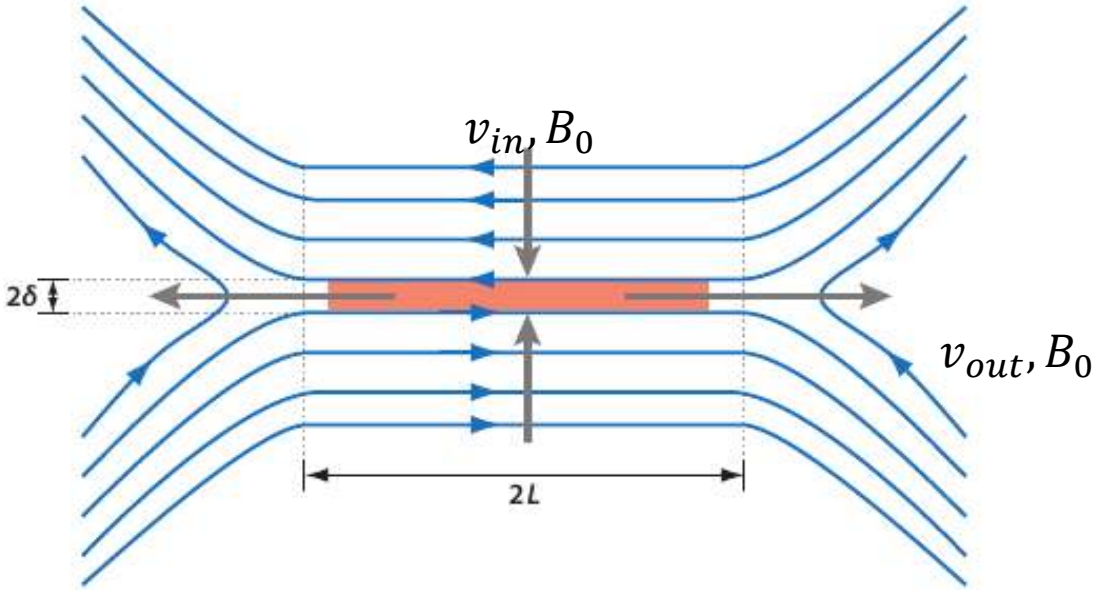


**Figure 1**

Sketch of magnetic field geometry in Sweet-Parker reconnection. Oppositely directed magnetic fields are brought together over a length  $2L$  and reconnect in a diffusion layer of width  $2\delta$ .

- continuity equation:  $v_{in}L = v_{out}\delta$ ;
- $v_{in}B_0 = \eta J = \eta \frac{B_0}{\delta}$
- stationary conditions

$$\frac{\delta}{L} = \frac{v_{in}}{v_{out}} = \frac{\eta}{\delta v_{out}}$$

$$\frac{\delta^2}{L^3} = \frac{\eta}{L^2 v_{out}}$$

$$\frac{\delta^2}{L^3} = \frac{1}{\tau_R v_{out}}$$

multiply by  $L^{-2}$

$$\tau_R \sim \frac{L^2}{\eta}$$

# Sweet Parker: force balance equation

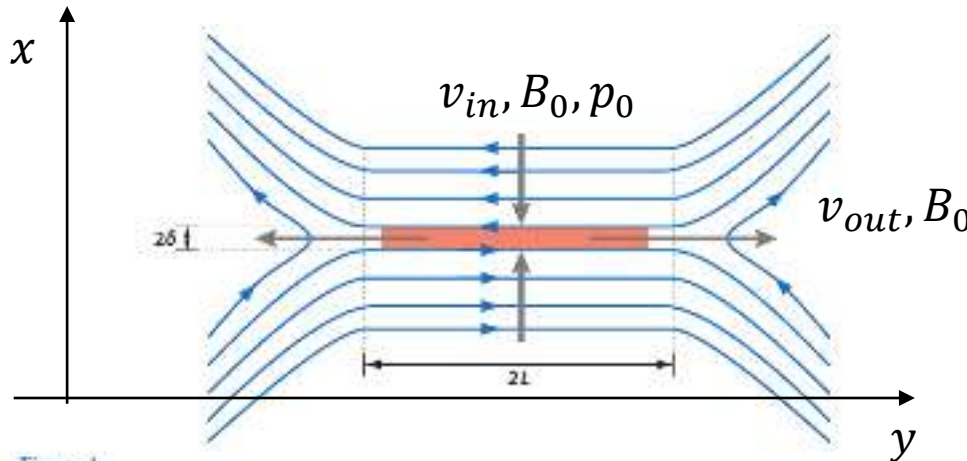


Figure 1

Sketch of magnetic field geometry in Sweet-Parker reconnection. Oppositely directed magnetic fields are brought together over a length  $2L$  and reconnect in a diffusion layer of width  $\delta$ .

$$\frac{\delta}{L} = \frac{v_{in}}{v_{out}} = \frac{\eta}{\delta v_{out}}$$

$$\frac{\delta^2}{L^3} = \frac{\eta}{L^2 v_{out}}$$

$$\frac{\delta^2}{L^3} = \frac{1}{\tau_R v_{out}}$$

force balance along vertical  $x$  direction:

$$\frac{d\mathbf{v}}{dt} = -\nabla p + \mathbf{J} \times \mathbf{B} \Big|_x$$

neglect inertial term

$$-\partial_x p + \nabla \times \mathbf{B} \times \mathbf{B} \Big|_x = 0$$

$$-\partial_x p + (-\nabla \mathbf{B} \mathbf{B} + (\mathbf{B} \cdot \nabla) \mathbf{B}) \Big|_x = 0$$

$$-\partial_x p + B \partial_x B = 0$$

$$\partial_x \left( \frac{B^2}{2} - p \right) = 0$$

integrate from the center,  
where  $B = 0$  and  $p = p_m$  to the outside where  
 $B = B_0$  and  $p = p_0$

$$\frac{B_0^2}{2} = p_m - p_0$$

# Sweet Parker: force balance equation

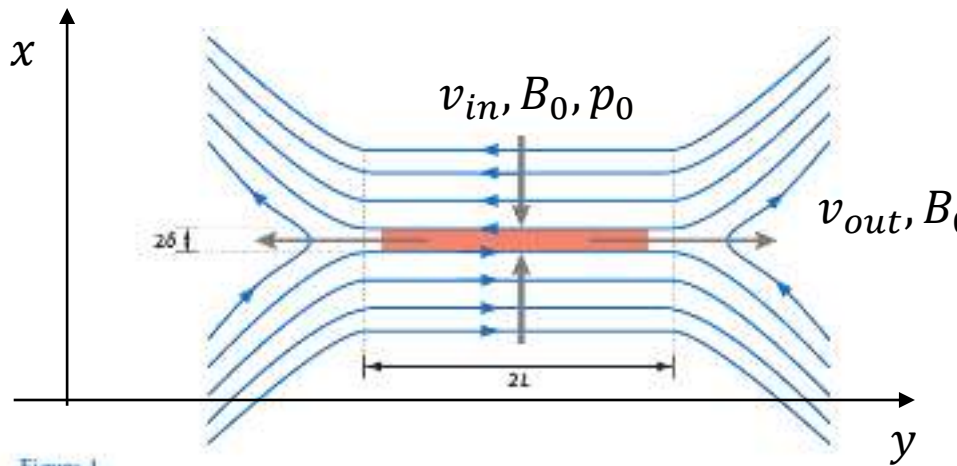


Figure 1

Sketch of magnetic field geometry in Sweet-Parker reconnection. Oppositely directed magnetic fields are brought together over a length  $2L$  and reconnect in a diffusion layer of width  $2\delta$ .

$$\frac{\delta}{L} = \frac{v_{in}}{v_{out}} = \frac{\eta}{\delta v_{out}}$$

$$\frac{\delta^2}{L^3} = \frac{\eta}{L^2 v_{out}}$$

$$\frac{\delta^2}{L^3} = \frac{1}{\tau_R v_{out}}$$

force balance along horizontal  $y$  direction, where  $\mathbf{B}$  vanishes

$$\frac{d\mathbf{v}}{dt} = -\nabla p + \mathbf{J} \times \mathbf{B} \Big|_y$$

$$\mathbf{v}_y \cdot \nabla v_y = -\partial_y p$$

$$\partial_x \left( \frac{v_y^2}{2} + p \right) = 0$$

integrate from the center, where  $v_y = 0$  and  $p = p_m$  to the outside where  $v_y = v_{out}$  and  $p = p_0$

$$\frac{v_{out}^2}{2} = p_m - p_0$$

together with eq. from previous slide

$$\frac{B_0^2}{2} = p_m - p_0$$

# Sweet Parker: a scaling for the reconnection rate

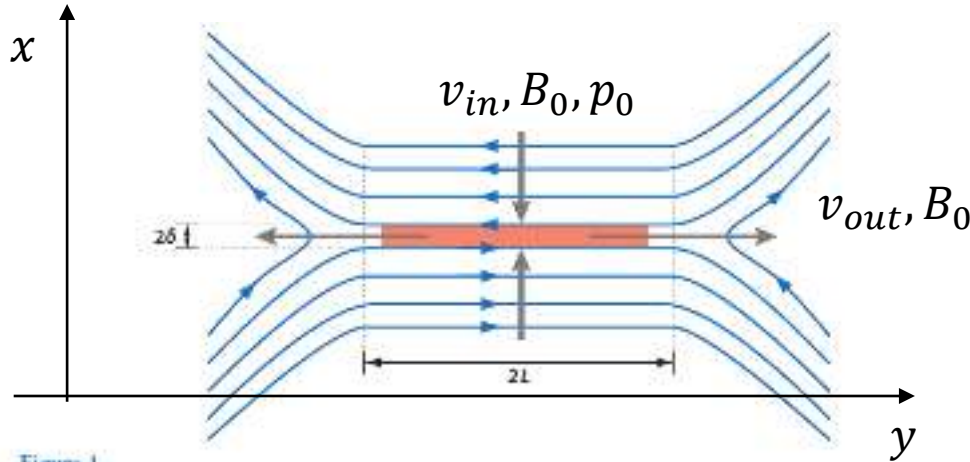


Figure 1

Sketch of magnetic field geometry in Sweet-Parker reconnection. Oppositely directed magnetic fields are brought together over a length  $2L$  and reconnect in a diffusion layer of width  $2\delta$ .

$$\frac{\delta}{L} = \frac{v_{in}}{v_{out}} = \frac{\eta}{\delta v_{out}}$$

$$\frac{\delta^2}{L^3} = \frac{\eta}{L^2 v_{out}}$$

$$\frac{\delta^2}{L^3} = \frac{1}{\tau_R v_{out}}$$

together with

$$\frac{v_{out}^2}{2} = p_m - p_0$$

implies

$$v_{out} = B_0 = v_A$$

the velocity outside can be assumed as the Alfvén velocity  $v_A$ , and so

$$\frac{\delta^2}{L^3} = \frac{1}{\tau_R v_{out}} = \frac{\tau_A}{\tau_R L}$$

and thus

$$\frac{v_{in}}{v_A} = \frac{\delta}{L} = S^{-\frac{1}{2}}$$

$$S = \frac{\tau_R}{\tau_A}$$

reconnection rate  $\tau^{-1}$  proportional to  $S^{-1/2}$

# optional: the issue of "fast reconnection"

- A long-standing problem in reconnection theory is briefly discussed here, i.e., the fast reconnection rates (proportional to the inverse Alfvén time) observed in astrophysical and laboratory systems like in the solar flares and in the tokamak sawtoothing instability.
- A resistive diffusion process would give too slow reconnection rates,  $\tau^{-1} \propto S^{-1}$
- magnetohydrodynamic (MHD) regime: Sweet and Parker<sup>1</sup> consider a two-dimensional current sheet and an incompressible inflow of plasma in the reconnection region gives a faster rate  $\tau^{-1} \propto S^{-0.5}$
- Later, the occurrence of instabilities of the current sheet itself<sup>2</sup>, discovering the possibility of reconnection rates independent of resistive effects  $\tau^{-1} \propto S^0$
- It was also shown that collisionless effects<sup>3</sup> could speed-up the reconnection rate to values compatible with observations
- Boozer<sup>4</sup> claims that the most overlooked feature in modeling fast magnetic reconnection is three-dimensionality.

<sup>1</sup> Parker EN (1957) Sweet's mechanism for merging magnetic fields in conducting fluids. *J Geophys Res (1896–1977)* 62(4):509–520.

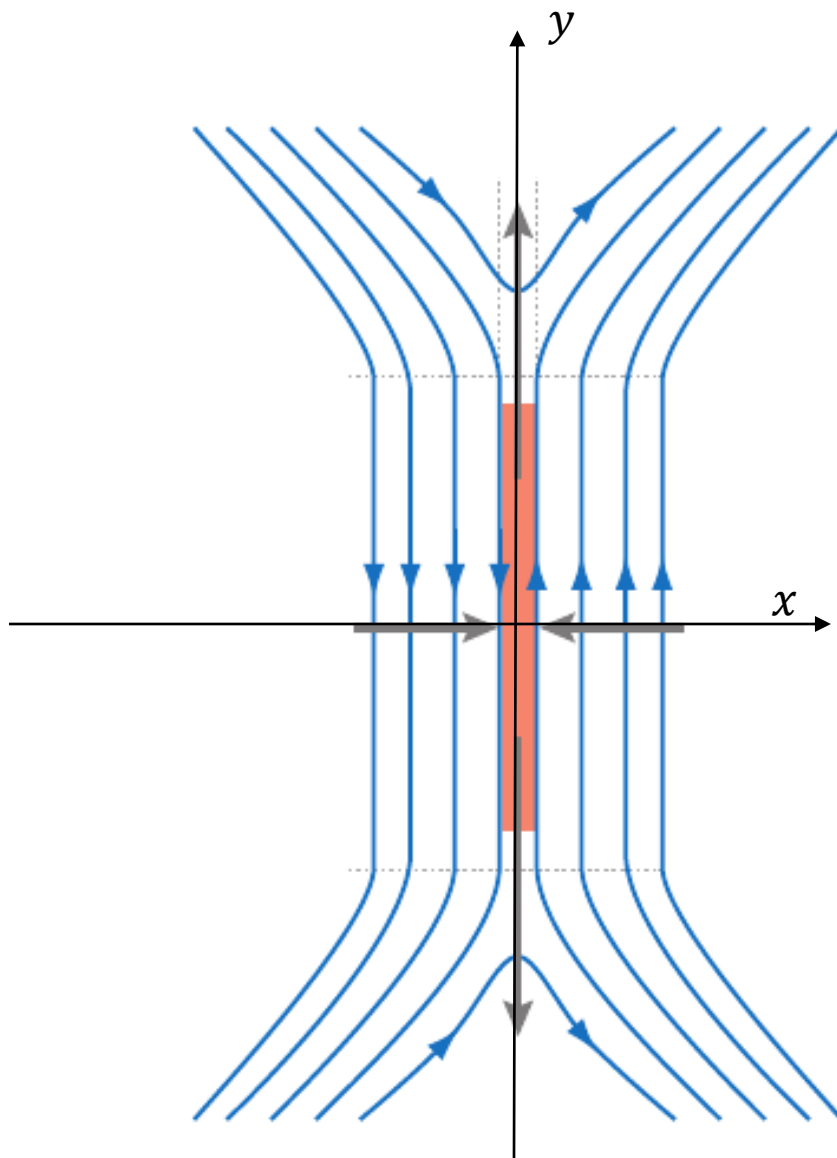
<sup>2</sup> Bhattacharjee A, Huang YM, Yang H, Rogers B (2009) Fast reconnection in high-Lundquist-number plasmas due to the plasmoid instability. *Phys Plasmas* 16(11):112102

<sup>3</sup> Biskamp D, Schwarz E, Drake JF (1995) Ion-controlled collisionless magnetic reconnection. *Phys Rev Lett* 75:3850–3853.

<sup>4</sup> Boozer AH (2018) Why fast magnetic reconnection is so prevalent. *J Plasma Phys* 84(1):715840102.

# magnetic islands: naive.

Modello semplificato



- aim of the instability: reconnect the magnetic field in the  $x \sim 0$  region;
- a small perturbation in the  $\hat{x}$  direction arises, active in the resistive layer.
- For simplicity we write it like this:

•  $B_x \sim B_{x0}(x) e^{yt} \sin(ky)$

Consideriamo una perturbazione del campo che cresce nella direzione x. Aumenta nel tempo.

- for small perturbations the magnetic field in the  $\hat{y}$  direction can be approximated by

Facciamo un'assunzione sulla componente y del campo

•  $B_y \sim B'_{y0} x$

$B_{x0}$  cambia muovendosi con x; l'esponenziale cresce lambda è il growth rate. La variazione lungo y è una sinusoida.

# magnetic islands: naive.

$$B_x \sim B_{x0} e^{\gamma t} \sin(ky)$$

$$B_y \sim B'_{y0} x$$

- compute magnetic field lines ( $\mathbf{B} \times d\mathbf{l} = 0$ ):

$$\frac{dx}{dl} = B_x , \quad \frac{dy}{dl} = B_y \quad ?$$

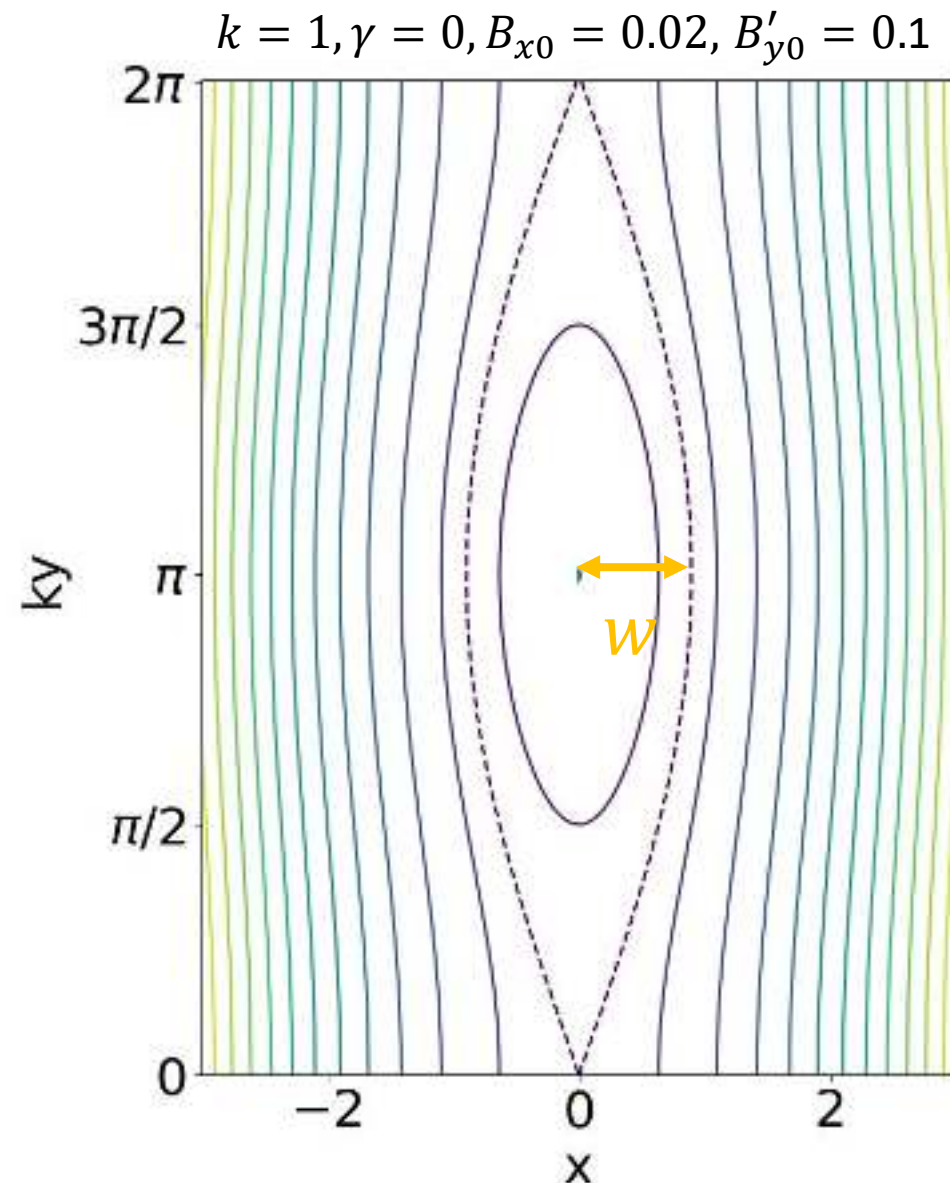
- and thus:

$$\frac{dx}{dy} = \frac{B_x}{B_y} = \frac{B_{x0}}{B'_{y0} x} e^{\gamma t} \sin(ky)$$

- integration gets you:

$$\rightarrow B'_{y0} \frac{x^2}{2} + B_{x0} e^{\gamma t} \frac{\cos(ky)}{k} = cost$$

# magnetic islands: half width $w$



$$B_x \sim B_{x0} e^{\gamma t} \sin(ky)$$

$$B_y \sim B'_{y0} x$$

$$B'_{y0} \frac{x^2}{2} + B_{x0} e^{\gamma t} \frac{\cos(ky)}{k} = c_0$$

- dashed separatrix @ $x = 0, y = 0$ :

$$c_0 = B_{x0} \frac{e^{\gamma t}}{k}$$

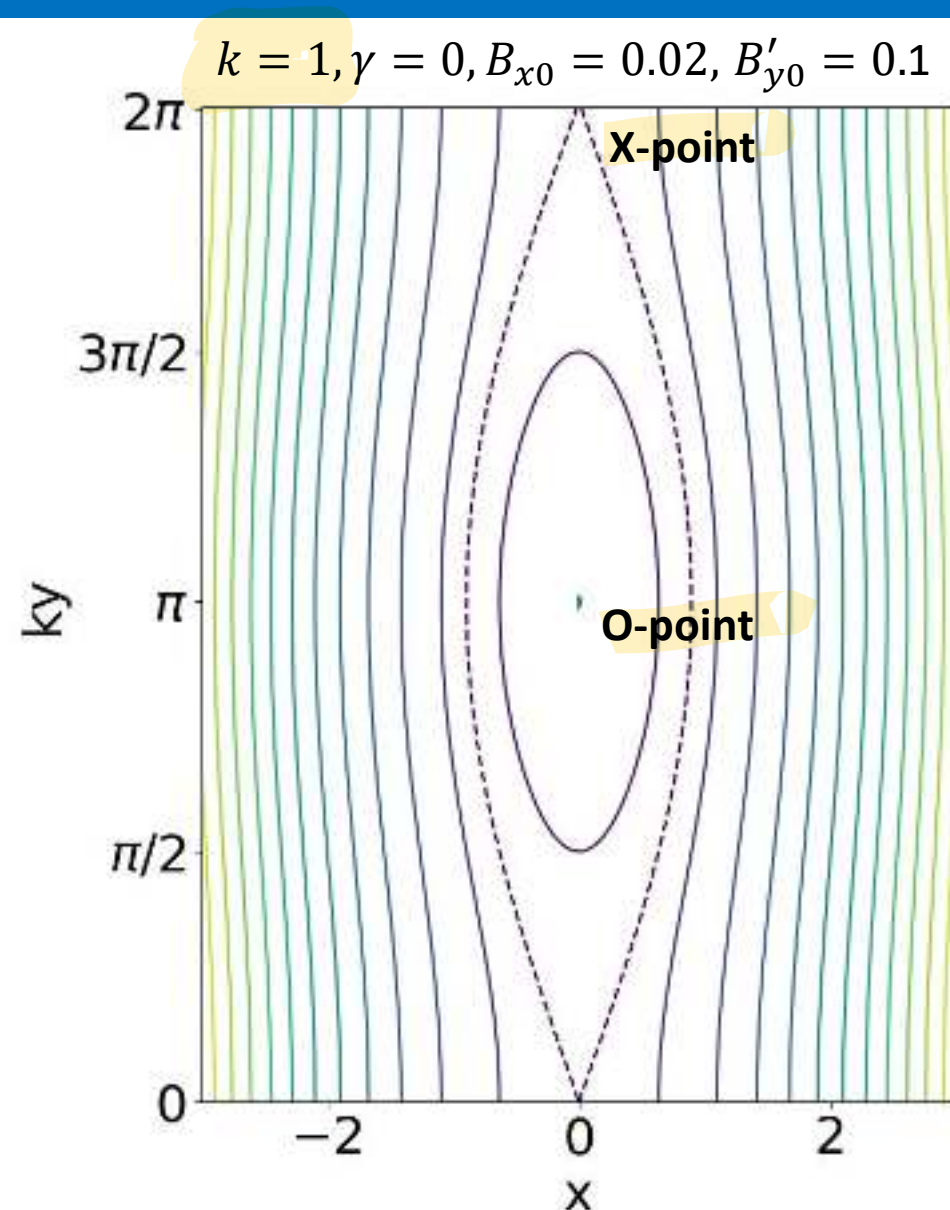
- follow the contour level until  $ky = \pi$ :

$$x^2 = \frac{2c_0}{B'_{y0}} \rightarrow x = \sqrt{\frac{2B_{x0} e^{\gamma t}}{B'_{y0} k}}$$

i.e. WIDTH  
 $w \propto \sqrt{B_{x0}}$

?

# magnetic islands: half width $w$



$$B_x \sim B_{x0} e^{\gamma t} \sin(ky)$$

$$B_y \sim B'_{y0} x$$

$$B'_{y0} \frac{x^2}{2} + B_{x0} e^{\gamma t} \frac{\cos(ky)}{k} = c_0$$

- dashed separatrix @ $x = 0, y = 0$ :

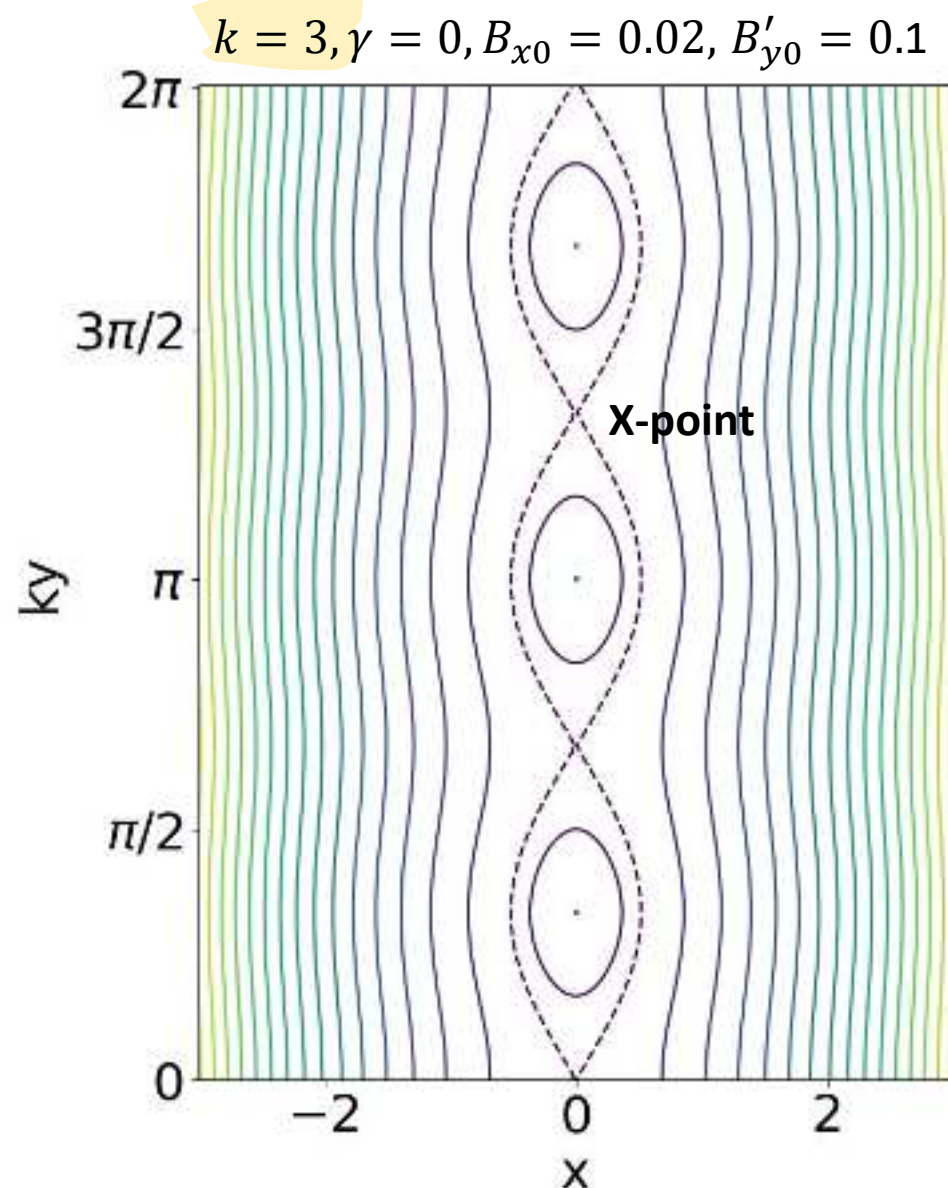
$$c_0 = B_{x0} \frac{e^{\gamma t}}{k}$$

- follow the contour level until  $ky = \pi$ :

$$x^2 = \frac{2c_0}{B'_{y0}} \rightarrow x = \sqrt{\frac{2B_{x0} e^{\gamma t}}{B'_{y0} k}}$$

i.e.  $w \propto \sqrt{B_{x0}}$

# magnetic islands



$$B_x \sim B_{x0} e^{\gamma t} \sin(ky)$$

$$B_y \sim B'_{y0} x$$

$$B'_{y0} \frac{x^2}{2} + B_{x0} e^{\gamma t} \frac{\cos(ky)}{k} = c_0$$

- dashed separatrix @ $x = 0, y = 0$ :

$$c_0 = B_{x0} \frac{e^{\gamma t}}{k}$$

- follow the contour level until  $ky = \pi$ :

$$x^2 = \frac{2c_0}{B'_{y0}} \rightarrow x = \sqrt{\frac{2B_{x0} e^{\gamma t}}{B'_{y0} k}}$$

i.e.  $w \propto \sqrt{B_{x0}}$

# magnetic islands: where magnetic reconnection can happen in a tokamak

- If we Fourier decompose every perturbation in a "cylindrical tokamak" (always in the spirit of keeping things simple) we can categorize them using two wave numbers for the two periodic coordinates  $\theta$  and  $z$ , i.e.  $\mathbf{k} = (m, n)$ , i.e. a generic perturbation is of the form  $B_{pert} \sim e^{\gamma t} e^{m\theta + \frac{nz}{R}}$  with  $R$  representing the axial height of the cylinder and the aspect ratio of the rectified torus.
- the condition for instability is the so-called resonance condition  $\mathbf{k} \cdot \mathbf{B} = 0$
- In pinches this happens locally when the safety factor has a rational value, i.e. magnetic field lines close on themselves after a certain number of turns in toroidal and poloidal direction. Because of the shear of the magnetic field, if we follow the field lines on both sides of the resonant surface with  $q = q_r = 2$  (we choose a particular case) they will either lag behind or advance the field line on the resonant surface, creating a component of the magnetic field relative to the  $q = q_r$  surface which changes sign across it. A transversal magnetic field, manifesting itself as a current-driven "tearing" instability results in the opening of a magnetic island, as observed looking at the helical flux function contour levels.
- Clearly, infinitely many rational numbers can be 'fitted in' between  $q(0)$  and  $q(a)$ . However, another rule, found by more refined analysis, is that only large wavelengths tend to be unstable to resistive-tearing modes.

# nonlinear evolution / saturation

- In practice, nonlinear effects will limit the growth of magnetic islands when significant modifications are produced in the underlying magnetic configuration on which our stability analysis was based.
- Such effects begin to appear as soon as the island width becomes comparable to the width of the resistive layer, as was shown in a paper (P.H. Rutherford 1973 Phys. Fluids **16** 1903).
- When the island grows to a significant fraction of the size of the overall configuration, it can affect the gross current profile tending to stabilize the tearing mode.

# nonlinear evolution: Rutherford equation

- a basic equation: Faraday in radial direction
- integrate along the island width  $w$  (and consider  $B_r$  approximately constant in the island)
- remind that  $w^2 \propto B_r$
- define the "linear stability index"  $\Delta' = \frac{1}{B_r} \partial_r B_r|_{r_s-w/2}^{r_s+w/2}$

(this index depends only on the ideal MHD of the system)

Instability occurs when  $\Delta'$  exceeds a critical value,  
 $\Delta' > \Delta_c \geq 0$

$$\partial_t B_r = \frac{\eta}{\mu_0} \frac{\partial^2 B_r}{\partial r^2}$$

$$w \partial_t B_r = \frac{\eta}{\mu_0} \partial_r B_r|_{r_s-w/2}^{r_s+w/2}$$

$$w \partial_t w^2 = \sim \frac{\eta}{\mu_0} \partial_r B_r|_{r_s-w/2}^{r_s+w/2}$$

$$\partial_t w = \frac{\eta}{2\mu_0} \frac{1}{B_r} \partial_r B_r|_{r_s-w/2}^{r_s+w/2}$$

$$\partial_t w \sim \frac{\eta}{\mu_0} \Delta'(w)$$

# nonlinear evolution: Rutherford equation

- but, for sufficient island width the previous linear estimates of  $\Delta'$  are no more correct, in fact tearing modes can affect the underlying equilibrium parameters in two ways:
  - i) flattening of the current density gradient
  - ii) flattening of temperature profiles.
- thus, the minimal estimate is (without proof) that

$$\Delta'(w) = \Delta'(0) \left( 1 - \frac{w}{w_{sat}} \right)$$

$$\partial_t w \sim \frac{\eta}{\mu_0} \Delta'(w)$$

- giving a solution of Rutherford equation

$$w(t) = w_{sat} \left( 1 - e^{-t \frac{r^2 \Delta'(0)}{\tau_R w_{sat}}} \right)$$

# nonlinear evolution: Rutherford equation

- further effects: plasma finite pressure, toroidicity (and thus non-inductive currents like:
  - bootstrap current due to the pressure gradient of trapped particles;
  - Pfirsch-Schlüter current that guarantees  $\nabla \cdot \mathbf{J} = 0$  even on the torus

$$\frac{\tau_R}{r_{\text{res}}} \frac{dW}{dt} = r_{\text{res}} \Delta'(W) + c_{\text{sat}} \frac{r_{\text{res}}^{3/2}}{R_0^{1/2}} \frac{L_q}{L_p} f_{\text{GGJ}} \beta_p \frac{1}{W} \quad *$$

- increases the possibility for tearing modes instability (neoclassical tearing modes) with increased plasma pressure

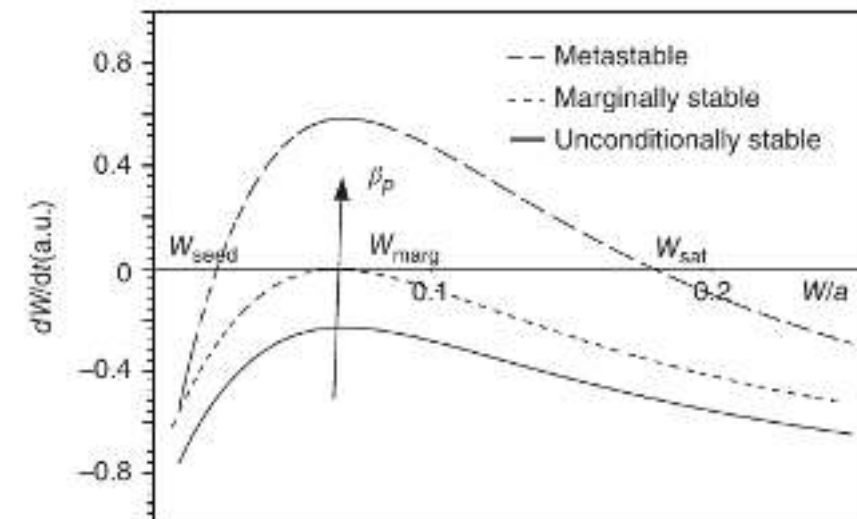


Figure 12.2 Schematic stability diagram for NTMs, indicating the existence of unconditional stability (no stationary point), marginal stability (one stationary point), and

metastability (two stationary points of which only  $W_{\text{sat}}$  is stable). For simplicity, only  $W_0$  has been included as small island term for this plot.

\*remind the definition of "decay length", for example  $L_p = -\frac{n}{\frac{dp}{dr}} = \frac{-1}{d\ln(p(r))}$

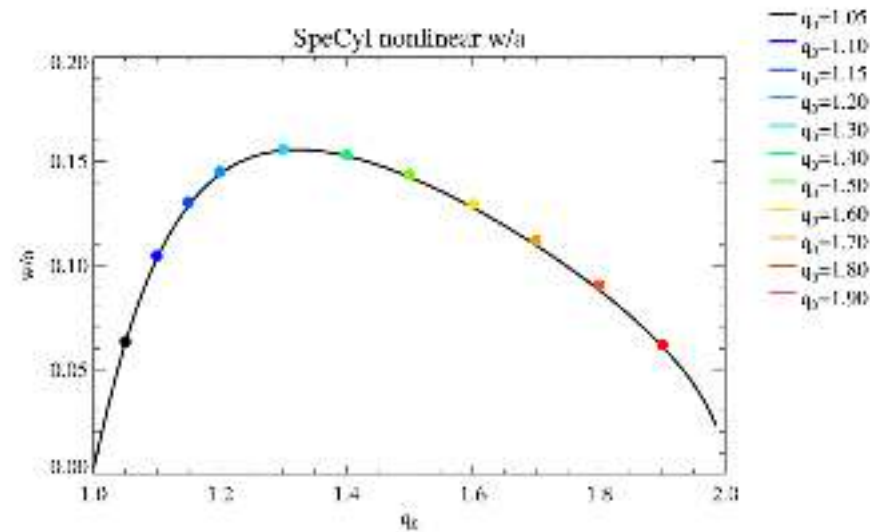
# nonlinear evolution: more advanced models

The saturation of the tearing mode is a difficult issue, and its solution has been a stepwise process covering almost three decades, starting from 1977 [a],

Many effects involved: plasma finite pressure, toroidicity (and thus non-inductive currents like Pfirsch-Pfirsch-Schlüter current that guarantees  $\nabla \cdot \mathbf{J} = 0$  even on the torus and others) .

A rigorous solution to the simple tearing mode problem in cylindrical geometry is given in [b]:

$$\frac{\mu_0}{\eta_{eq}(r_s)} \frac{dw}{dt} = 1.22V' + w \left\{ \frac{A^2}{2} \ln \frac{w}{w_0} - 2.21A^2 + 0.4 \frac{A}{r_s} + \frac{B}{2} + 0.17\lambda \frac{A^2 s}{2-s} \right\} + o(w)$$



comparison between the saturation width given by analytical formula (60) and 3D nonlinear MHD computations, varying on axis safety factor  $q(0)$ .

[a] R. B. White, D. A. Monticello, and M. N. Rosenbluth, Phys. Fluids 20, 800 (1977).

[b] Arcis, Escande, Ottaviani, Rigorous approach to the nonlinear saturation of the tearing mode in cylindrical and slab geometry, Physics of Plasma 13, 052305 (2006)

# magnetic islands: numerical solution

- numerically solved with main approximations:
  - zero-pressure;
  - constant and stationary density;
- for this purpose we use the SpeCyl MHD-code, (IPP, Consorzio RFX [a])
- using  $\eta = 10^{-6}$ ,  $\nu = 10^{-3}$

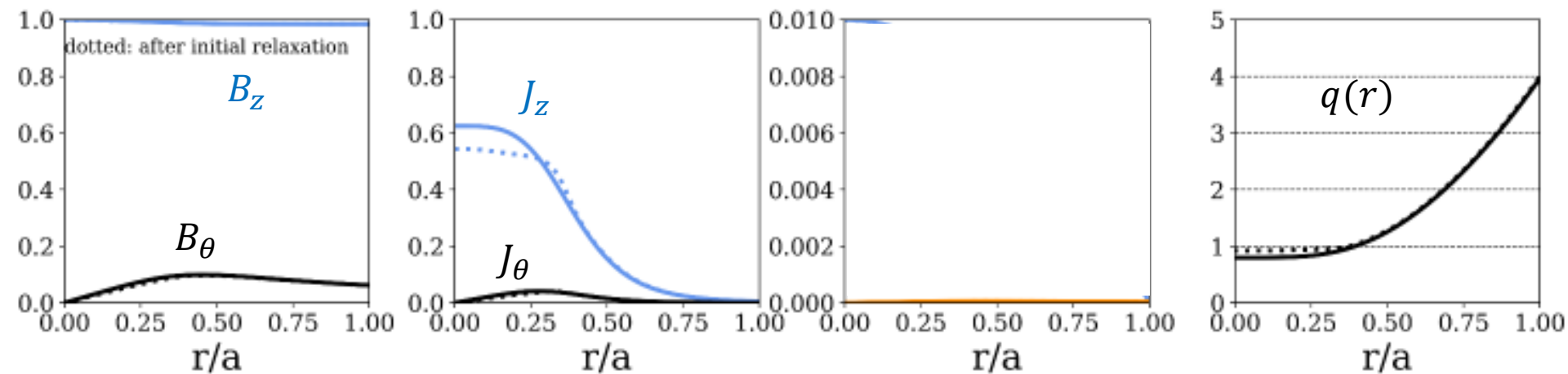
$$\frac{\partial \boldsymbol{v}}{\partial t} + \boldsymbol{v} \cdot \nabla \boldsymbol{v} = \boldsymbol{J} \times \boldsymbol{B} + \nu \nabla^2 \boldsymbol{v}$$

$$\boldsymbol{E} + \boldsymbol{v} \times \boldsymbol{B} = \eta \boldsymbol{J}$$

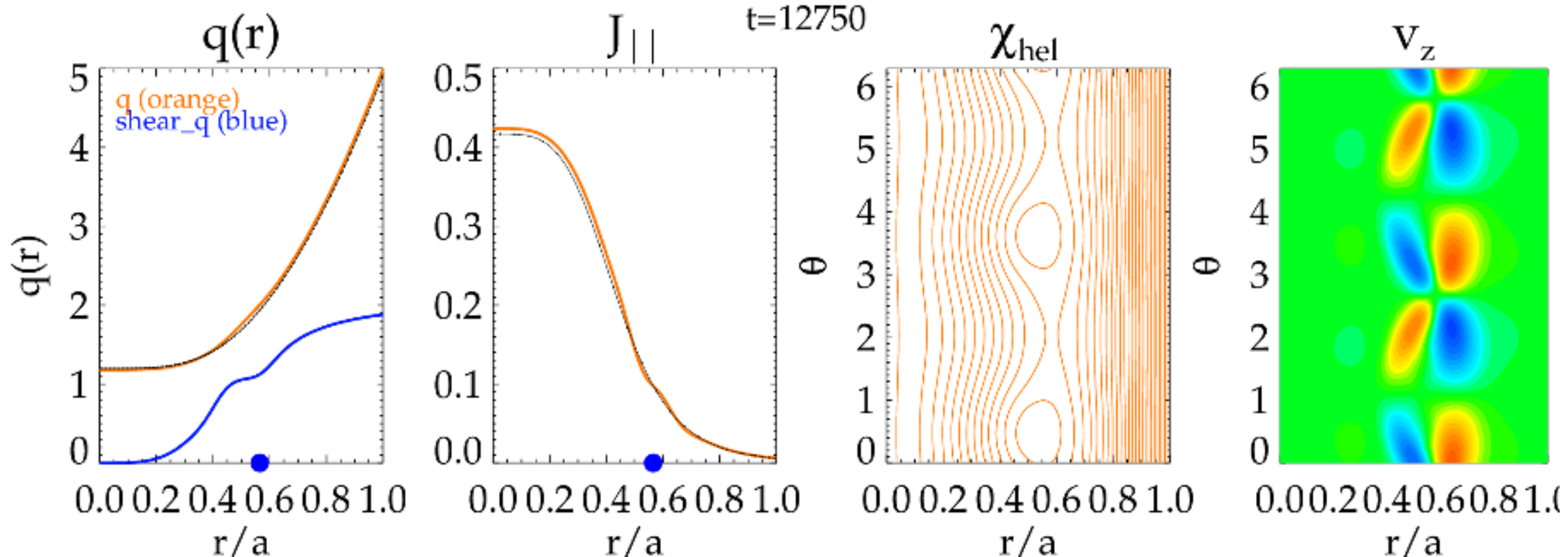
$$\nabla \times \boldsymbol{E} = -\frac{\partial \boldsymbol{B}}{\partial t}$$

$$\nabla \times \boldsymbol{B} = \boldsymbol{J}$$

$$\nabla \cdot \boldsymbol{B} = 0$$



# video: nonlinear evolution of a tearing mode with m=2 n=-1



remind: safety factor in cylindrical geometry  $q(r) = \frac{rB_z(r)}{RB_\theta(r)}$

$$\text{magnetic shear } s = \frac{rd(\ln q)}{dr}$$

# nonlinear evolution: effect on kinetic profiles

- Electron heat transport in constant-density, zero flow magnetized plasmas is:

$$\partial_t T + \nabla \cdot \mathbf{q} = S = \eta J^2 \quad (1)$$

- the heat flux  $\mathbf{q}$  is given by:  $\mathbf{q}[T] = -\chi_{\perp}(T)\nabla_{\perp}T + \mathbf{q}_{\parallel}[T]$

$$\partial_t T - \frac{\chi_{\parallel}}{\chi_{\perp}} \partial_s^2 T = \nabla_{\perp}^2 T + S$$

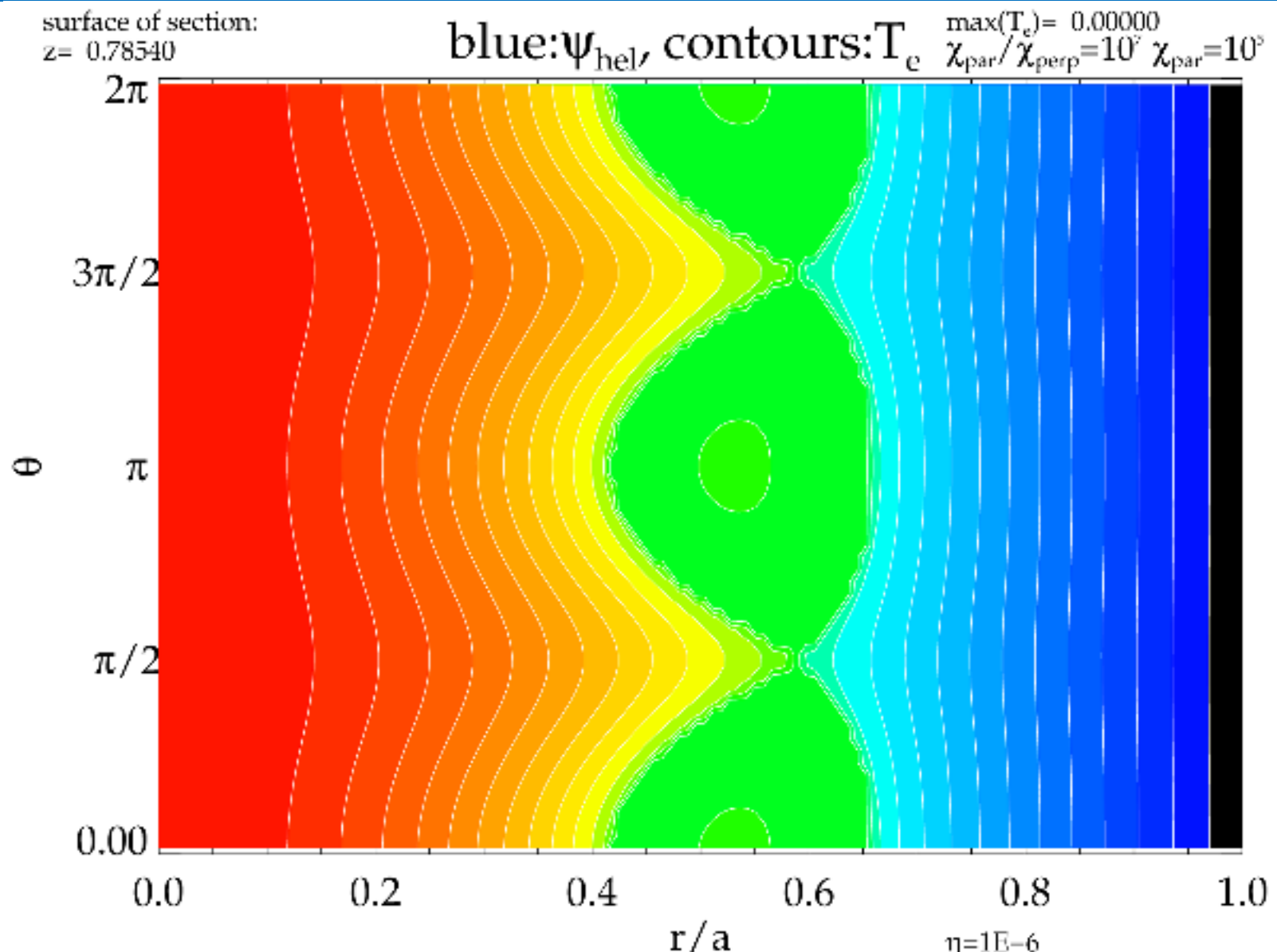
$$\epsilon = \frac{\chi_{\perp}}{\chi_{\parallel}} \approx 10^{-8:-10}$$

high anisotropy ratio in hot magnetized plasmas.  
 We consider uniform and constant diffusion coefficient

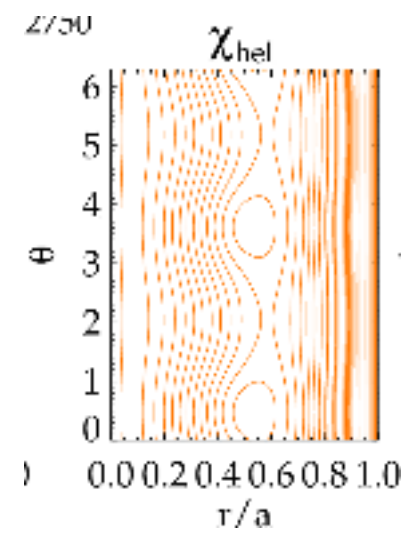
- Lagrangian approach, follow magnetic field lines wandering
- We solve equation (1) with the T3D code [a]

[a] L. Chacón, D. del-Castillo-Negrete, C.D. Hauck **JCP** 272 (2014)

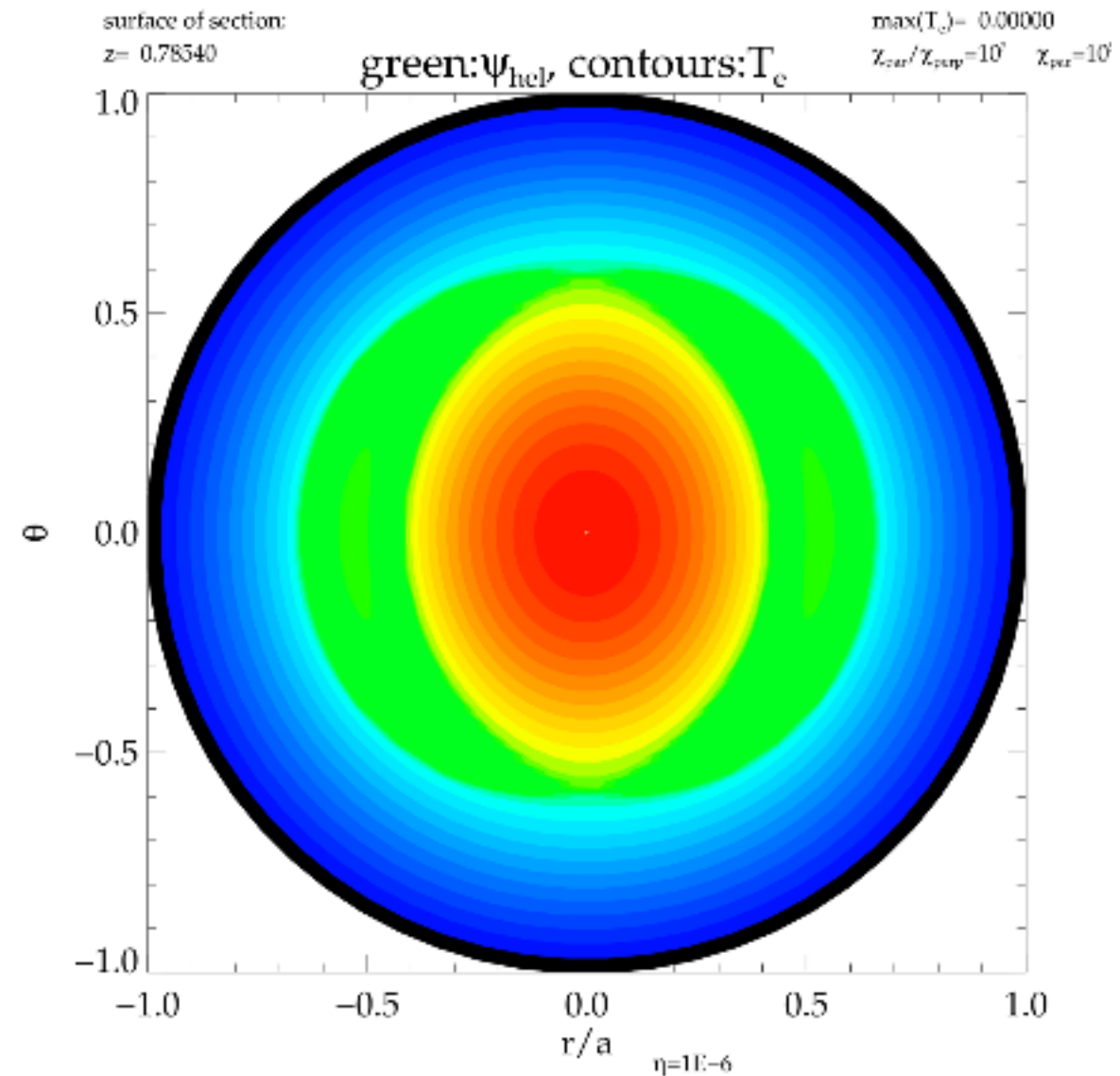
# nonlinear evolution: effect on kinetic profiles



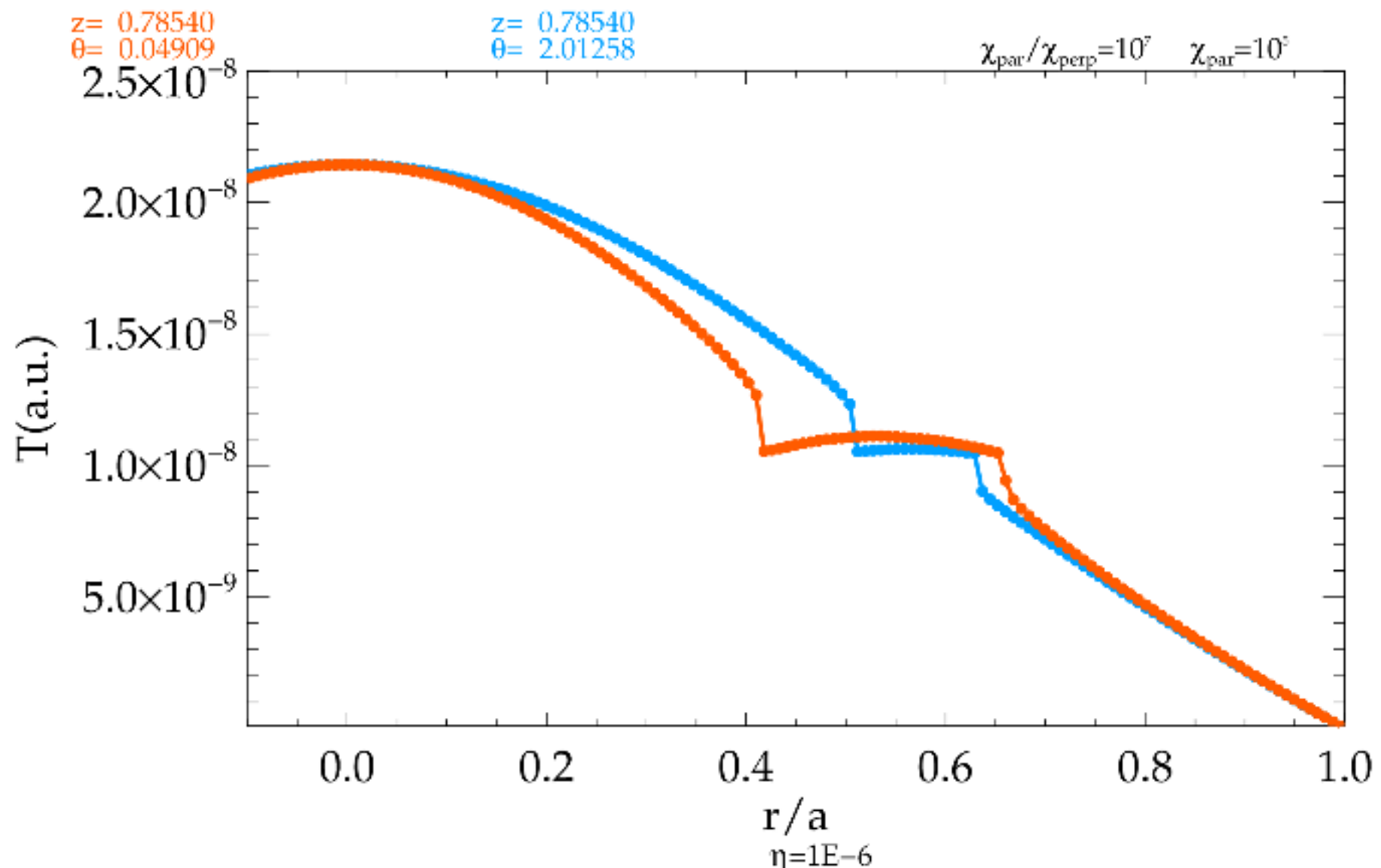
short circuit of magnetic field lines averages out temperature



# nonlinear evolution: effect on kinetic profiles



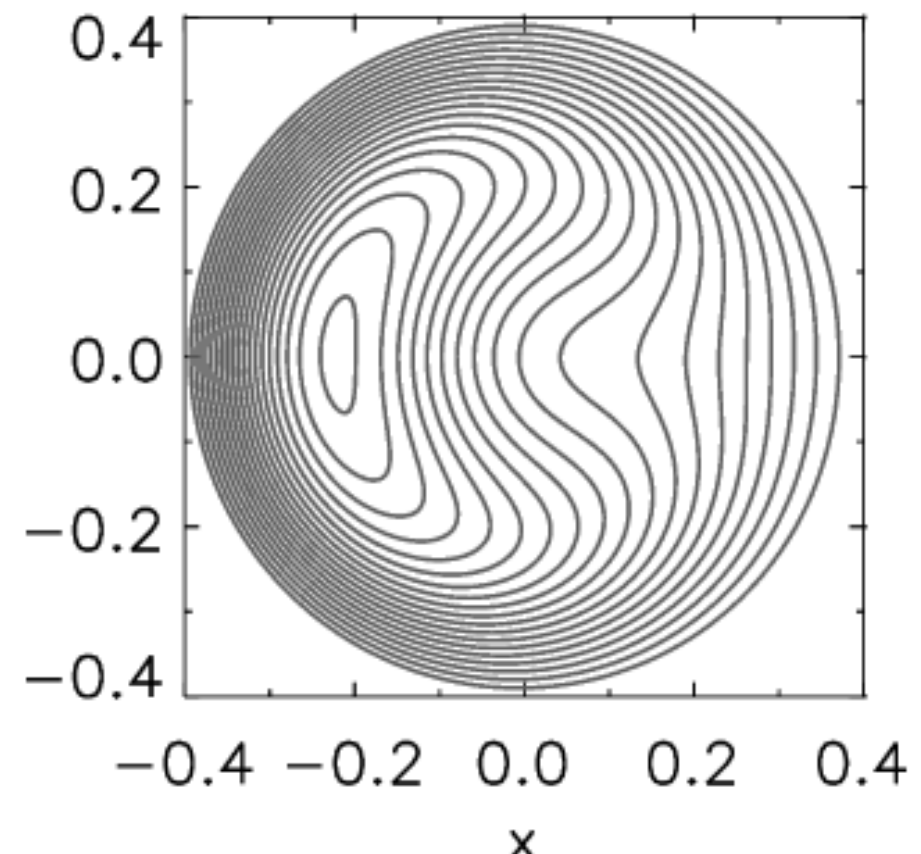
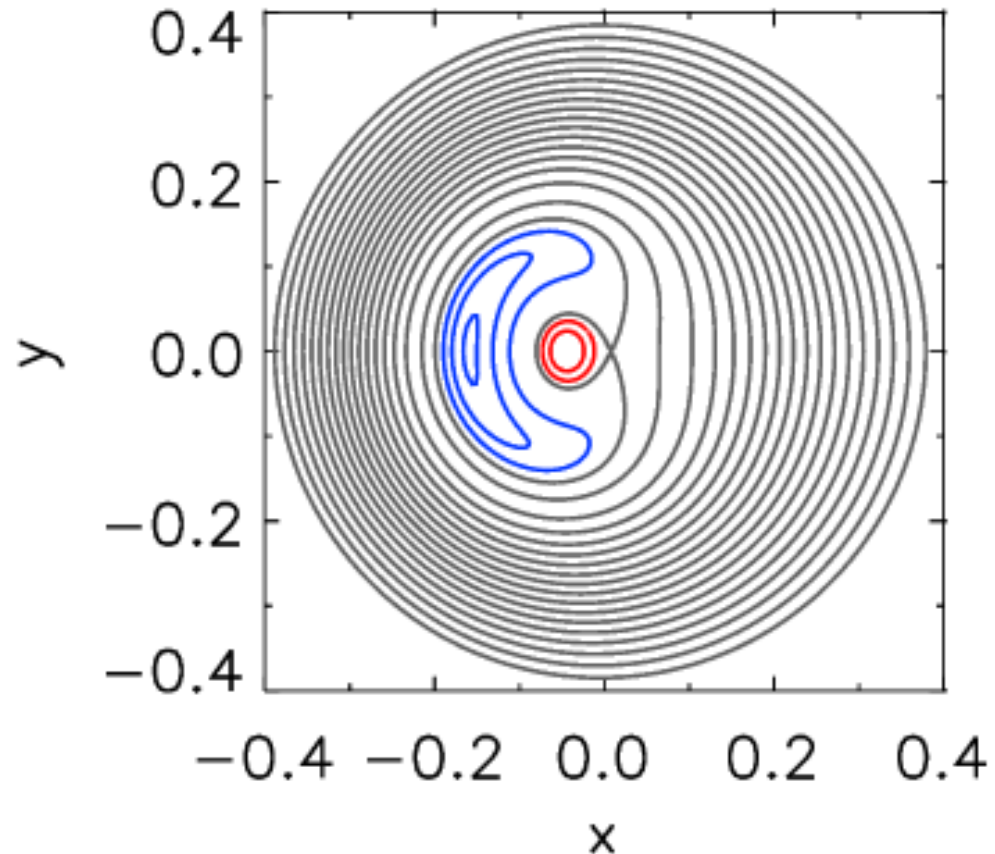
# nonlinear evolution: effect on kinetic profiles



# when plasma current is 10x higher than in tokamaks: reversed-field pinches

the magnetic island becomes so unstable that in the end it completely change the topology of the magnetic field and the original red axisymmetric red axis is destroyed and the new axis of the magnetic field is given by the O-point of the island (blue).

More on Thursday afternoon, RFP theory, S. Cappello.



pause

The sawtooth instability

i.e. effect of the «special» 1,1 mode

Subtle: non-ideal effects; nonlinear cycles;

Fishbone instability: 1,1+energetic particles

## Remind: linear theory of internal kink modes

- One of the basic tokamak instabilities: found by analytically solving the energy equation imposing  $\xi_a = 0$  and using a step-function for  $\xi(r)$ . Expansion of energy equation to fourth order → subtle (finite resistivity, two fluids effect, finite Larmor radius can change stability)

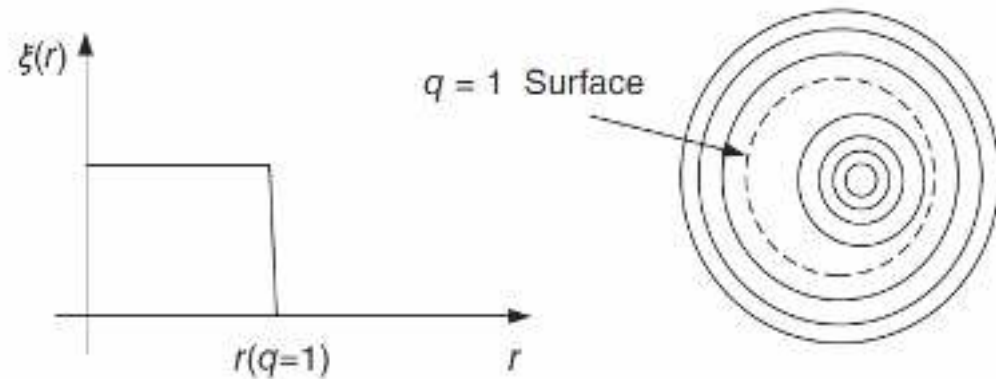


Figure 4.5 Test function used to minimize  $\delta W$  for internal kink analysis.

Necessary condition not to have an internal kink mode:  $q(0) > 1$

$$q(r) = \frac{rB_z}{RB_\theta}$$

$$\int dr B_\theta = \mu_0 I_P \rightarrow \frac{2B_\theta}{r} = \mu_0 J(r)$$

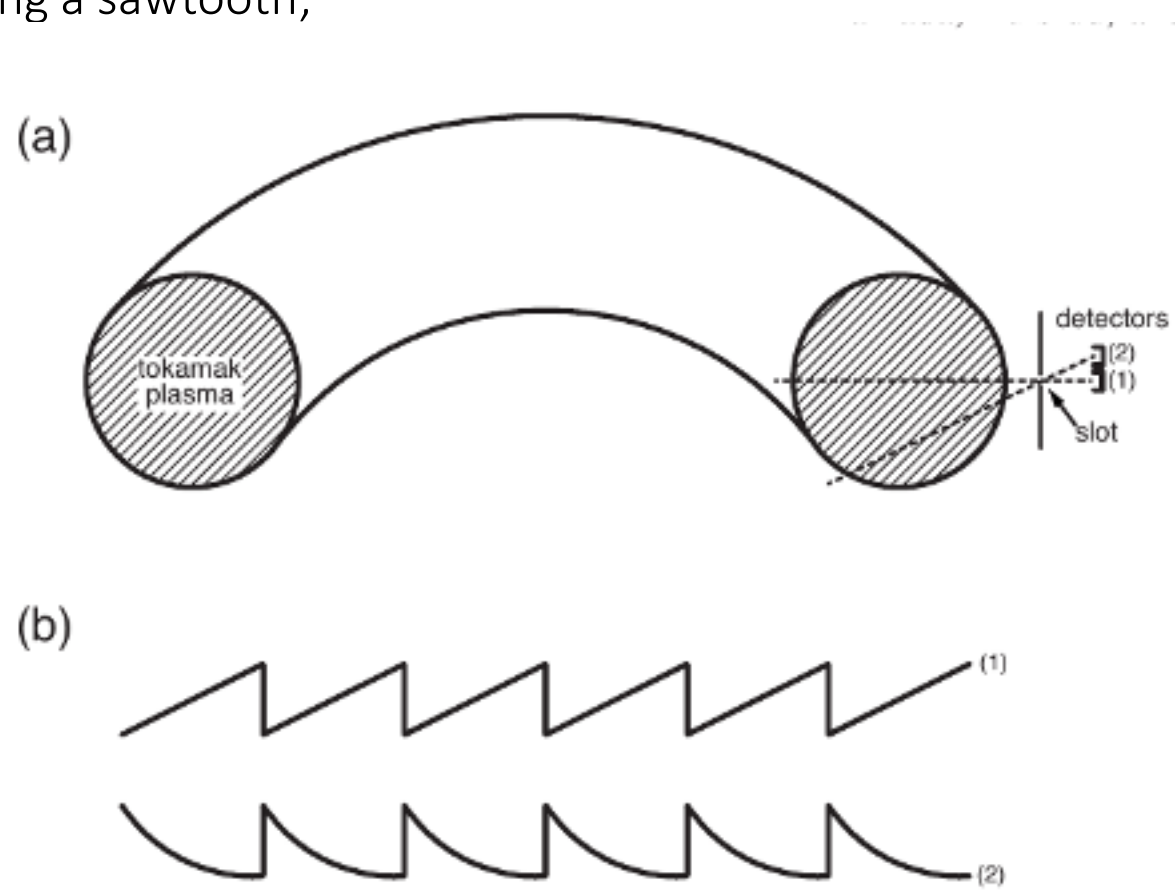
$$\rightarrow \text{around } r \sim 0 : q(0) = \frac{2B_z(0)}{R\mu_0 J(0)}$$

$$q(0) > 1 \rightarrow J(0) < \frac{2B_z}{\mu_0 R}$$

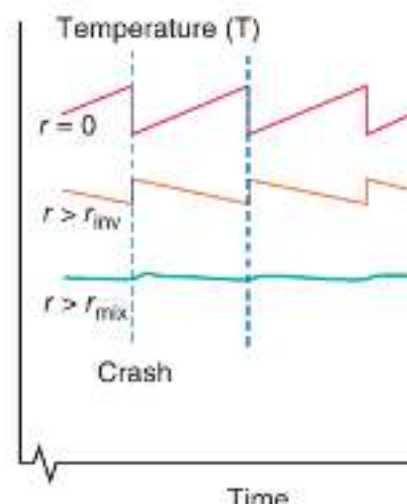
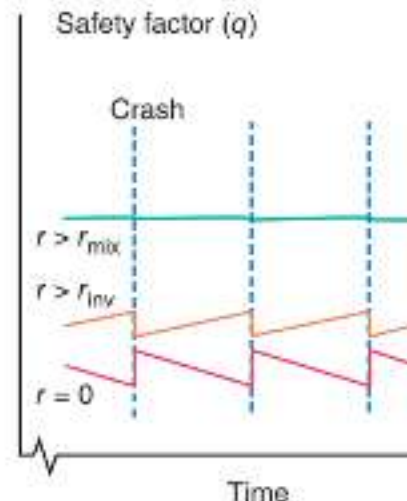
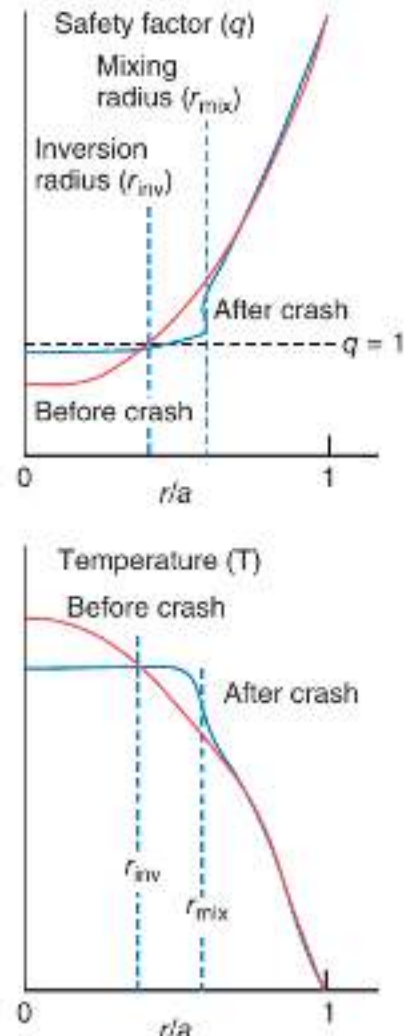
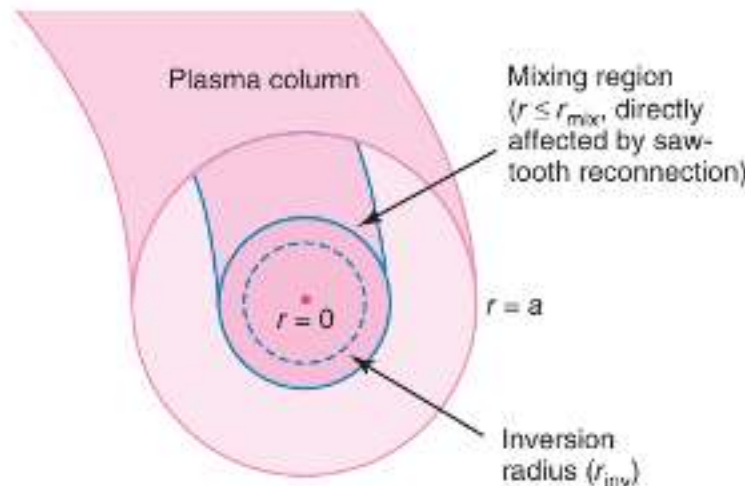
Limit on maximum  $I_P$ , i.e. limit on confinement time.

# internal kink modes: nonlinearity

- The sawtooth instability is observed in most conventional tokamak scenarios at reasonably high current, that is when a  $q = 1$  surface is present in the plasma;
- a periodic modulation of the central temperature and density is seen, with a time trace resembling a sawtooth;



# internal kink modes: nonlinearity

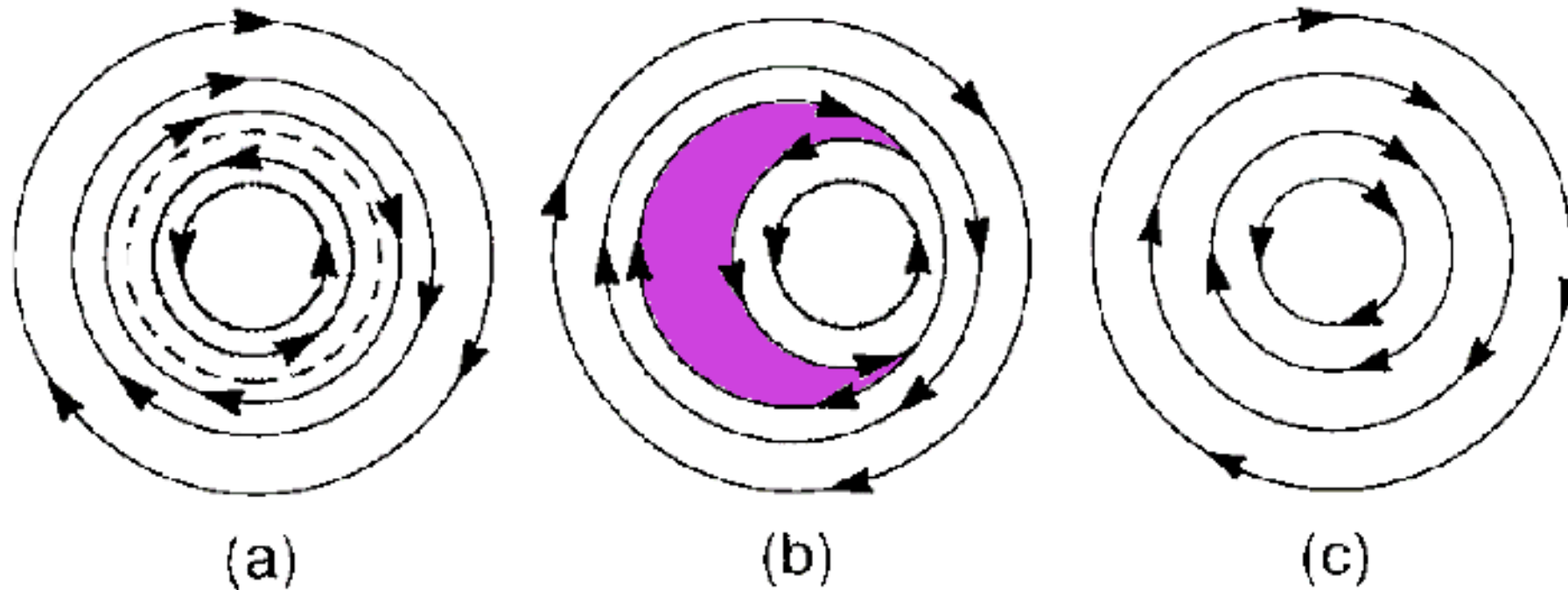


from Zohm,  
 Magnetohydrodynamic  
 Stability of Tokamaks  
 Wiley (2015)

# some physics

- Good energy confinement in the core  $\rightarrow T_e$  increases;
- Resistivity decreases ( $\eta \propto T_e^{-3/2}$ )
- Ohmic heat deposition increases ( $P_\Omega \propto \eta J^2 \sim \frac{E_0^2}{\eta}$ ), with  $E_0$  toroidal electric field and  $E_0 \sim \eta J$
- Electron temperature further increase and thus also plasma current
- this implies that  $J$  is further peaked
- A peaked current profile means that  $q_0$  decreases (below 1), the **1,1 mode becomes unstable**, it mixes the plasma inside the resonance radius redistributing its energy outside.
- redistribution of heat, particles, and poloidal flux
- instability plays an important role in determining the quasi-stationary (i.e. sawtooth-cycle averaged) parameters of tokamak discharges. In particular, it limits the peaking of temperature, density, and current density profiles.

# Resistive internal kink: reconnection and island formation



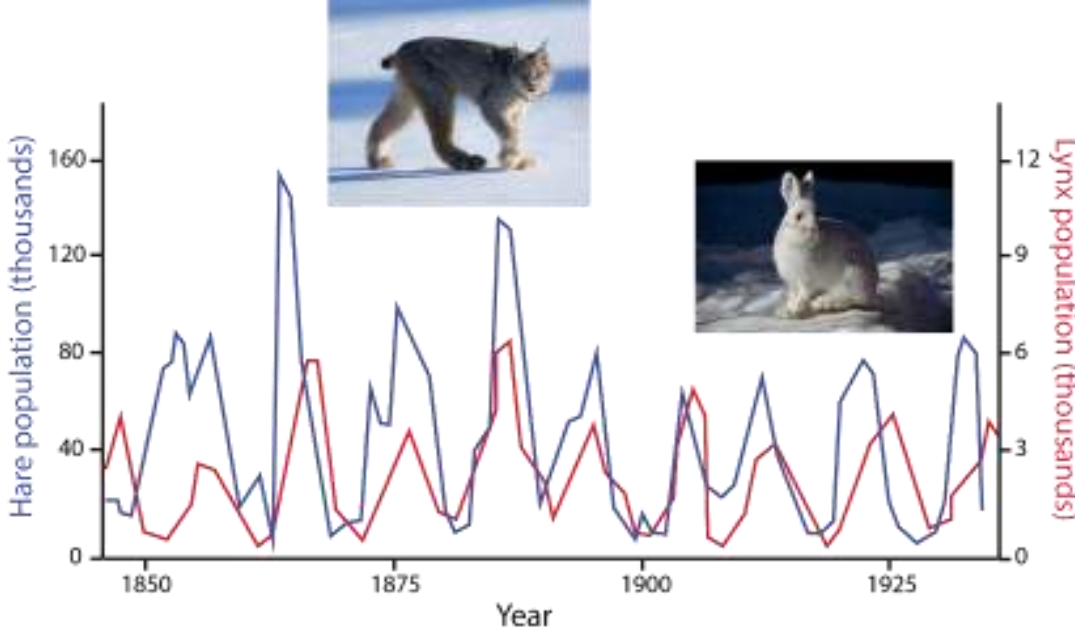
# effects of nonlinearity: nonlinear cycles and stochasticity

Non-linear cycles can arise from a system in which the **driving force** is continuously supplied and an **instability** that acts to remove the drive is triggered above a certain threshold.

Such a system can have different stationary solutions: one possibility is a state in which all time derivatives vanish and an equilibrium value is reached where the system just sits at marginal stability.

Another, more interesting case is the possibility of limit cycles: these are a periodic growth of an instability which removes the driving force such that it needs some time to be restored.

Basic example:  
Lotke-Volterra  
equations for  
predator-prey  
systems.  
not possible  
linearly

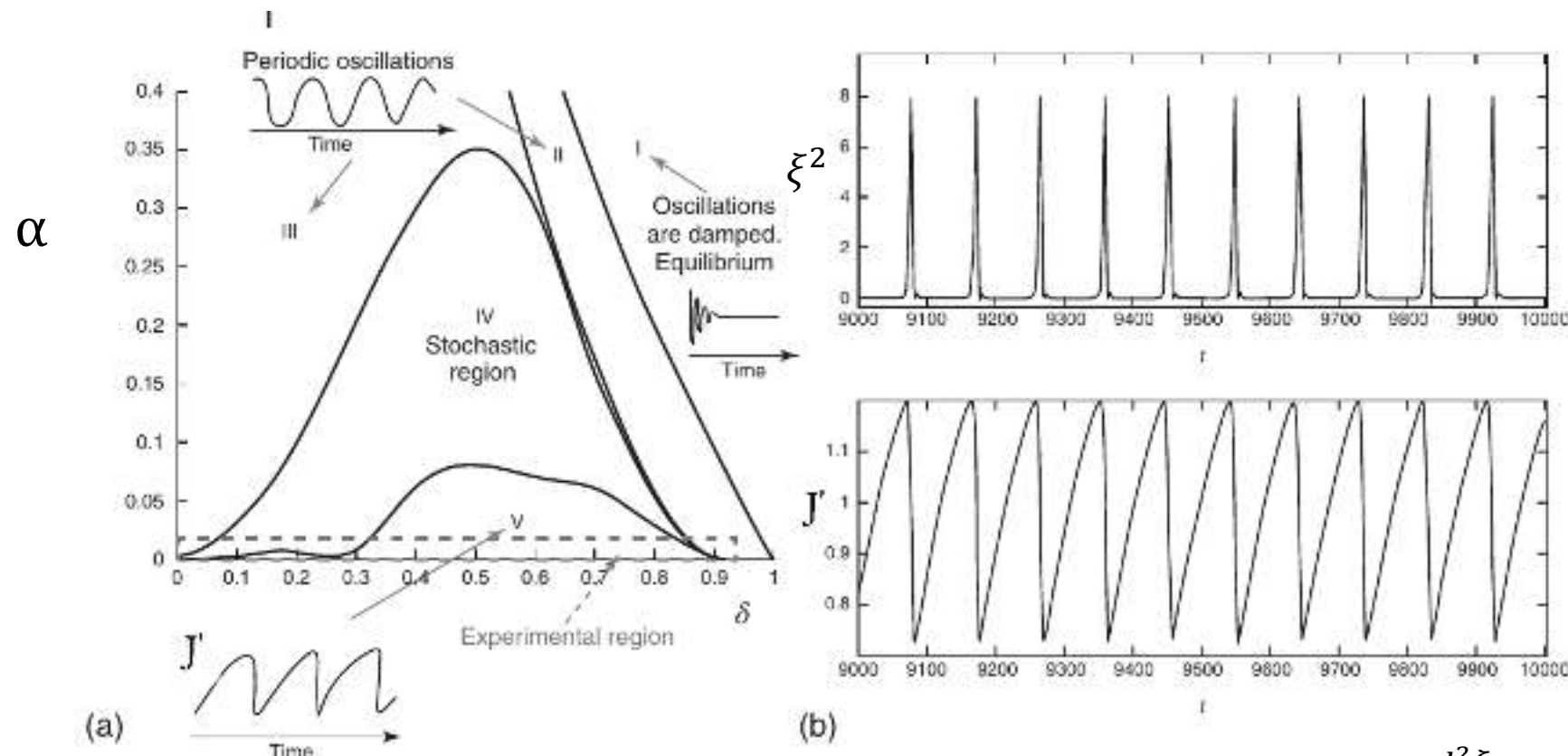


$$\frac{dx}{dt} = ax + \beta xy$$
$$\frac{dy}{dt} = \gamma y - \beta xy$$

# a simple nonlinear model to describe sawtoothing

- limit cycles can be obtained from a set of two non-linearly coupled differential equations representing the temporal evolution of the instability drive and the MHD mode (amplitude  $\xi$ ).
- In our case: the drive is the current density gradient  $J'$
- $\frac{d^2\xi}{dt^2} = (J' - 1)\xi - \delta \frac{d\xi}{dt}$  : equation for temporal evolution of MHD instability.  $\delta$  is a normalized damping.
- We need an equation for the temporal evolution of the drive:
- $\frac{dJ'}{dt} = \alpha(P - J' - \beta \xi^2 J')$
- the first two terms on the rhs represents a balance between power  $P$  increasing  $J'$  and  $J'$  itself, plus the **nonlinear term** providing the coupling between the two equations.
- $\alpha$  represents the ratio between transport timescale (which tends to resolve high  $J'$ ) and timescale related to the growth of MHD mode.

# some solutions of the micro-model



$$\frac{d^2\xi}{dt^2} = (J' - 1)\xi - \delta \frac{d\xi}{dt}$$

From H. Zohm, 2015, Magnetohydrodynamics stability of tokamaks, Wiley-VCH.  
 From D. Constantinescu et al (2011) A low-dimensional model system for quasi-periodic plasma perturbations. Phys. Plasmas, 18, 062307

$$\frac{dJ'}{dt} = \alpha(P - J' - \beta \xi^2 J')$$

- if no coupling, i.e.  $\beta = 0$ , temporal evolution moves towards a stationary state:  $J'(t) = P - e^{-\alpha t}$
- If no damping mechanism of instability is present, i.e.  $\delta = 0$ , harmonic oscillator if  $J' < 1$ , exponential growth if  $J' > 1$
- If high damping is present, oscillations are damped → equilibrium
- If  $\alpha \rightarrow 0$ , a regime of nonlinear oscillations can be found. Short MHD time scales compared to transport can evolve in a sawtooth way.

$$\frac{d^2\xi}{dt^2} = (J' - 1)\xi - \delta \frac{d\xi}{dt}$$

$$\frac{dJ'}{dt} = \alpha(P - J' - \beta \xi^2 J')$$

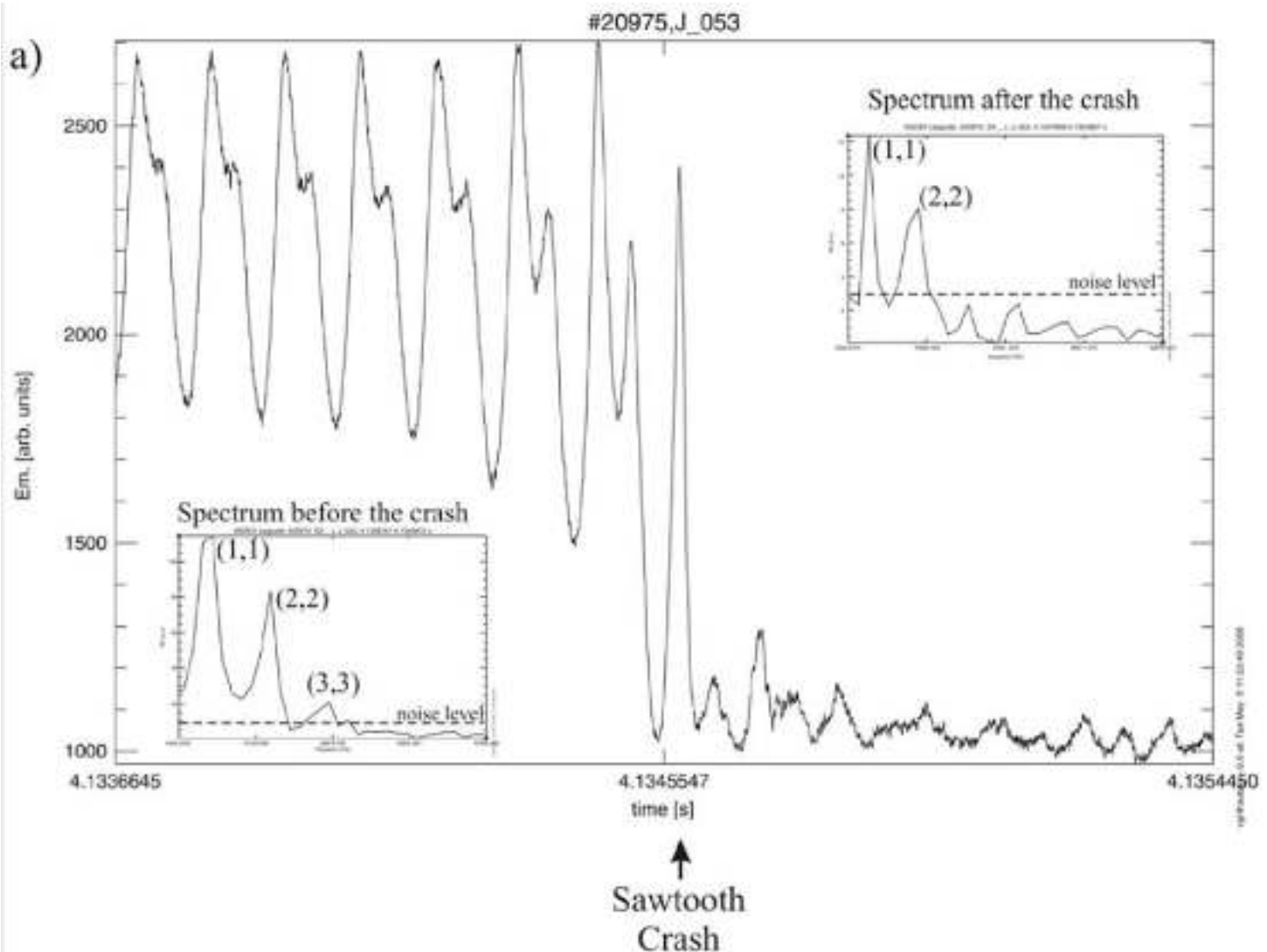
- very simplified: more advanced criteria to measure the steepness of the current gradient rely on the so-called "normalized magnetic shear at the  $q = 1$  surface", the normalized shear being defined as

$$s(r) = r \frac{d \ln q(r)}{dr} = \frac{r}{q} \frac{dq(r)}{dr}.$$

- Instability sets in only over a threshold in  $s(r|_{q(r)=1})$  [a]

[a] Porcelli, Boucher, Rosenbluth PPCF 38, 2163 (1998)

# Nonlinearity in (1,1) mode before sawtooth crash



From Igochine et al Nucl. Fusion **47** (2007) 23–32

# Stochasticization during sawtooth crash

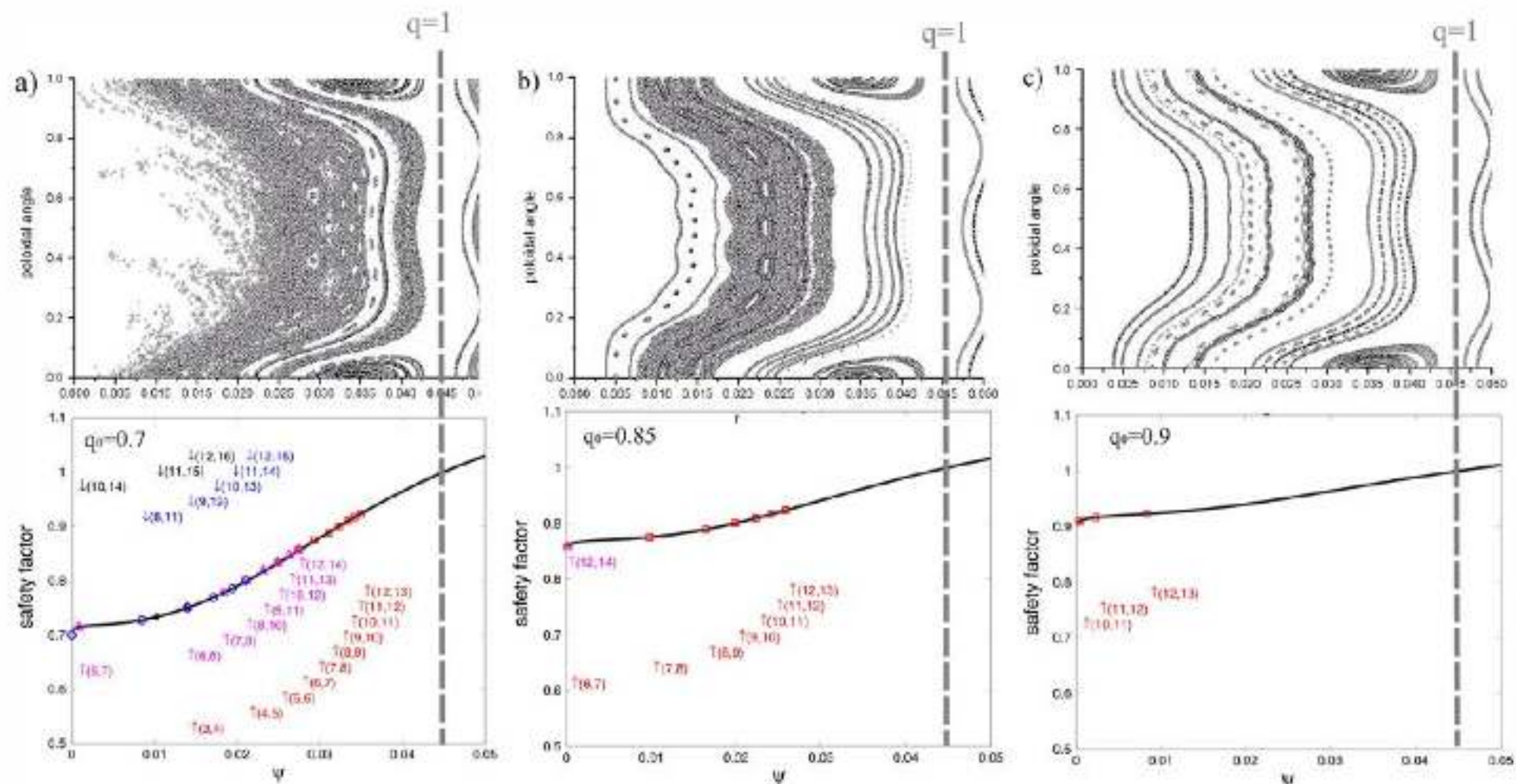


**Figure 9.** Poincaré plots for the same perturbations  $(1, 1) + (2, 2) + (3, 3)$  as in figure 4 but for different safety factor profiles. Note that stochasticization strongly depends on the existence of the low-order rational surfaces which are marked on the safety factor curves.

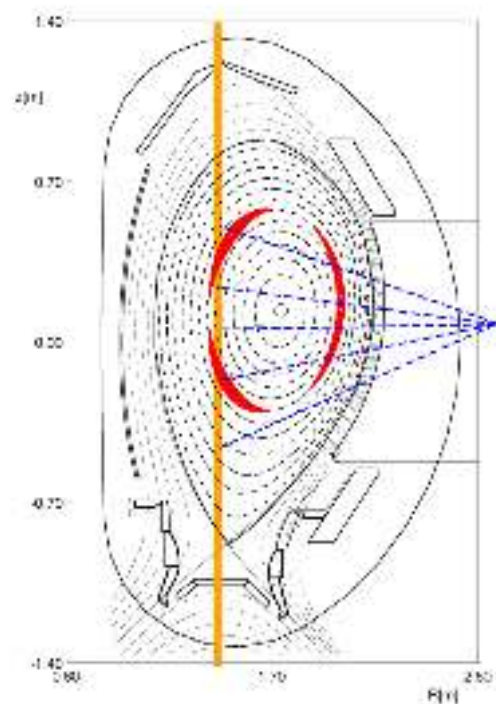
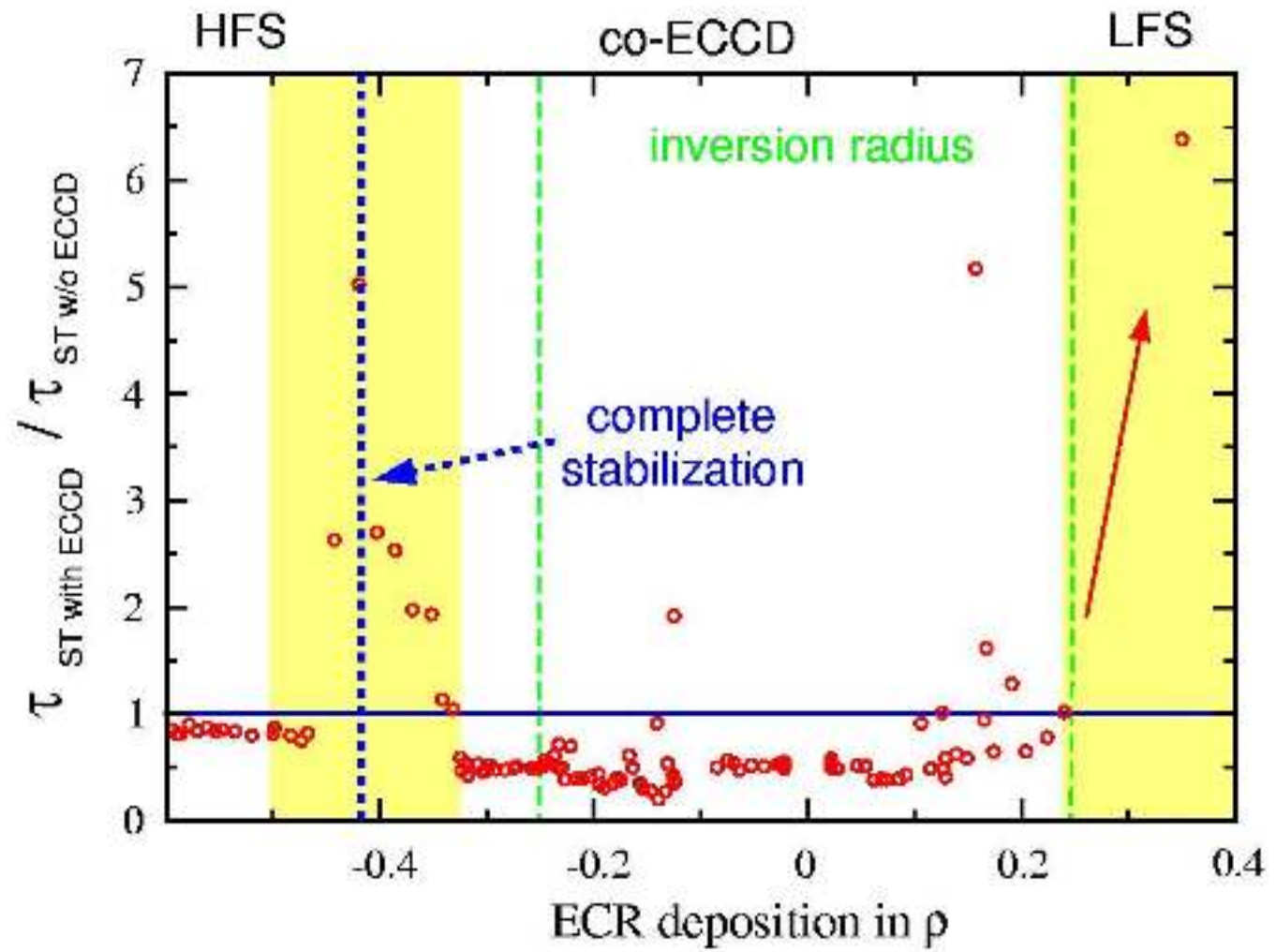
(a) Central  $q$ -value is 0.7; (b) central  $q$ -value is 0.85; (c) central  $q$ -value is 0.9

From Igochine et al Nucl. Fusion **47** (2007) 23–32

# more info about sawtoothing

- roles of sawtoothing: limit the peaking of temperature, density, and current density profiles;
- redistribution of energy and particles from core to edge: NEGATIVE;
- redistribution of impurities and He ashes (from fusion): POSITIVE.
- → need of **active control scheme to tailor** exactly the energy loss & core impurities control
- fast particles have stabilizing effects, alfa particles expected to stabilize.

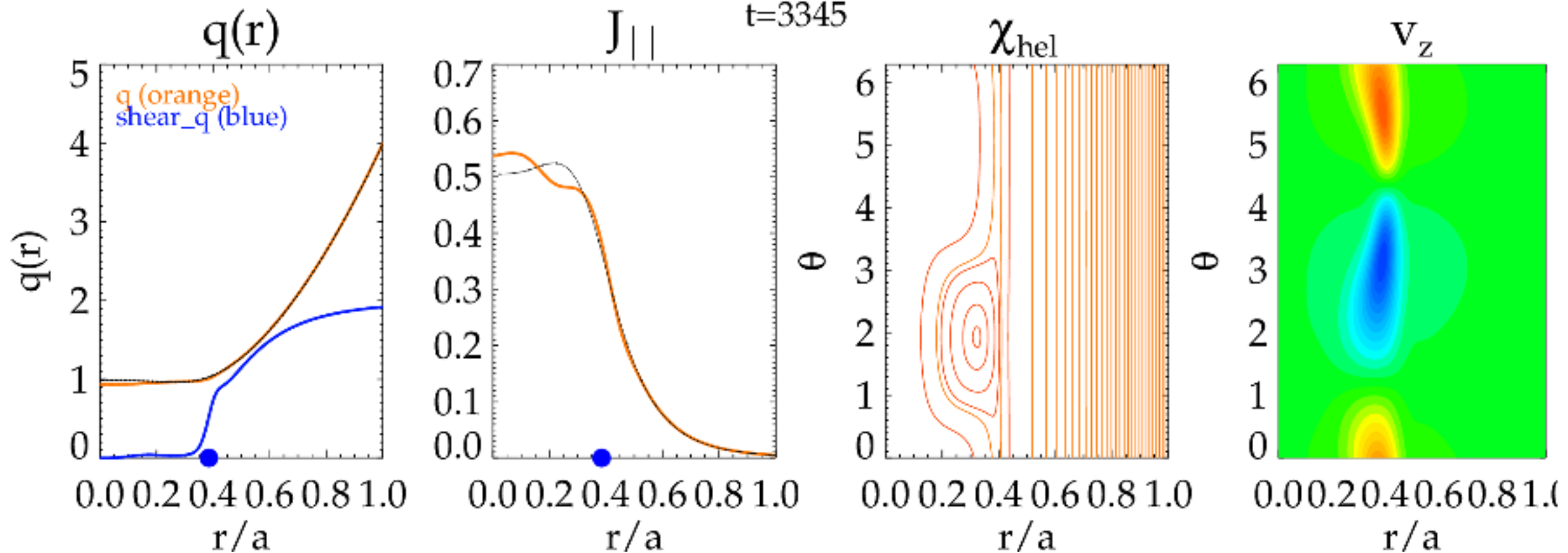
# Sawtooth tailoring by Electron Cyclotron Current Drive



$$\omega_{ECCD} \sim \omega_{ce} = \frac{eB}{m_e}$$

resonant interaction between wave and  $e^-$

# video: nonlinear evolution of a tearing mode with $m=1 n=-1$



questions?



pause

# HPC physics

# Evolution drives: technological constraints

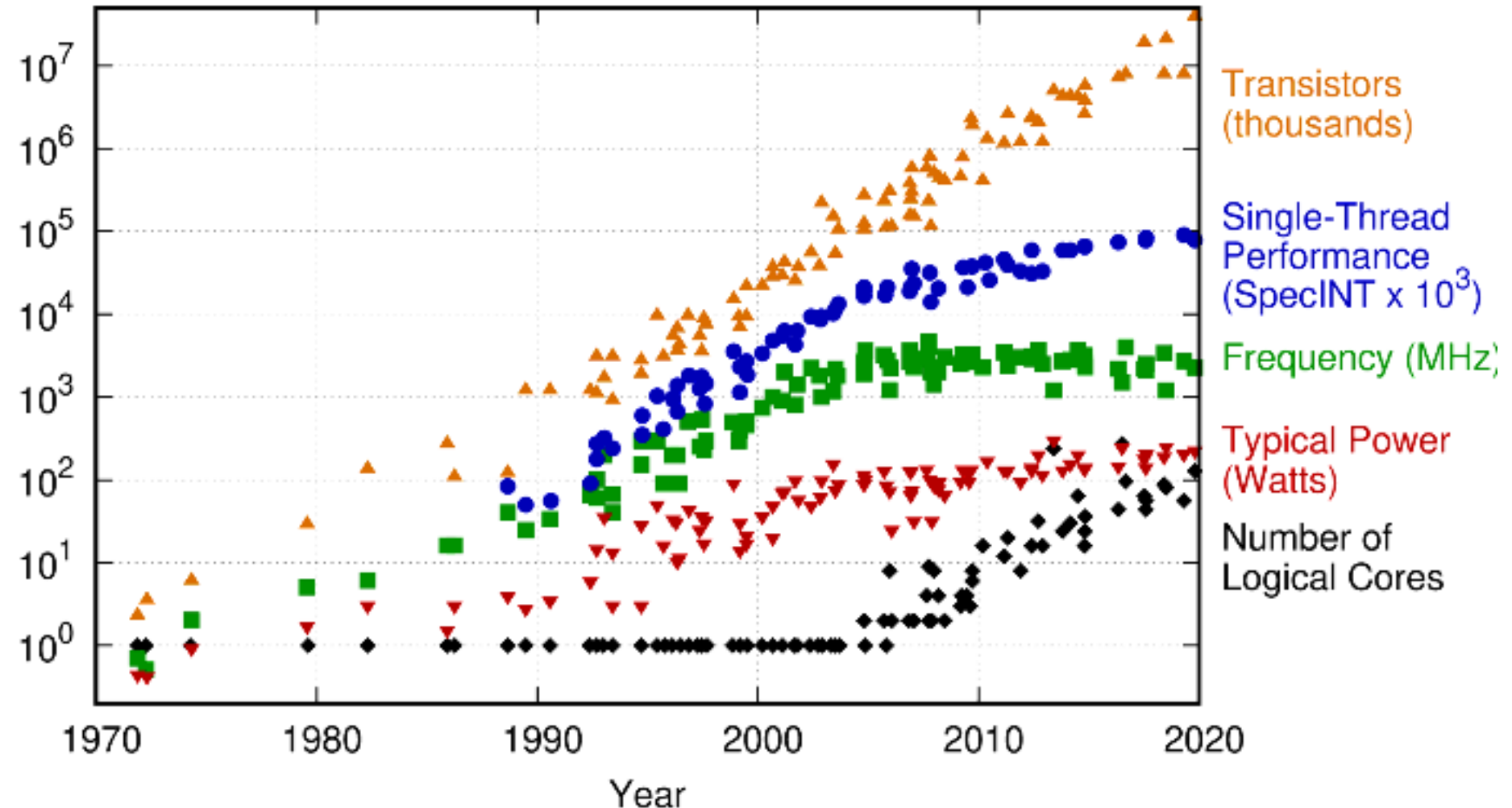
- Power wall
- Scaling wall
- Memory wall
- Towards accelerated architectures

- remind:  $P = cV^2f$

with  $P$ : power,  $V$ : voltage,  $f$ : frequency

# microprocessors in time: trends

48 Years of Microprocessor Trend Data

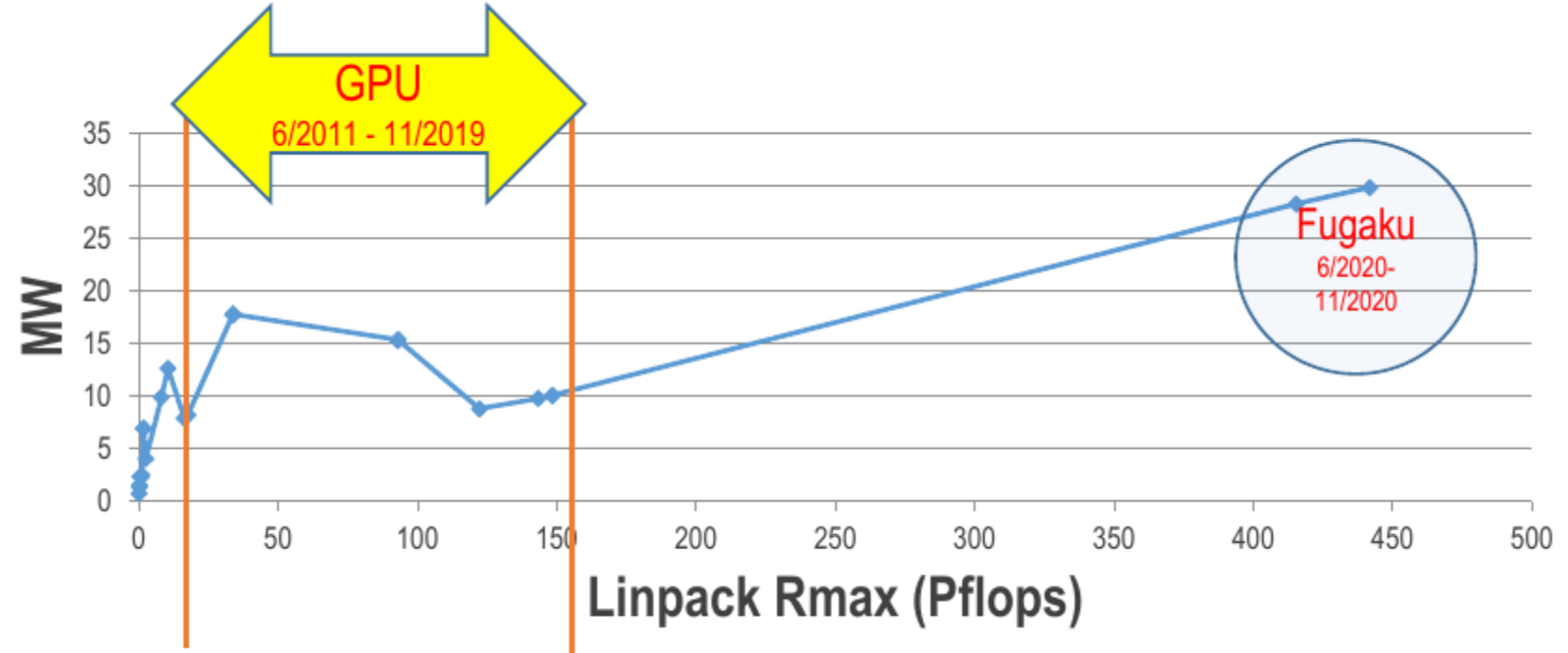


Original data up to the year 2010 collected and plotted by M. Horowitz, F. Labonte, O. Shacham, K. Olukotun, L. Hammond, and C. Balten  
New plot and data collected for 2010-2019 by K. Rupp

# future trends

- Moore's law comes to an end. Probable limit of transistor's size around 3 - 5 nm
- Need to design new structure for transistors
- Limit of circuit size: yield decrease with the increase of surface, chiplets will dominate
- Data movement will be the most expensive operation;
- Exaflop with regular CPUs will be too power hungry
  - One or more accelerator per node
  - Accelerator type will depend on applications
  - GPU (AI)
  - FPGA (Field-Programmable Gate Array)
  - Neuromorphic computing (<https://www.intel.com/content/www/us/en/research/neuromorphic-computing.html>)
  - Quantum accelerator

# acceleration is needed to save power



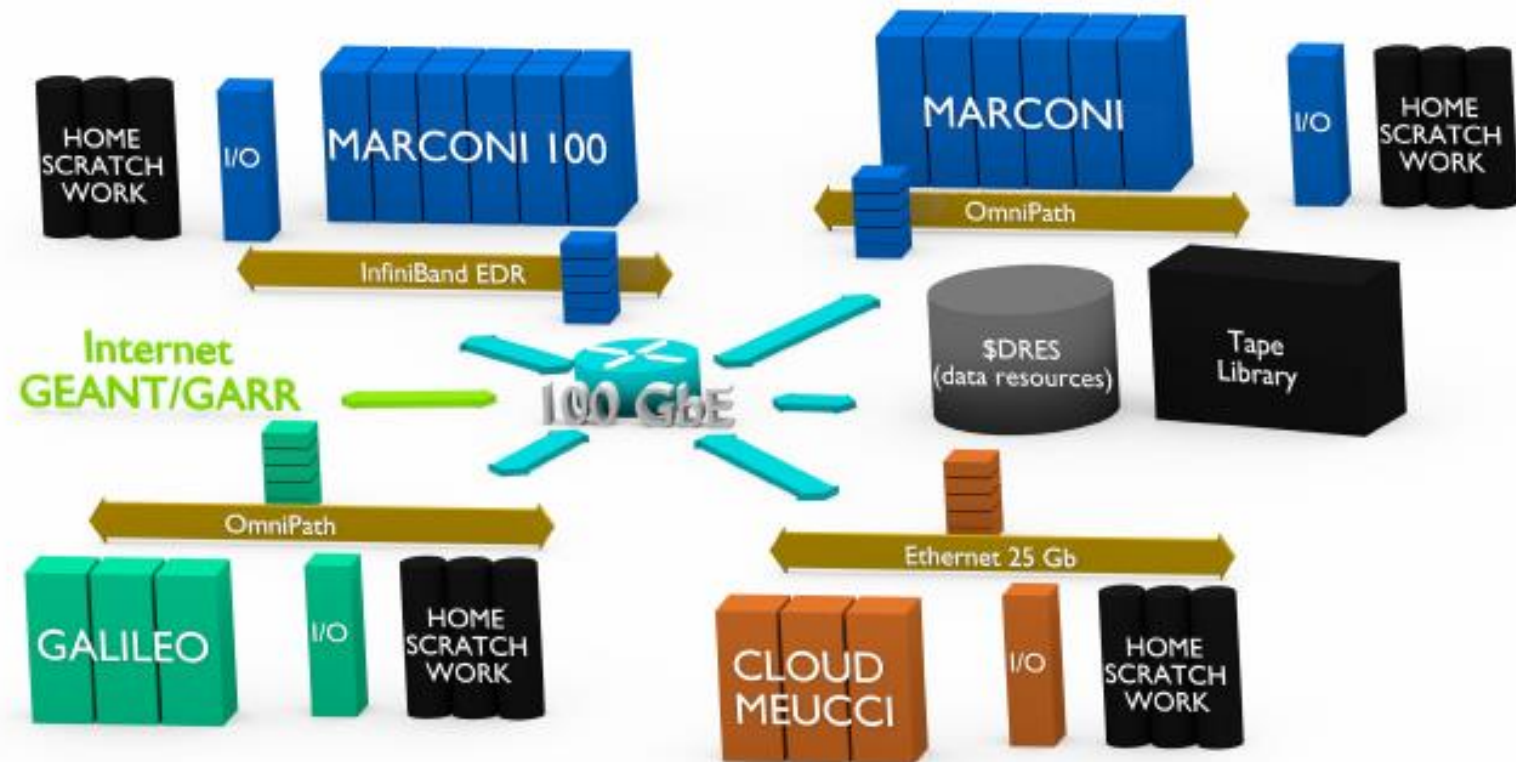
all (pre)Exascale machines to be built in the next few years are accelerated with GPUs

# future trends / 2

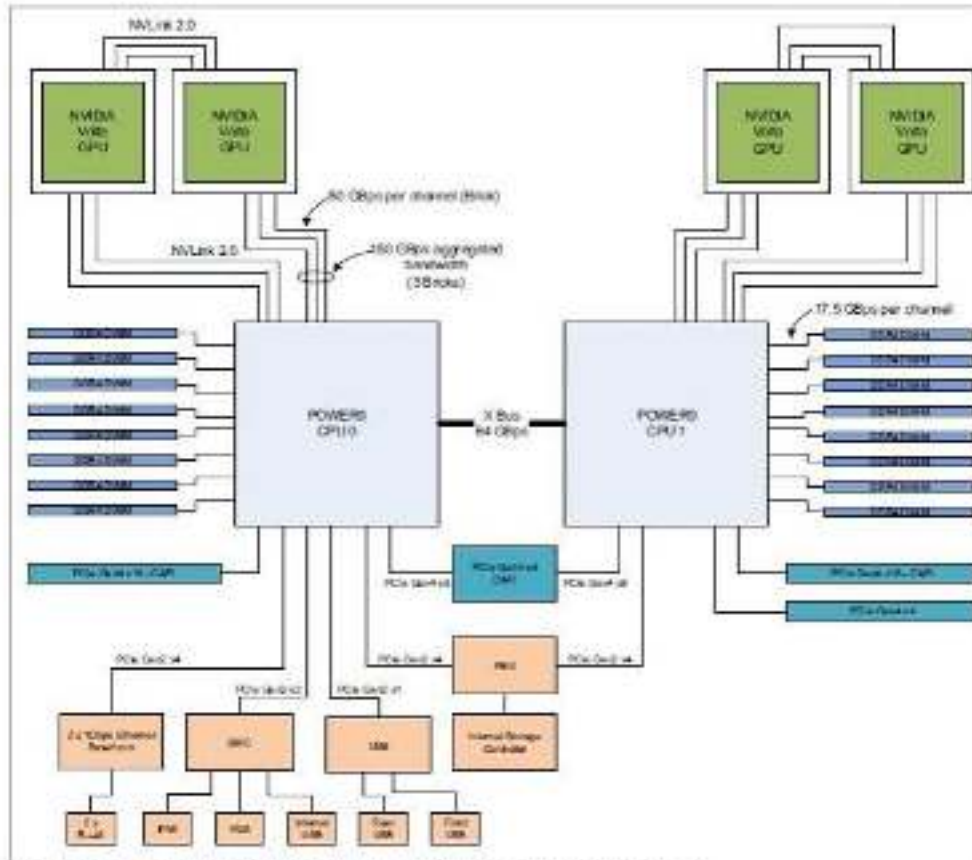
- Big trends:
  - C++ is getting momentum → new codes
  - Fortran is losing attraction
- It is high time to program for GPUs
- OpenMP looks like the best bet for the future
  - Especially for Legacy codes and Fortran codes
- C++ might be the best option in the long run

example of a HPC infrastructure

# CINECA Infrastructure



## Marconi100: the Power AC922 model



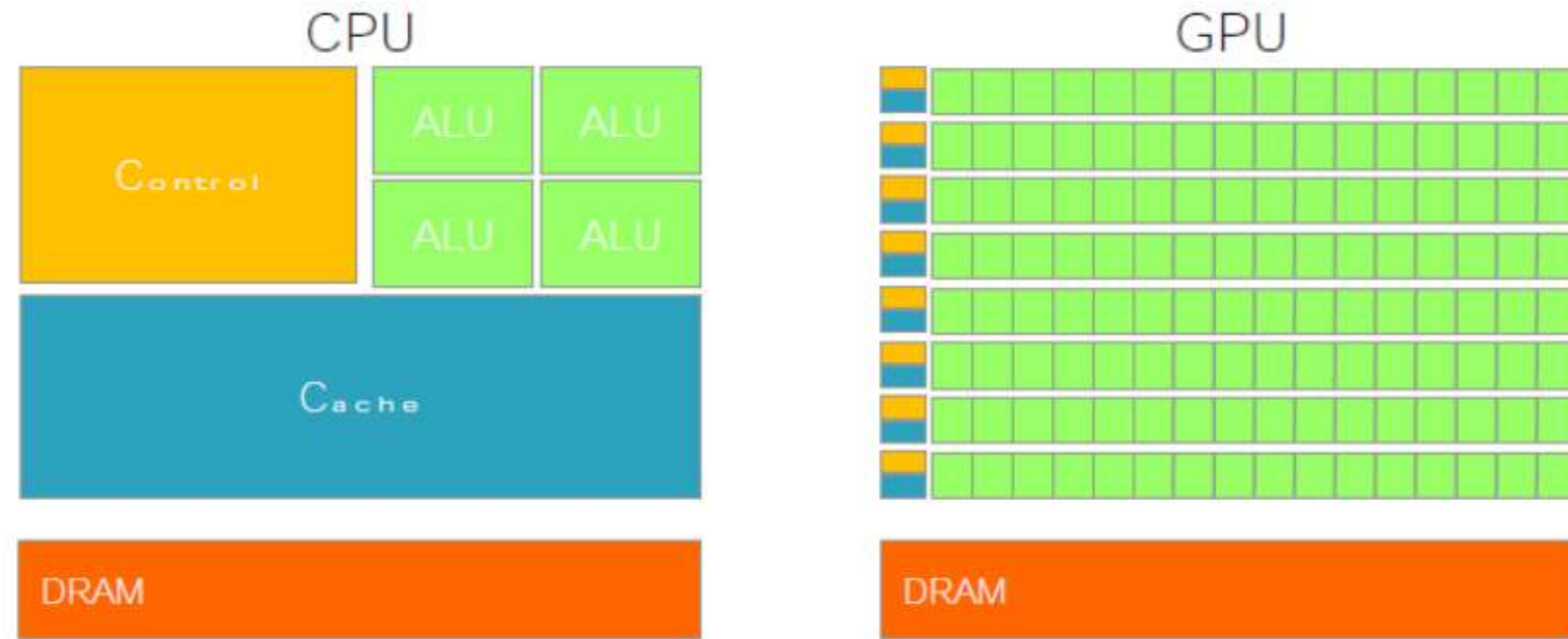
- AC922 "Whiterspoon"
- **32 PFlops peak**
- Nodes: 980 compute + 3 login nodes, 32 TFlops each
- Processors: 2x16 cores IBM 8335-GTG 2.6 (3.1) GHz
- Accelerators: **4xNVIDIA V100 GPUs**, Nvlink 2.0, 16GB
- RAM: 256 GB/node
- Local disk: 1.6TB NVMe
- Internal Network: Mellanox Infiniband EDR DragonFly+
- Disk Space: 8PB storage

# what is a GPU

- Graphic Processing Unit
  - a device equipped with an highly parallel microprocessor(many-core) and a private memory with very high bandwidth
- GPUS are designed to render complex 3D scenes composed of millions of data points/vertex in a very fast frate rate (60/120 FPS)
- the rendering process requires a set of transformations based on linear algebra operations
- the same set of operations are applied on each point of the scene
- each operation is independent with respect to data
- all operations are performed in parallel using a huge number of threads which process all data independently

# what is a GPU

- GPUs are specialized for intense data-parallel computations
- in GPUs more transistors are devoted to data processing rather than data caching and flow control
- main global memory: 32-64GB; high bandwidth: 250-800GB/s

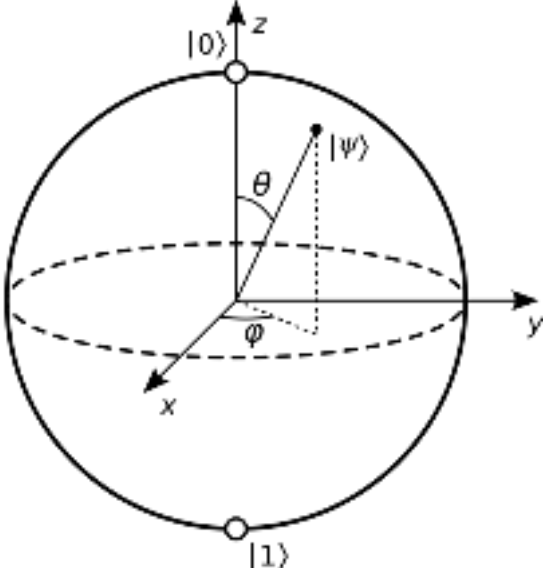


\*ALU=Arithmetic Logic Unit

# Quantum Computing

- a classical bit is a binary digit, either 0 or 1, used to represent information in classical computers;
- A pure qubit state is a coherent superposition of the basis states, I'd write it as  $|\psi\rangle = \alpha|0\rangle + \beta|1\rangle$ , with  $\alpha^2 + \beta^2 = 1$ , it can be represented as a point on the so-called Bloch sphere.
- There are two possible outcomes for the measurement of a qubit—usually taken to have the value "0" and "1", like a bit. However, the general state of a qubit according to quantum mechanics can arbitrarily be a coherent superposition of all computable states simultaneously → possibility to store much more information;
- But a measurement of a qubit would destroy its coherence and irrevocably disturb the superposition state
- Fundamental part of the success would be to harness the process of “quantum entanglement”, but this is rapidly destroyed by noise (produced, for example, by random oscillations of the ions or molecules used as qubits).
- As written in Nature: “Quantum computers: what are they good for? For now, absolutely nothing. But researchers and firms are optimistic about the applications.”

[<https://www.nature.com/articles/d41586-023-01692-9>]



**Bloch sphere** representation of a qubit. In fact, a qubit requires two complex numbers to describe its two probability amplitudes

- Whatever the design, the clever stuff happens when qubits are carefully coaxed into ‘superposition’ states of indefinite character — essentially a mix of digital ones and zeroes.
- Running algorithms on a quantum computer involves directing the evolution of these superposition states. The quantum rules of this evolution allow the qubits to interact to perform computations that are, in practical terms, impossible using classical computers.
- That said, useful computations are possible only on quantum machines with a huge number of qubits, and those do not yet exist. What’s more, qubits and their interactions must be robust against errors introduced through the effects of thermal vibrations, cosmic rays, electromagnetic interference and other sources of noise. These disturbances can cause some of the information necessary for the computation to leak out of the processor, a situation known as decoherence. That can mean dedicating a large proportion of the qubits to error-correction routines that keep a computation on track.

# basics of parallel programming

- OpenMP
- MPI
- simple examples

# OpenMP: De-facto standard for Shared-Memory Parallelization.

## History:

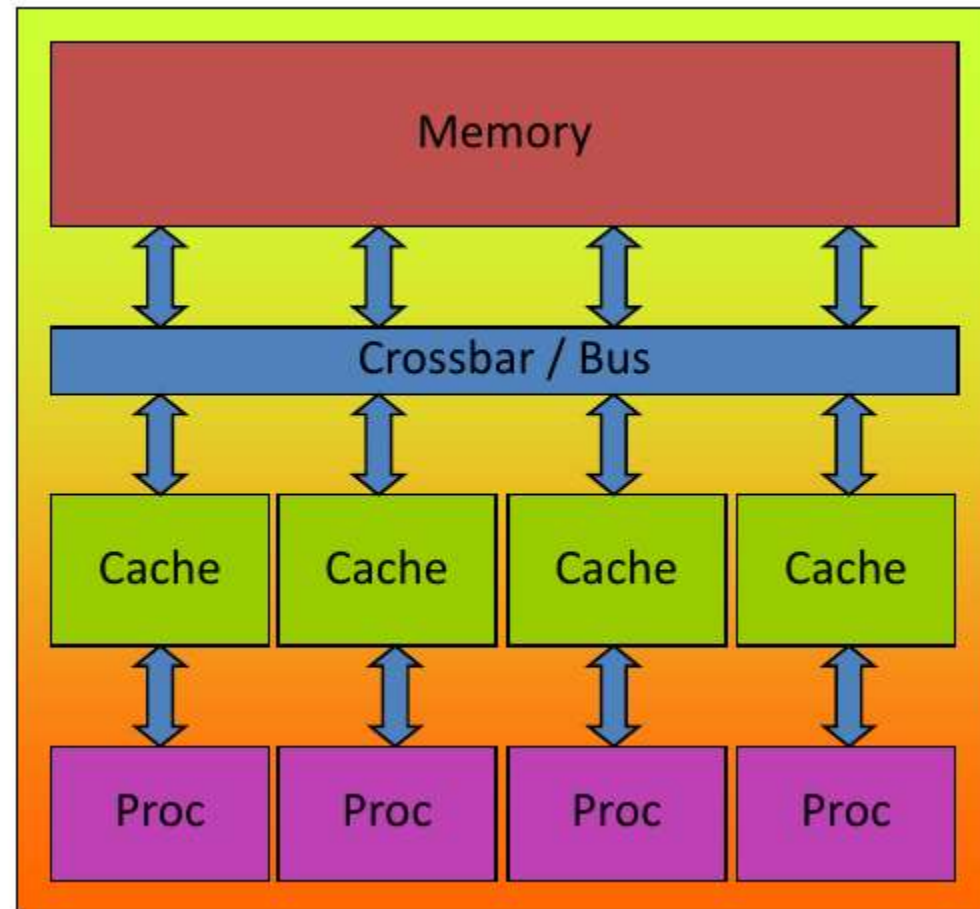
- 1997: OpenMP 1.0 for FORTRAN
- 2000: OpenMP 2.0 for FORTRAN
- 2002: OpenMP 2.0 for C and C++
- 2005: OpenMP 2.5 now includes both programming languages.
- 07/2013: OpenMP 4.0
- 11/2018: OpenMP 5.0
- 11/2020: OpenMP 5.1



- What is OpenMP?
  - Parallel Region & Worksharing
  - Tasking
  - SIMD / Vectorization
  - Accelerator Programming

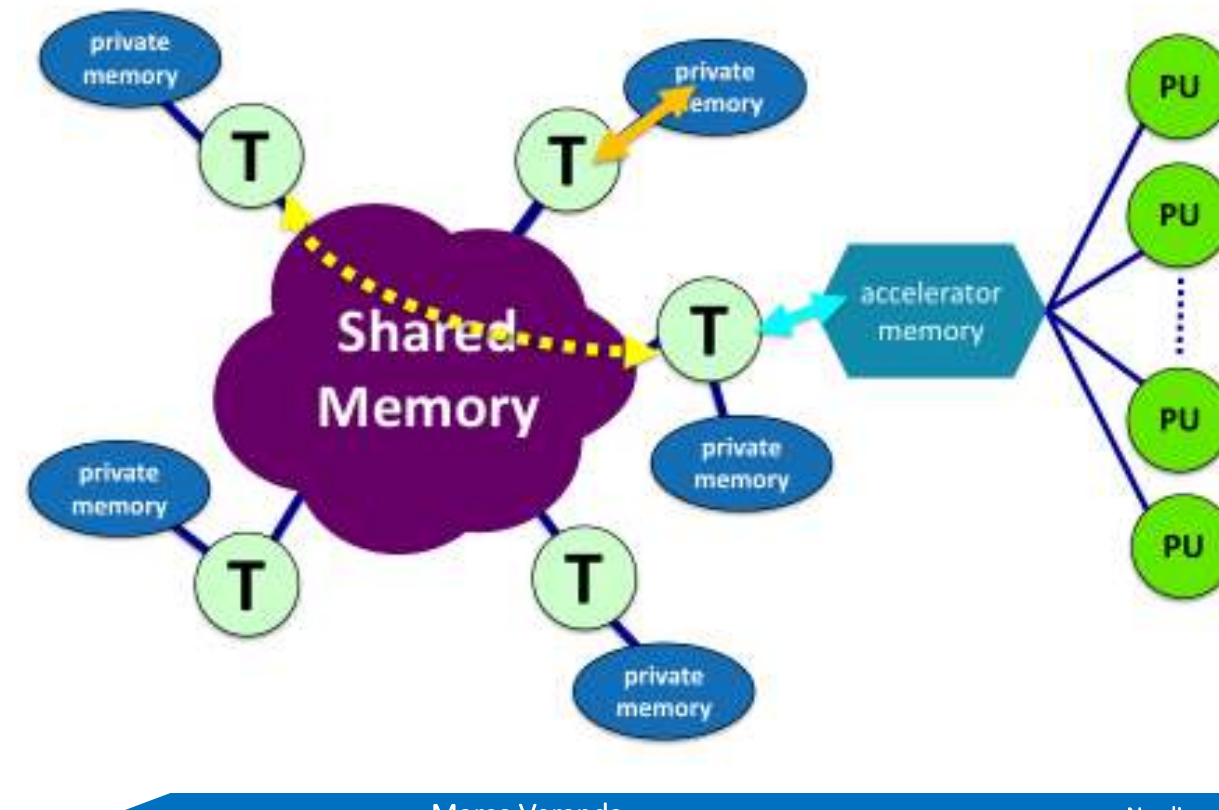
OpenMP: **Shared**-Memory Parallel Programming Model.

- All processors/cores access a shared main memory.
- Real architectures are more complex, as we have seen
- Parallelization in OpenMP employs multiple threads



# The OpenMP Memory Model

- All threads have access to the same, globally shared memory
- Data in private memory is only accessible by the thread owning this memory
- No other thread sees the change(s) in private memory
- Data transfer is through shared memory and is 100% transparent to the application

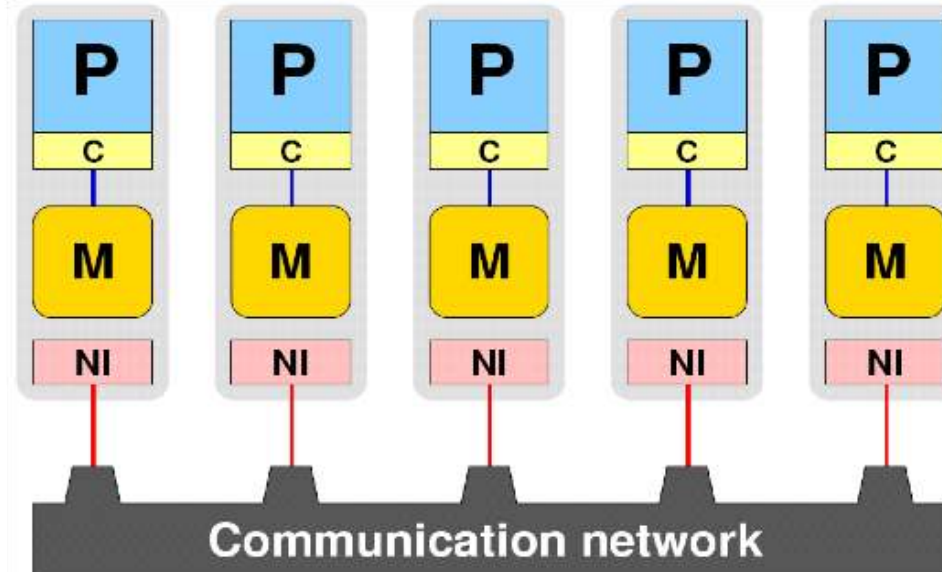


# Message Passing Interface (MPI)

[www.mpi-forum.org/](http://www mpi-forum.org/)

MPI: **Distributed**-Memory Parallel Programming Model.

- processors P do not share any topological entity with each other, they're equal
- Each one has its dedicated memory region (M)
- They are connected using one uniform network (NI)



# Parallel Region and Structured Blocks: simple OpenMP example

- The parallelism has to be expressed explicitly.

C/C++

```
#pragma omp parallel
{
...
structured block
...
}
```

Fortran

```
!$omp parallel
...
structured block
...
!$omp end parallel
```

- Structured Block
  - Exactly one entry point at the top
  - Exactly one exit point at the bottom
  - Branching in or out is not allowed
  - Terminating the program is allowed (abort / exit)

# example1: for worksharing

- OpenMP's most common worksharing construct: for

C/C++

```
int i;  
#pragma omp for  
for (i = 0; i < 100; i++)  
{  
    a[i] = b[i] + c[i];  
}
```

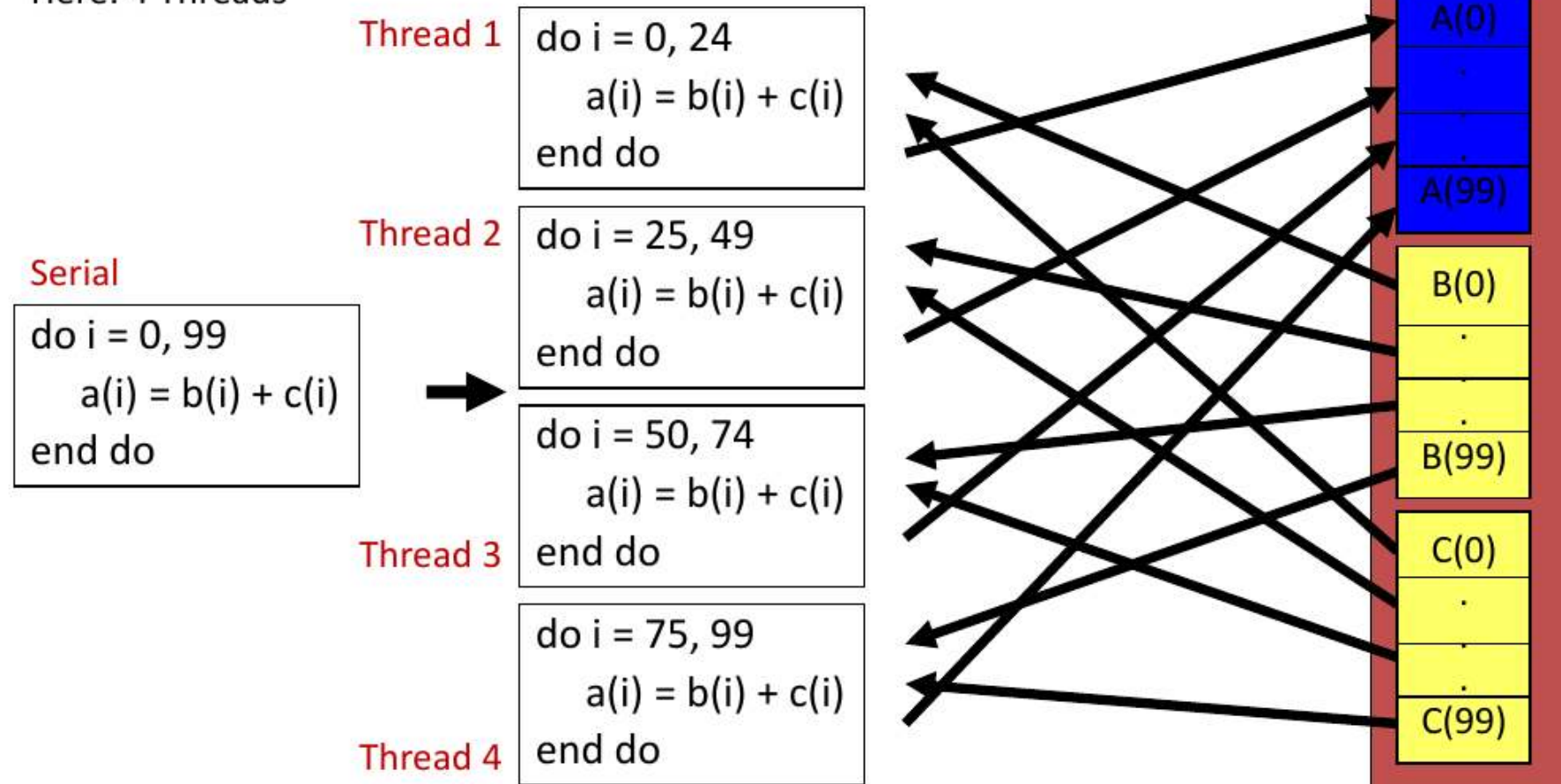
Fortran

```
INTEGER :: I  
!$omp do  
DO i = 0, 99  
    a[i] = b[i] + c[i]  
END DO
```

- Distribution of loop iterations over all threads in a Team.
- Scheduling of the distribution can be influenced.
- Loops often account for most of a program's runtime!

# worksharing illustrated

Pseudo-Code  
Here: 4 Threads



## example2: a more insidious for loop

- Can all loops be parallelized with for-constructs? No!
- Simple test: If the results differ when the code is executed backwards, the loop iterations are not independent. BUT: This test alone is not sufficient.

```
C/C++  
int i, int s = 0;  
#pragma omp parallel for  
for (i = 0; i < 100; i++)  
{  
    s = s + a[i];  
}
```

- Data Race: if between two synchronization points at least one thread writes to a memory location from which at least one other thread reads, the result is not deterministic (race condition).

## example2: a more insidious for loop

- A Critical Region is executed by all threads, but by only one thread simultaneously (Mutual Exclusion).

```
C/C++  
int i, s = 0;  
#pragma omp parallel for  
for (i = 0; i < 100; i++)  
{  
    #pragma omp critical  
    { s = s + a[i]; }  
}
```

- Does not scale well!

## example2: a more insidious for loop

- In a reduction-operation the operator is applied to all variables in the list. The variables have to be shared.
  - reduction(operator:list)
  - The result is provided in the associated reduction variable

```
C/C++  
int i, s = 0;  
#pragma omp parallel for reduction(+:s)  
for(i = 0; i < 99; i++)  
{  
    s = s + a[i];  
}
```

# final piece of code: compute $\pi$

```

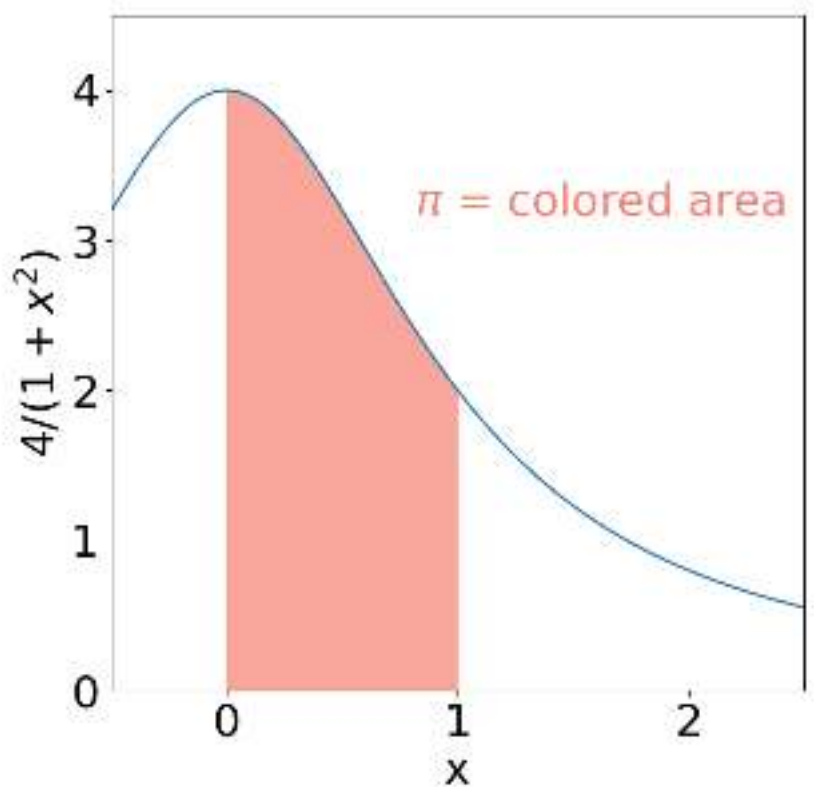
double f(double x)
{
    return (4.0 / (1.0 + x*x));
}

double CalcPi (int n)
{
    const double fH = 1.0 / (double) n;
    double fSum = 0.0;
    double fX;
    int i;

#pragma omp parallel for private(fX,i)
reduction(+:fSum)
    for (i = 0; i < n; i++)
    {
        fX = fH * ((double)i + 0.5);
        fSum += f(fX);
    }
    return fH * fSum;
}

```

$$\pi = \int_0^1 dx \frac{4}{1+x^2}$$



# how to work in an HPC infrastructure

- first you need to get some computational time, typically through a call for the use of resources;
- when you enter you find yourself in a LINUX environment

```
aurelio@r000u061015:~$ last login: Tue Mar  7 15:18:16 2023 from 150.178.181.4
*****
* Welcome to MARCONI / *
*   MARCONI-fusion 8 CINECA - NextScale cluster - CentOS 7.3   *
*   *
* SKL partition = 3124 nodes with:                                *
*   - 2x24-core Intel Xeon 8160 CPU @ 2.10GHz                   *
*   - 192 GB DDR4 RAM                                         *
*   *
* Intel OmniPath (100Gb/s) high-performance network           *
* SLURM 22.05                                                 *
*   *
* For a guide on Marconi:                                     *
* wiki.ugov.it/confluence/display/SCAIUS/UG3.1%2A+MARCONI+UserGuide *
* For support: superc@cinca.it                                 *
*****
IN EVIDENCE:
- An automatic cleaning procedure for the SCINECA_SCRATCH is active, each day
  all files older than 40 days will be cancelled.
- The "module" environment is installed and based on profiles. Use the modmap
  command to identify the correct profile ("modmap -h" for help).
[~/marconi_work/Flux3D_PTKIE3D/.veranda/nemato_1.6.3/runs/lcs-toc]
aurelio@r000u061015:~$
```

# how to work in an HPC infrastructure: the module system

- The **module system** is a concept available on most supercomputers,
- In most cases, a **supercomputer has far more software installed than the average user will ever use**. Each of these software packages need different settings in terms of \$PATH, \$LD\_LIBRARY\_PATH and other environment variables, which can adversely affect each other or even be mutually exclusive.
- Therefore, **the settings for all these software packages and their supported versions are encapsulated in “environment modules”** maintained by the module system.
- By means of the module system, all software currently available on your cluster can be listed, loaded, and unloaded, by using the command module.

[on Marconi HPC] use `module avail` to see all the available modules

# result of the module avail command

```
maurelio@000u061015: ~ module avail
-- /cineca/prod/opt/modulefiles/profiles --
profile/advanced profile/base profile/cheese profile/eng profile/knl profile/phys profile/unstable
profile/archive profile/bioinf profile/chem profile/global profile/lifesc profile/statistics
profile/astro profile/candidate profile/deeplrn profile/global_prove profile/neurosc profile/superc

-- /cineca/prod/opt/modulefiles/base/environment --
autoload env-bdw/1.0 env-knl/1.0 env-skl/1.0 prace/1.0

-- /cineca/prod/opt/modulefiles/base/libraries --
2decomp_fft/1.5.847--intelmpi--2018--binary matheval/1.1.11--intelmpi--2018--binary parmetis/4.0.3--intelmpi--2018--binary zlib/1.2.8--gnu--6.1.0
blas/3.8.0--intel--pe-xe-2018--binary metis/5.1.0--intel--pe-xe-2018--binary petsc/3.13.3--intelmpi--2018--binary zlib/1.2.11--gnu--8.3.0
boost/1.58--intelmpi--2018--binary mkl/2018--binary petsc/3.13.3_complex--intelmpi--2018--binary
boost/1.56.0--intelmpi--2018--binary mkl/2020--binary petsc/3.13.3_int64--intelmpi--2018--binary
boost/1.78.0--intelmpi--2018--binary mpi4py/3.0.0--python--3.6.4 petsc/3.16.0--intelmpi--2020--binary
cubelib/4.4--intelmpi--2018--binary nag/mark26--binary petsc/3.16.0_complex--intelmpi--2020--binary
cubelib/4.7--intelmpi--2020--binary nag/mark27--binary pnetcdf/1.11--intelmpi--2018--binary
fftw/3.3.5--intelmpi--2017--binary netcdf-cxx4/4.3.0--intel--pe-xe-2018--binary proj/8.0--intel--pe-xe-2018--binary
fftw/3.3.7--intelmpi--2018--binary netcdf-cxx4/4.3.0--intelmpi--2018--binary qt/5.7.0--intelmpi--2018--binary
fftw/3.3.8--intelmpi--2020--binary netcdf/4.6.1--intel--pe-xe-2018--binary qt/5.9.0--gnu--6.1.0
gdal/3.2.2--intel--pe-xe-2018--binary netcdf/4.6.1--intelmpi--2018--binary scalapack/2.0.2--intelmpi--2018--binary
geos/3.9.1--intel--pe-xe-2018--binary netcdf/4.9.0--intel--pe-xe-2020--binary scipy/1.2.2--python--2.7.12
gsl/2.5--intel--pe-xe-2018--binary netcdff/4.4.4--intel--pe-xe-2018--binary scipy/1.2.2--python--3.6.4
gts/0.7.6 netcdff/4.4.4--intelmpi--2018--binary slepc/3.13.3--intelmpi--2018--binary
hdf5/1.8.18--intel--pe-xe-2018--binary netcdff/4.6.0--intel--pe-xe-2020--binary slepc/3.13.3_int64--intelmpi--2018--binary
hdf5/1.8.18--intelmpi--2018--binary netcdff/4.6.0--intelmpi--2020--binary szip/2.1--gnu--6.1.0
hdf5/1.10.4--intel--pe-xe-2018--binary numpy/1.14.0--python--2.7.12 szip/2.1.1--gnu--8.3.0
hdf5/1.10.4--intelmpi--2018--binary udunits/2.2.28--intel--pe-xe-2018--binary
```

# result of the module avail command

- and the rest is up to your practice. but in case you're experiencing an issue ask me and I may help.

```
maurelio@000u061015: module avail
----- /cineca/prod/opt/modulefiles/profiles -----
profile/advanced profile/base profile/cheese profile/eng profile/knl profile/phys profile/unstable
profile/archive profile/bioinf profile/chem profile/global profile/lifesc profile/statistics
profile/astro profile/candidate profile/deeplrn profile/global_prove profile/neurosc profile/superc

----- /cineca/prod/opt/modulefiles/base/environment -----
autoload env-bdw/1.0 env-knl/1.0 env-skl/1.0 prace/1.0

----- /cineca/prod/opt/modulefiles/base/libraries -----
2decomp_fft/1.5.847--intelmpi--2018--binary blas/3.8.0--intel--pe-xe-2018--binary boost/1.58--intelmpi--2018--binary boost/1.66.0--intelmpi--2018--binary boost/1.78.0--intelmpi--2018--binary cubelib/4.4--intelmpi--2018--binary cubelib/4.7--intelmpi--2020--binary fftw/3.3.5--intelmpi--2017--binary fftw/3.3.7--intelmpi--2018--binary fftw/3.3.8--intelmpi--2020--binary gdal/3.2.2--intel--pe-xe-2018--binary geos/3.9.1--intel--pe-xe-2018--binary gsl/2.5--intel--pe-xe-2018--binary gts/0.7.6 hdf5/1.8.18--intel--pe-xe-2018--binary hdf5/1.8.18--intelmpi--2018--binary hdf5/1.10.4--intel--pe-xe-2018--binary hdf5/1.10.4--intelmpi--2018--binary
matheval/1.1.11--intelmpi--2018--binary metis/5.1.0--intel--pe-xe-2018--binary mkl/2018--binary mkl/2020--binary mpi4py/3.0.0--python--3.6.4 nag/mark26--binary nag/mark27--binary netcdf-cxx4/4.3.0--intel--pe-xe-2018--binary netcdf-cxx4/4.3.0--intelmpi--2018--binary netcdf/4.6.1--intel--pe-xe-2018--binary netcdf/4.6.1--intelmpi--2018--binary netcdf/4.9.0--intel--pe-xe-2020--binary netcdf/4.9.0--intelmpi--2020--binary netcdff/4.4.4--intel--pe-xe-2018--binary netcdff/4.4.4--intelmpi--2018--binary netcdff/4.6.0--intel--pe-xe-2020--binary netcdff/4.6.0--intelmpi--2020--binary numpy/1.14.0--python--2.7.12
parmetis/4.0.3--intelmpi--2018--binary petsc/3.13.3--intelmpi--2018--binary petsc/3.13.3_complex--intelmpi--2018--binary petsc/3.13.3_int64--intelmpi--2018--binary petsc/3.16.0--intelmpi--2020--binary petsc/3.16.0_complex--intelmpi--2020--binary pnetcdf/1.11--intelmpi--2018--binary proj/8.0--intel--pe-xe-2018--binary qt/5.7.0--intelmpi--2018--binary qt/5.9.0--gnu--6.1.0 scalapack/2.0.2--intelmpi--2018--binary scipy/1.2.2--python--2.7.12 scipy/1.2.2--python--3.6.4 slepc/3.13.3--intelmpi--2018--binary slepc/3.13.3_int64--intelmpi--2018--binary szip/2.1--gnu--6.1.0 szip/2.1.1--gnu--8.3.0 udunits/2.2.28--intel--pe-xe-2018--binary
```

questions?



## Q&A

- for any question mail to:

[marco.veranda@igi.cnr.it](mailto:marco.veranda@igi.cnr.it)

# Spare:

# magnetic islands. The helical flux function

- Let us consider a magnetic field  $\mathbf{B}(r)$  in a three-dimensional space with a curvilinear coordinate system whose coordinates are labeled as  $u_i = (u_1, u_2, u_3)$ .
- Let us suppose that the system has a symmetry, i.e.,  $\frac{\partial}{\partial u_3} = 0$ .
- The magnetic field can be written using the vector potential  $\mathbf{A}(r)$  as:  $\mathbf{B} = \nabla \times \mathbf{A} = \frac{\epsilon_{ijk}}{J} \frac{\partial A_j}{\partial u^i} \mathbf{e}_k$ , where  $\epsilon_{ijk}$  represents the Levi-Civita tensor,  $J$  the Jacobian of the coordinate transformation,  $A_j$  the covariant component of the vector potential and  $\mathbf{e}_k$  is the covariant basis vector.
- Imposing the relation  $\mathbf{B} \cdot \nabla \chi = 0$ , choosing a gauge  $A_1 = 0$  and remembering that  $\frac{\partial}{\partial u_3} = 0$  it is found that:

$$\frac{\partial A_3}{\partial u^2} \frac{\partial \chi}{\partial u^1} - \frac{\partial A_3}{\partial u^1} \frac{\partial \chi}{\partial u^2} = 0, \text{ meaning that the equality is satisfied if}$$

$$\chi = A_3 = \mathbf{A} \cdot \mathbf{e}_3$$

- In cylindrical geometry + choosing the most general symmetry in 2D (the helical one) we get  $A_3 = \chi = mA_z - \frac{n}{R_0} r A_\theta$

# Classical and Neoclassical Transport in Fusion Plasmas

M.Gobbin

Consorzio RFX, Padova, Italia

27/11/2024

PHD in Fusion Science and Engineering  
*Advanced course on plasma physics & diagnostics*



# Why Transport?

- Fusion on Earth requires a really hot plasma ( $\geq 10\text{keV}$ ).
- For a commercial use of fusion energy we need to *keep* that plasma hot, few meters away from the room temperature.
- Heat flows from hot to cold regions.
- Time and space scales of energy/particle transport contribute to determine the reactor dimension.

## Transport

These slides deal with the question of how well a magnetically confined plasma keeps itself hot.

This subject is called **plasma transport**.

# Outline

## 1 Classical Transport

- Diffusion and Random Walk
- Collisions
- Classical Diffusion coefficients

## 2 Neoclassical Transport

- Passing particles
- Trapped particles
- Diffusion regimes
- Bootstrap current

## 3 Transport in non-axisymmetric devices

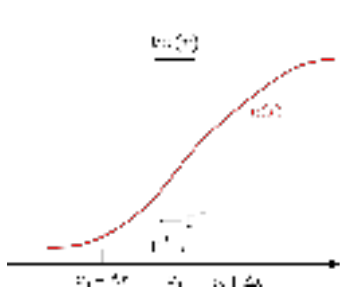
## 4 The kinetic equation

## 5 Bibliography

## 6 Extra

# Diffusion

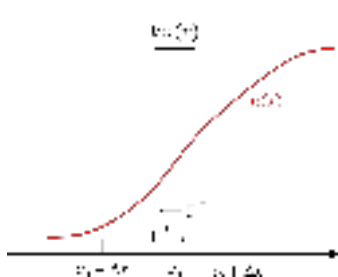
- 1D example with density gradient  $\nabla n(x)$  along the  $x$ -axis.
- Random walk of particle with step  $\pm \Delta x$  every time step  $\Delta t$ .
- Flux  $\Gamma^+$  at  $x_0$  from 1/2 particles in the region  $[x_0 - \Delta x, x_0]$ .
- Expand  $n(x) = n(x_0) + n'(x_0)(x - x_0)$ .



$$\begin{aligned}\Gamma^+ &= \frac{1}{2} \frac{1}{\Delta t} \int_{x_0 - \Delta x}^{x_0} n(x) dx = \\ &= \frac{1}{2\Delta t} \left[ n(x_0)x + \left( \frac{\partial n}{\partial x} \right)_{x_0} \frac{(x - x_0)^2}{2} \right]_{x_0 - \Delta x}^{x_0} = \\ &= \frac{1}{2\Delta t} \left[ n(x_0)\Delta x - \left( \frac{\partial n}{\partial x} \right)_{x_0} \frac{(\Delta x)^2}{2} \right]\end{aligned}$$

# Diffusion

- 1D example with density gradient  $\nabla n(x)$  along the  $x$ -axis.
- Random walk of particle with step  $\pm \Delta x$  every time step  $\Delta t$ .
- Flux  $\Gamma^-$  at  $x_0$  from 1/2 particles in the region  $[x_0, x_0 + \Delta x]$ .
- Expand  $n(x) = n(x_0) + n'(x_0)(x - x_0)$ .



$$\begin{aligned}\Gamma^- &= \frac{1}{2} \frac{1}{\Delta t} \int_{x_0}^{x_0 + \Delta x} n(x) dx = \\ &= \frac{1}{2\Delta t} \left[ n(x_0)x + \left( \frac{\partial n}{\partial x} \right)_{x_0} \frac{(x - x_0)^2}{2} \right]_{x_0}^{x_0 + \Delta x} = \\ &= \frac{1}{2\Delta t} \left[ n(x_0)\Delta x + \left( \frac{\partial n}{\partial x} \right)_{x_0} \frac{(\Delta x)^2}{2} \right] \\ \Gamma &= \Gamma^+ - \Gamma^-\end{aligned}$$

# Diffusion equation

- Total flux:  $\Gamma = \Gamma^+ - \Gamma^- = -\frac{(\Delta x)^2}{2\Delta t} n'(x_0) \rightarrow \Gamma = -\frac{(\Delta x)^2}{2\Delta t} \nabla n.$
- Diffusion coefficient  $D = \frac{(\Delta x)^2}{2\Delta t}$
- Fick Law:  $\Gamma = -D \nabla n$
- Conservation of particles number: variation in the volume  $V$  implies a flux  $\Gamma = n\mathbf{u}$  across the surface  $S$ :

$$-\frac{\partial}{\partial t} \int_V n dV = \int_S \Gamma dS = \int_V \nabla \cdot \Gamma dV \longrightarrow \frac{\partial n}{\partial t} + \nabla \cdot \Gamma = 0$$

- Using the Fick Law:  $\frac{\partial n}{\partial t} = \nabla \cdot (D \nabla n).$

# Diffusion equation: a solution in 1D

- In 1D and  $\nabla n$  along  $x$ :  $\frac{\partial n}{\partial t} = \frac{\partial}{\partial x}(D \frac{\partial}{\partial x} n)$ .
- Solution depends on the initial conditions, take  $n(x, 0) = \delta(x)N$ :

$$n(x, t) = \frac{N}{\sqrt{4\pi Dt}} e^{-\frac{x^2}{4Dt}}$$

- note that  $\langle x \rangle = \int xn(x, t)dx = 0$  but

$$\langle x^2 \rangle = \int n(x, t)x^2 dx = 2Dt \longrightarrow d = \sqrt{\langle x^2 \rangle} = \sqrt{2Dt}$$

## Classical Transport

Classical transport theory aims to calculate the diffusion coefficient  $D \approx \frac{(\Delta x)^2}{\Delta t}$  for particle and energy transport in magnetized plasmas due to collisions assuming a cylindrical geometry.

# Parallel diffusion

Consider a plasma with no magnetic field ( $\mathbf{B} = 0$ ).

- $\Delta x$  is proportional to the mean free path  $\lambda_m$  between two collisions.
- The collision frequency is  $\nu$  (i.e.  $1/\Delta t$ ).
- If  $v_{th} = \sqrt{T/m}$  is the thermal velocity:  $\lambda_m \sim v_{th} \Delta t$ , then:

$$D \sim \frac{(\Delta x)^2}{\Delta t} = \nu \lambda_m^2 \sim \frac{v_{th}^2}{\nu} = \frac{T}{m\nu}$$

- Transport along  $\mathbf{B}$  (i.e. *parallel*) is also characterized by the same  $D$ .

## Parallel transport

- Collisions reduce parallel transport.
- In a closed system with conserved flux surfaces parallel transport only smooths density variation along  $\mathbf{B}$  (no losses).

# Perpendicular diffusion

Without collisions:

- Particles orbit around the field lines, no losses.
- In axisymmetric toroidal systems like Tokamaks there are drifts ( $\nabla B$ ,  $R_c$  etc) but the resulting orbits are closed, no losses.

With Collisions:

- Collisions modify the gyration phase discontinuously.
- Guiding center position changes by random walk with step  $\Delta r_{gc}$ :

$$D_{\perp} \sim \nu(\Delta r_{gc})^2$$

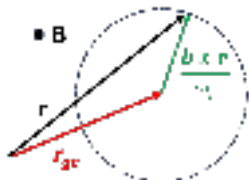
## Perpendicular transport

- Collisions enhance perpendicular transport and relative losses.
- Apparently  $D_{\perp,i} > D_{\perp,e}$  (for the same  $\nu$  and with  $\Delta r_{gc} \sim r_L$ ).

Which are the collisions relevant for transport?

# Collisions

Only unlike particle collisions contribute to particle transport.



$$m \frac{d\mathbf{v}}{dt} = q\mathbf{v} \times \mathbf{B} \longrightarrow \mathbf{r} = \mathbf{r}_{gc} + \frac{m}{qB} \mathbf{b} \times \mathbf{v}$$

$$\mathbf{r}_{gc} = \mathbf{r} + \frac{m}{qB} \mathbf{v} \times \mathbf{b}$$

- Conservation of momentum:  $(m_1 \Delta \mathbf{v}_1 + m_2 \Delta \mathbf{v}_2) = 0$ ;
- thus also:  $(m_1 \Delta \mathbf{v}_1 + m_2 \Delta \mathbf{v}_2) \times \mathbf{b} = 0$
- collision is fast:  $\Delta \mathbf{r} = 0$ , so  $\Delta \mathbf{r}_{gc} = \frac{m}{qB} \Delta \mathbf{v} \times \mathbf{b}$ ;
- replace in the momentum equation:

$$q_1 \Delta \mathbf{r}_{gc1} + q_2 \Delta \mathbf{r}_{gc2} = 0$$

# Like and unlike particle collisions

■ Unlike Particles:

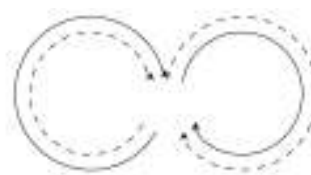
$$q_1 = -q_2 \longrightarrow \Delta \mathbf{r}_{gc2} = \Delta \mathbf{r}_{gc1}$$



the g.c. is moved of the same quantity and in the same direction!

■ Like Particles:

$$q_1 = q_2 \longrightarrow \Delta \mathbf{r}_{gc2} = -\Delta \mathbf{r}_{gc1}$$



just a position shift, no net diffusion!

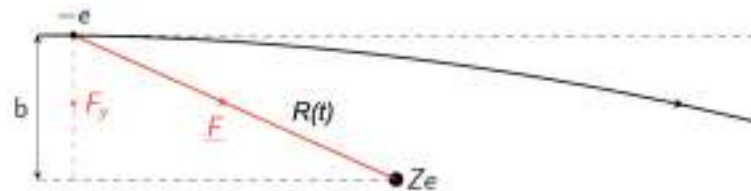
- Only e-i collisions contribute to particle diffusion;
- since  $m_e \ll m_i$  then:  $\Delta v_{e,\perp} \approx v_{e,\perp}$  and  $\Delta v_{i,\perp} \sim 0$ ;
- this gives:  $\Delta r_{gc} \approx \frac{mv_{e,\perp}}{eB} = r_{Le}$

$D$  evaluation still requires the e-i collision frequency  $\nu_{ei}$ .

# Coulomb collisions

In a fully ionized plasma charged particles have long range Coulomb interactions which dominate over collisions with neutrals.

- Consider an electron with initial velocity  $v_x = v$ :



- the force on the electron at the time  $t$  is:

$$F = \frac{Ze^2}{4\pi\epsilon_0 R^2(t)} \rightarrow F_y = \frac{Ze^2}{4\pi\epsilon_0 R^2(t)} \frac{b}{R(t)} = m_e \frac{dv_y}{dt}$$

- for small deflections:  $R^2 \approx b^2 + (vt)^2$ .

# Coulomb collisions - evaluation of $\Delta v_{\perp}$

- The velocity deflection along  $y$  is given by:

$$\Delta v_y = \frac{Ze^2 b}{4\pi\epsilon_0 m_e} \int_{-\infty}^{+\infty} \frac{1}{\sqrt{(b^2 + v^2 t^2)^3}} dt$$

- replace  $vt = b \cdot \sinh(\tau) \rightarrow dt = (b/v)\cosh(\tau)d\tau$  and use  $\cosh^2(\tau) - \sinh^2(\tau) = 1$ :

$$\begin{aligned}\Delta v_y &= \frac{Ze^2 b}{4\pi\epsilon_0 v m_e} \int_{-\infty}^{+\infty} \frac{d\tau}{\cosh^2(\tau)} = \frac{Ze^2}{4\pi\epsilon_0 v m_e b} [\tanh(\tau)]_{-\infty}^{+\infty} \\ &= \frac{Ze^2}{4\pi\epsilon_0 v m_e b} \left[ \frac{e^{2\tau} - 1}{e^{2\tau} + 1} \right]_{-\infty}^{+\infty} = \frac{Ze^2}{4\pi\epsilon_0 v m_e b} \frac{2}{b}\end{aligned}$$

- this result can be generalized to the perpendicular component of velocity variation  $\Delta v_{\perp}$ :

$$\Delta v_{\perp} = \frac{Ze^2}{4\pi\epsilon_0 v m_e} \frac{2}{b}$$

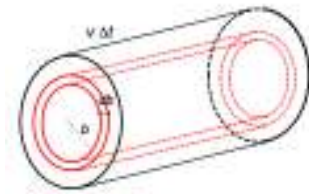
# Parallel force on the electron due to many collisions

- From energy conservation and small deflections  $(\Delta v_{||})^2 \sim 0$ :

$$(v + \Delta v_{||})^2 + (\Delta v_{\perp})^2 = v^2 \rightarrow (\Delta v_{||})^2 + 2v\Delta v_{||} + (\Delta v_{\perp})^2 = 0$$

$$\Delta v_{||} \approx -\frac{(\Delta v_{\perp})^2}{2v} \rightarrow \Delta v_{||} \approx -\frac{Z^2 e^4}{(4\pi\epsilon_0)^2 m_e^2 v^3} \frac{2}{b^2}$$

- the parallel force on the electron is  $F_{||} = m_e \Delta v_{||} / \Delta t$ ; sum up over all the collisions in the time  $\Delta t$  with ions of density  $n_i$  at the distance  $b$  i.e.  $dN_i = 2\pi b(db)n_i v \Delta t$ .



$$dF_{||} = dN_i \frac{m_e \Delta v_{||}}{\Delta t} = 2\pi m_e b n_i v \Delta v_{||} db$$

# Parallel force on the electron due to many collisions

- From energy conservation and small deflections  $(\Delta v_{||})^2 \sim 0$ :

$$(v + \Delta v_{||})^2 + (\Delta v_{\perp})^2 = v^2 \rightarrow (\Delta v_{||})^2 + 2v\Delta v_{||} + (\Delta v_{\perp})^2 = 0$$

$$\Delta v_{||} \approx -\frac{(\Delta v_{\perp})^2}{2v} \rightarrow \Delta v_{||} \approx -\frac{Z^2 e^4}{(4\pi\epsilon_0)^2 m_e^2 v^3} \frac{2}{b^2}$$

- the parallel force on the electron is  $F_{||} = m_e \Delta v_{||} / \Delta t$ ; sum up over all the collisions in the time  $\Delta t$  with ions of density  $n_i$  at the distance  $b$  i.e.  $dN_i = 2\pi b(db)n_i v \Delta t$ . Thus:

$$F_{||} = -2\pi m_e n_i v \frac{2Z^2 e^4}{(4\pi\epsilon_0)^2 m_e^2 v^3} \int_{b_{min}}^{b_{max}} \frac{1}{b} db$$

- $b_{max} \sim \lambda_D$  (Debye shielding)
- $b_{min}$  from small deflections condition i.e.  $|\Delta v_{||}| \leq |\Delta v_{\perp}|$ :

$$|\Delta v_{||}| = \frac{(\Delta v_{\perp})^2}{2v} \leq \Delta v_{\perp} \rightarrow \frac{Ze^2}{4v\pi\epsilon_0} \frac{2}{b} \leq 2v \rightarrow b \geq \frac{Ze^2}{4\pi\epsilon_0 v^2 m_e} = b_{min}$$

# The collision frequency $\nu_{ei}$

- The parallel force from the interaction with the ions is:

$$F_{\parallel} = -2\pi m_e n_i v \frac{2Z^2 e^4}{(4\pi\epsilon_0)^2 m_e^2 v^3} \ln \frac{\lambda_D}{b_{min}} = -\frac{4\pi n_i Z^2 e^4 \ln(\Lambda)}{(4\pi\epsilon_0)^2 m_e^2 v^3} m_e v$$

- $\ln(\Lambda) = \ln(\frac{\lambda_D}{b_{min}})$  is the Coulomb logarithm ( $\sim 15 - 20$ ).
- Define  $\nu_{ei} = \frac{n_i Z^2 e^4 \ln(\Lambda)}{4\pi\epsilon_0^2 m_e^2 v^3} \propto \frac{1}{T_e^{3/2}}$  so:

$$F_{\parallel} = m_e \frac{\Delta v_{\parallel}}{\Delta t} = -\nu_{ei} v m_e \rightarrow \Delta v_{\parallel} = -\nu_{ei} v \Delta t$$

in  $\Delta t = 1/\nu_{ei}$ ,  $\Delta v_{\parallel} = -v$  i.e. a deflection of  $90^\circ$ .

$\nu_{ei}$

The inverse of  $\nu_{ei}$  represents the time an electron takes to scatter  $90^\circ$  in velocity space due to the cumulative effect of small deflections.

# Neutral and charged particle trajectories

Neutral particle in a ionized gas:



Figure 2.1: The trajectory of a neutral particle in a partially ionized gas exhibits "straight-line" motion between abrupt atomic collisions. In this and the next figure, the (assumed stationary) random positions of "background" particles in the partially ionized plasma are indicated as follows: neutral particles (circles), electrons (minus signs) and ions (plus signs). The typical distance between neutral particle collisions is called the "collision mean free path."

Electron trajectory in a ionized gas:



Figure 2.2: The trajectory of a truly charged particle (electron) in a partially ionized gas shows the effects of the electric field due to the electron current. The linear motion occurs when there is no force due to nuclear charged particles. The "zig-zagging" of a charged particle is due mainly to the average effect of the many electric fields it passes through as it moves from one collision to the next.

from J.D. Callen, *Fundamentals of physics*

# Classical Diffusion coefficient

The classical diffusion coefficient  $D_{class}$  can be estimated as:

$$D_{class} = D_{\perp,i} = D_{\perp,e} \sim \frac{(\Delta x)^2}{\Delta t} \approx r_{Le}^2 \nu_{ei} = \left( \frac{mv}{eB} \right)^2 \frac{n_i Z^2 e^4 \ln(\Lambda)}{4\pi\epsilon_0^2 m_e^2 v^3} \propto \frac{1}{B^2 \sqrt{T_e}}$$

- ions and electrons diffuse at the same rate i.e. the transport is *intrinsically ambipolar*:  $\Gamma_i = \Gamma_e$ ;
- ambipolarity from momentum conservation during collisions;
- in other contexts  $D_i \neq D_e$  and a radial field  $E_r$  arises to balance the fluxes; the final  $D_{amb}$  is of the order of  $\min(D_e, D_i)$ ;

## Examples

$$B = 1T, n_e = 10^{20} m^{-3} \text{ and } T_e = 10keV, t = 1s$$

- $r_{Le} \approx 2.5 \cdot 10^{-4} m, \nu_{ei} \approx 5kHz$
- $d \sim \sqrt{D_{class} t} = r_{Le} \sqrt{\nu_{ei} t} \approx 1.8cm \quad \text{good, only few cm!}$

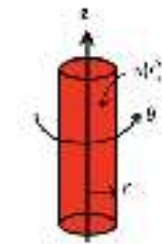
# MHD approach (1/2)

A more rigorous method to compute  $D_{class}$  by single fluid MHD.

- Fully ionized plasmas, cyl. geometry  $\partial_\theta = 0$ ,  $\partial_z = 0$ ;
- stationary equilibrium  $\partial_t = 0$ ;
- constant and uniform  $B$  along  $z$ ;

$$\mathbf{J} \times \mathbf{B} = \nabla p$$

$$\mathbf{E} + \mathbf{u} \times \mathbf{B} = \eta \mathbf{J}$$



- $\eta = \frac{m_e}{ne^2} < \nu_{ei} >$ , with  $< \dots >$  an average on velocity distribution ( $< \nu_{ei} > \approx 0.3\nu_{ei}$ );
- the components along  $r$  and  $\theta$  are:

$$\frac{dp}{dr} = J_\theta B$$

$$E_\theta - u_r B = \eta J_\theta$$

## MHD approach (2/2)

- note that  $E_\theta = 0$  ( $\nabla \times \mathbf{E} = 0$ ) thus:

$$\frac{dp}{dr} = J_\theta B = -\frac{u_r B^2}{\eta}$$

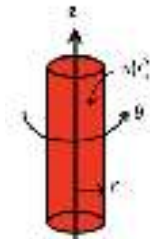
- since  $p = n(r)(T_e + T_i)$ , assuming constant  $T_{i,e}$ :

$$\nabla n(T_i + T_e) = -\frac{u_r B^2}{m_e \langle \nu_{ei} \rangle} e^2 n$$

- the radial flux is:

$$\Gamma_r = n u_r = - \langle \nu_{ei} \rangle \left( \frac{T_e m_e}{B^2 e^2} \right) \left( 1 + \frac{T_i}{T_e} \right) \nabla n = -D_{class} \nabla n$$

- which gives:  $D_{class} = r_{Le}^2 \langle \nu_{ei} \rangle \left( 1 + \frac{T_i}{T_e} \right)$



# Energy Transport

Like-particle (e-e, i-i) collisions do not contribute to net particle diffusion:

$$\langle \nu_{ee} \rangle \approx \frac{\langle \nu_{ei} \rangle}{n_i Z^2 / n_e} \quad \langle \nu_{ii} \rangle \approx \langle \nu_{ei} \rangle \sqrt{\frac{m_e}{m_i}}$$

They contribute to the heat flux  $Q = -\chi n \nabla T$  since their energy centroid ( $r_{cE} \propto (r_1 v_1^2 + r_2 v_2^2) / (v_1^2 + v_2^2)$ ) moves with a random walk:

$$\chi_{\parallel} \approx T/m\nu : T_e/m_e \nu_{ee} > T_i/m_i \nu_{ii} \rightarrow \chi_{e,\parallel} \sim \sqrt{m_i/m_e} \chi_{i,\parallel}$$

$$\chi_{\perp} \approx r_L^2 \nu : r_{Li}^2 \nu_{ii} > r_{Le}^2 \nu_{ee} \rightarrow \chi_{i,\perp} \sim \sqrt{m_i/m_e} \chi_{\perp,e}$$

## Examples

$B = 1T$ ,  $n_e = 10^{20} m^{-3}$  and  $T_e = 10 \text{keV} \rightarrow r_{Li} \approx 1 \text{cm}$ ,  $\nu_{ii} \approx 100 \text{Hz}$

$$D_{i,e} \approx \chi_{e,\perp} \sim 10^{-4} m^2/s, \chi_{i,\perp} \sim 10^{-2} m^2/s$$

■  $t = 1s \rightarrow d_E = \sqrt{\langle x^2 \rangle_E} \sim \sqrt{\chi_{\perp,i} t} = r_{Li} \sqrt{\nu_{ii} t} = 10 \text{cm}$

Good, we need a reactor with  $r$  of only  $\sim 50 - 100 \text{cm}$  radius! Or not?

# Summary on classical transport

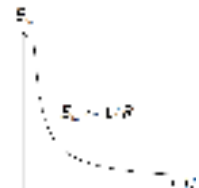
- Classical transport deals with particle/energy diffusion relative to a fully ionized plasmas in cylindrical geometry due to collisions.
- Only e-i Coulomb collisions contribute to the net particle diffusion.
- Intrinsic ambipolarity:  $\Gamma_e = \Gamma_i$ ,  $D_i = D_e = <\nu_{ei}> r_{Le}^2 \left(1 + \frac{T_i}{T_e}\right)$ .
- Perpendicular heat transport dominated by ions  $\chi_{i,\perp} \approx \nu_{ii} r_{Li}^2$  ( $\chi_{e,\perp} \approx \chi_{i,\perp} \sqrt{m_e/m_i}$ ) while the parallel one by electrons.
- Parallel transport in closed systems does not lead to losses.
- Efficient scaling with  $T$  and  $B$ :  $D, \chi \propto 1/\left(B^2 \sqrt{T}\right)$ .
- Classical diffusion is slow.
- Experimental measurements of diffusivities are quite larger!

# Neoclassical Transport

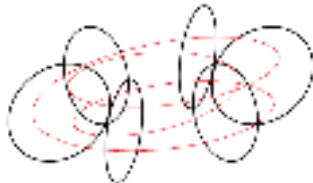
Real fusion devices are toroidal!

- Axisymmetry in Tokamaks:  $\partial_\phi = 0$ .
- The magnetic field depends on  $R = R_0 + r\cos(\theta)$ .
- Vertical drift due to  $R_c$  and  $\nabla B$ :

$$v_D = \frac{(v_{||}^2 + v_{\perp}^2/2)}{R_0\omega_c}$$



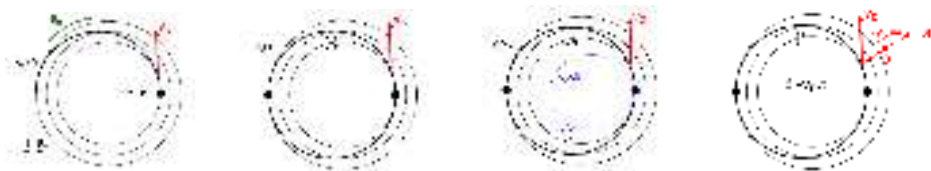
Vertical drift leads to charge separation and  $\mathbf{E} \times \mathbf{B}$  losses.



- add  $B_\theta$  (by a toroidal current);
- particles follow a helix;
- $q = \frac{d\phi}{d\theta} = \frac{rB_\phi}{R_0B_\theta}$ ;
- $q$ : number of toroidal turns for  $\Delta\theta = 2\pi$ ;
- distance along a field line:  $R_0 d\phi = q R_0 \Delta\theta$ .

## Passing particle trajectories ( $v_{\parallel} \gg v_{\perp}$ )

- With  $B_{\theta} \neq 0$  a particle still drifts vertically but the parallel motion along the helix moves it poloidally.
- This results in a closed shifted orbit with average displacement  $\sim \xi$ .



- suppose the particle collides at some point during the orbit: the g.c. is displaced with respect to  $\theta = 0$  of  $\sim \pm \xi$ ;
- the radial drift velocity is:  $v_{Dr} = v_D \sin(\theta) \approx v_D$ ;
- distance along  $\phi$  from  $\theta = 0$  to  $\pi/2$ :  $d = qR_0\pi/2 = \frac{\pi R_0 q}{2}$ ;
- corresponding time :  $\tau \approx \frac{\pi R_0 q}{2v_{\parallel}}$ .

# Neoclassical Diffusion coefficient

- The radial drift is  $\xi \approx v_D \tau \approx \frac{v_{\parallel}^2}{R_0 \omega_c} \frac{\pi R_0 q}{2v_{\parallel}} = \frac{v_{th} q m \pi}{2eB}$  with  $v_{\parallel} \sim v_{th}$ ;
- Coulomb collisions between un-like particles:  $\nu = \nu_{ei}$ ,  $\xi = \xi_e$ ;
- $\xi_e = \frac{\pi}{2} \frac{v_{th,e} m_e}{eB} q \approx r_{Le} q$ ;
- Evaluate  $D$  with  $\Delta x \sim \xi_e$  and  $\Delta t = 1/\nu_{ei}$ :

$$D_{NEO} = \frac{(\Delta x)^2}{\Delta t} \approx \nu_{ei} \xi_e^2 = q^2 r_{Le}^2 \nu_{ei} = D_{class} q^2$$

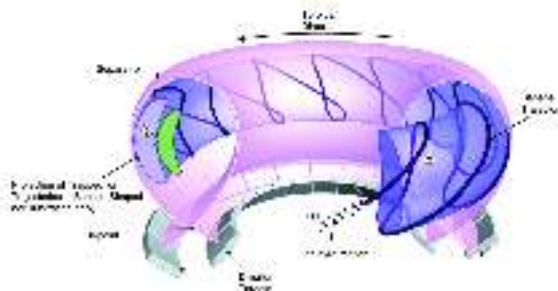
Note that:

- in Tokamaks  $q > 1$ , diffusion is higher than classical!
- Full derivation with MHD using  $B(r, \theta)$  gives:

$$D = \langle \nu_{ei} \rangle r_{Le}^2 (1 + q^2) \left( 1 + \frac{T_i}{T_e} \right) = D_{class} + D_{NEO} \left( 1 + \frac{T_i}{T_e} \right)$$

# Trapped particles ( $v_{\perp} \gg v_{\parallel}$ )

- $D_{NEO}$  ok for high collisionality but in fusion plasmas  $\nu_{ei} \propto 1/T_e^{3/2}$ ;
- particles are not all passing, a fraction might have  $v_{\parallel} = 0$  at some point and be reflected back (*trapped*);
- trapping condition + vertical drift  $v_D \rightarrow$  closed orbits with banana shape on the poloidal plane.
- By collisions a trapped particle might become passing and its g.c. is displaced of  $\sim$  banana width size.



# Fraction of trapped particles (1/2)

The fraction of trapped particles can be evaluated from magnetic moment and energy conservation:

$$\mu = \frac{mv_{\perp}^2}{2B}, \quad v^2 = v_{\parallel}^2 + v_{\perp}^2 = v_{\parallel,0}^2 + v_{\perp,0}^2, \quad v_{\parallel,0}, v_{\perp,0}(\theta = 0)$$

- Explicit  $B_{\phi} = \frac{R_0 B_0}{R} = \frac{R_0 B_0}{R_0 + r \cos \theta} = \frac{B_0}{1 + \epsilon \cos \theta} \approx B_0(1 - \epsilon \cos \theta)$ ,  $\epsilon = r/R_0$
- Conservation of magnetic moment,  $\mu = \text{constant}$ :

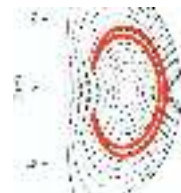
$$\begin{aligned} \frac{v_{\perp,0}^2}{1 - \epsilon} &= \frac{v_{\perp}^2}{1 - \epsilon \cos \theta} = \frac{v^2 - v_{\parallel}^2}{1 - \epsilon \cos \theta} \rightarrow v_{\parallel}^2 = v^2 \left[ 1 - \frac{v_{\perp,0}^2(1 - \epsilon \cos \theta)}{v^2(1 - \epsilon)} \right] \\ &\approx v^2 \left[ 1 - \frac{v_{\perp,0}^2}{v^2}(1 - \epsilon \cos \theta)(1 + \epsilon) \right] \approx v^2 \left[ 1 - \frac{v_{\perp,0}^2}{v^2} (1 + \epsilon(1 - \cos \theta) + o(\epsilon^2)) \right] \end{aligned}$$

## Fraction of trapped particles (2/2)

- since  $1 - \cos\theta = 2\sin^2\frac{\theta}{2}$ :

$$v_{\parallel}^2 = v^2 \left[ 1 - \frac{v_{\perp,0}^2}{v^2} \left( 1 + 2\epsilon \sin^2 \frac{\theta}{2} \right) \right]$$

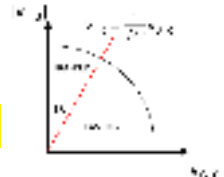
- consider a barely trapped particle  $v_{\parallel}^2 \leq 0$  at  $\theta = \pi$ :



$$1 - \frac{v_{\perp,0}^2}{v^2} (1 + 2\epsilon) \leq 0 \rightarrow \frac{v_{\parallel,0}^2 + v_{\perp,0}^2}{v_{\perp,0}^2} \leq 1 + 2\epsilon \rightarrow \frac{v_{\parallel,0}^2}{v_{\perp,0}^2} \leq 2\epsilon \rightarrow \left| \frac{v_{\parallel,0}}{v_{\perp,0}} \right| \leq \sqrt{2\epsilon}$$

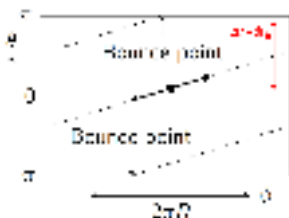
- isotropic velocity, trapped fraction is  $f_T \sim \alpha/(\pi/2)$ ;
- $\cot\alpha = 1/\sqrt{2\epsilon} \rightarrow \tan\alpha = \sqrt{2\epsilon}$  and for  $\epsilon \ll 1$ :

$$\tan(\alpha) \sim \alpha \sim \sqrt{2\epsilon} \rightarrow f_T \approx \frac{\sqrt{2\epsilon}}{\pi/2} \propto \sqrt{\epsilon}$$



# Bounce time and banana width

A trapped particle moves along the field with  $v_{\parallel} \approx v_{\perp}\sqrt{2\epsilon} \approx v_{th}\sqrt{2\epsilon}$  with also a vertical drift due to  $v_D$ .

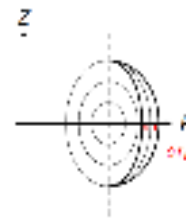


- A barely trapped particle moves from  $\theta = 0$  to  $\pi$  and back ( $\Delta\theta = 2\pi$ );
- from the distance in the toroidal direction  $2\pi R_0 q$  with velocity  $v_{\parallel} \approx v_{th}\sqrt{2\epsilon}$ :

$$t_b = \frac{2\pi R_0 q}{v_{th}\sqrt{2\epsilon}} \sim \frac{R_0 q}{v_{th}\sqrt{\epsilon}}$$

- banana width  $\delta r_b \approx v_D t_b$ :

$$\begin{aligned} \delta r_b &= \frac{v_{\parallel}^2 + v_{\perp}^2/2}{R_0 \omega_c} \frac{2\pi R_0 q}{v_{th}\sqrt{2\epsilon}} \approx \frac{m\pi q v_{th}^2}{eB v_{th}\sqrt{2\epsilon}} \\ &= \frac{\pi}{\sqrt{2}} \frac{q}{\sqrt{\epsilon}} \frac{v_{th} m}{eB} \approx \frac{qr_L}{\sqrt{\epsilon}} \end{aligned}$$



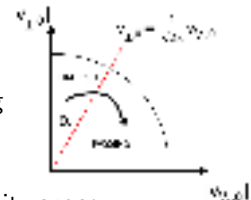
# Effective collision frequency

During the time  $t_b$  the particle drifts to a new surface at a distance  $\delta r_b$  from the original one.

- if at some point a collision occurs a trapped-passing conversion might happen with a step  $\delta r_b$  in g.c.;
- to become passing the particle doesn't need a  $\pi/2$  deflection but only to diffuse of  $\sim \alpha \sim \sqrt{2\epsilon}$  in velocity space;
- time for random walk in angular displacement  $t \propto \langle \alpha^2 \rangle$  (in analogy with  $t \propto \langle x^2 \rangle$ );
- the ratio for the respective collision times is thus:

$$\frac{t_{\text{trapped}}}{t_{\pi/2}} \propto \frac{\langle \alpha^2 \rangle}{(\pi/2)^2} \approx \frac{(\sqrt{2\epsilon})^2}{(\pi/2)^2} \approx \epsilon \rightarrow \frac{\nu_{\text{eff}}}{\nu_{ei}} = \frac{1}{\epsilon}$$

- larger collision frequency for trapped particles with respect to passing by a factor  $1/\epsilon$ .



# Banana particle and heat diffusion coefficients

The banana particle diffusion coefficient is:

$$D_{\text{ban}} = f_T \frac{(\Delta x)^2}{\Delta t} \approx f_T \delta r_b^2 \nu_{\text{eff}} = \sqrt{\epsilon} \frac{q^2 r_L^2 \nu}{\epsilon} \approx \frac{\nu_{ei} q^2 r_L^2}{\epsilon^{3/2}} \gg D_{\text{NEO}}.$$

- Axisymmetry ensures ambipolarity  $D_{\text{ban},i} \approx D_{\text{ban},e} = \frac{\nu_{ei} q^2 r_{Le}^2}{\epsilon^{3/2}}$ ;
- This is not true for energy where ions dominate:

$$\chi_{i,\perp} \sim \sqrt{\epsilon} \frac{\delta r_{b,i}^2 \nu_{ii}}{\epsilon} = \frac{q^2 r_{Li}^2 \nu_{ii}}{\epsilon^{3/2}}, \quad \chi_{e,\perp} \sim \sqrt{\epsilon} \frac{\delta r_{b,e}^2 \nu_{ei}}{\epsilon} = \frac{q^2 r_{Le}^2 \nu_{ee}}{\epsilon^{3/2}} = \chi_{i,\perp} \sqrt{\frac{m_e}{m_i}}$$

## Examples

For  $B = 1 T$ ,  $n_e = 10^{20} m^{-3}$ ,  $T = 10 \text{ keV}$ ,  $q = 2$ ,  $\epsilon = 0.1$ :

$$\delta r_{b,e} \approx 1.5 \text{ mm}, \quad \delta r_{b,i} \approx 6 \text{ cm}$$

$$D_{i,e} \approx \chi_{e,\perp} \sim 10^{-2} \text{ m}^2/\text{s}, \quad \chi_{i,\perp} \sim 1 \text{ m}^2/\text{s}$$

$$t = 1 \text{ s} \rightarrow d_E \sim \sqrt{t \chi_i} \sim \sqrt{t \nu_{\text{eff}} f_T \delta r_{b,i}} = 100 \text{ cm} \geq 10 d_{E,\text{class}}$$

## Definition of $\nu^*$

A useful quantity to characterize transport regimes in magnetic fusion devices is the collisionality  $\nu^*$  defined as:

$$\nu^* = \frac{t_b}{1/\nu_{eff}} \approx \frac{\nu_{ei} R_0 q}{\epsilon^{3/2} v_{th,e}} \propto \frac{n_e R_0 q}{\epsilon^{3/2} T_e^2}$$

which compares the banana orbit bounce time with the collision time.

- for  $\nu^* \ll 1 \rightarrow \nu_{eff} \ll 1/t_b$  trapped particles can complete many banana orbits before collide; the characteristic  $D$  is :

$$D_{ban} = \frac{\nu_{ei} r_{Le}^2 q^2}{\epsilon^{3/2}} = r_{Le}^2 \frac{\nu_{ei} R_0 q}{v_{th,e} \epsilon^{3/2}} \frac{q v_{th,e}}{R_0} = \frac{\nu^* v_{th,e} q r_{Le}^2}{R_0}$$

- at high collisionality both trapped/passing particles cannot complete their orbits before scattering since the time for a poloidal turn  $\tau_p \sim \frac{R_0 q}{v_{th}}$  is much longer of the collision time  $1/\nu_{ei}$ :

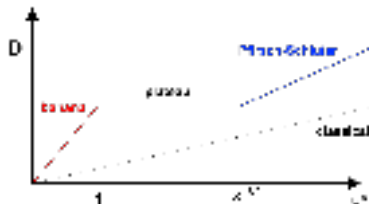
$$\nu_{ei} \tau_p \gg 1 \rightarrow \frac{\nu_{ei} R_0 q}{v_{th,e}} \gg 1 \rightarrow \nu^* \epsilon^{3/2} \gg 1 \rightarrow \nu^* \gg \epsilon^{-3/2}$$

# Diffusion regimes

- $\nu^* \gg \epsilon^{-3/2}$  corresponds to high collisional regime (*Pfirsch-Schluter*):

$$D_{PS} = D_{NEO} = \nu_{ei} r_{Le}^2 q^2 = \frac{\nu_{ei} q R_0}{\nu_{th,e} \epsilon^{3/2}} \frac{r_{Le}^2 q}{R_0} \nu_{th,e} \epsilon^{3/2} = \nu^* \nu_{th,e} \epsilon^{3/2} \frac{r_{Le}^2 q}{R_0}$$

- $\nu^* = 1 \rightarrow D_{ban} = r_{Le}^2 \frac{\nu_{th,e} q}{R_0}$
- $\nu^* = \epsilon^{-3/2} \rightarrow D_{PS} = r_{Le}^2 \frac{\nu_{th,e} q}{R_0}$
- *Plateau regime* for  $1 \leq \nu^* \leq \epsilon^{-3/2}$ : only passing particles can complete their orbits.

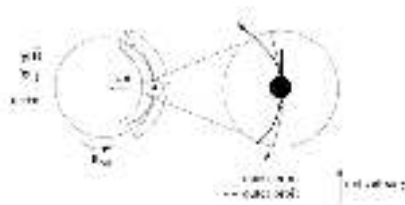


$$\begin{aligned} \nu_{th} &\propto \sqrt{T} \\ \nu_{ei} &\propto n/T^{3/2} \end{aligned} \rightarrow \nu^* \propto \frac{n}{T^2}$$

Trapped particles and banana regime dominant in hot Tokamaks!

## Banana current

Trapped particles are important in Tokamak also because they generate a toroidal current which contributes to the poloidal magnetic field.



- $n(r)$  decreases from the core → on a given flux surface more trapped particles circulate in the inner side;
- net flow in the toroidal direction;
- parallel current along the field lines  $J_{ban} \approx v_{\parallel} e \Delta n$

Since  $v_{\parallel} \sim v_{th} \sqrt{\epsilon}$  and  $\Delta n = \delta r_b \frac{d(n\sqrt{\epsilon})}{dr}$ :

$$J_{ban} = \delta r_b e v_{th} \sqrt{\epsilon} \frac{dn}{dr} \sqrt{\epsilon} = \frac{qr_L}{\sqrt{\epsilon}} e v_{th} \frac{dn}{dr} \epsilon = \frac{dn}{dr} \sqrt{\epsilon} v_{th} e \frac{r B_\phi}{R_0 B_\theta} \frac{m v_{th}}{e B_\phi} =$$

$$\frac{dn}{dr} \sqrt{\epsilon} v_{th}^2 \frac{rm}{R_0 B_\theta} = \frac{dn}{dr} \sqrt{\epsilon} \frac{T}{m} \frac{r}{R_0} \frac{m}{B_\theta} = \epsilon^{3/2} \frac{dn}{dr} \frac{T}{B_\theta}$$

# Bootstrap current

Trapped particles are in collisional equilibrium with the passing ones to which they transfer their momentum.

- The rate of transfer of parallel momentum by trapped particles for unit of time and volume is:  $\Delta P_{\parallel,t} = mv_{\parallel,t}(\Delta n)\nu_{eff} = mJ_{ban}/e$
- Collisions between passing particles with density  $n_p$  redistribute the momentum  $mv_{\parallel,p}$  with frequency  $\nu_{ei}$ :  $\Delta P_{\parallel,p} = mv_{\parallel,p}n_p\nu_{ei}$ .
- At the equilibrium:  $\Delta P_{\parallel,t} = \Delta P_{\parallel,p}$ :

$$mv_{\parallel,p}n_p\nu_{ei} = mv_{\parallel,t}\Delta n\nu_{eff} \rightarrow v_{\parallel,p}n_p = \frac{J_{ban}\nu_{eff}}{e\nu_{ei}}$$

$$J_{BS} = v_{\parallel,p}n_p e = J_{ban}\nu_{eff}/\nu_{ei} \rightarrow J_{BS} = J_{ban}/\epsilon$$

- Replacing the expression for  $J_{ban}$ :  $J_{BS} = \epsilon^{3/2} \frac{dn}{dr} \frac{T}{B_\theta} \frac{1}{\epsilon} = \boxed{\epsilon^{1/2} \frac{dn}{dr} \frac{T}{B_\theta}}$
- Collisions have a crucial role but do not appear in the result for  $J_{BS}$ .
- $J_{BS}$  mostly carried by passing particles but caused by those trapped.

# Bootstrap current in Tokamaks

Also the temperature gradient contributes to the banana current: if particles move faster on the inner than on the outer banana orbit, this generates a further toroidal current. The full computation leads to:

$$\langle \mathbf{J}_{BS} \cdot \mathbf{B} \rangle = \sqrt{2\epsilon} f(\psi) p(\psi) \left[ \frac{a_1}{n} \frac{\partial n}{\partial \psi} + \frac{a_2}{T_e} \frac{\partial T_e}{\partial \psi} + \frac{a_3}{T_i} \frac{\partial T_i}{\partial \psi} \right]$$

with  $\psi$  a flux function (e.g. toroidal flux) and  $a_{1,2,3}$  coefficients depending on geometry and collisionality. Advantages of  $J_{BS}$ :

- provides poloidal field;
- allows steady state operation reducing the current externally driven;

$$\frac{J_{BS}}{J_{OH}} \sim \frac{\sqrt{\epsilon} p}{B_\theta a} \frac{\pi a^2}{I_p} = \frac{\sqrt{\epsilon} p}{B_\theta r} \frac{\pi a^2 \mu_0}{B_\theta 2\pi a} = \sqrt{\epsilon} \frac{p}{4B_\theta^2/(2\mu_0)} \sim \sqrt{\epsilon} \beta_p$$

- $\beta_p \sim 1$ ,  $\epsilon = 0.3 - 0.4 \rightarrow J_{BS}/J_{OH} \sim 1/2$ ; in advanced scenario (JT-60,ITER) it can provide most of the current (60% – 80%).

# Summary of Neoclassical transport

- Neoclassical transport is the minimum achievable in fusion devices with toroidal geometry.
- Passing particles have a diffusion coefficient  $D_{NEO} \approx \nu_{ei} r_{Le}^2 q^2$ .
- Trapped particles move on banana shape orbits and increase the transport by a factor  $\sim (r/R_0)^{-3/2}$ .
- Intrinsic ambipolarity for axisymmetric systems and  $D \sim D_e$ .
- Heat transport dominated by ions with  $\chi_{i,\perp} \sim \delta r_{bi}^2 \nu_{ii} / \sqrt{\epsilon}$ .
- The values of  $n$  and  $T$  determine  $\nu^*$  and the particle diffusion regime: the banana regime is dominant at high temperature.
- Trapped particles are at the origin of the bootstrap current which can provide a significative fraction of the poloidal magnetic field.
- Higher diffusivities than neoclassical predictions are experimentally measured → anomalous transport.

# Stellarators

The poloidal field is a key element in axisymmetric devices to avoid the losses due to the vertical drift but is generated by driving a current: this is a *free energy* source which can trigger several kind of instabilities (current driven modes).

How can we twist the field lines without driving a current?

- A deformation (torsion) in 3D of the magnetic axis;
- Poloidally elongated and rotated magnetic surfaces in the toroidal direction;

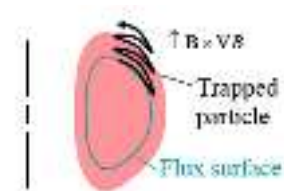
These systems are named Stellarators.



# Stellarators

## Advantages:

- steady state (no current needs to be driven);
- no instabilities like sawteeth, ELMS, disruption
- no density limit;



## Drawbacks:

- more complex geometry and coils design;
- no conservation of canonical momentum  $p_\phi = mv_\phi + e\psi$  ( $\partial_\phi \neq 0$ ): particles trajectories are not closed and can radially drift outward, also without collisions.

→ high level of neoclassical transport!

→ optimization required to reduce the particles drift!

# Toroidal and Helical ripple

In flux coordinates, the particle guiding center motion is determined by  $B(s, \theta, \zeta) = |\mathbf{B}|$ , with  $s$  a flux label (e.g.  $\propto \sqrt{\psi}$ ).

In general:  $B = \sum_{m,n} B_{m,n}(s) \cos(m\theta - n\zeta)$  or:

$$B = B_{00} + \sum_{m \neq 0, n=0} B_{m,0} \cos(m\theta) + \sum_{m \neq 0, n \neq 0} B_{m,n} \cos(m\theta - n\zeta) = \\ B_{00} \left[ 1 + \sum_{m \neq 0, n=0} \frac{B_{m,0}}{B_{00}} \cos(m\theta) + \sum_{m \neq 0, n \neq 0} \frac{B_{m,n}}{B_{00}} \cos(m\theta - n\zeta) \right]$$

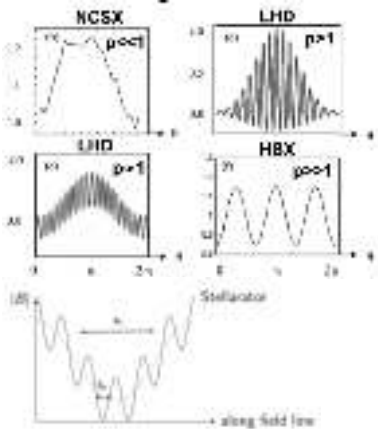
In many cases:  $B \sim B_{00} [1 - \epsilon_t(s)c(\theta) - \epsilon_h(s)f(M\theta - N\zeta)]$

- $\epsilon_t, \epsilon_h$  are flux surface averages;
- $\epsilon_t(s) \sim B_{m,0}$ : toroidal ripple ( $n = 0, m \neq 0$ );  
in a Tokamak  $\rightarrow \epsilon_t = \epsilon = r/R_0$ ,  $c(\theta) = \cos(\theta)$ ,  $B_{00} = B(R_0)$ ;
- $\epsilon_h(s) \sim B_{m,n}$ : helical ripple ( $n \neq 0, m \neq 0$ ).

# Examples

The ratio  $p = \epsilon_h/\epsilon_t$  estimates the distance from axisymmetry.

*B along a field line:*



from H.E. Mynick, Phys. Plasmas 13 (2006)

- $p \ll 1 \rightarrow$  quasi-axisymmetric stellarator;
- $p \gg 1 \rightarrow$  quasi-helical stellarator;
- $p = 0 \rightarrow$  Tokamak;
- $p = \infty \rightarrow$  helical stellarator.
  
- trapped particles like in tokamaks due to toroidicity;
- in stellarator other harmonics arise; particles get trapped also in local minima  $\rightarrow$  *superbananas*.

# Neoclassical Transport in Stellarators: $1/\nu$ regime

Superbanana drifts are important at low collisionality; the diffusion coefficient can be estimated replacing  $\epsilon_t = \epsilon$  with  $\epsilon_h$ . For electrons:

- effective collision frequency  $\nu_{\text{eff}} \approx \nu_e / \epsilon_h$ ;
- fraction of trapped particles in local minima :  $f_T \sim \sqrt{\epsilon_h}$ ;
- no closed orbits! in  $\Delta t = 1/\nu_{\text{eff}}$  the radial drift is  $\Delta r = v_D / \nu_{\text{eff}}$ ;

$$D_e = f_T \frac{(\Delta r)^2}{\Delta t} \approx \sqrt{\epsilon_h} v_D^2 \frac{\epsilon_h}{\nu_e} = \frac{\epsilon_h^{3/2}}{\nu_e} \left( \frac{v_{th,e}^2}{\omega_c R_0} \right)^2 = \frac{\epsilon_h^{3/2}}{\nu_e} \frac{v_{th,e}^4 m_e^2}{e^2 B^2 R_0^2}$$

$$\propto \epsilon_h^{3/2} \frac{\sqrt{m_e} T_e^2}{e^2 B^2 R_0^2} \frac{T_e^{3/2}}{n_e} \approx \epsilon_h^{3/2} \frac{\sqrt{m_e} T_e^{7/2}}{n_e B^2 R_0^2}$$

Note:

- $1/\nu_e$  regime and  $\Delta r \sim$  system scale length;
- strong  $T_e$  scaling: losses dominate at high temperature!
- higher values for ions: ambipolarity requires a radial electric field  $E_r$ !

# Neoclassical Transport in Stellarators: $\sqrt{\nu}$ regime

The ambipolar electric field  $E_r$  is negative since must prevent ions from diffusing to the wall and generates a poloidal  $\mathbf{E} \times \mathbf{B}/B^2$  drift.

- ions drift poloidally with a frequency  $\Omega_E \sim \frac{E_r}{rB}$ ;
- the radial distance traveled in the time  $1/\Omega_E$  is  $\Delta r \sim v_D/\Omega_E$ ;
- collisions make the ions move randomly out and in the local minima in a time  $t \propto (\alpha)^2$  with  $\alpha$  the distance from the trapping boundary in velocity space so that  $\nu_{\text{eff}} = \nu_i/(\alpha)^2$ ,  $f_T \sim \alpha$ ;
- $D_i \sim f_T(\Delta r)^2 \nu_{\text{eff}} = (\alpha) \frac{v_D^2}{\Omega_E^2} \frac{\nu_i}{(\alpha)^2} = \frac{v_D^2}{\Omega_E^2} \frac{\nu_i}{(\alpha)}$ ;
- condition for low collisionality:  $\nu_{\text{eff}} < \Omega_E$  gives  $\alpha \geq \left(\frac{\nu_i}{\Omega_E}\right)^{1/2}$ ;
- replacing in  $D_i$ :

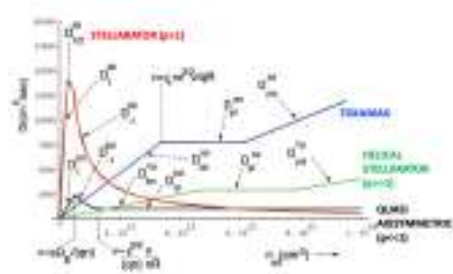
$$D_i = \frac{v_D^2 \nu_i}{\Omega_E^{3/2} \nu_i^{1/2}} = \frac{v_D^2 \sqrt{\nu_i}}{\Omega_E^{3/2}}$$

$E_r < 0 \rightarrow$  electrons in  $1/\nu$  regime while ions in  $\sqrt{\nu}$ .

# Optimization

Optimization reducing the drift:

- in presence of a symmetry a canonical momentum is conserved  
→ limit the deviation of particles from flux surfaces;
- make the radial drift average-out over a bounce orbit (*omnigeneous systems*).

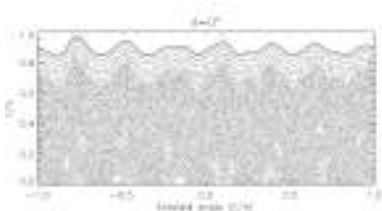


from H.E. Mynick, Phys. Plasmas 13 (2006)

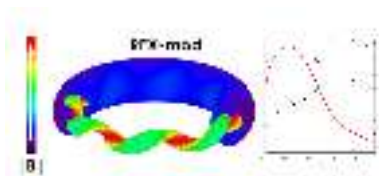
Ambipolarity  $\sum q_s \Gamma_s(r) = 0$  determines three solutions for  $E_r(r)$ :

- one unstable;
- $E_r < 0$ : ion root;
- $E_r > 0$ : electron root, large  $\Omega_E$  and transport reduction;  
→ optimization forcing the system in the electron root (ECRH, NBI).

# Transport in the Reversed Field Pinch (RFP)



- $B_T \approx B_P$ ,  $q \ll 1$ ;
- + resonant kink tearing modes  $\tilde{b}$ ;
- at low  $I_p$ : Multiple Helicity, no conserved flux surfaces → transport dominated by magnetic chaos  $D, \chi \propto (\tilde{b}/B)^{1.5}$   
( $D \sim 10 - 20 m^2/s$ );
  
- at high  $I_p$ : helical topology in the core;
- reduction of magnetic chaos and eITB formation;
- no superbanana  $1/\nu$  regime;
- neoclassical estimates:  $D_{ITB} < 0.5 m^2/s$ ,  
 $\chi_{e,ITB} \sim 1 m^2/s$ ;



Experimentally residual magnetic chaos still enhances particle/energy transport:  $D_{ITB} \sim 1 m^2/s$ ,  $\chi_{e,ITB} \sim 5 m^2/s$

# The kinetic theory

Kinetic theory provides a rigorous description of transport, commonly used to study several phenomena in plasma physics.

- A distribution function  $f(\mathbf{x}, \mathbf{v}, t)$  describes the particle density in a  $6D$  space with coordinates  $(x, y, z, v_x, v_y, v_z)$  at the time  $t$ ;
- the number of particles  $dN$  in the small  $6D$  volume  $dV = d\mathbf{x}d\mathbf{v}$  at  $(\mathbf{x}, \mathbf{v})$  at the time  $t$  is  $dN = f(\mathbf{x}, \mathbf{v}, t)d\mathbf{x}d\mathbf{v}$ ;
- every species  $\alpha$  has its own distribution  $f_\alpha$ ;
- $dV = d\mathbf{x}d\mathbf{v}$  contains a large number of particles.

Consider a volume  $V$  with surface  $S$  in  $6D$  space; without collisions, a variation of the number of particles in the volume  $V$  corresponds to a flux  $\Gamma = f\mathbf{U}dS$  across the surface  $S$ , where  $\mathbf{U} = (\dot{\mathbf{x}}, \dot{\mathbf{v}})$ :

$$\frac{\partial N}{\partial t} = - \int_S \Gamma ds \rightarrow \frac{\partial}{\partial t} \int_V f(\mathbf{x}, \mathbf{v}, t) d\mathbf{x}d\mathbf{v} = - \int_S f\mathbf{U}dS$$

# The Vaslov equation

The divergence theorem gives:

$$\int_V \left[ \frac{\partial f}{\partial t} + \nabla \cdot (f \mathbf{U}) \right] d\mathbf{x} d\mathbf{v} = 0$$

Note that:

- $\nabla \cdot (f \mathbf{U}) = \nabla f \cdot \mathbf{U} + f \nabla \cdot \mathbf{U}$
- $\nabla f \cdot \mathbf{U} = \nabla_x f \cdot \mathbf{v} + \nabla_{\mathbf{v}} f \cdot \dot{\mathbf{v}}$
- $f \nabla \cdot \mathbf{U} = f \nabla_x \cdot \mathbf{v} + f \nabla_{\mathbf{v}} \cdot \dot{\mathbf{v}} = 0 + f \nabla_{\mathbf{v}} \cdot \dot{\mathbf{v}}, \quad \dot{\mathbf{v}} = \mathbf{F}/m$
- $f \nabla_{\mathbf{v}} \cdot (\mathbf{F}/m) = 0$  if  $\mathbf{F} = q(\mathbf{E} + \mathbf{v} \times \mathbf{B})$ .

Thus we obtain the Vaslov equation:

$$\frac{\partial f}{\partial t} + \nabla_x f \cdot \mathbf{v} + \nabla_{\mathbf{v}} f \cdot \frac{q}{m} (\mathbf{E} + \mathbf{v} \times \mathbf{B}) = 0$$

and, once known  $f$ , the density  $n(\mathbf{x}, t)$  is given by:

$$n(\mathbf{x}, t) = \int f(\mathbf{x}, \mathbf{v}, t) d\mathbf{v}$$

# Collision operator

The Vaslov equation must be solved together with Maxwell equations using the density charge  $\rho_q$  and the density current  $\mathbf{J}$  self-consistently computed from  $f$ :

$$\rho_q = \sum_{\alpha} q_{\alpha} \int f_{\alpha} d\mathbf{v}, \quad \mathbf{J}(\mathbf{x}, t) = \sum_{\alpha} q_{\alpha} \int \mathbf{v} f_{\alpha} d\mathbf{v}$$

$$\nabla \times \mathbf{E} = -\frac{\partial \mathbf{B}}{\partial t} \quad \nabla \cdot \mathbf{E} = \rho_q / \epsilon_0 \quad \nabla \cdot \mathbf{B} = 0 \quad \nabla \times \mathbf{B} = \epsilon_0 \mu_0 \frac{\partial \mathbf{E}}{\partial t} + \mu_0 \mathbf{J}$$

- Vaslov equation is correct when studying phenomena evolving more rapidly than typical collision times.
- Collisions are included with a term  $(\partial f / \partial t)_c$  i.e. the particles variation per unit of time due to collisions with other species:

$$\frac{\partial f}{\partial t} + \nabla_{\mathbf{x}} f \cdot \mathbf{v} + \nabla_{\mathbf{v}} f \cdot \frac{q}{m} (\mathbf{E} + \mathbf{v} \times \mathbf{B}) = \left( \frac{\partial f}{\partial t} \right)_c$$

# Macroscopic quantities

Macroscopic parameters can be obtained by averages, like done for  $n$ :

- mean flow  $\mathbf{V}(\mathbf{x}, t) = \frac{1}{n} \int f \mathbf{v} d\mathbf{v}$  and particle flux  $\Gamma = \int f \mathbf{v} d\mathbf{v}$ ;
- pressure  $p(\mathbf{x}, t) = nT = \int f \frac{mv_r^2}{3} d\mathbf{v}, \quad \mathbf{v}_r = \mathbf{v} - \mathbf{V};$
- stress tensor:  $\pi(\mathbf{x}, t) = \int f m (\mathbf{v}_r \mathbf{v}_r - v_r^2 \mathbf{I}) d\mathbf{v}, \quad \mathbf{I} = \text{identity tensor}$
- conductive heat flux:  $\mathbf{q}(\mathbf{x}, t) = \int f \mathbf{v}_r \frac{mv_r^2}{2} d\mathbf{v};$
- the frictional force density:  $\mathbf{R} = \int d\mathbf{v} m \mathbf{v} \left( \frac{\partial f}{\partial t} \right)_c;$
- the collisions energy exchange:  $Q = \int d\mathbf{v} \frac{mv_r^2}{2} \left( \frac{\partial f}{\partial t} \right)_c;$

with their time evolution given by:

$$\int d\mathbf{v} g(\mathbf{v}) \left[ \frac{\partial f}{\partial t} + \nabla_{\mathbf{x}} f \cdot \mathbf{v} + \nabla_{\mathbf{v}} f \cdot \frac{q}{m} (\mathbf{E} + \mathbf{v} \times \mathbf{B}) - \left( \frac{\partial f}{\partial t} \right)_c \right] = 0$$

using different expression for  $g(\mathbf{v}) \propto \mathbf{v}^k$ .

# Moments

- $g(\mathbf{v}) = 1$ , continuity equation:

$$\frac{\partial n}{\partial t} + \nabla(n\mathbf{V}) = 0$$

- $g(\mathbf{v}) = m\mathbf{v}$ , motion equation:

$$mn\frac{\partial \mathbf{V}}{\partial t} = nq[\mathbf{E} + \mathbf{V} \times \mathbf{B}] - \nabla p - \nabla \cdot \boldsymbol{\pi} + \mathbf{R}$$

- $g(\mathbf{v}) = mv^2/2$ , heat transport:

$$\frac{3}{2}\frac{\partial p}{\partial t} + \frac{5}{2}p\nabla \cdot \mathbf{V} = -\nabla \cdot \mathbf{q} - \boldsymbol{\pi} : \nabla \mathbf{V} + Q$$

- higher moments have not a clear physical meaning;
- the system is not closed; at zero order  $n$  and  $\mathbf{V}$  are unknown, at first order also  $p = nT$  and  $\boldsymbol{\pi}$ , etc...

# Moments closure

- A closure can be obtained assuming a relation between  $\pi, \mathbf{q}, \mathbf{R}, Q, \Gamma \dots$  and  $n, T, \mathbf{V}$  phenomenologically.
- If variations are slow also kinetic methods can be used with  $f = f_0 + f_1$ ,  $f_0 = f_M(n, \mathbf{V}, T)$  a Maxwellian, and  $f_1 \ll f_0$ ;
- replacing  $f_0 + f_1$  in the K.E. and neglecting terms  $o(f_1^2)$  a new equation for  $f_1$  is obtained depending on spatial derivates of flow and temperature which describe the deviation from the Maxwellian;
- $f_1$  is used to calculate  $\pi, \mathbf{q}, \mathbf{R}, Q, \Gamma \dots$  which result proportional to the effects causing the deviations from  $f_0$  (e.g.  $Q \propto \nabla T, \Gamma \propto \nabla n$ );
- the corresponding coefficients of proportionality are called the *transport coefficients* and their determination is the basic goal of kinetic theory.
- An example of solution obtained by Braginskii (see Review of Plasma Physics 1, 205 (1965)).

# The Bhatnagar, Gross and Krook model (BGK)

A simple model for the collision operator:

- *Lorentz gas*: electrons scatter off infinitely heavy and stationary ions;
- at the equilibrium  $f_0 = n \left( \frac{m}{2\pi T} \right)^{3/2} e^{-m \frac{(v-v)^2}{2T}}$ ;
- deviation from equilibrium by small external perturbations;
- collisions drive  $f$  towards the equilibrium (BGK):

$$\left( \frac{\partial f}{\partial t} \right)_c = -\nu_c (f - f_0)$$

An example: the determination of resistivity.

- Apply an electric field  $\mathbf{E}$  in the  $x$  direction;
- Linearize the steady state K.E. with  $f = f_0 + f_1$ , assuming isotropy in space and  $\mathbf{V} = 0$ ; only terms  $\sim \mathbf{E} \sim f_1$  and note:  $\nabla_{\mathbf{v}} f_0 = -m \frac{\mathbf{v}}{T} f_0$

$$\frac{q\mathbf{E}}{m} \cdot \nabla_{\mathbf{v}} f_0 = -\nu_c f_1 \rightarrow \frac{q\mathbf{E}}{m} \cdot \frac{m\mathbf{v}}{T} f_0 = \nu_c f_1 \rightarrow f_1 = \frac{q\mathbf{E}}{T\nu_c} \cdot \mathbf{v} f_0$$

# Resistivity

Ohm law:  $\mathbf{E} = \eta \mathbf{J}$  used to determine the value of  $\eta$ .

- $\mathbf{J} = q \int f_1 \mathbf{v} d\mathbf{v} = \frac{q^2 \mathbf{E}}{T \nu_c} \cdot \int f_0 \mathbf{v} \mathbf{v} d\mathbf{v}$  (dyadic dot product);
- $\mathbf{E} \cdot \mathbf{v} = \sum_k E_k v_k = E v_x^2 \mathbf{e}_x + E v_x v_y \mathbf{e}_y + E v_x v_z \mathbf{e}_z$  ( $E_{y,z} = 0$ );
- the integral in space velocity is:

$$\int f_0 v_x v_y d\mathbf{v} = \int f_0 v_x v_z d\mathbf{v} = 0$$

$$\int f_0 v_x^2 d\mathbf{v}_x d\mathbf{v}_y d\mathbf{v}_z = n \left( \frac{m}{2\pi T} \right)^{3/2} \int e^{-m \frac{v_x^2}{2T}} v_x^2 d\mathbf{v}_x \int e^{-m \frac{v_y^2}{2T}} d\mathbf{v}_y \int e^{-m \frac{v_z^2}{2T}} d\mathbf{v}_z$$

- with  $v_k = s \sqrt{2T/m}$ :

$$\begin{aligned} n \left( \frac{m}{2\pi T} \right)^{3/2} \left( \frac{2T}{m} \right)^{3/2} \frac{2T}{m} \left( \int e^{-s^2} ds \right)^2 \int e^{-s^2} s^2 ds &= \frac{2Tn\pi}{m\pi^{3/2}} \int e^{-s^2} s^2 ds \\ &= \frac{2Tn}{m} \frac{1}{\sqrt{\pi}} \int (-2s) e^{-s^2} \frac{s}{2} ds = \frac{2Tn}{m} \frac{1}{\sqrt{\pi}} \frac{\sqrt{\pi}}{2} = \frac{Tn}{m} \end{aligned}$$

- $\mathbf{J} = \frac{q^2 \mathbf{E}}{T \nu_c} \frac{Tn}{m} \rightarrow \eta = \frac{m \nu_c}{n q^2}$

# Diffusion coefficient in a plasma with $\mathbf{B}=0$

To study particle diffusion we assume a spatial profile for the density in the initial Maxwellian so that:

$$f_0 = n(\mathbf{r}) \left( \frac{m}{2\pi T} \right)^{3/2} e^{-m\frac{\mathbf{v}^2}{2T}}$$

Assuming  $\mathbf{F} = 0$  the linearized kinetic equation becomes:

$$\mathbf{v} \cdot \nabla_{\mathbf{r}} f_0 = -\nu_c f_1 \rightarrow \frac{f_0}{n} \mathbf{v} \cdot \nabla_{\mathbf{r}} n = -\nu_c f_1 \rightarrow f_1 = -\frac{f_0}{n\nu_c} \mathbf{v} \cdot \nabla_{\mathbf{r}} n$$

and the flux of particles is given by:

$$\Gamma = \int f_1 \mathbf{v} d\mathbf{v} = -\frac{1}{n\nu_c} \nabla_{\mathbf{r}} n \int f_0 \mathbf{v} \mathbf{v} d\mathbf{v}$$

The integral in space velocity gives  $Tn/m$  so :

$$\Gamma = -\frac{T}{m\nu_c} \nabla_{\mathbf{r}} n \rightarrow D = \frac{T}{m\nu_c}$$

# Fokker-Planck collision operator

A general formulation for treating variations in the distribution function due to many collisional events producing small changes in the velocity.

- The starting point is the assumption that the distribution function at the time  $t$  depends on its value at the time  $t - \Delta t$  i.e.:

$$f(\mathbf{v}, t) = \int f(\mathbf{v} - \Delta\mathbf{v}, t - \Delta t) \phi(\mathbf{v} - \Delta\mathbf{v}, \Delta\mathbf{v}) d^3 \Delta\mathbf{v}$$

- $\phi(\mathbf{v}, \Delta\mathbf{v})$  is the probability that a particle with velocity  $\mathbf{v}$  acquires an increment of  $\Delta\mathbf{v}$  in the time  $\Delta t$ .
- From this definition the rate of change for  $f$  due to collisions can be derived and is called the Fokker-Planck collisional operator:

$$\begin{aligned} \left( \frac{\partial f}{\partial t} \right)_c &= \frac{f(\mathbf{v}, t) - f(\mathbf{v}, t - \Delta t)}{\Delta t} = \\ &- \frac{\partial}{\partial \mathbf{v}} \left( \frac{d \langle \Delta\mathbf{v} \rangle_f}{dt} \right) + \frac{1}{2} \frac{\partial^2}{\partial \mathbf{v} \partial \mathbf{v}} : \left( \frac{d \langle \Delta\mathbf{v} \Delta\mathbf{v} \rangle_f}{dt} \right) \end{aligned}$$

# Drift-kinetic equation

When the gyro-radius is much smaller than the system scale length ( $r_L \ll L$ ), a change of variable can be performed considering the g.c. motion:  $(\mathbf{x}, \mathbf{v}) \rightarrow (\mathbf{x}_{gc}, \mu, \epsilon_{gc}, \varphi)$ ; by a gyro-averaging procedure the evolution for the g.c. distribution  $f_{gc}$  is given by:

$$\frac{\partial f_{gc}}{\partial t} + (\mathbf{v}_{\parallel} \mathbf{b} + \mathbf{v}_{d\perp}) \cdot \nabla f_{gc} + \frac{d\epsilon_{gc}}{dt} \frac{\partial f_{gc}}{\partial \epsilon_{gc}} = \left\langle \left( \frac{\partial f}{\partial t} \right)_c \right\rangle$$

- $\mathbf{v}_{d\perp}$  is the drift velocity (including  $\mathbf{E} \times \mathbf{B}$  drift etc).
- with  $d\epsilon_{gc}/dt \approx q\partial\Phi/\partial t + \mu\partial B/\partial t - q\mathbf{v}_{\parallel}\mathbf{b} \cdot \partial\mathbf{A}/\partial t$
- $\left\langle \left( \frac{\partial f}{\partial t} \right)_c \right\rangle$  is the collision operator averaged over gyrophase.

In many applications the drift-kinetic equation is solved numerically to evaluate the transport coefficients in fusion plasmas.

More general and accurate gyrokinetic equations that include finite gyroradius effects have been also derived and are used when  $r_L/L \sim 1$ .

# Summary on non-axisymmetric devices and kinetic theory

- Stellarators as alternative to Tokamak: helical winding of the field lines obtained without recurring to the toroidal current.
- Lack of axisymmetry: orbits are not closed, higher level of neoclassical transport.
- If the system is not optimized often: electrons in the  $1/\nu$  regime while ions in  $\sqrt{\nu}$  regime.
- Optimization introducing a symmetry in the system or forcing it in the electron root regime.
- Kinetic equation to describe the particles distribution of a plasma.
- Macroscopic quantities and their time evolution obtained by integration over the velocity space.
- Closure of the equations system by assuming small deviations from the equilibrium and the linearization of the K.E.
- Examples of collision operators: BGK and Fokker-Planck.

# Bibliography (1/2)

## Diffusion and collisions:

- R.J.Goldston, Introduction to plasma physics, CRC Press (1995)  
Chapter 11-12
- J.D. Callen, Fundamental of plasma physics, Chapter 2 [link](#)  
<http://homepages.cae.wisc.edu/~callen/book.html>

## Classical Transport

- Nick McGreivy, General plasma physics notes, Chapter 6 [link](#)  
<https://scholar.princeton.edu/sites/default/files/nickmcgreivy/files/>
- Ben Dudson, lectures on plasma physics online n.2 [link](#)  
<https://www-users.york.ac.uk/~bd512/teaching/media>

## Neoclassical Transport and Bootstrap Current:

- T.J.Boyd and J.J.Sanderson, The physics of plasmas, Cambridge University Press (2003) pp 304-307
- Ben Dudson, lectures on plasma physics online n.3 and n.5
- Nick McGreivy, General plasma physics notes, Chapter 6

## Bibliography (2/2)

### Stellarators:

- H.E.Mynick, Phys.Plasmas 13, 058102 (2006)
- P Helander et al Plasma Phys. Control. Fusion 54 124009 (2012)
- M.Landerman, Electric fields and transport in optimized stellarators, PHD thesis [link](https://dspace.mit.edu/handle/1721.1/68874) <https://dspace.mit.edu/handle/1721.1/68874>
- Ben Dudson, lectures on plasma physics online n.6

### Kinetic Theory

- R.J.Goldston, Introduction to plasma physics, CRC Press (1995) Chapter 22
- T.J.Boyd and J.J.Sanderson, The physics of plasmas, Cambridge University Press (2003) pp 296-300
- S.I.Braginskii, Review of Plasma Physics 1 (1965)
- J.D. Callen, Fundamental of plasma physics, Chapter 5

Some figures in the slides have been adapted from these papers/books.

Email:[marco.gobbin@igi.cnr.it](mailto:marco.gobbin@igi.cnr.it)

# EXTRA

# Transport in a weakly ionized gas

An example of a system not-intrinsically ambipolar: a weakly ionized gas.

- $\nabla n$  in the  $x$  direction,  $\mathbf{B}$  along  $z$ , focus on perpendicular transport.
- Collisions mainly with neutral atoms at frequency  $\nu_0 \propto \sqrt{m}$ ;
- In steady state ( $d/dt \sim 0$ ) the motion equation for each species is:

$$qn(\mathbf{E} + \mathbf{u} \times \mathbf{B}) - T \nabla n - mn\nu_0 \mathbf{u} = 0$$

- along the  $x$  and  $y$  directions this becomes:

$$qnE_x + qnu_yB - T \frac{dn}{dx} - mn\nu_0 u_x = 0$$

$$-qnu_xB - mn\nu_0 u_y = 0 \rightarrow u_y = -\frac{u_x B}{m\nu_0}$$

- which gives for  $u_x$ :

$$u_x = \frac{1}{\frac{q^2 B^2}{m\nu_0} + m\nu_0} \left[ qE_x - T \frac{\nabla n}{n} \right] = \frac{\nu_0}{m(\omega_c^2 + \nu_0^2)} \left[ qE_x - T \frac{\nabla n}{n} \right]$$

# Ambipolar Electric field

The effect of the magnetic field becomes important when  $\omega_c \gg \nu_0$ :

$$u_x \approx \frac{\nu_0}{m\omega_c^2} \left[ qE_x - T \frac{\nabla n}{n} \right] \propto \sqrt{m} \left[ qE_x - T \frac{\nabla n}{n} \right]$$

- apply to ions, which diffusion is dominant across the field ( $\propto r_{L,i}^2$ );
- an electric field  $E_x$  arises to retard ions and largely reduces  $u_{x,i}$  by a factor  $\sqrt{m_i/m_e}$ , at zero order:  $E_x \approx \frac{T_i}{n_e} \nabla n$ ;
- replacing for electrons:  $n u_{x,e} = -\frac{\nu_{0e}}{m_e \omega_{ce}^2} (T_i + T_e) \nabla n = -D_a \nabla n$
- so that the ambipolar diffusion coefficient is :

$$D_a = \frac{\nu_{0e}(T_e + T_i)}{m_e \omega_{ce}^2} = \nu_{0e} r_{Le}^2 \left( 1 + \frac{T_i}{T_e} \right)$$

## Note:

- Diffusion rate is controlled by the species that diffuses more slowly!
- For diffusion along the field or in unmagnetized plasmas,  $D_a \approx D_i$ .

# Diffusion coefficient in a plasma with $\mathbf{B} \neq 0$ (1/3)

Consider a steady state plasma with  $\mathbf{B} = B_0 \mathbf{e}_z$  and density profile  $n(x, z)$  with gradients in the direction parallel ( $z$ ) and perpendicular ( $x$ ) to  $\mathbf{B}$ .

- The corresponding  $f_0$  is a bi-Maxwellian since in a plasma the temperature can be different along and across  $\mathbf{B}$ :

$$f_0 = n(x, z) \left( \frac{m}{2\pi T_{\perp}} \right) \left( \frac{m}{2\pi T_{\parallel}} \right)^{1/2} \exp \left[ -\frac{m(v_x^2 + v_y^2)}{2T_{\perp}} - \frac{mv_z^2}{2T_{\parallel}} \right]$$

- the linearized KE is:

$$\begin{aligned} \mathbf{v} \cdot \nabla_{\mathbf{r}} f_0 + \frac{q}{m} (\mathbf{v} \times \mathbf{B}) \cdot \nabla_{\mathbf{v}} f_1 &= -\nu_c f_1 \rightarrow \\ \left( v_x \frac{\partial n}{\partial x} + v_z \frac{\partial n}{\partial z} \right) \frac{f_0}{n} + \frac{qB_0}{m} \left( v_y \frac{\partial f_1}{\partial v_x} - v_x \frac{\partial f_1}{\partial v_y} \right) &= -\nu_c f_1 \end{aligned}$$

- Take the  $v_x$ ,  $v_y$  and  $v_z$  moments. For instance with  $v_x$ :

$$\int \left[ \left( v_x^2 \frac{\partial n}{\partial x} + v_z v_x \frac{\partial n}{\partial z} \right) \frac{f_0}{n} + \omega_c \left( v_y v_x \frac{\partial f_1}{\partial v_x} - v_x^2 \frac{\partial f_1}{\partial v_y} \right) - \nu_c v_x f_1 \right] dv_x dv_y dv_z = 0$$

## Diffusion coefficient in a plasma with $\mathbf{B} \neq 0$ (2/3)

- note that  $\int f_0 v_x v_z dv_x dv_z dv_y = 0$  and  $\int v_x^2 \frac{f_0}{n} dv_x dv_y dv_z = \frac{T_{\perp}}{n}$ ;
- $\int v_x^2 \frac{\partial f_1}{\partial v_y} dv_x dv_y dv_z \propto \int \frac{\partial f_1}{\partial v_y} dv_y = 0$  since  $f_1 \rightarrow 0$  at  $\pm\infty$ ;
- $-\int v_x \nu_c f_1 dv_x dv_y dv_z = -\nu_c \int v_x f_1 dv_x dv_y dv_z = -\nu_c \Gamma_x$ ;
- the term in  $\nabla_v$  includes the particle flux along  $y$ :

$$\begin{aligned} \int v_x v_y \frac{\partial f_1}{\partial v_x} dv_x dv_y dv_z &= \int v_y dv_y dv_z \left[ (v_x f_1)_{-\infty}^{+\infty} - \int f_1 dv_x \right] = \\ &\quad - \int f_1 v_y dv_x dv_y dv_z = -\Gamma_y \end{aligned}$$

Repeating the same procedure for  $v_y$  and  $v_z$ , the moments are:

$$\frac{T_{\perp}}{m} \frac{\partial n}{\partial x} - \omega_c \Gamma_y = -\nu_c \Gamma_x$$

$$\omega_c \Gamma_x = -\nu_c \Gamma_y$$

$$\frac{T_{\parallel}}{m} \frac{\partial n}{\partial z} = -\nu_c \Gamma_z$$

## Diffusion coefficient in a plasma with $\mathbf{B} \neq 0$ (3/3)

Solving for  $\Gamma_x$  and  $\Gamma_z$ :

$$\Gamma_x = -\frac{T_{\perp}}{m} \frac{\nu_c}{\nu_c^2 + \omega_c^2} \frac{\partial n}{\partial x} \quad \Gamma_z = -\frac{T_{\parallel}}{m\nu_c} \frac{\partial n}{\partial z}$$

From the definition of the parallel and perpendicular diffusion coefficients:

$$\Gamma_x = -D_{\perp} \frac{\partial n}{\partial x} \quad \Gamma_z = -D_{\parallel} \frac{\partial n}{\partial z}$$

their values are:

$$D_{\perp} = \frac{T_{\perp}}{m} \frac{\nu_c}{\nu_c^2 + \omega_c^2} \quad D_{\parallel} = \frac{T_{\parallel}}{m\nu_c}$$

- $D_{\parallel}$  is the same obtained for transport in an unmagnetized plasma;
- for  $\omega_c \gg \nu_c \rightarrow D_{\perp} \approx \frac{T_{\perp}}{m} \frac{\nu_c}{\omega_c^2} = r_L^2 \nu_c$  (classical result).

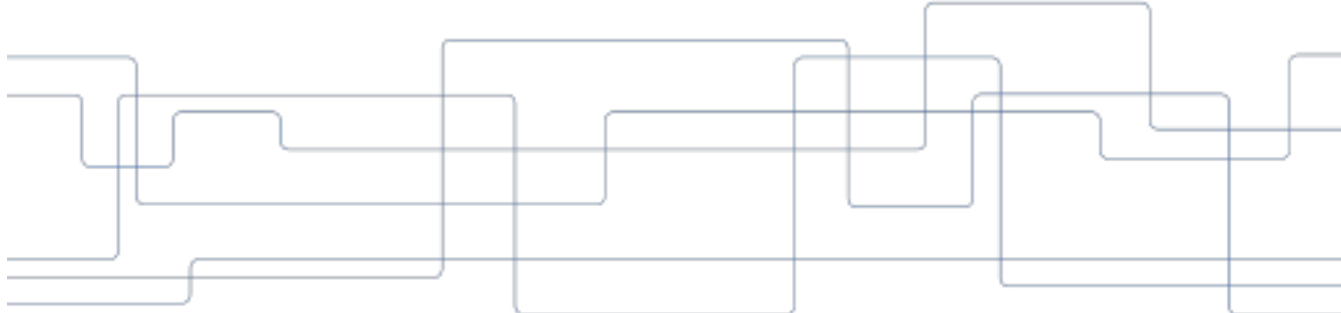


KTH ROYAL INSTITUTE  
OF TECHNOLOGY  
Stockholm, Sweden

# PEDESTAL PHYSICS

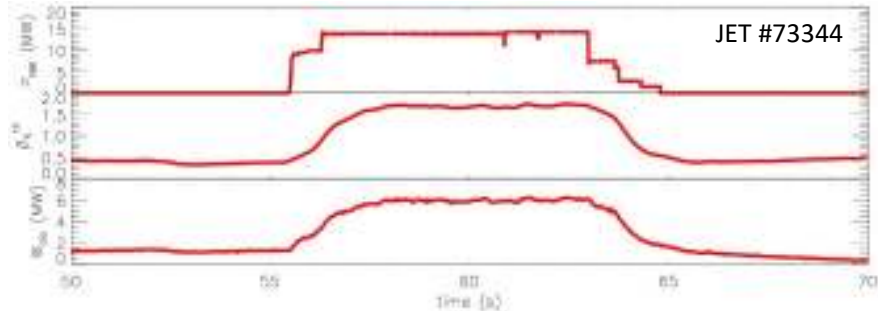
## a phenomenological introduction

L. Frassinetti



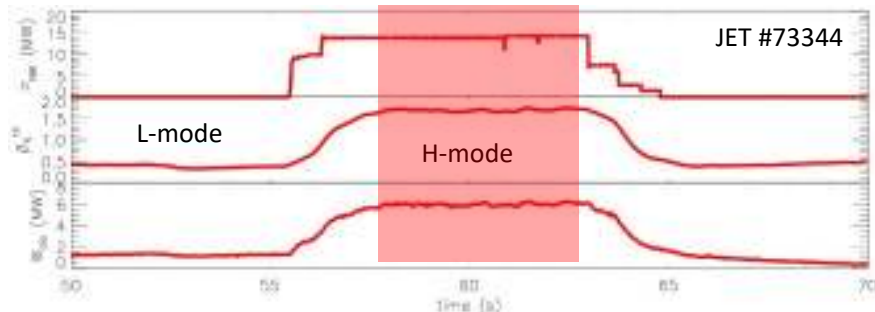
# H-mode plasma

- When the input power to the plasma is above a specific threshold, the plasma has a transition from a low confinement regime (L-mode) to a high confinement regimes (H-mode).

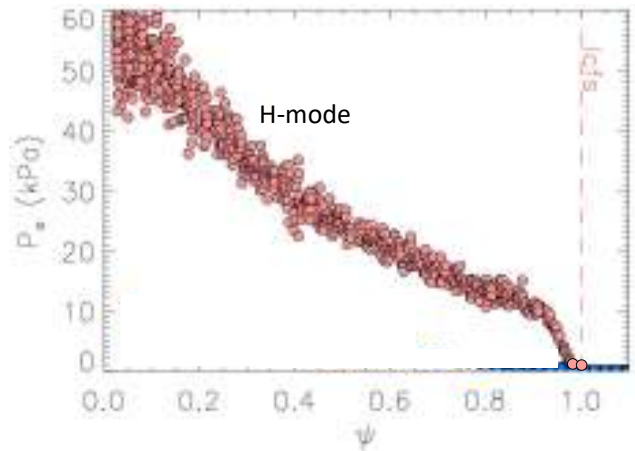


# H-mode plasma

- When the input power to the plasma is above a specific threshold, the plasma has a transition from a low confinement regime (L-mode) to a high confinement regimes (H-mode).

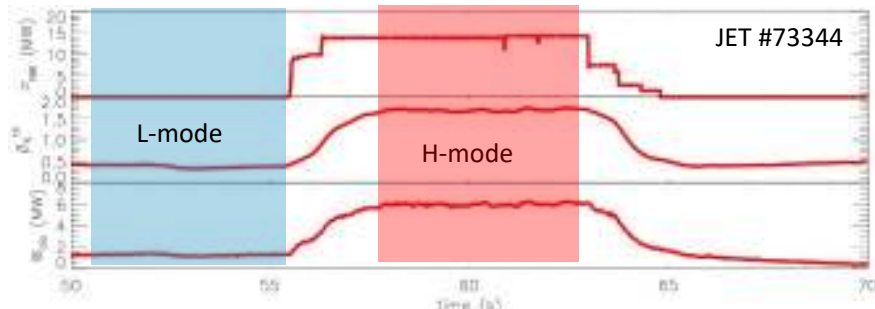


- The H-mode is characterized by:
  - steep gradients in the pressure "near" the edge of the plasma.This region is named "**pedestal**".

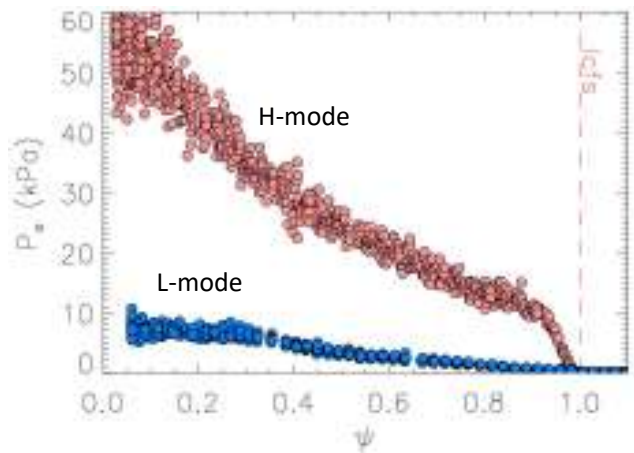


# H-mode plasma

- When the input power to the plasma is above a specific threshold, the plasma has a transition from a low confinement regime (L-mode) to a high confinement regimes (H-mode).

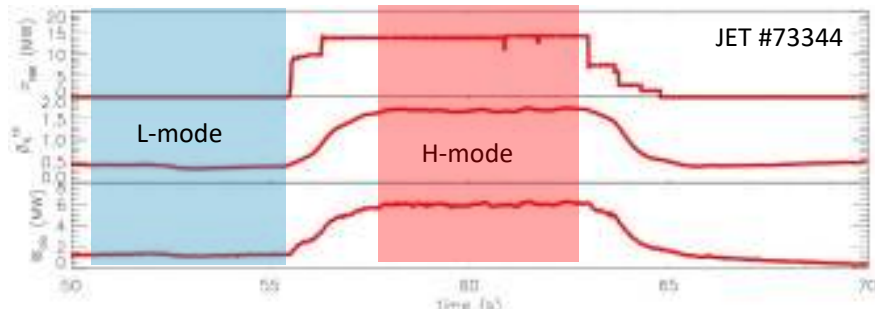


- The H-mode is characterized by:
  - steep gradients in the pressure "near" the edge of the plasma. This region is named "**pedestal**".

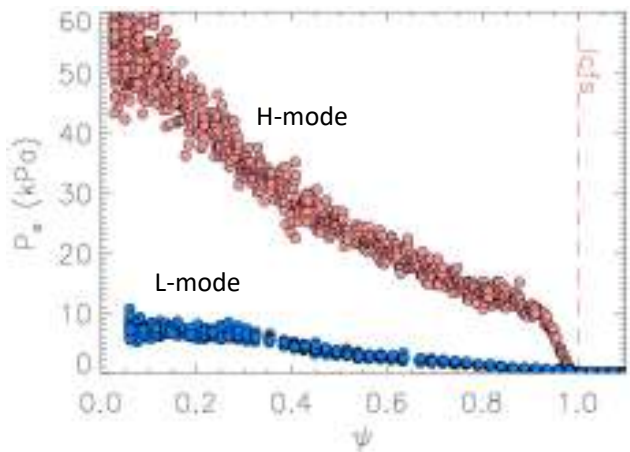


# H-mode plasma

- When the input power to the plasma is above a specific threshold, the plasma has a transition from a low confinement regime (L-mode) to a high confinement regimes (H-mode).



- The H-mode is characterized by:
  - steep gradients in the pressure "near" the edge of the plasma. This region is named "**pedestal**".
  - sudden releases of energy and particles from the pedestal region to the SOL and the divertor. These events are triggered by MHD instabilities and are named **edge localized modes (ELMs)**



# OUTLINE

- L-H transition
- Pedestal structure
- Edge localized modes (ELMs)
  - ELM energy losses
  - ELM types
- MHD stability of the pedestal
  - Role of MHD stability (and few words on transport)
  - The peeling-ballooning (PB) model
  - The ELM cycle within the PB model
  - Parameters that influences the pedestal
- Pedestal predictions
  - The EPED model:
    - The PB constraint
    - The KBM constraint
  - Non-linear MHD modelling
- Some of the most active research areas in pedestal physics

# OUTLINE

- **L-H transition**
- Pedestal structure
- Edge localized modes (ELMs)
  - ELM energy losses
  - ELM types
- MHD stability of the pedestal
  - Role of MHD stability (and few words on transport)
  - The peeling-balloonning (PB) model
  - The ELM cycle within the PB model
  - Parameters that influences the pedestal
- Pedestal predictions
  - The EPED model:
    - The PB constraint
    - The KBM constraint
  - Non-linear MHD modelling
- Some of the most active research areas in pedestal physics

# L-H transition

- Above a specific threshold in power ( $P_{LH}$ ), the plasma enters the H-mode
- The  $P_{LH}$  threshold depends on several parameters.
- A scaling law based on results from several machines produces:

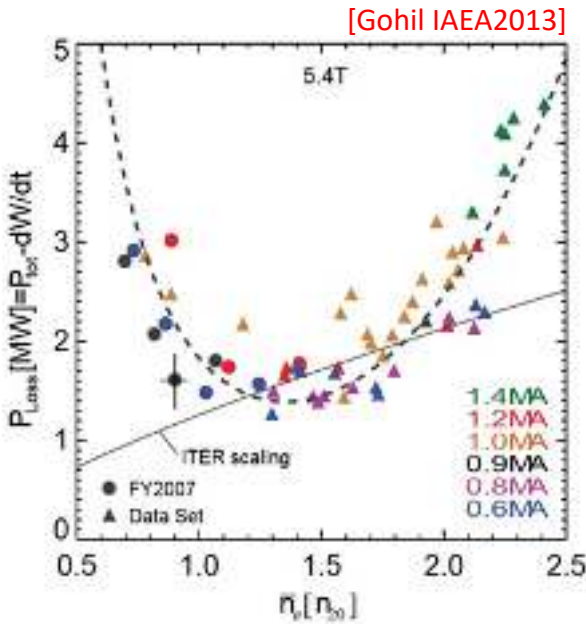
$$P_{LH} = 0.049 n_e^{0.72} B^{0.8} S^{0.94} \quad [\text{Martin JPC2008}]$$

# L-H transition

- Above a specific threshold in power ( $P_{LH}$ ), the plasma enters the H-mode
- The  $P_{LH}$  threshold depends on several parameters.
- A scaling law based on results from several machines produces:

$$P_{LH} = 0.049 n_e^{0.72} B^{0.8} S^{0.94} \quad [\text{Martin JPC2008}]$$

- However, the links between engineering/plasma parameters and  $P_{LH}$  is more complex.

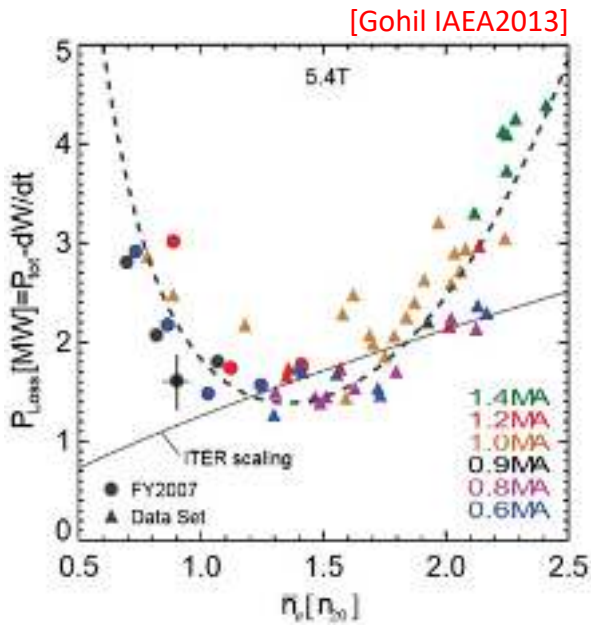


# L-H transition

- Above a specific threshold in power ( $P_{LH}$ ), the plasma enters the H-mode
- The  $P_{LH}$  threshold depends on several parameters.
- A scaling law based on results from several machines produces:

$$P_{LH} = 0.049 n_e^{0.72} B^{0.8} S^{0.94} \quad [\text{Martin JPC2008}]$$

- However, the links between engineering/plasma parameters and  $P_{LH}$  is more complex. Some of the main parameters that affects  $P_{LH}$  are:
  - Magnetic field
  - Isotope mass ( $P_{LH}$  decreases with isotope mass) [Righi NF1999]
  - Divertor geometry [Delabie EPS2015]
  - Wall material ( $P_{LH}$  reduced from carbon to metal walls) [Neu JNM2013]
  - Plasma density [Martin JPC2008]
    - Minimum around  $0.2\text{-}0.4n_{GW}$
    - Non-monotonic behavior seem related to edge ion heating [Ryter NF2014]



# L-H transition

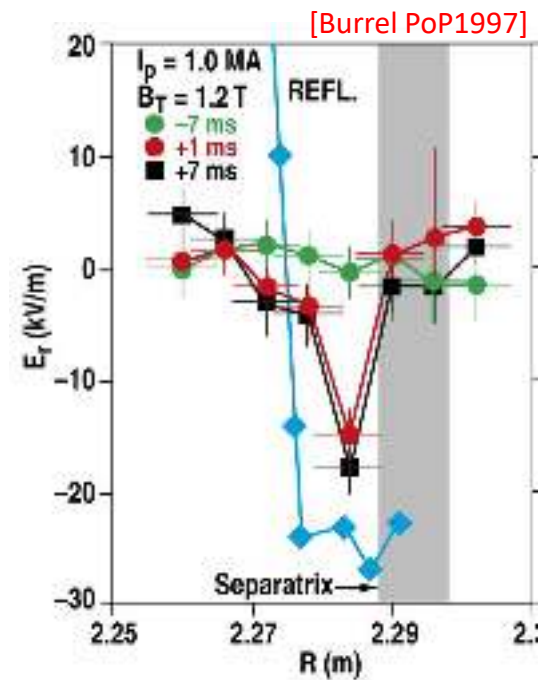
- The physics of L-H transition is not yet fully understood
  - several models have been proposed to explain the experimental results
  - but a physics based model of the L-H transition with full predictive capabilities has not been developed yet.

# L-H transition

- The physics of L-H transition is not yet fully understood
  - several models have been proposed to explain the experimental results
  - but a physics based model of the L-H transition with full predictive capabilities has not been developed yet.
- Some key experimental and theoretical concepts to explain the L-H transition are well established:
  - The L-H transition is due to stabilization of the turbulence near the plasma edge  
[Burrel PoP1997], [Terry RMP2000]
  - $\vec{E} \times \vec{B}$  shear stabilization plays a key role

# L-H transition

- The physics of L-H transition is not yet fully understood
  - several models have been proposed to explain the experimental results
  - but a physics based model of the L-H transition with full predictive capabilities has not been developed yet.
- Some key experimental and theoretical concepts to explain the L-H transition are well established:
  - The L-H transition is due to stabilization of the turbulence near the plasma edge [Burrel PoP1997], [Terry RMP2000]
  - $\vec{E} \times \vec{B}$  shear stabilization plays a key role
    - higher  $\vec{E} \times \vec{B}$  in L-mode  $\rightarrow$  lower  $P_{LH}$ .
    - The formation of a  $E_r$  well, just inside the separatrix, occurs as the plasma enters H-mode
    - The well has to reach a certain depth to allow the transition

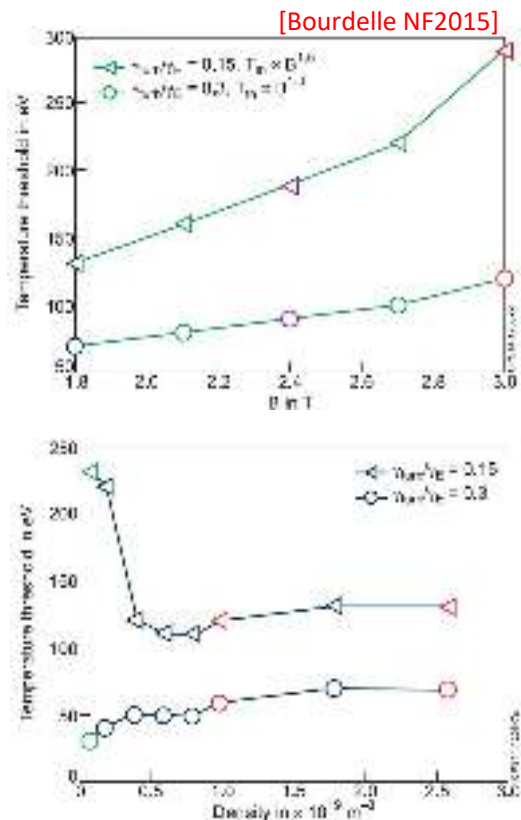


# L-H transition

- Many of the theoretical works are based on the interplay between the L-mode turbulence and  $E_r$  shearing. [Connor PPCF2000]
- A large part of other theoretical works are based on the stabilization of RBM via increased pressure gradient. [Rogers PRL1997]
- An example:

# L-H transition

- Many of the theoretical works are based on the interplay between the L-mode turbulence and  $E_r$  shearing. [Connor PPCF2000]
- A large part of other theoretical works are based on the stabilization of RBM via increased pressure gradient. [Rogers PRL1997]
- An example: [Bourdelle NF2015]
  - $\gamma_{\text{turb}}$  (growth rate of the turbulence) can be modeled from theory (either analytically or numerically)
  - $\gamma_E$  ( $E_r$  shear) can be obtained by modelling the  $E_r$  profiles.
  - $\gamma_{\text{turb}}/\gamma_E$  can be used to identify at which temperature the transition occurs  
→ Qualitative trends can be tested
- For a recent review on L-H transition: [Bourdelle NF2020]

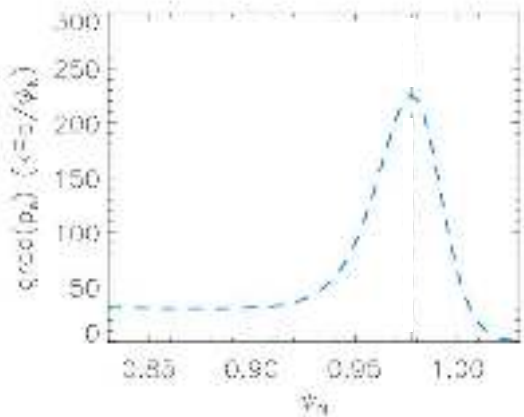
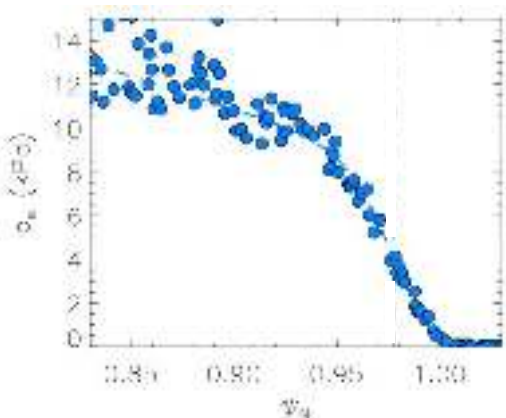


# OUTLINE

- L-H transition
- **Pedestal structure**
- Edge localized modes (ELMs)
  - ELM energy losses
  - ELM types
- MHD stability of the pedestal
  - Role of MHD stability (and few words on transport)
  - The peeling-balloonning (PB) model
  - The ELM cycle within the PB model
  - Parameters that influences the pedestal
- Pedestal predictions
  - The EPED model:
    - The PB constraint
    - The KBM constraint
  - Non-linear MHD modelling
- Some of the most active research areas in pedestal physics

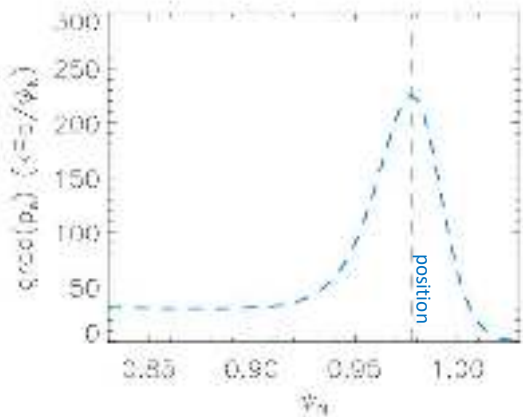
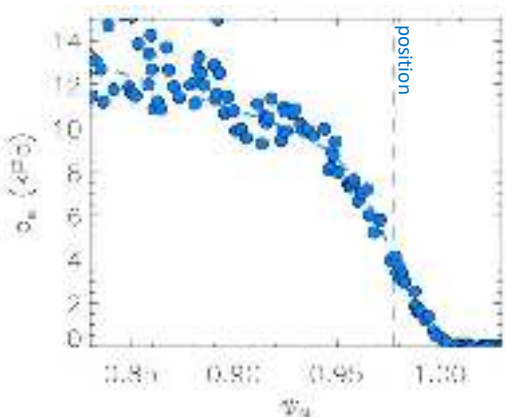
# Pedestal structure

- To study the pedestal, it is necessary to quantify the parameters that identify its structure.
- The key parameters are
  - pedestal height
  - pedestal width
  - pedestal position (often defined as the position of the maximum gradient).
  - maximum gradient
- These parameters are determined by fitting an analytical function (typically, a modified hyperbolic tangent) to the experimental data.



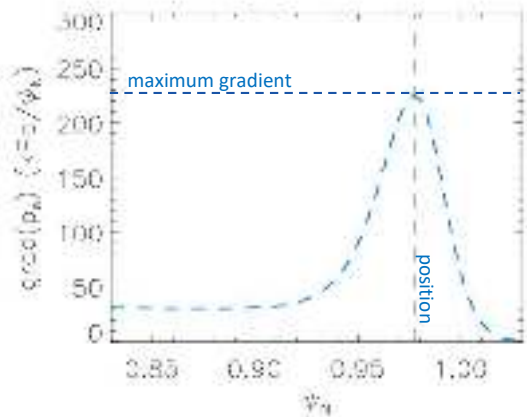
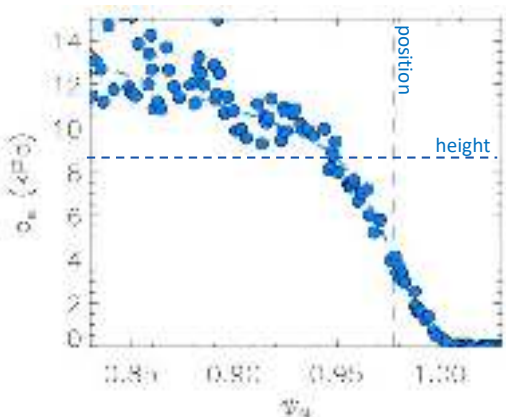
# Pedestal structure

- To study the pedestal, it is necessary to quantify the parameters that identify its structure.
- The key parameters are
  - pedestal height
  - pedestal width
  - pedestal position (often defined as the position of the maximum gradient).
  - maximum gradient
- These parameters are determined by fitting an analytical function (typically, a modified hyperbolic tangent) to the experimental data.



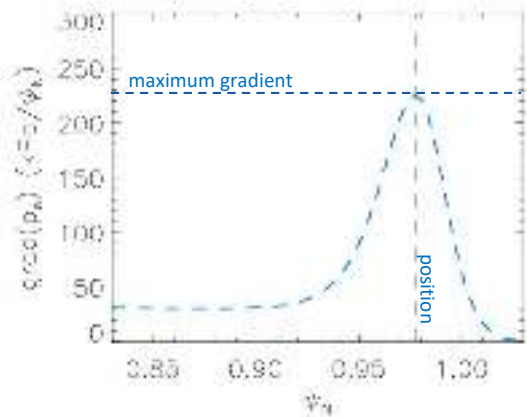
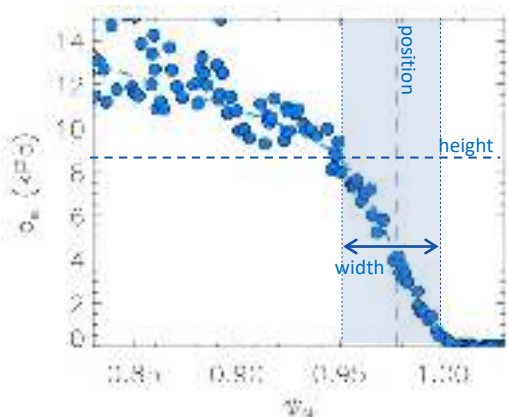
# Pedestal structure

- To study the pedestal, it is necessary to quantify the parameters that identify its structure.
- The key parameters are
  - pedestal height
  - pedestal width
  - pedestal position (often defined as the position of the maximum gradient).
  - maximum gradient
- These parameters are determined by fitting an analytical function (typically, a modified hyperbolic tangent) to the experimental data.



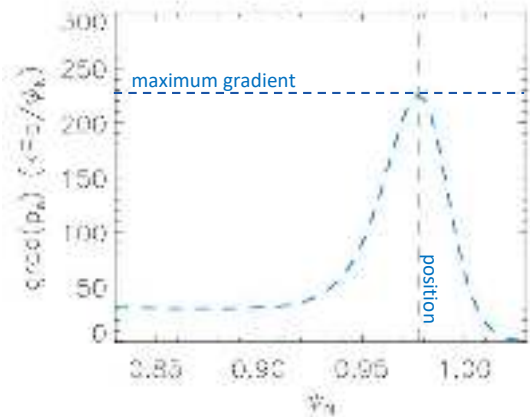
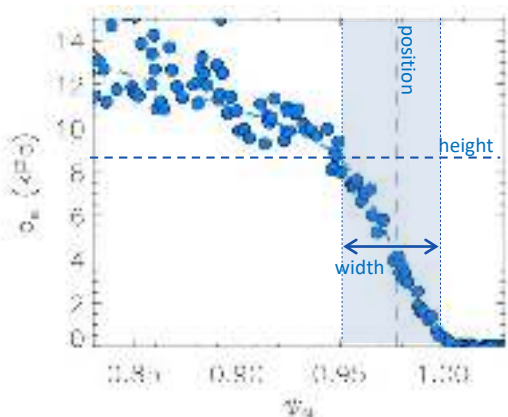
# Pedestal structure

- To study the pedestal, it is necessary to quantify the parameters that identify its structure.
- The key parameters are
  - pedestal height
  - pedestal width
  - pedestal position (often defined as the position of the maximum gradient).
  - maximum gradient
- These parameters are determined by fitting an analytical function (typically, a modified hyperbolic tangent) to the experimental data.



# Pedestal structure

- To study the pedestal, it is necessary to quantify the parameters that identify its structure.
- The key parameters are
  - pedestal height
  - pedestal width
  - pedestal position (often defined as the position of the maximum gradient).
  - maximum gradient
- The pedestal parameters are determined for:
  - pressure
  - temperature
  - density
- These parameters are determined by fitting an analytical function (typically, a modified hyperbolic tangent) to the experimental data.

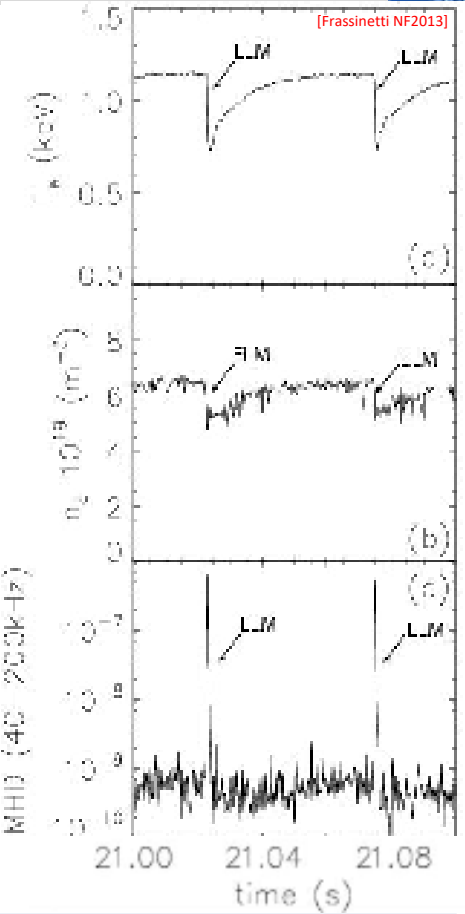


# OUTLINE

- L-H transition
- Pedestal structure
- **Edge localized modes (ELMs)**
  - **ELM energy losses**
  - **ELM types**
- MHD stability of the pedestal
  - Role of MHD stability (and few words on transport)
  - The peeling-balloonning (PB) model
  - The ELM cycle within the PB model
  - Parameters that influences the pedestal
- Pedestal predictions
  - The EPED model:
    - The PB constraint
    - The KBM constraint
  - Non-linear MHD modelling
- Some of the most active research areas in pedestal physics

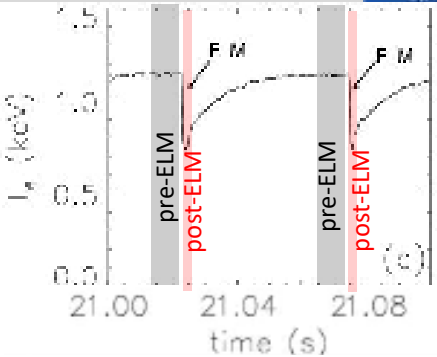
# Edge Localized Modes (ELMs)

- The pedestal is characterized by sudden events, triggered by MHD instabilities, called edge localized modes (ELMs).
- The ELM triggers the collapse of the pedestal temperature and density, which in turn leads to the release of energy and particles to the divertor.



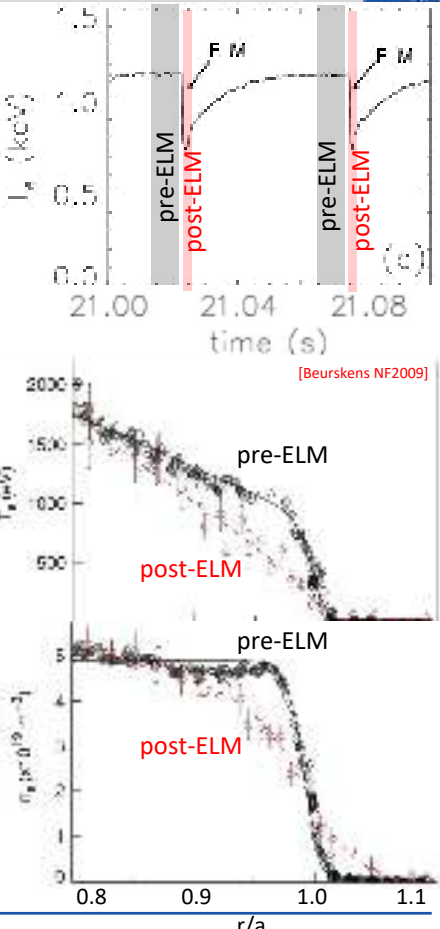
# Edge Localized Modes (ELMs)

- The pedestal is characterized by sudden events, triggered by MHD instabilities, called edge localized modes (ELMs).
- The ELM triggers the collapse of the pedestal temperature and density, which in turn leads to the release of energy and particles to the divertor.
- The ELM collapse affects the kinetic profiles only in the pedestal region.



# Edge Localized Modes (ELMs)

- The pedestal is characterized by sudden events, triggered by MHD instabilities, called edge localized modes (ELMs).
- The ELM triggers the collapse of the pedestal temperature and density, which in turn leads to the release of energy and particles to the divertor.
- The ELM collapse affects the kinetic profiles only in the pedestal region.

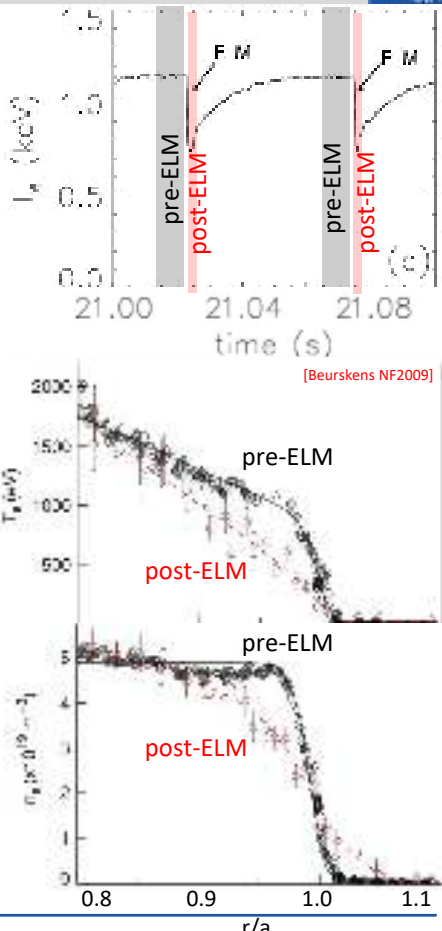


# Edge Localized Modes (ELMs)

- The pedestal is characterized by sudden events, triggered by MHD instabilities, called edge localized modes (ELMs).
- The ELM triggers the collapse of the pedestal temperature and density, which in turn leads to the release of energy and particles to the divertor.
- The ELM collapse affects the kinetic profiles only in the pedestal region.
- The ELM losses can be calculated by integrating the profiles just before and soon after the ELMs:

[Beurskens NF2009]

$$\begin{aligned}\Delta W_{ELM} &= W_{pre} - W_{post} = \\ &= \frac{3}{2} k \int (n_{pre} T_{pre} - n_{post} T_{post}) dV \approx \\ &\approx \frac{3}{2} k \underbrace{\int \Delta n T dV}_{\text{convective losses}} + \frac{3}{2} k \underbrace{\int n \Delta T dV}_{\text{conductive losses}}\end{aligned}$$



# ELM types: definitions

- H-mode plasma can be characterized by several types of ELMs. The ELM frequency ( $f_{\text{ELM}}$ ) is often used to identify the most common ELMs.
- The most common are:
  - **Type I ELMs.**
  - **Type III ELMs.**
  - **Type II (or "grassy" ELMs).**

# ELM types: definitions

- H-mode plasma can be characterized by several types of ELMs. The ELM frequency ( $f_{\text{ELM}}$ ) is often used to identify the most common ELMs.

- The most common are:

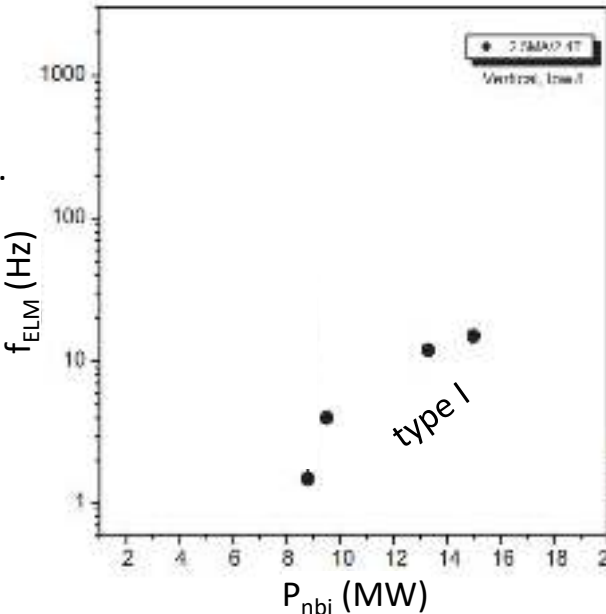
- Type I ELMs.**

- $f_{\text{ELM}}$  increases with  $P_{\text{sep}} = P_{in} - P_{rad} - dW/dt$ .
    - typically occurs at  $P_{\text{sep}} \gg P_{LH}$ .
    - they are triggered by ideal MHD.
    - they appear as sharp burst on the  $D_\alpha$ .

- Type III ELMs.**

- Type II (or "grassy" ELMs).**

[Sartori PPCF2004]



# ELM types: definitions

- H-mode plasma can be characterized by several types of ELMs. The ELM frequency ( $f_{\text{ELM}}$ ) is often used to identify the most common ELMs.

- The most common are:

- Type I ELMs.**

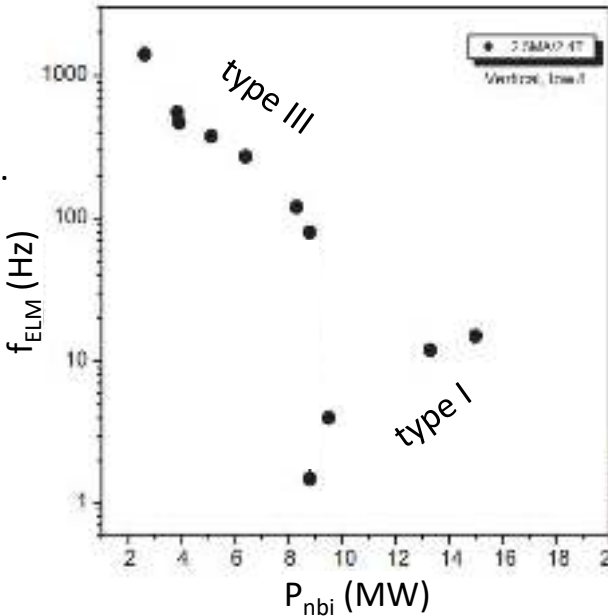
- $f_{\text{ELM}}$  increases with  $P_{\text{sep}} = P_{in} - P_{rad} - dW/dt$ .
    - typically occurs at  $P_{\text{sep}} \gg P_{LH}$ .
    - they are triggered by ideal MHD.
    - they appear as sharp burst on the  $D_\alpha$ .

- Type III ELMs.**

- $f_{\text{ELM}}$  decreases with  $P_{\text{sep}}$ .
    - typically occurs  $P_{\text{sep}} \approx P_{LH}$ .
    - they are not triggered by ideal MHD.

- Type II (or "grassy" ELMs).**

[Sartori PPCF2004]



# ELM types: definitions

- H-mode plasma can be characterized by several types of ELMs. The ELM frequency ( $f_{\text{ELM}}$ ) is often used to identify the most common ELMs.

- The most common are:

- Type I ELMs.**

- $f_{\text{ELM}}$  increases with  $P_{\text{sep}} = P_{in} - P_{rad} - dW/dt$ .
    - typically occurs at  $P_{\text{sep}} \gg P_{LH}$ .
    - they are triggered by ideal MHD.
    - they appear as sharp burst on the D <sub>$\alpha$</sub> .

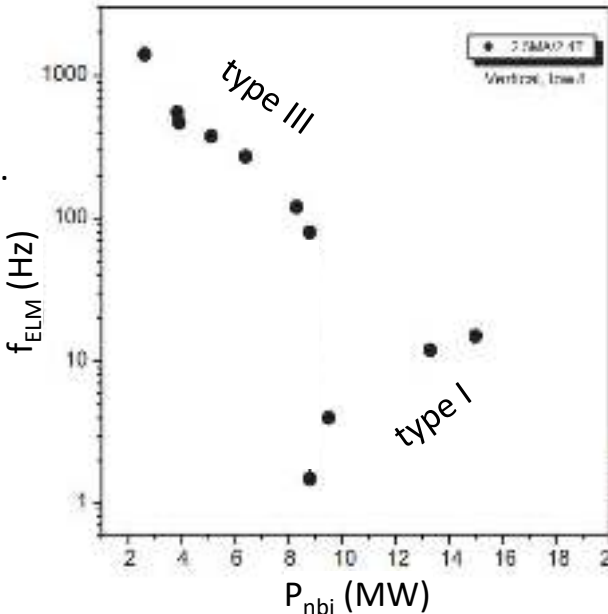
- Type III ELMs.**

- $f_{\text{ELM}}$  decreases with  $P_{\text{sep}}$ .
    - typically occurs  $P_{\text{sep}} \approx P_{LH}$ .
    - they are not triggered by ideal MHD.

- Type II (or "grassy" ELMs).**

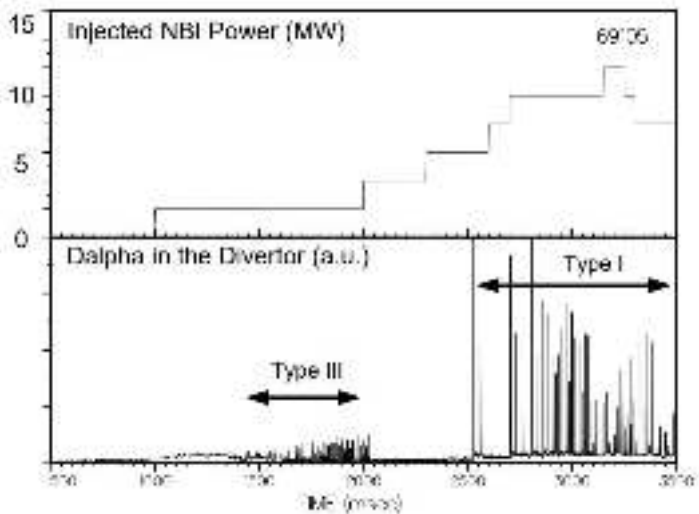
- Not achieved in all machines.
    - Occurs at high confinement and high triangularity.
    - They lead to small but frequent energy losses.

[Sartori PPCF2004]

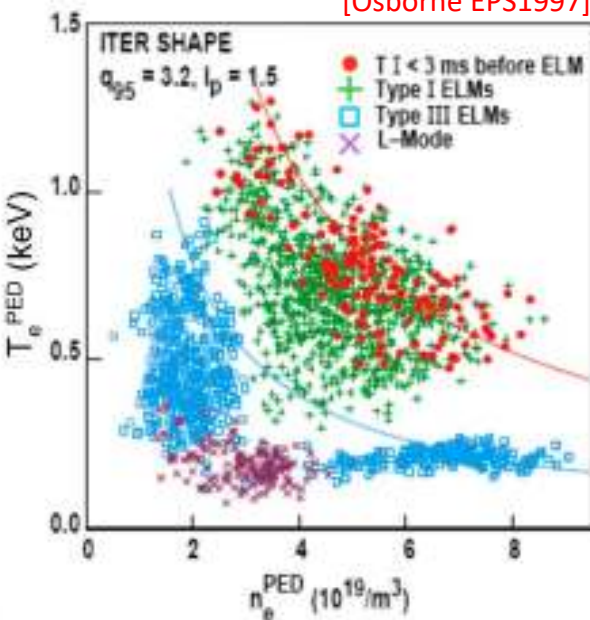


# ELM types: examples

[Zohm PPCF1996]



[Osborne EPS1997]



## ○ Type I ELMs.

- $f_{\text{ELM}}$  increases with  $P_{sep} = P_{in} - P_{rad} - dW/dt$ .
- typically occurs at  $P_{sep} \gg P_{LH}$ .

## ○ Type III ELMs.

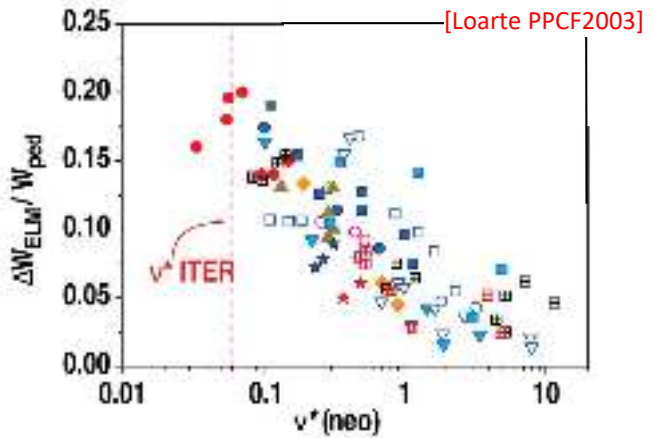
- $f_{\text{ELM}}$  decreases with  $P_{sep}$ .
- typically occurs  $P_{sep} \approx P_{LH}$ .

For reviews of ELM types:

- [Zohm PPCF1996]
- [Leonard PoP2014]

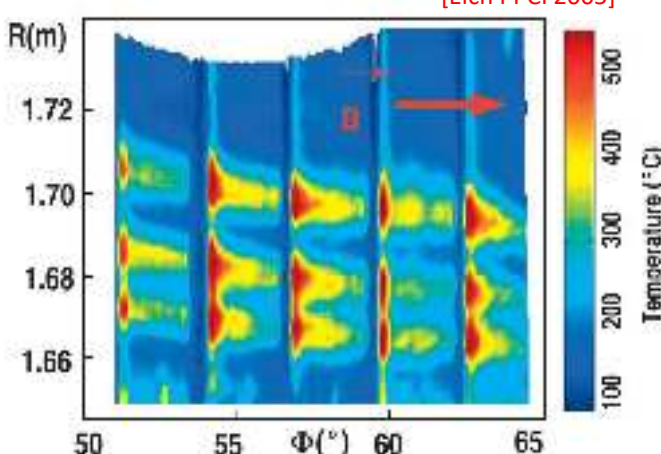
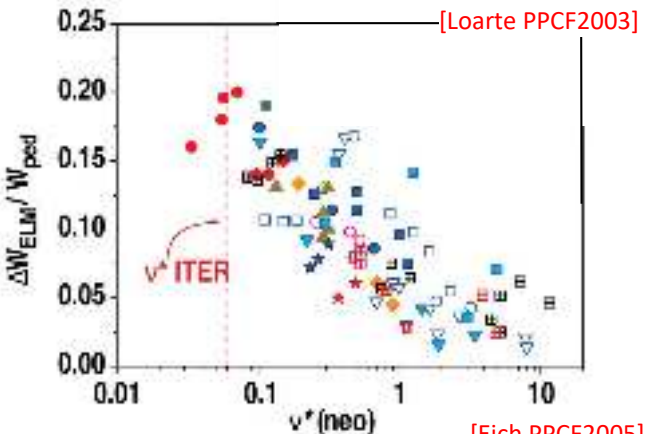
# ELMs: energy losses and heat loads

- ELM losses tend to increase with decreasing collisionality.
- At ITER collisionalities, the ELM energy losses might be 15%-20% of the pedestal stored energy.



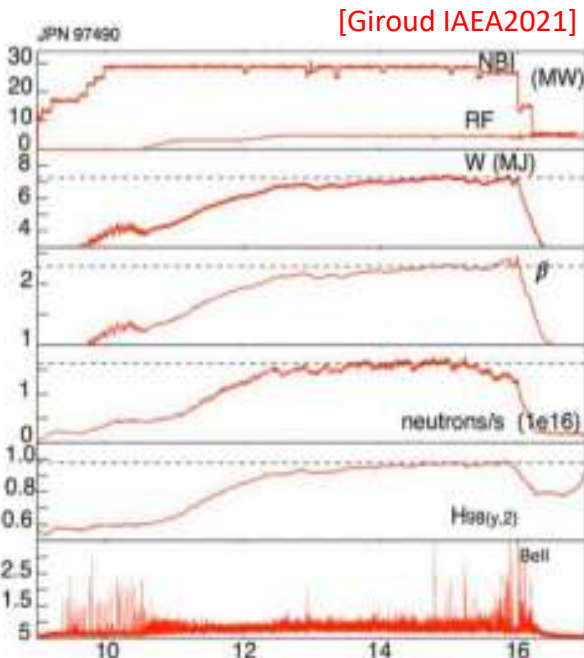
# ELMs: energy losses and heat loads

- ELM losses tend to increase with decreasing collisionality.
- At ITER collisionalities, the ELM energy losses might be 15%-20% of the pedestal stored energy.
- ELMs lead to fluxes of energy and particles to the divertor.
- The divertor can be damaged or could even melt. This could pose a problem for ITER. [Pitts JNM2013]
- It is essential to understand ELM pedestal physics to:
  - Minimize ELM energy losses
  - Develop techniques for ELM mitigation/suppressions. Some of the most developed techniques are:
  - RMPs for a review: [Evans JNM2013]
  - ELM pacing with pellets [Baylor NF2009]



# ELM types: small ELMs scenarios

- Type I ELMs have been the most studies, so far
- In recent years, significant experimental efforts have been devoted to identify and study alternatives to type I ELMs that might be useful for a fusion reactor:
  - Small ELMs (SE)**
    - at very low-gas and high performance baseline plasmas in JET [Garcia PoP2022]
  - Quasi Continuous Exhaust (QCE)**
    - at high triangularity and high gas rate (type II ELMs) [Stober NF2001]
  - Enhanced D-alpha (EDA) and quasi coherent mode (QCM)** [Greenwald PoP1999]
    - at high triangularity, low gas rate and power
  - Quiescent H-mode (QH)** [Chen NF2020]
    - At high NBI torque, which excites a edge harmonic oscillation EHO which increase transport.
  - Seeded small ELMs** [Giroud IAEA2021]
    - High power seeded plasmas.



Advantage compared to standard type I ELM scenarios:  
small ELMs, small heat loads on the divertor but good confinement

# OUTLINE

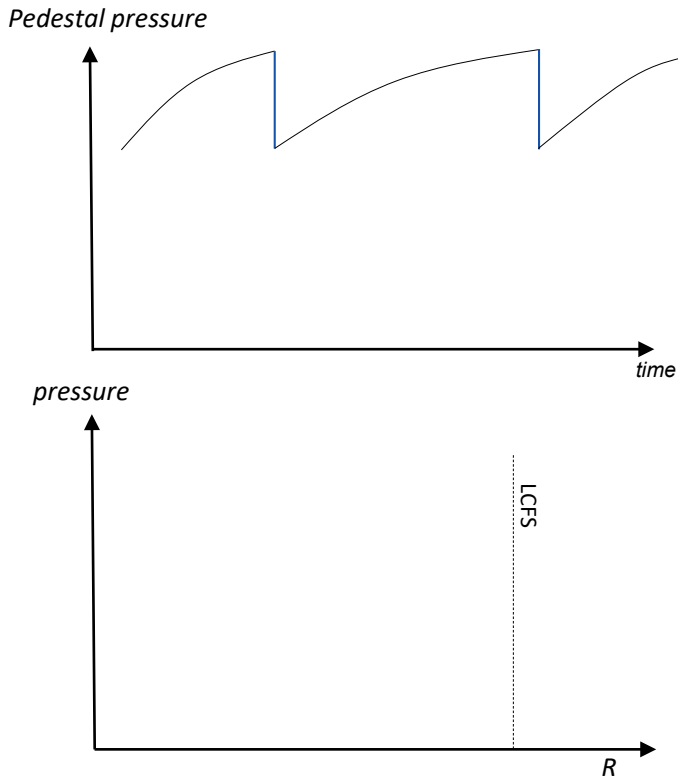
- L-H transition
- Pedestal structure
- Edge localized modes (ELMs)
  - ELM energy losses
  - ELM types
- **MHD stability of the pedestal**
  - **Role of MHD stability (and few words on transport)**
  - **The peeling-ballooning (PB) model**
  - **The ELM cycle within the PB model**
  - **Parameters that influences the pedestal**
- Pedestal predictions
  - The EPED model:
    - The PB constraint
    - The KBM constraint
  - Non-linear MHD modelling
- Some of the most active research areas in pedestal physics

# OUTLINE

- L-H transition
- Pedestal structure
- Edge localized modes (ELMs)
  - ELM energy losses
  - ELM types
- **MHD stability of the pedestal**
  - **Role of MHD stability (and few words on transport)**
  - **The peeling-ballooning (PB) model**
  - **The ELM cycle within the PB model**
  - **Parameters that influences the pedestal**
- Pedestal predictions
  - The EPED model:
    - The PB constraint
    - The KBM constraint
  - Non-linear MHD modelling
- Some of the most active research areas in pedestal physics

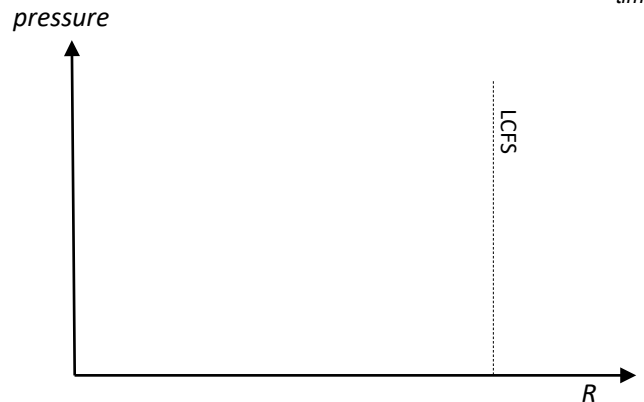
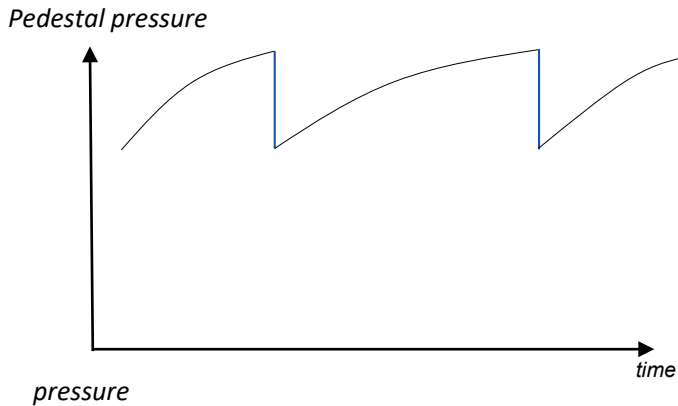
# MHD stability and transport

- What are the physical mechanisms that determines the pedestal structure and trigger the ELMs?
- Two main concepts
  - MHD stability
  - Heat and particle transport



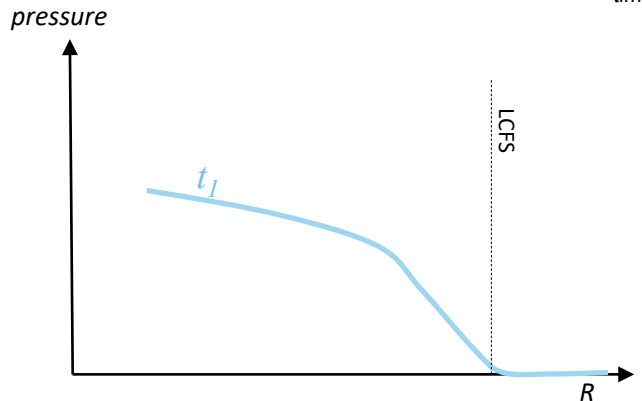
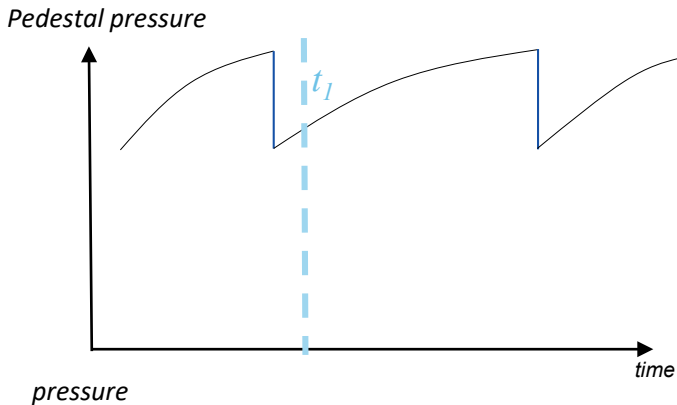
# MHD stability and transport

- What are the physical mechanisms that determines the pedestal structure and trigger the ELMs?
- Two main concepts
  - MHD stability
  - Heat and particle transport
- The time evolution is set by transport
  - Transport determines time evolution of
    - pedestal gradients
    - pedestal heights



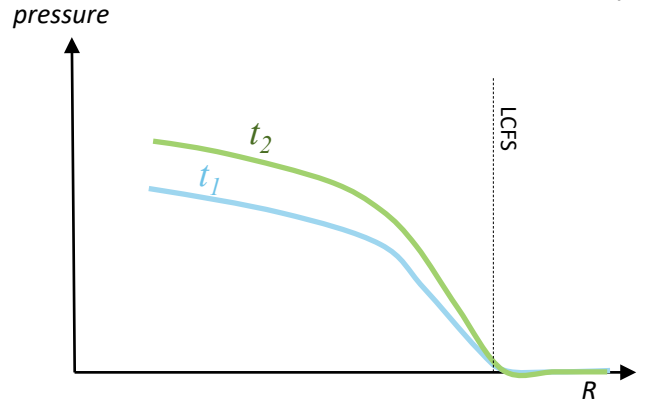
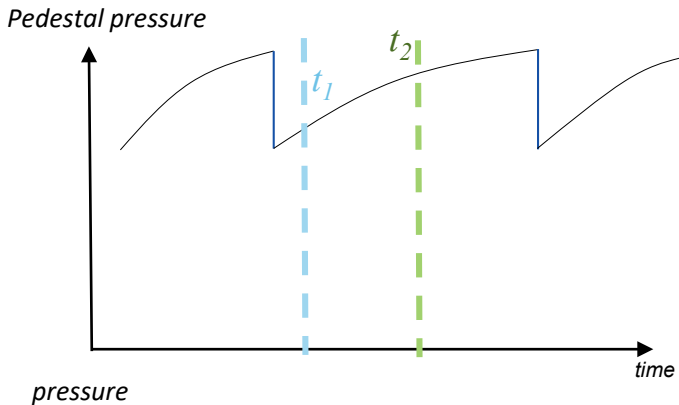
# MHD stability and transport

- What are the physical mechanisms that determines the pedestal structure and trigger the ELMs?
- Two main concepts
  - MHD stability
  - Heat and particle transport
- The time evolution is set by transport
  - Transport determines time evolution of
    - pedestal gradients
    - pedestal heights



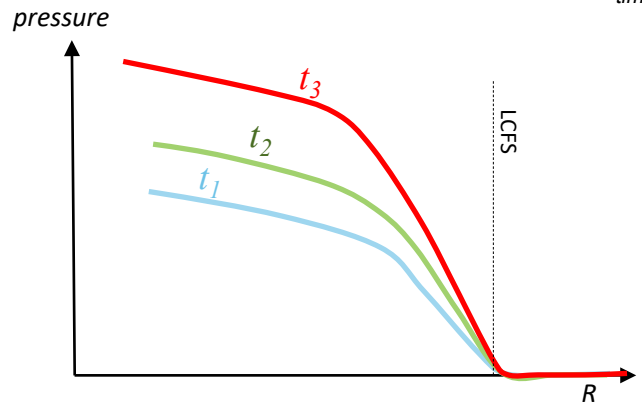
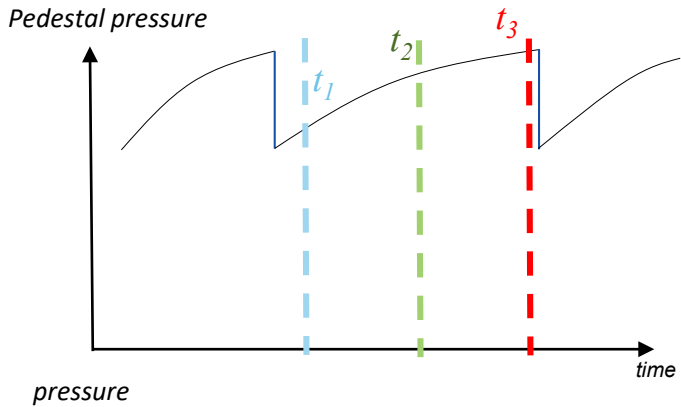
# MHD stability and transport

- What are the physical mechanisms that determines the pedestal structure and trigger the ELMs?
- Two main concepts
  - MHD stability
  - Heat and particle transport
- The time evolution is set by transport
  - Transport determines time evolution of
    - pedestal gradients
    - pedestal heights



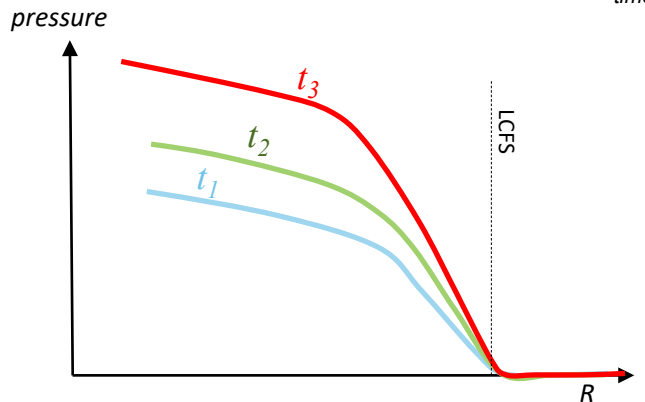
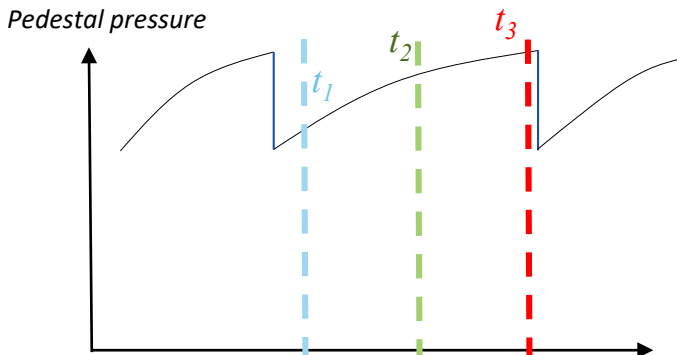
# MHD stability and transport

- What are the physical mechanisms that determines the pedestal structure and trigger the ELMs?
- Two main concepts
  - MHD stability
  - Heat and particle transport
- The time evolution is set by transport
  - Transport determines time evolution of
    - pedestal gradients
    - pedestal heights



# MHD stability and transport

- What are the physical mechanisms that determines the pedestal structure and trigger the ELMs?
- Two main concepts
  - MHD stability
  - Heat and particle transport
- The time evolution is set by transport
  - Transport determines time evolution of
    - pedestal gradients
    - pedestal heights
- The pedestal grows till a critical threshold in pressure. Then, the MHD stability triggers an ELM.
  - MHD stability determines:
    - pedestal height
    - the maximum gradient.
  - In the pedestal, the main MHD instabilities are:
    - ballooning (B) modes
    - peeling (P) modes
    - coupled PB modes

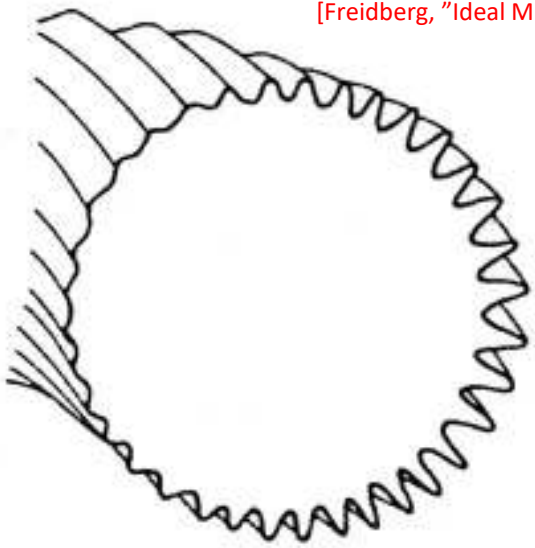


# OUTLINE

- L-H transition
- Pedestal structure
- Edge localized modes (ELMs)
  - ELM energy losses
  - ELM types
- **MHD stability of the pedestal**
  - **Role of MHD stability (and few words on transport)**
  - **The peeling-ballooning (PB) model**
  - **The ELM cycle within the PB model**
  - **Parameters that influences the pedestal**
- Pedestal predictions
  - The EPED model:
    - The PB constraint
    - The KBM constraint
  - Non-linear MHD modelling
- Some of the most active research areas in pedestal physics

# The ballooning modes

- The ballooning instabilities are pressure driven: they are triggered when the pressure gradient exceeds a critical threshold.
- They arise from toroidicity
- $B$  has an unfavourable curvature low field side → ballooning modes develop mainly on the LFS



[Freidberg, "Ideal MHD"]

# The ballooning modes

- The ballooning instabilities are pressure driven: they are triggered when the pressure gradient exceeds a critical threshold.
- They arise from toroidicity
- $B$  has an unfavourable curvature low field side → ballooning modes develop mainly on the LFS

- Two key parameters define the ballooning stability

- the normalized pressure gradient  $\alpha$

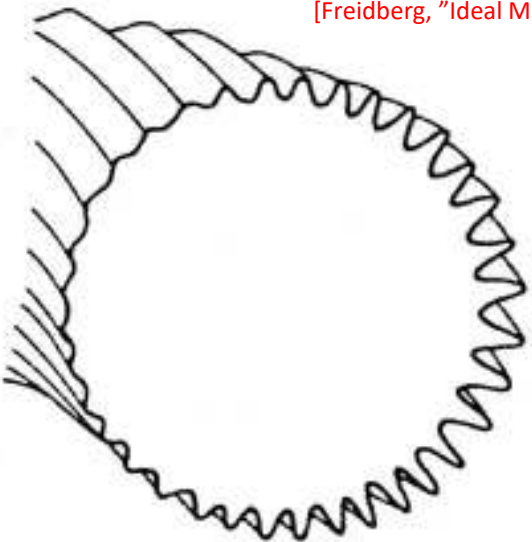
$$\alpha = -\frac{2\mu_0 R q^2}{B^2} \frac{dp}{dr}$$

has a destabilizing effect.

- the magnetic shear

$$s = -\frac{r}{q} \frac{dq}{dr}$$

$s$  has a stabilizing effect.



[Freidberg, "Ideal MHD"]

# The ballooning modes

- The ballooning instabilities are pressure driven: they are triggered when the pressure gradient exceeds a critical threshold.
- They arise from toroidicity
- $B$  has an unfavourable curvature low field side → ballooning modes develop mainly on the LFS
- Two key parameters define the ballooning stability
  - **the normalized pressure gradient  $\alpha$**

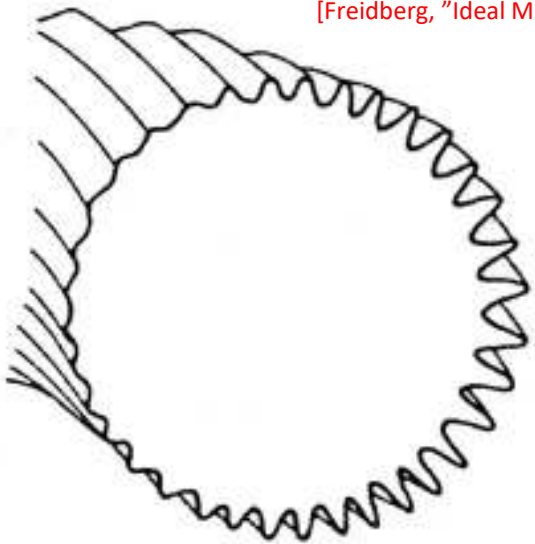
$$\alpha = -\frac{2\mu_0 R q^2}{B^2} \frac{dp}{dr}$$

has a destabilizing effect.

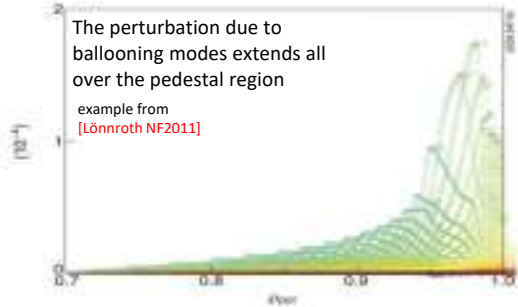
- **the magnetic shear**

$$s = -\frac{r}{q} \frac{dq}{dr}$$

$s$  has a stabilizing effect.



[Freidberg, "Ideal MHD"]



# The ballooning modes

- the normalized pressure gradient  $\alpha$

$$\alpha = -\frac{2\mu_0 R q^2}{B^2} \frac{dp}{dr}$$

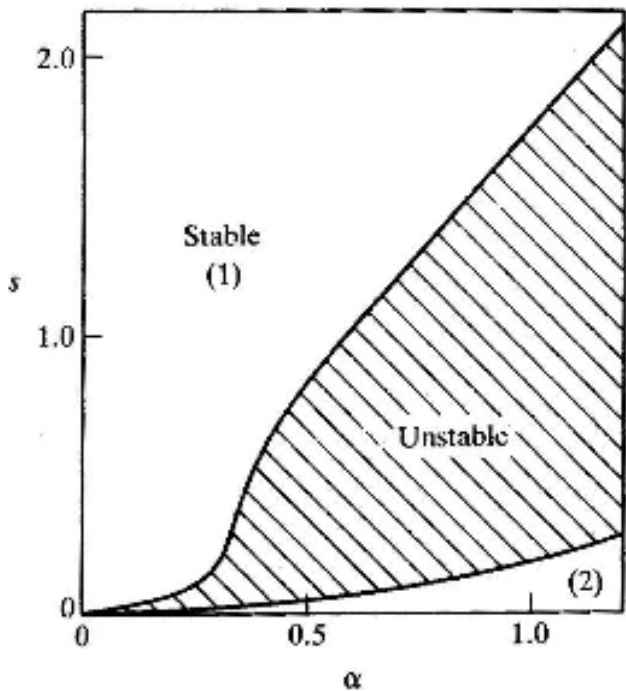
- the increase of  $\alpha$  destabilizes ballooning modes
- at a certain threshold in  $\alpha$  ( $\alpha_{\text{crit}}$ ) , the mode is unstable

- the magnetic shear

$$s = -\frac{r}{q} \frac{dq}{dr}$$

- the shear has a stabilizing effect
- Increasing the shear leads to an increase in  $\alpha_{\text{crit}}$ .

[Wesson "tokamaks"]



# The ballooning modes

- the normalized pressure gradient  $\alpha$

$$\alpha = -\frac{2\mu_0 R q^2}{B^2} \frac{dp}{dr}$$

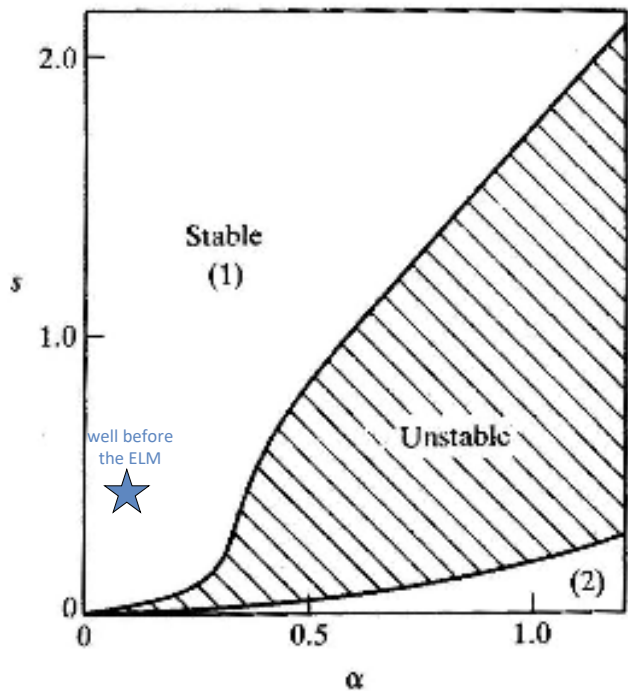
- the increase of  $\alpha$  destabilizes ballooning modes
- at a certain threshold in  $\alpha$  ( $\alpha_{\text{crit}}$ ) , the mode is unstable

- the magnetic shear

$$s = -\frac{r}{q} \frac{dq}{dr}$$

- the shear has a stabilizing effect
- Increasing the shear leads to an increase in  $\alpha_{\text{crit}}$ .

[Wesson "tokamaks"]



# The ballooning modes

- the normalized pressure gradient  $\alpha$

$$\alpha = -\frac{2\mu_0 R q^2}{B^2} \frac{dp}{dr}$$

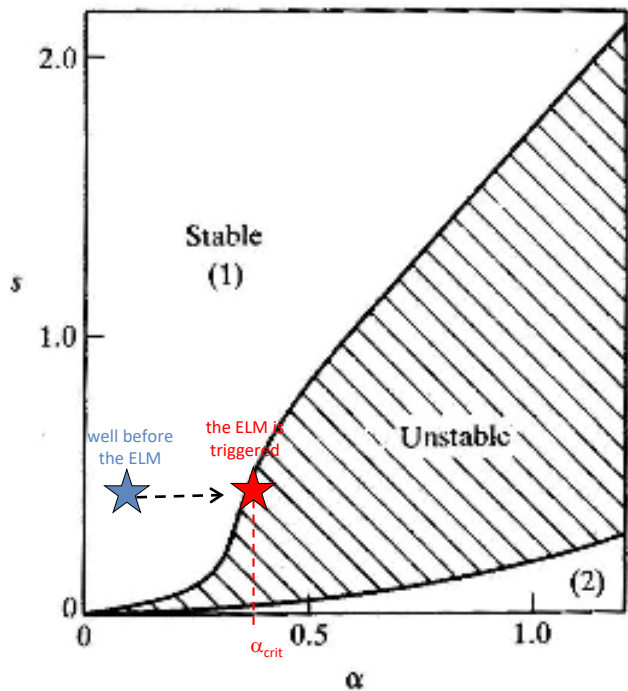
- the increase of  $\alpha$  destabilizes ballooning modes
- at a certain threshold in  $\alpha$  ( $\alpha_{\text{crit}}$ ) , the mode is unstable

- the magnetic shear

$$s = -\frac{r}{q} \frac{dq}{dr}$$

- the shear has a stabilizing effect
- Increasing the shear leads to an increase in  $\alpha_{\text{crit}}$ .

[Wesson "tokamaks"]



# The ballooning modes

- the normalized pressure gradient  $\alpha$

$$\alpha = -\frac{2\mu_0 R q^2}{B^2} \frac{dp}{dr}$$

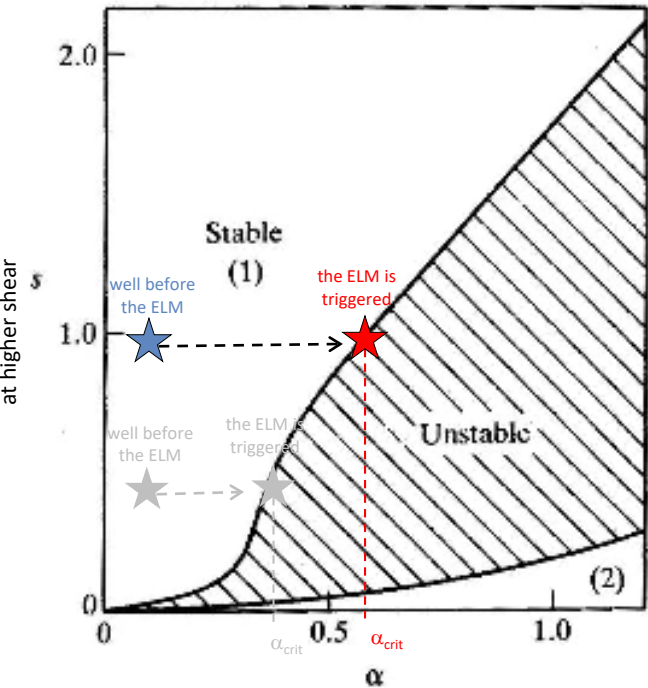
- the increase of  $\alpha$  destabilizes ballooning modes
- at a certain threshold in  $\alpha$  ( $\alpha_{\text{crit}}$ ) , the mode is unstable

- the magnetic shear

$$s = -\frac{r}{q} \frac{dq}{dr}$$

- the shear has a stabilizing effect
- Increasing the shear leads to an increase in  $\alpha_{\text{crit}}$ .

[Wesson "tokamaks"]



# The ballooning modes

- the normalized pressure gradient  $\alpha$

$$\alpha = -\frac{2\mu_0 R q^2}{B^2} \frac{dp}{dr}$$

- the increase of  $\alpha$  destabilizes ballooning modes
- at a certain threshold in  $\alpha$  ( $\alpha_{\text{crit}}$ ) , the mode is unstable

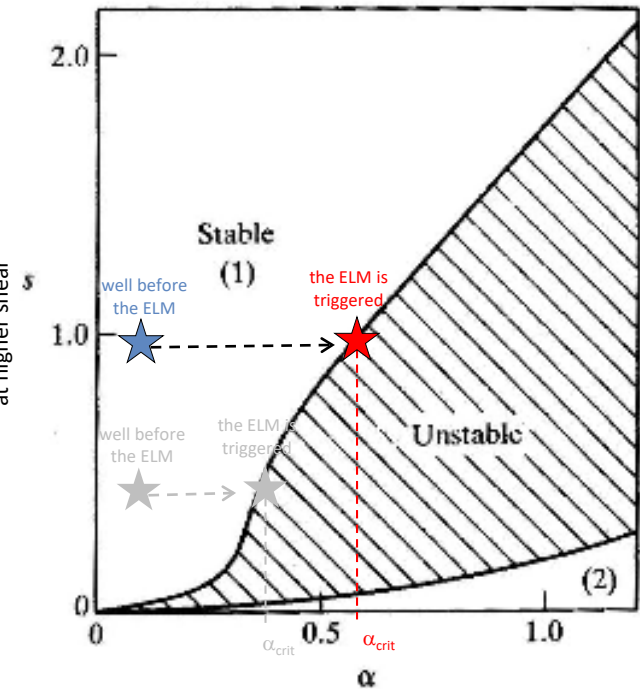
- the magnetic shear

$$s = -\frac{r}{q} \frac{dq}{dr}$$

- the shear has a stabilizing effect
- Increasing the shear leads to an increase in  $\alpha_{\text{crit}}$ .

- Most of the machines have a pedestal in region (1): the first stability region
- However, theory predicts a second stability region, at high  $\alpha$  and low shear

[Wesson "tokamaks"]



# The ballooning modes

- the normalized pressure gradient  $\alpha$

$$\alpha = -\frac{2\mu_0 R q^2}{B^2} \frac{dp}{dr}$$

- the increase of  $\alpha$  destabilizes ballooning modes
- at a certain threshold in  $\alpha$  ( $\alpha_{\text{crit}}$ ) , the mode is unstable

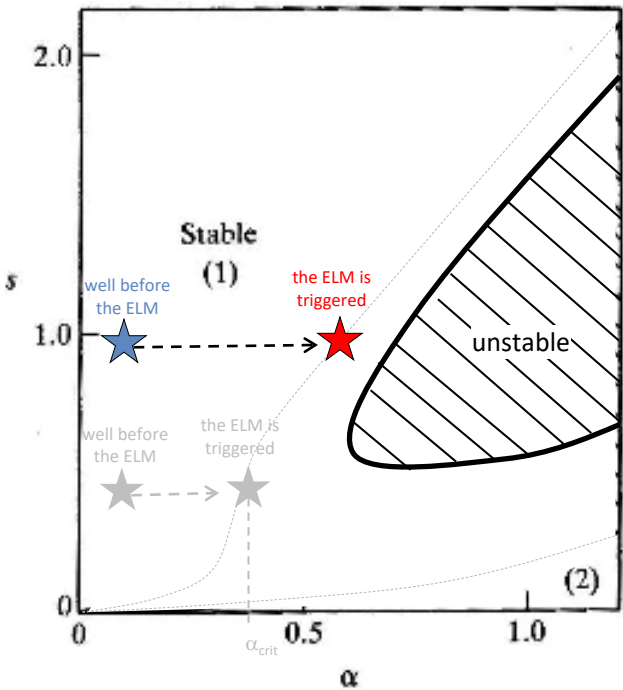
- the magnetic shear

$$s = -\frac{r}{q} \frac{dq}{dr}$$

- the shear has a stabilizing effect
- Increasing the shear leads to an increase in  $\alpha_{\text{crit}}$ .

- Most of the machines have a pedestal in region (1): the first stability region
- However, theory predicts a second stability region, at high  $\alpha$  and low shear
- Finite Larmor radius effects have a stabilizing effects and reduce the unstable region

adapted from  
[Wesson "tokamaks"]



# The ballooning modes

- the normalized pressure gradient  $\alpha$

$$\alpha = -\frac{2\mu_0 R q^2}{B^2} \frac{dp}{dr}$$

- the increase of  $\alpha$  destabilizes ballooning modes
- at a certain threshold in  $\alpha$  ( $\alpha_{\text{crit}}$ ) , the mode is unstable

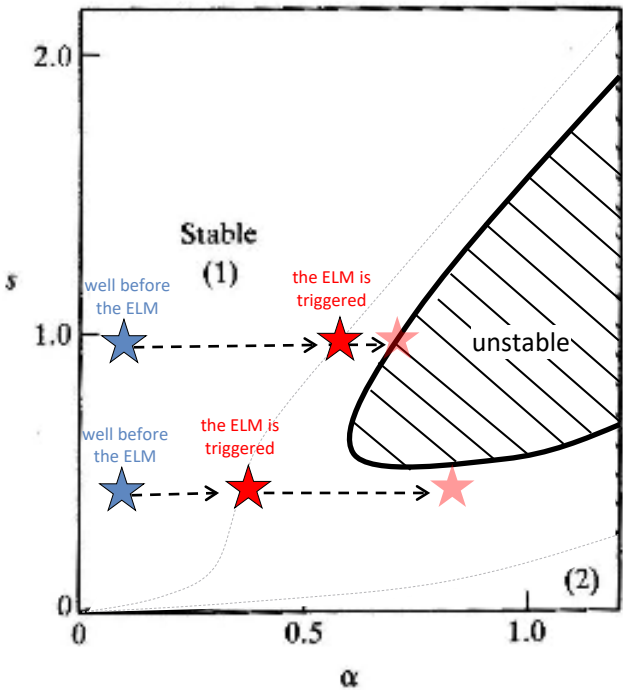
- the magnetic shear

$$s = -\frac{r}{q} \frac{dq}{dr}$$

- the shear has a stabilizing effect
- Increasing the shear leads to an increase in  $\alpha_{\text{crit}}$ .

- Most of the machines have a pedestal in region (1): the first stability region
- However, theory predicts a second stability region, at high  $\alpha$  and low shear
- Finite Larmor radius effects have a stabilizing effects and reduce the unstable region

adapted from  
[Wesson "tokamaks"]



# The ballooning modes

- the normalized pressure gradient  $\alpha$

$$\alpha = -\frac{2\mu_0 R q^2}{B^2} \frac{dp}{dr}$$

- the increase of  $\alpha$  destabilizes ballooning modes
- at a certain threshold in  $\alpha$  ( $\alpha_{\text{crit}}$ ) , the mode is unstable

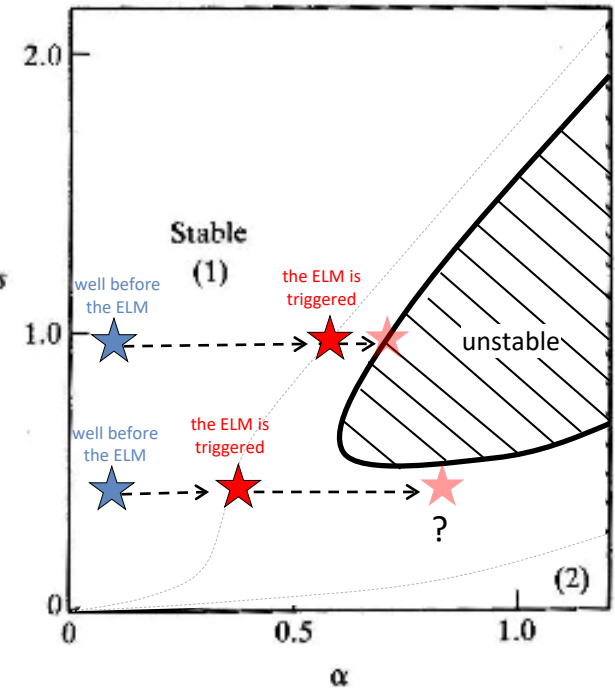
- the magnetic shear

$$s = -\frac{r}{q} \frac{dq}{dr}$$

- the shear has a stabilizing effect
- Increasing the shear leads to an increase in  $\alpha_{\text{crit}}$ .

- Most of the machines have a pedestal in region (1): the first stability region
- However, theory predicts a second stability region, at high  $\alpha$  and low shear
- Finite Larmor radius effects have a stabilizing effects and reduce the unstable region

adapted from  
[Wesson "tokamaks"]

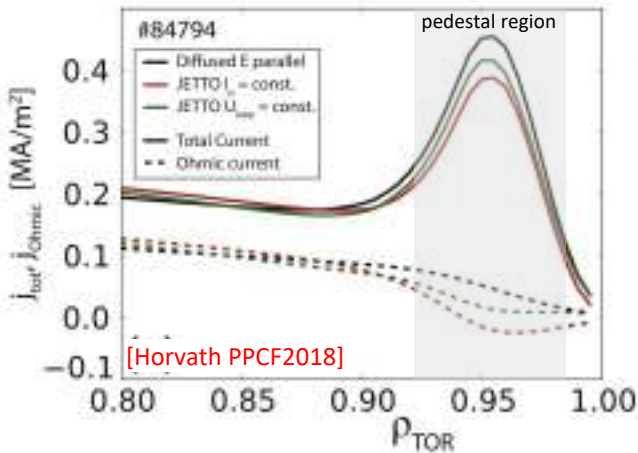


No!

There are further instabilities → see later.  
But first...

# The bootstrap current

- Due to the steep gradients in the pedestal region, the bootstrap current ( $j_{bs}$ ) can give a significant contribution to the total current density.
- For an expression of  $j_{bs}$ : [Sauter PoP1999]



# The bootstrap current

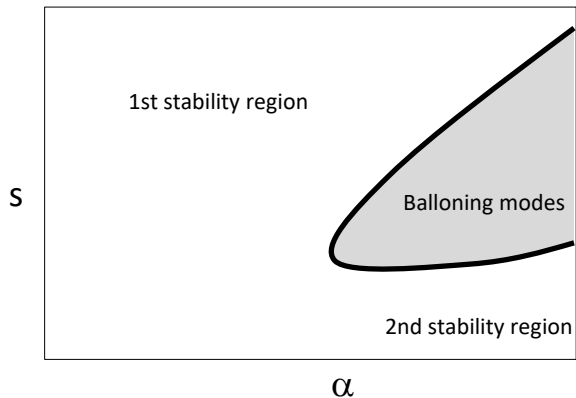
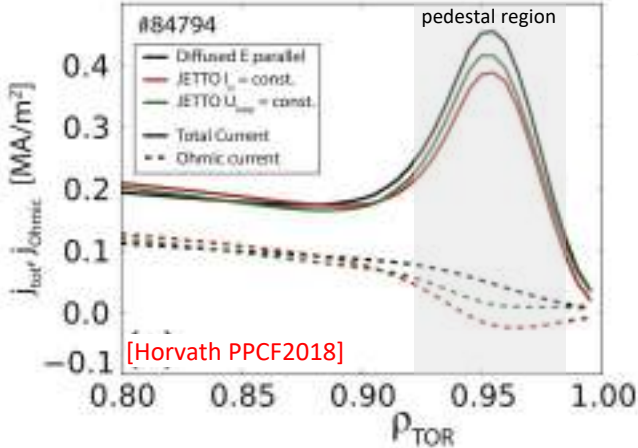
- Due to the steep gradients in the pedestal region, the bootstrap current ( $j_{bs}$ ) can give a significant contribution to the total current density.
- For an expression of  $j_{bs}$ : [Sauter PoP1999]
- The increase in the current density affects the shear [Miller PoP1999]

→  $j_{bs}$  has an effect on the pedestal stability.

[Snyder PoP2002]

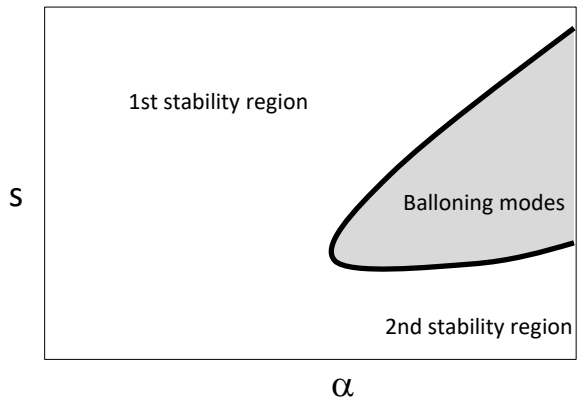
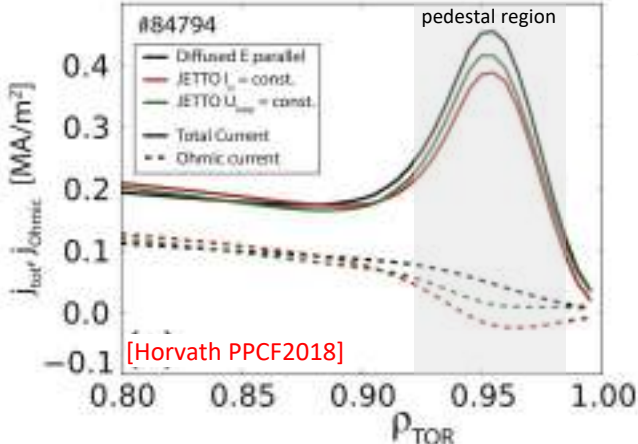
→ the parameters that affects  $j_{bs}$  will affect also the ballooning stability:

- collisionality
- plasma shape



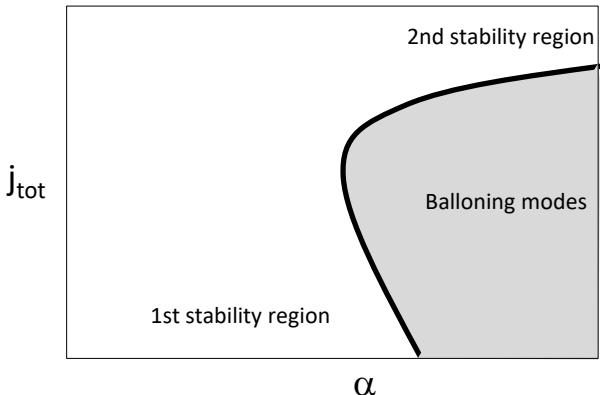
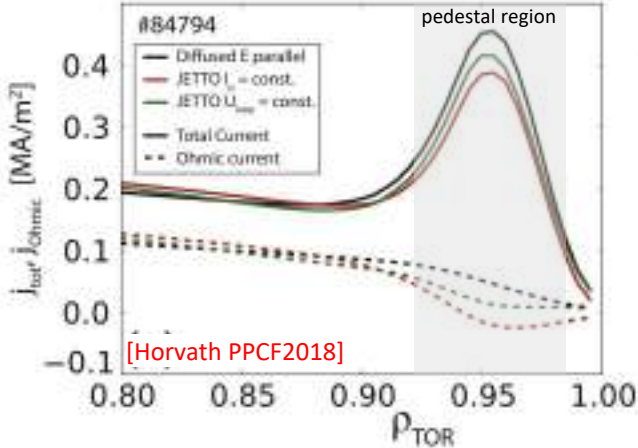
# The bootstrap current

- Due to the steep gradients in the pedestal region, the bootstrap current ( $j_{bs}$ ) can give a significant contribution to the total current density.
- For an expression of  $j_{bs}$ : [Sauter PoP1999]
- The increase in the current density affects the shear [Miller PoP1999]
- $j_{bs}$  has an effect on the pedestal stability. [Snyder PoP2002]
- the parameters that affects  $j_{bs}$  will affect also the ballooning stability:
  - collisionality
  - plasma shape
- It is common to use  $j_{tot}$  instead of the shear in the stability diagram



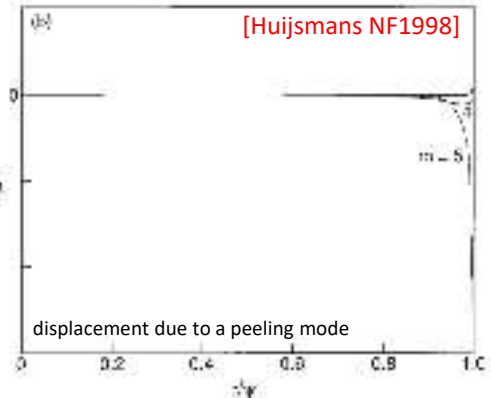
# The bootstrap current

- Due to the steep gradients in the pedestal region, the bootstrap current ( $j_{bs}$ ) can give a significant contribution to the total current density.
- For an expression of  $j_{bs}$ : [Sauter PoP1999]
- The increase in the current density affects the shear [Miller PoP1999]
- $j_{bs}$  has an effect on the pedestal stability. [Snyder PoP2002]
- the parameters that affects  $j_{bs}$  will affect also the ballooning stability:
  - collisionality
  - plasma shape
- It is common to use  $j_{tot}$  instead of the shear in the stability diagram



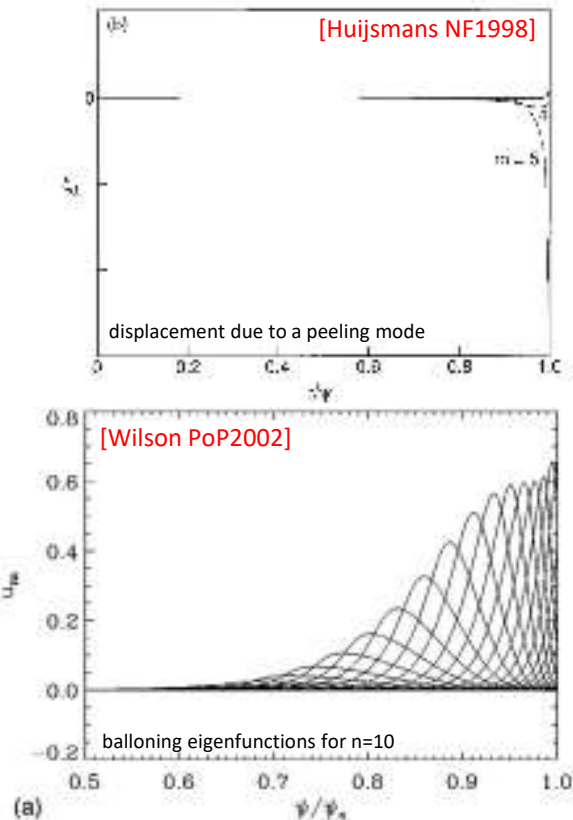
# The external kink / peeling mode

- The external kink mode is current driven
- The kink mode ( $m, n$ ) is destabilized when  $q$  at the plasma edge is low enough that  $q_{edge} < m/n$  and the resonance is very close to the plasma
  - the kink mode is resonant outside the plasma
  - the kink mode is strongly localized at the plasma edge.



# The external kink / peeling mode

- The external kink mode is current driven
- The kink mode ( $m, n$ ) is destabilized when  $q$  at the plasma edge is low enough that  $q_{edge} < m/n$  and the resonance is very close to the plasma
  - the kink mode is resonant outside the plasma
  - the kink mode is strongly localized at the plasma edge.  
For comparison, the ballooning modes have a more global structure.

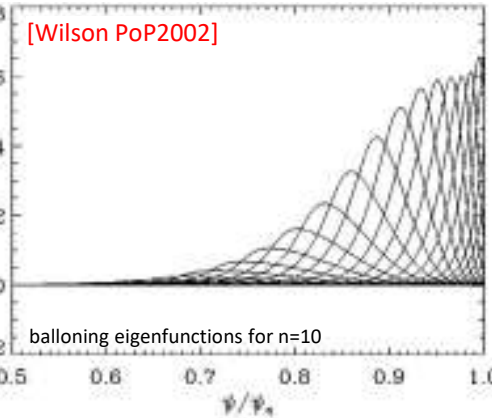
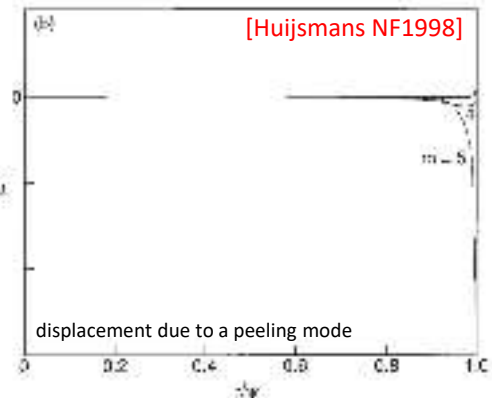
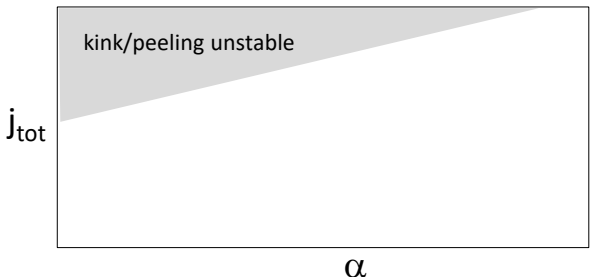


# The external kink / peeling mode

- The external kink mode is current driven
- The kink mode ( $m, n$ ) is destabilized when  $q$  at the plasma edge is low enough that  $q_{edge} < m/n$  and the resonance is very close to the plasma
  - the kink mode is resonant outside the plasma
  - the kink mode is strongly localized at the plasma edge.

For comparison, the ballooning modes have a more global structure.
- The kink mode depends on the edge current  
 $\rightarrow j_{bs}$  has a strong role

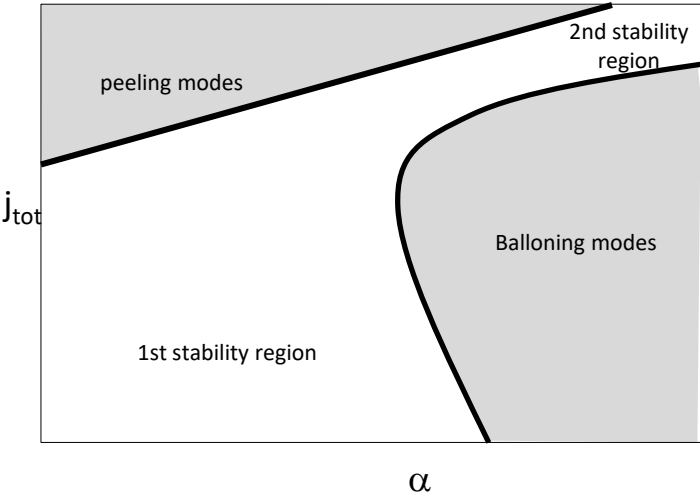
[Huijsmans NF1998]



(a)

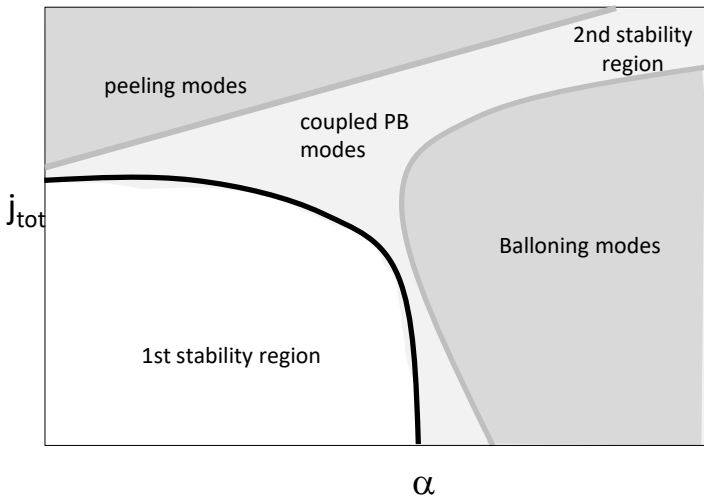
# The peeling-balloonning (PB) modes

- Toroidicity and shaping effects can couple peeling and ballooning (PB) modes.



# The peeling-balloonning (PB) modes

- Toroidicity and shaping effects can couple peeling and ballooning (PB) modes.
- The coupled PB modes can be destabilized even if the single peeling mode and ballooning are stable.  
[Connor PoP1998]
- The PB stability are driven by both pressure gradient and current density.

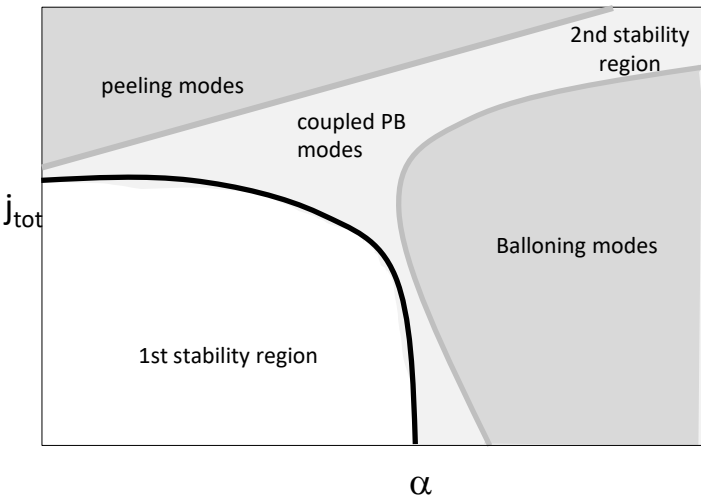


# The peeling-balloonning (PB) modes

- Toroidicity and shaping effects can couple peeling and ballooning (PB) modes.
- The coupled PB modes can be destabilized even if the single peeling mode and ballooning are stable.

[Connor PoP1998]

- The PB stability are driven by both pressure gradient and current density.
- The PB stability is the leading theory to explain the pedestal behvaior in type I ELM My H-modes. [Snyder PoP2002]  
[Wilson PoP2002]
- The PB modes strongly limit the stable region.
- The access to the 2nd stability region is closed (most of the times).

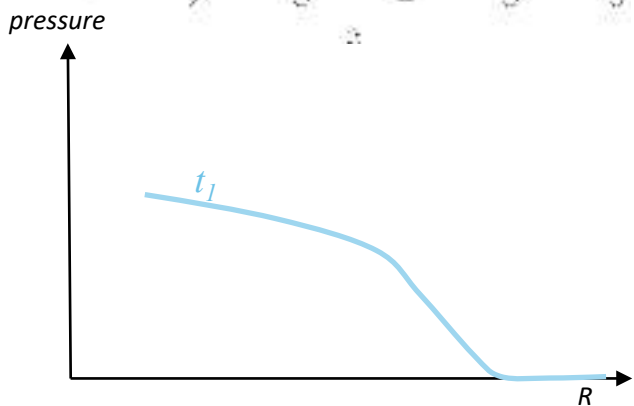
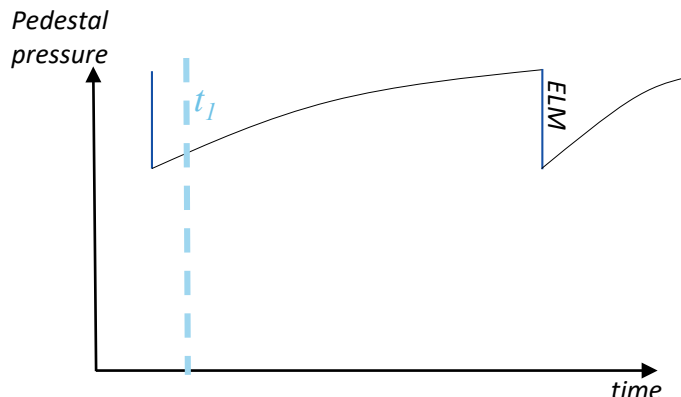
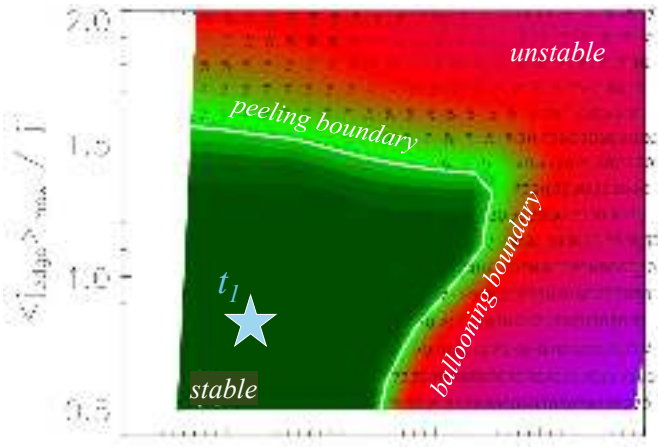


# OUTLINE

- L-H transition
- Pedestal structure
- Edge localized modes (ELMs)
  - ELM energy losses
  - ELM types
- **MHD stability of the pedestal**
  - **Role of MHD stability (and few words on transport)**
  - **The peeling-ballooning (PB) model**
  - **The ELM cycle within the PB model**
  - **Parameters that influences the pedestal**
- Pedestal predictions
  - The EPED model:
    - The PB constraint
    - The KBM constraint
  - Non-linear MHD modelling
- Some of the most active research areas in pedestal physics

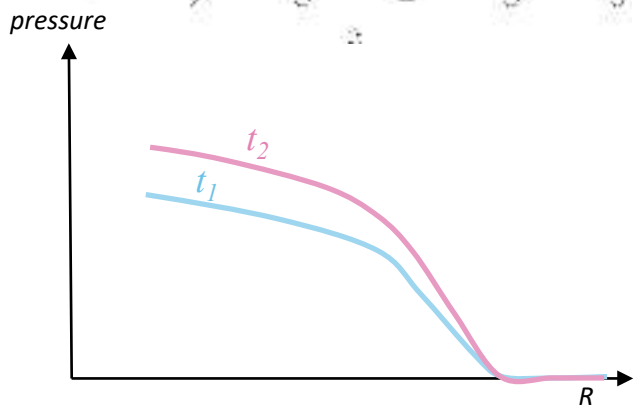
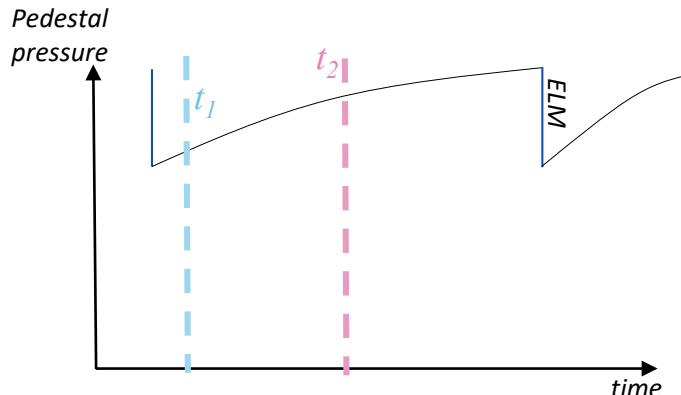
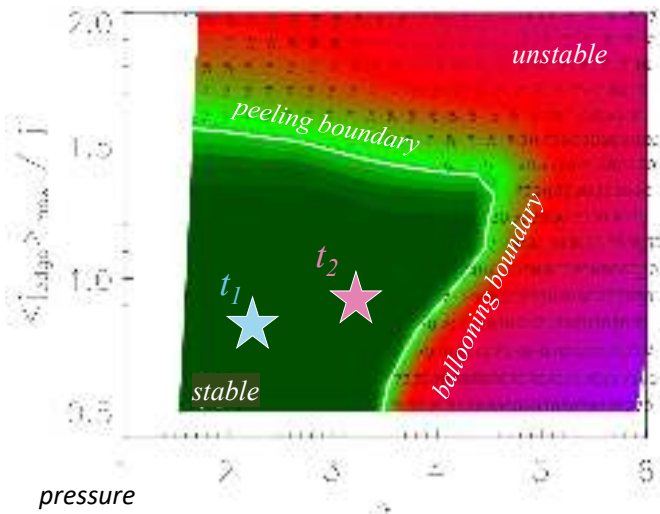
# The PB model for the ELM cycle

- 1 Just after an ELM, the pedestal has low gradient and low  $j_{bs}$ .



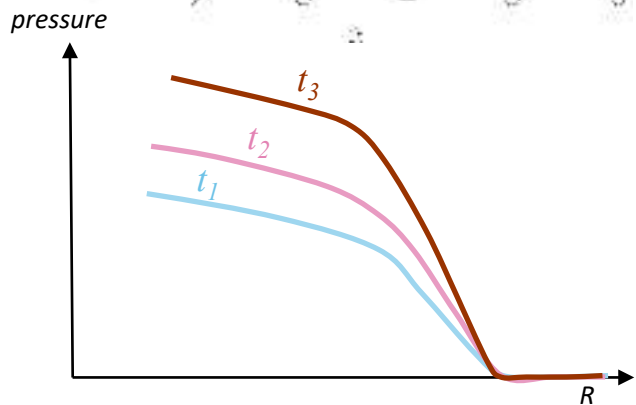
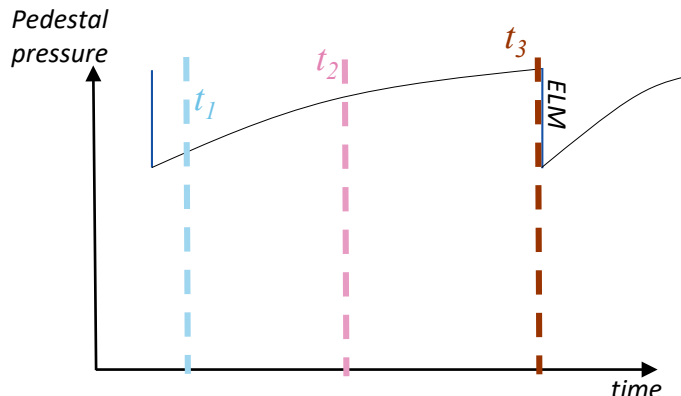
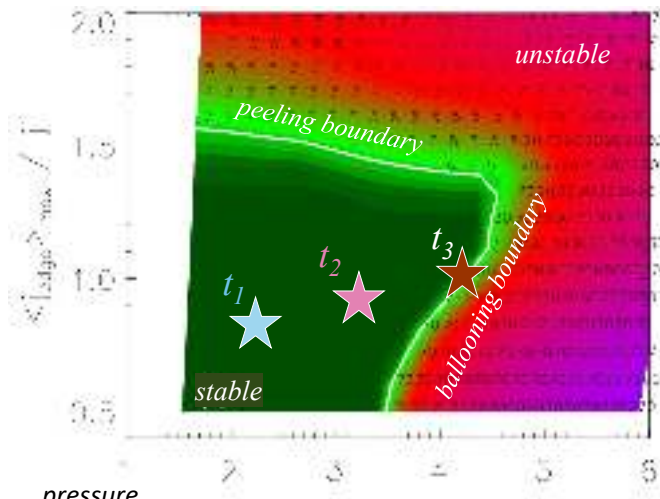
# The PB model for the ELM cycle

- 1 Just after an ELM, the pedestal has low gradient and low  $j_{bs}$ .
- 2 During the ELM cycle, the pressure gradient (and hence  $j_{bs}$ ) increases



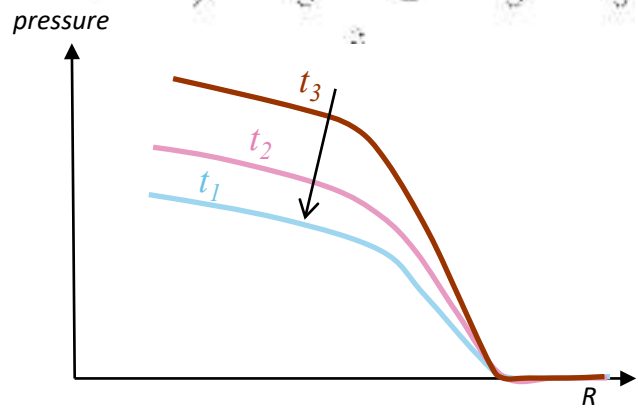
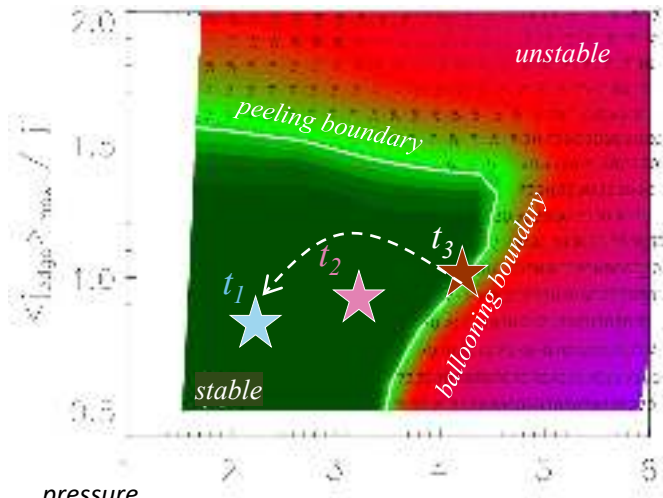
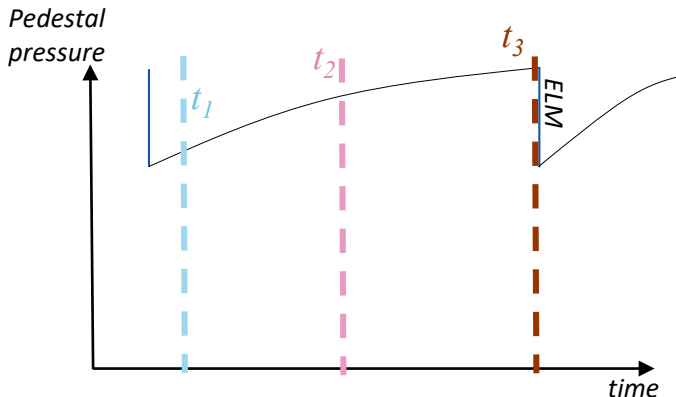
# The PB model for the ELM cycle

- 1 Just after an ELM, the pedestal has low gradient and low  $j_{bs}$ .
- 2 During the ELM cycle, the pressure gradient (and hence  $j_{bs}$ ) increases
- 3 The process continues till the PB boundary is reached.



# The PB model for the ELM cycle

- 1 Just after an ELM, the pedestal has low gradient and low  $j_{bs}$ .
- 2 During the ELM cycle, the pressure gradient (and hence  $j_{bs}$ ) increases
- 3 The process continues till the PB boundary is reached.
- 4 Then an ELM is triggered:
  - o the pressure gradient and the  $j_{bs}$  collapse.
  - o the process starts again.

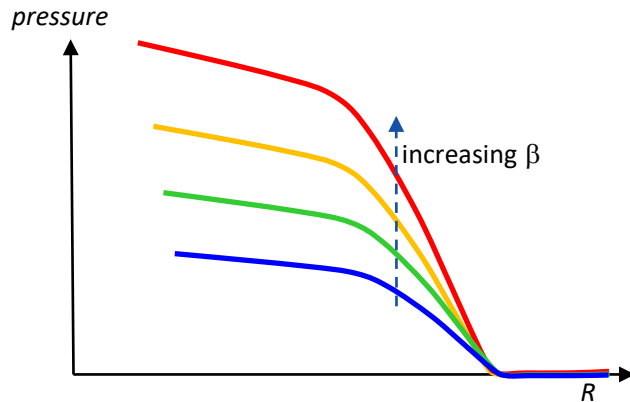
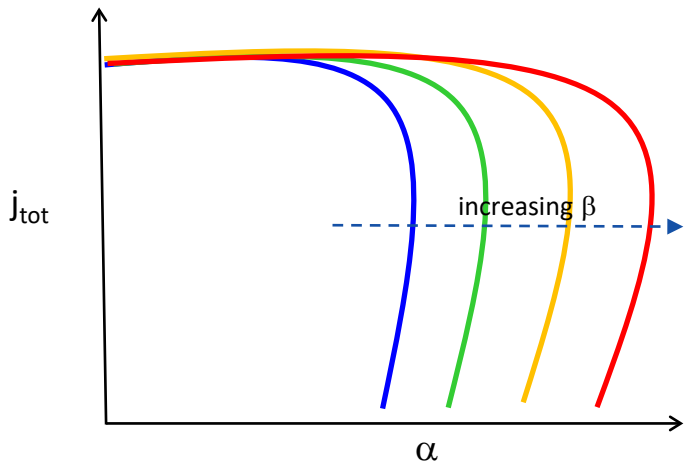


# OUTLINE

- L-H transition
- Pedestal structure
- Edge localized modes (ELMs)
  - ELM energy losses
  - ELM types
- **MHD stability of the pedestal**
  - **Role of MHD stability (and few words on transport)**
  - **The peeling-ballooning (PB) model**
  - **The ELM cycle within the PB model**
  - **Parameters that influences the pedestal**
- Pedestal predictions
  - The EPED model:
    - The PB constraint
    - The KBM constraint
  - Non-linear MHD modelling
- Some of the most active research areas in pedestal physics

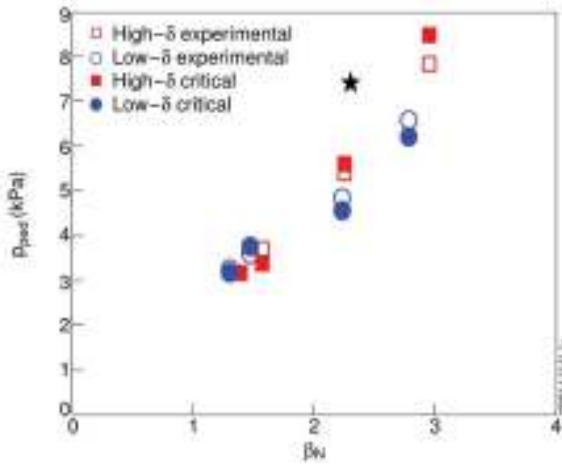
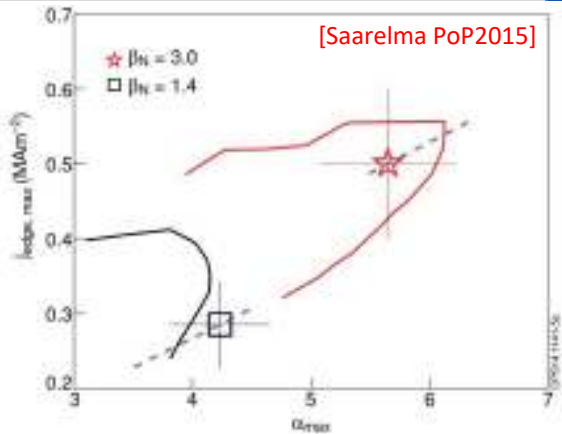
# Parameters that affect the pedestal: $\beta$

- $\beta = \frac{\langle p \rangle}{B^2/(2\mu_0)}$
  - the increase of  $\beta$  leads to the increases of the Shafranov shift.
    - the Shafranov shift has a stabilizing effect on the ballooning modes.
    - the ballooning modes boundary moves to higher  $\alpha$
    - the pre-ELM pedestal pressure gradient increases
- $p^{\text{ped}}$  increases with increasing  $\beta$ .



# Parameters that affect the pedestal: $\beta$

- $\beta = \frac{\langle p \rangle}{B^2/(2\mu_0)}$
  - the increase of  $\beta$  leads to the increases of the Shafranov shift.
    - the Shafranov shift has a stabilizing effect on the ballooning modes.
    - the ballooning modes boundary moves to higher  $\alpha$
    - the pre-ELM pedestal pressure gradient increases
- $p^{\text{ped}}$  increases with increasing  $\beta$ .



# Parameters that affect the pedestal: $\nu^*$

- Collisionality

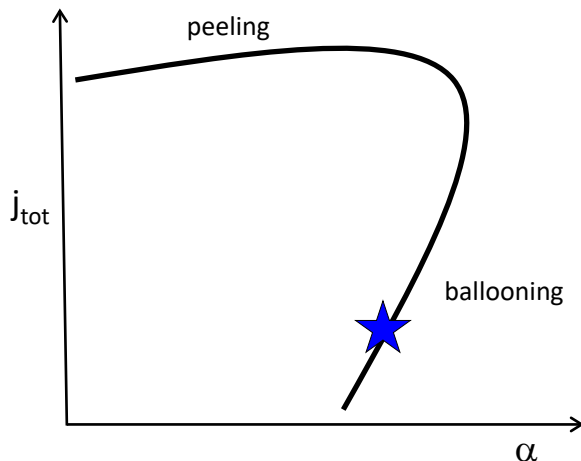
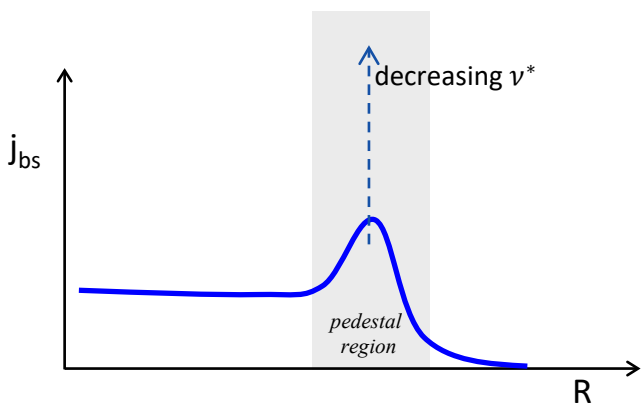
$$\nu^* = c \ln \Lambda \frac{R q n_e}{\varepsilon^{3/2} (T_e)^2}$$

- the collisionality has a major effect on  $j_{bs}$ .

[Sauter PoP1999] [Redl PoP2021]

- Approximately:

$$j_{bs} \approx \nu^{*-1}$$



- The reduction of collisionality tends to increase  $\nabla p$ , if the pedestal is near the ballooning boundary

# Parameters that affect the pedestal: $\nu^*$

- Collisionality

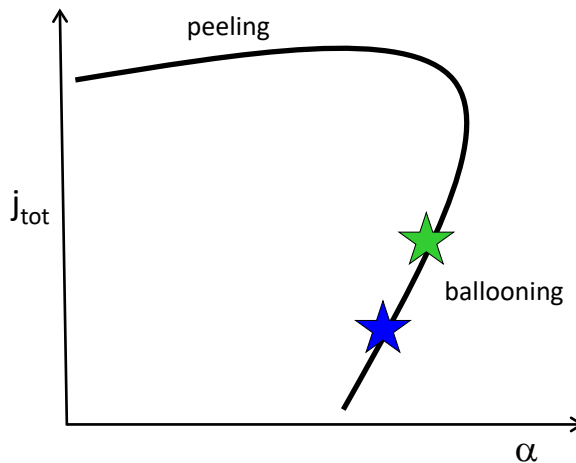
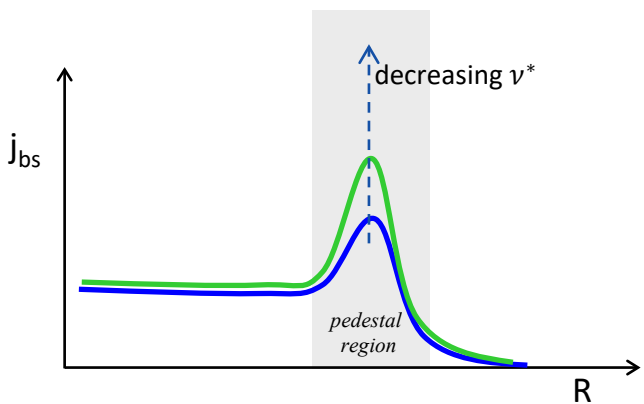
$$\nu^* = \text{cln} \Lambda \frac{R q n_e}{\varepsilon^{3/2} (T_e)^2}$$

- the collisionality has a major effect on  $j_{bs}$ .

[Sauter PoP1999] [Redl PoP2021]

- Approximately:

$$j_{bs} \approx \nu^{*-1}$$



- The reduction of collisionality tends to increase  $\nabla p$ , if the pedestal is near the ballooning boundary

# Parameters that affect the pedestal: $\nu^*$

- Collisionality

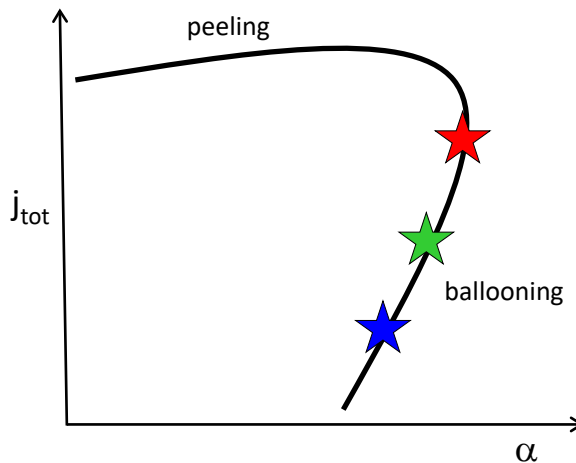
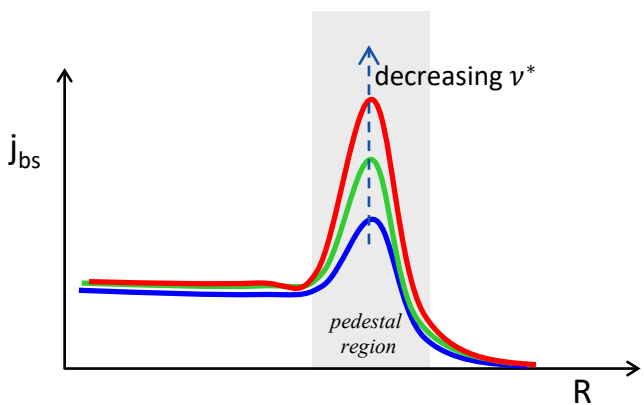
$$\nu^* = c \ln \Lambda \frac{R q n_e}{\varepsilon^{3/2} (T_e)^2}$$

- the collisionality has a major effect on  $j_{bs}$ .

[Sauter PoP1999] [Redl PoP2021]

- Approximately:

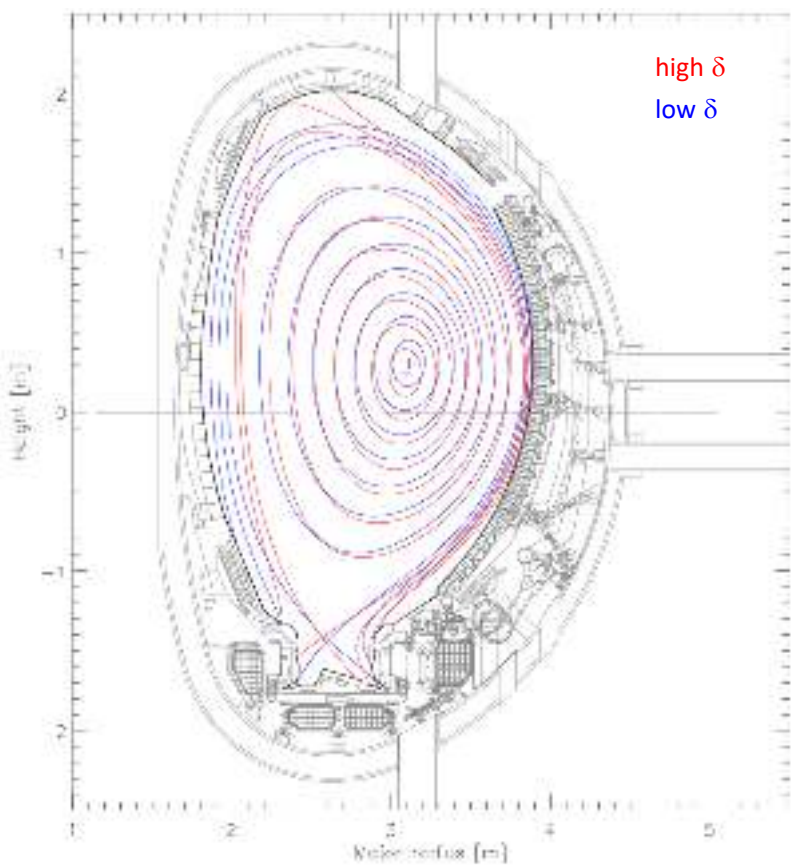
$$j_{bs} \approx \nu^{*-1}$$



- The reduction of collisionality tends to increase  $\nabla p$ , if the pedestal is near the ballooning boundary

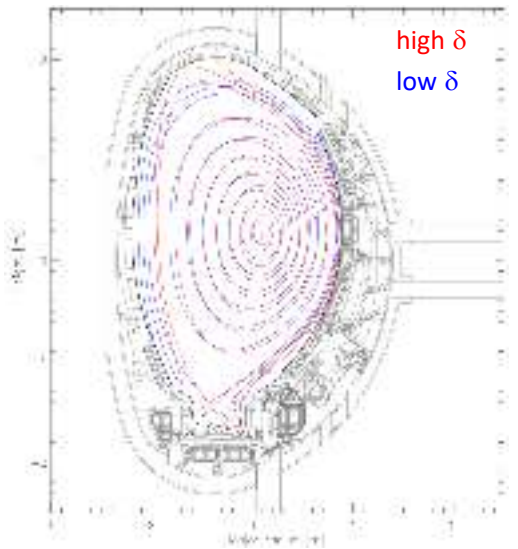
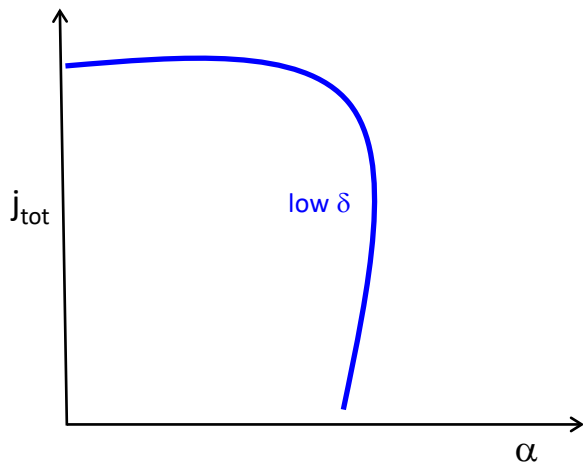
# Parameters that affect the pedestal: $\delta$

- $\delta$ : plasma triangularity



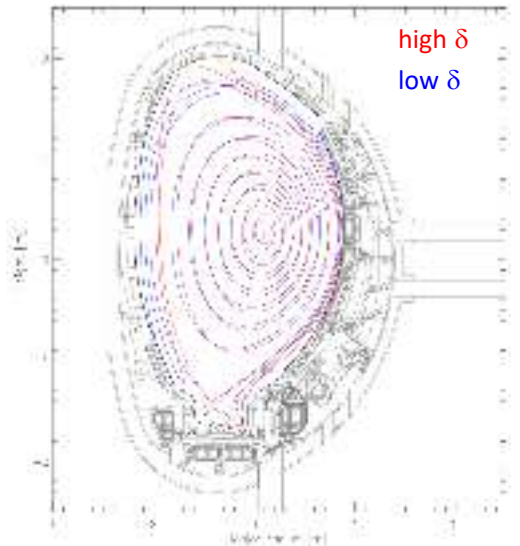
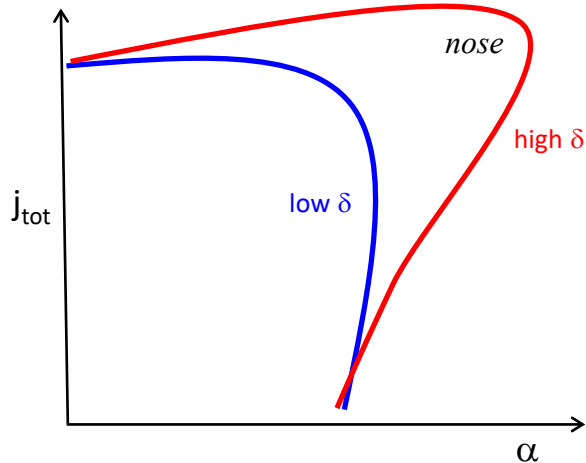
# Parameters that affect the pedestal: $\delta$

- $\delta$ : plasma triangularity
- the increase of  $\delta$  stabilizes part of the ballooning modes.



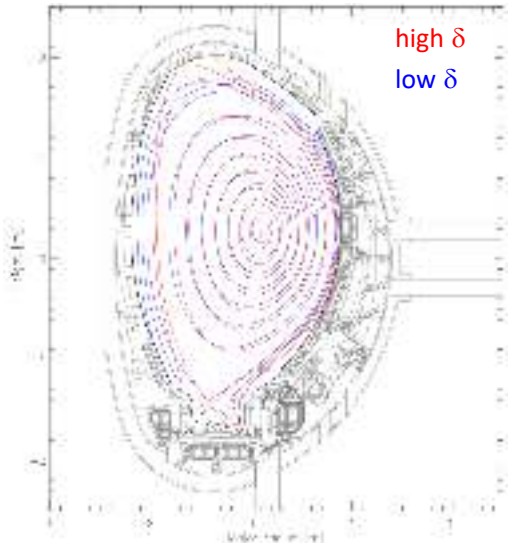
# Parameters that affect the pedestal: $\delta$

- $\delta$ : plasma triangularity
- the increase of  $\delta$  stabilizes part of the ballooning modes.
- the PB is strongly shaped at high  $\delta$  and a so called "nose" is formed:
  - high  $j_{bs}$   $\rightarrow \nabla p$  increases with increasing  $\delta$ .
  - low  $j_{bs}$   $\rightarrow \nabla p$  does not change much with  $\delta$ .

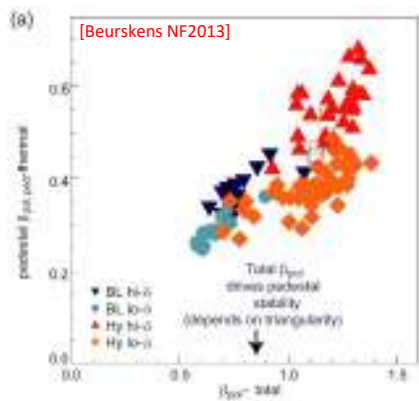
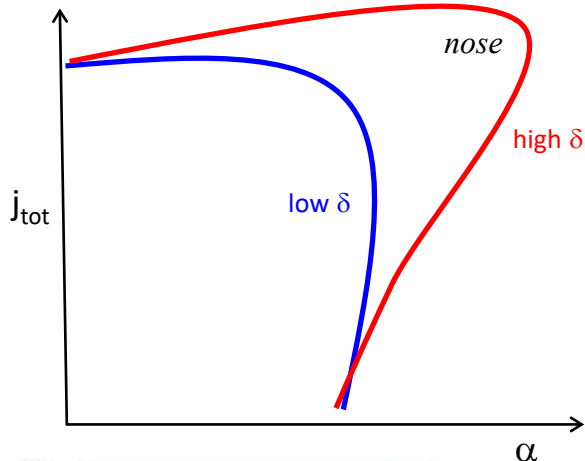


# Parameters that affect the pedestal: $\delta$

- $\delta$ : plasma triangularity
- the increase of  $\delta$  stabilizes part of the ballooning modes.
- the PB is strongly shaped at high  $\delta$  and a so called "nose" is formed:
  - high  $j_{bs}$   $\rightarrow \nabla p$  increases with increasing  $\delta$ .
  - low  $j_{bs}$   $\rightarrow \nabla p$  does not change much with  $\delta$ .

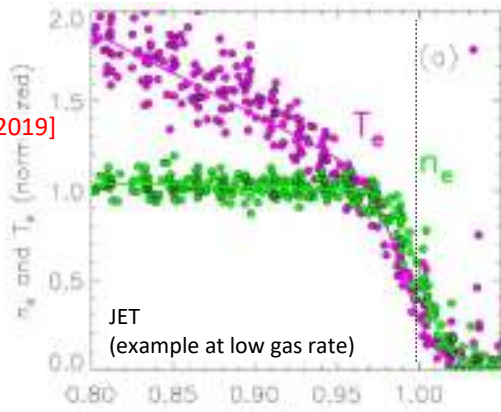


[Saibene PPCF2002]  
 [Beurskens NF2013]  
 [Urano NF2014]

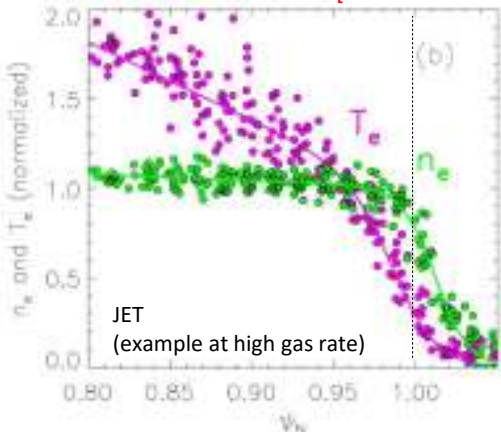


# Parameters that affect the pedestal: $n_e^{\text{sep}}/n_e^{\text{ped}}$

- Separatrix density and pedestal position:
  - The pedestal position can vary significantly depending on engineering parameters [Stefanikova NF2019]

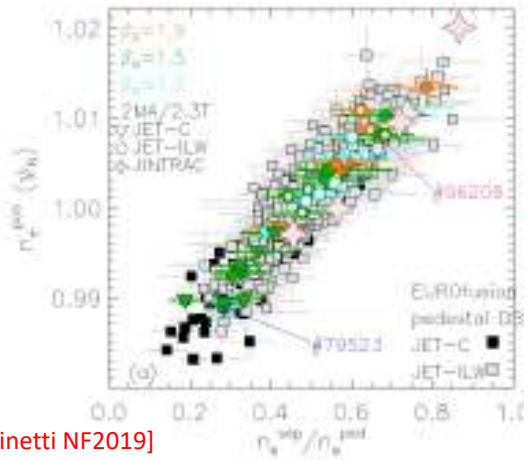


[Stefanikova NF2019]

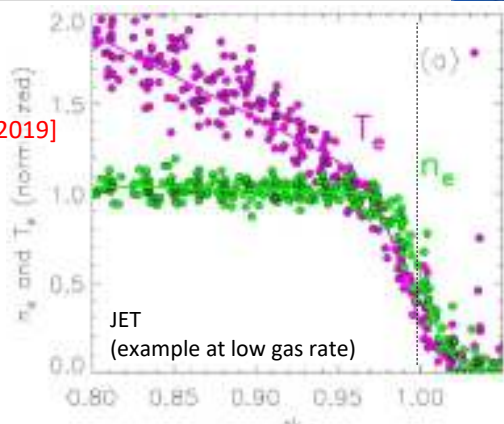


## Parameters that affect the pedestal: $n_e^{sep}/n_e^{ped}$

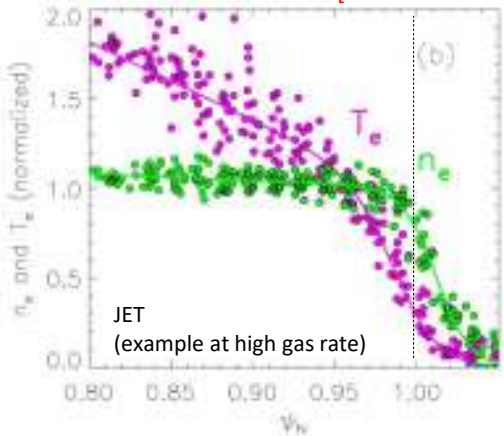
- Separatrix density and pedestal position:
    - The pedestal position can vary significantly depending on engineering parameters [Stefanini et al. 2018]
    - $n_e$  pedestal position and separatrix density are strongly correlated. [Frassinetti NF2021]



[Frassineti NF2019]

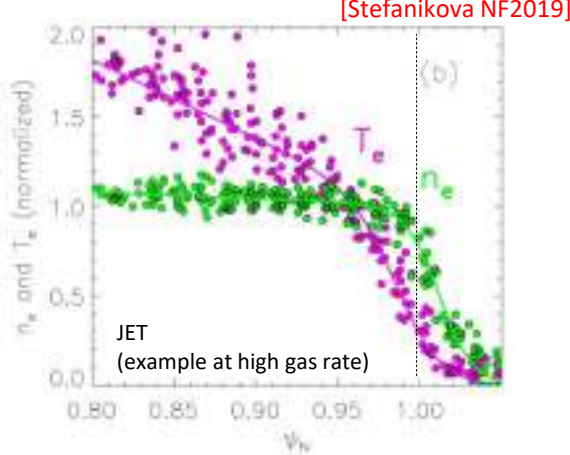
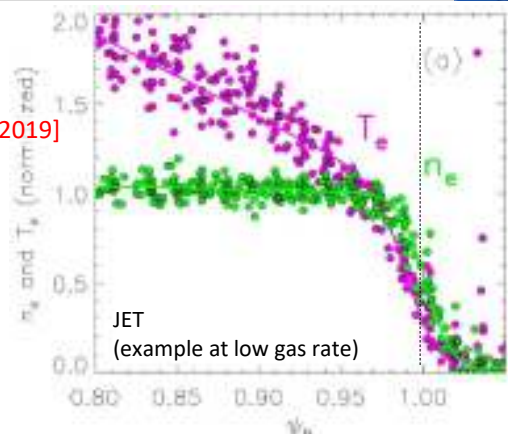
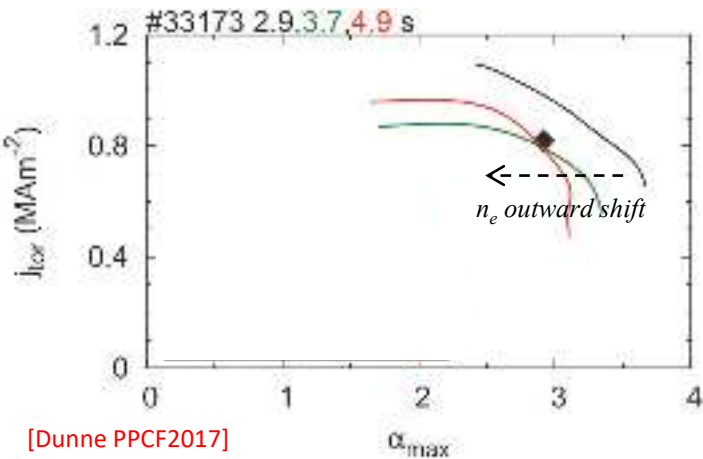


[Stefanikova NF2019]



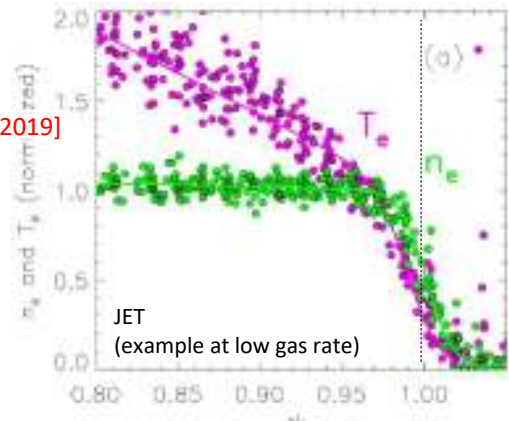
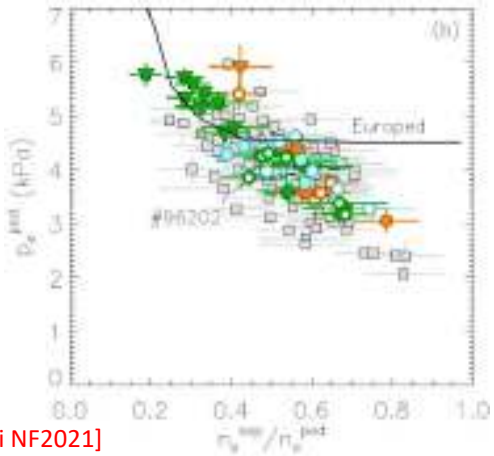
# Parameters that affect the pedestal: $n_e^{\text{sep}}/n_e^{\text{ped}}$

- Separatrix density and pedestal position:
  - The pedestal position can vary significantly depending on engineering parameters [Stefanikova NF2019]
  - $n_e$  pedestal position and separatrix density are strongly correlated. [Frassinetti NF2021]
  - The increase of  $n_e^{\text{sep}}/n_e^{\text{ped}}$  and the outward shift of the pedestal position destabilizes ballooning modes and reduces the pedestal height [Dunne PPCF2017][Frassinetti NF2019]

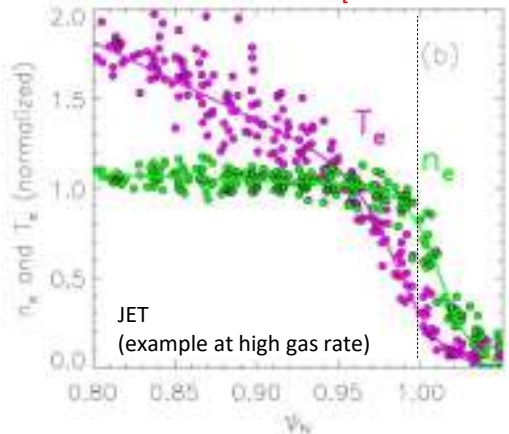


# Parameters that affect the pedestal: $n_e^{sep}/n_e^{ped}$

- Separatrix density and pedestal position:
  - The pedestal position can vary significantly depending on engineering parameters [Stefanikova NF2019]
  - $n_e$  pedestal position and separatrix density are strongly correlated. [Frassinetti NF2021]
  - The increase of  $n_e^{sep}/n_e^{ped}$  and the outward shift of the pedestal position destabilizes ballooning modes and reduces the pedestal height [Dunne PPCF2017][Frassinetti NF2019]



[Stefanikova NF2019]

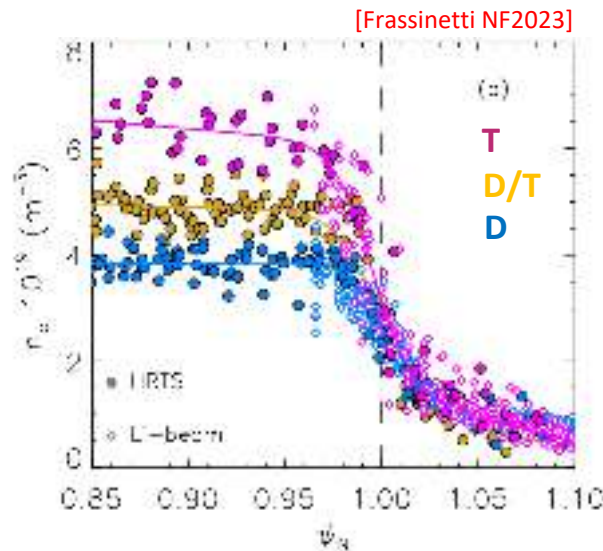


# Parameters that affect the pedestal: isotope



- Isotope mass ( $A$ ) can affect the pedestal:
  - pedestal density
    - $n_e^{\text{ped}}$  increases with increasing  $A$  (JET, DIII-D, AUG, JT60-U...)
    - Effect observed both from  $H \rightarrow D$  and from  $D \rightarrow T$

[Urano NF2013] [Horvath NF2021]  
[Gohil IAEA2008] [Schneider PPCF2021]  
[Maggi PPCF2018] [Schneider NF2022]  
[Frassinetti NF2023]



# Parameters that affect the pedestal: isotope



- Isotope mass ( $A$ ) can affect the pedestal:
  - pedestal density
    - $n_e^{\text{ped}}$  increases with increasing  $A$  (JET, DIII-D, AUG, JT60-U...)
    - Effect observed both from  $H \rightarrow D$  and from  $D \rightarrow T$ 
      - [Urano NF2013] [Horvath NF2021]
      - [Gohil IAEA2008] [Schneider PPCF2021]
      - [Maggi PPCF2018] [Schneider NF2022]
      - [Frassinetti NF2023]
  - pedestal pressure
    - In JET and AUG:  $p_e^{\text{ped}}$  increases with increasing  $A$ . [Maggi PPCF2018, Schneider NF2023]
    - In DIII-D and JT60-U: no significant effect related to  $A$ 
      - [Urano NF2013]
      - [Gohil IAEA2008]

# Parameters that affect the pedestal: isotope

- Isotope mass ( $A$ ) can affect the pedestal:
  - pedestal density
    - $n_e^{\text{ped}}$  increases with increasing  $A$  (JET, DIII-D, AUG, JT60-U...)
    - Effect observed both from  $H \rightarrow D$  and from  $D \rightarrow T$
  - pedestal pressure
    - In JET and AUG:  $p_e^{\text{ped}}$  increases with increasing  $A$ . [Maggi PPCF2018, Schneider NF2023]
    - In DIII-D and JT60-U: no significant effect related to  $A$

[Urano NF2013]

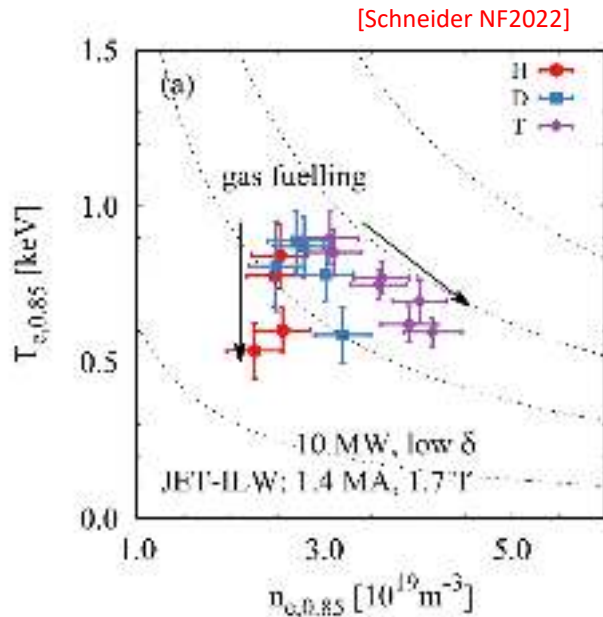
[Gohil IAEA2008]

[Maggi PPCF2018]

[Horvath NF2021]

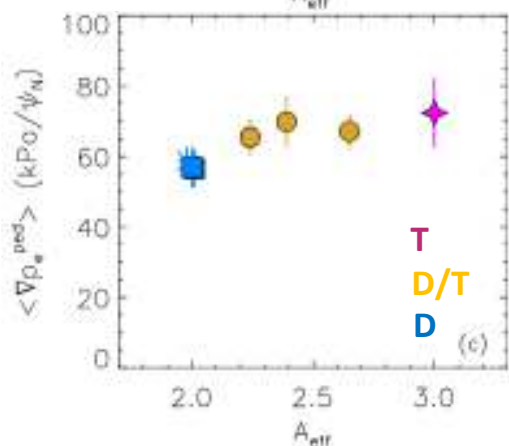
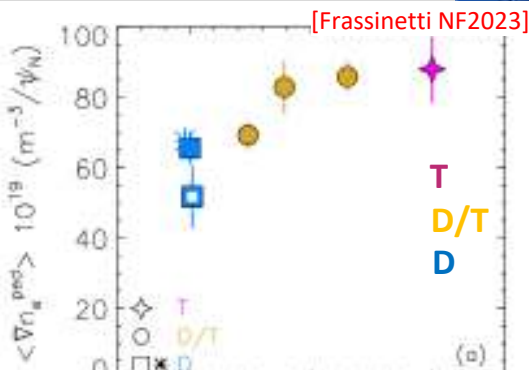
[Schneider PPCF2021]

[Frassinetti NF2023]



# Parameters that affect the pedestal: isotope

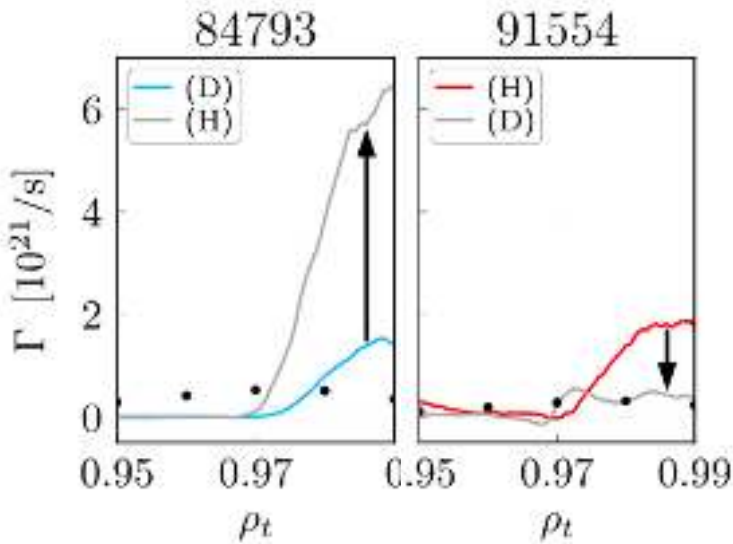
- Isotope mass ( $A$ ) can affect the pedestal:
  - pedestal density
    - $n_e^{\text{ped}}$  increases with increasing  $A$  (JET, DIII-D, AUG, JT60-U...)
    - Effect observed both from  $H \rightarrow D$  and from  $D \rightarrow T$
  - pedestal pressure
    - In JET and AUG:  $p_e^{\text{ped}}$  increases with increasing  $A$ . [Maggi PPCF2018, Schneider NF2023]
    - In DIII-D and JT60-U: no significant effect related to  $A$  [Urano NF2013]  
[Gohil IAEA2008]
  - Pedestal gradients:
    - The increase in  $n_e^{\text{ped}}$  is due to an increase in  $\nabla n_e \rightarrow$  likely,  $A$  affects the transport (but other reasons cannot be excluded yet) [Frassinetti NF2023]
    - The increase in  $p_e^{\text{ped}}$  is due to an increase in  $\nabla p_e \rightarrow A$  can affects the stability [Frassinetti NF2023]
  - Pedestal width: no significant variation



# Parameters that affect the pedestal: isotope



- Understandings of the effects of A
  - pedestal density
    - Sources: experimental estimate very challenging
    - GK results show in H vs D plasmas in JET-ILW show reduction of particle transport with increasing mass [Predebon NF2023] (due to reduced ITG turbulence)
    - Further work on-going before conclusive claims

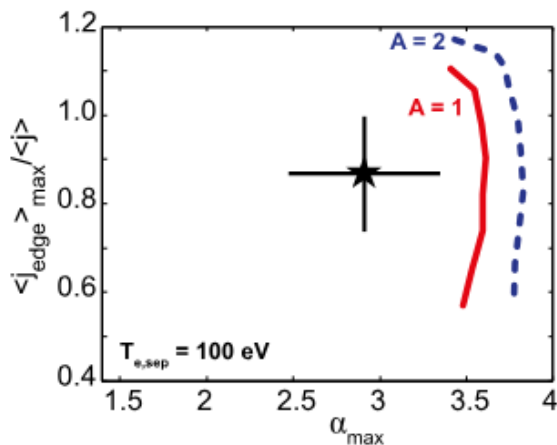


[Predebon NF2023]

# Parameters that affect the pedestal: isotope



- Understandings of the effects of A
  - pedestal density
    - Sources: experimental estimate very challenging
    - GK results show in H vs D plasmas in JET-ILW show reduction of particle transport with increasing mass [Predebon NF2023] (due to reduced ITG turbulence)
    - Further work on-going before conclusive claims
  - pedestal pressure
    - Ideal MHD cannot explain the increase of  $\nabla p_e$  [Horvath NF2021]

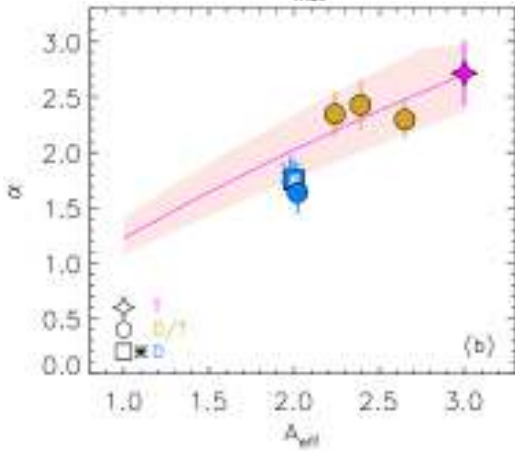
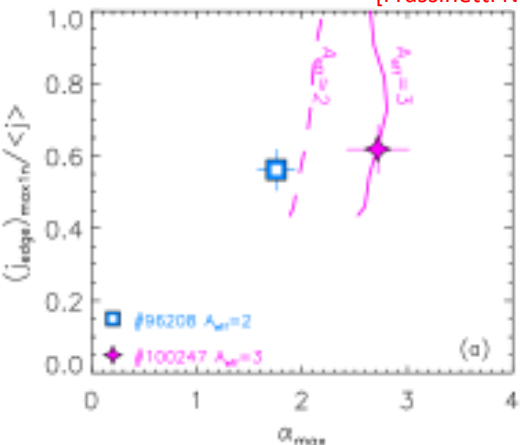


[Horvath NF2021]

# Parameters that affect the pedestal: isotope

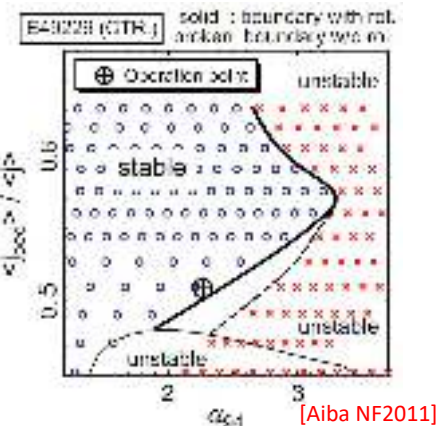
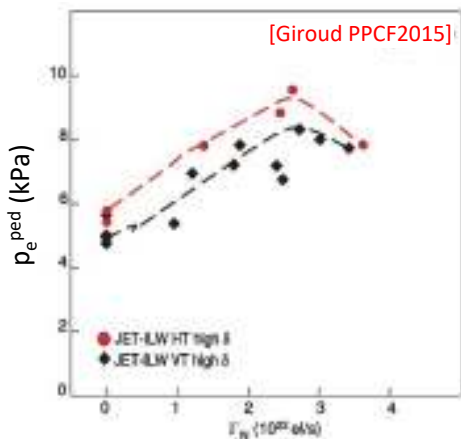
[Frassinetti NF2023]

- Understandings of the effects of A
  - pedestal density
    - Sources: experimental estimate very challenging
    - GK results show in H vs D plasmas in JET-ILW show reduction of particle transport with increasing mass [Predebon NF2023] (due to reduced ITG turbulence)
    - Further work on-going before conclusive claims
  - pedestal pressure
    - Ideal MHD cannot explain the increase of  $\nabla p_e$  [Horvath NF2021]
    - Resistive MHD shows a reasonable agreement with experimental results [Frassinetti NF2023]



# Parameters that affect the pedestal

- Other parameters that affect the pedestal stability are:
  - Impurities and seeding.**  $Z_{\text{eff}}$  affects collisionality and  $j_{\text{bs}}$ . It affects the electron pressure via the dilution effect. It can affect turbulent transport. Not fully understood yet.  
 [Giroud NF2013, PPCF2015, IAEA2018, Dunne PPCF2017]  
 [Saarela PoP2015]
  - q-profile.** A change in q-profiles affects the shear. [Snyder PoP2002]
  - Pedestal width.** A wider pedestal can contain more ballooning modes, so it is more unstable  
 [Snyder PoP2002]
  - Plasma rotation.** [Aiba NF2018]
  - Density at the pedestal top.** Not trivial effects, see later  
 [Snyder NF2011]



[Aiba NF2011]

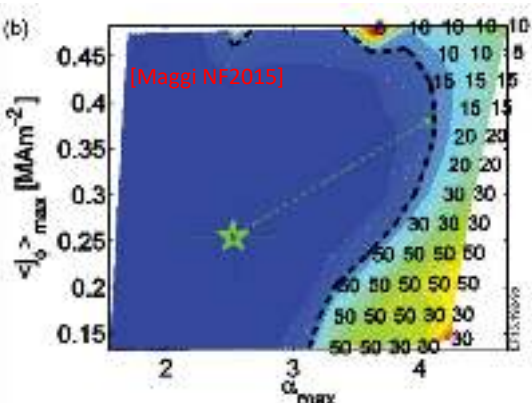
# OUTLINE

- L-H transition
- Pedestal structure
- Edge localized modes (ELMs)
  - ELM energy losses
  - ELM types
- MHD stability of the pedestal
  - Role of MHD stability (and few words on transport)
  - The peeling-balloonning (PB) model
  - The ELM cycle within the PB model
  - Parameters that influences the pedestal
- **Pedestal predictions**
  - **The EPED model:**
    - **The PB constraint**
    - **The KBM constraint**
  - **Non-linear MHD modelling**
- Some of the most active research areas in pedestal physics

# Pedestal predictions: the PB constraint



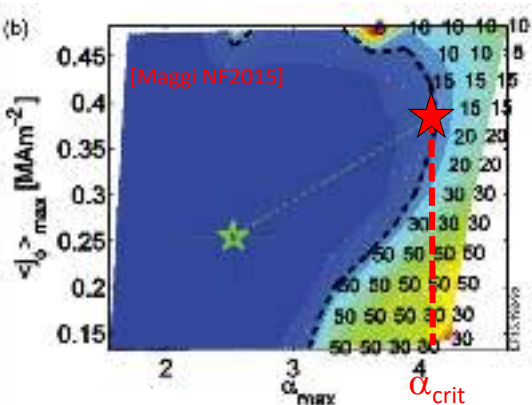
- Can we use the PB model to predict the pedestal pressure height before the ELM?



# Pedestal predictions: the PB constraint

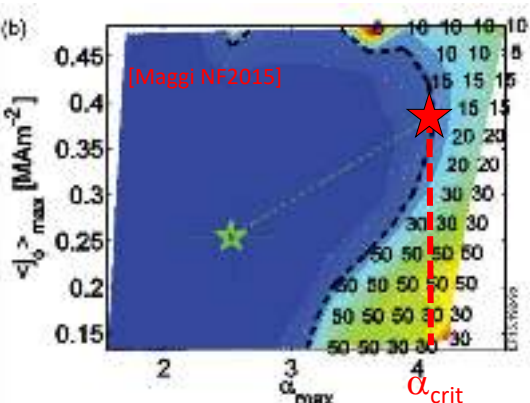
- Can we use the PB model to predict the pedestal pressure height before the ELM?
- The PB model identify the critical normalized pressure gradient ( $\alpha_{\text{crit}}$ ) above which the PB modes are destabilized.

➤ It can be used to determine  $\nabla p$ .



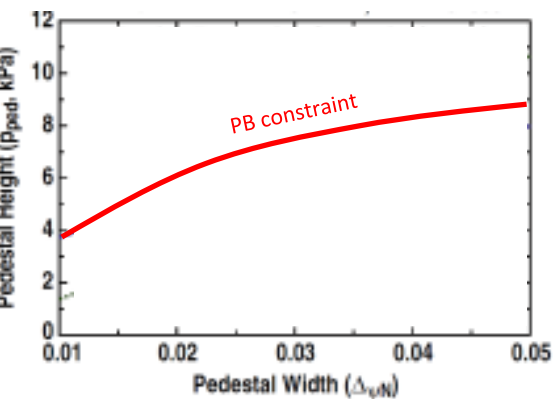
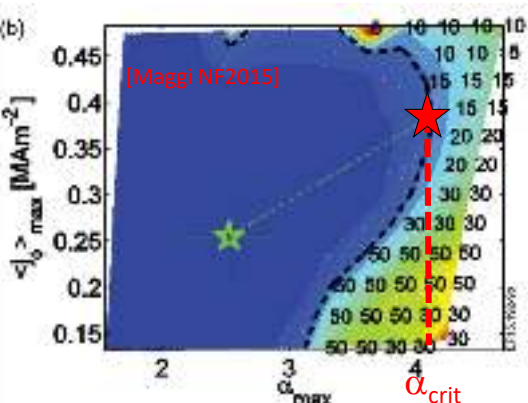
# Pedestal predictions: the PB constraint

- Can we use the PB model to predict the pedestal pressure height before the ELM?
- The PB model identify the critical normalized pressure gradient ( $\alpha_{\text{crit}}$ ) above which the PB modes are destabilized.
  - It can be used to determine  $\nabla p$ .
- For a specific pedestal width, the PB model can determine the critical  $\nabla p$  at which the PB modes are destabilized.
  - for this specific width, the critical pressure height can determined from  $(\nabla p)_{\text{crit}}$ .



# Pedestal predictions: the PB constraint

- Can we use the PB model to predict the pedestal pressure height before the ELM?
- The PB model identify the critical normalized pressure gradient ( $\alpha_{\text{crit}}$ ) above which the PB modes are destabilized.
  - It can be used to determine  $\nabla p$ .
- For a specific pedestal width, the PB model can determine the critical  $\nabla p$  at which the PB modes are destabilized.
  - for this specific width, the critical pressure height can determined from  $(\nabla p)_{\text{crit}}$ .
  - A correlation between width and critical pressure can be obtained. This is often called "PB constraint"
- More information is necessary to predict pedestal height and width.



# Pedestal predictions: the KBM constraint



- The other constraint can come from pedestal transport
- The problem is that the pedestal transport is (often) driven by turbulence.  
Turbulence studies are not trivial and very time consuming

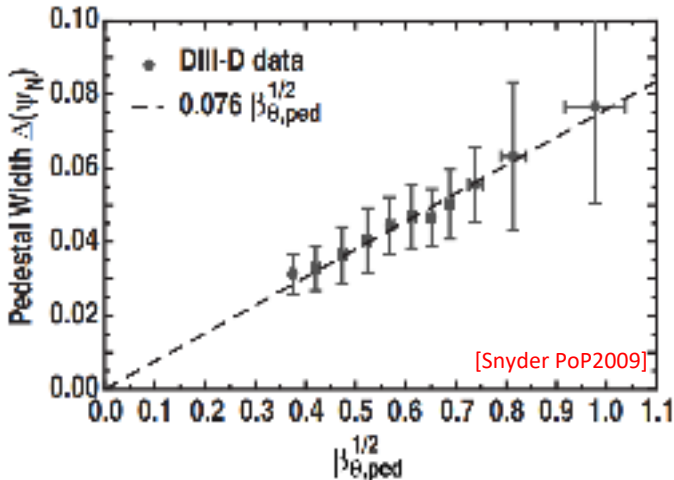
# Pedestal predictions: the KBM constraint

- The other constraint can come from pedestal transport
- The problem is that the pedestal transport is (often) driven by turbulence. Turbulence studies are not trivial and very time consuming
- The most successful approach, so far, has been developed in DIII-D [Snyder PoP2009]
  - experimental results suggest that DIII-D pedestal transport is driven by kinetic ballooning modes (KBMs)
  - from the theoretical arguments, it can be derived that for pedestals limited by the KBM turbulence:

$$w_{ped} = c \sqrt{\beta_\theta^{ped}}$$

- an experimental fit from DIII-D data gives:

$$w_{ped} = 0.076 \sqrt{\beta_\theta^{ped}}$$



[Snyder PoP2009]

# Pedestal predictions: the KBM constraint

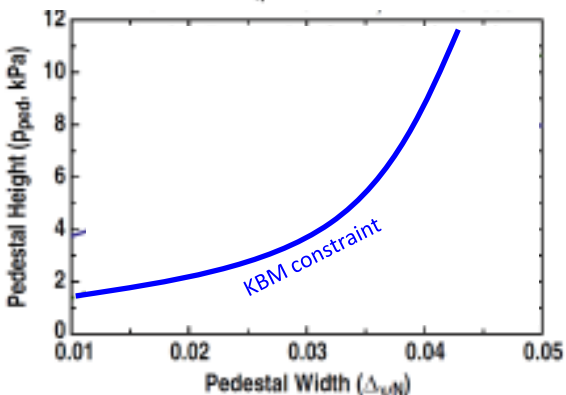
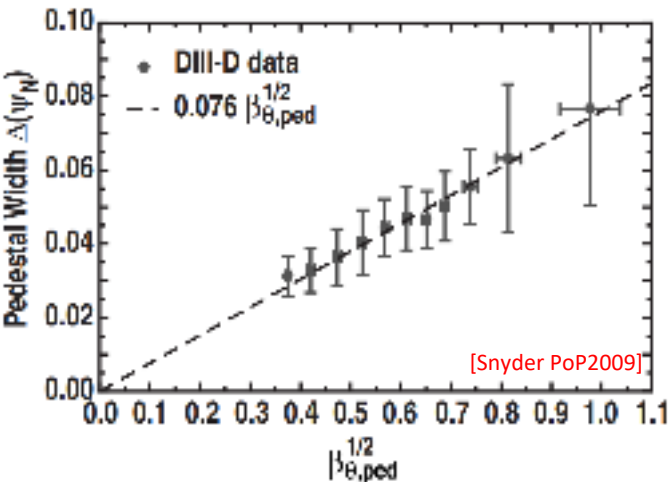
- The other constraint can come from pedestal transport
- The problem is that the pedestal transport is (often) driven by turbulence. Turbulence studies are not trivial and very time consuming
- The most successful approach, so far, has been developed in DIII-D [Snyder PoP2009]
  - experimental results suggest that DIII-D pedestal transport is driven by kinetic ballooning modes (KBMs)
  - from the theoretical arguments, it can be derived that for pedestals limited by the KBM turbulence:

$$w_{ped} = c \sqrt{\beta_\theta^{ped}}$$

- an experimental fit from DIII-D data gives:

$$w_{ped} = 0.076 \sqrt{\beta_\theta^{ped}}$$

KBM constraint



# Pedestal predictions: the KBM constraint

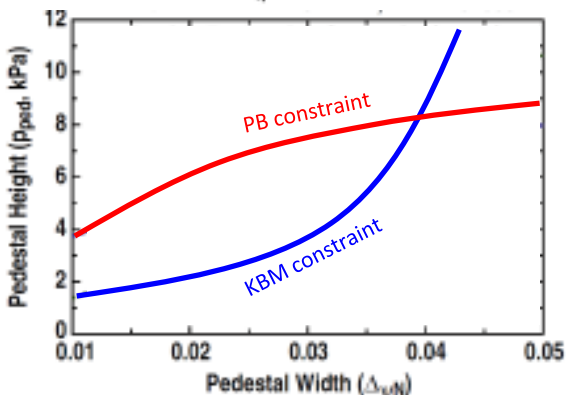
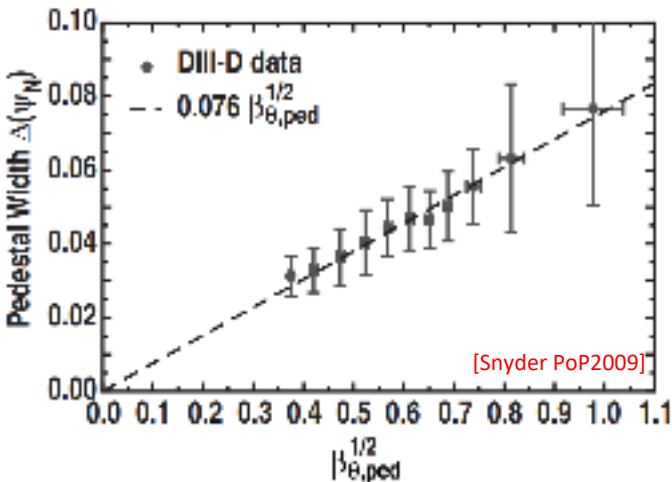
- The other constraint can come from pedestal transport
- The problem is that the pedestal transport is (often) driven by turbulence. Turbulence studies are not trivial and very time consuming
- The most successful approach, so far, has been developed in DIII-D [Snyder PoP2009]
  - experimental results suggest that DIII-D pedestal transport is driven by kinetic ballooning modes (KBMs)
  - from the theoretical arguments, it can be derived that for pedestals limited by the KBM turbulence:

$$w_{ped} = c \sqrt{\beta_\theta^{ped}}$$

- an experimental fit from DIII-D data gives:

$$w_{ped} = 0.076 \sqrt{\beta_\theta^{ped}}$$

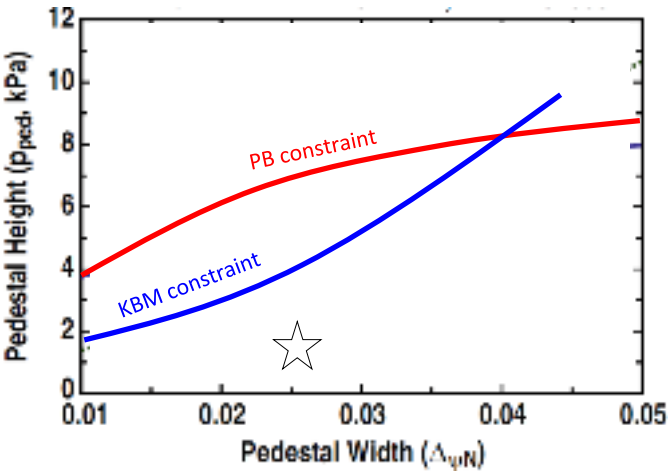
KBM constraint



# The EPED1 model

- The EPED1 model predicts pedestal pressure height and pedestal pressure width using the
  - KBM constraint:  
local KBM stability → "clamps"  $\nabla p$
  - PB constraint:  
global PB stability → triggers the ELM

[Snyder PoP2009]  
[Snyder NF2011]



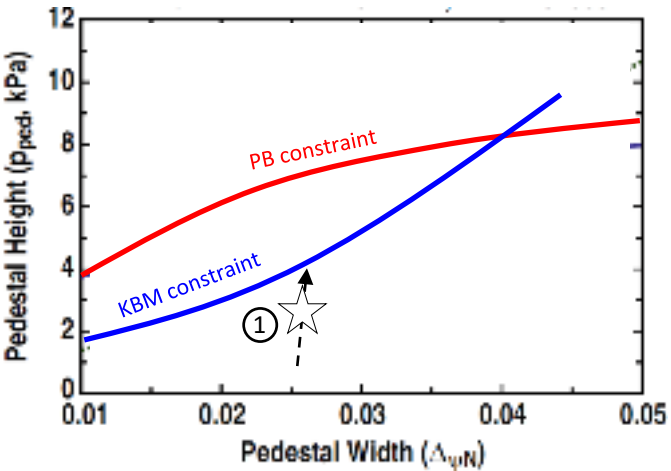
# The EPED1 model

- The EPED1 model predicts pedestal pressure height and pedestal pressure width using the
  - KBM constraint:  
local KBM stability  $\rightarrow$  "clamps"  $\nabla p$
  - PB constraint:  
global PB stability  $\rightarrow$  triggers the ELM

[Snyder PoP2009]  
[Snyder NF2011]

## THE ELM CYCLE ACCORDING TO EPED1:

- ①  $\nabla p$  grows unconstrained

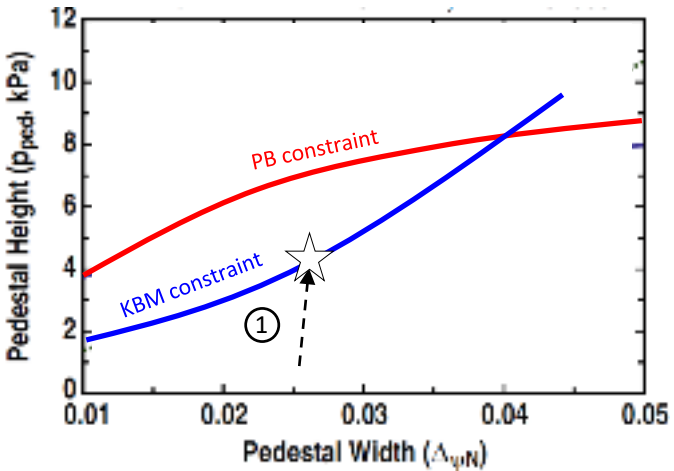


# The EPED1 model

- The EPED1 model predicts pedestal pressure height and pedestal pressure width using the
  - [Snyder PoP2009]
  - [Snyder NF2011]
- KBM constraint:  
local KBM stability → "clamps"  $\nabla p$
- PB constraint:  
global PB stability → triggers the ELM

## THE ELM CYCLE ACCORDING TO EPED1:

- 1  $\nabla p$  grows unconstrained
- 2 KBM boundary is reached:
  - $\nabla p$  is "clamped"



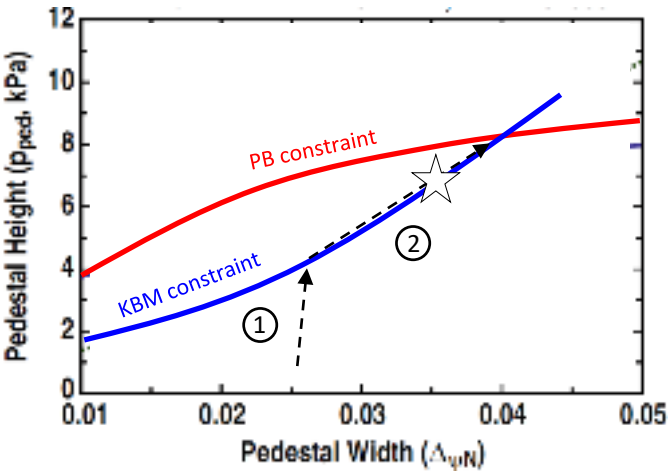
# The EPED1 model

- The EPED1 model predicts pedestal pressure height and pedestal pressure width using the
  - [Snyder PoP2009]
  - [Snyder NF2011]
- KBM constraint:  
local KBM stability → "clamps"  $\nabla p$
- PB constraint:  
global PB stability → triggers the ELM

## THE ELM CYCLE ACCORDING TO EPED1:

- $\nabla p$  grows unconstrained
- KBM boundary is reached:
  - $\nabla p$  is "clamped"
  - The pedestal height grows via the increase of the pedestal width:

$$w_{ped} = 0.076 \sqrt{\beta_\theta^{ped}}$$

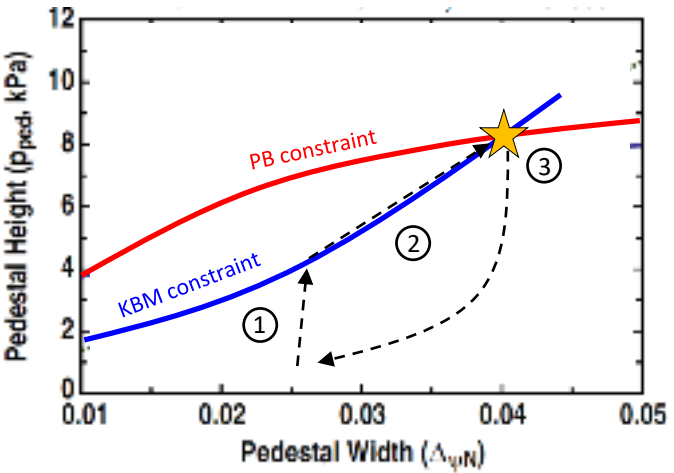


# The EPED1 model

- The EPED1 model predicts pedestal pressure height and pedestal pressure width using the
  - [Snyder PoP2009]
  - [Snyder NF2011]
- KBM constraint:  
local KBM stability → "clamps"  $\nabla p$
- PB constraint:  
global PB stability → triggers the ELM

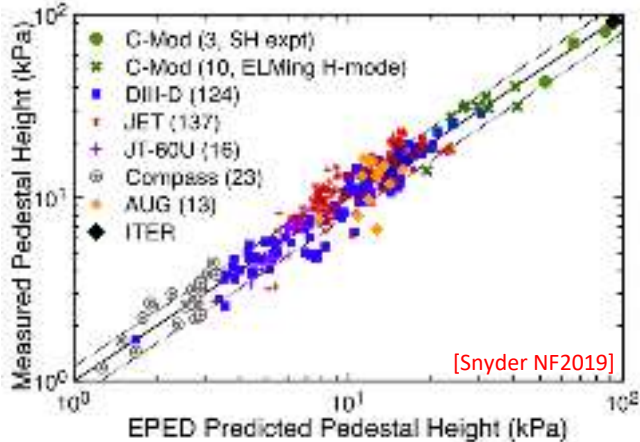
## THE ELM CYCLE ACCORDING TO EPED1:

- ①  $\nabla p$  grows unconstrained
- ② KBM boundary is reached:
  - $\nabla p$  is "clamped"
  - The pedestal height grows via the increase of the pedestal width:
- ③ PB boundary is reached
  - ELM triggered



# The EPED1 model

- EPED1 tends to predict the pedestal pressure height rather well, for a large of parameters and in many machines.  
[Snyder NF2019]
- EPED1 is a useful tool to test the PB model.



# The EPED1 model

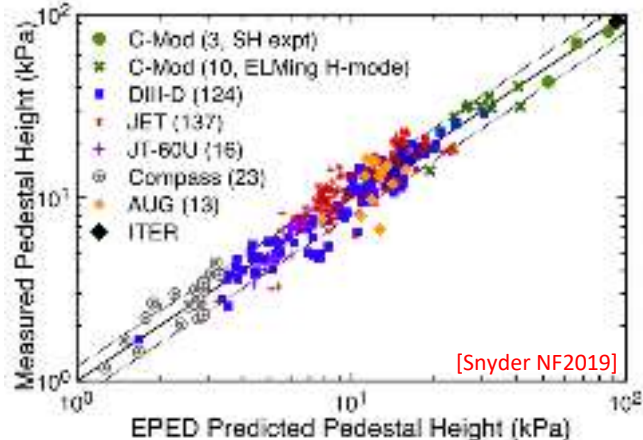
- EPED1 tends to predict the pedestal pressure height rather well, for a large of parameters and in many machines.

[Snyder NF2019]

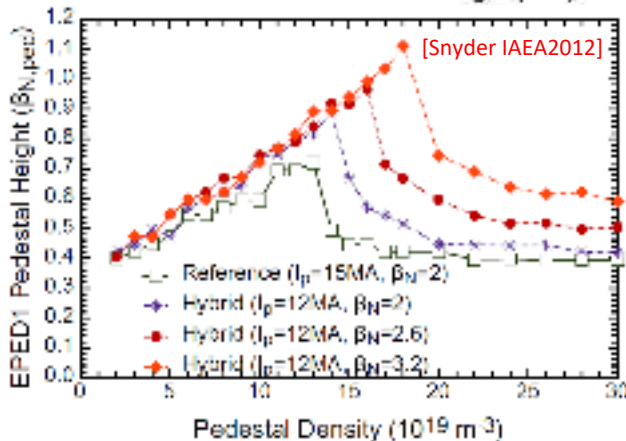
- EPED1 is a useful tool to test the PB model.

- EPED1 is widely used to predict the pedestal height (also in ITER).
- Example: prediction of pedestal pressure dependence with:

- density
- $\beta$



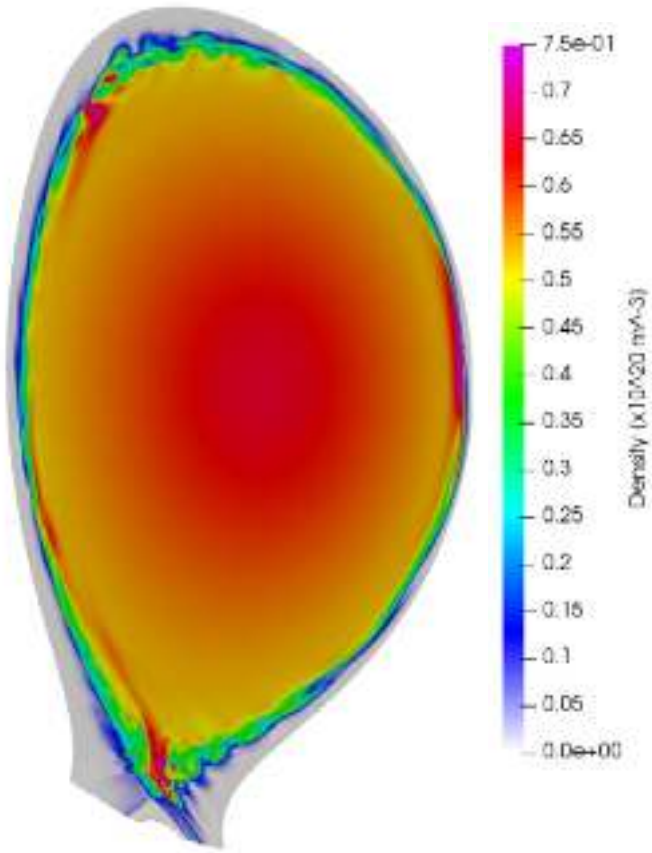
[Snyder NF2019]



[Snyder IAEA2012]

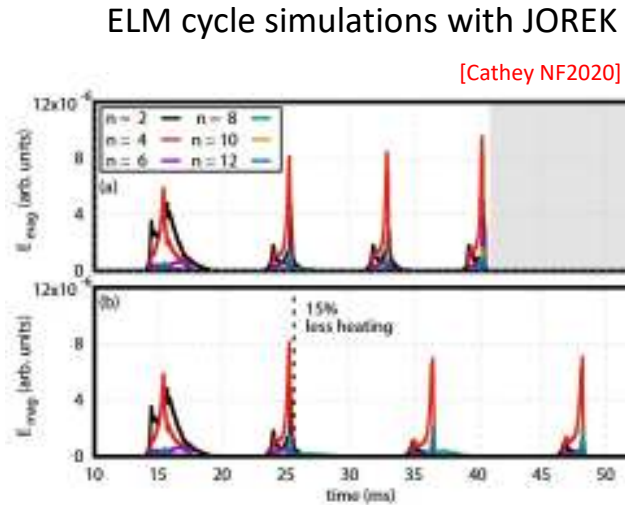
# Non-linear MHD modelling

- EPED1 works relatively well, but it is a linear model:
  - it does not predict time evolutions
  - cannot predict ELM energy losses
- Non-linear codes are necessary for modelling the details of the ELMs.
- Recent results with the JOREK code are very promising: [\[Huijsmans NF2007\]](#)



# Non-linear MHD modelling

- EPED1 works relatively well, but it is a linear model:
  - it does not predict time evolutions
  - cannot predict ELM energy losses
- Non-linear codes are necessary for modelling the details of the ELMs.
- Recent results with the JOREK code are very promising:
  - type I ELMs start to be modeled rather well  
[Cathey NF2021]
  - ELMs similar to those in small ELMs scenarios have also been modelled.  
[Cathey PPCF2022]



# OUTLINE

- L-H transition
- Pedestal structure
- Edge localized modes (ELMs)
  - ELM energy losses
  - ELM types
- MHD stability of the pedestal
  - Role of MHD stability (and few words on transport)
  - The peeling-balloonning (PB) model
  - The ELM cycle within the PB model
  - Parameters that influences the pedestal
- Pedestal predictions
  - The EPED model:
    - The PB constraint
    - The KBM constraint
  - Non-linear MHD modelling
- Some of the most active research areas in pedestal physics

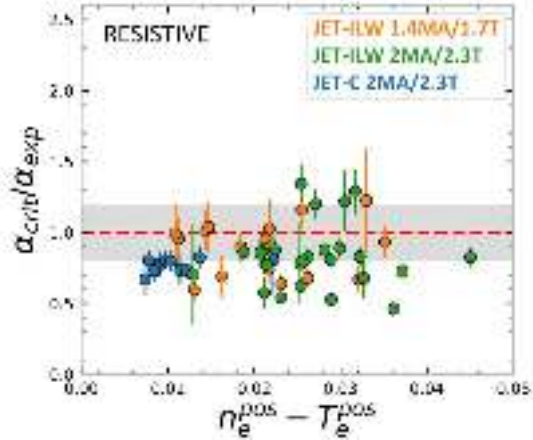
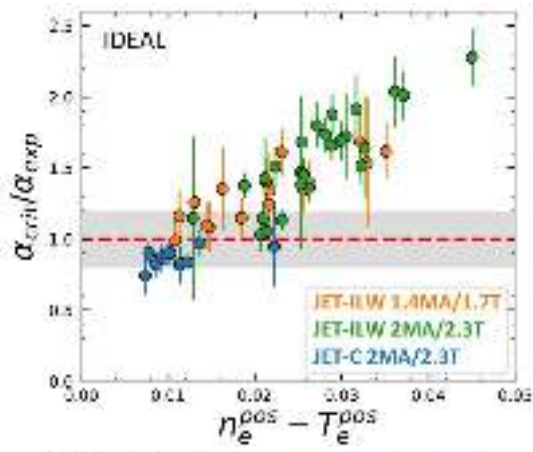
# Some active research areas

- Discrepancies between PB stability and experimental results, especially in JET-ILW, have been observed.
  - [Frassinetti NF2019], [Frassinetti NF2021], [Nyström NF2022]
  - Resistive MHD might play a role
- Super H-mode: DIII-D results show that at high  $\delta$  the 2nd stability region can be accessed. [Snyder NF2015]
  - can other experiments reach this region?
- Peeling limited pedestals
  - Reach peeling limited pedestals and validate pedestal predictions in view of ITER [Frassinetti, in preparation]
- Small ELMs
  - will operation with good pedestals and small ELMs be possible in ITER? [Viezzer NF2018] [Dunne NF2024]
- ELM mitigation
  - develop and test ELM mitigation techniques that can be used in ITER

# Some active research areas

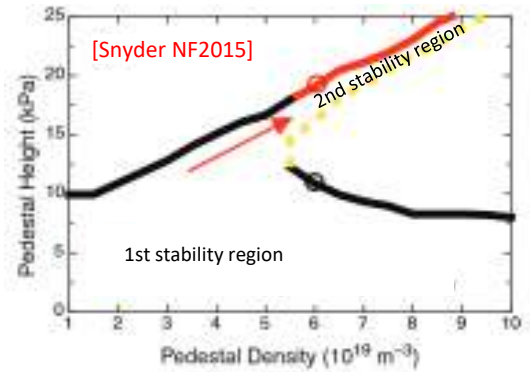
[Nyström NF2022]

- Discrepancies between PB stability and experimental results, especially in JET-ILW, have been observed.  
[Frassinetti NF2019], [Frassinetti NF2021], [Nyström NF2022]
  - Resistive MHD might play a role
- Super H-mode: DIII-D results show that at high  $\delta$  the 2nd stability region can be accessed. [Snyder NF2015]
  - can other experiments reach this region?
- Peeling limited pedestals
  - Reach peeling limited pedestals and validate pedestal predictions in view of ITER [Frassinetti, in preparation]
- Small ELMs
  - will operation with good pedestals and small ELMs be possible in ITER? [Viezzini NF2018] [Dunne NF2024]
- ELM mitigation
  - develop and test ELM mitigation techniques that can be used in ITER



# Some active research areas

- Discrepancies between PB stability and experimental results, especially in JET-ILW, have been observed.
  - [Frassinetti NF2019], [Frassinetti NF2021], [Nuström NF2022]
  - Resistive MHD might play a role
- Super H-mode: DIII-D results show that at high  $\delta$  the 2nd stability region can be accessed. [Snyder NF2015]
  - can other experiments reach this region?
- Peeling limited pedestals
  - Reach peeling limited pedestals and validate pedestal predictions in view of ITER
- [Frassinetti, in preparation]
- Small ELMs
  - will operation with good pedestals and small ELMs be possible in ITER? [Viezzer NF2018]
  - [Dunne NF2024]
- ELM mitigation
  - develop and test ELM mitigation techniques that can be used in ITER



# Some active research areas

[Frassinetti, in preparation]

- Discrepancies between PB stability and experimental results, especially in JET-ILW, have been observed.

[Frassinetti NF2019], [Frassinetti NF2021], [Nuñez NF2022]

- Resistive MHD might play a role
- Super H-mode: DIII-D results show that at high  $\delta$  the 2nd stability region can be accessed. [Snyder NF2015]
- can other experiments reach this region?

- Peeling limited pedestals

- Reach peeling limited pedestals and validate pedestal predictions in view of ITER

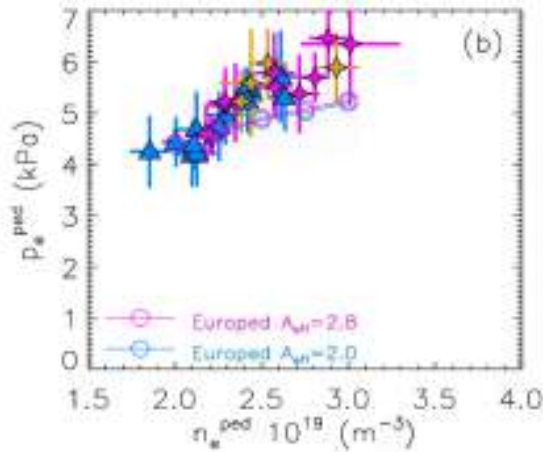
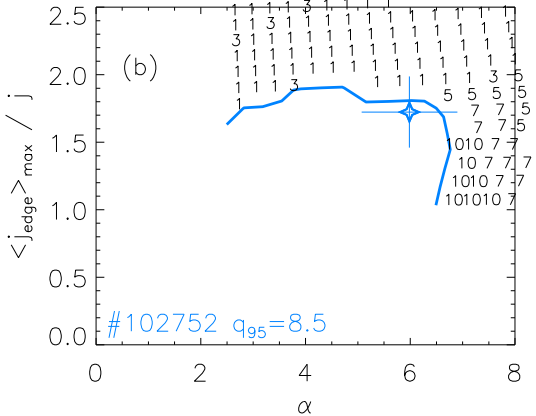
[Frassinetti, in preparation]

- Small ELMs

- will operation with good pedestals and small ELMs be possible in ITER? [Viezzini NF2018]  
[Dunne NF2024]

- ELM mitigation

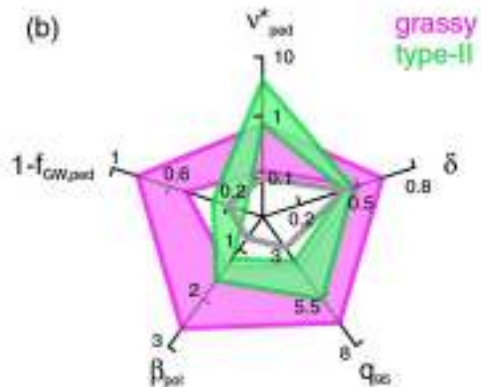
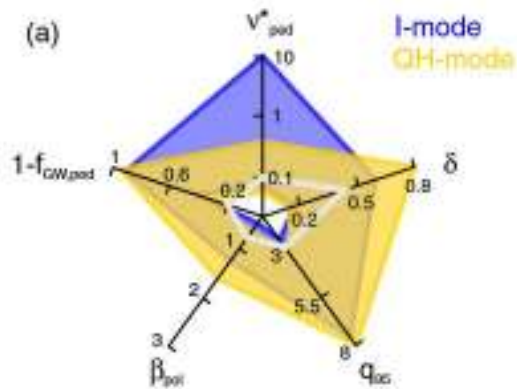
- develop and test ELM mitigation techniques that can be used in ITER



# Some active research areas

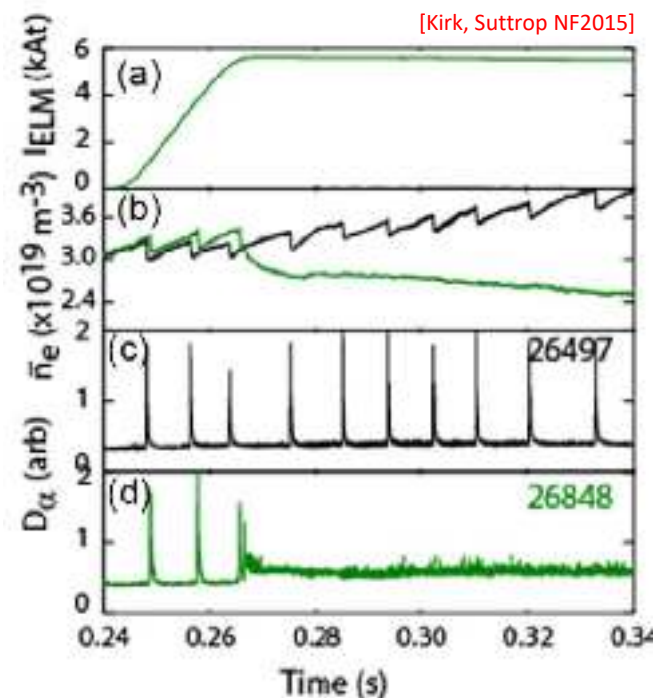
- Discrepancies between PB stability and experimental results, especially in JET-ILW, have been observed.
  - [Frassinetti NF2019], [Frassinetti NF2021], [Nuström NF2022]
- Resitive MHD might play a role
- Super H-mode: DIII-D results show that at high  $\delta$  the 2nd stability region can be accessed. [Snyder NF2015]
  - can other experiments reach this region?
- Peeling limited pedestals
  - Reach peeling limited pedestals and validate pedestal predictions in view of ITER

[Frassinetti, in preparation]
- Small ELMs
  - will operation with good pedestals and small ELMs be possible in ITER? [Viezzini NF2018] [Dunne NF2024]
- ELM mitigation
  - develop and test ELM mitigation techniques that can be used in ITER



# Some active research areas

- Discrepancies between PB stability and experimental results, especially in JET-ILW, have been observed.
  - Frassinetti NF2019], [Frassinetti NF2021], [Nuñez NF2022]
- Super H-mode: DIII-D results show that at high  $\delta$  the 2nd stability region can be accessed. [Snyder NF2015]
  - can other experiments reach this region?
- Peeling limited pedestals
  - Reach peeling limited pedestals and validate pedestal predictions in view of ITER [Frassinetti, in preparation]
- Small ELMs
  - will operation with good pedestals and small ELMs be possible in ITER? [Viezzini NF2018] [Dunne NF2024]
- ELM mitigation
  - develop and test ELM mitigation techniques that can be used in ITER



# Some useful references

The choice of the following papers is based on two criteria:

- overview papers, when possible.
- most recent papers.

This list does not necessarily cite the original papers on the topic.  
Many excellent papers have not been included.

- Pedestal physics: [Groebner PPCF2023]  
[Urano NF2014]  
[Leonard PoP2014]
- LH transition: [Bourdelle NF2020]
- Pedestal structure: [Frassinetti NF2021]
- Isotope effect: [Maggi PPCF2018]
- ELMs: [Zohm PPCF1996]  
[Leonard PoP2014]
- PB model: [Wilson PoP1999]  
[Snyder PoP2002]  
[Snyder NF2004]
- EPED model: [Snyder PoP2009]  
[Snyder NF2011]

# ANOMALOUS TRANSPORT

---

Nicola Vianello

28 November 2024

ISTP-CNR and Consorzio RFX

## INTRODUCTION

---

## TRANSPORT IN TOKAMAK PLASMAS

- (i) The topic of **transport** is dedicated to the physical processes by which, particles momentum and energy are moved in real (or in phase space) domain
- (ii) The goal of transport theory is to identify the relationship between the thermodynamic fluxes and the thermodynamics forces
- (iii) Thermodynamic fluxes are particle, momentum and energy (heat) presently driven mainly by external sources (particle sources, torques or heating power)
- (iv) Thermodynamics forces are the spatial gradients, i.e. of density, temperature or momentum density
- (v) Transport determines plasma reaction to imposed gradients and subsequent relaxing to final thermodynamics fluxes gradients.

## REMIND

- In tokamak plasmas collisional transport produced a level of minimum (unavoidable) level of transport  $\chi_i^{CL} \sim 10^{-3} \text{m}^2/\text{s}$

$$\chi_i \approx \nu_{ii} r_{L,i}^2 \quad \chi_e \approx \nu_{ee} r_{L,e}^2 \quad \chi_i \sim \sqrt{\frac{M}{m}} \chi_e$$

- Neoclassical correction due to toroidicity increase the level of observed transport but still lower then observed:

$$\chi_{i,p}^{NC} \sim q^2 \chi_i^{CL} \sim 10^{-2} \text{m}^2/\text{s} \quad \chi_{i,t}^{NC} \sim q^2 \left( \frac{R_0}{r} \right)^{3/2} \chi_i^{CL} \sim 1 \text{m}^2/\text{s}$$

## REMIND

- In tokamak plasmas collisional transport produced a level of minimum (unavoidable) level of transport  $\chi_i^{CL} \sim 10^{-3} \text{m}^2/\text{s}$

$$\chi_i \approx \nu_{ii} r_{L,i}^2 \quad \chi_e \approx \nu_{ee} r_{L,e}^2 \quad \chi_i \sim \sqrt{\frac{M}{m}} \chi_e$$

- Neoclassical correction due to toroidicity increase the level of observed transport but still lower then observed:

$$\chi_{i,p}^{NC} \sim q^2 \chi_i^{CL} \sim 10^{-2} \text{m}^2/\text{s} \quad \chi_{i,t}^{NC} \sim q^2 \left( \frac{R_0}{r} \right)^{3/2} \chi_i^{CL} \sim 1 \text{m}^2/\text{s}$$

- Apart from improved confinement regimes where thermal conductivity approaches values close to NC transport is higher and can only be explained by turbulence

## TURBULENT OR ANOMALOUS TRANSPORT

---

## TRANSPORT RELEVANT SCALES

- Although the most conspicuous instabilities observed in tokamaks are long-wavelength low-m MHD modes, their contributions to particle and heat transport is general low away from their resonant surface
- Microturbulence then main player contributing to transport through:
  - (i)  $E \times B$  drift across the confining lines resulting from fluctuating electric fields
  - (ii) Motion along magnetic field lines with a fluctuating radial component

## DERIVATION OF TRANSPORT FROM KINETIC EQUATIONS

- We try to derive the influence of perturbation on particle transport directly from the Vlasov equation neglecting the collisional operator, which we already observed is unable to describe the level of transport observed.
- We will assume to be in the condition:

$$f = f_0 + \tilde{f} \quad E = E_0 + \tilde{E} \quad B = B_0 + \tilde{B}.$$

where average is defined in term of ensemble average and fluctuating component is defined as the deviation from the ensemble average.

- For the average quantities we will consider the following spatial dependence

$$f_0 = f_0(x) \quad E_0 = E_0(x) \quad B = B_0(x)\hat{z} \quad (1)$$

## DERIVATION OF TRANSPORT FROM KINETIC EQUATIONS

- We try to derive the influence of perturbation on particle transport directly from the Vlasov equation neglecting the collisional operator, which we already observed is unable to describe the level of transport observed.
- We will assume to be in the condition:

$$f = f_0 + \tilde{f} \quad E = E_0 + \tilde{E} \quad B = B_0 + \tilde{B}.$$

where average is defined in term of ensemble average and fluctuating component is defined as the deviation from the ensemble average.

- Thus taking the average of the Vlasov with perturbation kept at first order one obtain:

$$\frac{\partial f_0}{\partial t} + \frac{\partial}{\partial x}(v_x f_0) + \frac{\partial}{\partial v} \cdot \left[ \frac{q}{m} (E_0 + v \times B_0) f_0 \right] + \frac{\partial}{\partial v} \cdot \left[ \frac{q}{m} \langle \tilde{E} \tilde{f} \rangle + \frac{q}{m} \langle (v \times \tilde{B}) \tilde{f} \rangle \right] = 0 \quad (1)$$

where the highlighted quantities are responsible for turbulent transport

## TURBULENT PARTICLE TRANSPORT

- Following what is customary done for average quantities we can derive the various moments also for fluctuating components

$$n_0 = \int f_0 dv \quad \tilde{n} = \int \tilde{f} dv \quad (2)$$

$$\mathbf{\Gamma}_0 = \int \mathbf{v} f_0 dv \quad \tilde{\mathbf{\Gamma}} = \int \mathbf{v} \tilde{f} dv \quad (3)$$

$$\mathbf{u}_0 = \frac{1}{n_0} \int \mathbf{v} f_0 dv \quad \tilde{\mathbf{u}} = \frac{1}{n_0} \int \mathbf{v} \tilde{f} dv \quad (4)$$

- We can also derive the first order momentum of equation:

$$\frac{\partial \mathbf{\Gamma}_0}{\partial t} + \frac{\partial}{\partial x} \int v_x \mathbf{v} f_0 dv - \frac{q}{m} \int (\mathbf{E}_0 + \mathbf{v} \times \mathbf{B}_0) f_0 dv - \frac{q}{m} \int \langle \tilde{\mathbf{E}} \tilde{f} \rangle dv - \frac{q}{m} \int \langle (\mathbf{v} \times \tilde{\mathbf{B}}) \tilde{f} \rangle dv = 0 \quad (5)$$

## TURBULENT PARTICLE FLUX 2

- In deriving particle flux we will use the following ordering  $\omega_c \gg 1/T$        $\rho_L \ll L$  where  $T$  and  $L$  are the typical turbulence time and length

## TURBULENT PARTICLE FLUX 2

- In deriving particle flux we will use the following ordering  $\omega_c \gg 1/T$        $\rho_L \ll L$  where  $T$  and  $L$  are the typical turbulence time and length
- Particle flux along the  $x$  direction can be computed considering the evolution along the  $y$  direction:

$$\frac{\partial \Gamma_{0y}}{\partial t} + \frac{\partial}{\partial x} \int v_x v_y f_0 d\mathbf{v} + \frac{q}{m} \Gamma_{0x} B_0 + \frac{q}{m} E_{0y} n_0 - \frac{q}{m} \langle \tilde{E}_y \tilde{n} \rangle - \frac{q}{m} \langle \tilde{\boldsymbol{\Gamma}} \times \tilde{\mathbf{B}} \rangle_y = 0$$

## TURBULENT PARTICLE FLUX 2

- In deriving particle flux we will use the following ordering  $\omega_c \gg 1/T$        $\rho_L \ll L$  where  $T$  and  $L$  are the typical turbulence time and length
- Particle flux along the  $x$  direction can be computed considering the evolution along the  $y$  direction:

$$\frac{\partial \Gamma_{0y}}{\partial t} + \frac{\partial}{\partial x} \int v_x v_y f_0 d\mathbf{v} + \frac{q}{m} \Gamma_{0x} B_0 + \frac{q}{m} E_{0y} n_0 - \frac{q}{m} \langle \tilde{E}_y \tilde{n} \rangle - \frac{q}{m} \langle \tilde{\boldsymbol{\Gamma}} \times \tilde{\mathbf{B}} \rangle_y = 0$$

- With the defined ordering we have

$$\frac{\partial v_y f_0}{\partial t} \sim \frac{v_y f_0}{T} \ll \frac{q}{m} \Gamma_{0x} B_0 \sim v f_0 \omega_c$$

$$\frac{\partial v_x v_y f_0}{\partial x} \sim v^2 f_0 / L \ll \frac{q}{m} \Gamma_{0x} B_0 \sim v^2 f_0 / r_L$$

## TURBULENT PARTICLE FLUX 2

- In deriving particle flux we will use the following ordering  $\omega_c \gg 1/T$        $\rho_L \ll L$  where  $T$  and  $L$  are the typical turbulence time and length
- Particle flux along the  $x$  direction can be computed considering the evolution along the  $y$  direction:

$$\frac{\partial \Gamma_{0y}}{\partial t} + \frac{\partial}{\partial x} \int v_x v_y f_0 d\mathbf{v} + \frac{q}{m} \Gamma_{0x} B_0 + \frac{q}{m} E_{0y} n_0 - \frac{q}{m} \langle \tilde{E}_y \tilde{n} \rangle - \frac{q}{m} \langle \tilde{\boldsymbol{\Gamma}} \times \tilde{\mathbf{B}} \rangle_y = 0$$

- Thus neglecting the pinch effects proportional to  $E_0$  the particle flux induced by turbulent effects may be written:

$$\Gamma_{0x} = \frac{\langle \tilde{E}_y \tilde{n} \rangle}{B_0} + \frac{\langle \tilde{\boldsymbol{\Gamma}} \times \tilde{\mathbf{B}} \rangle_y}{B_0} = \frac{\langle \tilde{E}_y \tilde{n} \rangle}{B_0} + \frac{n}{B} \langle \tilde{\mathbf{u}}_z \tilde{\mathbf{b}}_x \rangle$$

## RANDOM WALK ESTIMATE OF TURBULENT DIFFUSION

- In the case of electrostatic turbulence we can suppose fluctuation in electrostatic potential to be written in the form  $\delta\phi = \sum_k \delta\phi_k e^{k \cdot x}$  so that  $\delta v_k = -i \frac{k \times B}{B^2} \delta\phi_k$  (see (Wesson 2004))

## RANDOM WALK ESTIMATE OF TURBULENT DIFFUSION

- In the case of electrostatic turbulence we can suppose fluctuation in electrostatic potential to be written in the form  $\delta\phi = \sum_k \delta\phi_k e^{k \cdot x}$  so that  $\delta v_k = -i \frac{k \times B}{B^2} \delta\phi_k$  (see (Wesson 2004))
- If the particle velocity persists for a correlation time  $\tau_k$  causes a displacement  $\delta r_k \sim \delta v_k \tau_k \implies$

$$D = \sum_k \frac{(\delta r_k)^2}{\tau_k} = \sum_k \left( \frac{k_{\perp} \delta\phi_k}{B} \right)^2 \tau_k \quad (6)$$

## RANDOM WALK ESTIMATE OF TURBULENT DIFFUSION

- In the case of electrostatic turbulence we can suppose fluctuation in electrostatic potential to be written in the form  $\delta\phi = \sum_k \delta\phi_k e^{k \cdot x}$  so that  $\delta v_k = -i \frac{k \times B}{B^2} \delta\phi_k$  (see (Wesson 2004))
- If the particle velocity persists for a correlation time  $\tau_k$  causes a displacement  $\delta r_k \sim \delta v_k \tau_k \implies$

$$D = \sum_k \frac{(\delta r_k)^2}{\tau_k} = \sum_k \left( \frac{k_{\perp} \delta\phi_k}{B} \right)^2 \tau_k \quad (6)$$

- The correlation time is determined by the process which limits more rapidly the  $E \times B$  drift. Among these:
  - The time variation of the fluctuations  $\tau_k \sim 1/\omega_k$

## RANDOM WALK ESTIMATE OF TURBULENT DIFFUSION

- In the case of electrostatic turbulence we can suppose fluctuation in electrostatic potential to be written in the form  $\delta\phi = \sum_k \delta\phi_k e^{k \cdot x}$  so that  $\delta v_k = -i \frac{k \times B}{B^2} \delta\phi_k$  (see (Wesson 2004))
- If the particle velocity persists for a correlation time  $\tau_k$  causes a displacement  $\delta r_k \sim \delta v_k \tau_k \implies$

$$D = \sum_k \frac{(\delta r_k)^2}{\tau_k} = \sum_k \left( \frac{k_{\perp} \delta\phi_k}{B} \right)^2 \tau_k \quad (6)$$

- The correlation time is determined by the process which limits more rapidly the  $E \times B$  drift. Among these:
  - The effect of the linear motion of the particle as the parallel transit  $1/k_{\parallel} v_T$

## RANDOM WALK ESTIMATE OF TURBULENT DIFFUSION

- In the case of electrostatic turbulence we can suppose fluctuation in electrostatic potential to be written in the form  $\delta\phi = \sum_k \delta\phi_k e^{k \cdot x}$  so that  $\delta v_k = -i \frac{k \times B}{B^2} \delta\phi_k$  (see (Wesson 2004))
- If the particle velocity persists for a correlation time  $\tau_k$  causes a displacement  $\delta r_k \sim \delta v_k \tau_k \implies$

$$D = \sum_k \frac{(\delta r_k)^2}{\tau_k} = \sum_k \left( \frac{k_{\perp} \delta\phi_k}{B} \right)^2 \tau_k \quad (6)$$

- The correlation time is determined by the process which limits more rapidly the  $E \times B$  drift. Among these:
  - The time  $1/\nu_{eff}$  for collisions to change the particle orbit

## RANDOM WALK ESTIMATE OF TURBULENT DIFFUSION

- In the case of electrostatic turbulence we can suppose fluctuation in electrostatic potential to be written in the form  $\delta\phi = \sum_k \delta\phi_k e^{k \cdot x}$  so that  $\delta v_k = -i \frac{k \times B}{B^2} \delta\phi_k$  (see (Wesson 2004))
- If the particle velocity persists for a correlation time  $\tau_k$  causes a displacement  $\delta r_k \sim \delta v_k \tau_k \implies$

$$D = \sum_k \frac{(\delta r_k)^2}{\tau_k} = \sum_k \left( \frac{k_{\perp} \delta\phi_k}{B} \right)^2 \tau_k \quad (6)$$

- The correlation time is determined by the process which limits more rapidly the  $E \times B$  drift. Among these:
  - At high level of fluctuations the fastest limiting process is the turbulent velocity  $\delta v_k$  carrying a particle a perpendicular wavelength  $\tau_k = \Omega_k^{-1}$  with  $\Omega_k = k_{\perp} \delta v_k = \frac{k_{\perp}^2 \delta\phi_k}{B}$ . Thus if  $\Omega_k \ll \omega_{eff} = \max(\omega_k, k_{\parallel} v_T, \nu_{eff}) \rightarrow D = \sum_k \frac{1}{\omega_{eff}} \left( \frac{k_{\perp} \delta\phi_k}{B} \right)^2$  otherwise for  $\Omega_k \gtrsim \omega_{eff,k}$ ,  $D = \sum_k \frac{\delta\phi_k}{B}$

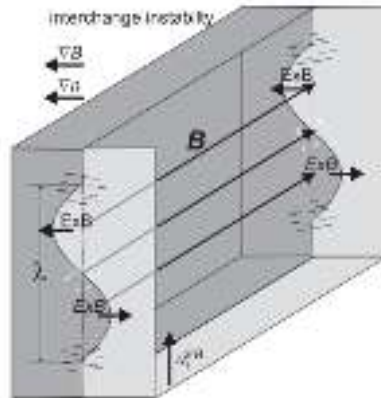
## PHENOMENOLOGY OF TURBULENT PLASMA TRANSPORT

- Net advected transport requires both density and electrostatic potential perturbation
- These perturbation needs to be out of phase



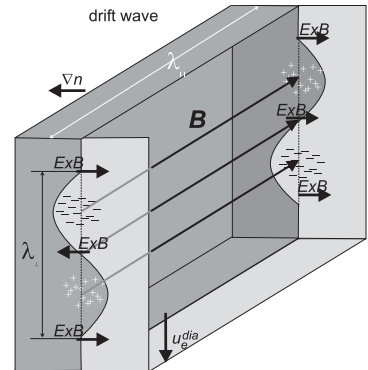
## INTERCHANGE INSTABILITY

- Interchange instability intrinsically 2D with  $k_{\parallel} = 0$  and dynamics restricted to the plane perpendicular to  $\mathbf{B}$
- Occurring in the region of bad-curvature
- In the figure instability driven by the charge-dependent curvature drift. Given the different motions of  $e^-/i$  w.r.t. the density perturbation a potential perturbation with  $\pi/2$  phase difference with density builds up.
- The resulting  $\mathbf{E} \times \mathbf{B}$  drift amplifies the original density perturbations.



## DRIFT-WAVE INSTABILITY

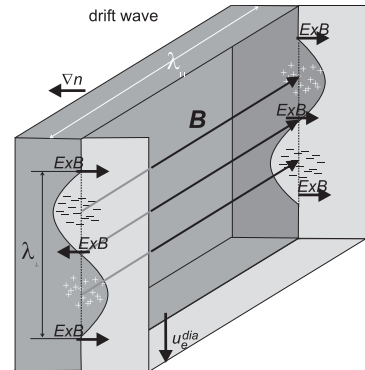
- Three dimensional perturbation of the pressure equilibrium with  $k_{\parallel} \neq 0, k_{\perp} \gg k_{\parallel}$
- Electron faster response create positive charges in the region of positive density and vice versa. Creates an electric field and an advective  $E \times B$  drift



## DRIFT-WAVE INSTABILITY

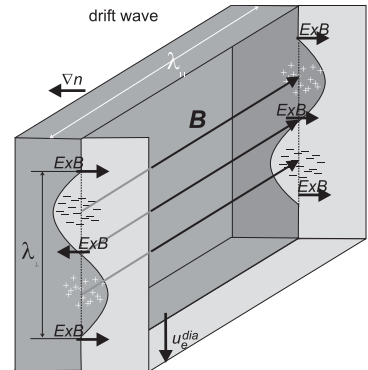
- Three dimensional perturbation of the pressure equilibrium with  $k_{\parallel} \neq 0, k_{\perp} \gg k_{\parallel}$
- Electron faster response create positive charges in the region of positive density and vice versa. Creates an electric field and an advective  $E \times B$  drift
- With adiabatic electrons ( $\frac{\tilde{n}}{n} \simeq \frac{e\phi}{T_e}$ ) (instantaneous response) only a displacement of the perturbation which moves in the  $e$ -diamagnetic direction

$$\omega_{*,e} = -\frac{k_y T_e}{e B n} \frac{dn}{dx}$$



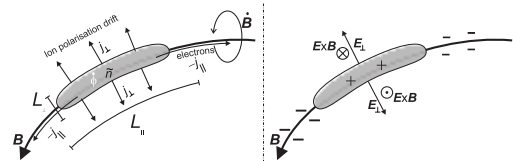
## DRIFT-WAVE INSTABILITY

- Three dimensional perturbation of the pressure equilibrium with  $k_{\parallel} \neq 0, k_{\perp} \gg k_{\parallel}$
- Electron faster response create positive charges in the region of positive density and vice versa. Creates an electric field and an advective  $E \times B$  drift
- With adiabatic electrons ( $\frac{\tilde{n}}{n} \simeq \frac{e\phi}{T_e}$ ) (instantaneous response) only a displacement of the perturbation which moves in the  $e$ -diamagnetic direction  
$$\omega_{*,e} = -\frac{k_y T_e}{e B n} \frac{dn}{dx}$$
- Electron dissipation through collisions or geometry effects break adiabatic response. With a small lag or delayed electron response the drift-wave is unstable.  $E \times B$  amplifies the initial perturbation.



## DRIFT-WAVE MODEL

- We start from an elongated positive density perturbation
- Due to their smaller inertia electrons respond faster and creates a positive potential inside the positive density
- Time constant defined by the polarization drift which drives ions in the perpendicular direction counteracting the charging building up
- The resulting  $E_{\perp}$  causes the density perturbation advection driving transport
- The perturbation is intrinsically 3D. Parallel dynamics sets by electrons, perpendicular one by the ion drifting.
- Consider the simplest case with cold ions  $T_i = 0$  and a density gradient with decay length  $L_n = -n_0/\nabla n_0$



## DRIFT-WAVE MODEL: THE HASEGAWA WAKATANI MODEL

- A simplified model for drift-wave turbulence may be built starting from the Generalized Ohm's law and Parallel Electric field equation

$$\frac{m_e}{e} \frac{\partial j_{\parallel}}{\partial t} = enE_{\parallel} + \nabla_{\parallel}p - en\frac{j_{\parallel}}{\sigma} \quad \text{Generalized Ohm's law}$$

$$E_{\parallel} = -\nabla_{\parallel}\phi - \frac{\partial A_{\parallel}}{\partial t} \text{ with } \nabla_{\perp}^2 A_{\parallel} = \mu_0 j_{\parallel} \quad \text{Parallel Electric Field}$$

## DRIFT-WAVE MODEL: THE HASEGAWA WAKATANI MODEL

- A simplified model for drift-wave turbulence may be built starting from the Generalized Ohm's law and Parallel Electric field equation

$$\frac{m_e}{e} \frac{\partial j_{\parallel}}{\partial t} = enE_{\parallel} + \nabla_{\parallel}p - en\frac{j_{\parallel}}{\sigma} \quad \text{Generalized Ohm's law}$$

$$E_{\parallel} = -\nabla_{\parallel}\phi - \frac{\partial A_{\parallel}}{\partial t} \text{ with } \nabla_{\perp}^2 A_{\parallel} = \mu_0 j_{\parallel} \quad \text{Parallel Electric Field}$$

- The two previous equations may be combined in the following

$$en\frac{\partial A_{\parallel}}{\partial t} + \frac{m}{e} \frac{\partial j_{\parallel}}{\partial t} = -en\nabla_{\parallel}\phi + \nabla_{\parallel}p_e - 0.511\frac{m_e\nu}{e}j_{\parallel}$$

## DRIFT-WAVE MODEL: THE HASEGAWA WAKATANI MODEL

- The previous equation may be considered together with the Perpendicular ion drift

$$\mathbf{u}_{i\perp} = \frac{\mathbf{E} \times \mathbf{B}}{B^2} + \frac{m_i}{eB^2} \left( \frac{\partial \mathbf{E}_\perp}{\partial t} + \mathbf{u}^{\mathbf{E} \times \mathbf{B}} \cdot \nabla \mathbf{E}_\perp \right)$$

- Where we have recognize that the only ion contribution to the electric current come from the ion polarization current

$$\mathbf{j}_\perp = \frac{m_i n}{B^2} \left( \frac{\partial \mathbf{E}_\perp}{\partial t} + \mathbf{u}^{\mathbf{E} \times \mathbf{B}} \cdot \nabla \mathbf{E}_\perp \right)$$

## DRIFT-WAVE MODEL: THE HASEGAWA WAKATANI MODEL

- The previous equation may be considered together with the Perpendicular ion drift

$$\mathbf{u}_{i\perp} = \frac{\mathbf{E} \times \mathbf{B}}{B^2} + \frac{m_i}{eB^2} \left( \frac{\partial \mathbf{E}_\perp}{\partial t} + \mathbf{u}^{\mathbf{E} \times \mathbf{B}} \cdot \nabla \mathbf{E}_\perp \right)$$

- Where we have recognize that the only ion contribution to the electric current come from the ion polarization current

$$\mathbf{j}_\perp = \frac{m_i n}{B^2} \left( \frac{\partial \mathbf{E}_\perp}{\partial t} + \mathbf{u}^{\mathbf{E} \times \mathbf{B}} \cdot \nabla \mathbf{E}_\perp \right)$$

- From the quasi-neutrality condition  $\nabla_\perp \mathbf{j}_\perp + \nabla_\parallel j_\parallel = 0$  and with  $E_\perp = -\nabla_\perp \phi$  we derive the vorticity equation

$$\frac{m_i n}{B^2} \left( \frac{\partial}{\partial t} + \mathbf{u}^{\mathbf{E} \times \mathbf{B}} \cdot \nabla \right) \nabla_\perp^2 \phi = \nabla_\parallel j_\parallel$$

## DRIFT-WAVE MODEL: THE HASEGAWA WAKATANI MODE II

- Vorticity equation is coupled with the continuity equation

$$\left( \frac{\partial}{\partial t} + \mathbf{u}^{\mathbf{E} \times \mathbf{B}} \cdot \nabla \right) n = -n \nabla_{\parallel} u_{e\parallel} \approx \nabla_{\parallel} j_{\parallel} / e$$

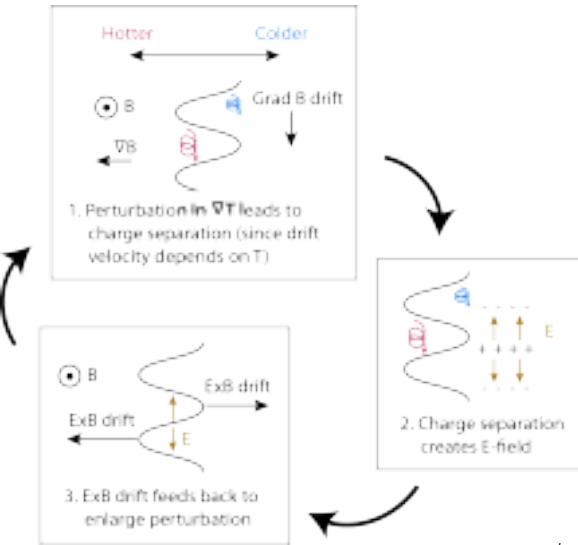
- In the electrostatic limit we have an explicit definition of  $j_{\parallel}$ . The two coupled equations are:

$$\begin{aligned} \left( \frac{\partial}{\partial t} + \mathbf{u}^{\mathbf{E} \times \mathbf{B}} \cdot \nabla \right) n &= \frac{1}{m_e \nu_e} \nabla_{\parallel} (\nabla_{\parallel} p_e - e n \nabla_{\parallel} \phi) \\ \frac{m_i n}{B^2} \left( \frac{\partial}{\partial t} + \mathbf{u}^{\mathbf{E} \times \mathbf{B}} \cdot \nabla \right) \nabla_{\perp}^2 \phi &= \frac{e}{m_e \nu_e} \nabla_{\parallel} (\nabla_{\parallel} p_e - e n \nabla_{\parallel} \phi) \end{aligned}$$

- The linearized normalized form of these two coupled equations is known as Hasegawa-Wakatani equations

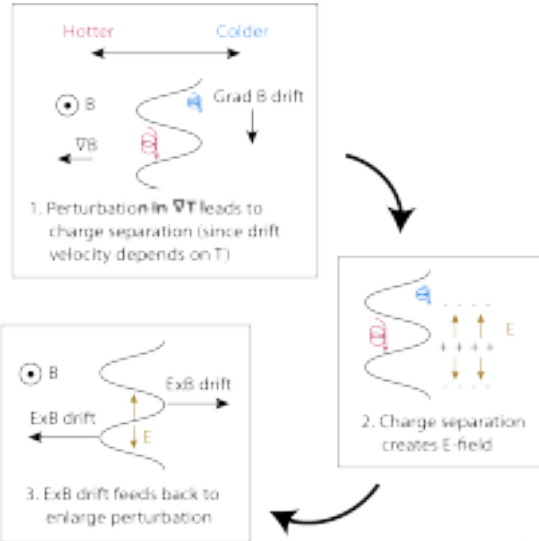
# ITG TURBULENCE

- Instability drive could arise as well from temperature gradients as the case of **Ion Temperature Gradient (ITG) modes**
- Assuming a temperature perturbation occurs on an isothermal flux surface



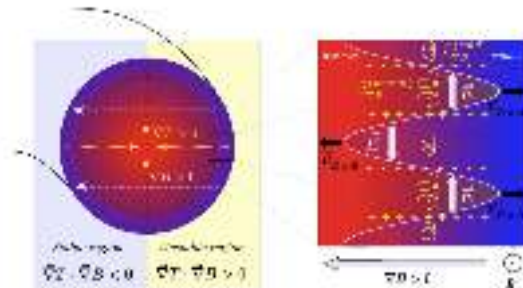
# ITG TURBULENCE

- The grad-B drift,  $v_{\nabla B} = \pm \frac{v_{\perp}^2}{\omega_c} \frac{\mathbf{B} \times \nabla \mathbf{B}}{B^2} \propto T$  is proportional to the temperature
- Corresponding density perturbation builds up → *interchange like density perturbation*
- Assuming that  $\omega \ll \omega_b$ , and  $\omega \ll k_{\parallel} v_{T_e}$ , adiabatic response of the passing particle population
- Parallel force balance ensures the build up of a potential perturbation and corresponding  $\mathbf{E} \times \mathbf{B}$  drift which enhance the perturbation



## ITG TURBULENCE

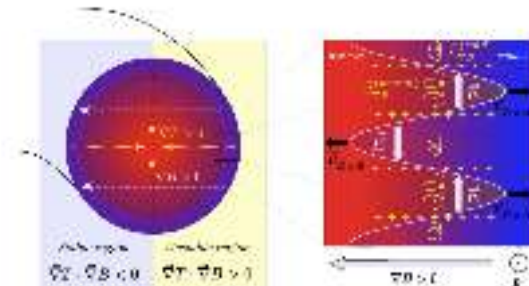
- Clear ballooning character since favorable/unfavorable curvatures in the HFS/LFS of the Torus



## ITG TURBULENCE

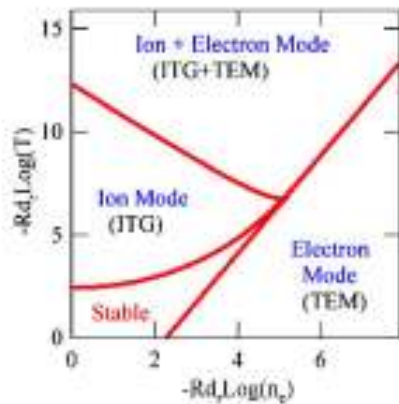
- Clear ballooning character since favorable/unfavorable curvatures in the HFS/LFS of the Torus
- ITG exhibit a **critical threshold** for  $R/L_{T_i}$ , being  $L_{T_i} = |T_i/\nabla T_i|^{-1}$
- The threshold increases with increasing  $T_i/T_e$  and for adiabatic electrons increasing with increasing  $R/L_n$
- For  $\eta_i = L_n/L_{T_i} > \frac{2}{3}$  analytical formula found for critical gradient (Romanelli 1989)

$$\frac{R}{L_{T_i}} > \frac{4}{3} \left( 1 + \frac{T_i}{T_e} \right)$$



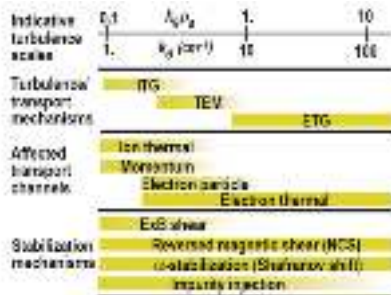
## OTHER INSTABILITIES, CORRESPONDING SCALES AND STABILIZING MECHANISM

- So far we have explored the (electrostatic) ITG mode with adiabatic electrons
- The inclusion of the electron dynamics leads to several other modes as trapped electron mode (TEM) and the electron temperature gradient (ETG) mode
- Both the two instabilities exhibit still a critical electron temperature gradient
- The TEM , still at  $r_{L_i}$  scale include the effect of electron slower inertial along field line because of trapping
- The ETG is an analogous of ITG at electron larmor radius effects
- Plasma conditions determine the stability diagram  
(Garbet et al. 2004)



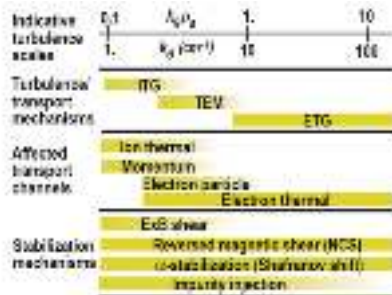
## OTHER INSTABILITIES, CORRESPONDING SCALES AND STABILIZING MECHANISM

- Plasma turbulence is a multiscale process where different instabilities may coexist



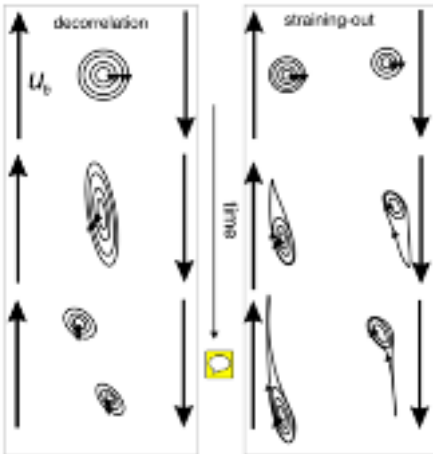
## OTHER INSTABILITIES, CORRESPONDING SCALES AND STABILIZING MECHANISM

- Plasma turbulence is a multiscale process where different instabilities may coexist
- Main stabilizing mechanisms are the  $E \times B$  shear and the magnetic shear



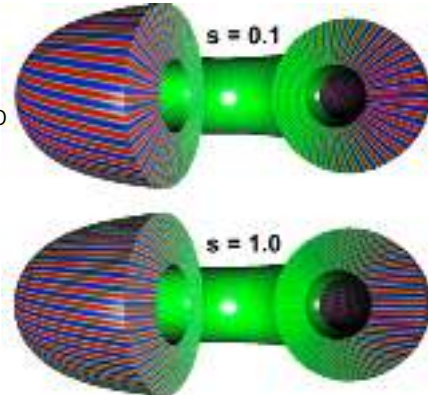
## OTHER INSTABILITIES, CORRESPONDING SCALES AND STABILIZING MECHANISM

- Any sheared flow (gradient in rotation velocity) can produce a reduction of the turbulence and associated transport
- The mechanism is identified as the key player producing the transport barrier at the edge during the transition to H-Mode



## OTHER INSTABILITIES, CORRESPONDING SCALES AND STABILIZING MECHANISM

- Magnetic shear is due to different winding numbers of the field lines (non constant safety factor)
- Since most of the instabilities are field aligned due to the strong anisotropy in velocity it has a strong stabilizing effect
- It basically lead to a deformation of the structures



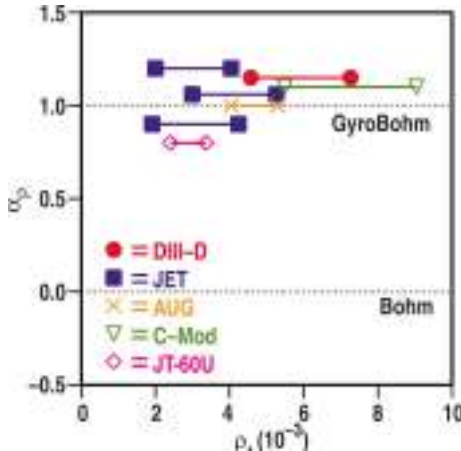
## RELEVANT TRANSPORT SCALING

- Reference diffusivity is the Bohm like diffusion  $D_B \propto \frac{T_e}{B}$  (Horton 1999) arising from mesoscale toroidal drift-wave structures near marginal stability
- Drift-wave diffusivity exhibit a gyro-Bohm scaling of the form

$$D_{dw} = \frac{\rho_s}{L_n} \frac{T_e}{B} \propto \rho^* D_b$$

being  $\rho^* \approx \frac{\rho_s}{a}$

- However  $\rho^*$  scaling is more Bohm-like for
  - High  $q_{95} > 4$
  - Heating power close to L-H power threshold
  - Low (L) confinement mode



(Petty 2008)

## WHAT WE LEARNED

- (i) We introduce the concept of **anomalous transport** showing how a perturbation in the particle distribution function may contribute to particle and heat transport
- (ii) We introduce two of the basic linear instabilities responsible for transport showing how collisionality and geometry could contribute to their non-linear evolution
- (iii) We empirically describe one of the major player in the core transport as the ITG and as well the characteristic scale lengths for smaller scale turbulence
- (iv) We provide proper scaling of turbulence induce diffusivities
- (v) We introduce the basic mechanisms for turbulence suppression
- (vi) Clearly all presented is just an attempt to scrap the surface and we are still far for a proper understanding of anomalous transport to provide adequate predictive capabilities

## BIBLIOGRAPHY I

1. Garbet, X. et al. **Physics of transport in tokamaks.** *Plasma Physics and Controlled Fusion* **46**, B557 (2004).
2. Horton, W. **Drift waves and transport.** *Reviews of Modern Physics* **71**, 735 (1999).
3. Petty, C. C. **Sizing up plasmas using dimensionless parameters.** *Physics of Plasmas* **15**, 080501 (2008).
4. Romanelli, F. **Ion temperature gradient driven modes and anomalous ion transport in tokamaks.** *Physics of Fluids B: Plasma Physics* **1**, 1018 (1989).
5. Wesson, J. **Tokamaks.** ISBN: 0199592233 (Oxford University Press, 2004).

# **SOL and Divertor physics**

---

Nicola Vianello

28 November 2024

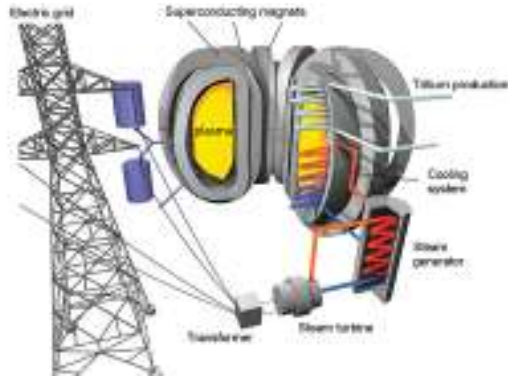
ISTP-CNR and Consorzio RFX

# **Introduction**

---

# The motivation for a divertor: the exhaust problem

- Nuclear reaction

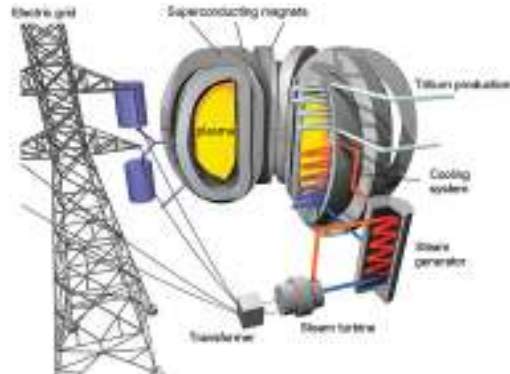


## The motivation for a divertor: the exhaust problem

- Nuclear reaction



- Neutrons leave the plasma into power conversion system and will be used for net energy production

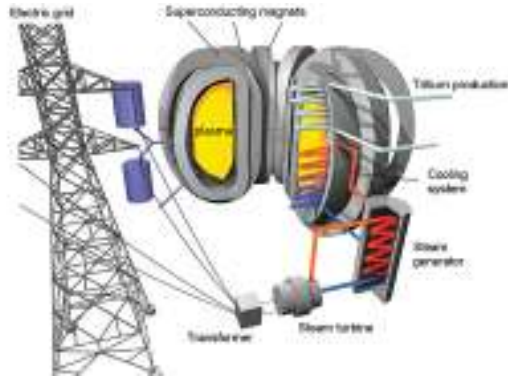


## The motivation for a divertor: the exhaust problem

- Nuclear reaction



- Neutrons leave the plasma into power conversion system and will be used for net energy production
- Alphas heat the plasmas and then need to be exhausted

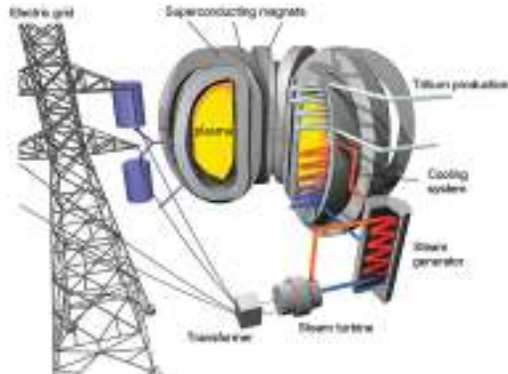


# The motivation for a divertor: the exhaust problem

- Nuclear reaction



- Neutrons leave the plasma into power conversion system and will be used for net energy production
- Alphas heat the plasmas and then need to be exhausted
- The roles:
  - Helium ash removal
  - Impurity control
  - Fueling Neutral particle control
  - Heat Exhaust
  - Minimize material damage as erosion and melting



## Severity of the exhaust problem



### ASDEX-Upgrade

Major radius: 1.65m

$$q_{\perp} \approx 40 \text{ MW/m}^2$$

## Severity of the exhaust problem



**ASDEX-Upgrade**

Major radius: 1.65m

$q_{\perp}$  40 MW/m<sup>2</sup>



**ITER**

Major radius: 6.2m

$q_{\perp}$  100 MW/m<sup>2</sup>

## Severity of the exhaust problem



**ASDEX-Upgrade**

Major radius: 1.65m

$q_{\perp}$  40 MW/m<sup>2</sup>



**ITER**

Major radius: 6.2m

$q_{\perp}$  100 MW/m<sup>2</sup>



**DEMO**

Major radius: ~ 9m

$q_{\perp}$  350 MW/m<sup>2</sup>

## Severity of the exhaust problem



$$q_{\perp} \sim 1 \text{ MW}^2$$



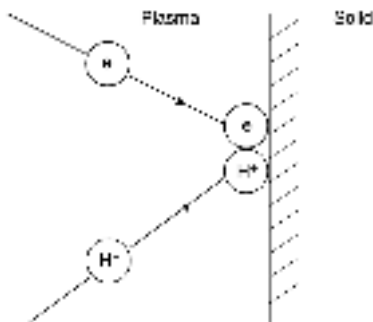
$$q_{\perp} \sim 5 \text{ MW}^2$$



$$q_{\perp} \sim 80 \text{ MW}^2$$

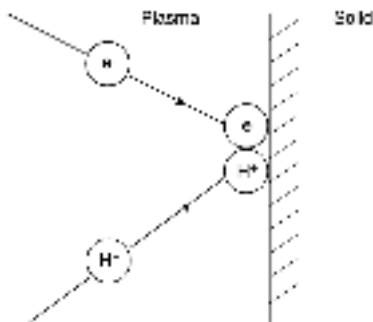
## Solid surface interaction with a plasma: PWI

- Any solid surface inserted into a plasma constitutes a very strong particle sink
- If charged particles strike a solid surface they tend to stick long enough to recombine
- For insulating or electrically isolated surfaces, opposite charges stick and produce *surface recombination*
- The neutrals are generally weakly bound to the solid and are thermally re-emitted as neutrals



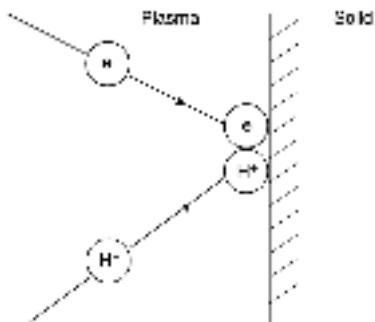
## Solid surface interaction with a plasma: PWI

- Any solid surface inserted into a plasma constitutes a very strong particle sink
- If charged particles strike a solid surface they tend to stick long enough to recombine
- For insulating or electrically isolated surfaces, opposite charges stick and produce *surface recombination*
- Thus we have a plasma sink not a mass sink



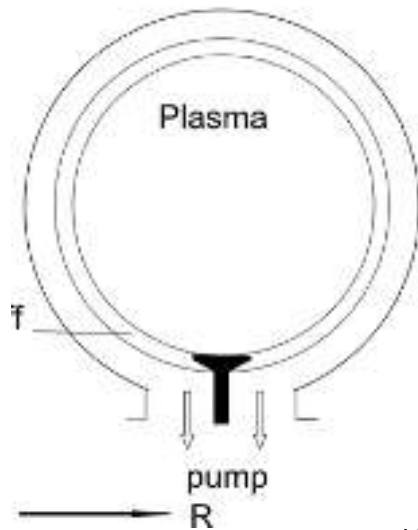
## Solid surface interaction with a plasma: PWI

- Any solid surface inserted into a plasma constitutes a very strong particle sink
- If charged particles strike a solid surface they tend to stick long enough to recombine
- For insulating or electrically isolated surfaces, opposite charges stick and produce *surface recombination*
- Thus we have a plasma sink not a mass sink
- This *recycling* process can happen in steady-state condition whereby plasma charged pairs are lost at the same rate as recombined neutrals re-enter the plasma



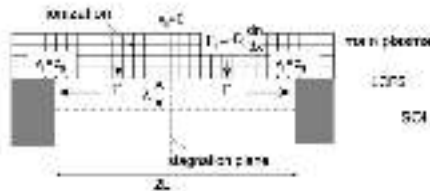
## The Limiter configuration and simple SOL

- Solid surface eventually inserted by purpose to provide controlled Plasma Wall Interaction
- Historically first solution proposed is the **limiter solution** (with toroidal or poloidal limiters)
- Clear identification of the **LCFS** and the SOL
- Can be described by **fluid approach** as far as **self collisional mean free paths of electrons and ions lower than parallel connection length  $\lambda_{ee}, \lambda_{ii} \ll L_{||}$**



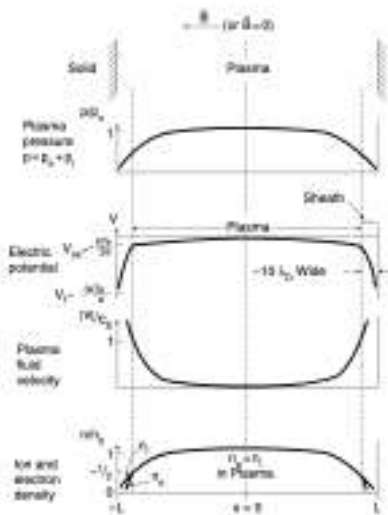
## The Limiter configuration and simple SOL

- If the neutral m.f.p. is long enough to pass through the SOL and they are ionized inside the main plasm, then we are in the condition of **Simple SOL**
- To describe the characteristics of simple SOL we need to describe better the interaction of a plasma with solid wall



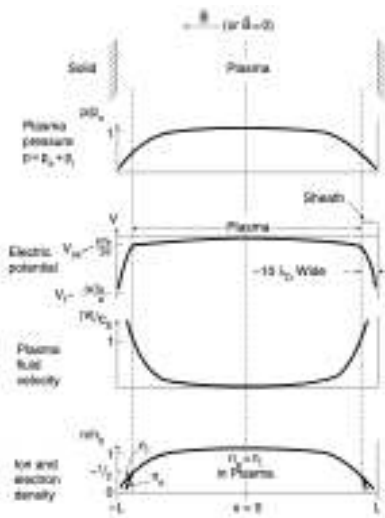
## The Limiter configuration and simple SOL

- In presence of a solid wall higher electron mobility charge up the wall negatively  $\Rightarrow$  ambipolar electric field builds up to ensure equal ion/electron loss  $\rightarrow V_{wall} \approx -3kT_e/e$  w.r.t. plasma potential



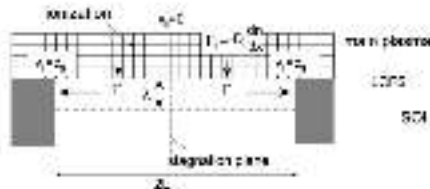
## The Limiter configuration and simple SOL

- In presence of a solid wall higher electron mobility charge up the wall negatively  $\Rightarrow$  ambipolar electric field builds up to ensure equal ion/electron loss  $\rightarrow V_{wall} \approx -3kT_e/e$  w.r.t. plasma potential
- Electrostatic potential shielded within a Debye length  $\lambda_D = \sqrt{\frac{\epsilon_0 k T_e}{n_e e^2}}$
- Shielding is not perfect. pre-sheath electric field of the order of  $E \approx kT_e/2eL$
- Ions are accelerated in the pre-sheath up to the sheath entrance velocity  $v_{se} = c_s = \sqrt{\frac{k(T_e + T_i)}{m_i}} \Rightarrow$  Bohm criterion
- At sheath entrance density is  $n_{se} = \frac{1}{2} n_0$



## The Limiter configuration and simple SOL

- In the **simple SOL approximation** with no source of particle in the SOL, simple relation holds between **diffusion** and **SOL width**
- This is obtained by the equality between the **Total particle outflow crossing the LCFS**  $\phi_{\perp}$  to the **total particle flow towards the 2 solid surfaces**  $\phi_{\parallel}$

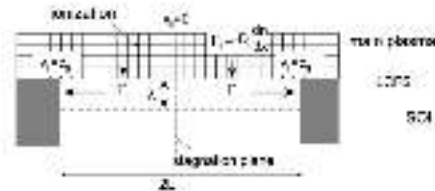


$$\phi_{\perp} = -D_{\perp}^{SOL} \frac{dn}{dr}_{LCFS} 2Lw = -D_{\perp}^{SOL} \frac{n_{LCFS}}{\lambda_n} 2Lw$$

$$\phi_{\parallel} = 2w \int_{r=LCFS}^{\infty} n c_s dr \approx 2w \frac{1}{2} n_{LCFS} c_s \lambda_n \quad \text{with} \quad n(r) = n_{LCFS} e^{-\frac{r}{\lambda_n}}$$

## The Limiter configuration and simple SOL

- In the simple SOL approximation with no source of particle in the SOL, simple relation holds between diffusion and SOL width
- This is obtained by the equality between the Total particle outflow crossing the LCFS  $\phi_{\perp}$  to the total particle flow towards the 2 solid surfaces  $\phi_{\parallel}$



$$\lambda_n = \sqrt{\frac{2D_{\perp}^{SOL} L}{c_s}}$$

## The Limiter configuration and simple SOL

- The corresponding ion and electron parallel flux to the target can be estimated remembering that electrons distributions remains Maxwellian even in retarding electric field

$$\Gamma_t^i = n_{se} c_s, \quad \Gamma_t^e = \frac{1}{4} n_{es} \exp(eV_s/kT_e) \sqrt{\frac{8kT_e}{\pi m_e}} \quad \Rightarrow \frac{eV_s}{kT_e} = 0.5 \ln \left( 2\pi \frac{m_e}{m_i} \right) (1 + T_i/T_e) \approx 3$$

## The Limiter configuration and simple SOL

- The corresponding ion and electron parallel flux to the target can be estimated remembering that electrons distributions remains Maxwellian even in retarding electric field

$$\Gamma_t^i = n_{se} c_s, \quad \Gamma_t^e = \frac{1}{4} n_{es} \exp(eV_s/kT_e) \sqrt{\frac{8kT_e}{\pi m_e}} \quad \Rightarrow \frac{eV_s}{kT_e} = 0.5 \ln \left( 2\pi \frac{m_e}{m_i} \right) (1 + T_i/T_e) \approx 3$$

- Heat flux related to particle flux through the **sheath transmission coefficients**  $\gamma_{i,e} = \frac{q_{i,e}}{kT_e \Gamma_t}$

## The Limiter configuration and simple SOL

- The corresponding ion and electron parallel flux to the target can be estimated remembering that electrons distributions remains Maxwellian even in retarding electric field

$$\Gamma_t^i = n_{se} c_s, \quad \Gamma_t^e = \frac{1}{4} n_{es} \exp(eV_s/kT_e) \sqrt{\frac{8kT_e}{\pi m_e}} \quad \Rightarrow \frac{eV_s}{kT_e} = 0.5 \ln \left( 2\pi \frac{m_e}{m_i} \right) (1 + T_i/T_e) \approx 3$$

- Heat flux related to particle flux through the **sheath transmission coefficients**  $\gamma_{i,e} = \frac{q_{i,e}}{kT_e \Gamma_t}$
- For electrons considering sheath and pre-sheath drop  $\gamma_e = 5.5$
- For the ion the computation is not straightforward: if ion distribution is maxwellian then  $\gamma_i = 3.5$

## The Limiter configuration and simple SOL

- The corresponding ion and electron parallel flux to the target can be estimated remembering that electrons distributions remains Maxwellian even in retarding electric field

$$\Gamma_t^i = n_{se} c_s, \quad \Gamma_t^e = \frac{1}{4} n_{es} \exp(eV_s/kT_e) \sqrt{\frac{8kT_e}{\pi m_e}} \quad \Rightarrow \frac{eV_s}{kT_e} = 0.5 \ln \left( 2\pi \frac{m_e}{m_i} \right) (1 + T_i/T_e) \approx 3$$

- Heat flux related to particle flux through the **sheath transmission coefficients**  $\gamma_{i,e} = \frac{q_{i,e}}{kT_e \Gamma_t}$
- For electrons considering sheath and pre-sheath drop  $\gamma_e = 5.5$
- For the ion the computation is not straightforward: if ion distribution is maxwellian then  $\gamma_i = 3.5$
- The flux is then computed as  $q_t^{i,e} = \gamma_{i,e} n_{es} c_s kT_e$

## General description of the parallel transport in the SOL

- Identified the ion and electron heat flux to the target as related to the corresponding particle flux
- Need to determine the eventual spatial distribution. 1D approach with detail description in (P. C. Stangeby 2000; Unterberg 2017)

## General description of the parallel transport in the SOL

- Density conservation equation in steady-state

$$\frac{\partial}{\partial z} (n_{i,e} V_{\parallel i,e}) = S_p$$

- Ion momentum conservation in steady state

$$\frac{\partial}{\partial z} (m_i n v_{\parallel i}^2 + p_i) = e n E + R_{ie} + R_n$$

- $R_{ie}$  being the friction force caused by electron collisions:

$$R_{ie} = m_e (v_e - v_i) \nu_{ei} n + 0.71 n \partial k T_e / \partial z$$

- $R_n$  being the friction force due to collisions with neutrals

$$R_n = -m_i (v_i - v_n) \langle \sigma v \rangle_{CX} n_n n + m_i v_n S_p \text{ where we implicitly assumed that momentum loss due to Charce eXchange is dominant mechanism for ions}$$

## General description of the parallel transport in the SOL

- Density conservation equation in steady-state

$$\frac{\partial}{\partial z} (n_{i,e} V_{\parallel i,e}) = S_p$$

- For the electron we rely on the small inertia and momentum balance is written as

$$\frac{\partial p_e}{\partial z} + enE = -m_e(v_e - v_i)\nu_{ei} - 0.71n \frac{\partial kT_e}{\partial z}$$

where we kept the friction term for ion-electron momentum exchange

## General description of the parallel transport in the SOL

- Density conservation equation in steady-state

$$\frac{\partial}{\partial z} (n_{i,e} V_{\parallel i,e}) = S_p$$

- The total plasma momentum equation results then in

$$\frac{\partial}{\partial z} (m_i n v^2 + p_i + p_e) = -m_i (v_i - v_n) \langle \sigma v \rangle n_n n + m_i v_n S_p(z)$$

- We recognize that the main force acting on  $m_i n v^2$  is the pressure gradient with no effect from electric field. Strong uncertainty come from the unknown of  $T_{\parallel}$
- We need to move to higher momentum and compute the parallel energy equation

## General description of the parallel transport in the SOL

- Ion energy conservation

$$\frac{\partial q_{\parallel,i}}{\partial z} = \frac{\partial}{\partial z} \left[ \left( \frac{5}{2} T_i + \frac{1}{2} m_i v_i^2 \right) n v_i \begin{bmatrix} -\kappa_{0,i} T_i^{5/2} \frac{\partial T_i}{\partial z} \end{bmatrix} \right] = e n v_i E + Q_{eq} + Q_{Ei}$$

- Electron energy conservation equation

$$\frac{\partial q_{\parallel,e}}{\partial z} = \frac{\partial}{\partial z} \left[ \frac{5}{2} T_e n v_e \begin{bmatrix} -\kappa_{0,e} T_e^{5/2} \frac{\partial T_e}{\partial z} \end{bmatrix} \right] = -e n v_i E - Q_{eq} + Q_r + Q_{Ee}$$

- With  $Q_{eq}$  arising because of thermal equilibration collision between electrons and ions,  $Q_r$  the Joule heating term,  $Q_{Ei}$  resulting from ion-neutral interaction and  $Q_{Ee}$  is the energy loss for electrons because of inelastic collisions which ionize or excite neutrals
- Ion conduction  $\kappa_{0,i} \approx 60 \ll \kappa_{0,e} \approx 2000$  because of a  $m^{-1/2}$  dependence

## General description of the parallel transport in the SOL

- For  $T_e = T_i$ , defining the total pressure  $p = p_e + p_i$  we have a simplified form

$$\frac{\partial(nv)}{\partial z} = S_p$$

$$\frac{\partial}{\partial z}[(m_i v^2 + 2kT)n] = -m_i v \langle \sigma v \rangle n n_n$$

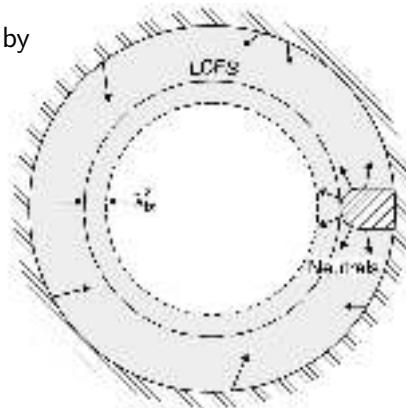
$$\frac{\partial}{\partial z} \left[ \left( \frac{1}{2} m_i v^2 + 5kT \right) nv - \kappa_{0,e} T_e^{5/2} \partial T_e / \partial z \right] = Q_r + Q_E$$

## **Divertor configuration**

---

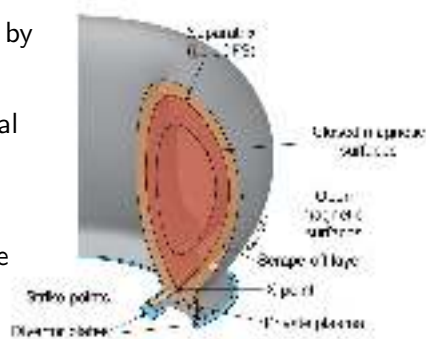
## Divertor configuration

- Limiter configuration not ideal to reduce plasma pollution by impurities generated by PWI



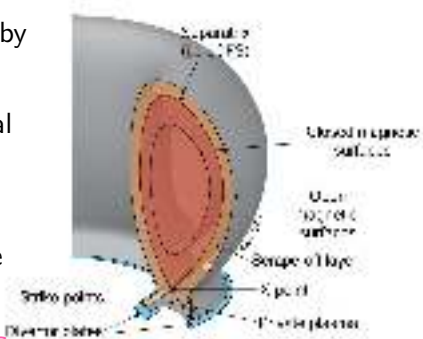
## Divertor configuration

- Limiter configuration not ideal to reduce plasma pollution by impurities generated by PWI
- Introduced the divertor configuration, generated by poloidal field coil where PWI occur far from confined region →  
**Ionization source in within SOL volume**
- Guarantee better pumping efficiency, lower heat flux at the target.



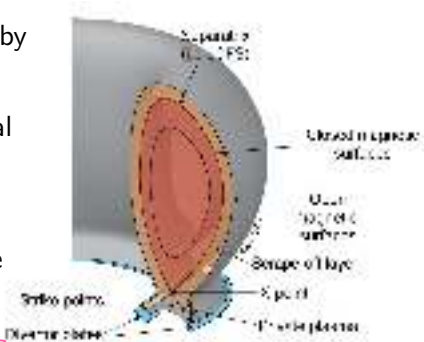
## Divertor configuration

- Limiter configuration not ideal to reduce plasma pollution by impurities generated by PWI
- Introduced the divertor configuration, generated by poloidal field coil where PWI occur far from confined region →  
**Ionization source in within SOL volume**
- Guarantee better pumping efficiency, lower heat flux at the target.
- Realized by reducing plasma temperature in front of the PFC and establishing a temperature gradient along the magnetic field



## Divertor configuration

- Limiter configuration not ideal to reduce plasma pollution by impurities generated by PWI
- Introduced the divertor configuration, generated by poloidal field coil where PWI occur far from confined region →  
**Ionization source in within SOL volume**
- Guarantee better pumping efficiency, lower heat flux at the target.
- Realized by reducing plasma temperature in front of the PFC and establishing a temperature gradient along the magnetic field
- Described by the **2 point model** (P. C. Stangeby 2018, 2000; P. Stangeby 2020a,b) which describe relation between upstream and target condition



## Divertor configuration

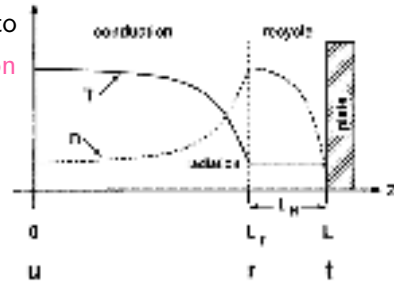
- Unfolding the SOL, if ionization occurs in a region close to the target, the **heat conduction** dominates  $\Rightarrow$  **conduction limited regime**
- The parallel heat flux is thus related to the parallel temperature gradient:

$$q_{\parallel} = \frac{P_{SOL}}{A_{\parallel}} = -\kappa_{0,e} T^{5/2} \frac{\partial T}{\partial z_{\parallel}}$$

- Integrating the previous equation

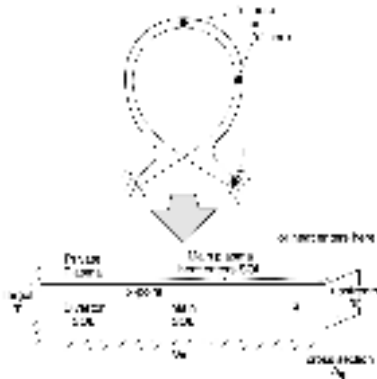
$$T(z_{\parallel}) = \left[ T_t^{7/2} + \frac{7}{2} \frac{P_{SOL}/A_{\parallel}(L_{\parallel} - s_{\parallel})}{\kappa_{0,e}} \right]$$

which for  $T_u \ll T_t$  we obtain  $T_u \simeq \left( \frac{7}{2} \frac{P_{SOL}/A_{\parallel} L_{\parallel}}{\kappa_{0,e}} \right)^{2/7}$



## Unfolding the SOL: 2 point model

- **Particle balance:** neutrals recycling from the targets are ionized in thin layer close to the target and parallel flow limited to the same region where particle accelerate up to sheath velocity entrance
- **Total pressure balance:**  $p + nmv^2 = \text{constant}$  which in the case of  $T_e = T_i$  implies  $p = 2nkT$  and dynamic pressure  $\neq 0$  only close to the target with  $v_t = c_{st} = \sqrt{2kT_t/m_i}$
- **Power balance:** Since  $v = 0$  almost entirely in the SOL then conduction dominated dynamic with  $T_u^{7/2} = T_t^{7/2} + \frac{7}{2}q_{\parallel}\frac{L_{\parallel}}{\kappa_{0e}}$ . No volumetric power loss assumed (very thin ionization layer) then  $q_{\parallel} = q_t = \gamma n_t k T_t c_{st}$



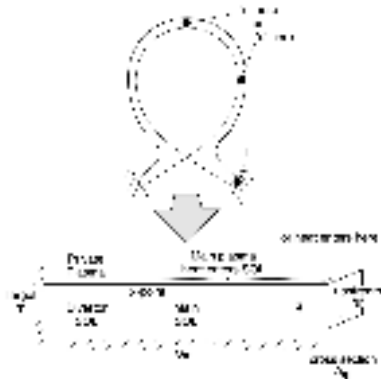
## Unfolding the SOL: 2 point model

- Combining all these information together we have:

$$2n_t T_t = n_u T_u$$

$$T_u^{7/2} = T_t^{7/2} + \frac{7}{2} q_{\parallel} \frac{L_{\parallel}}{\kappa_{0e}}$$

$$q_{\parallel} = q_t = \gamma n_t k T_t c_{st}$$



## Unfolding the SOL: 2 point model

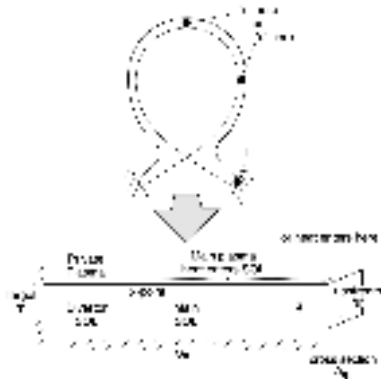
- We derive now  $n_t$ ,  $T_t$ ,  $T_u$  from  $n_u$  and  $q_{\parallel}$

$$T_u \simeq \left( \frac{7}{2} \frac{q_{\parallel} L_{\parallel}}{\kappa_{0e}} \right)^{2/7}$$

$$T_t = \frac{m_i}{2e} \frac{4q_{\parallel}^2}{\gamma^2 e^2 n_u^2 T_u^2} \simeq \frac{m_i}{2e} \frac{4q_{\parallel}^2 \left( \frac{7}{2} \frac{q_{\parallel} L_{\parallel}}{\kappa_{0e}} \right)^{-4/7}}{\gamma^2 e^2 n_u^2} \propto \frac{q_{\parallel}^{10/7}}{L_{\parallel}^{4/7} n_u^2}$$

$$n_t = \frac{n_u^3}{q_{\parallel}^2} \left( \frac{7}{2} \frac{q_{\parallel} L_{\parallel}}{\kappa_{0e}} \right)^{6/7} \frac{\gamma^2 e^3}{4m_i} \propto n_u^3 q_{\parallel}^{-8/7} L_{\parallel}^{6/7}$$

$$\Gamma_t = \frac{q_{\parallel}}{\gamma e T_T} = \frac{n_u^2}{q_{\parallel}} \left( \frac{7}{2} \frac{q_{\parallel} L_{\parallel}}{\kappa_{0e}} \right)^{4/7} \frac{\gamma e^2}{2m_i} \propto n_u^2 q_{\parallel}^{-3/7} L_{\parallel}^{4/7}$$



## Modified 2Point Model

- We need to account the effect of **Volumetric power losses due to radiation and charge exchange losses**,  $q_{rad}^{SOL} + q_{CX}^{SOL} = f_{pow} q_{||}$  which modify the power balance equation as

$$(1 - f_{pow}) q_{||} = q_t = \gamma k T_t n_t c_{st}$$

- The momentum equation is modified to account for **momentum losses** which are due to volumetric momentum losses (e.g. friction with neutrals, viscous forces, volume recombination ) as well as *effective volumetric losses* due for example by cross-field transport:

$$2n_t T_t = f_{mom} n_u T_u$$

- Some residual convection still remain, which tend to reduce the temperature gradient. We therefore introduce a conduction factor  $f_{cond}$  so that  $q_{||,cond} = f_{cond} q_{||}$

## Modified 2Point Model

- The upstream temperature is modified accordingly and in the condition of  $T_t \ll T_u$  we have

$$T_u \simeq \left( \frac{2}{7} \frac{f_{cond} q_{\parallel} L_{\parallel}}{\kappa_0 e} \right)^{2/7} \propto f_{cond}^{2/7}$$

$T_u$  unaffected by momentum loss or volumetric power loss and small variation due to the convection

## Modified 2Point Model

- The upstream temperature is modified accordingly and in the condition of  $T_t \ll T_u$  we have

$$T_u \simeq \left( \frac{2}{7} \frac{f_{cond} q_{||} L_{||}}{\kappa_0 e} \right)^{2/7} \propto f_{cond}^{2/7}$$

$T_u$  unaffected by momentum loss or volumetric power loss and small variation due to the convection

- Target temperature strongly reduced by **volumetric power loss** and increase by **momentum loss**

$$T_t \propto \frac{(1 - f_{pow})^2}{f_{mom}^2 f_{cond}^{4/7}}$$

## Modified 2Point Model

- Correspondingly the ratio of upstream and target temperature results in

$$\frac{T_u}{T_t} \propto \frac{f_{cond}^{6/7} f_{mom}^2}{(1 - f_{pow}^2)}$$

with the clear tendency of convection to reduce/eliminate the parallel temperature gradient

- The target density results in

$$n_t \propto \frac{f_{mom}^3 f_{cond}^{6/7}}{(1 - f_{pow})^2}$$

We recognize a robust effect of momentum dissipation in suppressing target density

## Modified 2Point Model

- Finally the target particle flux is modified as

$$\Gamma_t \propto \frac{f_{mom}^2 f_{cond}^{4/7}}{1 - f_{pow}}$$

and thus with a strong contribution of **momentum loss** in reducing fluxes to the target

## Divertor regimes

For a given  $q_{\parallel u}$  input in a flux tube it is generally observed that as  $n_u$  is increased the target  $T_t$  decreases and the corresponding flux tube passes through **different regimes**:

1. **Sheath limited Regimes** where small temperature gradients exists and  $q_{\parallel}$  is constrained by sheath condition.  $\Gamma_{\parallel}$  and pressure approximately constant along the flux tube

## Divertor regimes

For a given  $q_{\parallel u}$  input in a flux tube it is generally observed that as  $n_u$  is increased the target  $T_t$  decreases and the corresponding flux tube passes through **different regimes**:

1. **Sheath limited Regimes** where small temperature gradients exists and  $q_{\parallel}$  is constrained by sheath condition.  $\Gamma_{\parallel}$  and pressure approximately constant along the flux tube
2. **High Recycling Regime** a.k.a. *Conduction limited regime* where  $q_{\parallel}$  is constrained by sheath condition and temperature conduction. Significant drop of  $T_e$ ,  $T_t \ll T_u$ ,  $\Gamma_{\parallel,u} \ll \Gamma_{\parallel,t}$  but momentum is still constant along the flux tube

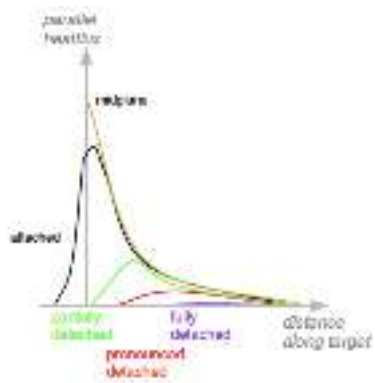
## Divertor regimes

For a given  $q_{\parallel u}$  input in a flux tube it is generally observed that as  $n_u$  is increased the target  $T_t$  decreases and the corresponding flux tube passes through **different regimes**:

1. **Sheath limited Regimes** where small temperature gradients exists and  $q_{\parallel}$  is constrained by sheath condition.  $\Gamma_{\parallel}$  and pressure approximately constant along the flux tube
2. **High Recycling Regime** a.k.a. *Conduction limited regime* where  $q_{\parallel}$  is constrained by sheath condition and temperature conduction. Significant drop of  $T_e$ ,  $T_t \ll T_u$ ,  $\Gamma_{\parallel,u} \ll \Gamma_{\parallel,t}$  but momentum is still constant along the flux tube
3. **Detachment regime** with significant reduction of the power and particle fluxes to the target with associated pronounced pressure drop

## Divertor regimes

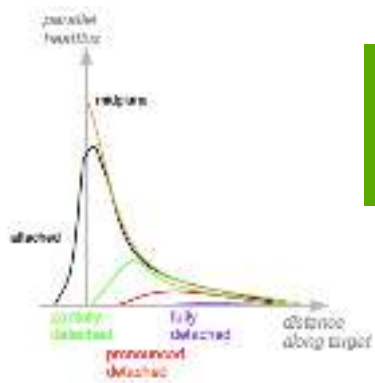
For a given  $q_{\parallel u}$  input in a flux tube it is generally observed that as  $n_u$  is increased the target  $T_t$  decreases and the corresponding flux tube passes through different regimes:



(Kallenbach et al. 2015)

## Divertor regimes

For a given  $q_{\parallel u}$  input in a flux tube it is generally observed that as  $n_u$  is increased the target  $T_t$  decreases and the corresponding flux tube passes through different regimes:

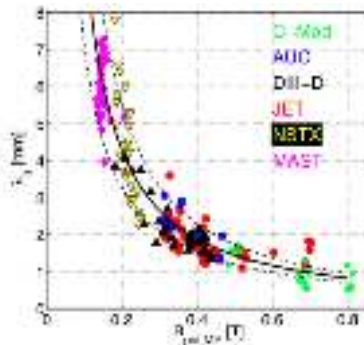


But what we can expect to be the  $\lambda_q$  in future devices?

## The need for exhaust solution: $\lambda_q$ scaling

- ITPA multi-machine database suggest **only the poloidal magnetic field is statistically important** (Eich *et al.* 2013)

$$\lambda_q = (0.63 \pm 0.08) B_{pol}^{-1.19 \pm 0.08}$$

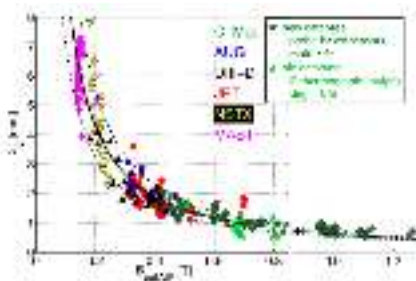


## The need for exhaust solution: $\lambda_q$ scaling

- ITPA multi-machine database suggest **only the poloidal magnetic field is statistically important** (Eich *et al.* 2013)

$$\lambda_q = (0.63 \pm 0.08) B_{pol}^{-1.19 \pm 0.08}$$

- Recent extension to ITER relevant poloidal magnetic field (Brunner *et al.* 2018) suggest the validity up to a predicted  $\lambda_q^{ITER} \leq 1\text{mm}$

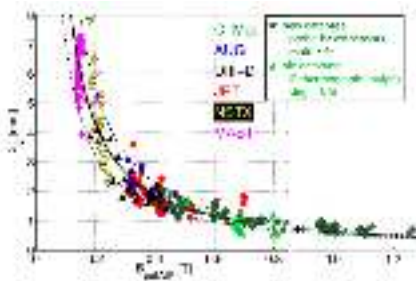


## The need for exhaust solution: $\lambda_q$ scaling

- ITPA multi-machine database suggest only the poloidal magnetic field is statistically important (Eich *et al.* 2013)

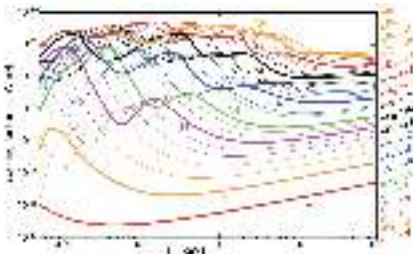
$$\lambda_q = (0.63 \pm 0.08) B_{pol}^{-1.19 \pm 0.08}$$

- Recent extension to ITER relevant poloidal magnetic field (Brunner *et al.* 2018) suggest the validity up to a predicted  $\lambda_q^{ITER} \leq 1\text{mm}$
- The predicted heat flux exceed the engineering material limit set to approximately  $10 \text{ M/m}^2$  or bit higher (to avoid W material re-crystallization (Pitts *et al.* 2019) ).  
We need mitigation strategy



## Radiative divertor

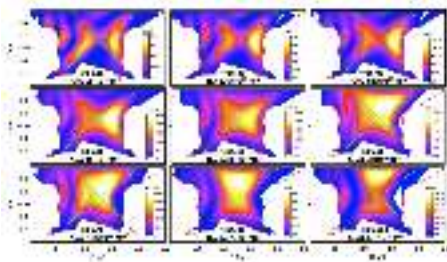
- Extrinsic impurity injected to increase radiation and provide tolerable heat load
- Scenario foreseen for ITER operation (Ne injection) to achieve partial detachment of the OSP
- For DEMO higher radiation fraction needed (90 % of  $P_{sep}$ ) needed



(Pütterich *et al.* 2019)

## Radiative divertor

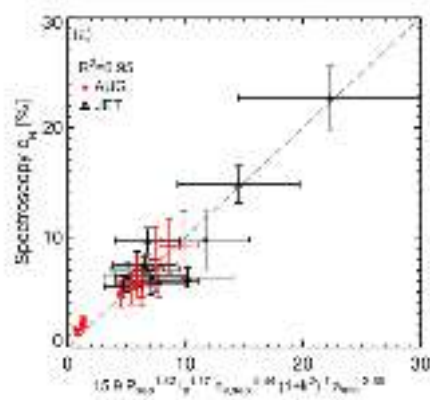
- Extrinsic impurity injected to increase radiation and provide tolerable heat load
- Scenario foreseen for ITER operation (Ne injection) to achieve partial detachment of the OSP
- For DEMO higher radiation fraction needed (90 % of  $P_{sep}$ ) needed
- Drawback appearance of a MARFE (multifaceted asymmetric radiation from the edge) and corresponding radiative collapse



(Huber *et al.* 2007)

## Radiative divertor

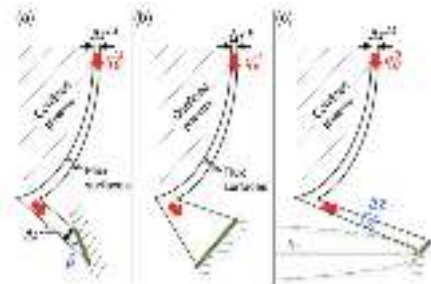
- Different models proposed for determining impurity concentration needed to provide detachment
  - Goldston scaling** which focus on separatrix density (Goldston *et al.* 2017)  $c_z \propto \frac{P_{sep}}{B_p(1+\kappa)^{1.5} f_{GW,sep}^2}$
  - Reinke scaling** which focus on machine size (Reinke 2017)  $c_z \propto B_T^{0.88} R^{1.33}$
  - Kallenbach scaling** which focus on momentum and energy loss  $c_z \propto \frac{P_{sep}/R}{p_{div} \lambda_{int} R^{rz}}$
- Experimental results on multimachine scaling provide hints towards Goldstone scaling with a further dependence on minor radius



(Henderson, IAEA 2020, IAEA2023)

## Geometrical effects on heat flux

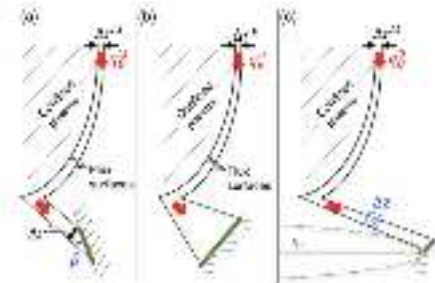
- Geometrical divertor modification can already provide tools for heat flux mitigation



(Theiler *et al.* 2017)

## Geometrical effects on heat flux

- Grazing angle reduce the amount of parallel heat flux perpendicular to the surface  $q_{\perp} = q_{\parallel} \sin \alpha$
- Tilting the divertor plate on the poloidal plane of an angle  $\beta$  already drastically reduce the perpendicular heat flux

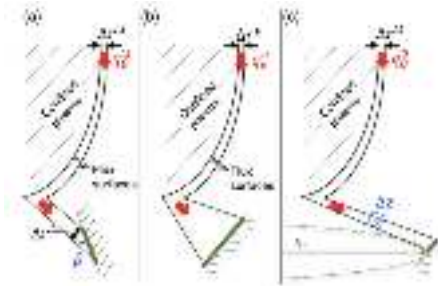


(Theiler *et al.* 2017)

## Geometrical effects on heat flux

- Grazing angle reduce the amount of parallel heat flux perpendicular to the surface  $q_{\perp} = q_{\parallel} \sin \alpha$
- Tilting the divertor plate on the poloidal plane of an angle  $\beta$  already drastically reduce the perpendicular heat flux
- Increase flux-surface separation at the target by increasing the **poloidal flux expansion**

$$f_x = \Delta r_t / \Delta r_u = B_{\theta}^u B_{\phi}^t / B_{\theta}^t B_{\phi}^u$$

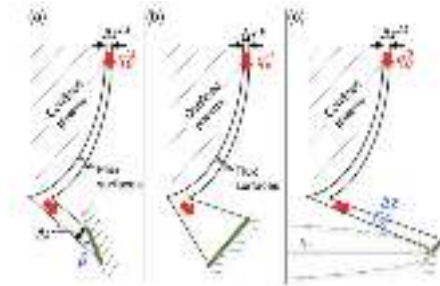


(Theiler *et al.* 2017)

## Geometrical effects on heat flux

- Grazing angle reduce the amount of parallel heat flux perpendicular to the surface  $q_{\perp} = q_{\parallel} \sin \alpha$
- Tilting the divertor plate on the poloidal plane of an angle  $\beta$  already drastically reduce the perpendicular heat flux
- Increase flux-surface separation at the target by increasing the **poloidal flux expansion**

$$f_x = \Delta r_t / \Delta r_u = B_\theta^u B_\phi^t / B_\theta^t B_\phi^u$$

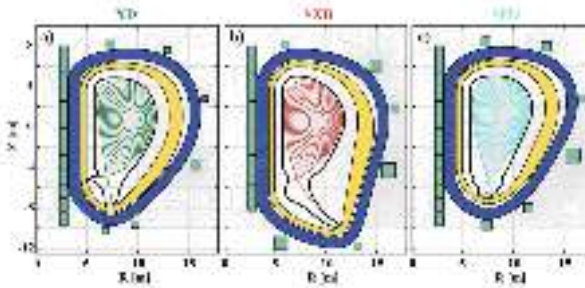


(Theiler *et al.* 2017)

- Increase the target radius. Extension of 2PM to include the variation of the major radius along the divertor leg brings (Kotschenreuther *et al.* 2010; Petrie *et al.* 2013)

$$T_e^t \propto \frac{q_{\parallel}^{10/7} (1 - f_{pow})^2}{n_u^2 L_{\parallel}^{4/7}} \frac{R_u^2}{R_t^2} \quad n_e^t \propto \frac{n_u^3 L_{\parallel}^{6/7}}{q_{\parallel}^{8/7} (1 - f_{rad})^2} \frac{R_t^2}{R_u^2}$$

## Alternative divertor configuration

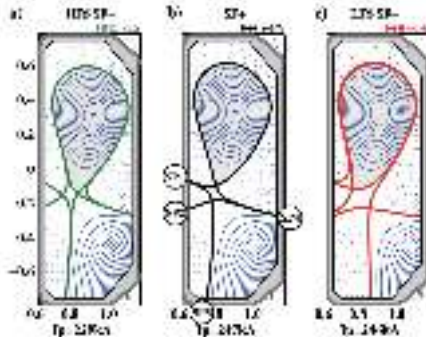


(Reimerdes, Ambrosino, et al. 2020)

- Alternative divertor proposed to the standard Lower Single Null adopted for present tokamaks and ITER
- Exploitation of flux flaring at the target (**X-divertor**), of large  $R_t$  effect (**Super-X divertor**)
- Additional solution known as **Snowflake configuration** suggested (Ryutov & Soukhanovskii 2015) with the inclusion of a second X-point

## Alternative divertor configuration

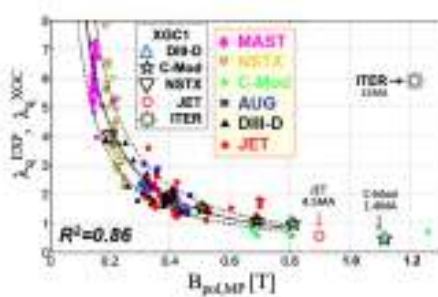
- Zoo of possible SF configuration exists, mainly SF+ and SF- (with second X-point in the private or common flux regione)
- Provide power sharing distribution among the 4 SPs (Maurizio *et al.* 2018), radiation mainly localized within the 2 X-points (Reimerdes, Duval, *et al.* 2017) and modification of SOL transport (Tsui *et al.* 2021)



(Reimerdes, Duval, *et al.* 2017)

## Extrapolation to future devices: the quest for anomalous transport

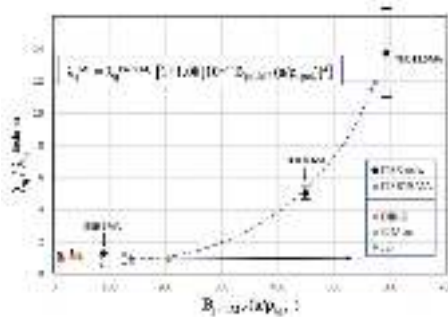
- Present state of the art gyrokinetic code able to mimic the observed scaling (Chang *et al.* 2021)
- Whenever extended to future devices higher  $\lambda_q$  foreseen due to a change of the underlying physical mechanism with TEM in weakly collisional plasma as efficient transported of electron heat and mass



(Chang *et al.* 2021)

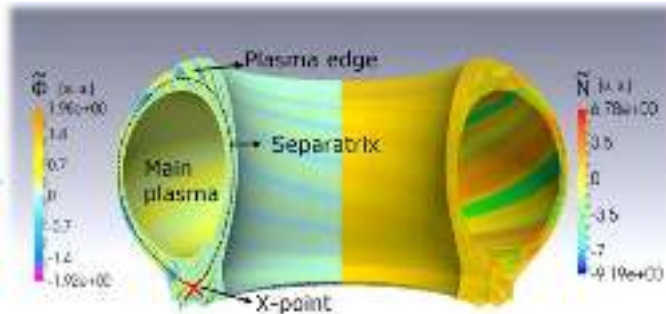
## Extrapolation to future devices: the quest for anomalous transport

- Present state of the art gyrokinetic code able to mimic the observed scaling (Chang *et al.* 2021)
- Whenever extended to future devices higher  $\lambda_q$  foreseen due to a change of the underlying physical mechanism with TEM in weakly collisional plasma as efficient transported of electron heat and mass
- Machine learning approach suggests a scaling compatible with the observed ITPA database as well as giving additional physical insight



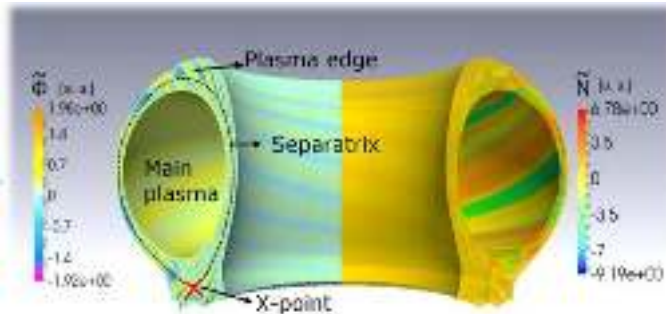
(Chang *et al.* 2021)

## Anomalous transport in the SOL



- In all the approach used so far we concentrate on parallel transport but SOL is a combination between **parallel, perpendicular and sources**.
- The perpendicular transport is strongly **anomalous** with source of free energy coming primarily from separatrix where strong gradient resides (as well as possible damping mechanism as  $\omega_{E \times B}$ ). SOL acts as well below the X-point

## Anomalous transport in the SOL



- In all the approach used so far we concentrate on parallel transport but SOL is a combination between **parallel, perpendicular and sources**.
- Various global code currently in development **Tokam3X, GBS, GRILLIX** as example, all including em effects as well as neutrals based on fluid approach. Extension to gyrofluid or gyrokinetic approach in progress

## Conclusions

- We clarify the importance of SOL and Divertor in view of Fusion exploitation
- Divertor and upstream conditions are tightly linked: density and upstream power set the conditions at the target as well as the regime. **True as well the opposite** (e.g. neutral pressure at the target set he  $n_{e,sep}$ )
- A global assessment need an experimental and modeling approach beyond the standard diffusive and 2D SOL approach.
- Remember that PEX is considered as a possible showstopper for fusion exploitation
- Remember this is clearly an incomplete review/lecture where we left apart many topics: PWI, Liquid Divertor, Proper atomic physics occurring at the target ...

## Bibliography i

1. Brunner, D. *et al.* **High-resolution heat flux width measurements at reactor-level magnetic fields and observation of a unified width scaling across confinement regimes in the Alcator C-Mod tokamak.** *Nuclear Fusion* **58**, 094002 (2018).
2. Chang, C. S. *et al.* **Constructing a new predictive scaling formula for ITER's divertor heat-load width informed by a simulation-anchored machine learning.** *Physics of Plasmas* **28**, 022501. ISSN: 1070-664X (2021).
3. Eich, T. *et al.* **Scaling of the tokamak near the scrape-off layer H-mode power width and implications for ITER.** *Nuclear Fusion* **53**, 093031 (2013).
4. Goldston, R. J. *et al.* **A new scaling for divertor detachment.** *Plasma Physics and Controlled Fusion* **59**, 055015 (2017).

5. Huber, A. *et al.* **Improved radiation measurements on JET – First results from an upgraded bolometer system.** *Journal of Nuclear Materials* **363**, 365 (2007).
6. Kallenbach, A. *et al.* **Partial detachment of high power discharges in ASDEX Upgrade.** *Nuclear Fusion* **55** (2015).
7. Kotschenreuther, M. *et al.* **The super X divertor (SXD) and a compact fusion neutron source (CFNS).** *Nuclear Fusion* **50**, 035003 (2010).
8. Maurizio, R. *et al.* **The effect of the secondary x-point on the scrape-off layer transport in the TCV snowflake minus divertor.** *Nuclear Fusion* **59**, 016014 (2018).
9. Petrie, T. W. *et al.* **Effect of changes in separatrix magnetic geometry on divertor behaviour in DIII-D.** *Nuclear Fusion* **53**, 113024 (2013).

10. Pitts, R. et al. **Physics basis for the first ITER tungsten divertor.** *Nuclear Materials and Energy*, 100696 (2019).
11. Pütterich, T. et al. **Determination of the tolerable impurity concentrations in a fusion reactor using a consistent set of cooling factors.** *Nuclear Fusion* **59**, 056013 (2019).
12. Reimerdes, H., Ambrosino, R., et al. **Assessment of alternative divertor configurations as an exhaust solution for DEMO.** *Nuclear Fusion* **60**, 066030 (2020).
13. Reimerdes, H., Duval, B. P., et al. **TCV experiments towards the development of a plasma exhaust solution.** *Nuclear Fusion* **57**, 126007 (2017).
14. Reinke, M. L. **Heat flux mitigation by impurity seeding in high-field tokamaks.** *Nuclear Fusion* **57**, 034004 (2017).

15. Ryutov, D. D. & Soukhanovskii, V. A. **The snowflake divertor.** *Physics of Plasmas (1994-present)* **22**, 110901 (2015).
16. Stangeby, P. C. **Basic physical processes and reduced models for plasma detachment.** *Plasma Physics and Controlled Fusion* **60**, 044022 (2018).
17. Stangeby, P. C. **The Plasma Boundary of Magnetic Fusion Devices.** ISBN: 9780750305594 (Taylor & Francis, 2000).
18. Stangeby, P. **The roles of power loss and momentum-pressure loss in causing particle-detachment in tokamak divertors: I. A heuristic model analysis.** *Plasma Physics and Controlled Fusion* **62**, 025012 (2020).
19. Stangeby, P. **The roles of power loss and momentum-pressure loss in causing particle-detachment in tokamak divertors: II. 2 Point Model analysis that includes recycle power-loss explicitly.** *Plasma Physics and Controlled Fusion* **62**, 025013 (2020).

20. Theiler, C. *et al.* **Results from recent detachment experiments in alternative divertor configurations on TCV.** *Nuclear Fusion* **57**, 072008 (2017).
21. Tsui, C. K. *et al.* **Parallel convection and  $E \times B$  drifts in the TCV snowflake divertor and their effects on target heat-fluxes.** *Nuclear Fusion* **61**, 046004 (2021).
22. Unterberg, B. **Overview of Plasma Edge Physics.** *Fusion Science and Technology* **49**, 215–233 (2017).

# Theory and Advanced Simulation

## The Reversed-Field Pinch case

## Helical Self-Organization processes

Susanna Cappello [susanna.cappello@igi.cnr.it](mailto:susanna.cappello@igi.cnr.it)

**Theory and Simulation physics group of Consorzio RFX**

*Consiglio Nazionale delle Ricerche – CNR – ISTP (Istitute for Plasma Science and Technology)  
CONSORZIO RFX*

*Associazione Euratom-ENEA sulla Fusione - PADOVA - ITALY  
partnership of CNR, ENEA, INFN, Padova University and Acciaierie Venete spa*



Preliminary considerations, a few slides:

RFP and RFX in Italy,  
Theory-Simulation EUROFusion context.

“Palazzo della Ragione”



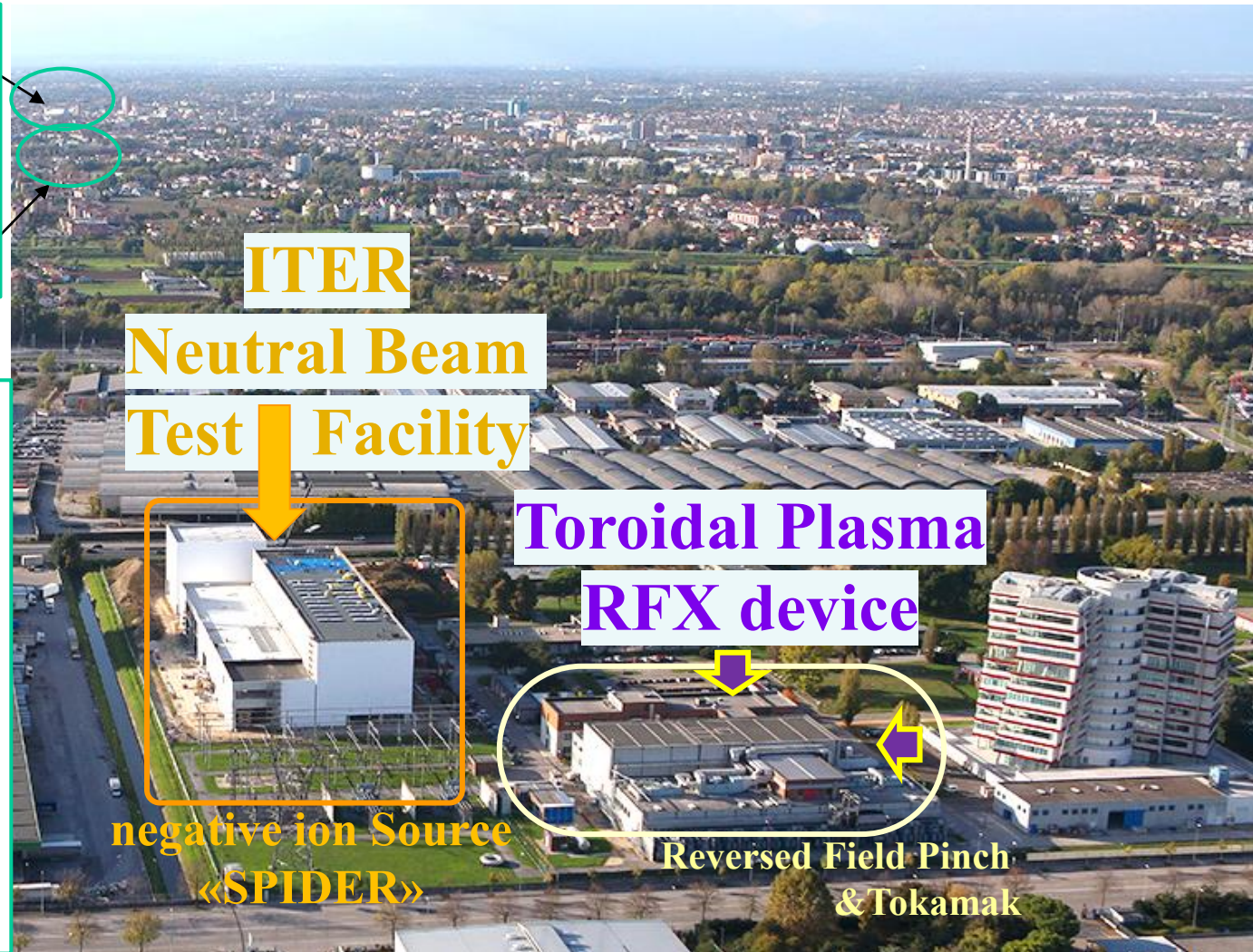
From the web

[https://en.wikipedia.org/wiki/Palazzo\\_della\\_Ragione,\\_Padua](https://en.wikipedia.org/wiki/Palazzo_della_Ragione,_Padua)

Padova University historical site



From the web



[https://en.wikipedia.org/wiki/University\\_of\\_Padua](https://en.wikipedia.org/wiki/University_of_Padua)

Reversed Field Pinch, RFP, partners:  
USA - Sweden - Japan – China

*High priorities infrastructures in Italy (for Fusion): DTT (ENEA) and RFX (CNR)*

NRRP (National Recovery and Resilience Plan):

project “**NEFERTARI**” based upon the **RFX** Research\_Infrastructure

Project title: ‘**NEFERTARI**’

(**New Equipment for Fusion Experimental Research & Technological Advancements with Rfx Infrastructure**)

Project aim: innovation of **experimental equipment** and **diagnostic systems** for RFX-mod2

Duration: 30 months (**2022 – 2025**) *with a perspective scientific exploitation for the next 10 years*

**EUROfusion** welcomes alternative approaches and intellectual diversity

*The Reversed Field Pinch research is an example*

*The Reversed Field Pinch research is an example*

## EUROPEAN RESEARCH ROADMAP

[https://euro-fusion.org/wp-content/uploads/2022/10/2018\\_Research\\_roadmap\\_long\\_version\\_01.pdf](https://euro-fusion.org/wp-content/uploads/2022/10/2018_Research_roadmap_long_version_01.pdf)

(2018 revision, FP9: 2021-27,  
after first release in 2013, FP8: 2014-20)

Preface by T. Donnè & W. Morris - page 3:

“ The strategy of the fusion roadmap is built on three main pillars:

- the international ITER tokamak
- a fusion neutron source facility for materials development and qualification
- demonstration power plant DEMO

In addition, a strong **research and innovation programme is needed** supporting these and looking towards commercial fusion power plants.

Parallel research and innovation programmes ... include **alternative approaches**, notably the stellarator.

In pursuing this goal, Europe should seek all the opportunities for international collaborations for mutual benefit from the **intellectual diversity** of the whole fusion community and from the sharing of resources and facilities.”

# Magnetic Configurations for fusion energy

The RFP magnetic configuration is produced mainly by plasma current itself  
In principle, no additional heating system appears necessary

## Stellarator

## Tokamak

## RFP

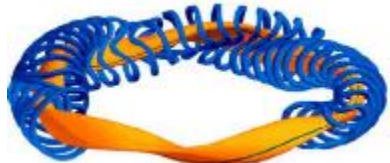
*Increasing plasma current*



Steady state



Coils Complexity

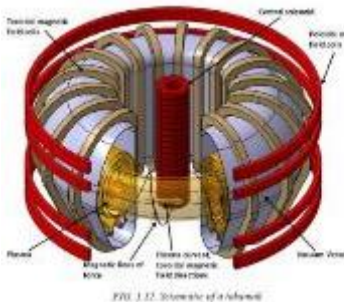


[\*]

FIG. 1.14. Schematic of stellarator magnetic field coils and plasma configuration (Ref. [1.65]).

**$R = 5.5 \text{ m }$  W7-X**

( $R = 3.9 \text{ m }$  LHD)



**$R = 1.65 \text{ m }$  AUG**  
 **$R = 3 \text{ m }$  JET**  
**( $R = 6.21 \text{ m }$  ITER)**

Light Tech expected

Confinement

## RFP

Global Helical self-organization



**$R = 2.0 \text{ m }$  RFX**

(1.5 m MST USA  
1.4 m KTX Hefei China)

<https://doi.org/10.1088/1741-4326/abc06c>

[\*] Fusion Physics IAEA 2012

[\*\*] Marrelli et al 2021 Nuclear Fusion

Magnetic configurations for fusion energy despite the differences  
display several **common physics issues**

Transition low–high confinement regimes

Transport barrier formation

Magnetic relaxation

RFP dynamo/Flux pumping effect

Density limit

Isotopic effect

“Anomalous” ion heating (like in Solar Corona?)

...

proficuous **challenge** for theories, models, understanding !

theories, models, understanding ... in EUROfusion

EUROfusion E-TASC groups **TSVV & ACH** aim at “validated predictive capability”

## Eurofusion Theory and Advanced Simulation Coordination effort (E-TASC):

<https://iopscience.iop.org/article/10.1088/1361-6587/ac44e4>

X. Litaudon et al PPCF (2022)

“ Therefore, it is timely to prepare this transition with a **coordinated, comprehensive: Theory, Simulation, Verification and Validation programme**

**TSVV**

to maximize the benefit delivered from investment in large facilities.

This aspect is recognized in the revised version of the Research Roadmap for the Realisation of Fusion Energy (Donné et al 2017, European Research Roadmap to the Realisation of Fusion Energy 2018) which states

'For all the missions, a **theory and modelling effort integrated tightly with the experimental programme will be crucial in providing the capability of extrapolating the available results to ITER, DEMO and commercial fusion power plants through carefully validated models and codes**'. An empirical approach will not be sufficient to bridge the gap between an experimental facility like ITER and a demonstration facility-like DEMO as stated in the EUROfusion 25 Research Roadmap ‘

It has become clear that a strong theory and modelling programme is essential because empirically-based predictions are uncertain in unexplored environments like ITER and particularly DEMO, and this will be a stronger focus than foreseen earlier.

It will make use of **Advanced Computational techniques and High performance computers.** ’ ”

**AC-Hubs**

## EUROfusion E-TASC groups: TSVV & ACH



TSVV

Develop state-of-the-art codes for the WPs to also be used for ITER and DEMO

ACH

Support the TSVVs in code development

**TSVV:**

*Theory, Simulation, Verification and Validation*

**ACH:**

*Advanced Computing Hubs*

E-TASC KOM: Introduction | April 23, 2021

[https://indico.euro-fusion.org/category/279/attachments/1700/3352/ETASC-KOM-Intro\\_Naulin\\_Jenko.pdf](https://indico.euro-fusion.org/category/279/attachments/1700/3352/ETASC-KOM-Intro_Naulin_Jenko.pdf)

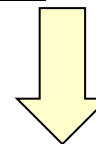
On a smaller scale, RFP research is a *proficuous* place for training and practicing *TSVV*:

## *“Theory, Simulation, Verification & Validation”*

Verification and validation are defined in the DOE Defense Programs (DOE/DP) program plan for the Strategic Computing & Simulation Validation & Verification Program [1] as:

**Verification** – The process of determining that a computer simulation correctly represents the conceptual model and its solution.

**Validation** – The process of determining the degree to which a computer simulation is an accurate representation of the real world.



Am I solving the model correctly?

Am I solving the proper model?

... Benchmarking against  
- analytical solutions  
- different codes

... Tight connection and comparison with experiments

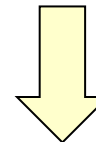
On a smaller scale, RFP research is a *proficuous* place for training and practicing:

## *“Theory, Simulation, Verification & Validation”*

Verification and validation are defined in the DOE Defense Programs (DOE/DP) program plan for the Strategic Computing & Simulation Validation & Verification Program [1] as:

**Verification** – The process of determining that a computer simulation correctly represents the conceptual model and its solution.

**Validation** – The process of determining the degree to which a computer simulation is an accurate representation of the real world.



Am I solving the model correctly?

Am I solving the proper model?

... Benchmarking against  
- analytical solutions  
- different codes

... Tight connection and comparison with experiments

‘Newcomers’,

## Uncertainty Quantification (UQ) Sensitivity Analysis (SA)

<https://pmc.ncbi.nlm.nih.gov/articles/PMC9232142/>

While scientific computing has undergone extraordinary increases in sophistication, a fundamental disconnect exists between simulations and practical applications. While most simulations are deterministic, engineering applications have many sources of uncertainty arising from a number of sources such as subject variability, initial conditions or system surroundings.

<https://pmc.ncbi.nlm.nih.gov/articles/PMC7304739/>

<https://www.sciencedirect.com/science/article/pii/S0017931022003957>

VVUQ...

# Some links/references (for those who are interested)

2021

[https://indico.euro-fusion.org/category/279/attachments/1700/3352/ETASC-KOM-Intro\\_Naulin\\_Jenko.pdf](https://indico.euro-fusion.org/category/279/attachments/1700/3352/ETASC-KOM-Intro_Naulin_Jenko.pdf)

2024

[https://finnfusion.fi/app/uploads/2024/06/mantsinen\\_c.pdf](https://finnfusion.fi/app/uploads/2024/06/mantsinen_c.pdf)

**Advanced Computing Hubs within EUROfusion E-TASC programme**

Mervi Mantsinen

ICREA and Barcelona Supercomputing Center (BSC)

FinnFusion Annual Seminar, Helsinki, Finland, 27-28 May 2024

- (2016) [https://geodynamics.org/resources/301/download/Oberkampf\\_Webinar\\_CIG-2016.pdf](https://geodynamics.org/resources/301/download/Oberkampf_Webinar_CIG-2016.pdf)

Dr. William L. Oberkampf Sandia National Laboratories (retired)

Verification, Validation, and Predictive Capability: 2021 What's What?

- (2010) M. Greenwald *Verification and validation for magnetic fusion* Phys. Plasmas 17, 058101;  
<https://doi.org/10.1063/1.3298884>

- (2008) P. W. Terry, M. Greenwald, J.-N. Leboeuf, G. R. McKee, D. R. Mikkelsen, W. M. Nevins, D. E. Newman, and D. P. Stotler, *Validation in fusion research: Towards guidelines and best practices* Physics of Plasmas 15, 062503  
<https://doi.org/10.1063/1.2928909>

- (1998). AIAA. "Guide for the Verification and Validation of Computational Fluid Dynamics Simulations." American Institute of Aeronautics and Astronautics, AIAA-G-077-1998 <https://arc.aiaa.org/doi/book/10.2514/4.472855>

# Preliminary considerations summary:

- Consorzio RFX site
- RFX high priority national infrastructure (NEFERTARI project)
- EUROFUSION welcomes:
  - alternative approaches – parallel research – intellectual diversity
- DIFFERENT configurations for Magnetic Confinement Fusion: Stellarator Tokamak RFP
- COMMON PHYSICS issues: challenging for theories models understanding
- Theory, Advanced Simulation, Verification & Validation and EUROFUSION: E-TASC
- RFX-RFP research:
  - Proficuous place for training and practicing Theory, Simulation, V & V ...UQ**

# Theory and Advanced Simulation

## The Reversed-Field Pinch *case*

### Helical Self-Organization processes

tightly integrated to past and future experimental programme:

- RFX / RFX-mod /
- RFX-mod2 device

(1992 – 1999)

RFX

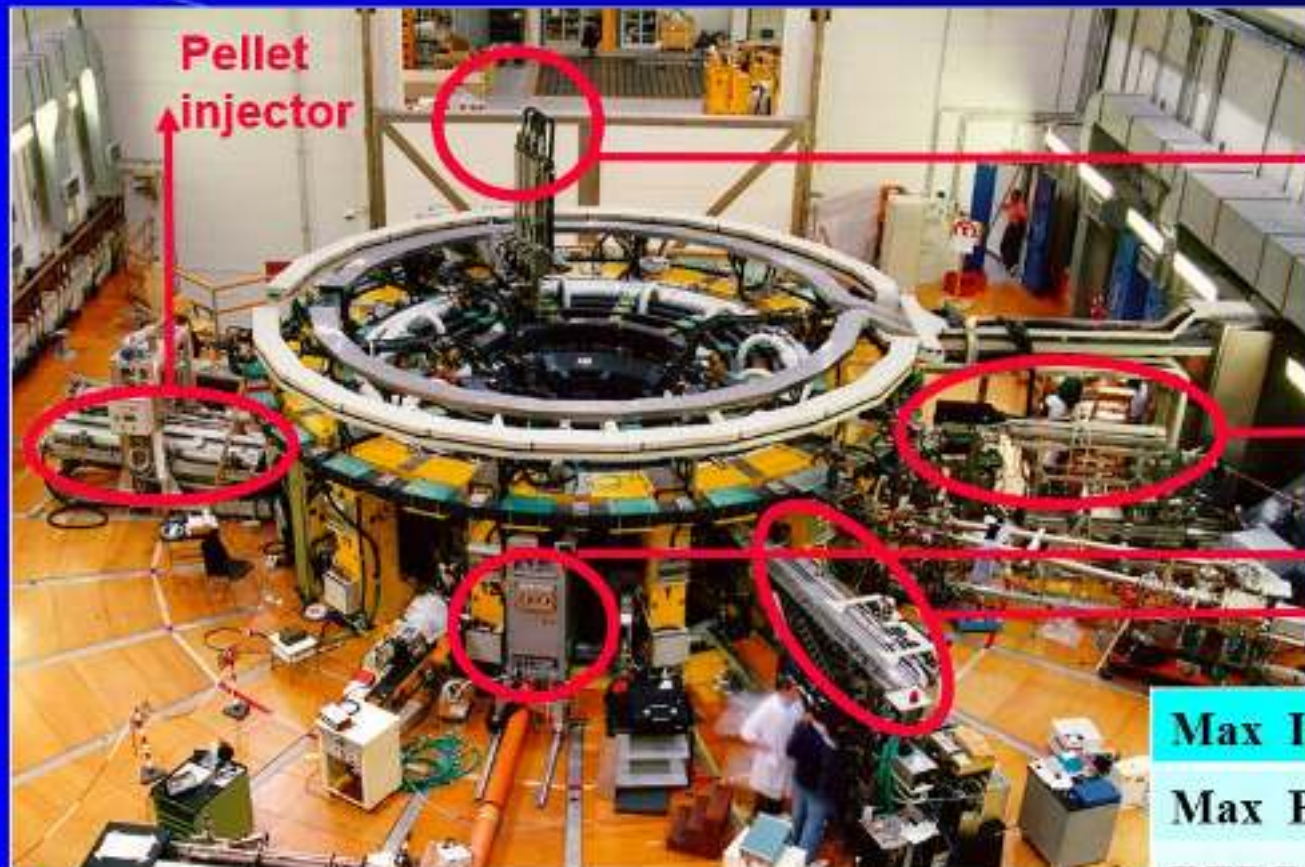
(2004 – 2015)

RFX-mod

(2026 ...)

RFX-mod2

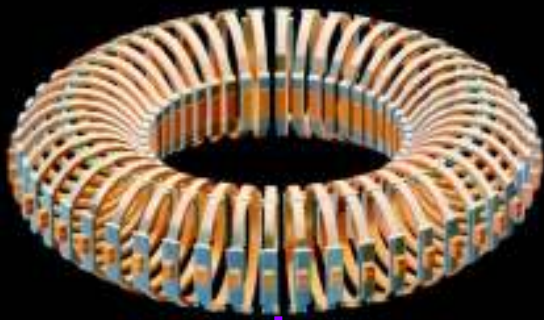
(MIAIVO project  
PNRR NEFERTARI project)



Max Ip	2 MA
Max Bz	0.7 T
RFP Pulse duration	0.6 s
Tokamak Pulse	1 s

**Pinch device** - plasma self-squeezes due to plasma current  $I$

## RFX device coils



toroidal magnetic field



poloidal magnetic field

Schematic RFP

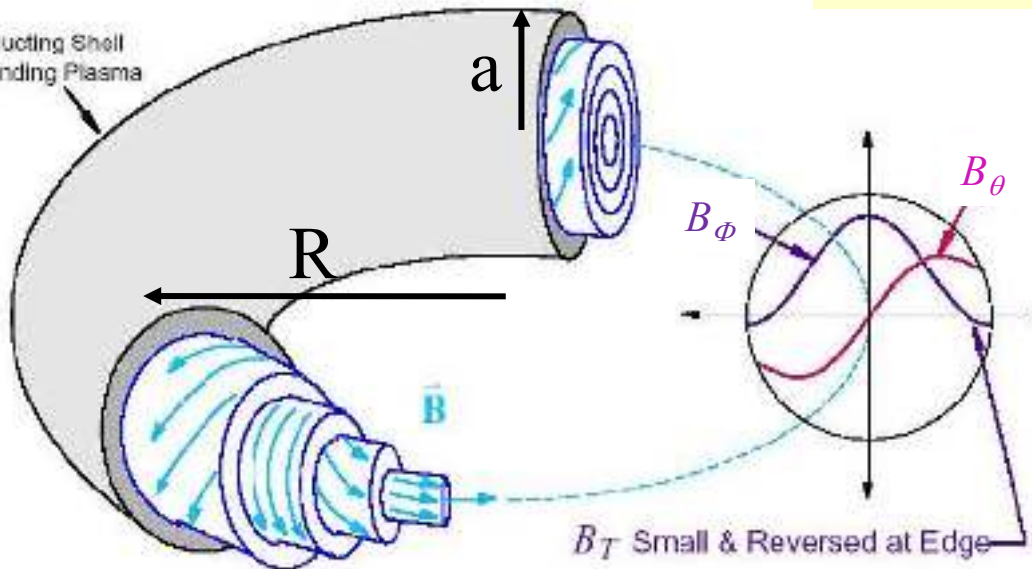
**RFX**

$R = 2.0\text{m}$

$a = 0.5\text{m}$

MST

Conducting Shell  
Surrounding Plasma



induction of  
plasma current

mean  
magnetic field  
radial profiles

# Schematic B(r)

axisymmetric components

## Tokamak and RFP

given  $B_\phi(r=0)$  and plasma radius “a”

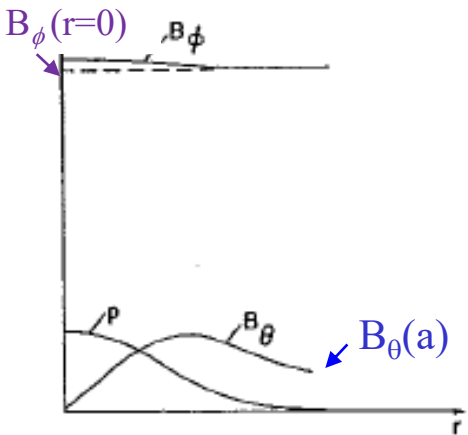


Figure 6.10. Typical radial profiles for an ohmically heated tokamak.

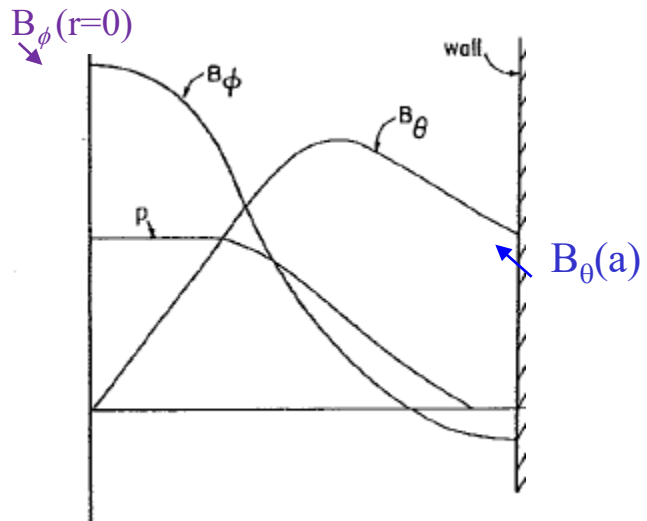
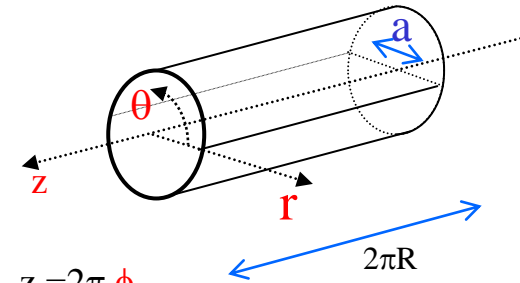


Figure 6.5. Schematic diagram of the  $B_\phi$ ,  $B_\theta$ , and  $p$  profiles providing radial pressure balance in an RFP.

Periodic cylinder:  
common approximation of the torus.

Usual coordinates:



Poloidal angle  $\theta$   
and  
 $z$  toroidal like, or  $\phi$

# Schematic B(r)

axisymmetric components

## Tokamak and RFP

given  $B_\phi(r=0)$  and plasma radius “a”

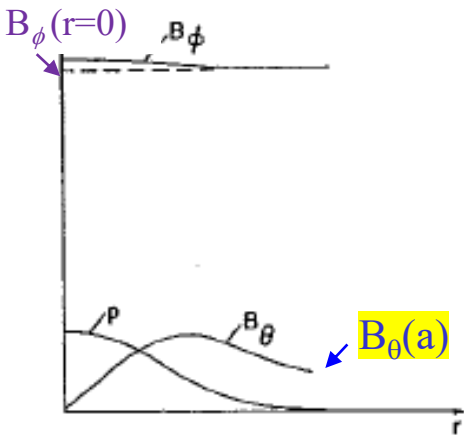


Figure 6.10. Typical radial profiles for an ohmically heated tokamak.

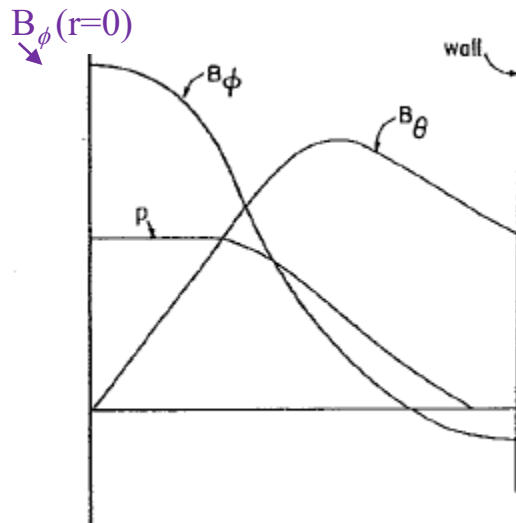


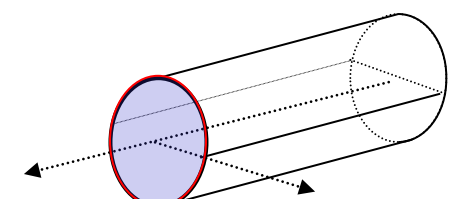
Figure 6.5. Schematic diagram of the  $B_\phi$ ,  $B_\theta$ , and  $p$  profiles providing radial pressure balance in an RFP.

RFP much larger plasma current I

$$\nabla \times \mathbf{B} = \mu_0 \mathbf{J}$$

$$aB_0(a) \sim I_p$$

$$\int_S dS \cdot \nabla \times \mathbf{A} = \oint_C dl \cdot \mathbf{A}$$



Reversal, F, and Pinch, Θ, parameters:

$$F \equiv \frac{\mathbf{B}_z(a)}{\langle \mathbf{B}_z \rangle} \quad \Theta \equiv \frac{\mathbf{B}_\phi(a)}{\langle \mathbf{B}_z \rangle} \sim \frac{I_p}{\Phi}$$

$$\text{Safety factor: } q(r) = \frac{d\Phi}{d\psi} \sim \frac{r B_z(r)}{R B_\theta(r)}$$

F has a similar relevance as  
q(a) in Tokamak “vocabulary”

Let's enter a little bit more into the RFP world

Right from its origin ('50), the RFP placed puzzling issues.

The configuration was discovered in early pinches when pushing plasma current to high enough values

1.  $B_z$  self-reversal was **unexpected**,  
... associated quiescent regime: **unexpected**
2. Call for an «*RFP dynamo*»

# 1. Quiescent regimes associated with $B_Z$ field reversal

Historical observations ('50ties several toroidal pinches) ZETA machine (UK):  
Pushing plasma current above “threshold” → toroidal  $B_Z$  self-reversal

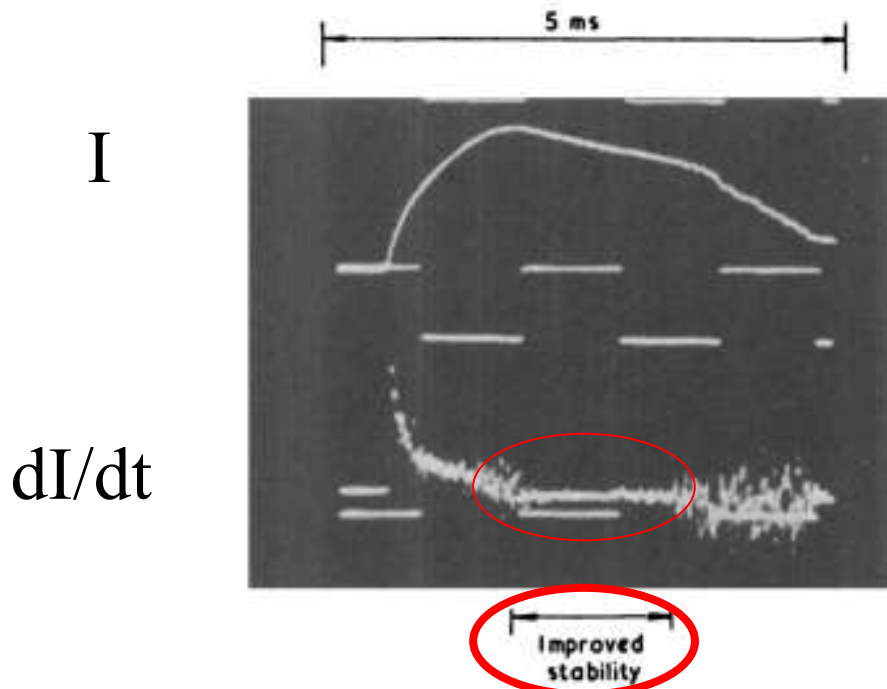


FIG.2. Oscilloscope record of ZETA discharge lasting 5 ms.  
Top trace is gas current  $I$ , reaching a maximum here of 420 kA,  
while lower trace is rate-of-change of current  $dI/dt$  and exhibits  
period of quiescence subsequently associated with magnetic-  
field reversal.

# 1. Quiescent regimes associated with $B_Z$ field reversal

*A few lines about Taylor's relaxation theory for the RFP.  
It was inspired by astrophysical dynamo theories*

# 1. Quiescent regimes associated with $B_Z$ field reversal

*A few lines about Taylor's relaxation theory for the RFP.  
It was inspired by astrophysical dynamo theories*

Taylor's relaxation theory for the RFP [\*]

boosted the RFP research due to its ability to provide a first understanding...

Taylor's conjecture can be considered a “weak formulation” of Woltjer theorem (1958) proposed to describe astrophysical magnetic fields of celestial bodies:  
***astrophysical dynamo***... in particular ***turbulent dynamo***

It considers a variational principle:

- search for the minimum of magnetic energy,
- compatible with a given conserved topological complexity (magnetic helicity).

(The topological complexity is an ideal invariant, due to the frozen-in law of magnetic field in perfectly conducting fluids... Alfvén theorem).

[\*]

*J. B. Taylor PRL 1974*

*J. B. Taylor Rev. Mod Phys. 1986*

# 1. Quiescent regimes associated with $B_Z$ field reversal

By solving the variational problem casted by Taylor's relaxation theory one finds "relaxed states" with **field reversal** for  $\Theta \geq 1.2$

The theory gained a great success, providing a first way to understand the experimental observations

... despite quantitative differences, significant in the external region around reversal...



Bessel analytical solutions

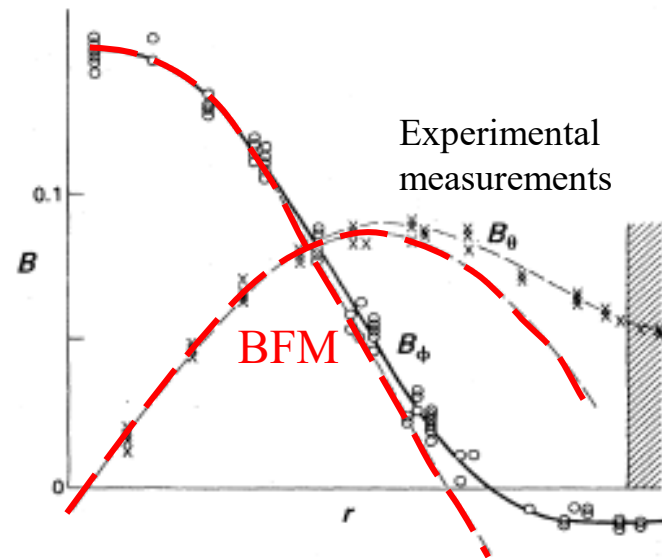


FIG. 2. Experimental and theoretical magnetic field profiles. HBTX-1A (from Bodin, 1984).

## Bessel Function Model (BFM)

Rev. Mod. Phys., Vol. 56, No. 3, July 1986

[\*]

J. B. Taylor PRL 1974

J. B. Taylor Rev. Mod Phys. 1986

For those interested in the Taylor Relaxation Theory: come to my office.  
I can suggest some material.

2. “RFP dynamo effect ” needed ... let's recall **the equations for conducting fluid:**

Ohm's law

$$\mathbf{E} + \mathbf{V} \wedge \mathbf{B} = \eta \mathbf{J}$$

(simple form for conducting fluid)

Induction equation

$$\frac{\partial \mathbf{B}}{\partial t} = -\nabla \wedge \mathbf{E}$$

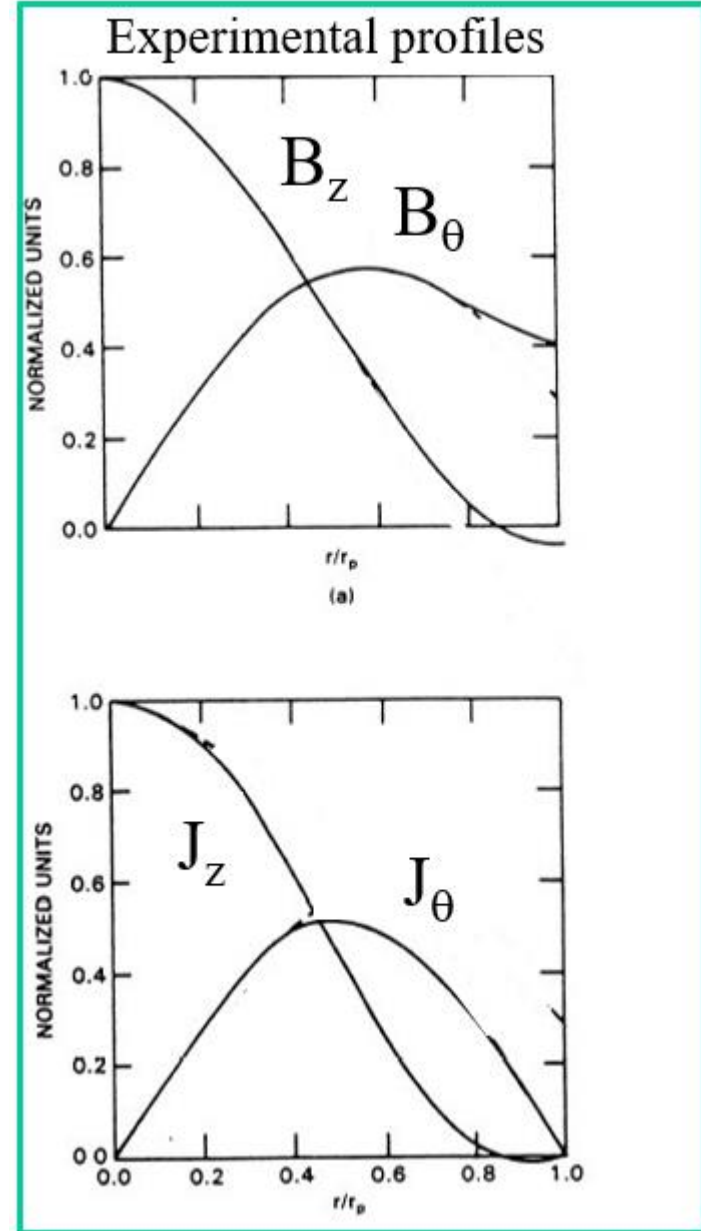
2. “RFP dynamo effect ” needed ... let's recall [the typical B and J profiles](#):

Ohm's law

$$\mathbf{E} + \mathbf{V} \wedge \mathbf{B} = \eta \mathbf{J}$$

Induction equation

$$\frac{\partial \mathbf{B}}{\partial t} = -\nabla \wedge \mathbf{E}$$



## 2. “RFP dynamo effect ” needed ... let's recall the typical B and J profiles:

Ohm's law

$$\mathbf{E} + \mathbf{V} \wedge \mathbf{B} = \eta \mathbf{J}$$

Induction equation

$$\frac{\partial \mathbf{B}}{\partial t} = -\nabla \wedge \mathbf{E}$$

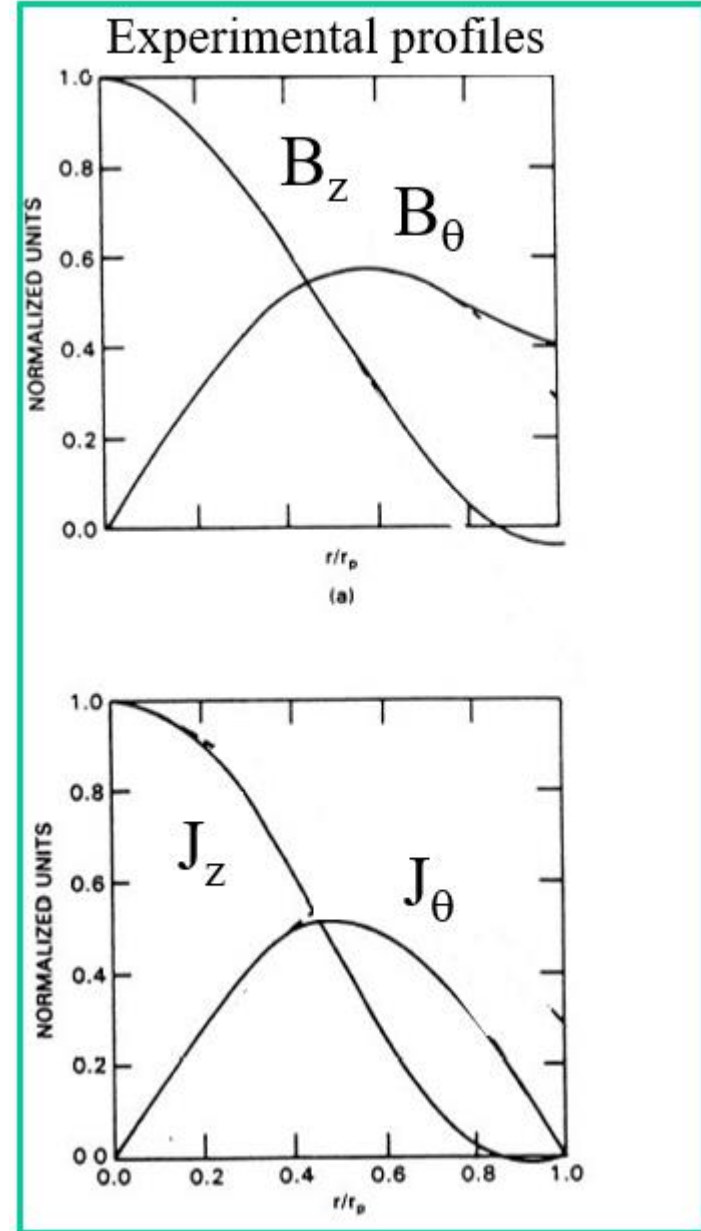
Consider stationary fields

stationarity  $\frac{\partial}{\partial t} = 0 \rightarrow$

$$E_\theta(r) \equiv 0$$

$$E_Z(r) \equiv E_o$$

*(Applied Voltage)*



## 2. “RFP dynamo effect” needed

!! Inconsistency

Project along poloidal coordinate

→ Ohm's law

$$\mathbf{E} + \mathbf{V} \wedge \mathbf{B} = \eta \mathbf{J}$$

at reversal  $B_z=0$

$$E_\theta(r) = \eta J_\theta + Vr B_z$$

→ Induction equation

$$J_\vartheta(r) = 0 !$$

!

$$\frac{\partial \mathbf{B}}{\partial t} = -\nabla \wedge \mathbf{E}$$

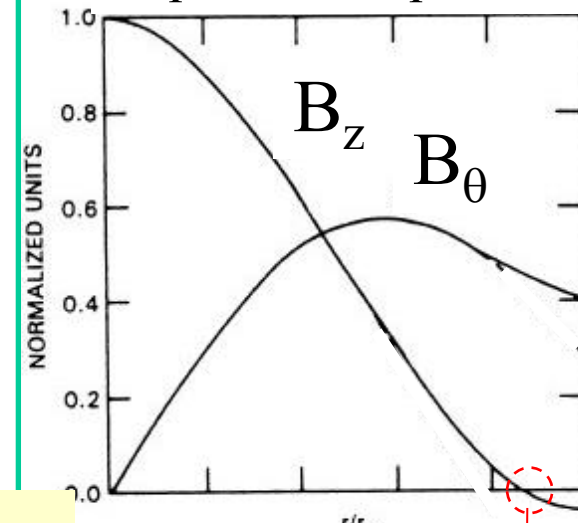
stationarity  $\frac{\partial}{\partial t} = 0 \rightarrow$

$$E_\theta(r) \equiv 0$$

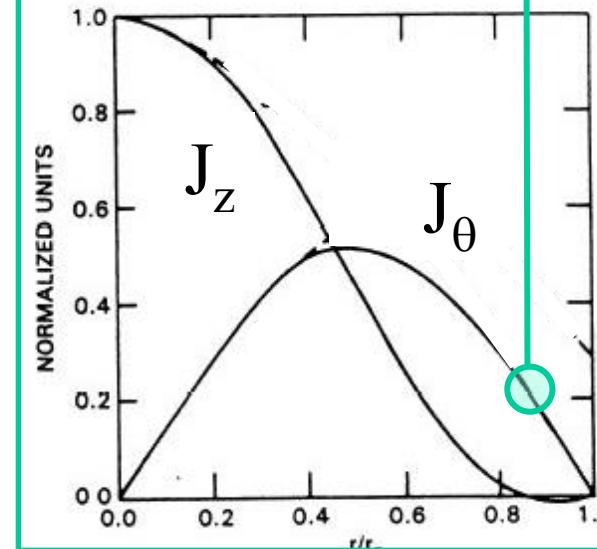
$$E_Z(r) \equiv E_o$$

(Applied Voltage)

Experimental profiles



$$J_\vartheta(r) \neq 0$$



## 2. “RFP dynamo effect” needed

an additional “**dynamo**” electric field is needed with respect to the one provided by axisymmetric  $B$  and  $v$  fields in order to balance Ohm’s law if a finite  $J_\theta$  is present at reversal radius:

within resistive MHD such a contribution comes through a  
coherent modulations  $V^1, B^1$  on top of the axisymmetric components  $V, B$

$$E_\theta(r) = \eta J_\theta + Vr B_z \langle V^1 \wedge B^1 \rangle_\theta$$

$E_{\text{dynamo}}$

*Thus, inspired by astrophysical studies, and supported by Taylor Relaxation Theory, a small scale turbulence has been deemed as necessary to get RFP dynamo effect ...*

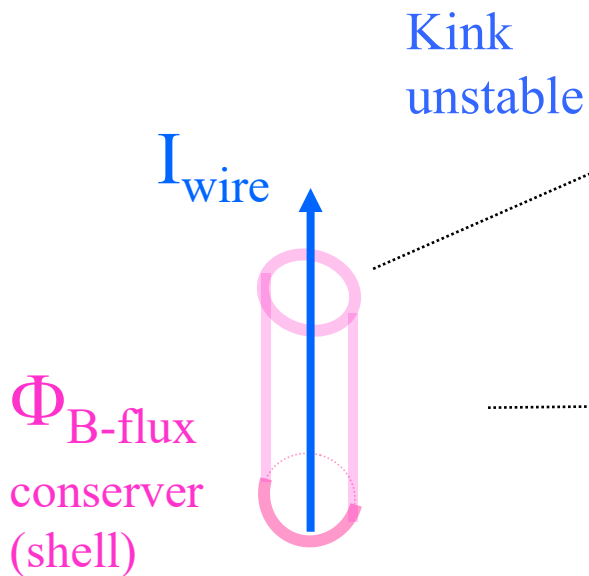
*We shall see that a laminar –steady- macroscopic helical dynamo can also be a solution of **3D nonlinear MHD** simulations for cylindrical RFP.*

## Toy model

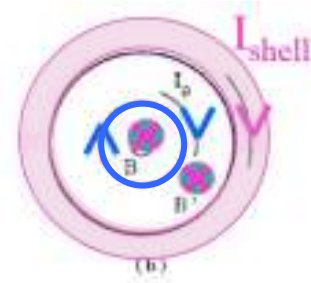
The toy model:  
intuitive and simplified understanding of self-reversal  
(schematic and intuitive RFP)  
... and of the global helical self-organization

# Toy model (1): a kink deformation of the current “path” pumps toroidal B-flux

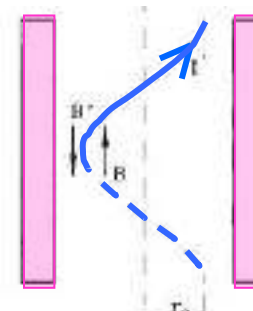
Think of a **current carrying wire** in a **flux conserver**:



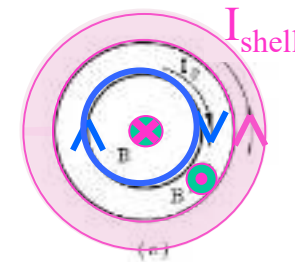
$\Phi_{\text{B-flux}}$   
conserver  
(shell)



$I_{\text{wire}} & I_{\text{shell}}$  attract each other



solenoidal effect  
by the wire itself:  
- core B increase



by flux conservation:  
- edge B decreases ..

Kink saturates when/if  
reversal of edge field  
is achieved

Elaborated in:

Benisti Escande EFTC 1998

Escande et al. PPCF 2000

See also Cappello et al Varenna 2008

$r_0 \rightarrow 1$  (disruption) for too small  $\frac{I_{\text{wire}}}{\Phi}$   
(Tokamak case)

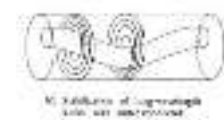
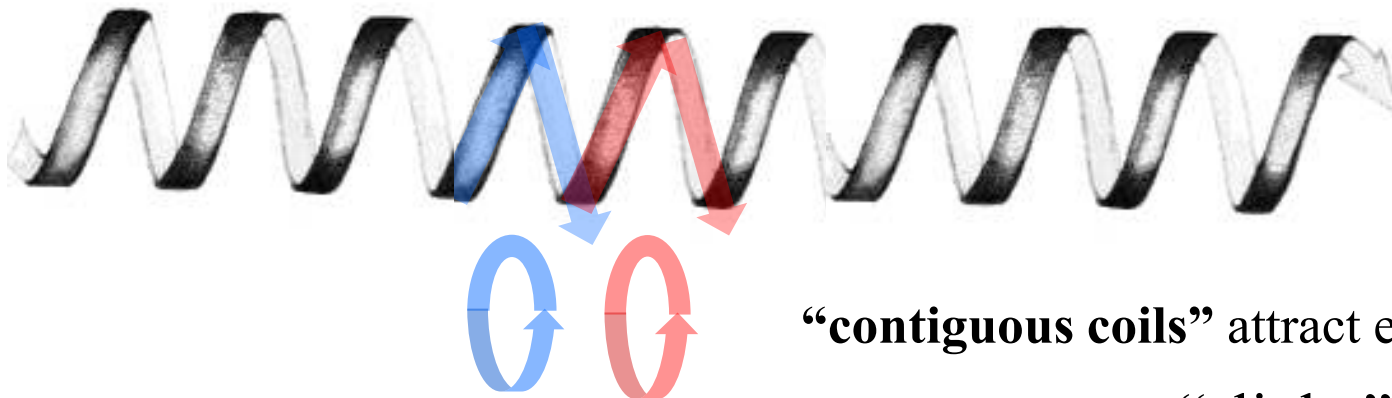
Early elements:

Verhage-Furzer-Robinson NF 1978

Kadomtsev 1992 (Sawer PoF 1959)

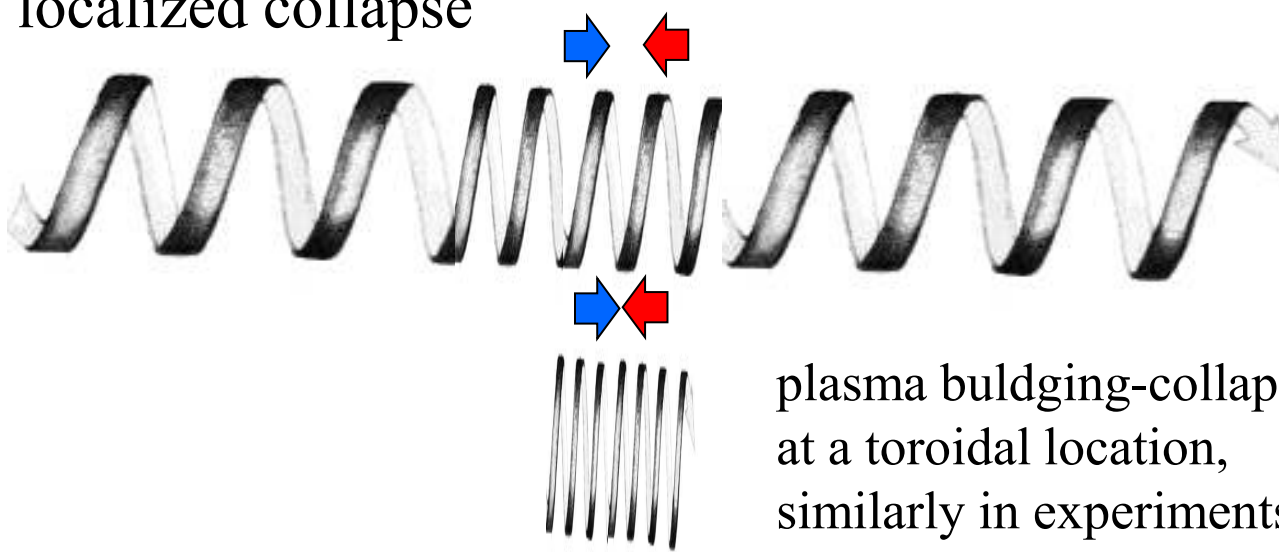
## Toy model (2): the kink deformation is subject to a secondary instability

After kinking ...

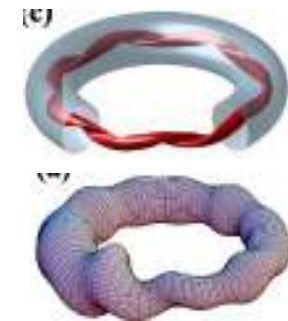


“contiguous coils” attract each other ...  
... “slinky” instability

... localized collapse



plasma bulging-collapse  
at a toroidal location,  
similarly in experiments  
and nonlinear modeling...



# Summary of first steps in RFP theory, modeling and understanding :

- ZETA experiment puzzling: quiescent regime & reversal of magnetic field ('60)
- Taylor relaxation theory ('70):
  - analytical «relaxed» solutions with  $B_z$  reversal
  - need for additional dynamo Electric field (small scale turbulence deemed necessary)
- Toy model schematic intuitive description of reversal effect (flux pumping by global kink)

# Modern era - Helical self-organization processes

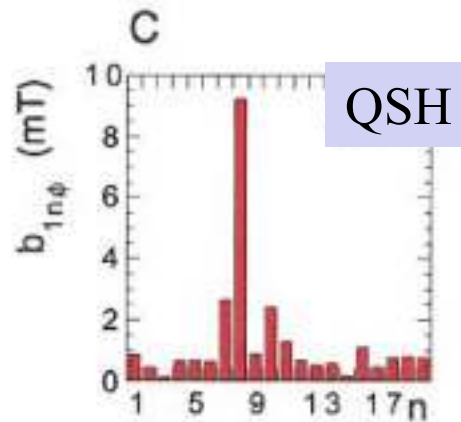
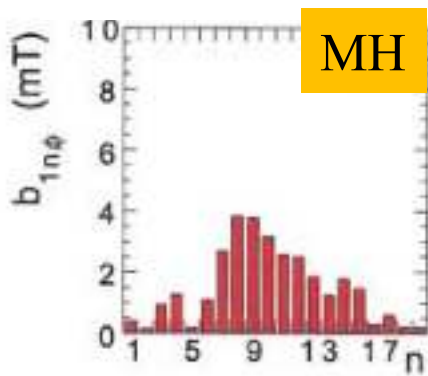
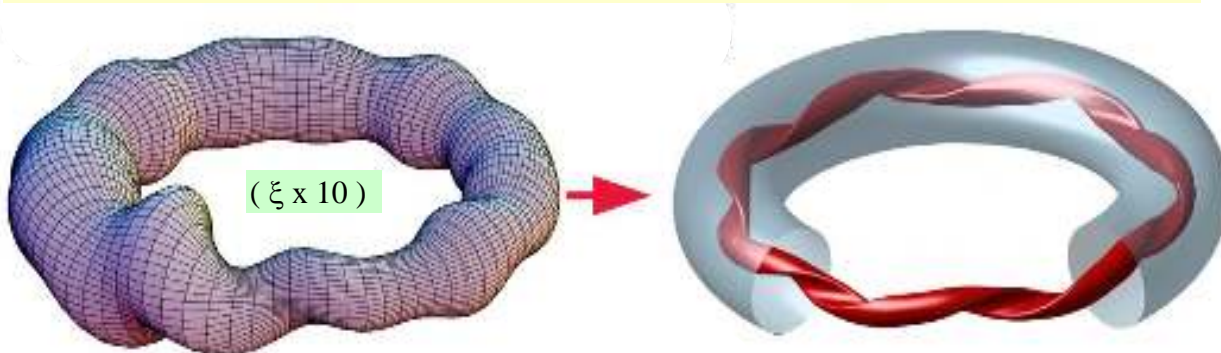
- Overview of RFX observations
- Description from **nonlinear MHD model:**  
**3D Numerical Simulation**

# RFP self-organization in brief

RFX

RFP  $\leftrightarrow$  saturated KINKED plasma

for  $I_p$  above  $\sim 1$  MA



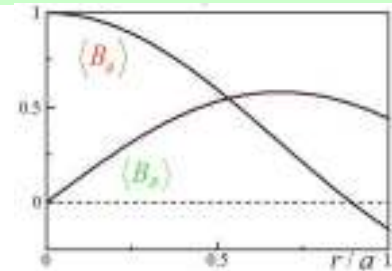
MHD spectrum: resistive kink-tearing modes

Advanced operation required in RFX-mod

CLEAN MODE CONTROL  
and/or  
NON-CONVENTIONAL SCENARIOS (PPCD-OPCD)



Feedback coils system  
Typical operation:  
 $I_p \sim 1.7$  MA  
 $T_e$  up to 1.2 keV

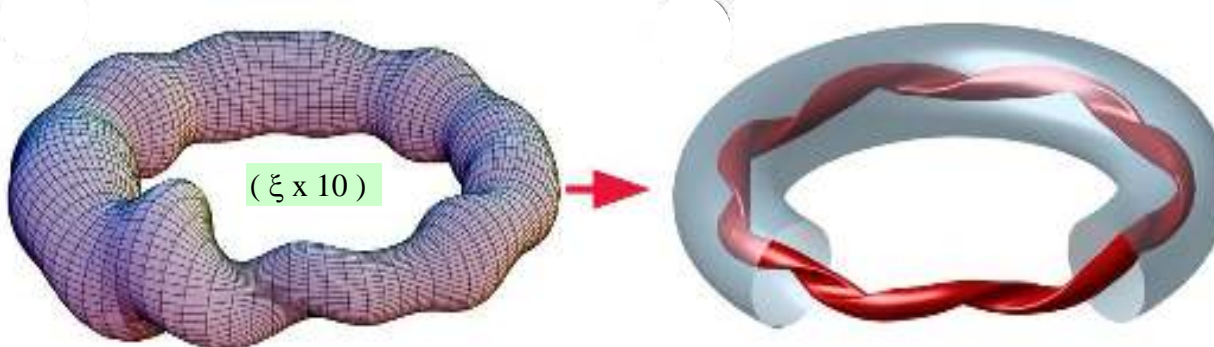


# RFP self-organization in brief

RFX

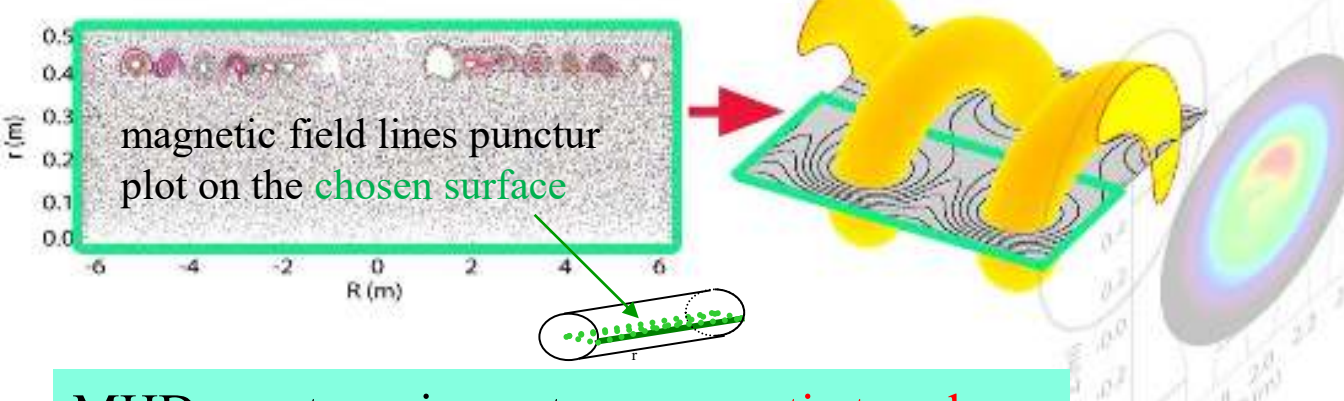
RFP  $\leftrightarrow$  saturated KINKED plasma

for  $I_p$  above  $\sim 1$  MA



MH

SH



MHD spectrum impact on magnetic topology  
Believed to rule transport properties in RFP

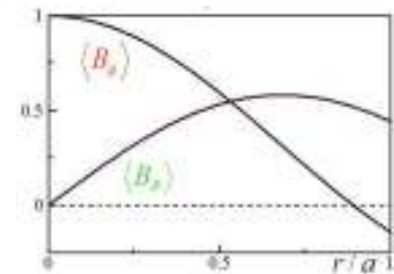
Advanced operation required in RFX-mod

CLEAN MODE CONTROL  
and/or  
NON-CONVENTIONAL SCENARIOS (PPCD-OPCD)

RFX-mod



Feedback coils system  
Typical operation:  
 $I_p \sim 1.7$  MA  
 $T_e$  up to 1.2 keV



# RFP helical self-organization – Experimental overview

- **First observations: one single MHD mode emerging**
- **Statistical robustness of the helical self-organization**
- **Electron Temperature (and density) Internal Transport barrier – eITB**
  - Relation with safety factor profile
  - Temporal behavior
- Impurity screening effect
- Isotopic effect: better performances when running Deuterium discharges

# RFP helical self-organization: several experiments RFX – TPE – MST – T2R



FIG. 3 (color). Schematic view of a  $n = 7$  helical structure inside the RFX vessel.

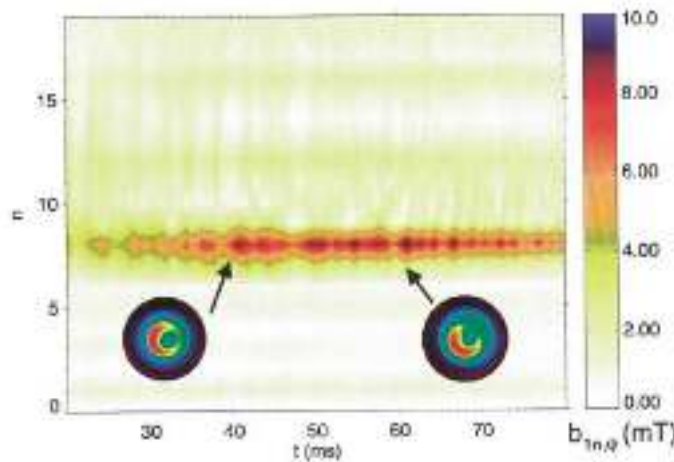
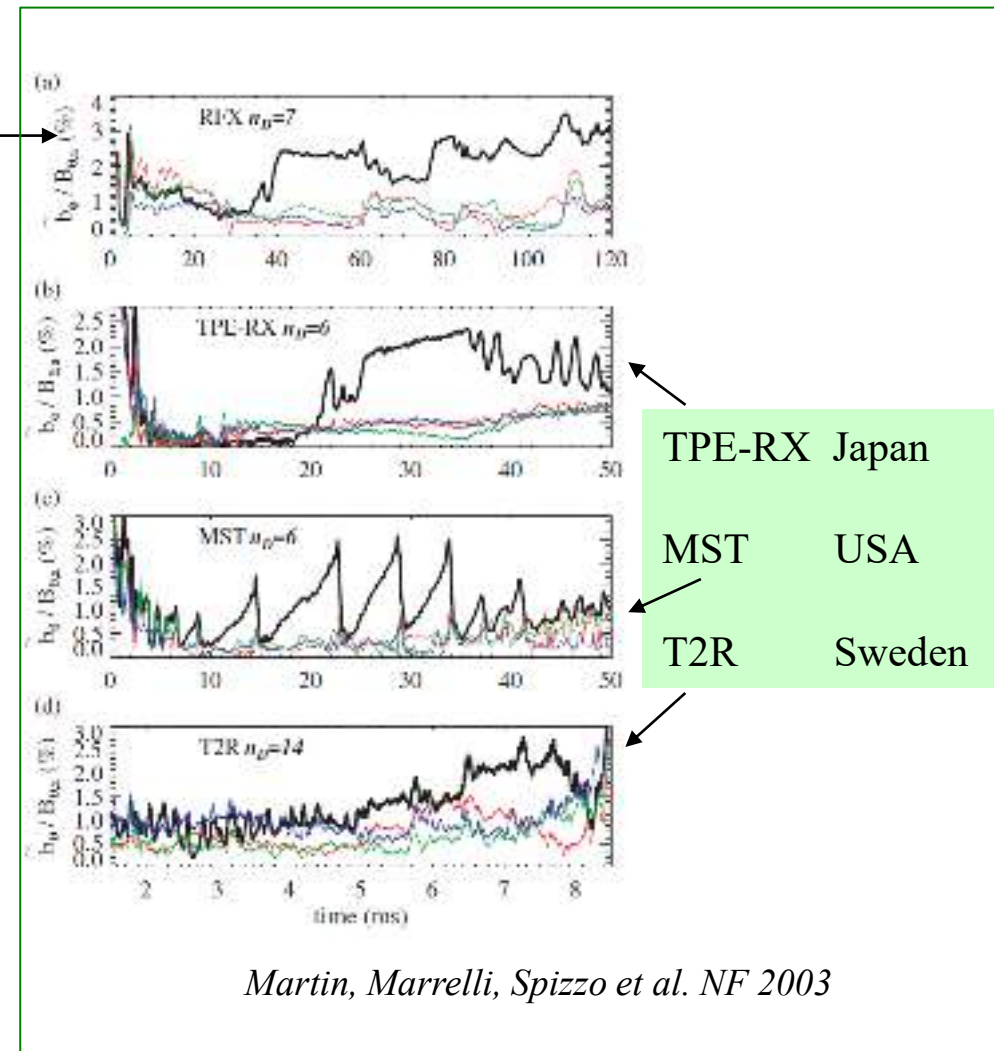


FIG. 5 (color).  $m = 1$  modes  $n$ -spectrum vs time and SXR emissivity patterns at selected times ( $t = 40$  ms and  $t = 60$  ms) in a plasma (No. 11336) where the QSH state is permanent. The dominant mode in this case is  $n = 8$ .

Escande, Martin, Ortolani et al. PRL 2000

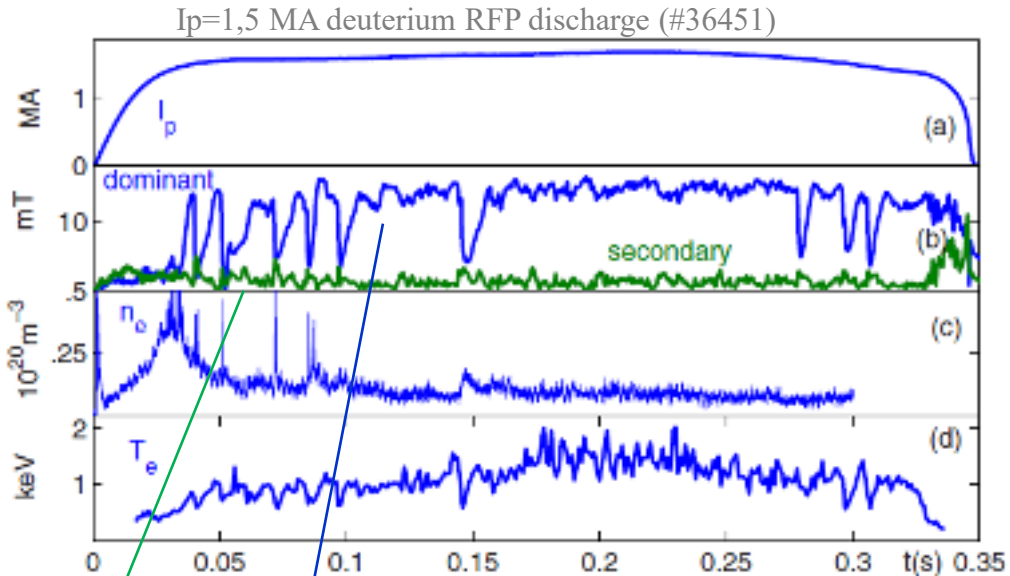


More recently also:  
RELAX (Japan), KTX (Hefei- China)

# RFP helical self-organization: a robust process

RFX -mod

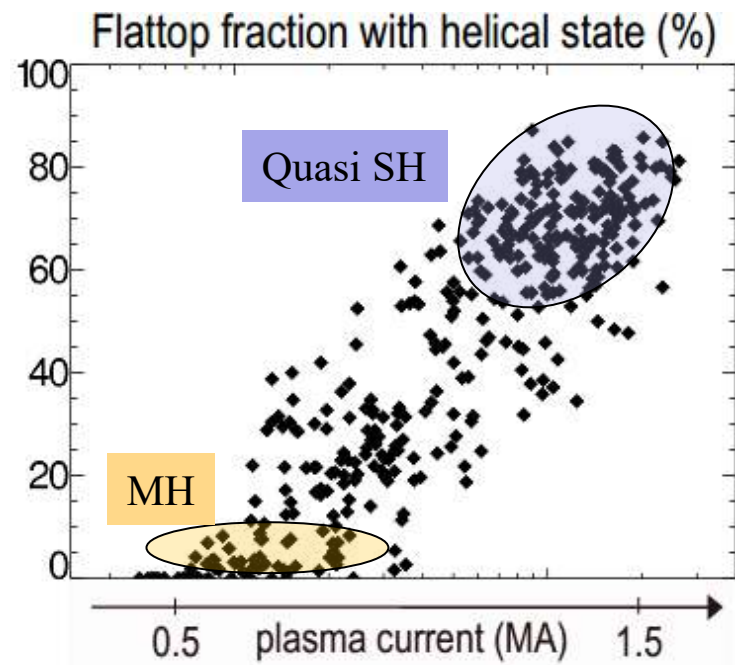
HELICAL persistency increases with current - up to > 85% of flat top



Dominant mode (internal)

ave secondary modes

Puiatti, Dal Bello, Marrelli et al. NF 2015



(hydrogen RFP discharges)

Piovesan, Zuin et al NuclFus 2009

Similar behavior in MST experiment:

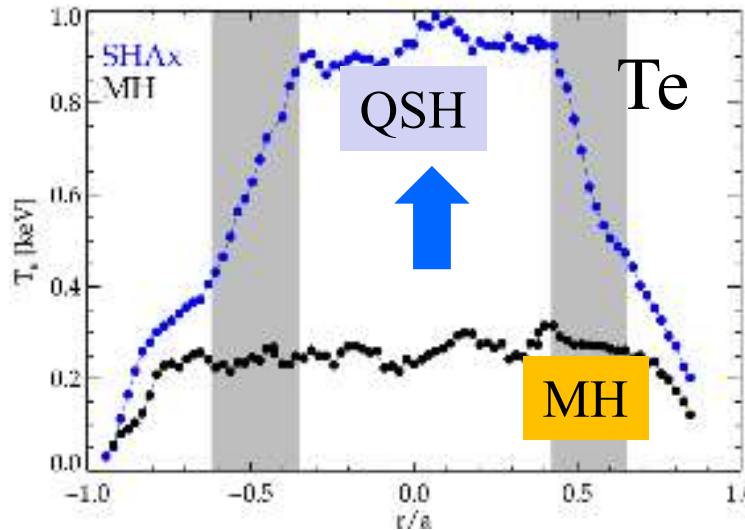
- Chapman et al IAEA EX/P6-01 (2012)
- Sarff et al Nucl Fus (2013)

# RFP helical self-organization: barriers formation

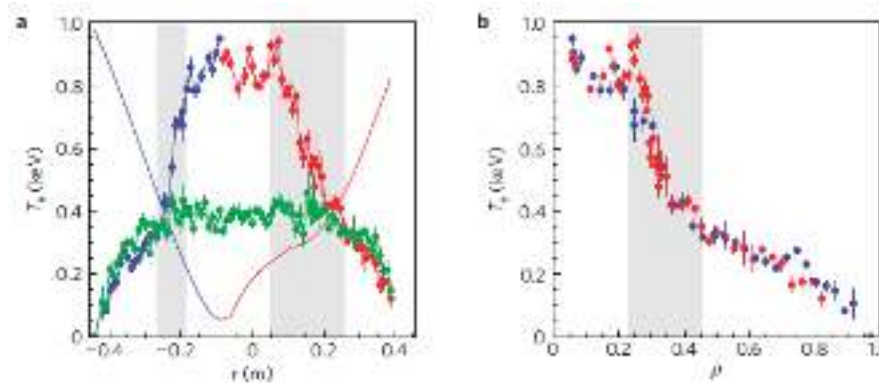
RFX -mod

## Formation of e-Internal Transport Barriers

24598, 117ms  
 $I_p=1.3\text{MA}$   
 $n/n_G=0.20$



22201, 35ms  
 $I_p=0.7\text{MA}$   
 $n/n_G=0.22$



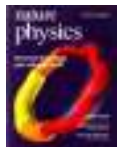
Barrier formation believed to be provided by magnetic chaos healing effect

Lorenzini, Martines, Piovesan et al NatPhys 2009

Piovesan, Zuin, Alfier et al NF 2009

Cappello et al Theory of Fusion Plasmas, 2008

Joint Varenna-Lausanne International Workshop



# RFP helical self-organization – 3D nonlinear MHD modeling

- SpeCyl code
- Verification benchmark vs PIXIE3D (LANL code)
- Relevant dimensionless parameters in governing dynamical regime transition  
Resistivity  $\eta$ , Viscosity  $\nu$ , and the Hartman number  $(\eta\nu)^{-1/2}$
- Role of non-ideal Boundary Condition:  
Magnetic Perturbation (Resonant MP / Non-Resonant MP) and sawtooth pacing
- ...
- Sensitivity Analysis vs viscosity profiles
- Magnetic chaos healing, Lagrangian Coherent Structures detection

# 3D nonlinear MHD modeling

$B(r,\theta,z,t), v(r,\theta,z,t)$

The “minimum” visco resistive 3D MHD approximation:

**Induction equation:** Faraday + Ohm's law

$$\frac{\partial \mathbf{B}}{\partial t} = \nabla \wedge (\mathbf{v} \wedge \mathbf{B}) - \nabla \wedge (\eta \mathbf{J})$$

**Momentum equation**

more or less *Navier Stokes* (*-pressure + Lorentz*)

$$\frac{d\mathbf{v}}{dt} = \mathbf{J} \wedge \mathbf{B} + \nu \nabla^2 \mathbf{v}$$

Implemented in the  
**SpeCyl** numerical code

# 3D nonlinear MHD

$$\frac{\partial \mathbf{B}}{\partial t} = \nabla \wedge (\mathbf{v} \wedge \mathbf{B}) - \nabla \wedge (\eta \mathbf{J})$$

$$\frac{d\mathbf{v}}{dt} = \mathbf{J} \wedge \mathbf{B} + \nu \nabla^2 \mathbf{v}$$

$$\rho \equiv 1, \quad \nabla p \equiv 0$$

$$\nabla \cdot \mathbf{B} \equiv 0 \quad \nabla \wedge \mathbf{B} \equiv \mathbf{J}$$

SpeCyl code - simple visco-resistive approx.

Cappello & Biskamp Nucl. Fus. 1996

$$\eta = \tau_A / \tau_R$$

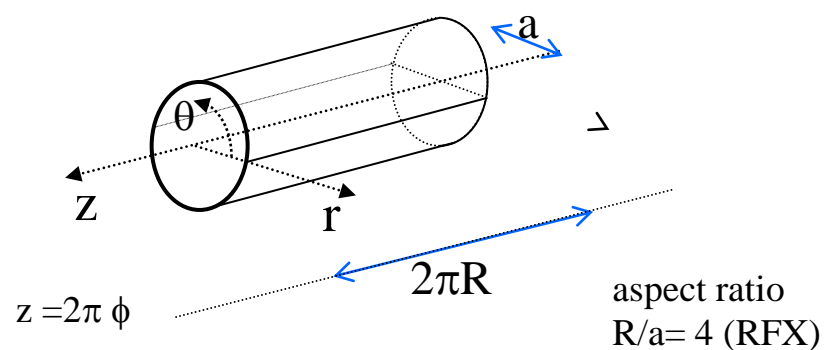
two dimensionless parameters  
with assigned radial profiles

$$\nu = \tau_A / \tau_v$$

$$\begin{cases} \text{Lundquist: } & \mathbf{S} = 1 / \eta \\ \text{Viscous Lundquist } & \mathbf{M} = 1 / \nu \end{cases}$$

r	Finite difference
$\theta, \phi$	Spectral formulation
t	Predictor-corrector + semi-implicit

Geometry: periodic cylinder



# 3D nonlinear MHD

$$\frac{\partial \mathbf{B}}{\partial t} = \nabla \wedge (\mathbf{v} \wedge \mathbf{B}) - \nabla \wedge (\eta \mathbf{J})$$

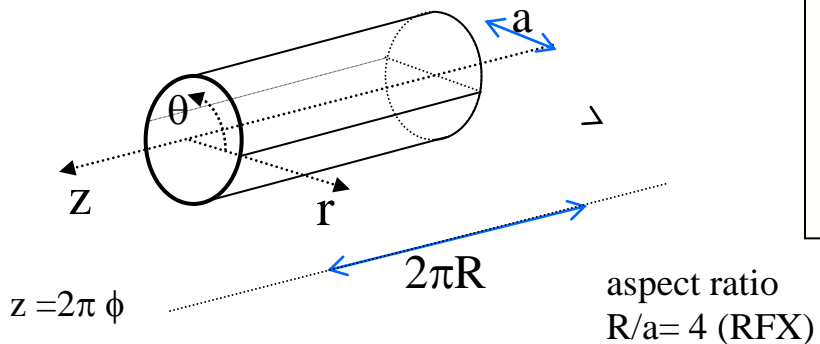
$$\frac{d\mathbf{v}}{dt} = \mathbf{J} \wedge \mathbf{B} + \nu \nabla^2 \mathbf{v}$$

$$\rho \equiv 1, \quad \nabla p \equiv 0$$

$$\nabla \cdot \mathbf{B} \equiv 0 \quad \nabla \wedge \mathbf{B} \equiv \mathbf{J}$$

r	Finite difference
$\theta, \phi$	Spectral formulation
t	Predictor-corrector + semi-implicit

Geometry: periodic cylinder



SpeCyl code - simple visco-resistive approx.

Cappello & Biskamp Nucl. Fus. 1996

$$\eta = \tau_A / \tau_R$$

two dimensionless parameters  
with assigned radial profiles

$$\nu = \tau_A / \tau_v$$

Lundquist:  $S = 1 / \eta$   
Viscous Lundquist  $M = 1 / \nu$

“typical” boundary conditions:

- $B'_z = 0$  (**constant magnetic flux  $\Phi$** )
- Constant  $E_z$  (or constant  $I_p$ )
  - m,n {
  - Ideal boundary
  - MP on  $B_{r,m,n}$  ( $\sim 1\%, 2\%, 4\% \dots$ )
  - Thin shell + vacuum layer +ideal wall
- velocity field: no slip/self consistent.

initial conditions define  $\Phi, I_z$

# Nonlinear **verification** benchmark SpeCyl – PIXIE3D

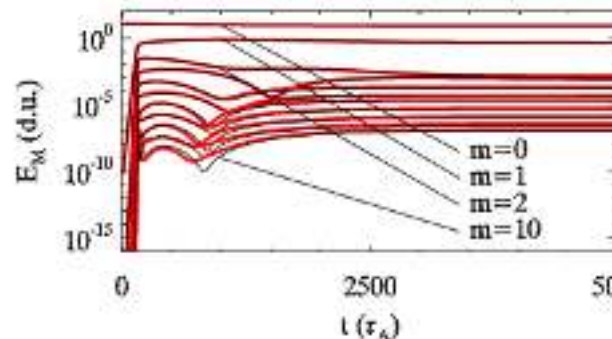
PIXIE3D is a massively parallel code in arbitrary curvilinear geometry  
conservative, solenoidal finite-volume discretization in space,  
fully implicit temporal advance.

PIXIE3D: Chacón CPC 2004, PoP 2008, Los Alamos NL -NM USA

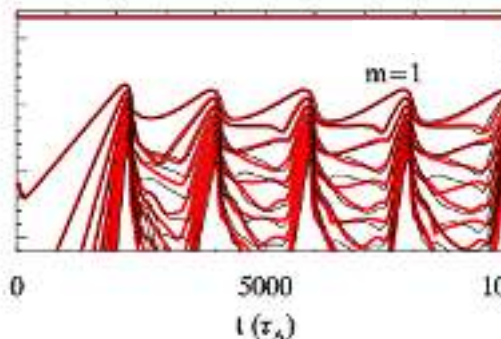
Bonfiglio, Chacón, Cappello POP 2010  
Spinicci, Bonfiglio, Chacón, et al, AIP Advances 2023

**2D**

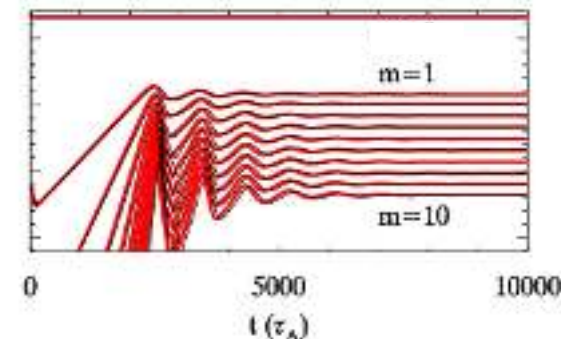
2D: single helicity (SH) RFP



2D: Tokamak sawtooth

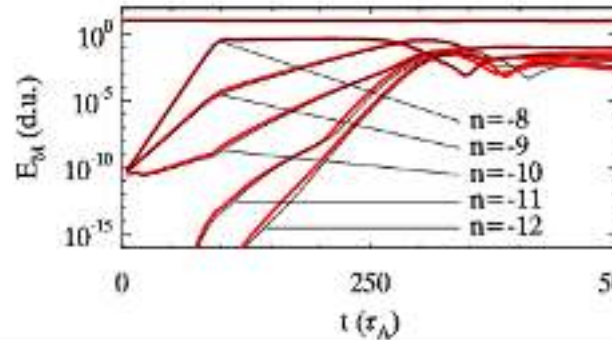


2D: Tokamak snake

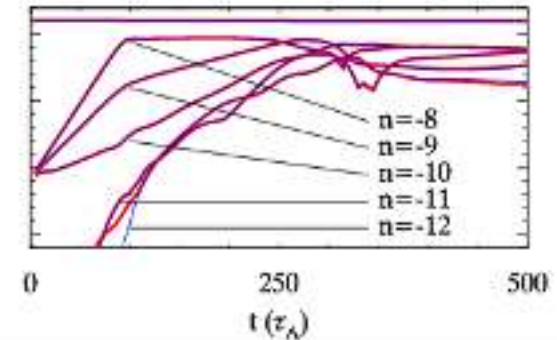
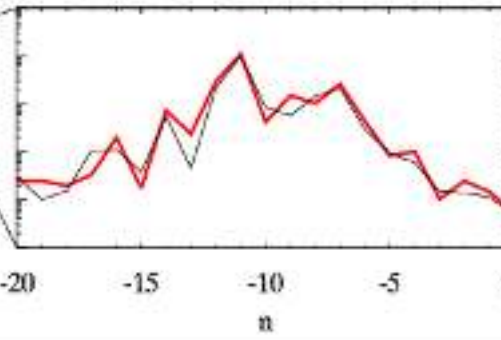


**3D**

3D: multiple helicity (MH) RFP



PIXIE3D:  $\Delta t = 1.0 \tau_A$



Magnetic energy evolution from SpeCyl and PIXIE3D (black and red curves respectively).

**Top panels 2D**) RFP and Tokamak.

**Bottom 3D**) left) RFP case, right) PIXIE3D with different time steps (red  $\Delta t = 5 \times 10^{-3}$  blue  $\Delta t = 1 \tau_A$ )

## Model equations transformation

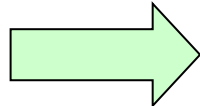
... re-scaling :

$$t \rightarrow \bar{t} = \sqrt{\frac{\eta}{\nu}} t$$

$$v \rightarrow \bar{v} = \sqrt{\frac{\nu}{\eta}} v$$

$(S, M)$

$(\eta, v)$



$(H, P)$

Magnetic Prandtl  $P = \nu/\eta = S/M$   
Hartmann number  $H = (\nu\eta)^{-1/2}$

Hartmann:  $H = (\nu\eta)^{-1/2}$

highlighted in

D. Montgomery et al. PPCF 92-93 (applied to linearized equations)

magnetic Prandtl:  $P = \nu / \eta$

Whenever inertia is negligible and/or magnetic Prandtl is large:  
the H number alone governs the solutions of the model equations

$$\frac{\partial \bar{B}}{\partial \bar{t}} = \nabla \wedge (\bar{v} \wedge \bar{B}) - \nabla \wedge (\bar{H}^{-1} \bar{J})$$

$$\frac{1}{P} \frac{d\bar{v}}{d\bar{t}} = \bar{J} \wedge \bar{B} + \nabla^2 (\bar{H}^{-1} \bar{v})$$

$$\rho \equiv 1, p \equiv 0$$

# 3D nonlinear MHD

Some examples of different regimes decided by  $H$

Spectrum of MHD modes:  $m=1$  resistive kink/tearing modes

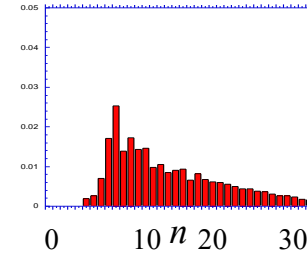
$m=1$  modes

$\delta B_{m=1, n}$

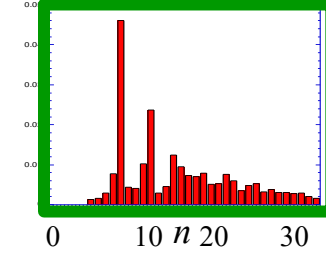
$m=1$  modes  
nonlinearly drive  
 $m=0$  modes

**$m = 0$  modes:**  
**signature of the dynamical regime**

**MH**

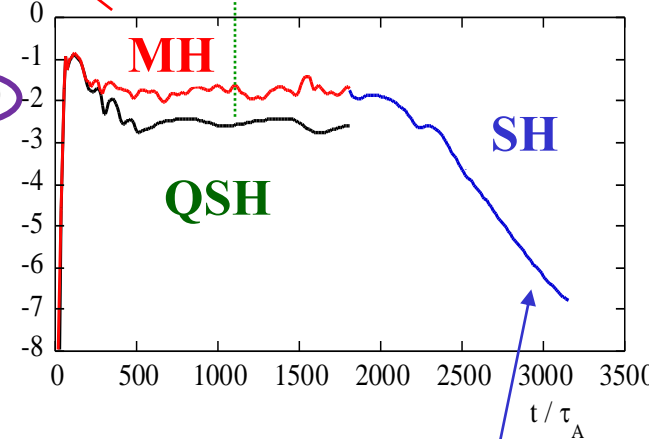


**QSH**



$m=1, n=1, 2, \dots$

**Log  $W_{m=0}$**



$m=0, \sum_n$

**Low  $H$ : SH Single Helicity regime**

$m=1$  ONE single  $m=1$  mode survives (and its harmonics)  
 $m=0$  modes decrease to vanishing values

# 3D nonlinear MHD

## The transition to helical regimes

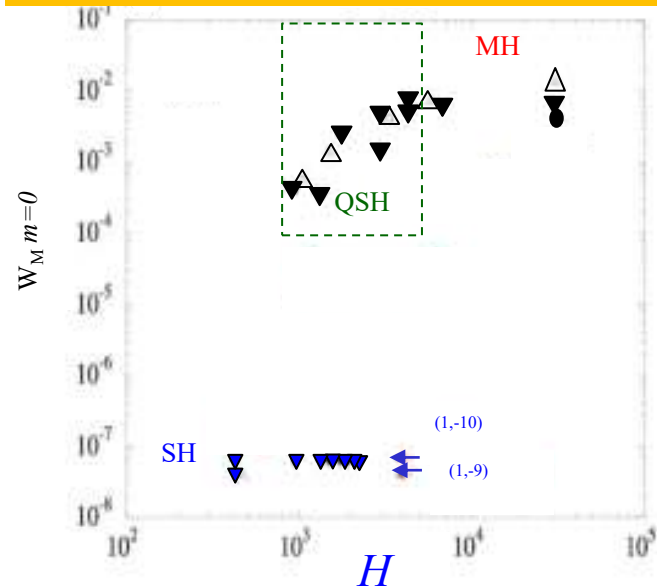
- is a continuous one ruled by: Hartmann number,  $H$ ,  $(\eta v)^{-1/2}$

$m = 0$  modes:  
signature of the dynamical regime

$\Delta S = 3.3 \times 10^3$  (P: 2/3-10)  
 $\nabla S = 3.0 \times 10^4$  (P: 1-5000)  
 $\bullet S = 10^5$  (P = 10)

SH  
W<sub>M</sub>=0 exponentially decaying: →  
conventional finite value assigned in the plot

A transition diagram can be drawn in terms of:  
- W<sub>M=0</sub> mode -time averaged- energy (order parameter)  
vs  
- H artmann number



Solutions with different values of the couple (S, P) lie on a single curve when plotted against H

Pinch Parameter  $\Theta = 1,6$

Cappello & Escande PRL2000  
Cappello PPCF 2004

# 3D nonlinear MHD

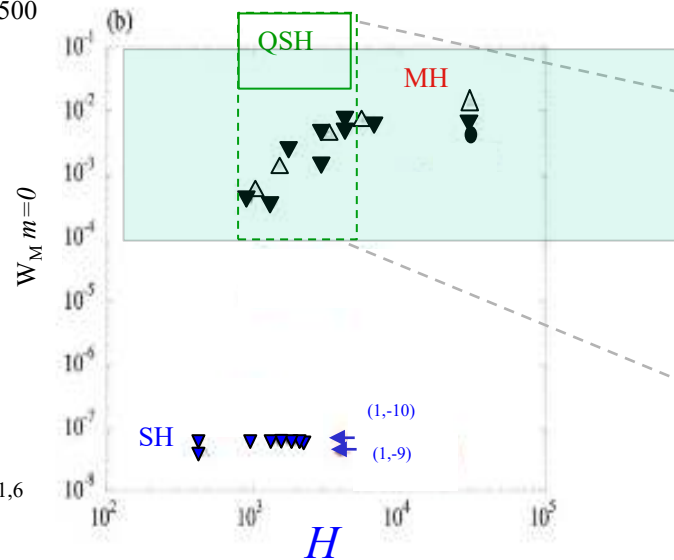
## The transition to helical regimes

- is a continuous one ruled by: Hartmann number,  $H$ ,  $(\eta v)^{-1/2}$
- is significantly favored by **seed** edge **Magnetic Perturbation**

$\Delta S = 3.3 \times 10^3$  (P: 2/3-10)

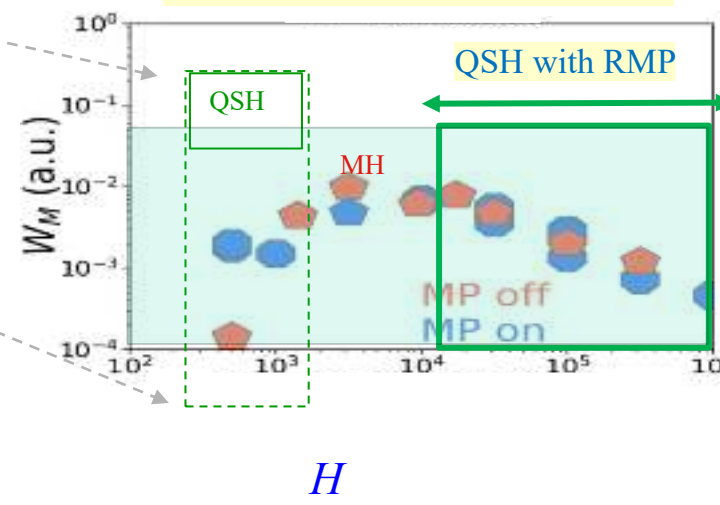
$\blacktriangledown S = 3.0 \times 10^4$  (P: 1-500)

$\bullet S = 10^5$  (P = 10)



Pinch Parameter  $\Theta = 1.6$

here additional set of simulations



$S = [10^4 : 10^7]$

$P = [1 - 10^5]$

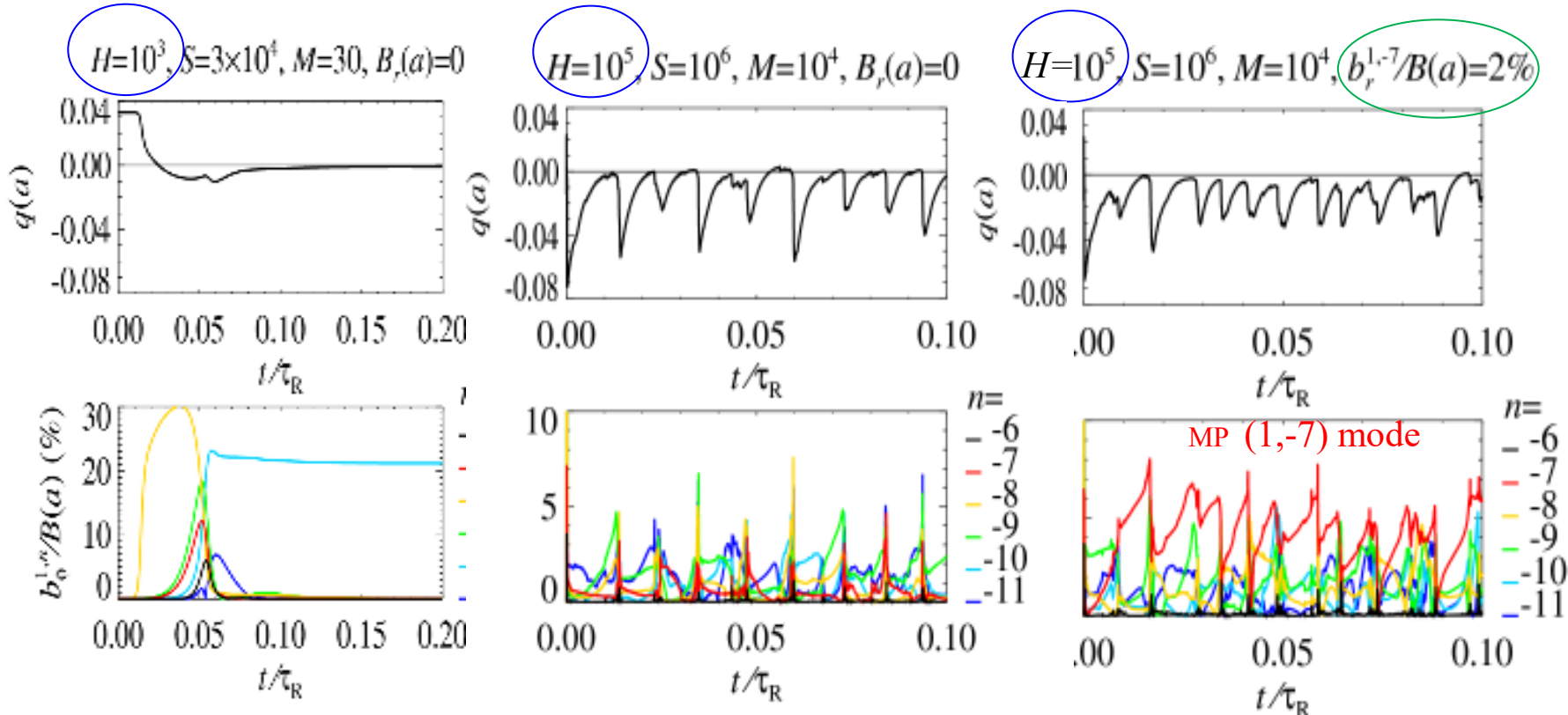
No QSH Without  
QSH With RMP

The higher  $H$  (lower dissipation)  
the smaller the MP required to  
excite QSH regimes

Trend with increasing H and applying MP

RFP “sawtooth” cycle excitation

“sawtooth” cycle pacing and QSH excitation



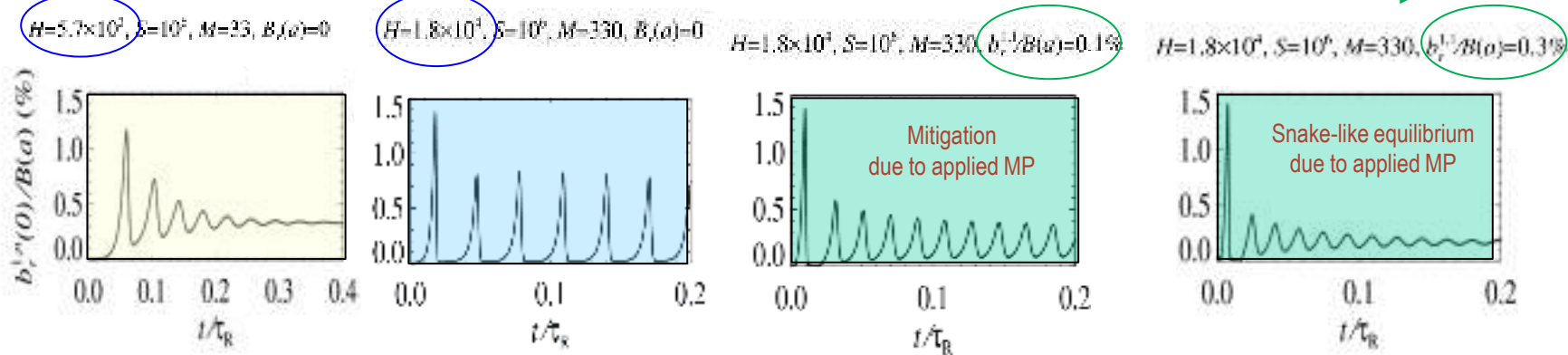
Similar to RFX-mod at  
“intermediate” values of  
plasma current

**Circular tokamak** in viscoresistive SpeCyl simulations: + MP  $(1,1)$

Snake like (high dissipation)  $\rightarrow$  periodic sawtoothing (low dissipation)

approaching snake (**same dissipation but MP applied**)

Trend with increasing  $H$  and applying MP



H & MP produce similar dynamical effects as in RFP

Bonfiglio, Chacon, Cappello PoP 2010

Bonfiglio, Escande , Zanca, Cappello NF 2011

Veranda, Bonfiglio Cappello et al EPS 2012

Bonfiglio, Veranda , Cappello et al PPCF 2015

Remarks:

- 3D nonlinear MHD simulations at realistic values of Lundquist parameters remain beyond present capabilities,
- indeed, the estimate of a realistic viscous Lundquist, i.e. theory of momentum transport, is still an open issue,
- Uncertainty in the estimate of Lundquist number appears less problematic, yet some debate still pop up here and there;

# 3D nonlinear MHD

Summary of the presented hints from viscoresistive approximation of RFP description:

Large and medium scale resistive-kink/tearing modes yield field reversal (dynamo effect);

**Resitivity and viscosity** (the product of them -  $\eta$ ) govern:

- the transition from magnetic chaos dominated to reduced chaos (QSH) regimes,
- the amplitude and frequency of sawtooting,

**Magnetic Perturbations (MP):**

- are capable of pacing sawtooth amplitude and frequency,
- favors the transition to QSH;

# Summary and Concluding remarks

J. B. Taylor theory of RFP relaxation ('70ties).

- Variational principle: provides analytical solutions of magnetic profiles similar to experimental measurements.

Toy model ('60ties and modern *revival*).

- Schematic model provides intuitive description of macroscopic helical self-organization.

3D nonlinear MHD numerical simulations.

- Despite the simple approximation adopted in SpeCyl code implementation, several characteristic features observed in experiments find a useful description and inspires directions to be studied.

It still remains challenging to achieve a quantitative predictive capability, needed for fusion research.

Additional hints are available from viscoresistive approximation of RFP description, and are briefly presented in the following slides:

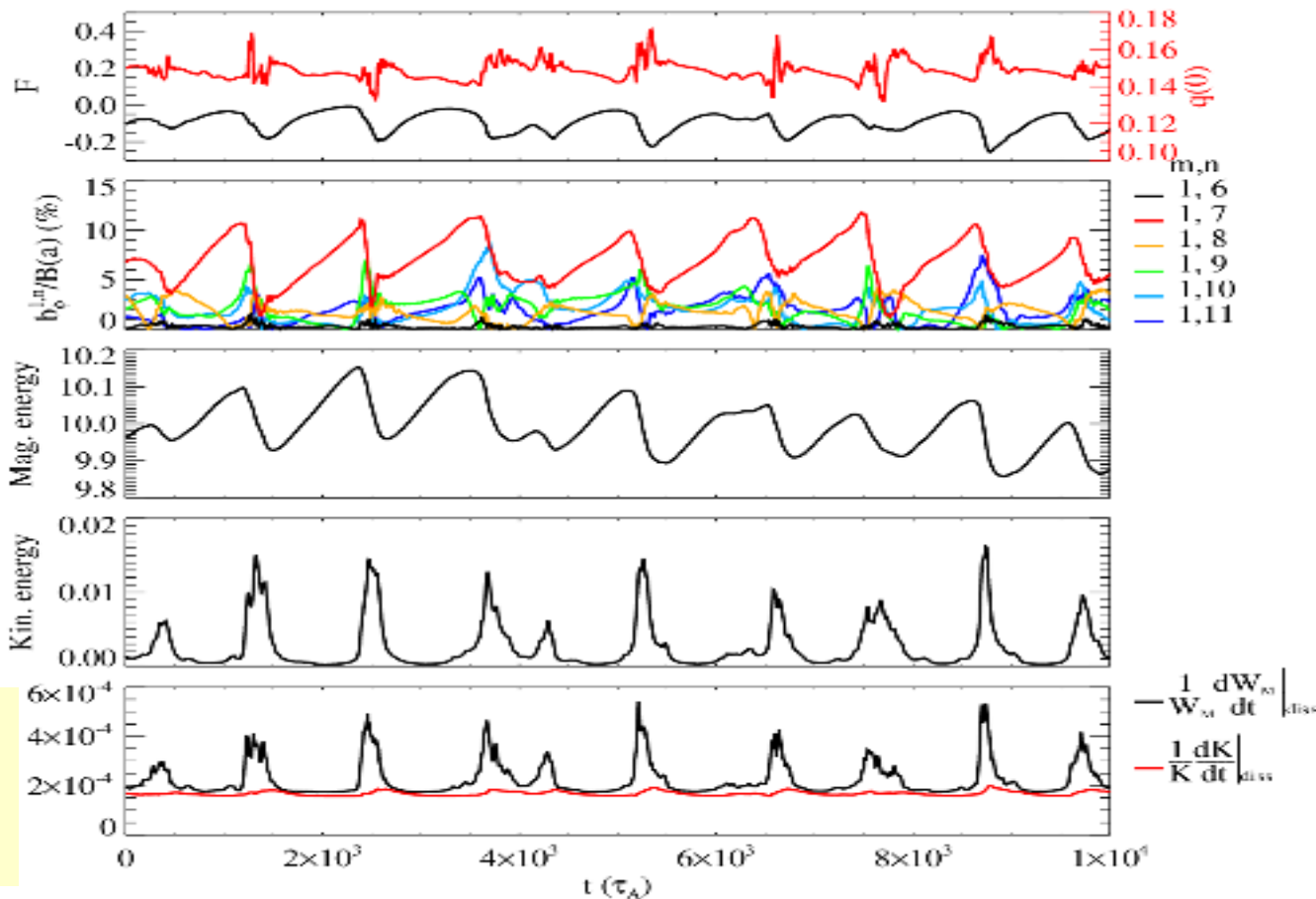
- Relaxation-reconnection events at sawtooth cycle
  - Magnetic into Kinetic energy conversion (possible ion heating?)
  - Current sheets formation – magnetic reconnection,
  - Mode phase locking, (toroidal collapse of the helix)
  - Excitation of Alfvén waves
- Transport Barrier formation and Magnetic chaos healing
- Some open issues

next slides: relaxation-reconnection cycles features (only mention)

- Magnetic into Kinetic energy conversion (possible ion heating?)
- Current sheets formation – magnetic reconnection,
- Mode phase locking, (toroidal collapse of the helix)
- Excitation of Alfvén waves

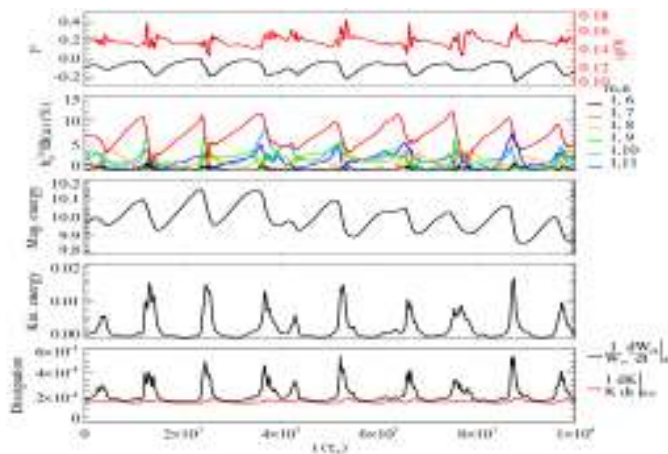
# - Magnetic into Kinetic energy conversion

RFP “sawtoothing” cycle



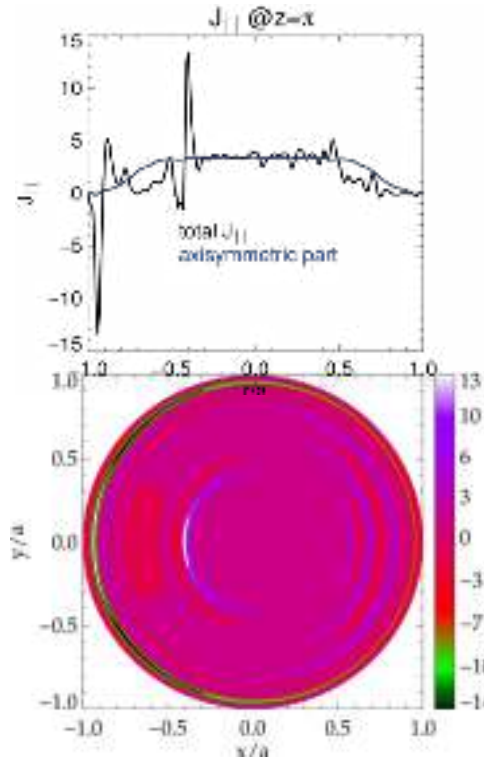
# current sheets formation mode phase locking and excitation of Alfvén waves

RFP S=10<sup>5</sup>, P=10



$J \cdot B$

3D



1D  
Radial  
profiles

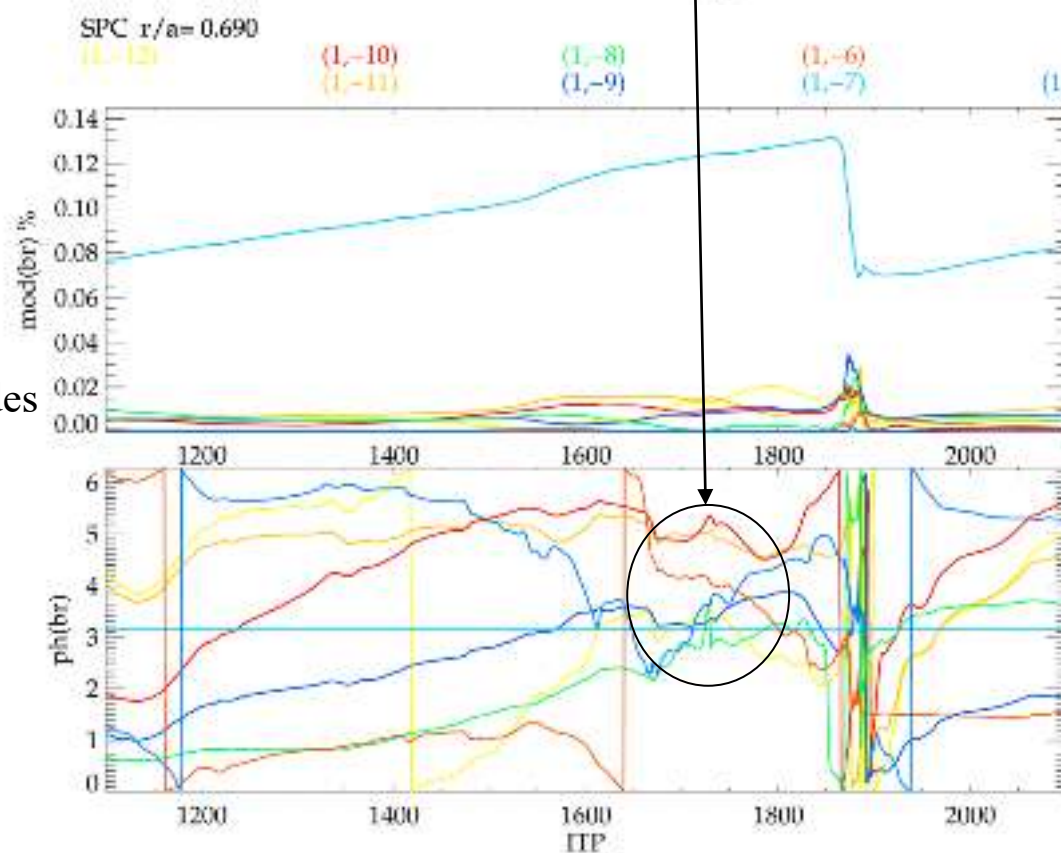
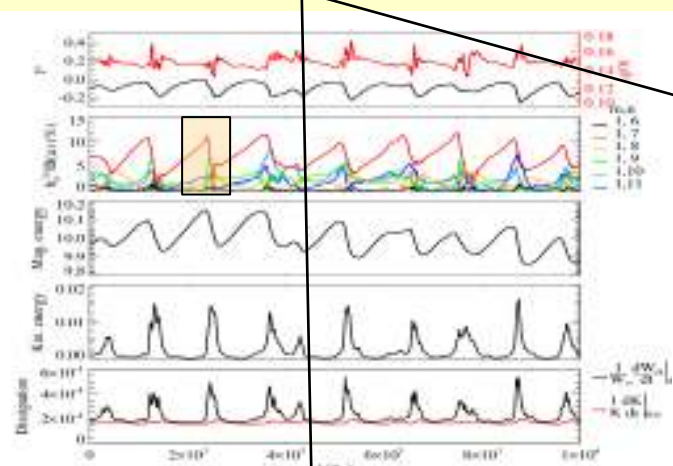
2D  
contour  
plot

1D  
Radial  
profiles

2D  
contour  
plot

current sheets formation **mode phase locking** and excitation of Alfvén waves

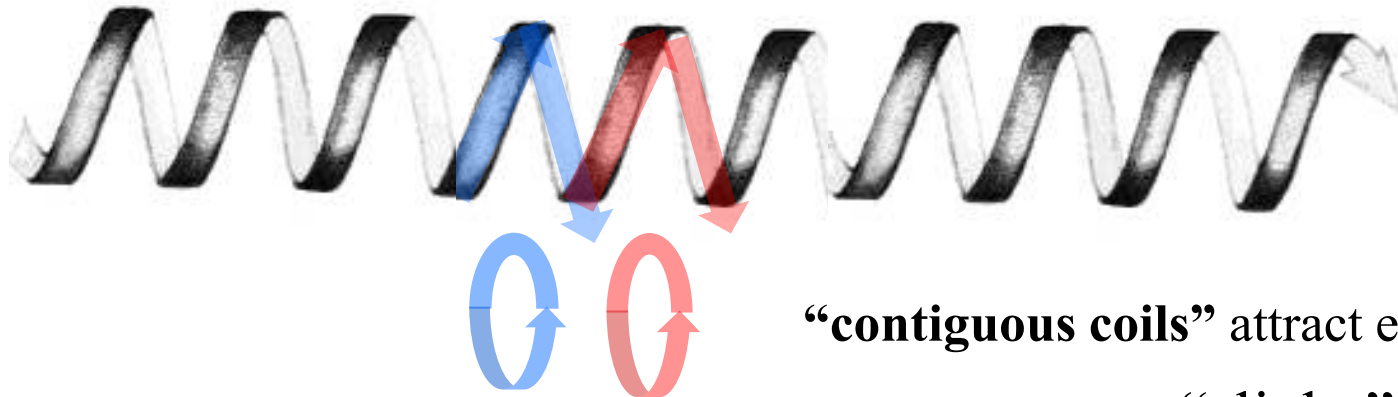
RFP S=10<sup>5</sup>, P=10



$J//$  contours

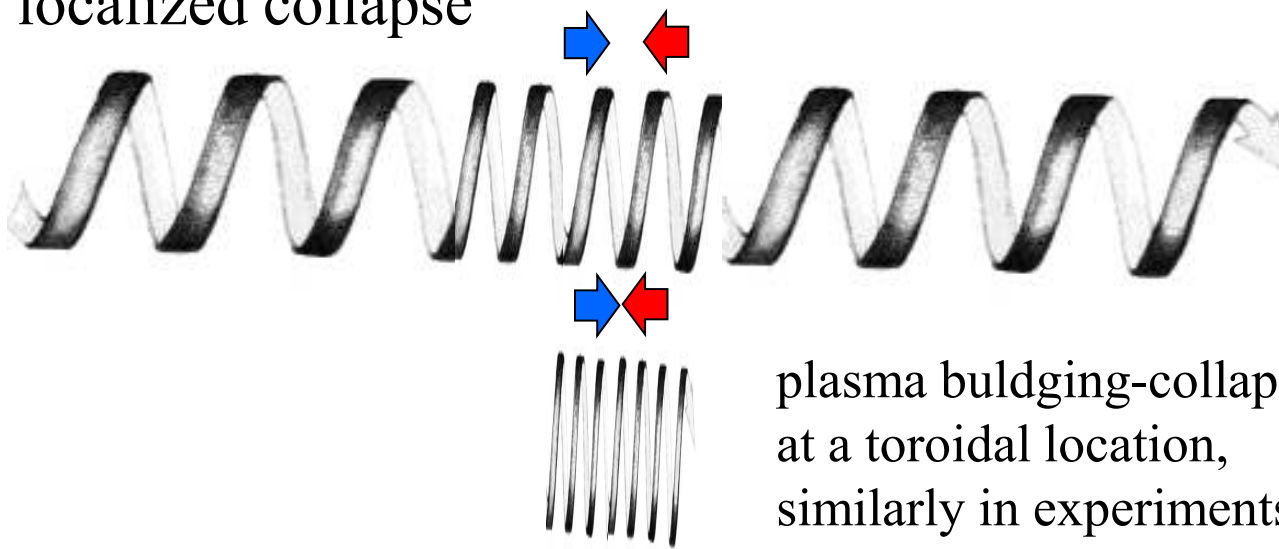
# RFP Toy model: useful to describe the “slinky -phase locking- effect”

After kinking ...



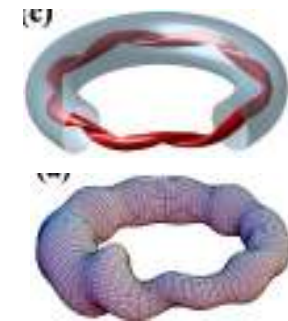
“contiguous coils” attract each other ...

... localized collapse



... “slinky” instability

plasma bulging-collapse  
at a toroidal location,  
similarly in experiments  
and nonlinear modeling...

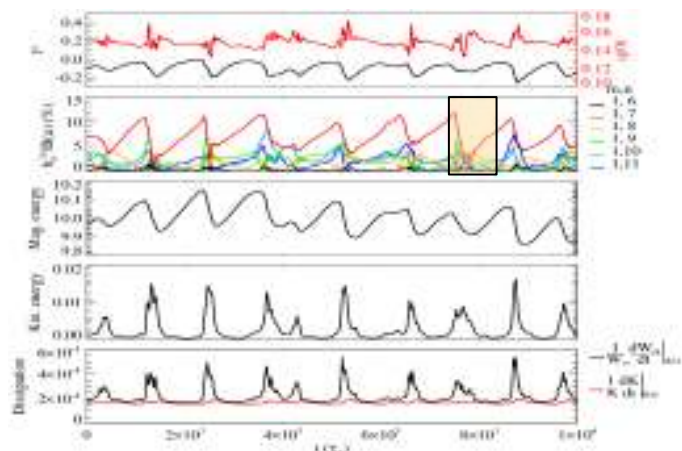


# current sheets formation mode phase locking and excitation of Alfvén waves

RFP S=10<sup>5</sup>, P=10

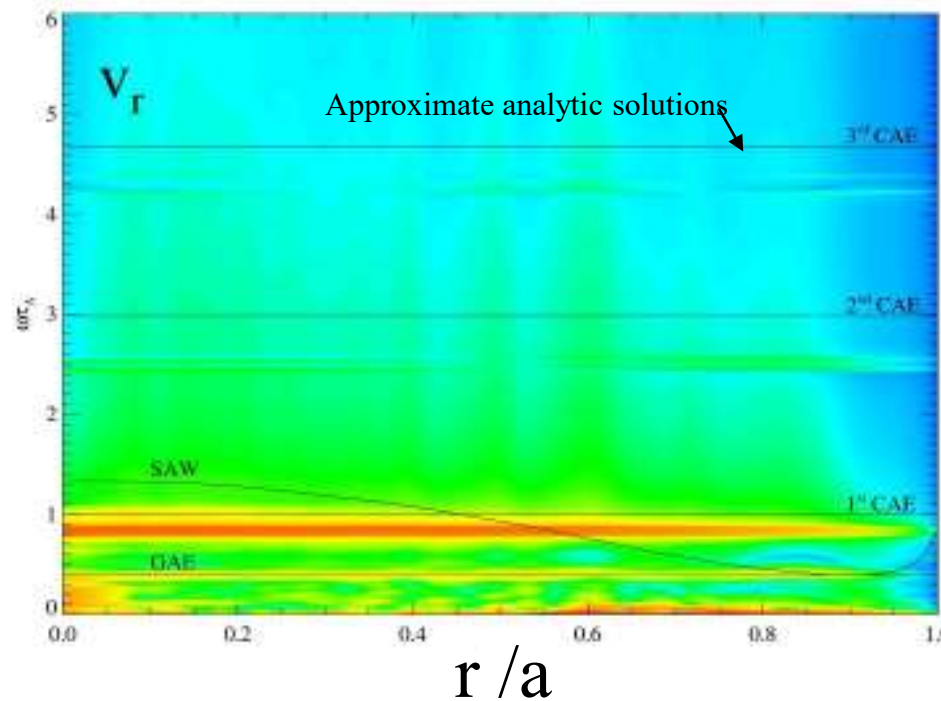
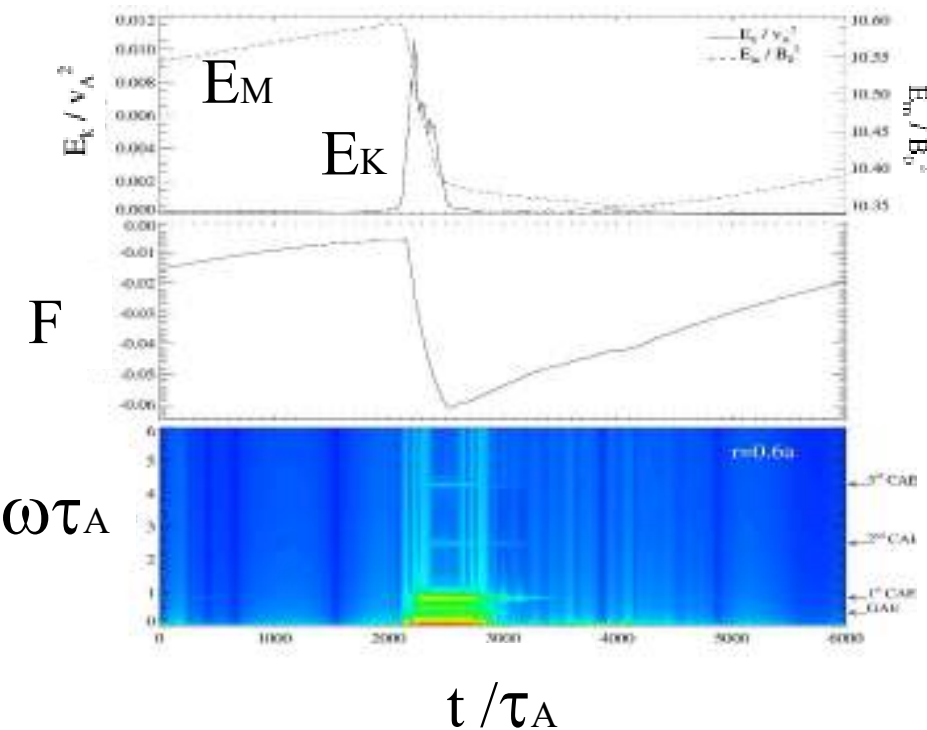
RFX-mod like density profile assigned

Alfvén waves spectrum  
( $m=1, n=0$ )  $r = 0.6a$



Kryzhanovskyy et al NF 2022

Alfvén Eigenmodes  
(in particular the GAE and the  
1<sup>st</sup> CAE) are excited by  
magnetic reconnection event.



Experimentally observed in RFPs:  
Spagnolo NF 2011 and therein refs, Koliner PRL 2012

Transport in RFP is believed to be ruled by **magnetic topology properties**:

Typical tool for topology inspection:

**Poincarè surface of section** approximated by **magnetic field lines punctur plot**:

Trace magnetic Field Line and mark intersection in chosen surface.

Chaotic magnetic field emerge in several conditions in RFP, Tokamak and Stellarator.

Magnetic Field line integration, numerical tools available at Consorzio RFX:

NEMATO [1]

benchmarked vs ORBIT code [2]

[1] Finn, Chacòn **PoP** 2005

[2] Ciaccio, Veranda, Bonfiglio, Cappello, Spizzo, White **PoP** (2013)

# Magnetic field lines and magnetic surfaces

The two extreme dynamical regimes:

MH

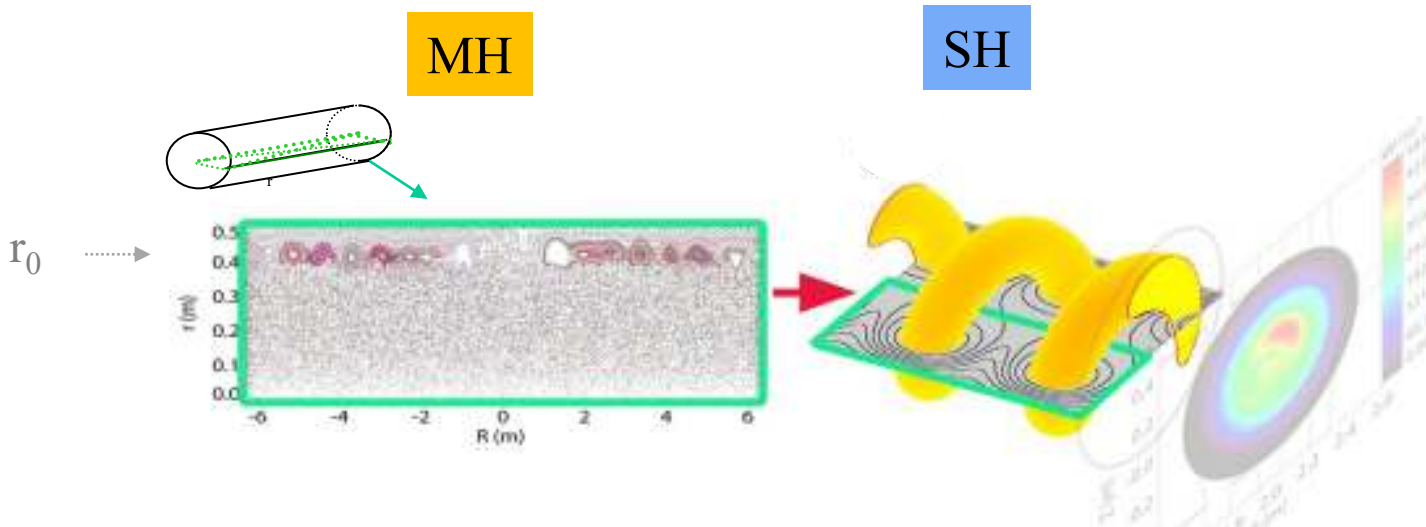
and SH (exist only in cylinder)

Magnetic field lines punctur plot:

- Magnetic chaos spreads in the core of the domain
- A chain of magnetic islands exist at reversal radius: magnetic lines lie on that surfaces, do not move from them.

Magnetic flux surfaces perfectly conserved

In helical symmetry you can find a helical flux function, the isosurfaces are magnetic flux surfaces:  
Magnetic field lines lie on flux surfaces.



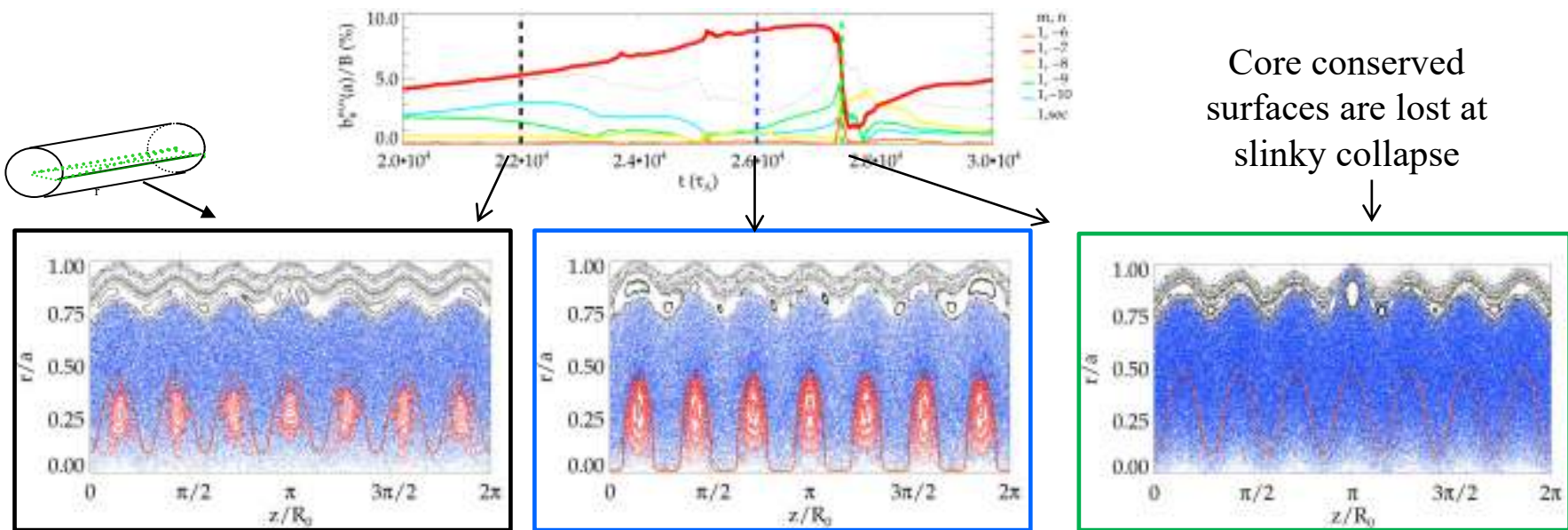
# Chaos healing effect thanks to helical structure

By inspection of magnetic topology during a typical QSH sawtooth cycle in simulations we find an intermediate situation in between MH and SH: partial chaos healing

# Chaos healing effect thanks to helical structure

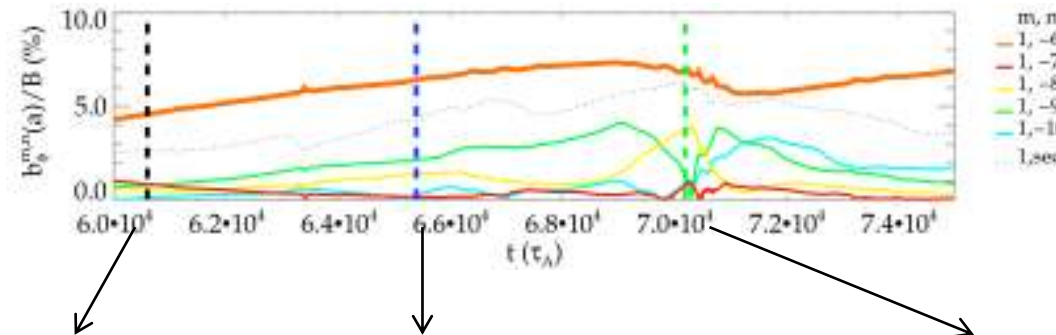
[Dominant mode  
separatrix expulsion  
Escande et al PRL (2000) ]

## The width of conserved helical core evolves

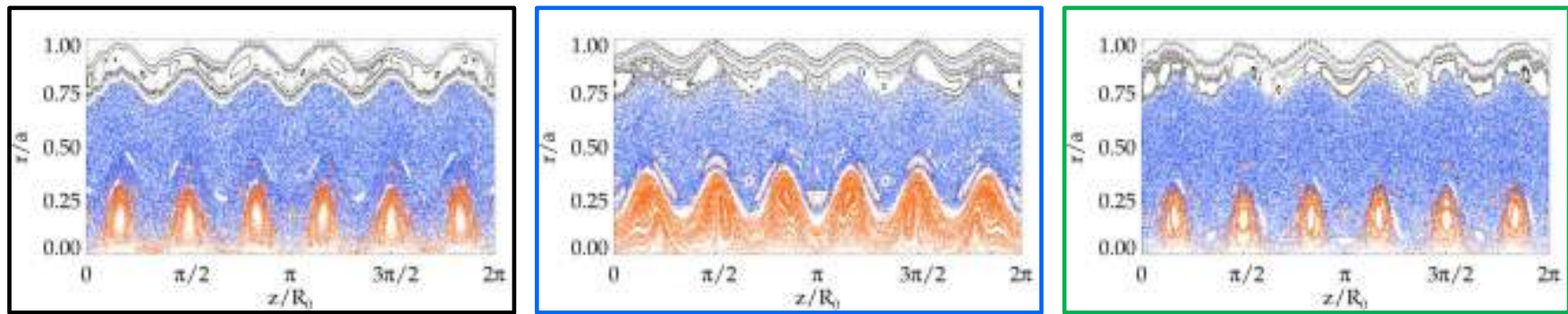


Inspired by indications obtained in topology studies of numerical simulations we studied a Non-Resonant helical regimes

# More efficient chaos healing by stimulating n=6 (Non Resonant)



Conserved surfaces  
are never lost



Poincaré plots: secondary modes divided by 5 to match experimental amplitudes (as scaled to  $S = 10^7$ )

# Lagrangian Coherent Structures, LCS, detected in simulation cases:

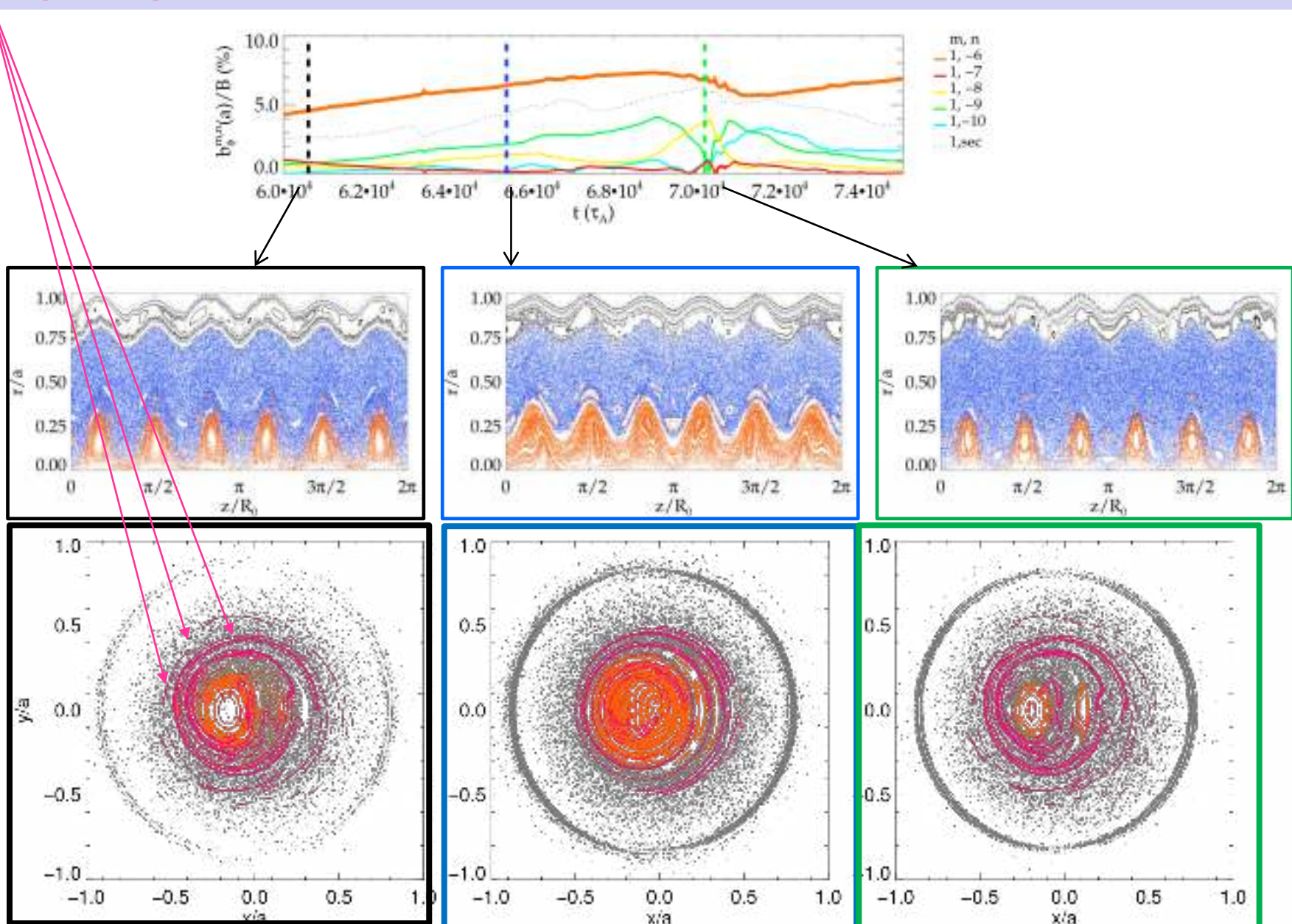
Barriers to the wandering magnetic field lines *embedded in chaotic domains*

- Di Giannatale, Bonfiglio, Cappello, Chacòn, Veranda NF (2021)
- Veranda, Bonfiglio, Cappello, Di Giannatale, Escande NF (2020)
- Pegoraro \*, PPCF (2019)
- Di Giannatale, et al POP a,b (2019)
- Rubino °, Borgogno°, Veranda, Bonfiglio, Cappello, Grasso°, PPCF (2015)

Collaboration with

- ° ISC (Institute for Complex Systems) - CNR Torino Italy – Politecnico Torino
- \* University of Pisa - Italy

# Lagrangian Coherent Structures nearby conserved surfaces

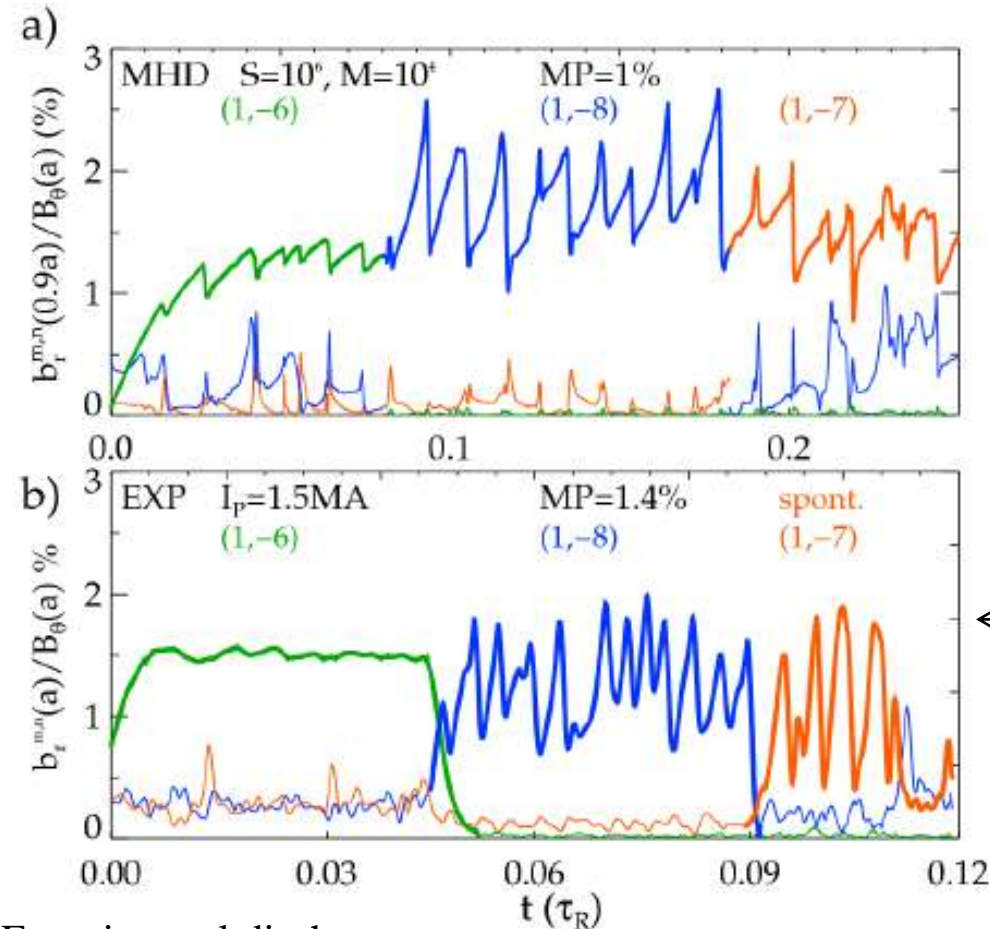


The possibility to convey the experimental discharge toward a “new” helical solution, in particular, low  $n$  non-resonant helix, has been tested in RFX-mod by applying suitable MP.

# Dynamics successfully confirmed in RFX-mod experiment

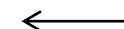
Small edge Magnetic Perturbations (MP) can drive new helical regimes, with different pitch:

## Validation example

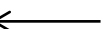


Experimental discharge  
#30932 RFX-mod

Veranda, Bonfiglio, Cappello et al NF 2017



simulation



Successful RFX-mod experiments:  
**alternative  $n_s$**   
**stimulated by seed MP**

# Some open issues, Ongoing work:

Implementation of more **realistic Boundary Conditions**

Verification SpeCyl – PIXIE3D (Chacòn-LosAlamos)

*Spinicci (PhD), Bonfiglio et al, EPS 2022*

Addressing **estimate of experimental effective Hartmann**

Heuristic approach (momentum transport in plasmas is a long standing open issue)

*Vivenzi (PhD) Veranda et al, EPS 2022 ; Vivenzi Veranda et al, Theory Fusion Plasmas 2022 submitted JPCS*

Assessing **magnetic LCS validation on experimental eITB**

*follow up of Veranda et al, NF 2017*

Further develop **analogies RFP – Tokamak - ...**

- **Alfven waves excitation at sawtoothing (ohmic)**

*Kryzhanovskyy (PostDoc), Bonfiglio et al, Nuclear Fusion 2022 <https://doi.org/10.1088/1741-4326/ac6ad3>*

*Kryzhanovskyy (PostDoc), Bonfiglio et al, paper under revision*

- **What is the role of visco-resistive “quality” in determining MHD mode coupling in Tokamak ?**

*Possible impact on density limit processes (both RFP and Tokamak) under discussion*

**What is the mechanism of “anomalous” ion heating in RFPs (observed at sawtoothing) ?**

*non resonant Alfvèn wave particle interaction*

spare slides

## Theory and Simulation Group at Consorzio RFX:

Susanna Cappello

[3D nonlinear MHD (head of the group)]

nome.cognome@igi.cnr.it

Fabio Sattin

[ particle statistics and wave-particle]

Daniele Bonfiglio

[ 3D nonlinear MHD]

Italo Predebon

[ gyrokinetics, MHD]

Marco Veranda

[ 3D nonlinear MHD, magnetic topology]

Emanuele Spada

[ high voltage holding (MITICA-NBTF) / theoretical studies]

+ 2 Post Doc (Kryzhanovskyy, Spinicci)

+ 1 PhD student (Calcagno)

+ international collaborators

# Main NUMERICAL TOOLS involved on the modeling side

- **3D nonlinear MHD** – viscoresistive approximation:  
SpeCyl <sup>[a]</sup> - PIXIE3D <sup>[b]</sup> (benchmarked codes) <sup>[c]</sup>
- **Magnetic Field line integration:**  
NEMATO <sup>[d]</sup> (benchmarked vs ORBIT code <sup>[e]</sup> )
- **Lagrangian Coherent Structures** detection <sup>[f, g]</sup>

[a] Cappello, Biskamp **NF** 1996

[b] Chacòn **CPC** 2004, Chacòn **PoP** 2008

[c] Bonfiglio, Chacon, Cappello **PoP** 2010

[d] Finn, Chacòn **PoP** 2005

[e] Ciaccio, Veranda, Bonfiglio, Cappello, Spizzo, White **PoP** (2013)

Recent collaboration with Borgogno (CNRS-Nice), Rubino and Grasso (CNR – ISC Torino, PoliTO) :

[f] Rubino, Borgogno, Veranda, Bonfiglio, Cappello, Grasso **PPCF** (2015)

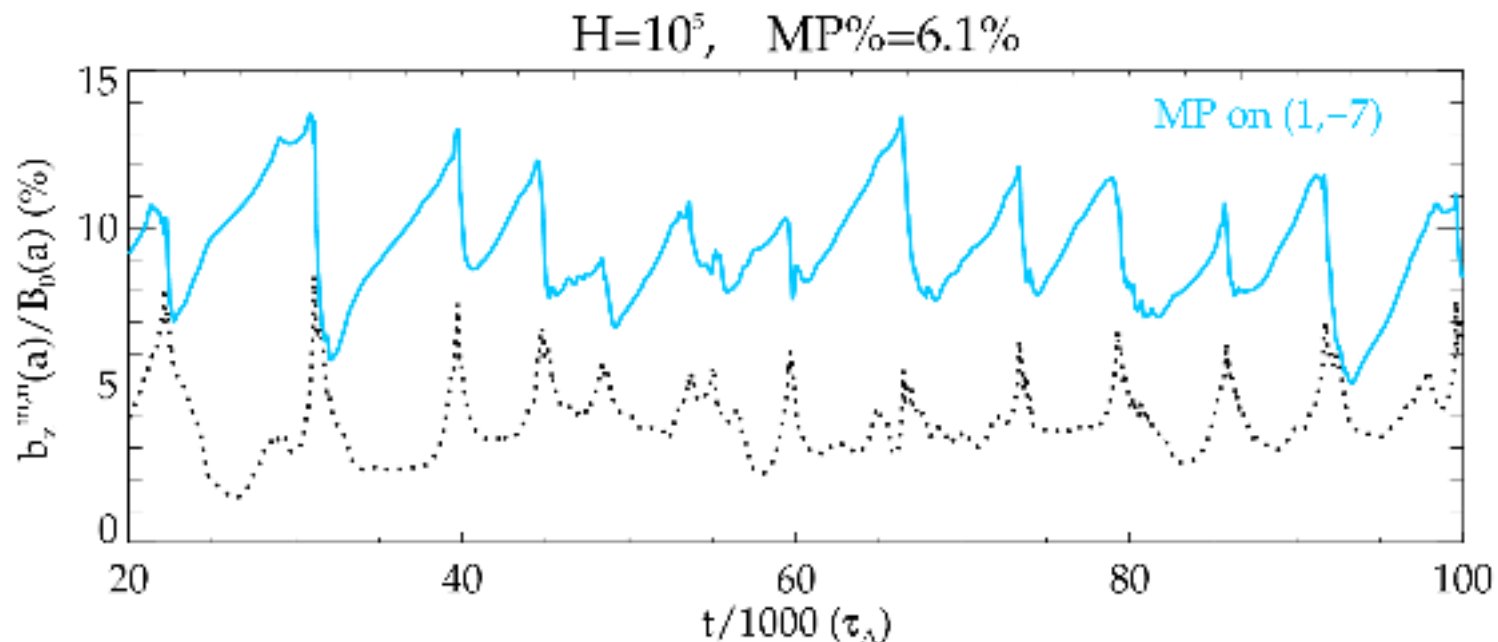
[f] Di Giannatale, et al **POP** a,b (2019)

[f] Pegoraro, **PPCF** (2019)

Possible to excite different  $ns$

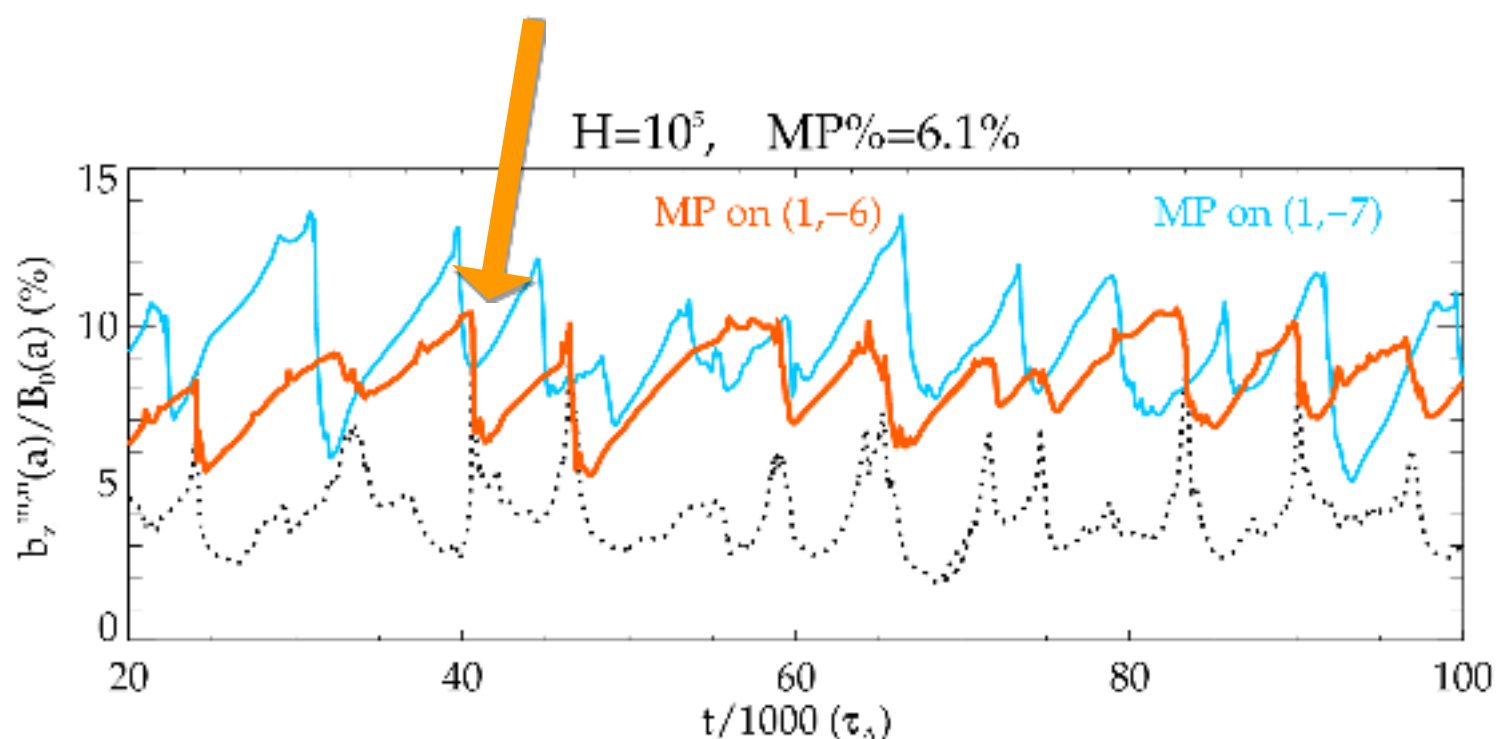
Dominant  $(1,-7)$  and sum of secondary modes

---



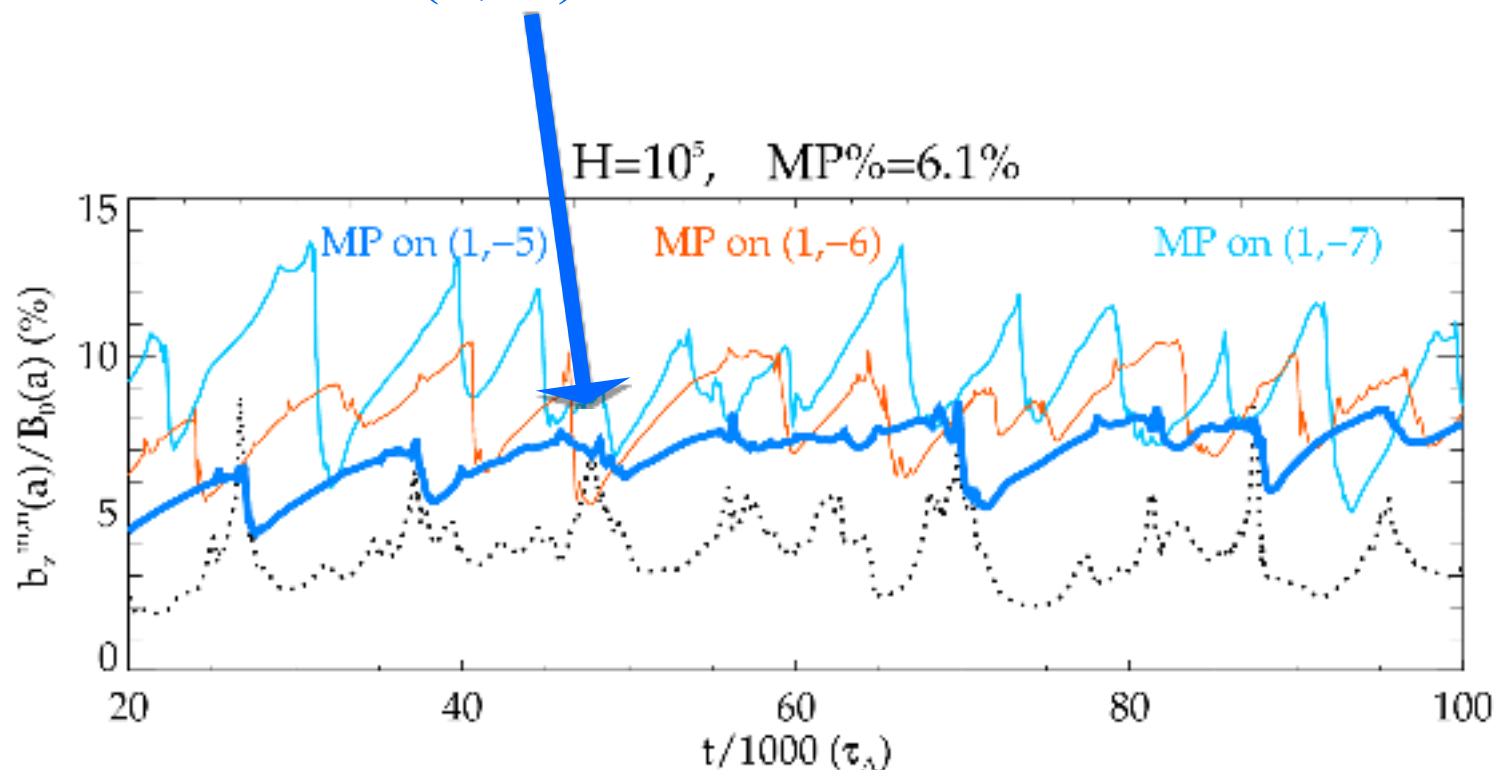
# Response to different MPs : comparison

Dominant (1,-6) less reactive than -7



# Response to different MPs : comparison

Dominant (1,-5) even less reactive

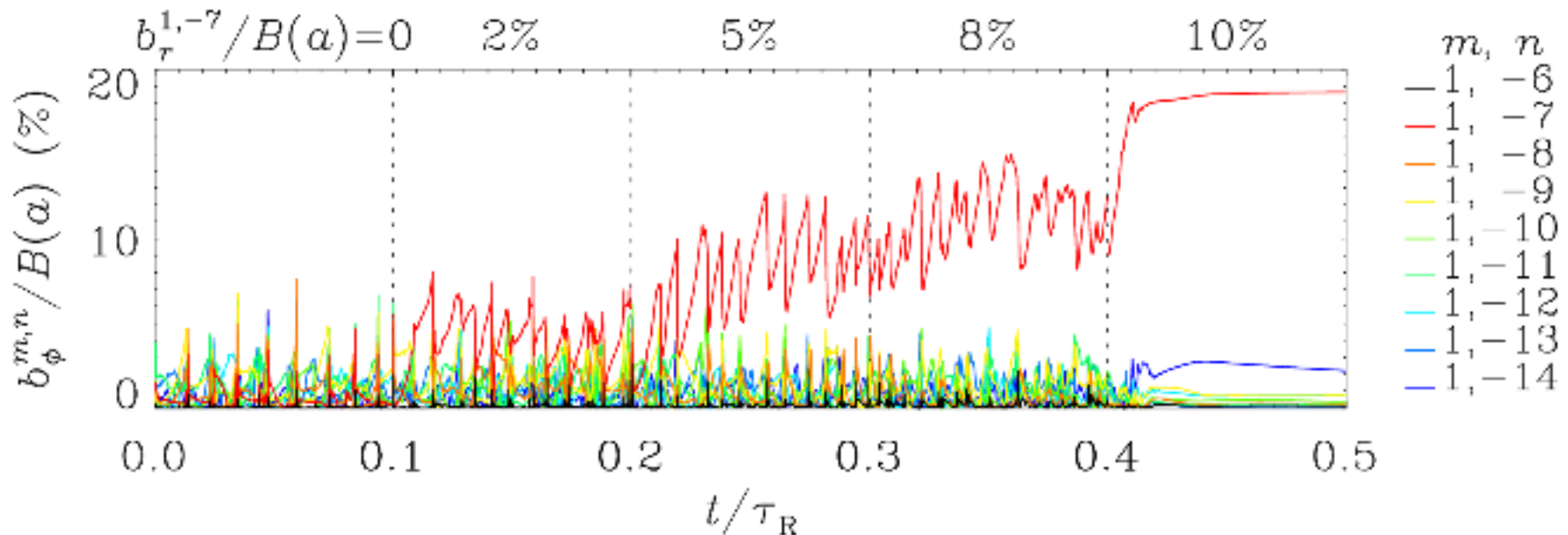


NOTE: the lower the  $n_{MP}$   $\rightarrow$  the smaller the **Frequency&Amplitude** of cyclic oscillations

# Larger MPs leads to steady helical saturation

(Similar to the ones obtained at high dissipation)

Veranda PPCF 2013  
Bonfiglio PPCF 2015



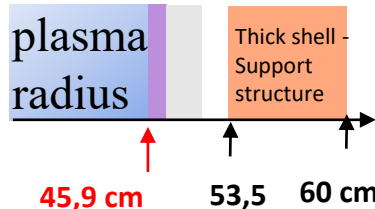
... to be explored in experiments

# RFX device evolution: plasma radius and magnetic front-end

(1992  
1999)

RFX

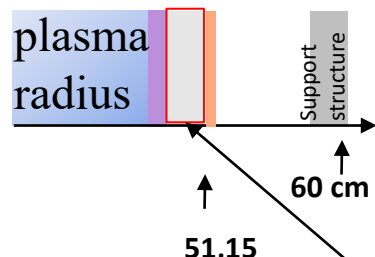
Tiles (18 mm)  
Vessel (30 mm)



**Thick shell**

(2004  
2015)

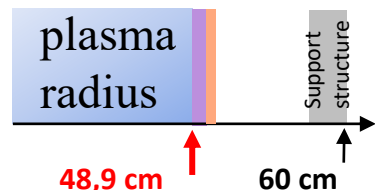
RFX-mod



**thin shell + control coils**

start  
2022...

**RFX-mod2**



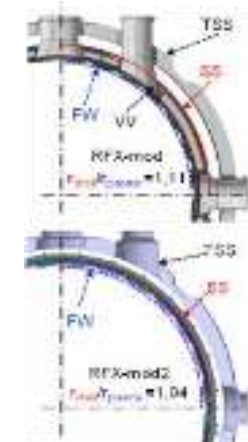
**Removed original vacuum vessel**

Shell proximity

$$b/a = 1.17$$

$$b/a = 1.11$$

$$b/a = \mathbf{1.04}$$



$r_{saddle\ sensors} = .5065$



$r_{saddle\ coils} = .5815$

$r_{pick\_up\ coils} = .510$



# RECONNECTION PROCESSES AND SCALING LAWS IN REVERSED FIELD PINCH MAGNETOHYDRODYNAMICS

S. CAPPELLO

Gruppo di Padova per Ricerche sulle Fusione,  
Associazioni Euratom-ENEA-CNR-Università' di Padova,  
Padova, Italy

D. RISKAMP

Max-Planck-Institut für Plasmaphysik,  
Euratom Association, Garching, Germany

**ABSTRACT.** Reversed field pinch (RFP) confinement is studied in the framework of three dimensional magnetohydrodynamic (MHD) numerical simulations. The scaling law for the magnetic fluctuation amplitude with Lundquist number  $S$  is  $\delta B \propto S^{-0.22}$ , which can be understood if the basic dynamic processes are governed by current sheet reconnection. Quasi-periodic oscillations are in fact found to be correlated with the presence of localized sheet currents, which for sufficiently large  $S$  make the major contribution to the average power dissipated by fluctuations. Special attention is paid to numerical convergence in the simulations. The results are compared with experimental observations.

The  $m = 0$  modes are found to contribute directly to the dynamo action. Figure 9 shows the radial profile (time averaged over  $3500\tau_A$ ) of the contributions to the poloidal electric field  $E_\theta^D(r) = -(\bar{v} \times \bar{b}_\theta)$  of the

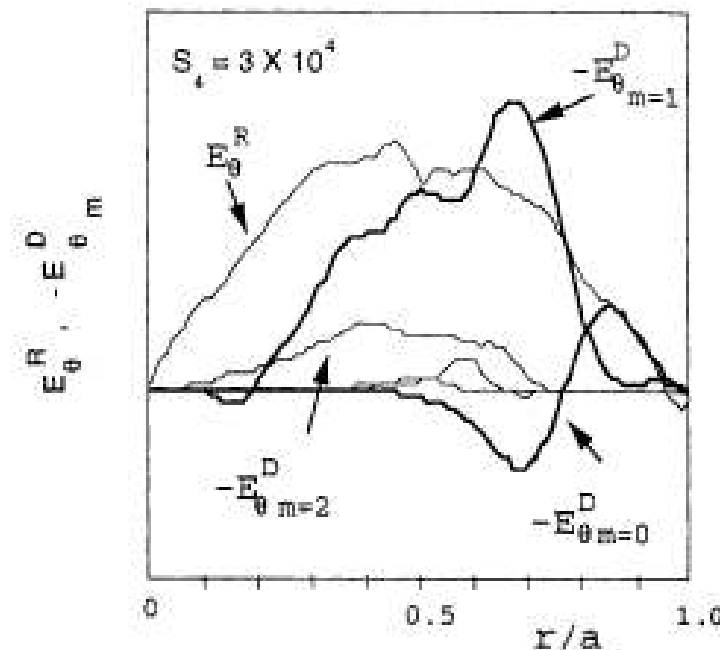
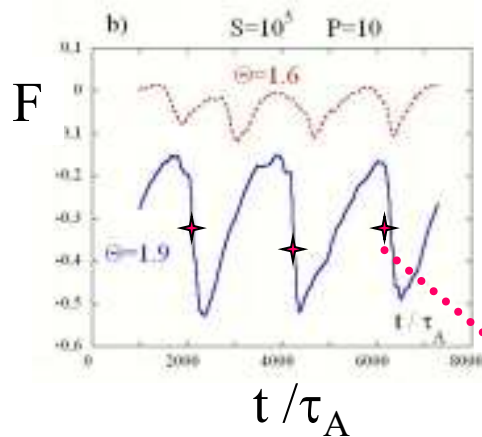


FIG. 9. Poloidal electric field along the radius: resistive and dynamo contributions:  $E_\theta^R(r)$  and  $-E_{\theta,m}^D(r)$ .

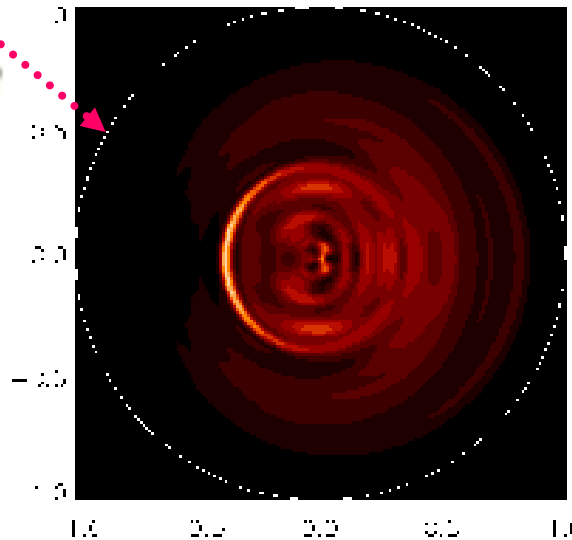
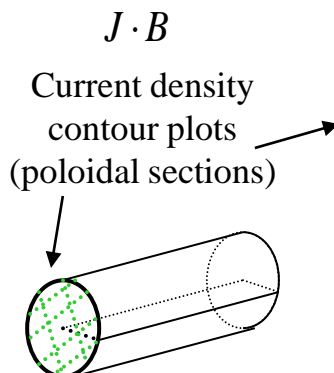
different  $m$  modes in the  $S = 3 \times 10^4$  case.  $E_\theta^D$  balancing the resistive term  $E_\theta^R(r) = \eta J_\theta$  in Ohm's law. The  $m = 1$  modes give the largest contribution to  $E_\theta^D$  over the major part of the plasma radius, but the  $m = 0$  contribution becomes comparable in amplitude in the outer half of the radius and, in particular, by changing sign in the vicinity of the reversal is the

MH regime:

Nearly-periodic relaxation events



(similarly to low current experimental observations)



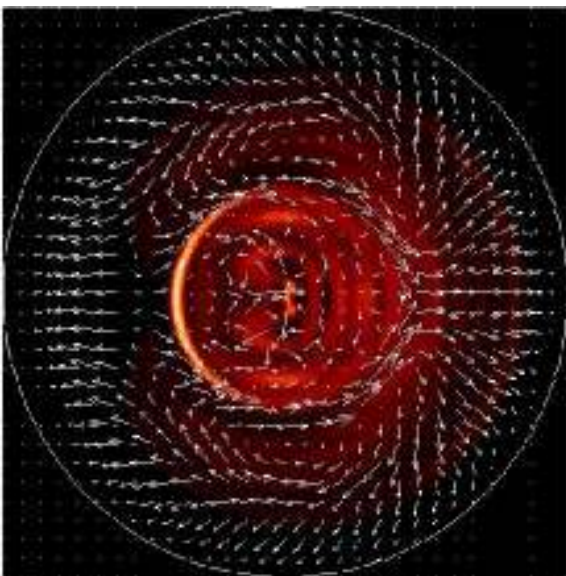
with formation of current sheets

(3D: all of the  
modes  
contribute)

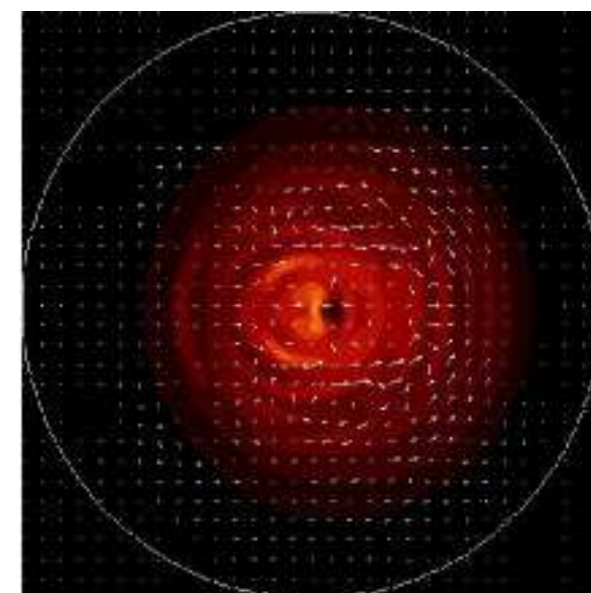
Bright colour =>  
high current

Cappello & Biskamp Nucl Fus 1996

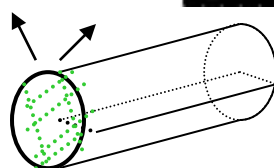
## $J \cdot B$ contour plot and flow pattern



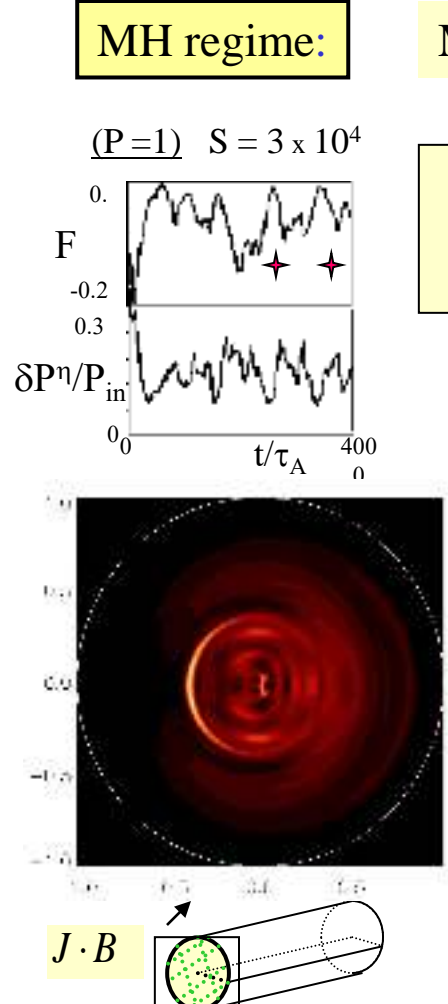
during RFP relaxation event



... in between relaxation events



Bright colour => high current



## MHD Reconnection and scaling laws

Cappello & Biskamp Nucl Fus 1996

**Quasi-periodic relaxation events  
with formation of current sheets (3D)**

NUMERICAL  
scaling law

$$\delta B \sim S^{-0.22}$$

( $P=1$ )

$$\delta B \sim S^{-1/4} (= H^{-1/4})$$

(at constant  $P$ )

...  $P \neq 1$  ...  
+  
RFX data  
→

ARGUMENT:

Sweet-Parker reconnection  
 $(\delta v_{perp} / \delta B = S^{-1/2})$   
dominates RFP dynamics

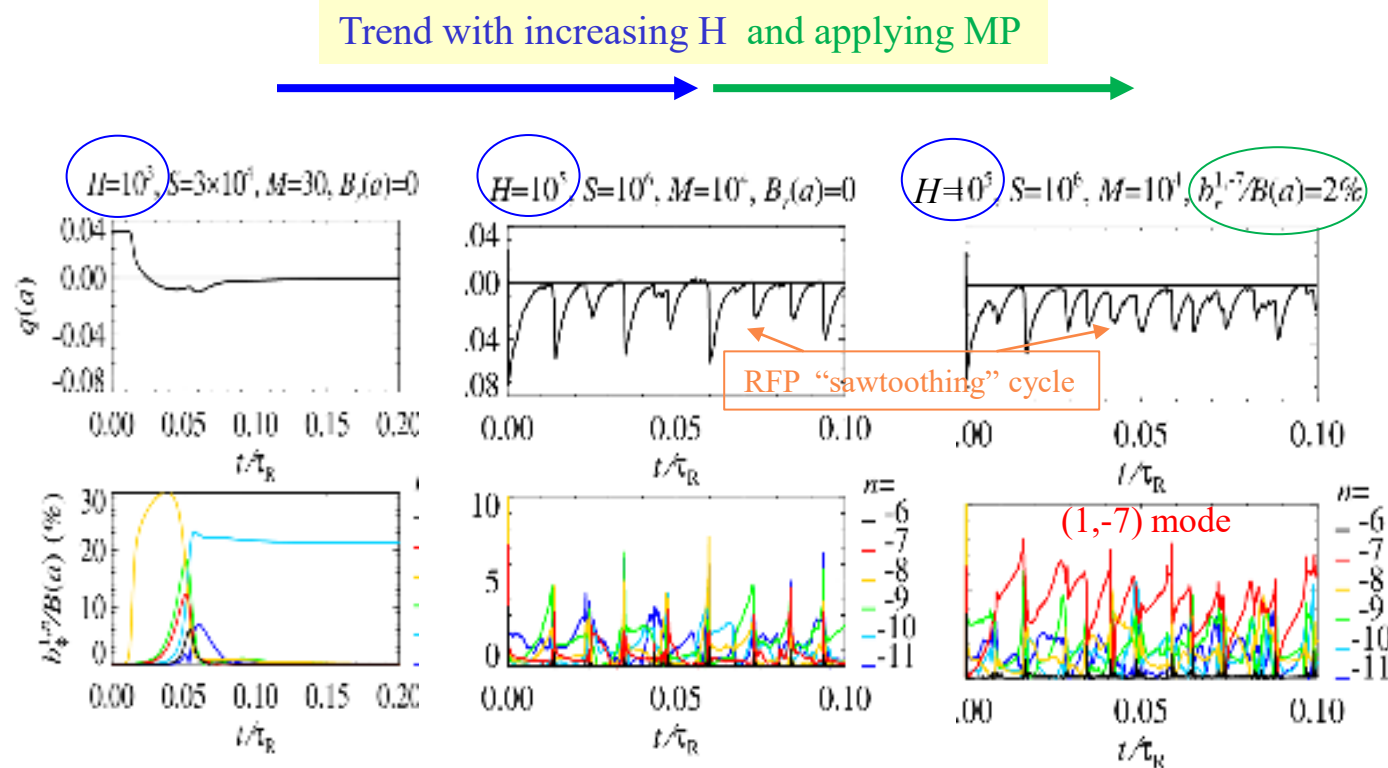
$$(S^{-1} J_{\theta 0} = \langle \delta v \times \delta B \rangle_{\theta \text{ at reversal}})$$

ITG turbulent  
viscosity may  
characterize  
the RFPs

Terranova et al. PPCF 2000

# 3D nonlinear MHD

## Reversed Field Pinch in viscoresistive SpeCyl simulations: + MP (1,-7)



Similar to RFX-mod discharges at  
“intermediate” values of plasma current

# 3D nonlinear MHD

**Circular tokamak** in viscoresistive SpeCyl simulations: + MP  $(1,1)$

Snake like (high dissipation)  $\rightarrow$  periodic sawtoothing (low dissipation)

approaching snake (**same dissipation but MP applied**)

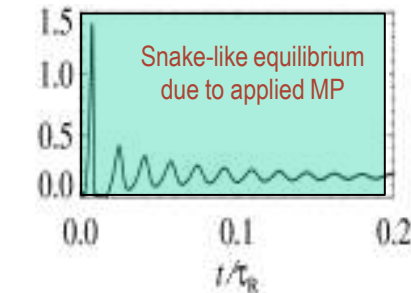
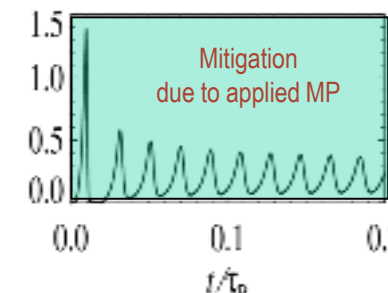
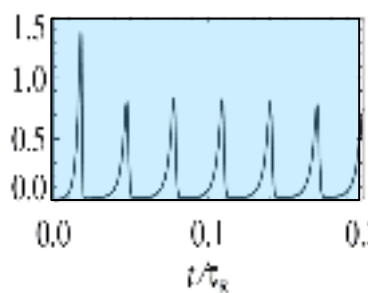
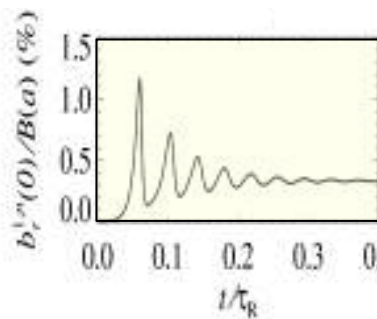
Trend with increasing  $H$  and applying MP

$$H=5.7 \times 10^3, S=10^5, M=23, B(a)=0$$

$$H=1.8 \times 10^4, S=10^5, M=330, B(a)=0$$

$$H=1.8 \times 10^4, S=10^5, M=330, b_r^{1/2}B(a)=0.1\%$$

$$H=1.8 \times 10^4, S=10^5, M=330, b_r^{1/2}B(a)=0.3\%$$



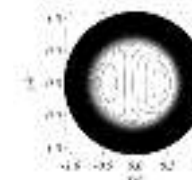
Dissipation & MP produce similar dynamical effects as in RFP

Bonfiglio, Chacon, Cappello PoP 2010

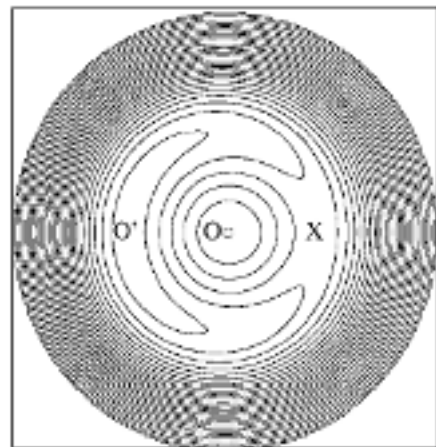
Bonfiglio, Escande , Zanca, Cappello NF 2011

Veranda, Bonfiglio Cappello et al EPS 2012

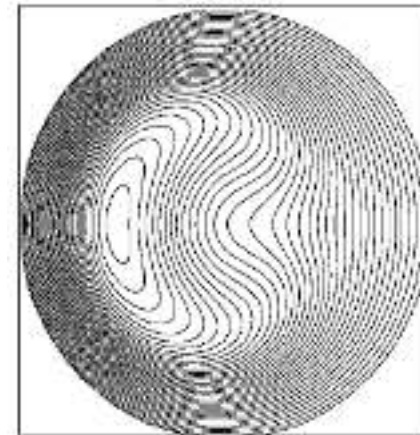
Bonfiglio, Veranda , Cappello et al PPCF 2015



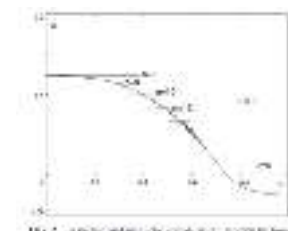
When QSH dominant mode GROWS: separatrix expulsion occurs, and



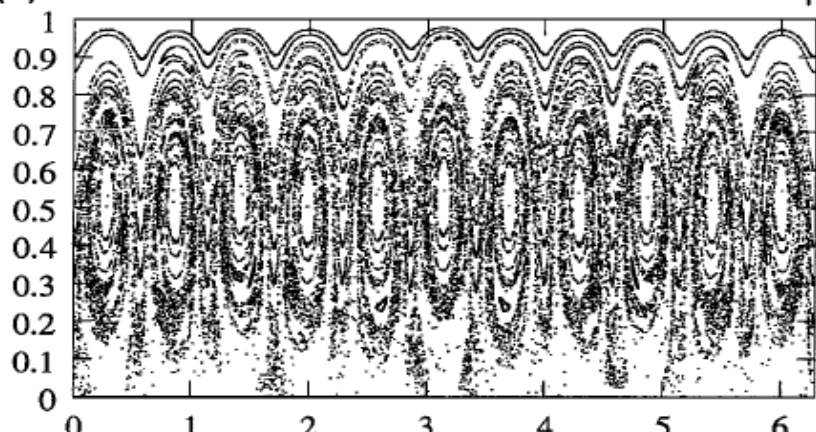
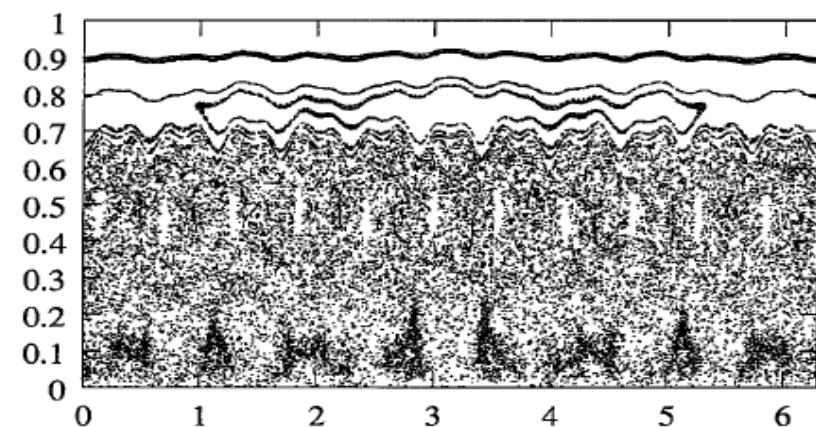
(a)



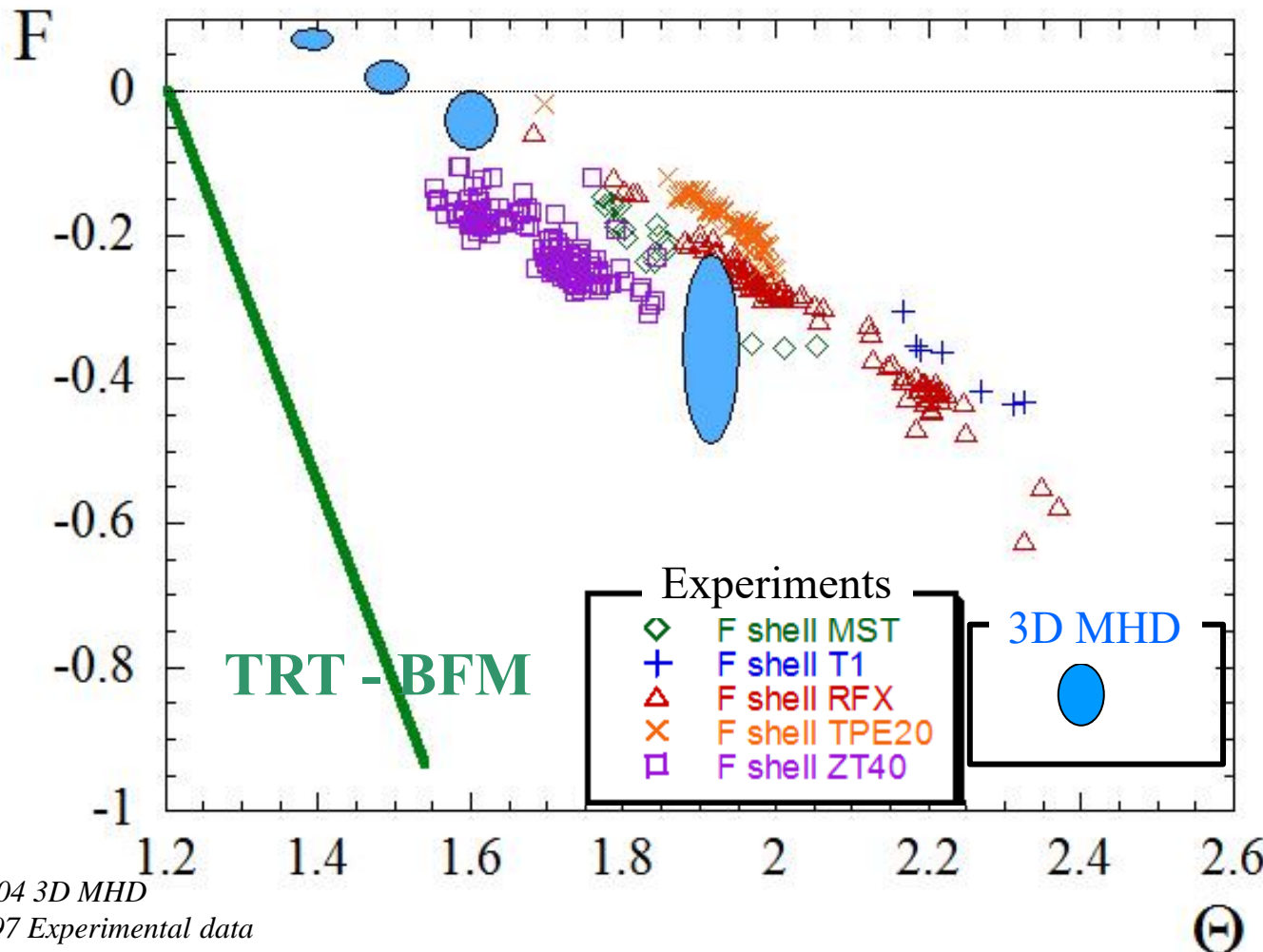
(b)



...clean helical topology emerges



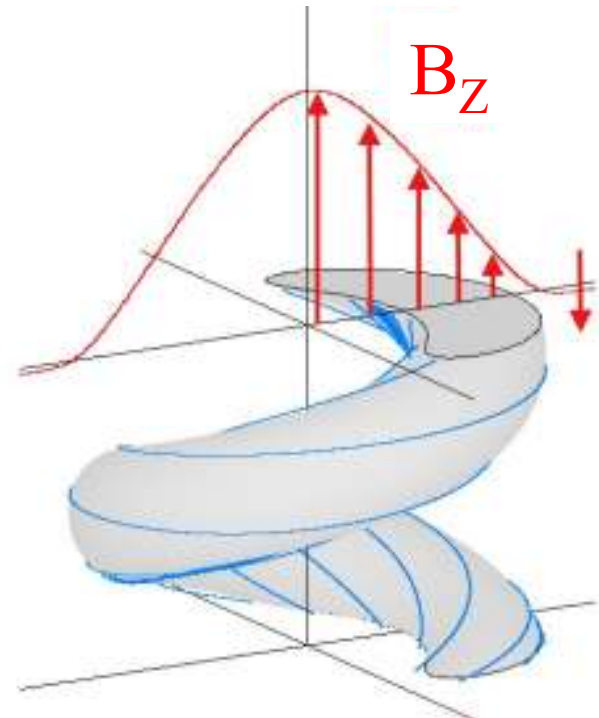
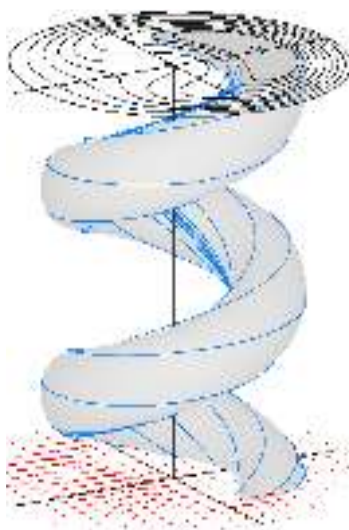
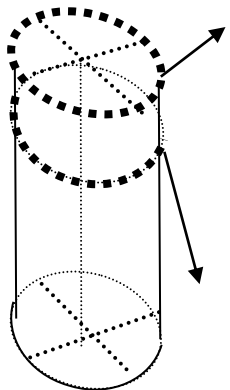
# Comparison “operational points”: Numerical modelling – Experiments - Taylor’s Theory



A finite radial magnetic field component at the boundary was suggested to favour attainment of helical ohmic equilibrium (Helical Grad-Shafranov problem)

## Magnetic flux surfaces & field lines

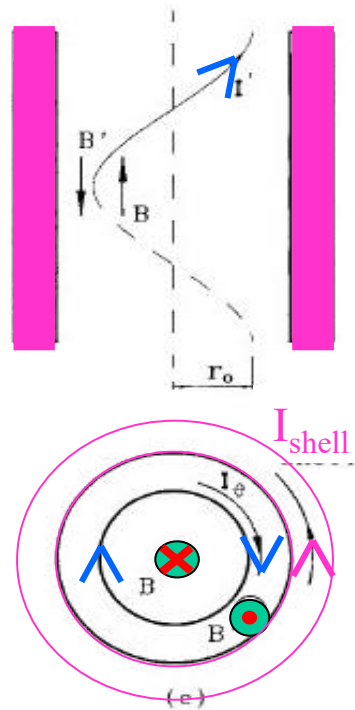
... and corresponding reversed mean profile of  $B_Z$



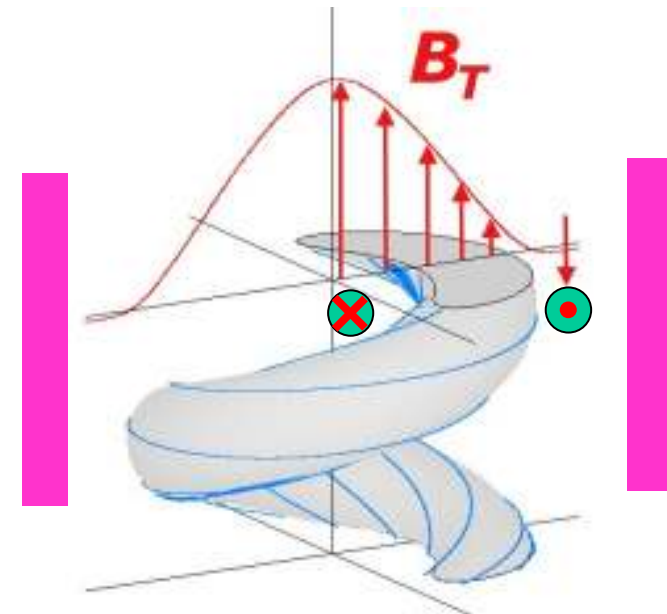
note the **velocity field** (red arrows), it is a helical pinch  
it provides the Edynamo = coherent modulation  $\langle \delta v \wedge \delta B \rangle$ )

→ drift velocity induced by the electrostatic potential ...

# SH solutions resemble the toy model



kinked wire



SH in viscoresistive modelling

# Nearly-periodic relaxations QSH akin to experimental ones

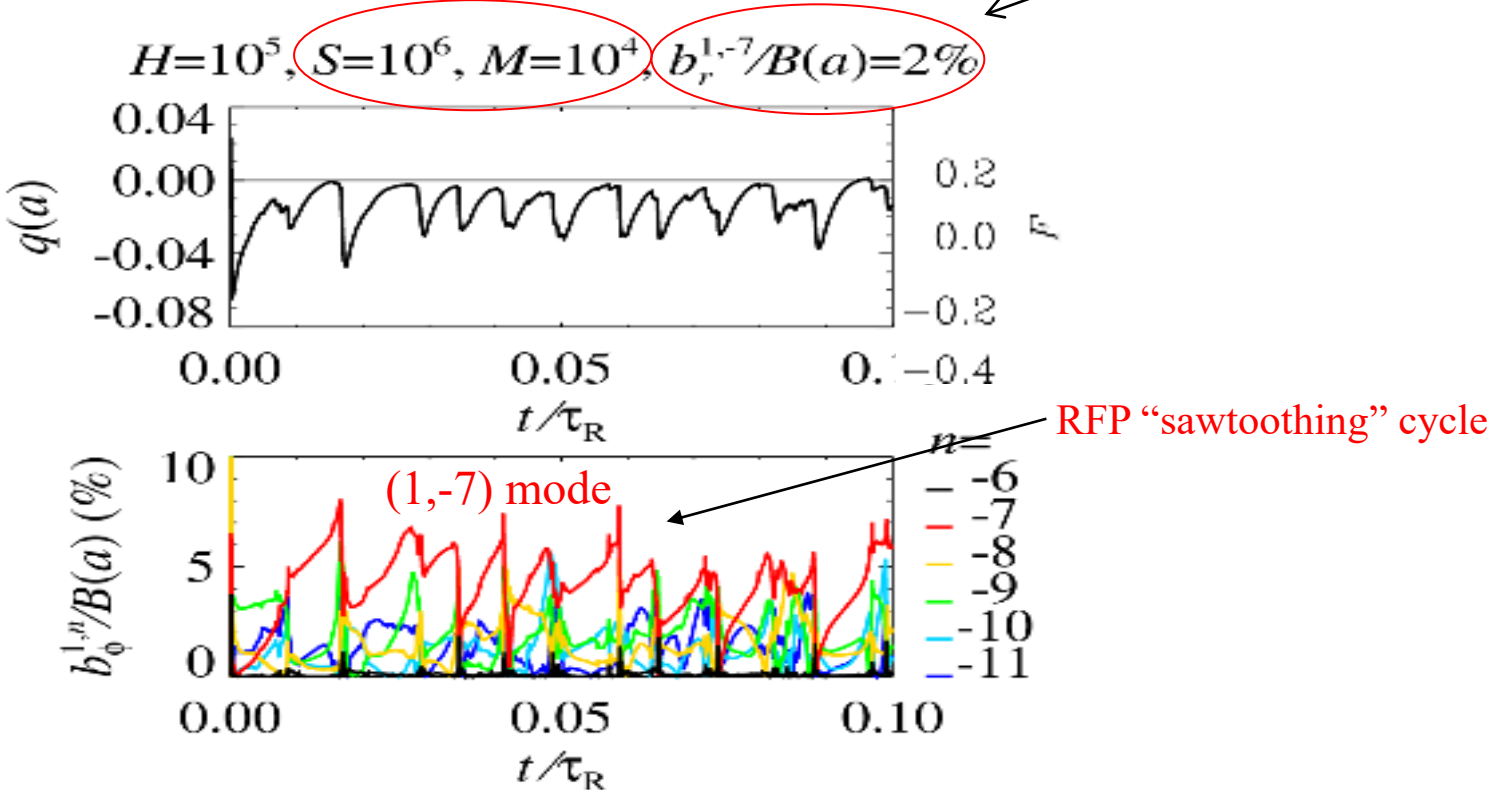
with MP (1,7)

(Ideal wall + MP)

Typical RFP sawtoothing

Mode amplitude

Bonfiglio NF 2011  
Veranda PPCF 2013  
Bonfiglio PRL 2013

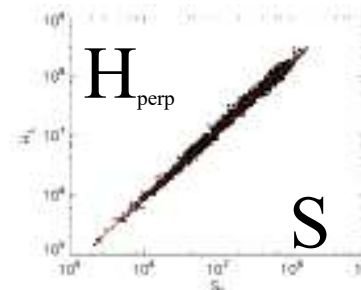
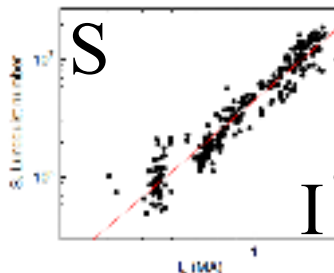


The amplitude of secondary modes decreases with Lundquist, S, and Hartmann H

**The threshold MP% to excite a dominant mode decreases with S (H) too,  
... explains the experimental trend of the helical regime emerging clearly at high currents.**

RFX-mod:  
 $I \geq 1\text{MA}$   
 $S \geq 5 \cdot 10^6$

Piovesan,  
Zuin et al  
NF 2009



Vivenzi, Spizzo, Veranda,  
Bonfiglio, Cappello et al  
Theory Fusion Plasmas  
Varenna 2022



CONSORZIO RFX  
*Ricerca Formazione Innovazione*

CENTRO RICERCHE FUSIONE

1222-2022  
**800**  
ANNI



UNIVERSITÀ  
DEGLI STUDI  
DI PADOVA

*Ph.D. Programme in Fusion Science and Engineering*

## Advanced course on Plasma Physics and Diagnostics (AC1)

Padova, Nov. 29<sup>th</sup> 2024

# Physics of NBI heating and current drive

P. Vincenzi\*

[pietro.vincenzi@igi.cnr.it](mailto:pietro.vincenzi@igi.cnr.it)

\*Consorzio RFX, Padova

\*CNR – ISTR, Padova

**Disclaimer:** The material and contents of this lesson are intended for personal use only and should not be reproduced or distributed (also electronically) outside the present Ph.D. Programme, except upon prior request.

# Contents

- Introduction
  - H&CD systems
  - Neutral Beam Injection (NBI)
- NBI: from generation to the plasma
  - Neutral beam generation
  - Neutral beam ionization
  - Fast ion orbits and slowing down
- Beam energetic particle losses
- NBI modelling techniques
- Conclusion

A special acknowledgement to Chiara De Piccoli for helping me with the material in this presentation



# Contents

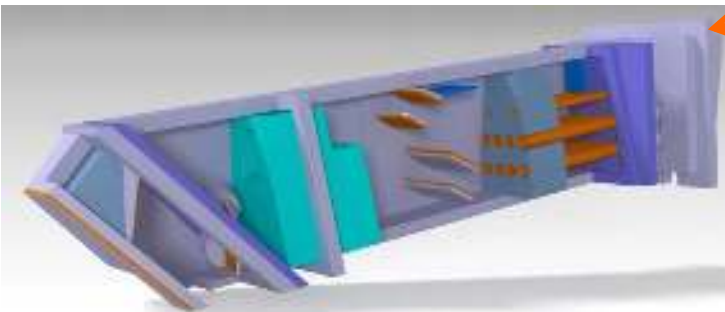
- **Introduction**
  - **H&CD systems**
  - **Neutral Beam Injection (NBI)**
- NBI: from generation to the plasma
  - Neutral beam generation
  - Neutral beam ionization
  - Fast ion orbits and slowing down
- Beam energetic particle losses
- NBI modelling techniques
- Conclusion



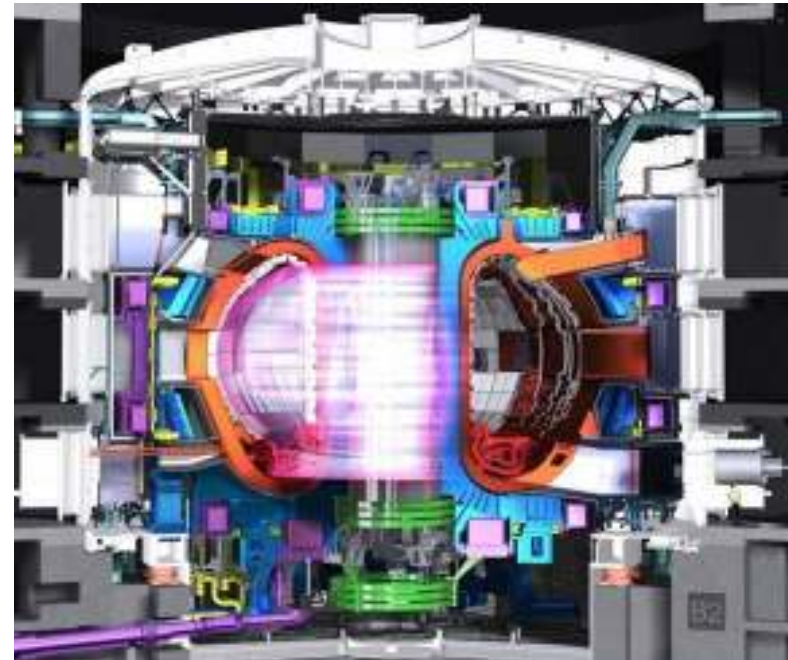
# The “additional” H&CD systems

ITER will use the so-called “additional” heating (& current drive) systems

Electron Cyclotron (EC) ITER Launcher

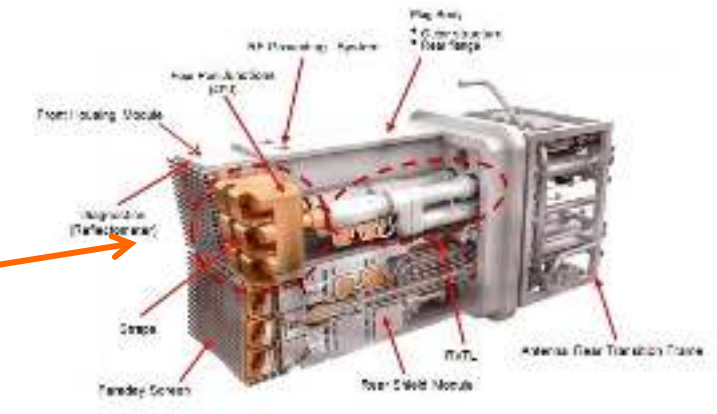


Radio Frequency Systems

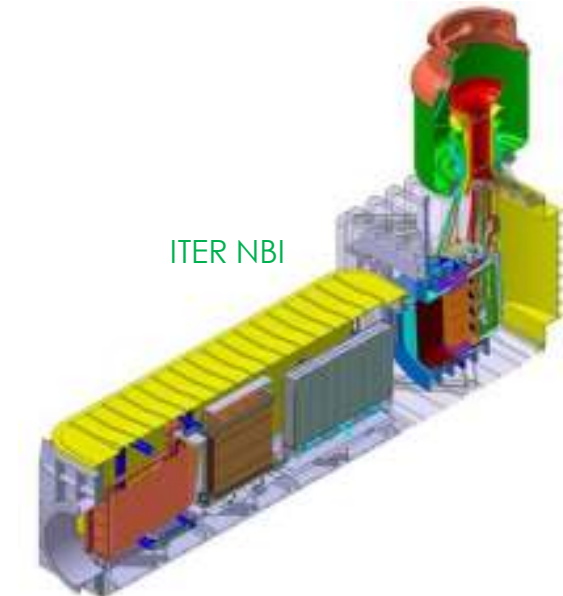


\*Lower Hybrid Current Drive (LHCD)  
system is not part of the ITER  
construction baseline

Images from [www.iter.org](http://www.iter.org), [www.inr.kit.edu](http://www.inr.kit.edu)



Ion Cyclotron (IC) ITER Antenna



ITER NBI

Neutral Beam Injection (NBI)



# A step back...

## **Additional to...what?**

- Let's assume here we are dealing with toroidal pinches (tokamak, RFP, ...). Initial considerations on stellarator devices would be a bit different.
- We will mention mainly **3 actions**: **heating**, **current drive**, and **momentum injection**. Spend some moments and try to think what this means in a plasma.
- There are fundamental quantities that can be linked to these actions:
  - heating → **temperature (T)**
  - current drive → **current density (j)**
  - momentum drive → **plasma fluid rotation (W)**
- You will see that not only average values, but also **radial profiles** (and their time evolution!) are important to understand H&CD role.



# 0D power balance

0D power balance in stationary conditions

$$P_{\text{aux}} + P_a + P_{\text{ohmic}} = P_{\text{loss}}$$

$P_{\text{aux}}$  = External heating sources

$P_a$  = Alpha power ( $\sim 1/5 P_{\text{fus}}$ )

$P_{\text{ohmic}}$  = Ohmic power

$P_{\text{loss}}$  = Power losses (radiation, conduction)

J. D. Lawson, (1957) Proc. Phys. Soc. B 70 303

Current experiments (tokamaks):

$$P_a \sim 0$$

$$\rightarrow P_{\text{aux}} + P_{\text{ohmic}} = P_{\text{loss}}$$

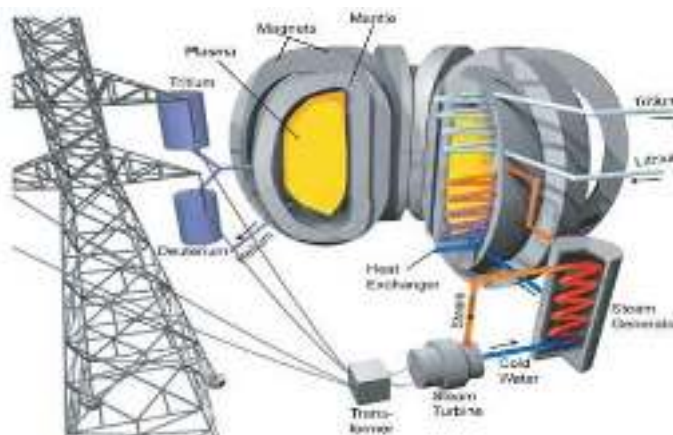


JT-60SA experiment

Future reactors:

Aiming at ignition (plasma self-sustainment)

$$\rightarrow P_{\text{ohmic}} \text{ negligible}, P_{\text{aux}} = 0 \rightarrow P_a = P_{\text{loss}}$$



P. Vincenzi – Physics of NBI heating and current drive



# 0D power balance

0D power balance in stationary conditions

$$P_{\text{aux}} + P_a + P_{\text{ohmic}} = P_{\text{loss}}$$

$P_{\text{aux}}$  = External heating sources

$P_a$  = Alpha power ( $\sim 1/5 P_{\text{fus}}$ )

$P_{\text{ohmic}}$  = Ohmic power

$P_{\text{loss}}$  = Power losses (radiation, conduction)

J. D. Lawson, (1957) Proc. Phys. Soc. B 70 303

Current experiments (RFP):

If  $P_{\text{aux}} = 0$  and  $P_a \sim 0$

$$\rightarrow P_{\text{ohmic}} = P_{\text{loss}}$$

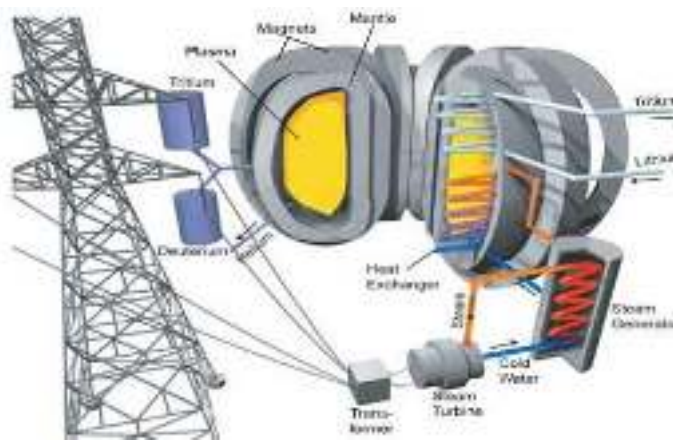


RFX-mod experiment, IT

Future reactors:

Aiming at ignition (plasma self-sustainment)

➤  $P_{\text{ohmic}}$  negligible,  $P_{\text{aux}} = 0 \rightarrow P_a = P_{\text{loss}}$



# 0D power balance

0D power balance in stationary conditions

$$P_{\text{aux}} + P_a + P_{\text{ohmic}} = P_{\text{loss}}$$

$P_{\text{aux}}$  = External heating sources

$P_a$  = Alpha power ( $\sim 1/5 P_{\text{fus}}$ )

$P_{\text{ohmic}}$  = Ohmic power

$P_{\text{loss}}$  = Power losses (radiation, conduction)

J. D. Lawson, (1957) Proc. Phys. Soc. B 70 303

Current experiments (stellarator):

If  $I_p = 0 \rightarrow P_{\text{ohmic}} = 0$  and  $P_a \sim 0$

$\rightarrow P_{\text{aux}} = P_{\text{loss}}$

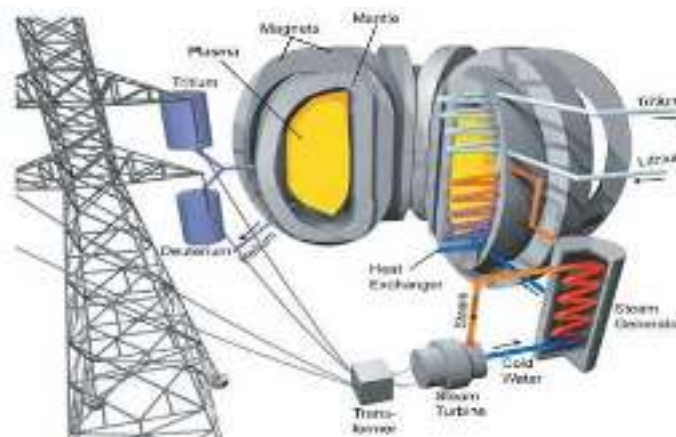


W7-X experiment, DE

Future reactors:

Aiming at ignition (plasma self-sustainment)

➤  $P_{\text{ohmic}}$  negligible,  $P_{\text{aux}} = 0 \rightarrow P_a = P_{\text{loss}}$



# Why do we need additional heating power?

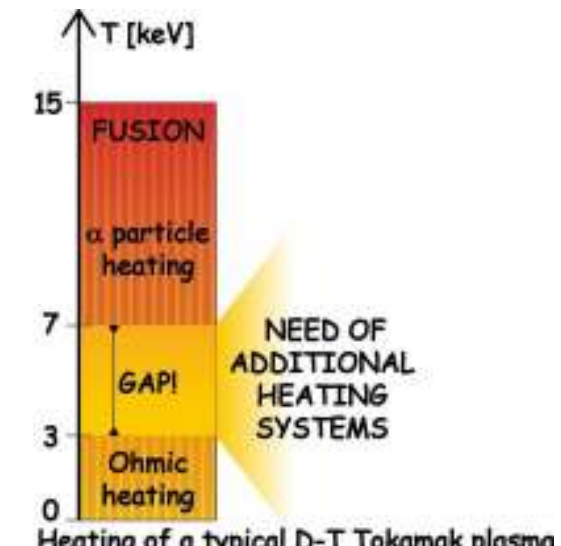
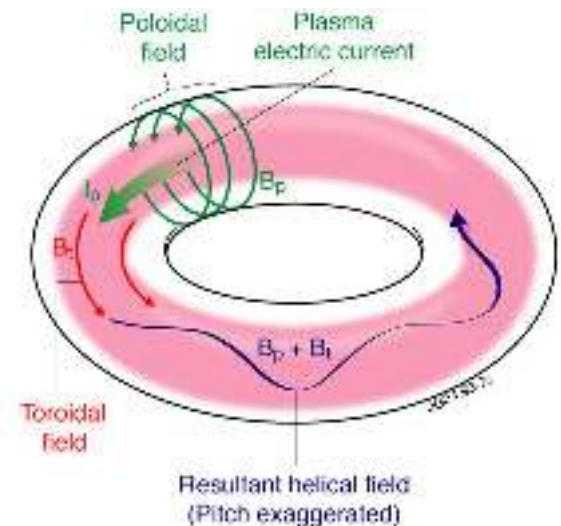
If we aim at ignition ( $P_{aux} = 0$ ), why do we need additional heating power?

Let's take a step back

- For ignition, we need to reach a high enough ion temperature ( $\sim 10 - 15$  keV)
- Alpha power becomes dominant from  $T > 5 - 7$  keV

We need additional heating to reach fusion-relevant temperatures:

- The simplest one is **ohmic heating**: plasma is a conductor
- Unfortunately, plasma **ohmic heating decreases with temperature** (due to plasma resistivity  $\propto T^{-3/2}$ )
- Maximum current for a given toroidal field is limited by MHD stability
- For typical tokamak reactor parameters, the maximum temperature reached only by ohmic heating is  $T \sim 3$  keV

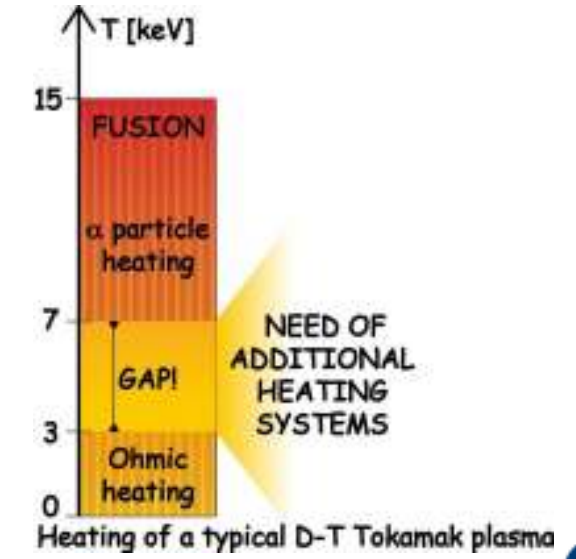
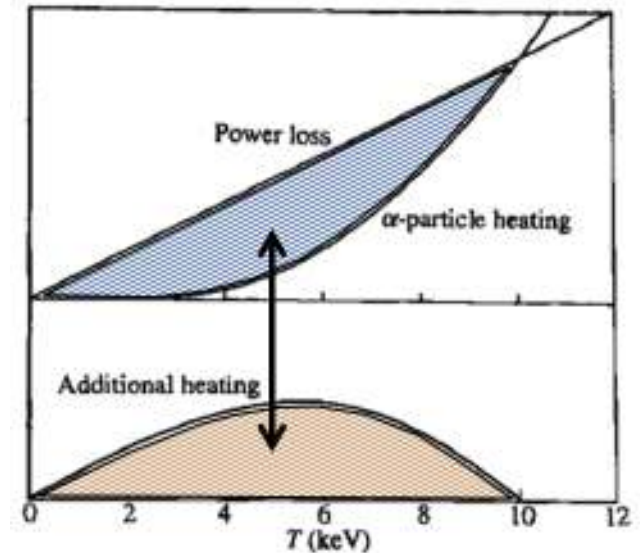


# Why do we need additional heating power?

If we aim at ignition ( $P_{aux} = 0$ ), why do we need additional heating power?

- Ohmic heating is not sufficient to reach fusion-relevant temperatures
- Access to H-mode or target confinement regimes
- Energy loss channels must be balanced, e.g.: thermal conduction, radiation (line radiation, bremsstrahlung...)

→ Additional (external) heating systems are necessary!  
(additional to self-heating by ohmic power and alpha power)



# ...not only heating

Actually, we will see that we don't only need heating for 0D power balance, but also localized heating (change of temperature radial profile) to have generally better performance and control/suppress MHD instabilities. Moreover, **additional heating systems are able** not only to heat the plasma but also **to sustain the plasma in many other ways**, if specifically designed. These capabilities are well-known and exploited in fusion experiments.

Additional H&CD systems can **drive plasma current** (both RF and NBI).

It is helpful for non-inductive plasma scenarios and to ramp-up plasma current.

Current drive (CD) is achieved:

- Accelerating a plasma species (RF systems)
- Injecting fast particles, which become fast ions with a preferential toroidal direction of their velocity (tangential NBI)

**Other general capabilities** (different system by system):

- Torque generation
- Temperature and current profile shaping
- Plasma control (instability suppression, core impurity accumulation counteraction, assisted discharge initiation and termination...)
- Plasma fuelling
- Wall cleaning and conditioning
- Stabilize MHD modes
- ...



# ...and not only Tokamaks

## Helical devices:

The main aim is to heat the plasma (no  $P_{\text{ohmic}}$ ) and balance power losses. A careful set of the systems is necessary to keep  $I_p = 0$

- [W7-X](#) stellarator: ECRH, NBI, ICRH
- [LHD](#) heliotron: NBI, ICRH, ECRH
- ...



## RFP devices:

H&CD systems mainly to increase performances (temperature, current)

- [MST](#), Madison: NBI + Electron Bernstein wave current drive
- [RFX-mod2?](#) NBI?



# H&CD system capabilities

Tasks	EC	NBI	IC
<b>Break down &amp; Plasma start up</b>	X		
<b>Plasma Current Ramp up and H-mode access</b>	X	partially	X
<b>Electron Heating</b>	X	X	X
<b>Ion Heating</b>		X	X
<b>Current drive</b>	X	X	*
<b>MHD Control (NTM &amp; ST)</b>	X	partially	
<b>Fast Particle Generation</b>		X	X
<b>Profiles Control (locally)</b>	X		X
<b>Impurity Accumulation Avoidance</b>	X	X	X
<b>Momentum injection &amp; Control</b>		X	
<b>Transport Studies</b>	X	X	
<b>Diagnostics</b>	X	X	
<b>Wall Cleaning</b>	X		X

\*fast, low frequency, ICRF waves, low efficiency



# Neutral Beam Injection (NBI)

In this lesson we will focus on **Neutral Beam Injection (NBI)** and particularly on the interaction of this system with the plasma.



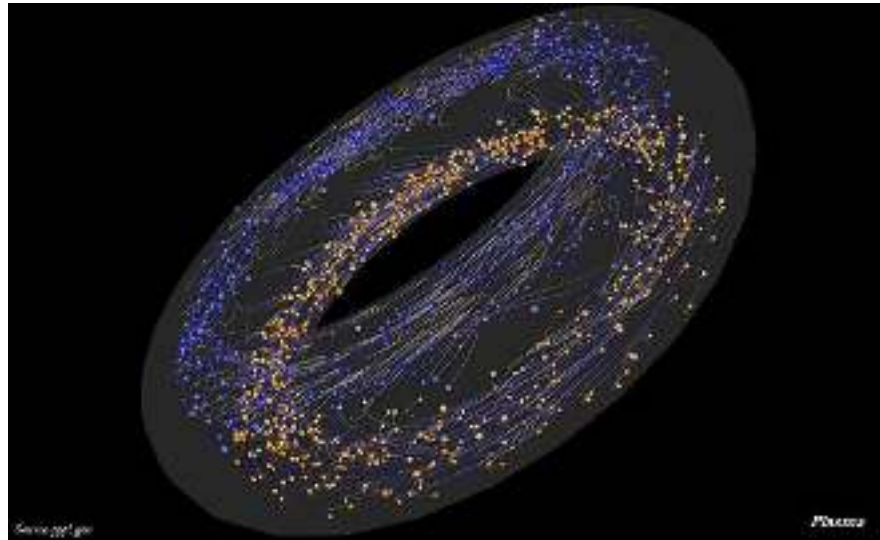
Interaction of the NBI with the plasma (this lesson)

NBI system (here only a few words)



# Neutral Beam Injection principle

- The idea is to inject high energy particles >> energy of the plasma thermal particles
- First of all, entering beam particles must be neutral otherwise they would be deflected by magnetic fields in the plasma region (and surrounding zone).
- Fast neutral particles follow straight lines (injection direction) until they are ionized by the plasma, becoming fast ions.
- Then, thanks to Coulomb collisions, the energy is transferred to the plasma (slowing down process).
- Since “fast” electrons and ions coming from NBI neutral particles have the same injection velocity, the more massive ions carry almost all the beam energy (we will only speak about fast ions).



# NBI often dominant in experiments

	$R_0$ [m]	$a$ [m]	$I_p$ [MA]	$B_t$ [T]	Installed heating power [MW]				
					P-NBI	N-NBI	ECRH	ICRH	LH
ITER	6.2	2.0	15	5.3	-	33-50	<u>60-67</u>	10-20	-
DTT	2.19	0.7	5.5	6	-	10	<u>32</u>	8	-
JT60-SA	2.97	1.17	5	2.25	<u>24</u>	<u>10</u>	7	-	-
JET	2.96	1.25	4.8	3.45	<u>34</u>	-	-	10	7
AUG	1.65	0.5	1.2	3.1	<u>20</u>	-	5	4	-
DIII-D	1.67	0.67	2.0	2.2	<u>20</u>	-	6	8	-
EAST	1.7	0.4	1.0	3.5	8	-	4	<u>12</u>	10



# NBI is on fire!

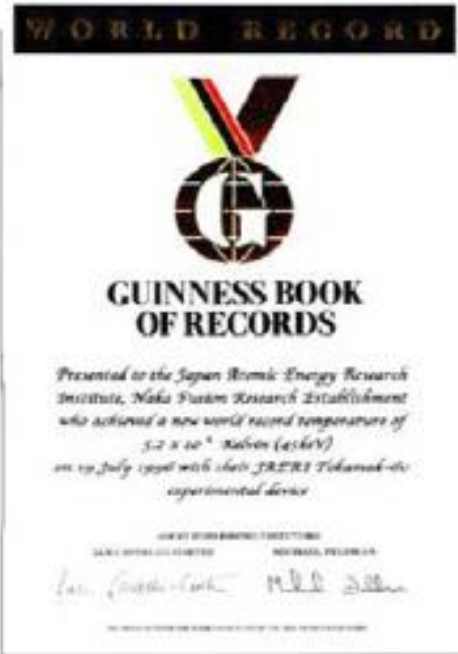
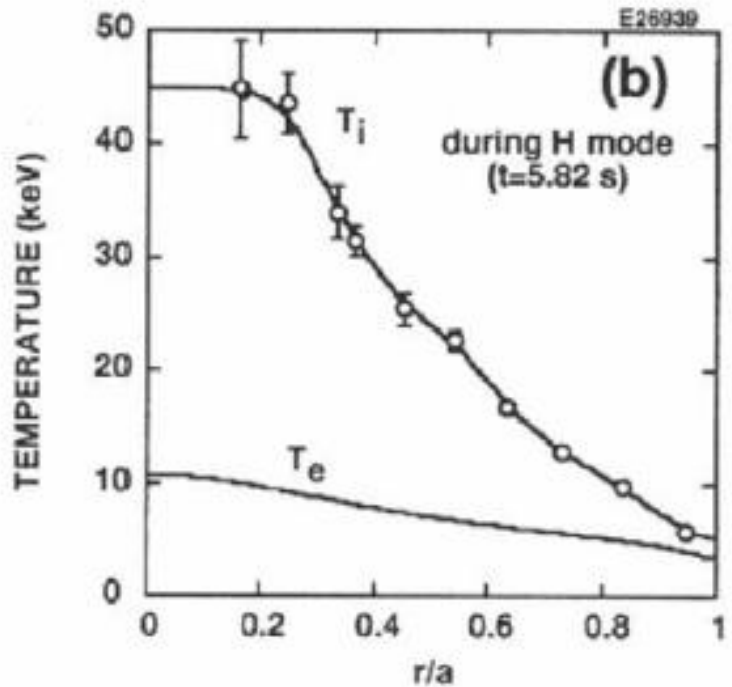


FIG. 5.12.  $T_i$  and  $T_e$  profiles for the world's highest central ion temperature in JT-60U and Guinness Book of Records on achievement of 45 keV in 1996 [5.22].

$$P_{NBI} = 27 \text{ MW}$$
$$E_{NBI} = 92 \text{ keV} \text{ (ion heating mainly)}$$



# Contents

- Introduction
- H&CD systems
- Neutral Beam Injection (NBI)
- **NBI: from generation to the plasma**
  - **Neutral beam generation**
  - **Neutral beam ionization**
  - **Fast ion orbits and slowing down**
- Beam energetic particle losses
- NBI modelling techniques
- NBI-related diagnostics



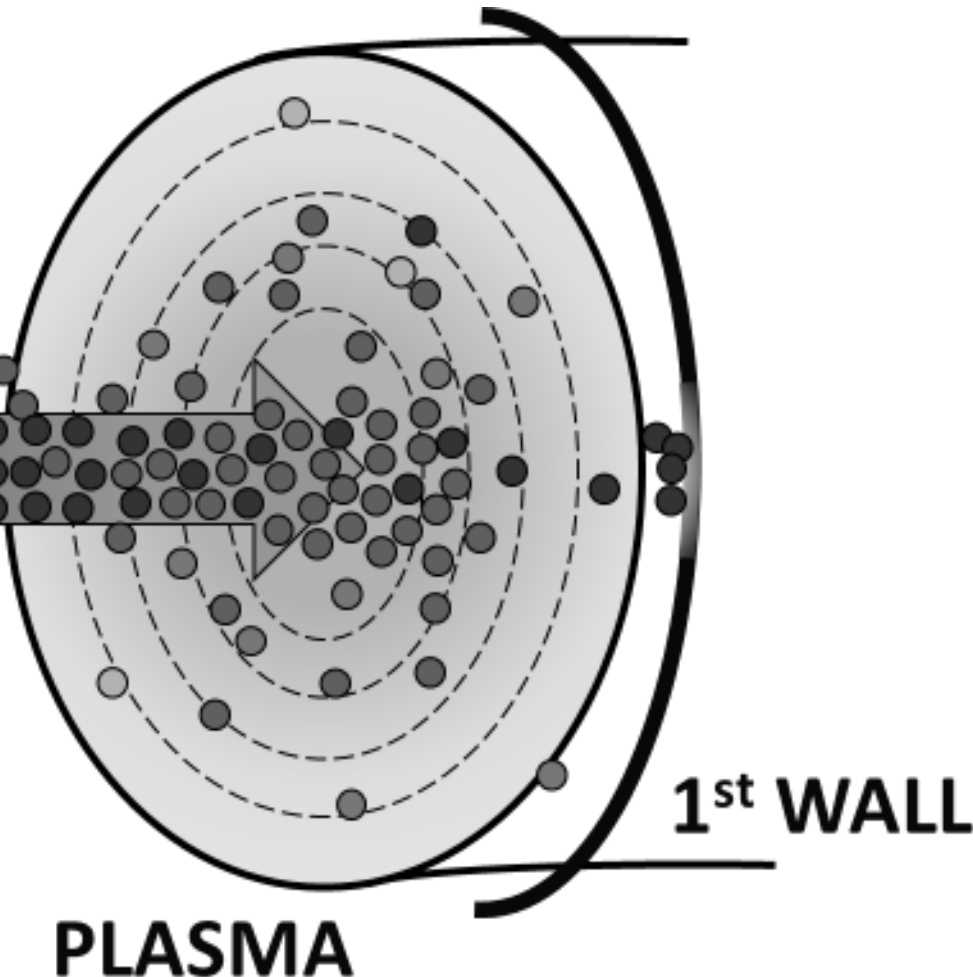
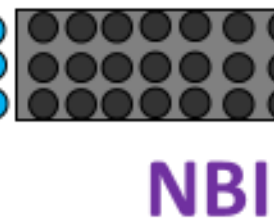
# Beam generation

● **neutral particles**

● **fast ions**

● **slowing down fast ions**

● **background neutrals**



— Neutral beam generation —

Neutral particle journey —

Beam ionization —

Fast particle slowing down →

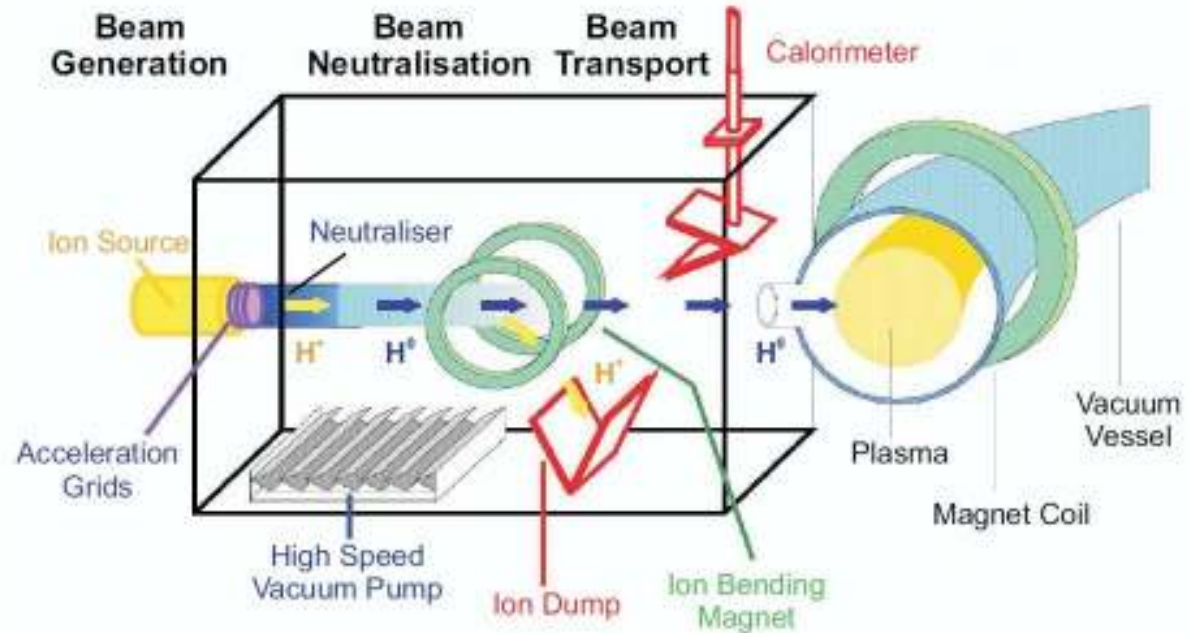


# Beam generation

This topic will be covered in AC3 course

The **NBI system** is composed by:

- Ion source (positive or negative)
- Acceleration grids
- Neutralizer
- Residual ion dump



The objective of the system is to provide a **stable** and possibly **uniform** fast particle **beam** (usually composed by several beamlets) for the duration of the plasma discharge, of a given **species**, at a selected **energy\*** and **power**, injected in a **direction** determined by the system geometry.

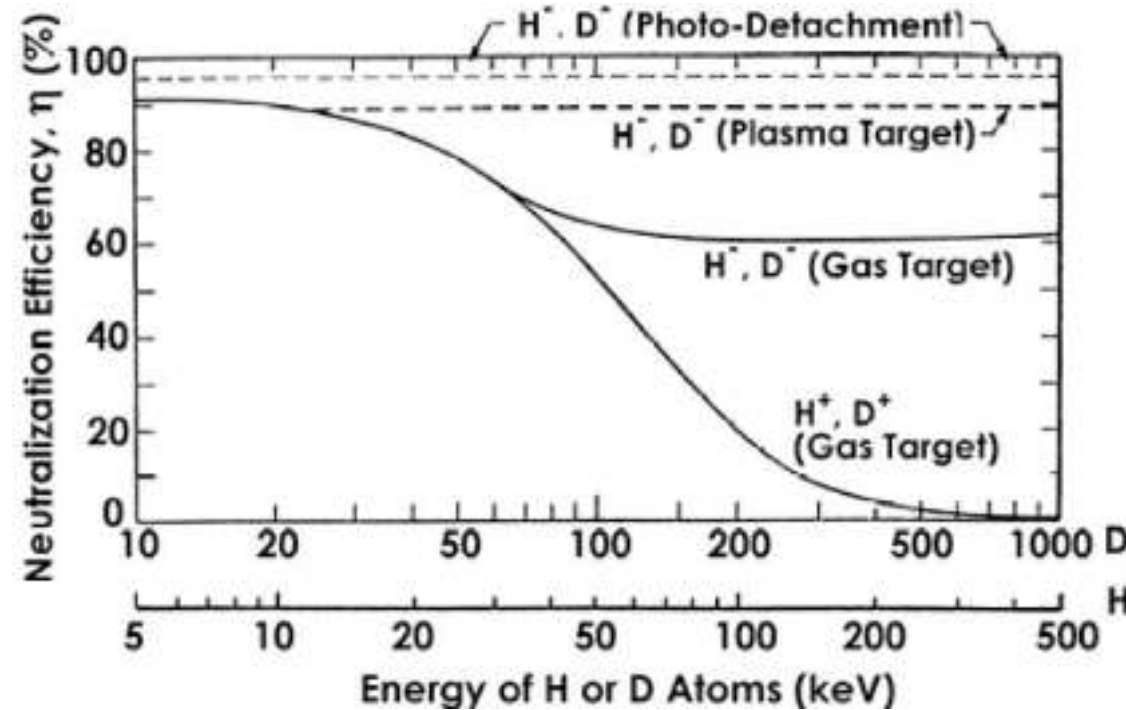
\*or energies in case of positive ion source (ionized molecules)



# Beam generation

This topic will be covered in AC3 course

NBI system: negative or positive ion source depending on the designed  $E_{NBI}$



For positive ion sources we have different energy components of the beam:

**molecular ions** are created (side effect), and are accelerated with the same voltage

→ when e.g. a molecular  $H_n$  is first dissociated and then ionized, each  $H^+$  will have energy  $E_0/n$  (shorter plasma penetration)



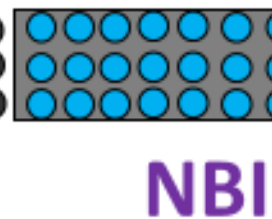
# Neutral particle journey

● **neutral particles**

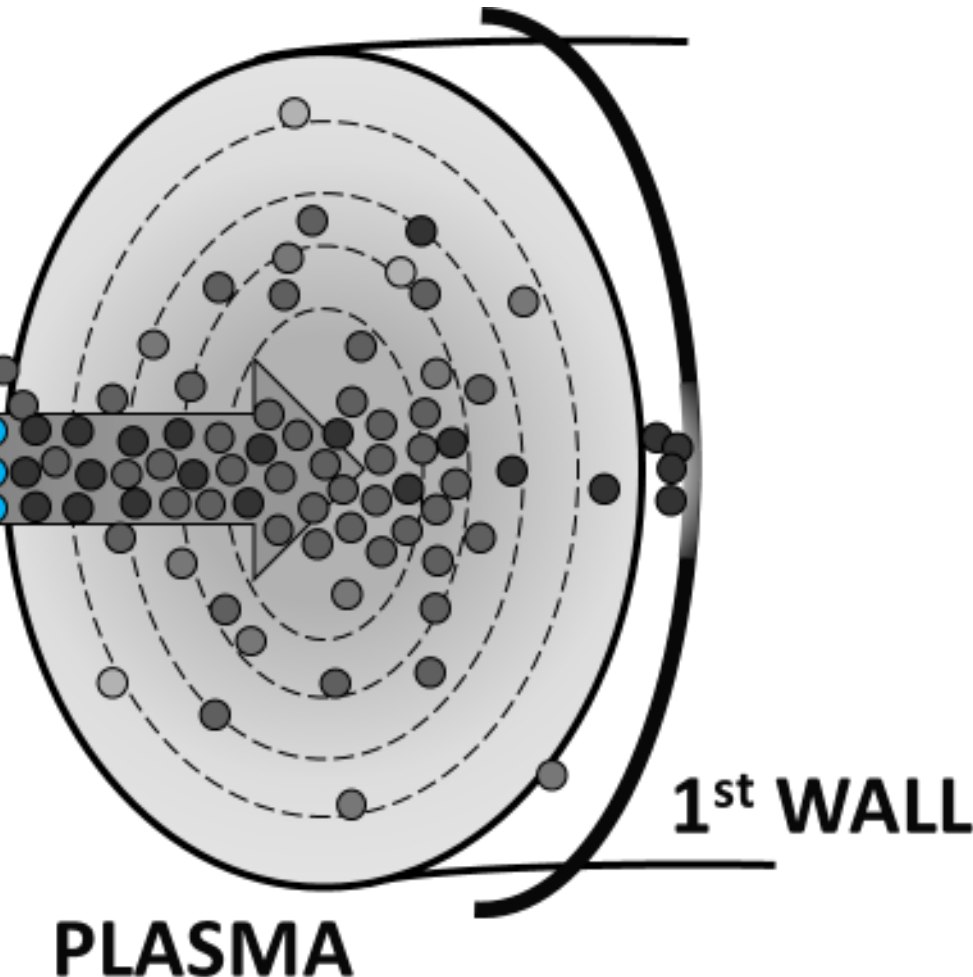
● **fast ions**

● **slowing down fast ions**

● **background neutrals**



**NBI**



— Neutral beam generation

— **Neutral particle journey**

— Beam ionization

— Fast particle slowing down

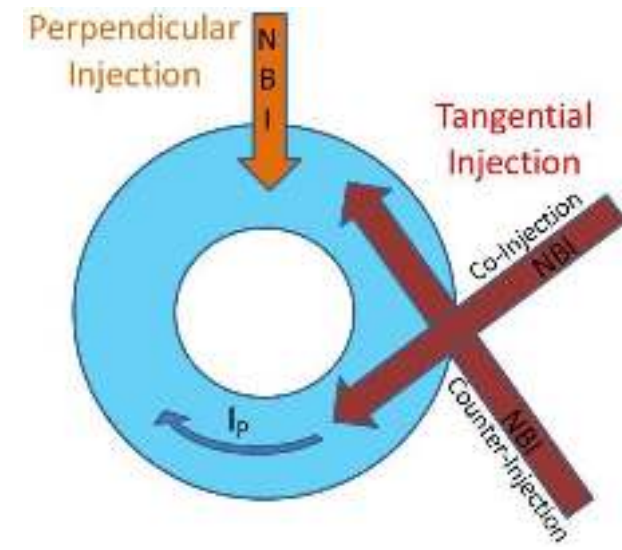
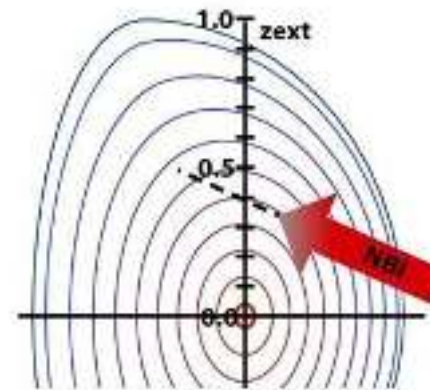
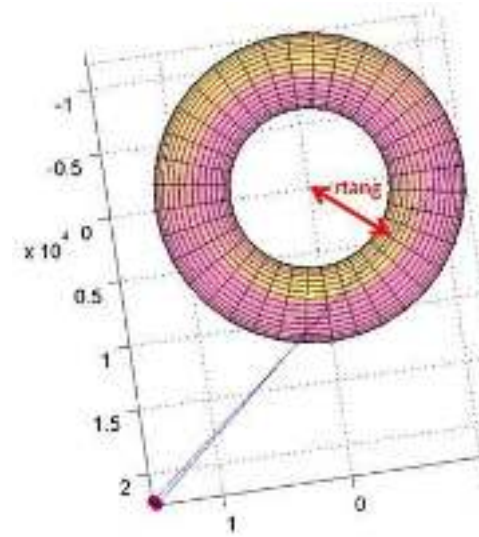


# Aimed beam of fast particles

We have a beam (usually composed of different beamlets) of fast neutral particles travelling through the **NBI system duct**, passing the **wall opening** (port) and entering the plasma.

Relevant NBI parameters from plasma point of view are:

- Energy ( $E_{NBI}$ )
- Power ( $P_{NBI}$ )
- **Injection geometry**: tangency radius, vertical tilt, beam focus, beamlet divergence



Recently some NBI systems have been designed to be able to **modulate power and energy** during the discharge, within certain constraints (e.g. in DIII-D tokamak and planned for ITER and DTT)



# How NBI parameters are chosen?

## Energy

- **Low:** small plasma/low density, high input torque
- **High:** big plasma/high density, current-drive

## Direction

- (Nearly) **Parallel** to magnetic field: longer path into dense plasma, current-drive/torque input
  - **Co-current** (usual choice): current drive, good coupling with plasma
  - **Counter-current**: counter torque/current to control rotation and plasma current, larger losses
- (Nearly) **Perpendicular** to magnetic field: technologically easier, shorter path in the plasma, risk of larger losses
- **On-axis** (usual choice): longer path through dense plasma, central heating
- **Off-axis**: current-drive



# Neutral beam ionization

● neutral particles

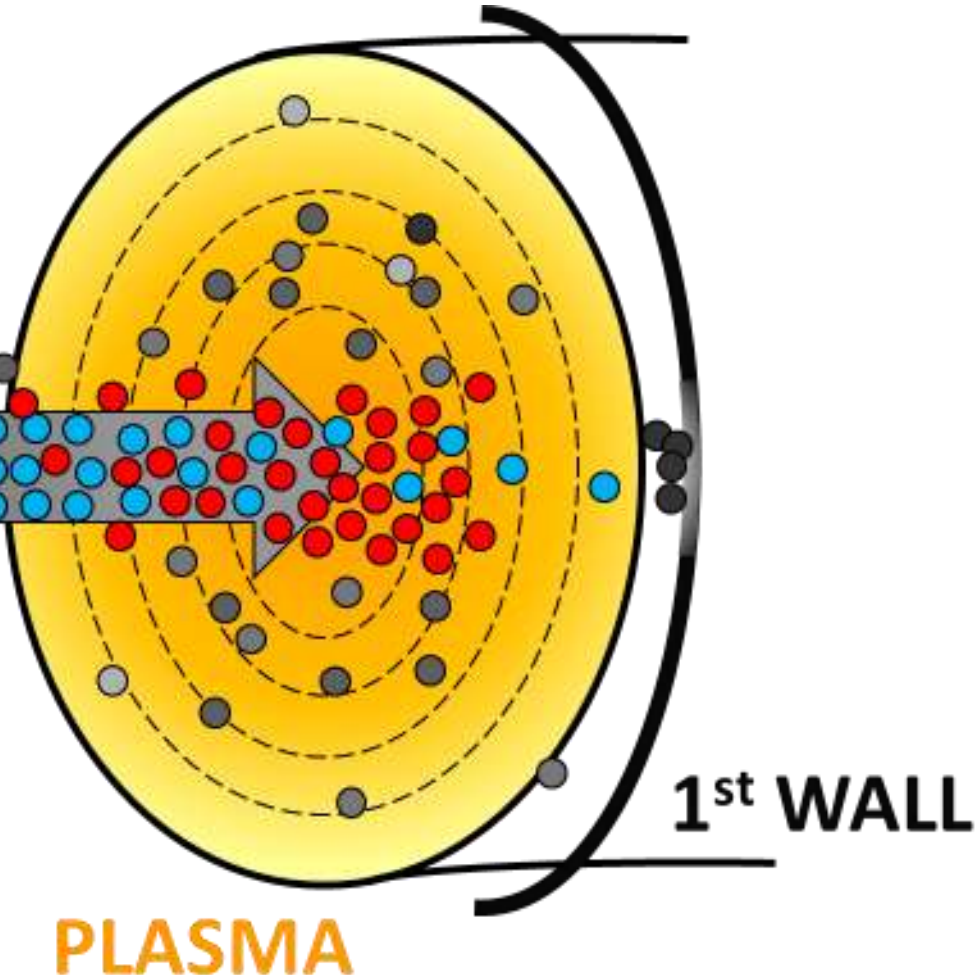
● fast ions

● slowing down fast ions

● background neutrals



NBI



— Neutral beam generation

— Neutral particle journey

— Beam ionization

— Fast particle slowing down



# Neutral beam ionization

Neutral particles from the beam are ionised in the plasma by mainly 3 processes:

- $H_0^{fast} + H^+ \rightarrow H^{+}_{fast} + H^0$  **charge exchange (CX)**
- $H_0^{fast} + H^+ \rightarrow H^{+}_{fast} + H^+ + e^-$  **ionization by ions (ii)**
- $H_0^{fast} + e^- \rightarrow H^{+}_{fast} + 2e^-$  **ionization by electrons (ie)**

The total cross section depends on the relative velocity:

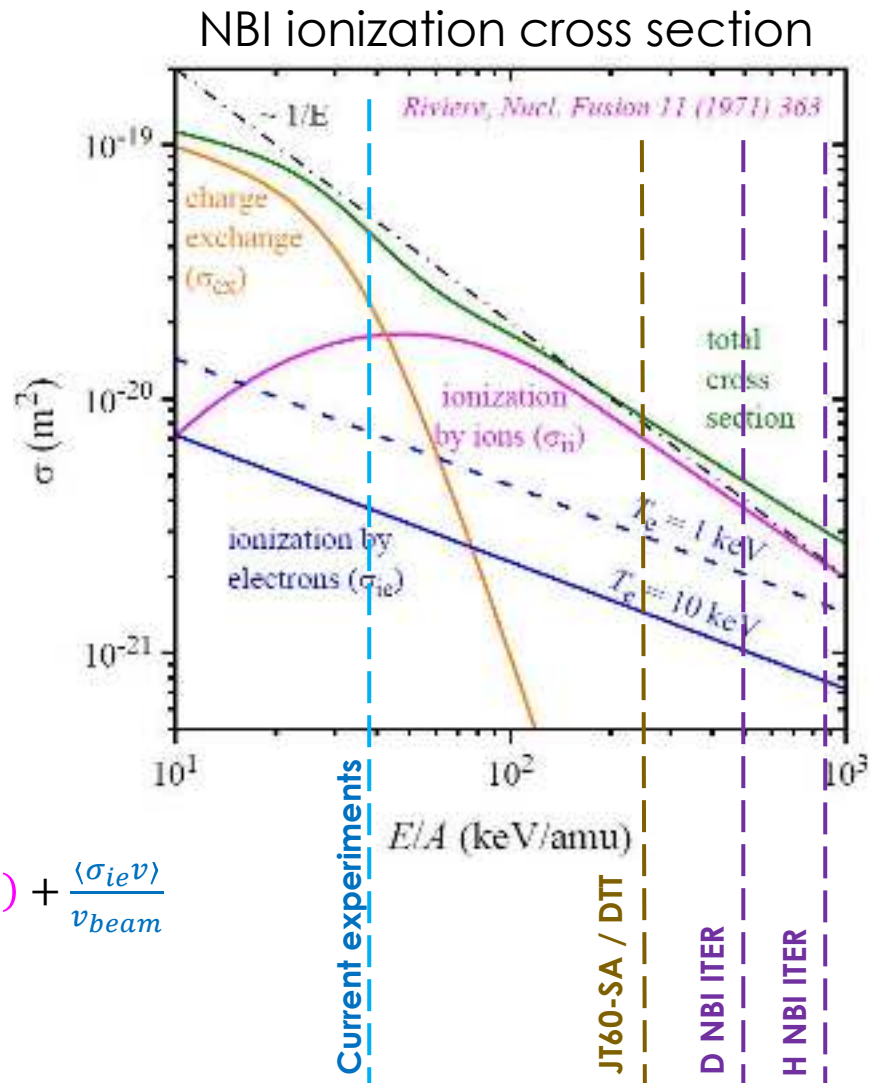
$$v_{rel} = |v_{beam} - v_{(ions/el.)}|$$
 and results:

$$\sigma_{tot} = \sum_{k=cx,ii,ie} \frac{\langle \sigma_k v \rangle}{v_{beam}} \quad \text{with} \quad \langle \sigma_k v \rangle = \frac{\int \sigma_k(v_{rel}) v_{rel} f(v_{rel}) dv_{rel}}{\int f(v_{rel}) dv_{rel}}$$

But since  $v_i \ll v_{beam} \ll v_e$  we can approximate:  $\sigma_{tot} = \sigma_{cx}(v_{beam}) + \sigma_{ii}(v_{beam}) + \frac{\langle \sigma_{ie} v \rangle}{v_{beam}}$

If the plasma rotation is not negligible:  $v_{rel} = |\vec{v}_{beam} - \vec{v}_{rotation}|$

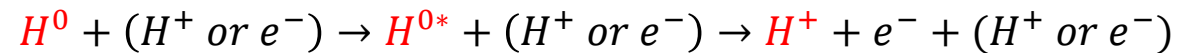
Mean free path:  $\lambda = 1/n\sigma_{tot}$  ( $n = n_i = n_e$ ,  $Z = 1$ ):  $\sigma_{tot} \sim 1/E_{NBI} \rightarrow \lambda \sim E_{NBI}/n$



# Fast ion birth

The ionization cross section is modified by two other effects:

- multi-step ionization (MSI) from **excited states**



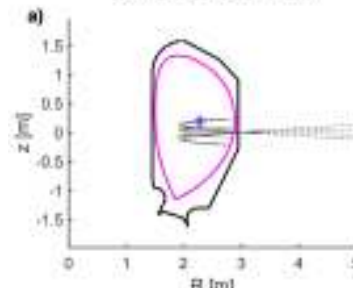
$$\rightarrow \text{Enhancement factor } \delta: \sigma_{tot_{MSI}} = \sigma_{tot}(1 + \delta)$$

$\rightarrow$  Relevant for high  $E_{NBI}$  and high density plasmas (collisional time  $\ll$  excited state lifetime)  
current small experiments, P-NBI:  $\delta < 0.2$   
ITER:  $\delta \sim 0.5-0.6$

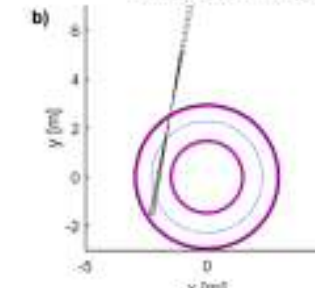
- **impurity ionization** (proportional to their concentration)

E.g.: DTT NBI ionization  
C. De Piccoli et al., 2024, Front. Phys. 12:1492095

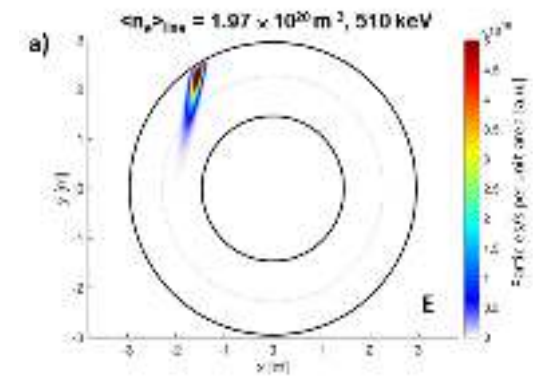
DTT NBI poloidal view



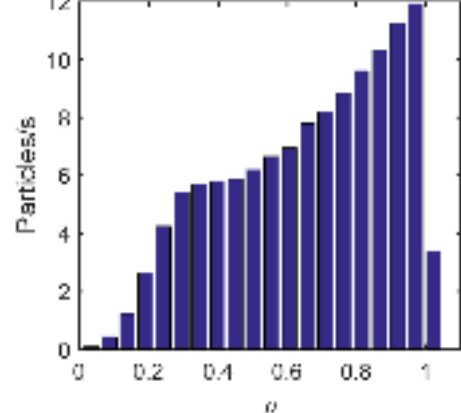
DTT NBI toroidal view



$\langle n_e \rangle_{\text{gas}} = 1.97 \times 10^{20} \text{ m}^{-3}, 510 \text{ keV}$

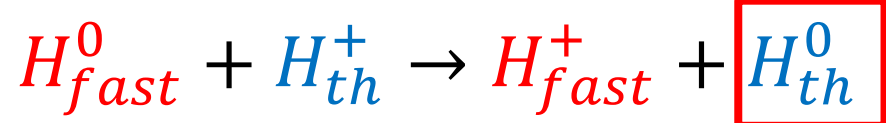


$\times 10^{12} \text{ Fast ion birth (510keV)}$

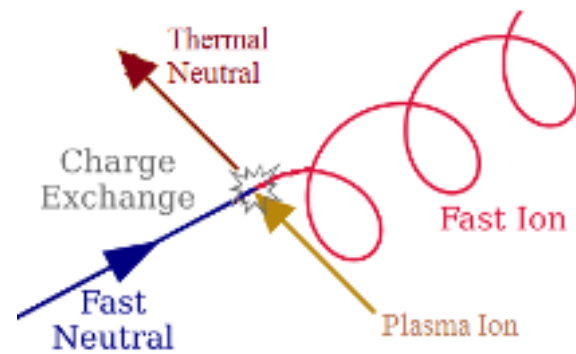


# Beam halo

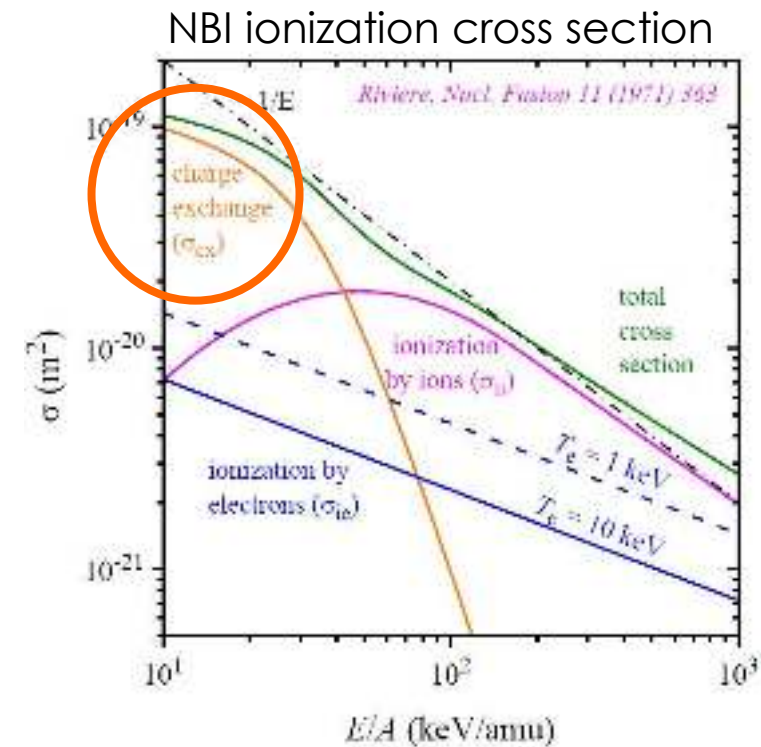
Beam halo: a side effect of CX ionization process



creation of a thermal neutral at plasma temperature



- Creation of a thermal neutral which travels ballistically and charge exchanges with other thermal ions, creating other neutrals (Halo)
- This process is then recursively repeated multiple times, producing fewer and fewer neutrals
- Halo of neutrals surrounding the neutral beam



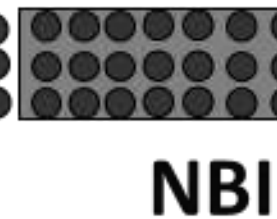
# Fast particle slowing down

- neutral particles

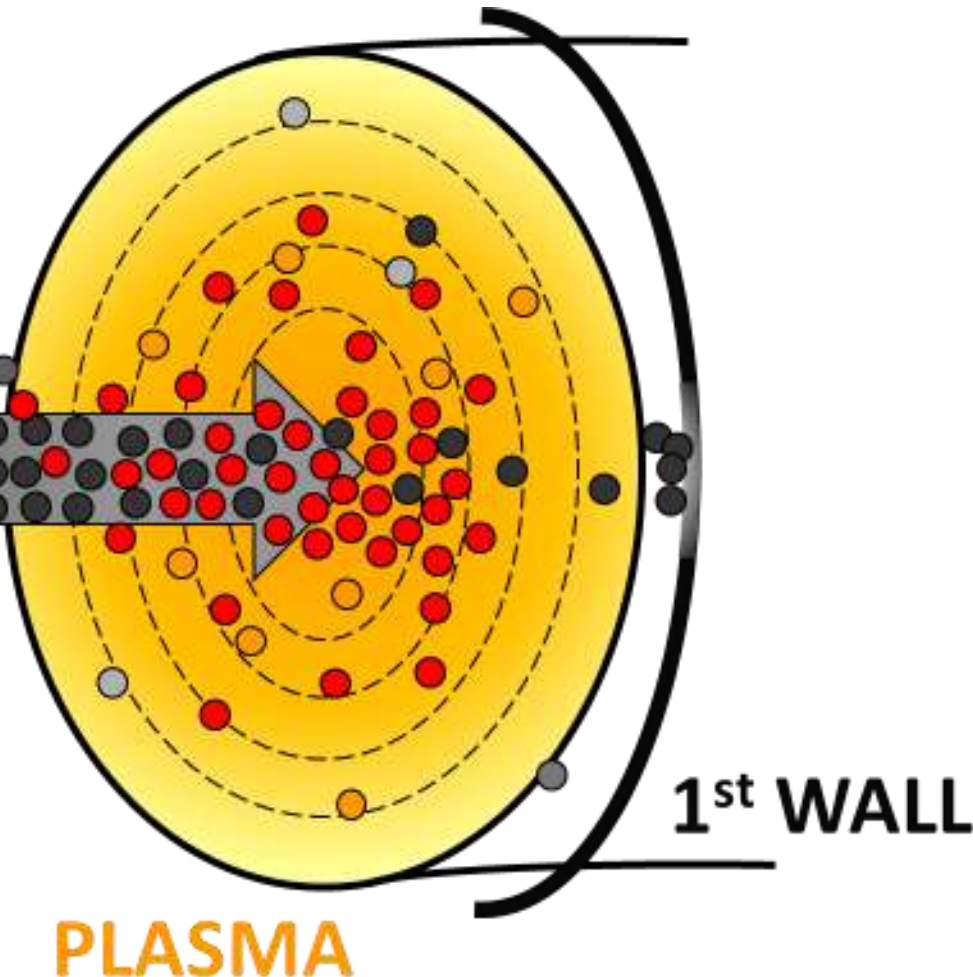
- fast ions

- slowing down fast ions

- background neutrals



NBI



— Neutral beam generation

— Neutral particle journey

— Beam ionization

— Fast particle slowing down



# Ion orbits

After NBI ionization, newly born **fast ions** start experiencing the magnetic field. What are their orbits?

(refreshing single particle motion)

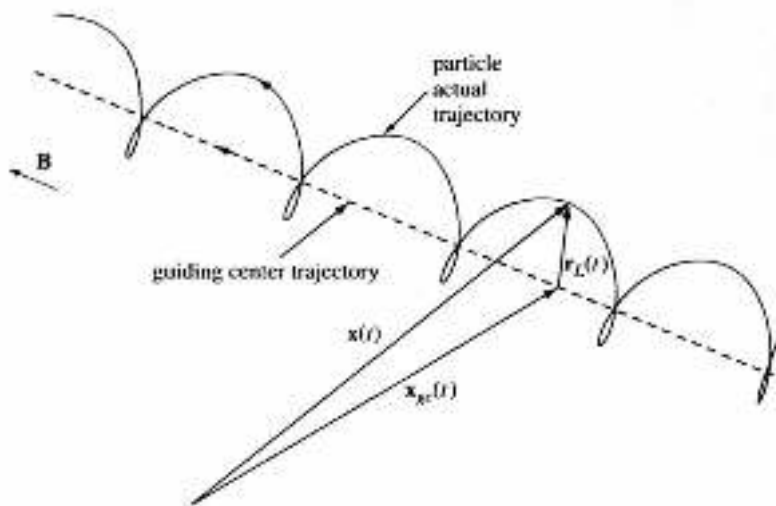
Charged particle motion into a homogeneous magnetic field  $B$ : the **Lorentz force**

Lorentz force       $m \frac{d\vec{v}}{dt} = q_e \cdot \vec{v} \times \vec{B}$

$\parallel \vec{B}$        $\frac{dv_{||}}{dt} = 0$

$\perp \vec{B}$ : Larmor radius       $\rho_L = \frac{mv_{\perp}}{q_e B}$

Cyclotron frequency       $\omega_c = \frac{q_e B}{m}$



In an arbitrary magnetic field with a force  $F$ :

$$m \frac{d\vec{v}}{dt} = \vec{F} + q_e \cdot \vec{v} \times \vec{B}$$

**Guiding center motion**, we can split into:

- Motion along  $\vec{B}$  field lines (if  $|v_{||}| > 0$ )
- Drift motion due to the presence of force  $F$  (if  $F=0$ , we step back to Lorentz motion)

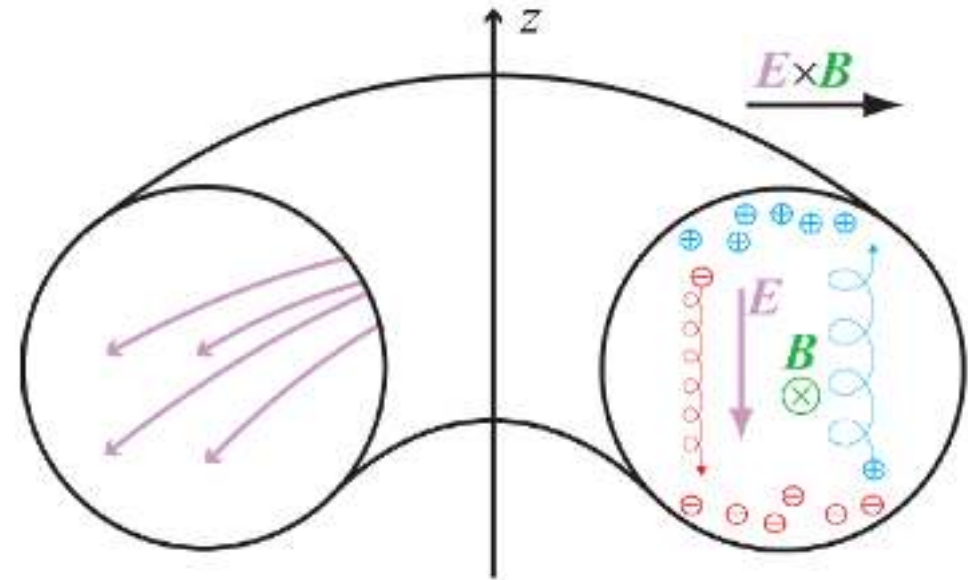


# Ion motion: drifts

Different **drifts due to different forces** in the plasma:

- B-field gradient → **Grad-B drift**
- Curvature of B → **Curvature drift**

they are vertical drifts and bring to **charge separation**

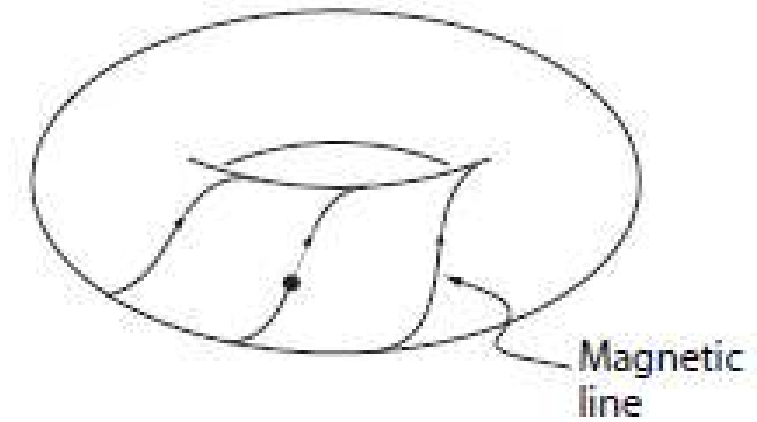


- formation of electric field →  **$E \times B$  drift** (outward drift for both electrons and ions)

This is the reason of the forced **helical twist of the magnetic field lines** in fusion experiments

(other drifts are present: e.g. diamagnetic drift...)

→ Guiding center **orbits are shifted** with respect to magnetic surfaces



# Orbit topology: passing and trapped

In charged particle motion **kinetic energy** is constant and **magnetic moment** an adiabatic invariant:

$$E_k = \frac{1}{2} m(v_{par}^2 + v_{perp}^2) = const$$

$$\mu = \frac{mv_{perp}^2}{2B} \approx const$$

In a tokamak, the **magnetic field varies** as  $B(R) = B_0 \frac{R_0}{R}$

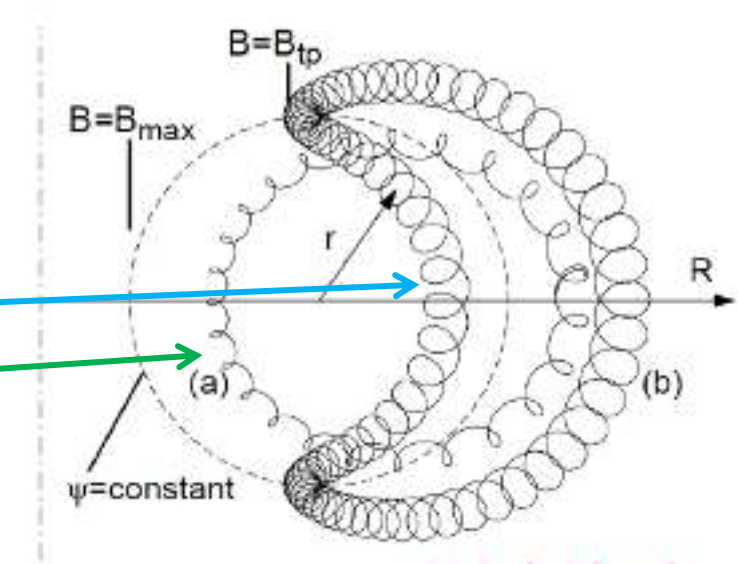
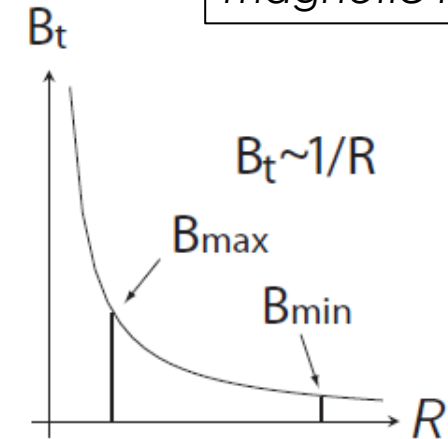
In its (drifted) orbit, the **fast ion experiences varying B**  
→ particle energy is transferred between parallel and perpendicular direction

Depending on the initial fast ion pitch ( $\epsilon = v_{par}/v$ ), the particle may be reflected (condition  $v_{par} = 0$  at  $B_{max}$ ) when travelling towards the inner side of the plasma (as in a magnetic mirror): **trapped particle (banana orbits)** —

Otherwise, the fast ion is a **passing particle** —

$$\text{passing particle: } \frac{v_{perp}}{v_{par}} < \left( \frac{B_{max}}{B_{min}} - 1 \right)^{-1/2}$$

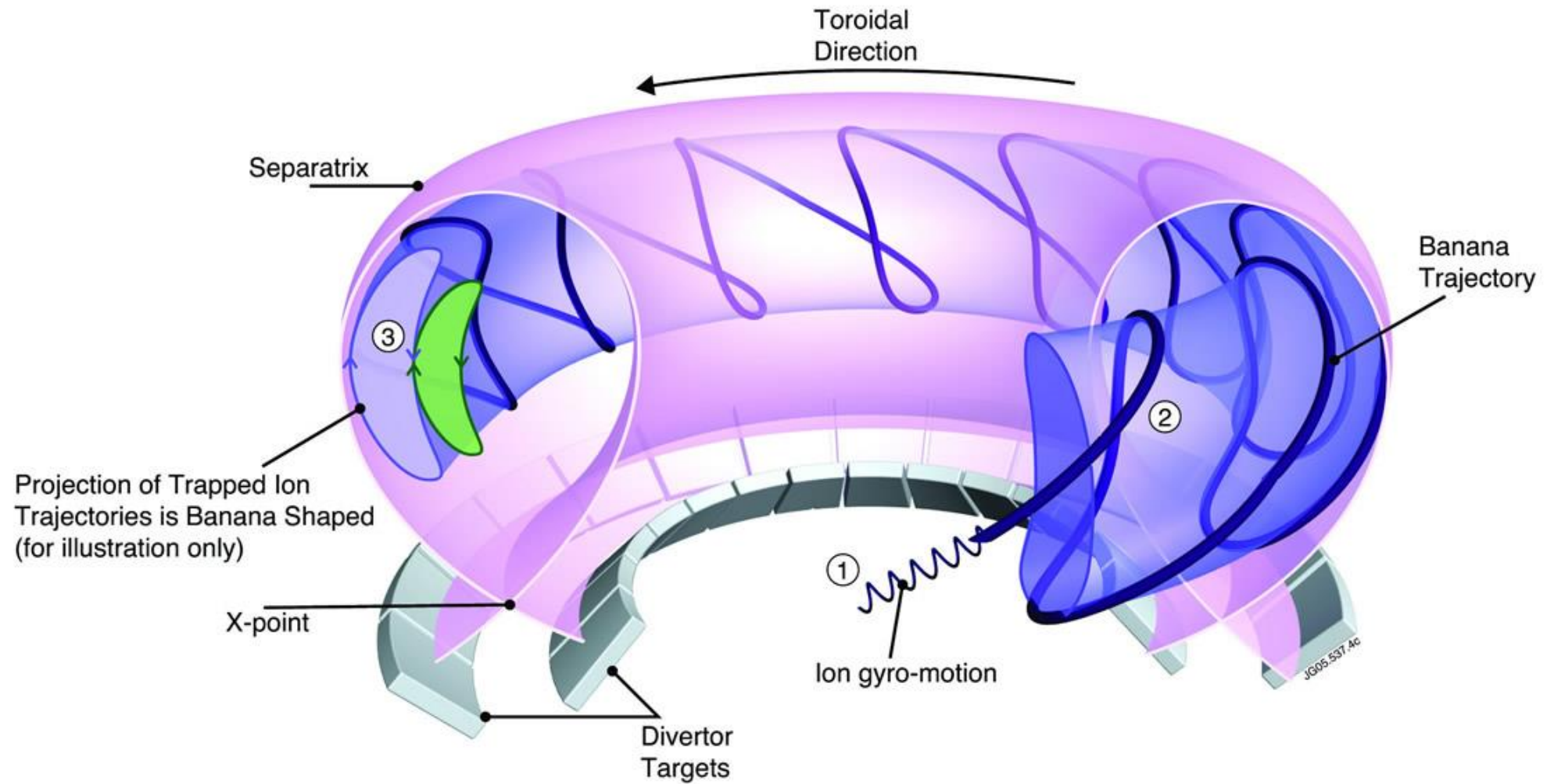
$v_{par}, v_{perp}$  with respect to magnetic field



(H.J. de Blanck)



# Banana orbits



# Let's ask to the greengrocer: Bananas!

## Trapped Banana orbits

- **Banana width** (half width):  $\Delta r \sim \frac{mv_{par}}{eB_{pol}}$   
→ proportional to the mass (we consider only ions)
- Fast ions have larger bananas than thermal ions, and so trapped fast ion **banana orbits should be inward** to reduce fast ion losses.

## How can I say if beam ions will have inward or outward bananas?

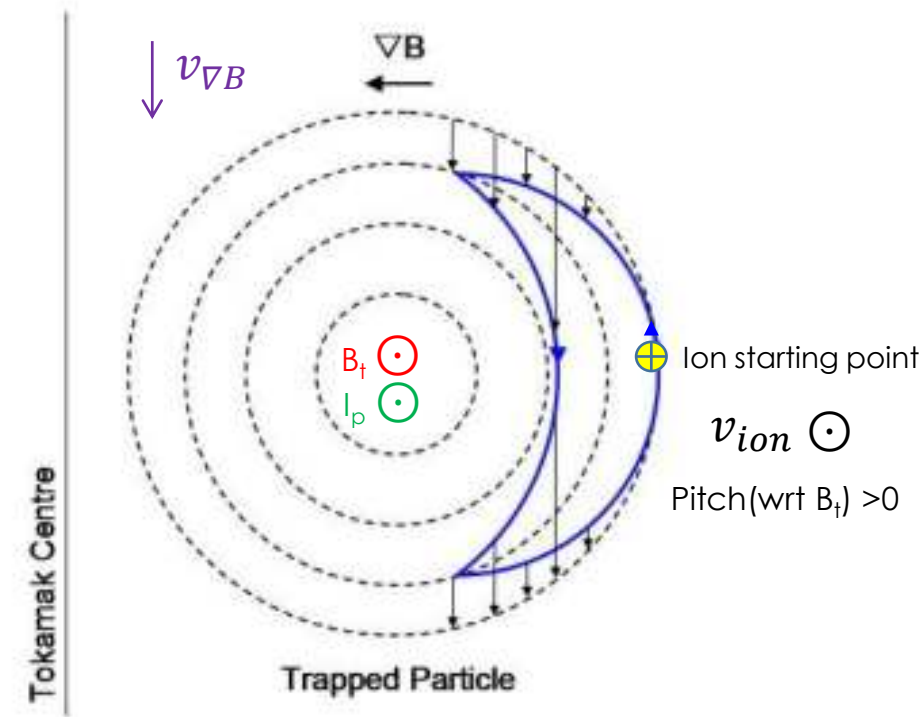
1) First of all, the **direction of the  $\nabla B$  drift** should be determined (up or down). It depends on the sign of the charge.

The  $\nabla B$  drift will shift the particle inwards or outwards with respect to the starting magnetic flux surface.

$$\nabla B \text{ drift (ion } \rightarrow q>0\text{)} \quad \vec{v}_{\nabla B} = \frac{mv_{\perp}^2}{2qB^3} \vec{B} \times \nabla \vec{B}$$

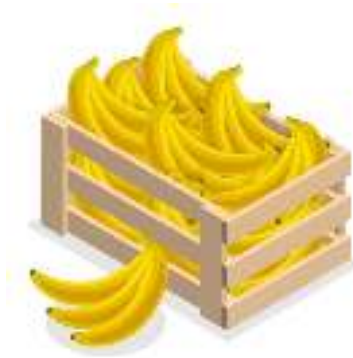
2) The second step is to determine the **direction of the poloidal magnetic field  $\mathbf{B}_p$**  (determined by the plasma current) at the considered particle starting point. Then we must separate the cases of particles with a velocity in the same direction of the toroidal magnetic field (positive **pitch**) or opposite (negative pitch):

- **positive pitch trapped particles** will start the banana orbit in the same direction of  $\mathbf{B}_p$
- **negative pitch particles** in the opposite direction.

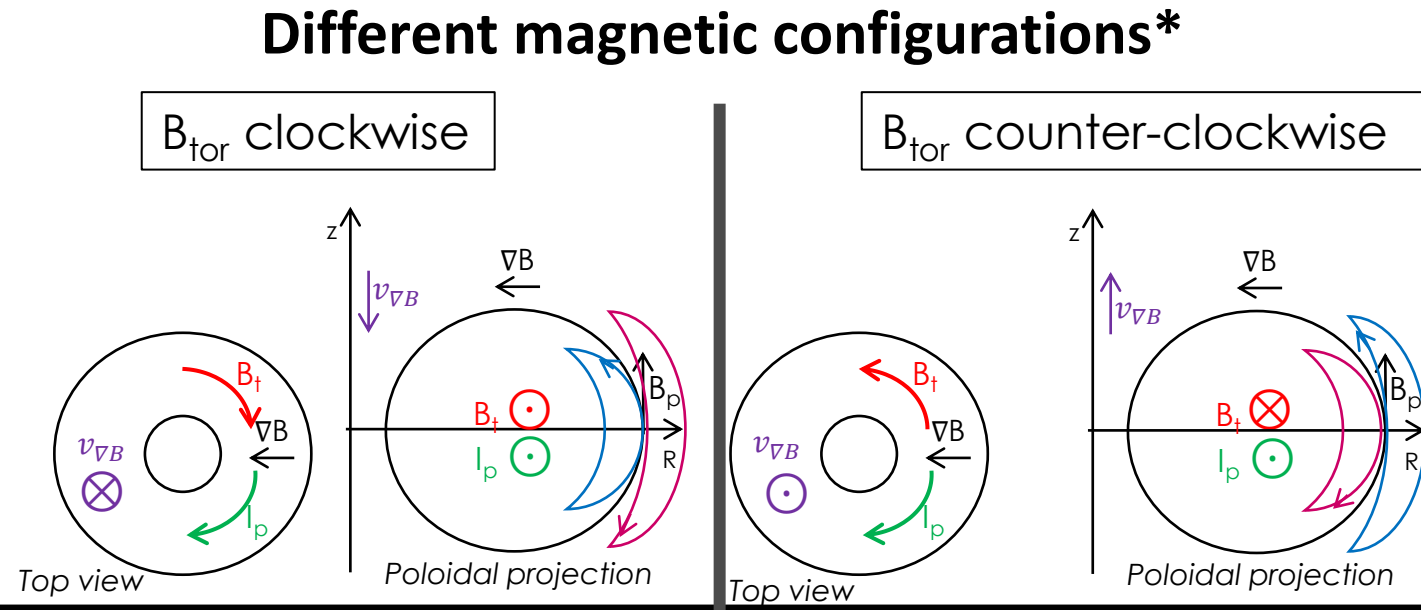


# Let's ask to the greengrocer: Bananas!

Ions,  $q > 0$



$I_p$  clockwise

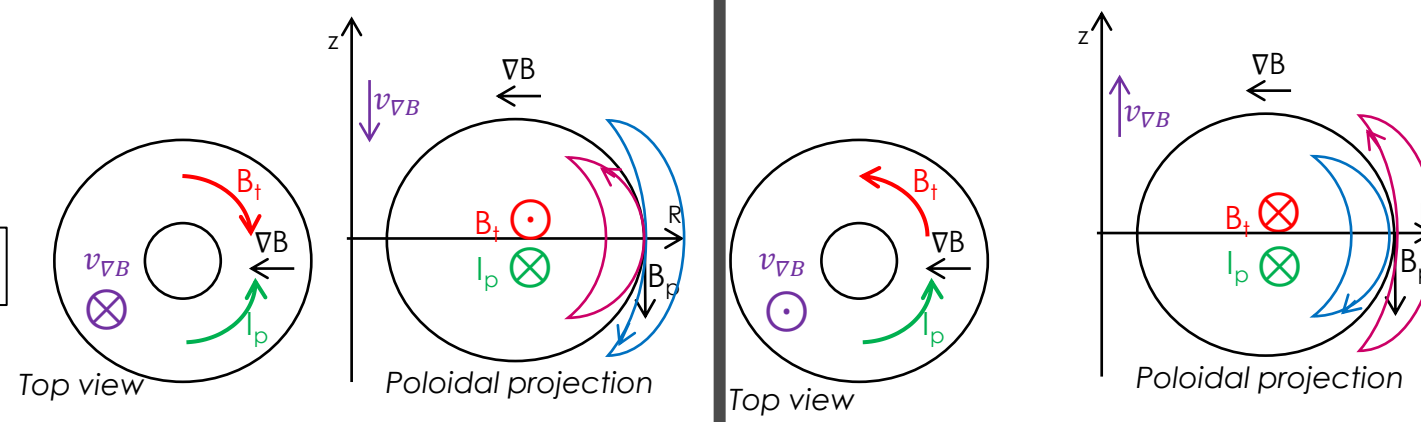


Different magnetic configurations\*

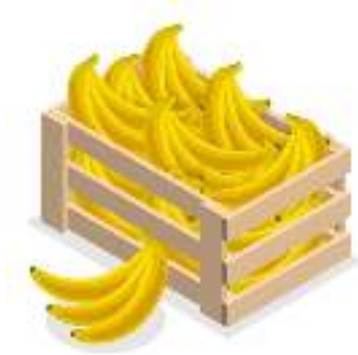
$B_{\text{tor}}$  counter-clockwise

Trapped ion velocity:  
 $\text{Pitch(wrt } B) > 0$   
 $\text{Pitch(wrt } B) < 0$

$I_p$  counter-clockwise



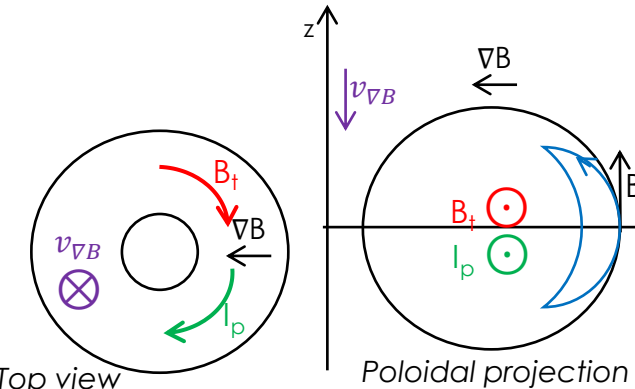
# Let's ask to the greengrocer: Bananas!



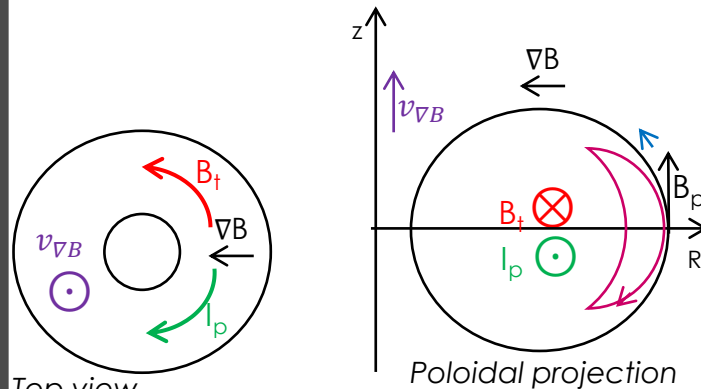
NBI co-current injection is preferable!\*

$I_p$  clockwise

$B_{\text{tor}}$  clockwise

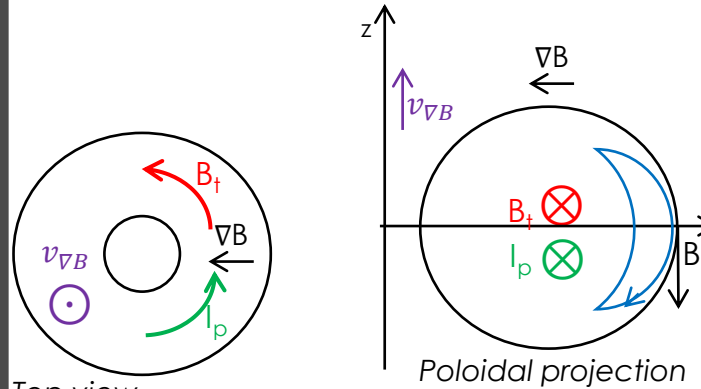
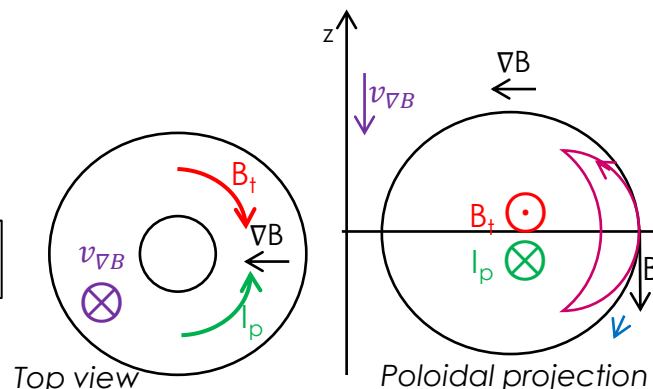


$B_{\text{tor}}$  counter-clockwise



Trapped ion velocity:  
 $\text{Pitch(wrt } B) > 0$   
 $\text{Pitch(wrt } B) < 0$

$I_p$  counter-clockwise



\*because bananas point inwards always (do not mix current direction and pitch which is determined with respect to  $B$ ).

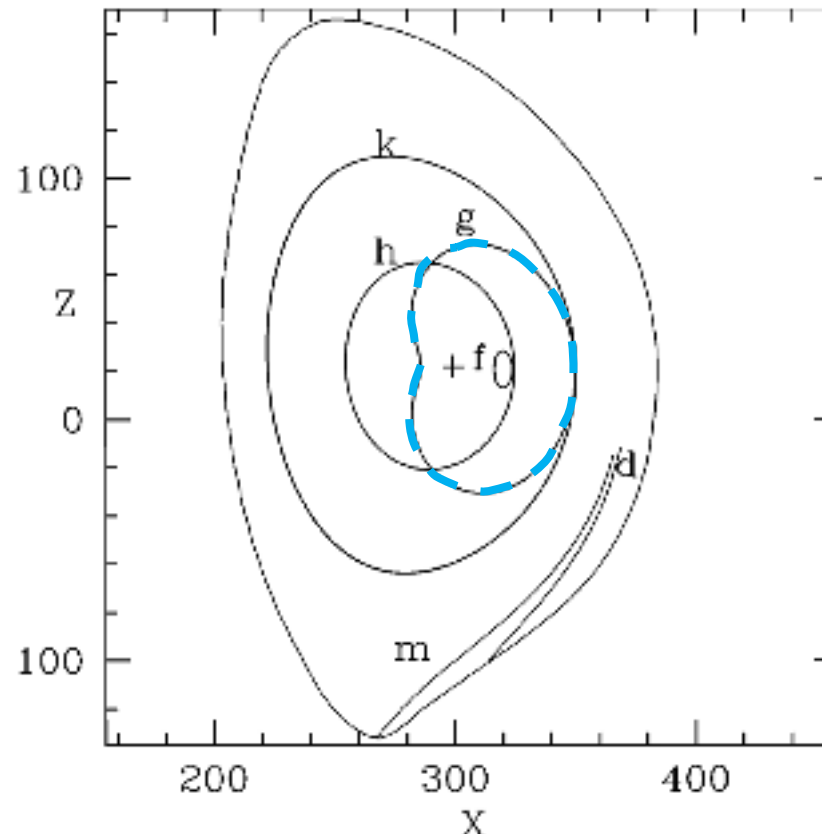


# Other peculiar fast ion orbits

Due to the larger energy with respect to thermal particles, fast ions can experience also other type of orbits:

- **Potato orbits**

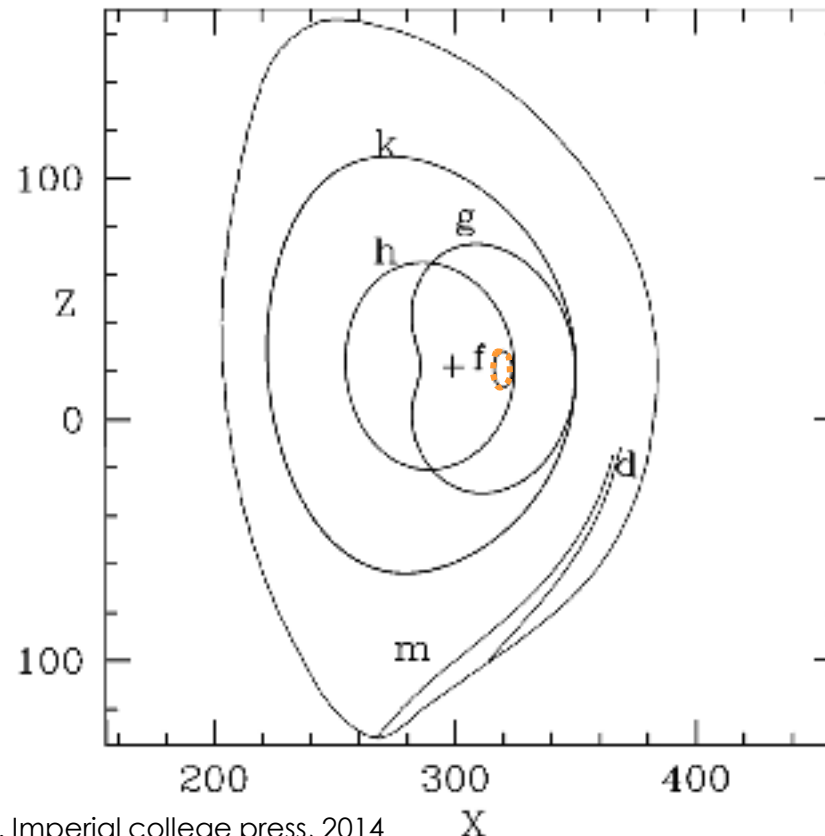
- trapped orbit
- on a poloidal projection, the orbit passes close to the magnetic axis (often, encircles magnetic axis)
- potatoes has larger width than bananas



# Other peculiar fast ion orbits

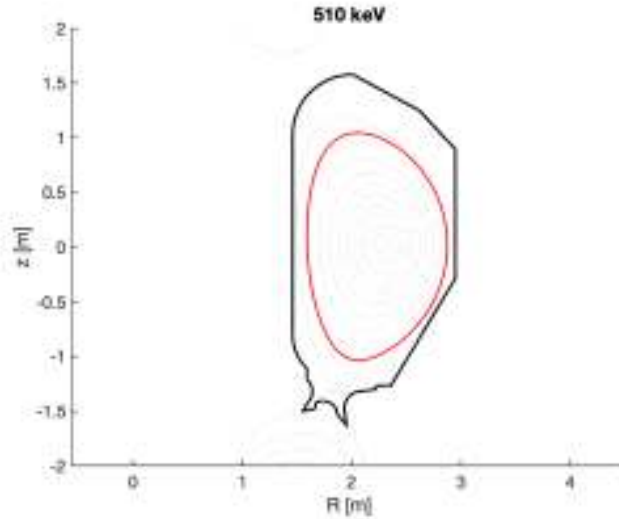
Due to the larger energy with respect to thermal particles, fast ions can experience also other type of orbits:

- **Potato orbits**
- **Stagnation orbits**
  - passing orbit
  - fast ion completing a toroidal orbit scarcely moving poloidally

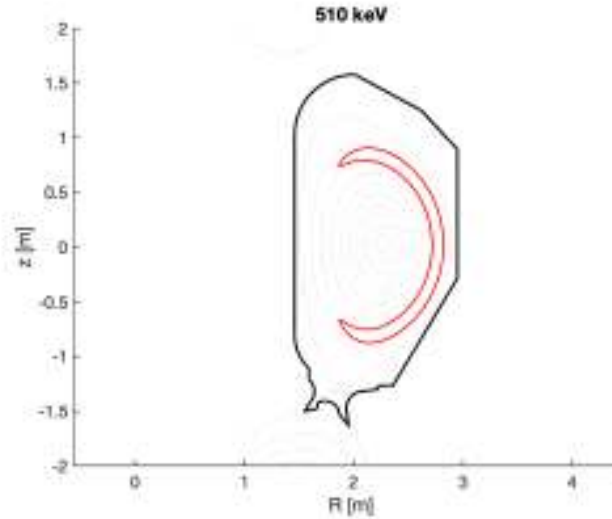


# Example of DTT NBI EP orbits

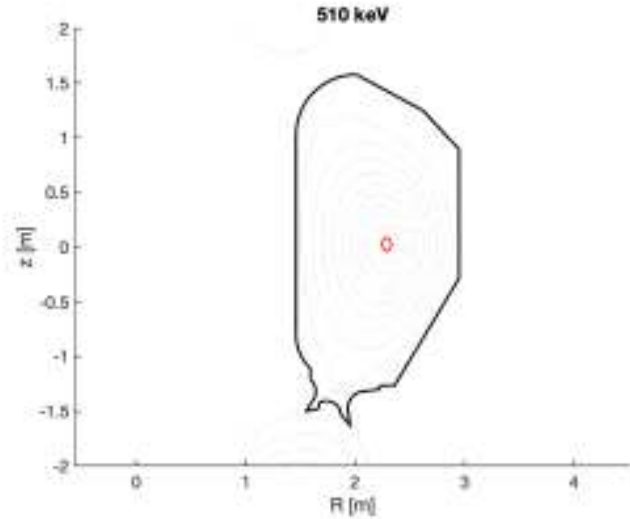
ASCOT simulations (C. De Piccoli)



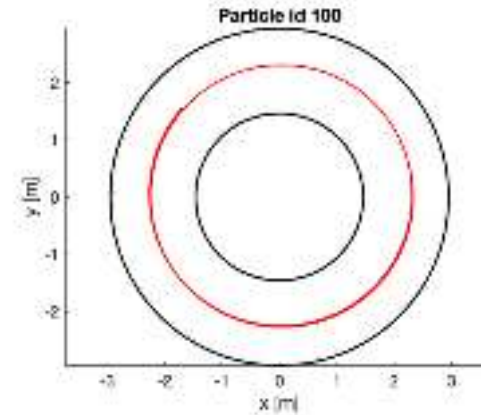
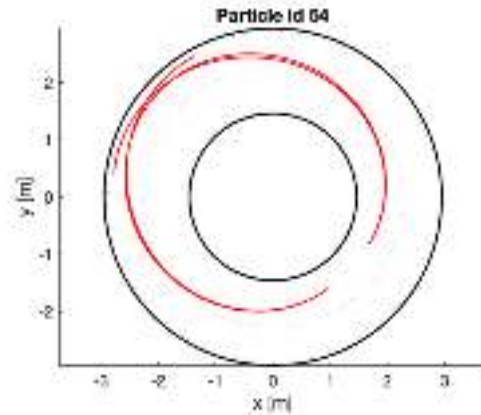
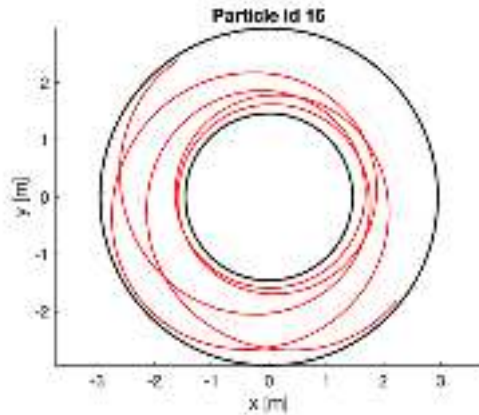
Confined passing orbit



Confined trapped orbit

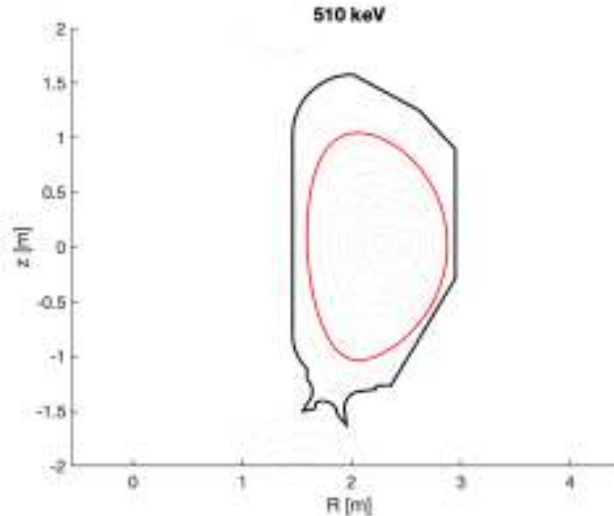


Stagnation orbit

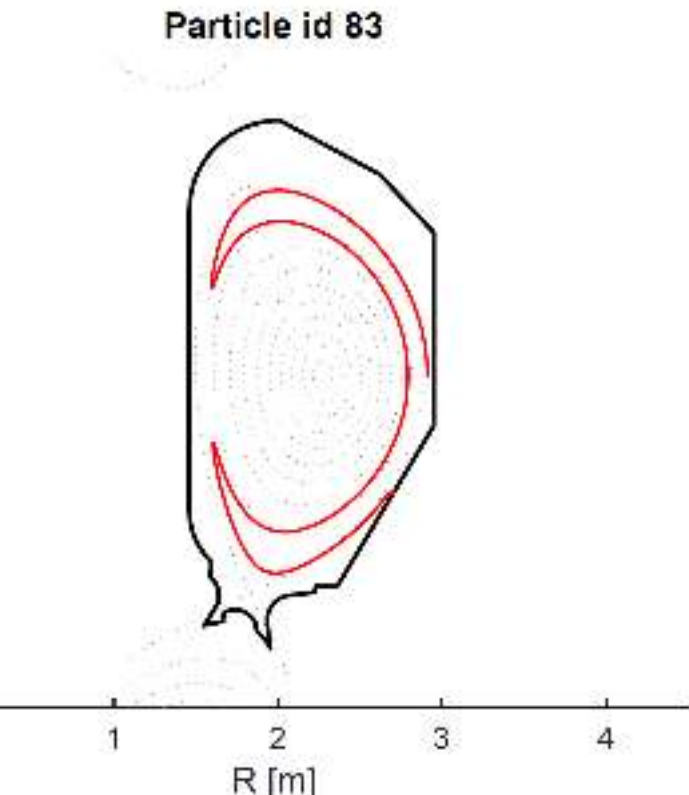
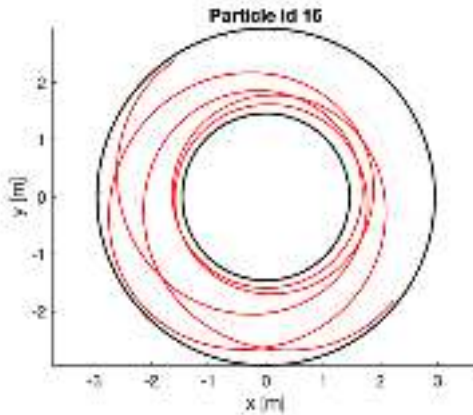


# Example of DTT NBI EP orbits

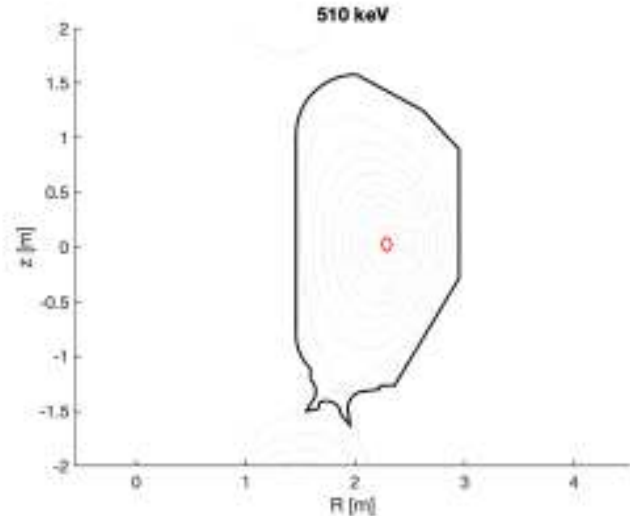
ASCOT simulations (C. De Piccoli)



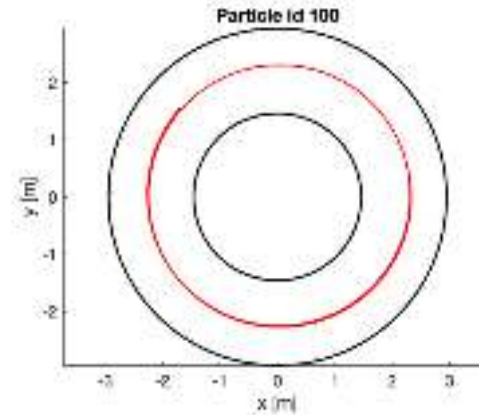
Confined passing orbit



Lost trapped orbit

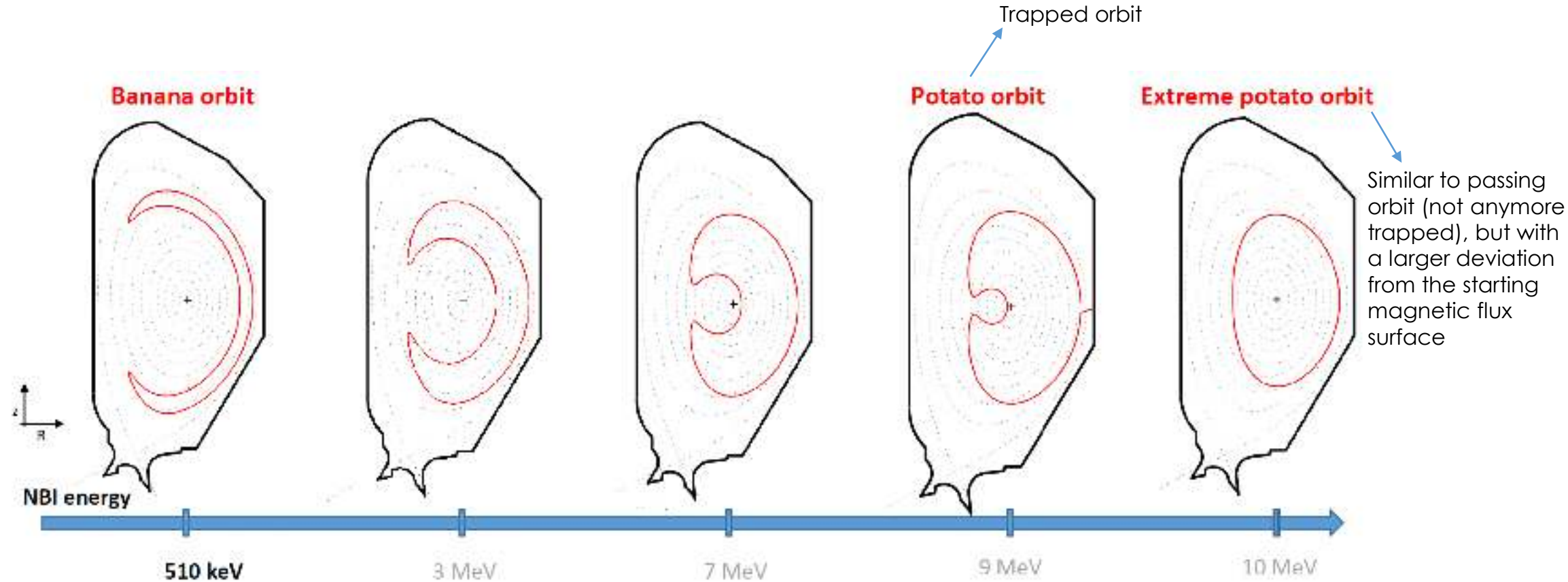


Stagnation orbit



# Example of DTT NBI EP orbits

ASCOT simulations (C. De Piccoli)



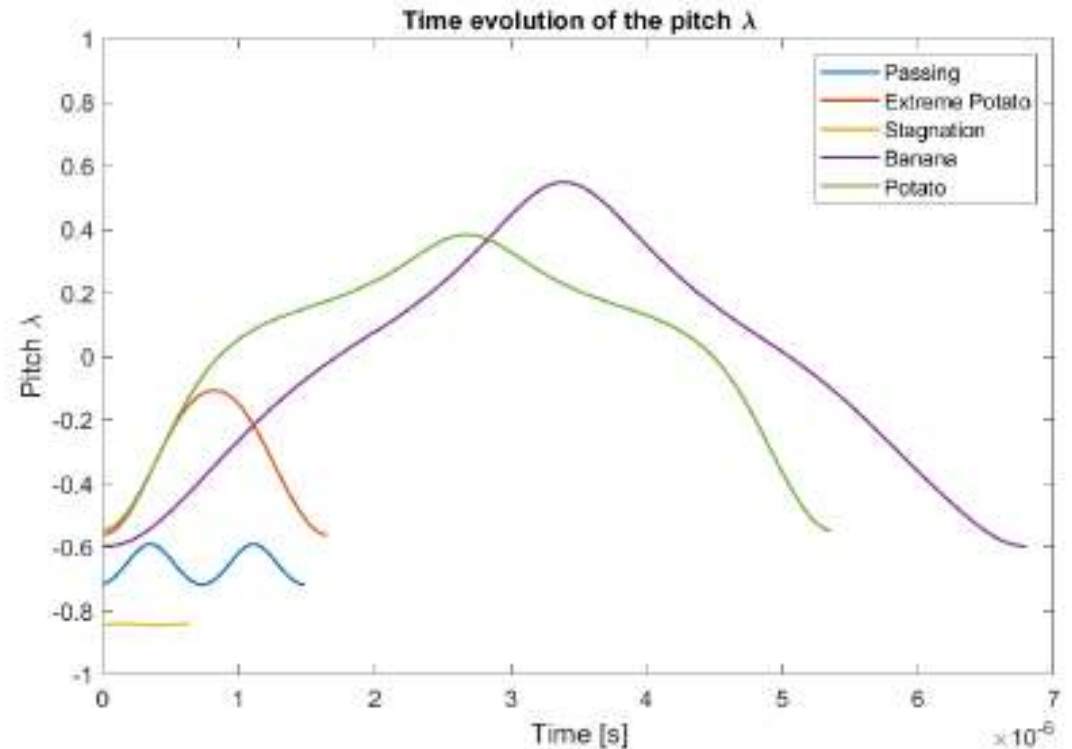
# Pitch evolution of non-standard orbits

ASCOT simulations (C. De Piccoli)

Pitch:  $\lambda = v_{\text{par}}/v_{\text{tot}}$  with respect to magnetic field B

Example of different orbits of imaginary\* NBI EP in DTT

- Pitch changes sign → particle turning back:
  - Banana
  - Potato
- Pitch does not change sign:
  - Passing
  - Stagnation
  - Extreme potato



\*EP energy increased arbitrarily to see these exotic orbits, NBI EP in DTT will be mostly passing



# Fast ion slowing down and energy transfer

During their motion, **fast ions transfer their energy to plasma species** through **Coulomb collisions (slowing down process)**:

- To ions, including impurities
- To electrons

How the energy is transferred?  
(approximation valid for  $v_i \ll v_{beam} \ll v_e$ )

$$\frac{dE}{dx} = -\underbrace{\frac{\alpha}{E}}_{\text{to ions}} - \underbrace{\beta\sqrt{E}}_{\text{to electrons}}$$

We can define a fast ion energy corresponding to equal stopping from electrons and ions:

$$\frac{\alpha}{E} = \beta\sqrt{E}$$

And define therefore this energy as the **critical energy  $E_c$** :  $E_c = \left(\frac{\alpha}{\beta}\right)^{2/3} = 14.8 \left[ \sum_{j=\text{species}} \frac{n_j Z_j^2}{n_e A_j} \right]^{2/3} A_b T_e [\text{keV}]$

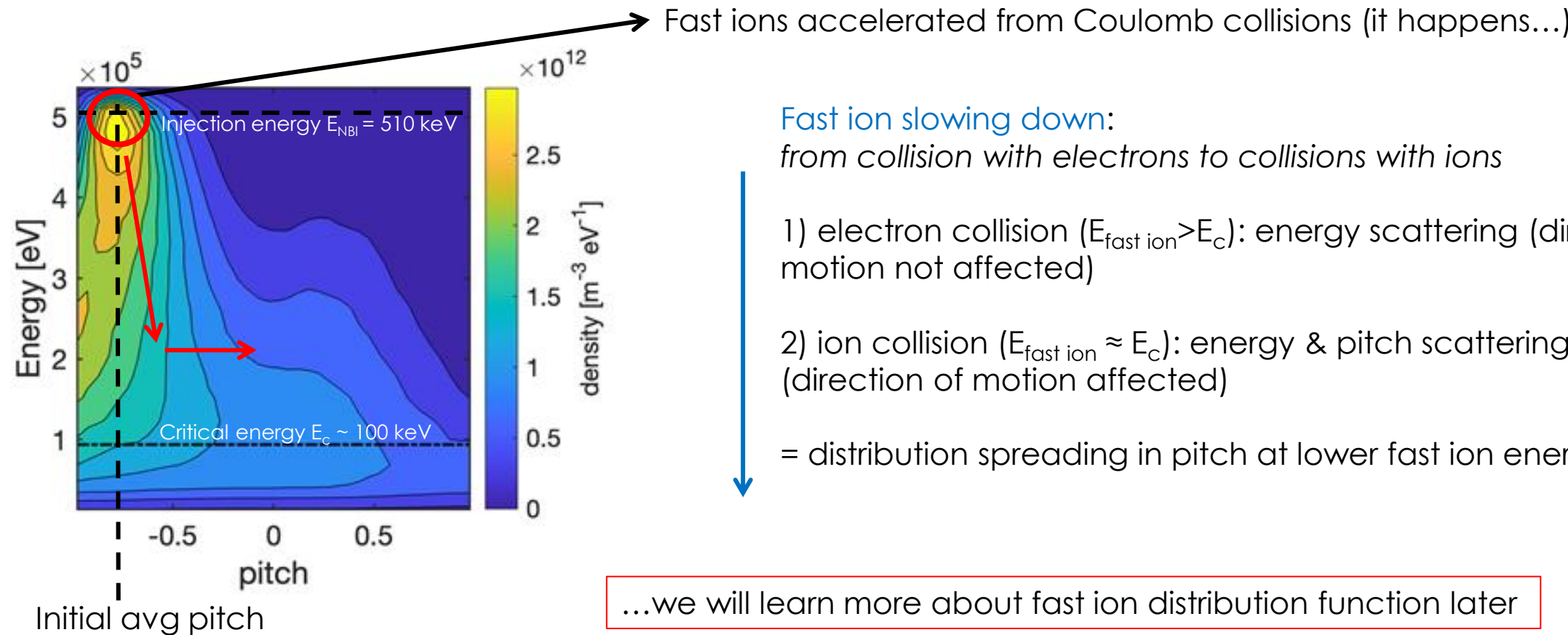
- It **depends** only **on plasma** (temperature, density, plasma species, except dependence on NBI species)
- At time  $t$  during a fast ion slowing down lasting  $\tau_s > t$ :
  - $E_{\text{fast ion}}(t) > E_c$  dominant energy transfer to plasma electrons
  - $E_{\text{fast ion}}(t) < E_c$  dominant energy transfer to plasma ions



# Fast ion energy transfer

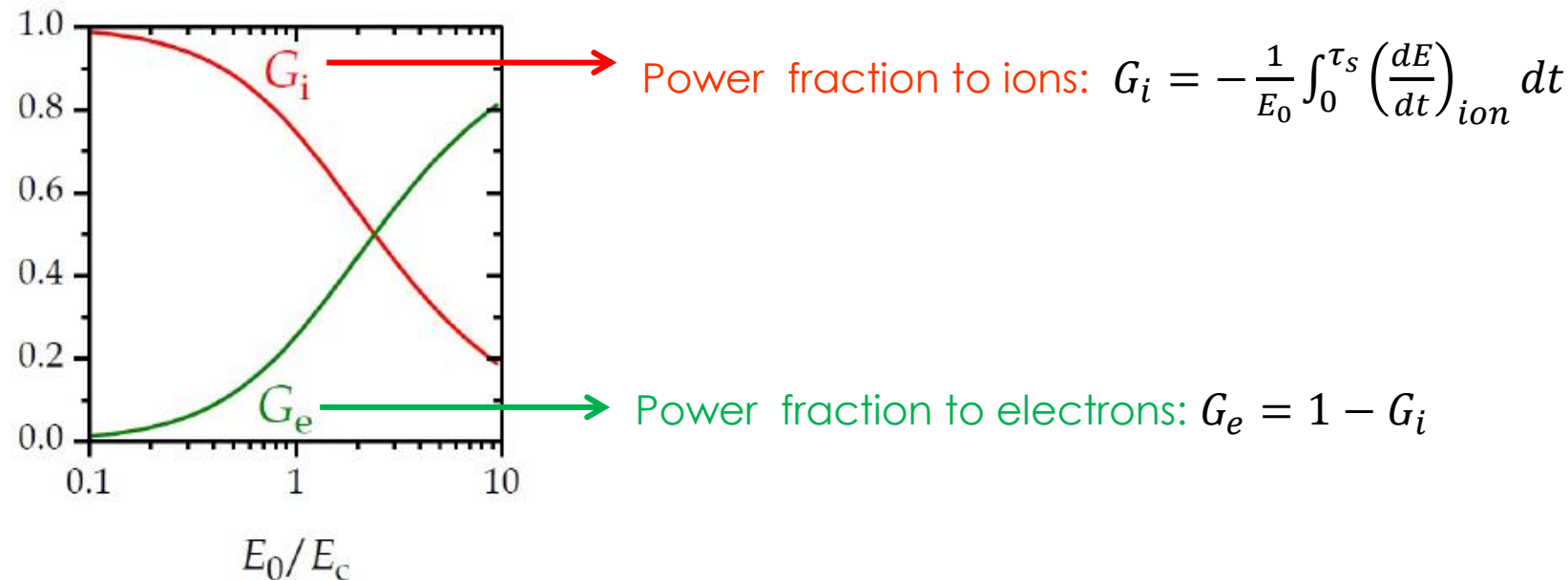
In steady state conditions, we have a **fast ion population** composed of newly ionised particles, fast ions in the middle of slowing down, scattered, almost thermalized...

An example of the steady state numerical solution of the **fast ion particle distribution function** (density of ions in  $E+dE$  and  $\varepsilon+d\varepsilon$ ):



# Fast ion energy transfer

If we want to estimate the **NBI power** (for a NBI with energy  $E_0$ ) going to **electrons** and **ions** we have to **integrate the energy transferred in time**:



For  $E_0 > 2.5 E_c$ , electron heating dominates (future reactors, alpha heating...)

In current experiments (low  $E_{NBI}$ ), ion heating is dominant, also due to lower energy components of the beam, in future reactors it will be the other way round



# Slowing down time

The **time** a fast ion spends to transfer its energy (from  $E_0$  to  $E \sim E_{\text{thermal}}$ , **thermalization**) is:

Slowing down time: 
$$\tau_{\text{sd}} = \int_{t(E_0)}^{t(E=0)} dt = \int_{E_0}^{E=0} \left[ \frac{dE}{dx} \frac{dx}{dt} \right]^{-1} dE = \int_0^{E_0} \left[ -\frac{dE}{dx} \sqrt{\frac{2E}{m}} \right]^{-1} dE =$$
$$= \frac{t_s}{3} \ln \left[ 1 + \left( \frac{E_0}{E_c} \right)^{\frac{3}{2}} \right]$$

with the Spitzer slowing down time defined as:  $t_s [\text{s}] = \frac{\sqrt{2m_i}}{\beta} = 6.28 \times 10^{14} \cdot \frac{A T_e [\text{eV}]^{\frac{3}{2}}}{Z^2 n_e [\text{m}^{-3}] \ln \Lambda}$

For current experiments  $\tau_{\text{sd}} \sim 100\text{-}200 \text{ ms}$ , in future reactors (larger  $T_e$ , larger  $E_{\text{NBI}}$ ) it will be up to seconds



# Current-drive

## Inducing plasma current

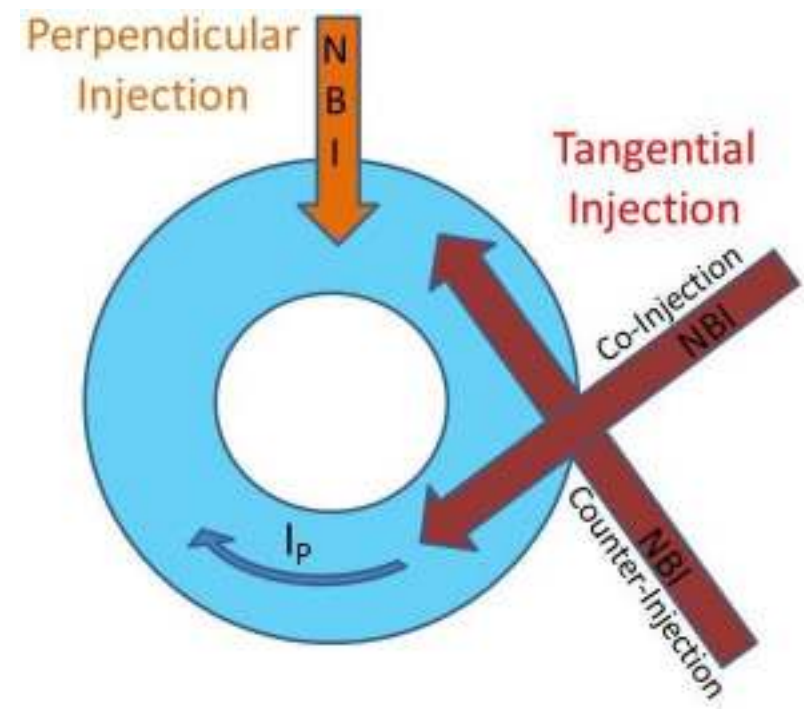
In tokamaks plasma current is currently sustained mainly by the central solenoid → pulsed, inductive operations with **limited pulse length**, cycles

The generation of **non-inductive currents** (bootstrap, or by external H&CD systems) could extend discharge duration:

- fully non-inductive plasma current (steady state tokamak)
- partially non-inductive (extended pulse length)

NBI, as other systems, can drive current in the plasma.

**NBI must have tangential injection** to drive current



# NBI current drive

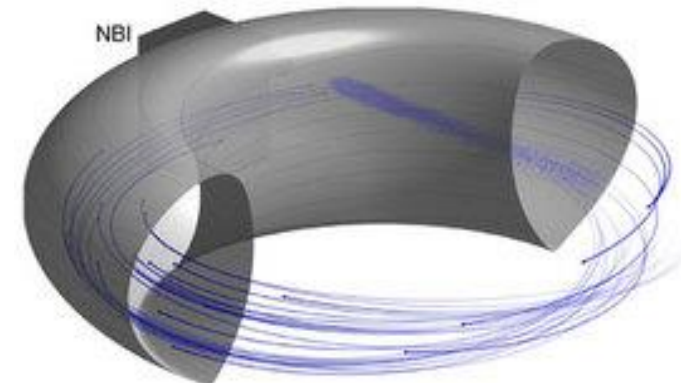
## A simple estimation of the driven current

The tangentially injected fast particles, becoming fast ions, generate a circulating **fast ion current**:

$$I_{circ} = I_0 \frac{\langle v_{par} \rangle \tau_{sd}}{2\pi R_o}$$

average number of toroidal laps ( $\langle v_{||} \rangle \sim v_0/2$ )

$I_0 = P_{NBI}/E_0$  injected particles



But we miss:

- correct averaging over slowing down
- pitch angle scattering
- electrons dragged by fast ions

→ Back electron current: could cancel all the fast ion current if we do not consider toroidal effects and if  $Z_{beam} = Z_{eff}$ . Luckily these conditions are not present in experiments.

$$\rightarrow I_{NBCD} = I_{circ} \left( 1 - \frac{Z_{beam}}{Z_{eff}} \right)$$

- trapped electrons that cannot be dragged along with fast ions (this would give some current also for  $Z_{beam} = Z_{eff}$ )

$$\rightarrow I_{NBCD} = I_{circ} \left( 1 - \frac{Z_{beam}}{Z_{eff}} (1 - f(Z_{eff}, \varepsilon)) \right) \quad \varepsilon = \text{aspect ratio}$$



# Current drive efficiency

The **efficiency** of an auxiliary current drive system can be defined as the current driven per power injected  $I_{CD}/P_{NBI}$ .

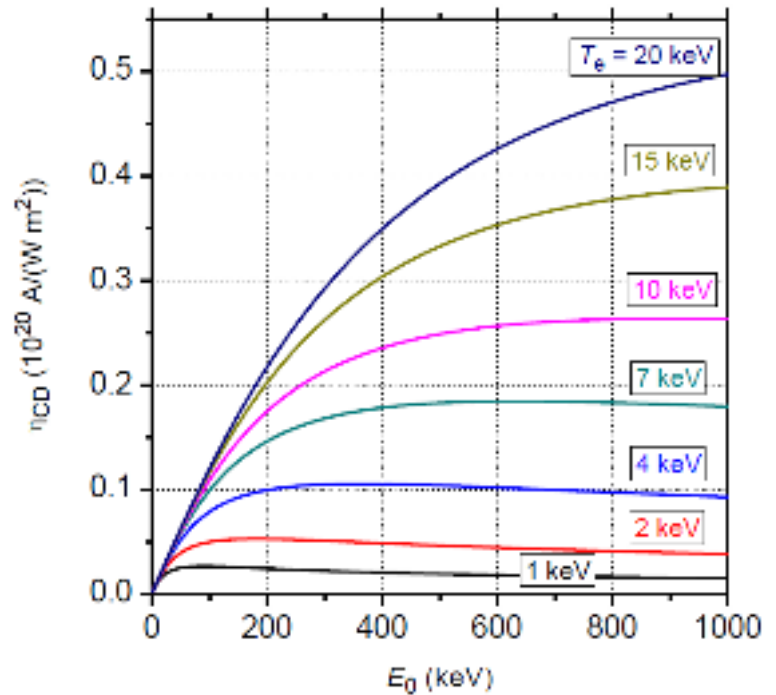
But since:

$$I_{CD} \propto P \frac{1}{R_0 n_e}$$

the **current drive efficiency** is defined as:

$$\eta_{CD} = R_0 n_e \frac{I_{CD}}{P} \quad \text{usually in } \left[ \frac{10^{20} A}{W m^2} \right]$$

- The **NBI CD efficiency** increases with  $E_{NBI}$  and plasma temperature:  
 $\max(\eta_{NBI,CD})$  increases linearly with  $T_e$
- 90% of  $\max(\eta_{NBI,CD})$  at considerably lower  $E_{NBI}$ :  $E_{0.9\max} \sim 0.5 \cdot E_{\max}$
- In current experiments  $\eta_{NBI,CD} \sim 0.05 - 0.1$  (record in JT60-SA: 0.15)
- For future reactors (ITER, DEMO)  $\eta_{NBI,CD} \sim 0.3 - 0.4$
- NBI has usually the highest CD efficiency



Ex. for D tangential injection



# NBI is also a source of...

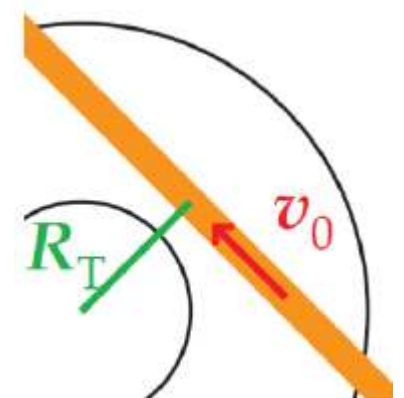
## Source of particle N (plasma fuelling)

$$\frac{dN_{NBI}}{dt} = \frac{P_{NBI}}{eE_0}$$

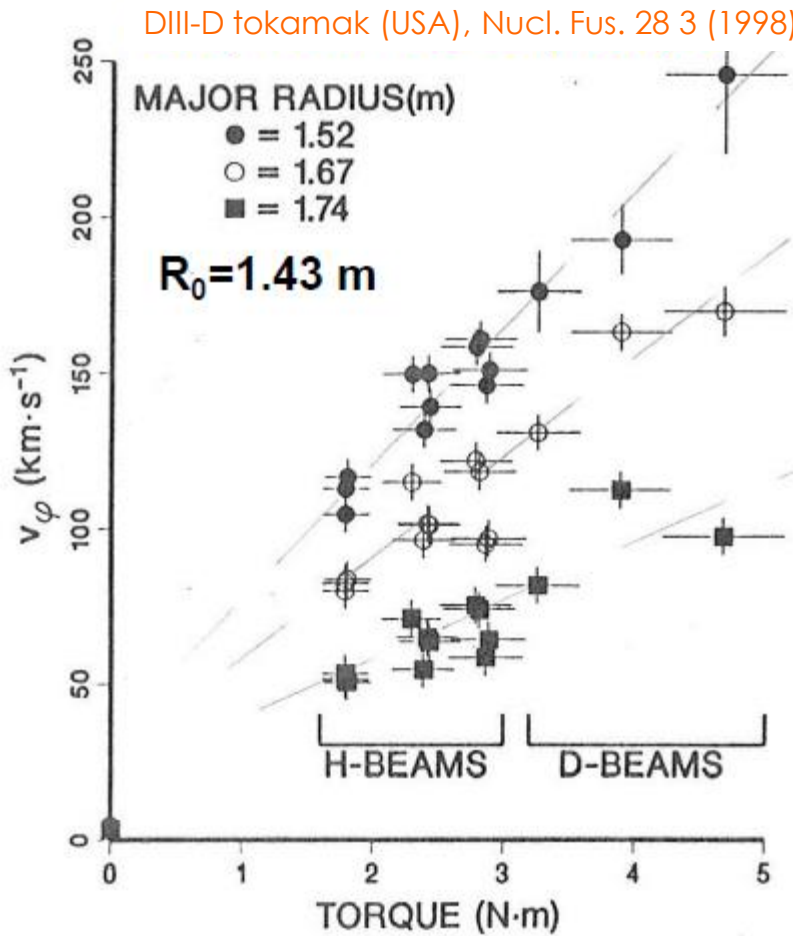
- useful for core plasma fueling (efficient)
- relevant for current experiments
- negligible for future reactor-like experiments ( $V_{\text{plasma}}$  two order of magnitude larger,  $E_{\text{NBI}}$  1 order of magnitude higher,  $P_{\text{NBI}}$  almost the same)

## Source of toroidal torque (only for tangential injection)

- Due to a combination of collisional torque and  $j \times B$  torque (due to fast ion current)
- Collisional torque:  $M = \frac{I_0}{e} A_{\text{beam}} m_p v_0 R_T e_\phi$   
since  $I_0 = P_{\text{NBI}}/E_0$  and  $v_0 \propto \sqrt{E_0/A_{\text{beam}}}$   $\rightarrow \frac{M}{P_{\text{NBI}}} \propto E_0^{-1/2}$
- Torque induces plasma rotation depending also on the momentum confinement time



# NBI torque and plasma rotation



- Control of plasma rotation by NBI torque
- In case of counter-current injection, the plasma rotation can be reduced (decreasing it to condition similar to future reactors)
- plasma rotation and rotation shear ( $dv_{\text{rot}}/dr$ ) can suppress turbulence and help plasma stability



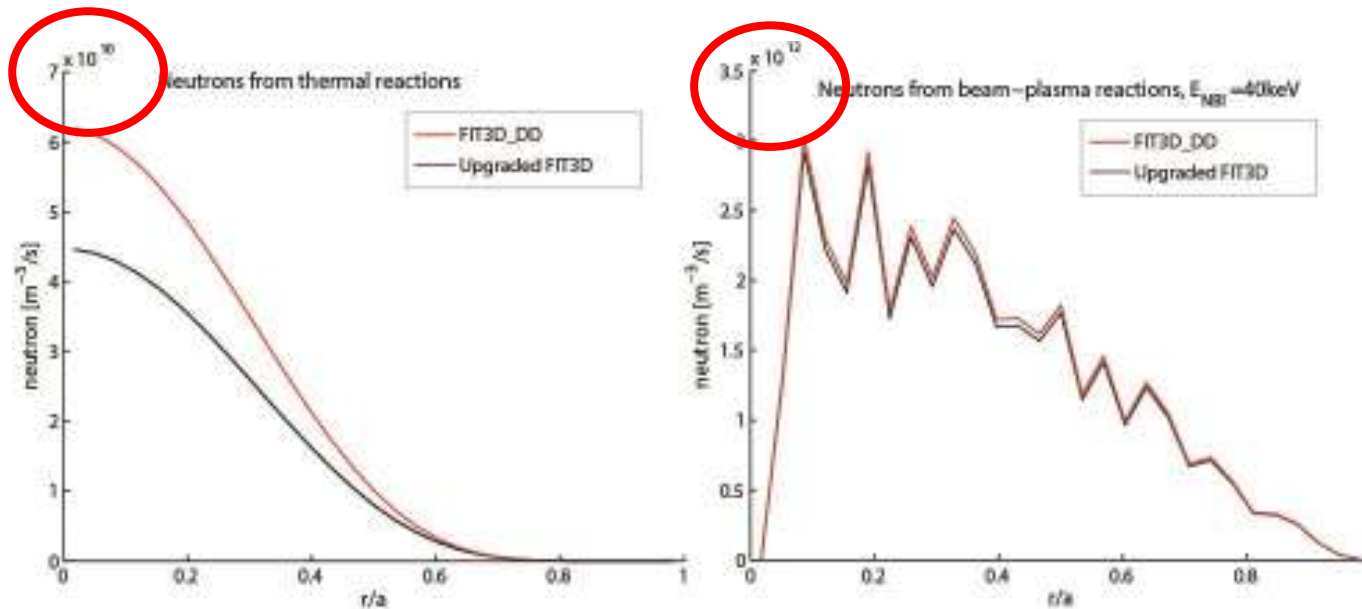
# Beam-plasma fusion reactions

In case of reactive species (D-D, D-T), the interaction between NBI and plasma is a **source of fusion reactions (beam-plasma reactions)**, additional to background plasma reactions (**thermal reaction**).

In world-record JET and TFTR D-T experiments, beam-plasma reactions dominated.

Simulation for D campaign of LHD experiment (“stellarator family”,  $P_{NBI} \sim 20\text{MW}$ ,  $E_{NBI} = 50\text{-}200\text{ keV}$ ,  $n_{e,0} = 3e19\text{ m}^{-3}$ ,  $T_{e,0} = 1\text{keV}$ )  
P. Vincenzi et al., Plasma Phys. Control. Fusion 58 (2016) 125008

- $D + D \rightarrow p$  (3.02MeV) + T (1.01 MeV)      proton production
- $D + D \rightarrow n$  (2.45 MeV) +  $^3\text{He}$  (0.82 MeV)      neutron production



Also the fast ions of the beam itself can react (beam-beam reactions)



# Energetic particle physics: a few words

NBI fast ions represent a particular ion population in the plasma: **suprathermal ions** (or Energetic Particles EPs)

- NBI fast ions can be a relevant part (tens %) of plasma ions in current experiments, while they will be a **small population in larger tokamaks**
- NBI fast ions are **different from fusion alphas** not only for the energy but also for the anisotropy in velocity space
- fast ions can drive **instabilities** such as Alfvén Eigenmodes (AEs), if their velocity  $\approx$  Alfvén velocity  $v_A = \frac{B}{\sqrt{\mu_0 n m}}$
- **fast ions** can be affected by instabilities and fast ions can be lost
- Experimental findings on fast ion AEs that reduce thermal ion micro-turbulence in JET and AUG (very interesting for  $T_i$  increase and reactor performance)

A. Di Siena et al., "New high-confinement regime with fast ions in the core of fusion plasmas", arXiv:2010.14839

Mazzi, S. et al. Enhanced performance in fusion plasmas through turbulence suppression by megaelectronvolt ions. Nat. Phys. 18, 776–782 (2022)



# Summary: NBI is a source of...

Neutral Beam injection is a source in the plasma of:

- **Energy** ( $\rightarrow$  heating)
- **Current** (in case of tangential injection)
- **Particles** ("plasma fueling")
- **Torque** (acting on plasma rotation, in case of tangential injection)
- **Fusion reactions** (beam-plasma reactions, in case of reactive species)
- "**Beam halo**" (= thermal neutrals), in case of relevant CX ionization process
- **Fast particles** (peculiar particle population with their own **instabilities** and interaction with thermal plasma, used also for diagnostics)



# NBI...towards future

		Present day	ITER/Reactors (?)
NBI technology	Energy	Low-middle (40-200 up to ~500 keV - JT60SA & DTT)	High ~1000 keV
	Power	Tens MW	Tens MW
NBI physics	Heating source	✓	✓
	Current source	✓	✓
	Particle source	✓	Negligible
	Torque source	✓	✓
	Fusion reactions (beam-plasma) source	✓	Relatively low



# Contents

- Introduction
- H&CD systems
- Neutral Beam Injection (NBI)
- NBI: from generation to the plasma
  - Neutral beam generation
  - Neutral beam ionization
  - Fast ion orbits and slowing down
- **Beam energetic particle losses**
- NBI modelling techniques
- Conclusion



# Fast particle losses

- neutral particles
- fast ions
- slowing down fast ions
- background neutrals



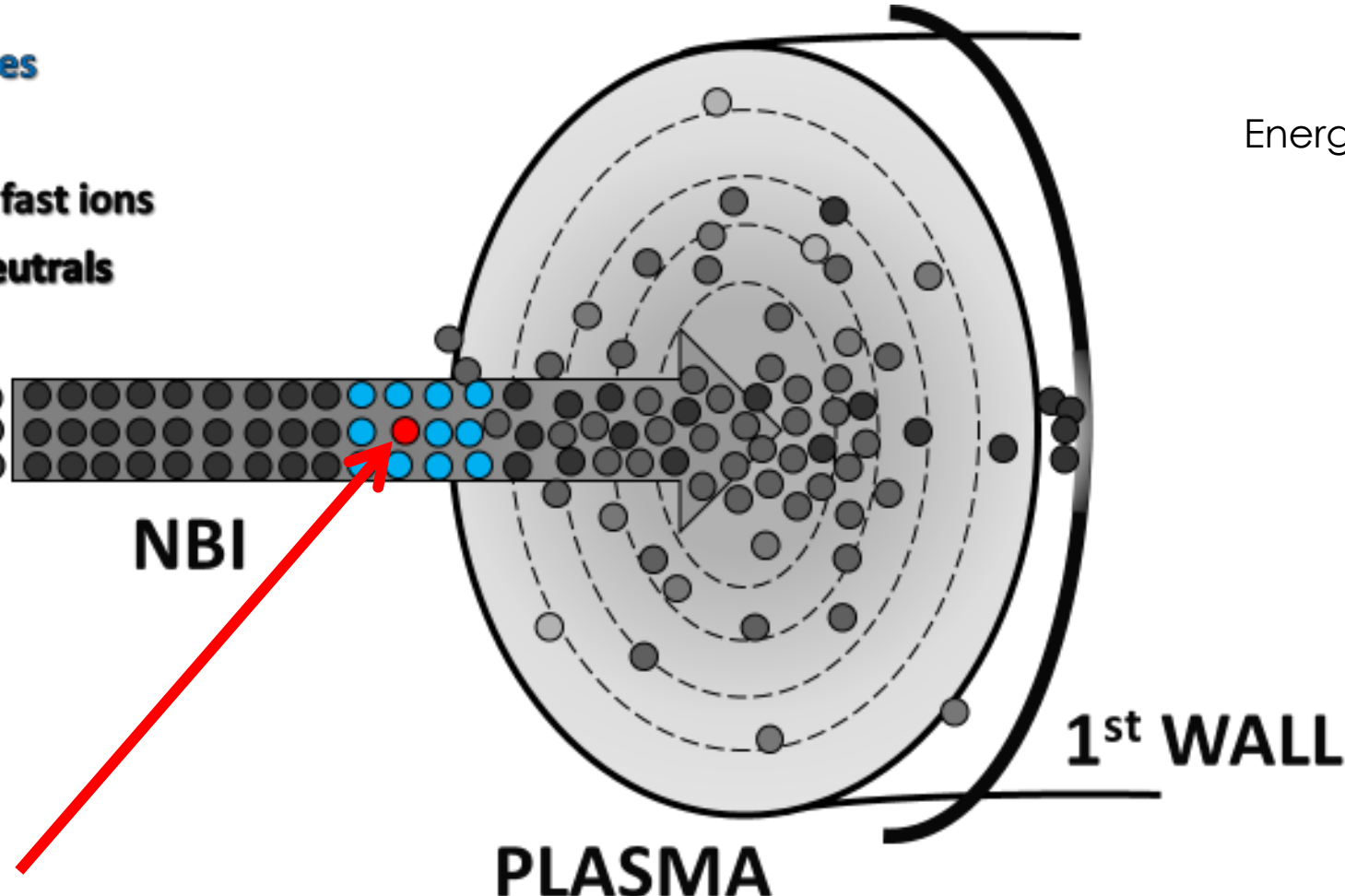
## Fast particle losses

NBI



# Energetic particle losses

- neutral particles
- fast ions
- slowing down fast ions
- background neutrals



Scrape-off layer (SOL) losses:

Fast ions born inside the tokamak chamber but outside confined plasma

Energetic particle losses:

Scrape-off layer

First orbit

Charge-exchange

Orbit

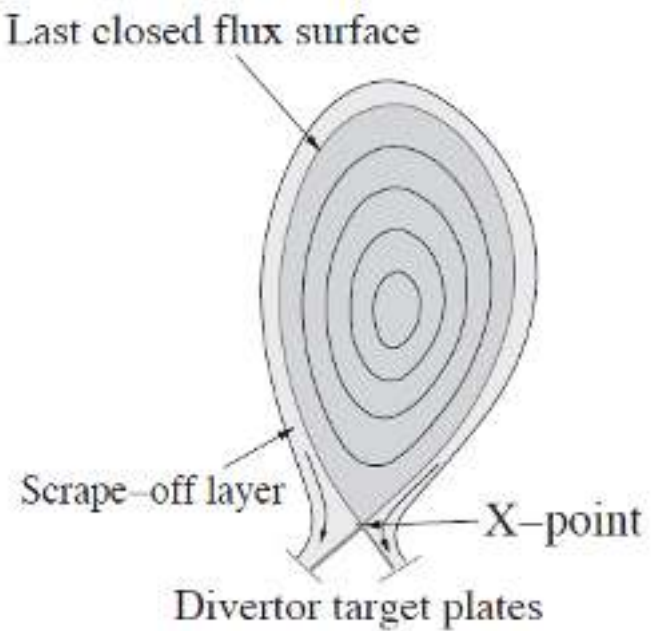
Shine-through



# Scape-off layer losses

Scrape-off layer (SOL) losses:

- SOL is characterized by open magnetic flux surfaces
- If a fast neutral particle is ionized in the SOL, its orbit will **collide with divertor plates**
- In this region we find **neutral particles** (e.g. gas puff) and ions entering/escaping from the plasma. It is usually difficult to estimate SOL density: if it is known, SOL losses can be easily estimated by numerical modelling



# Energetic particle losses

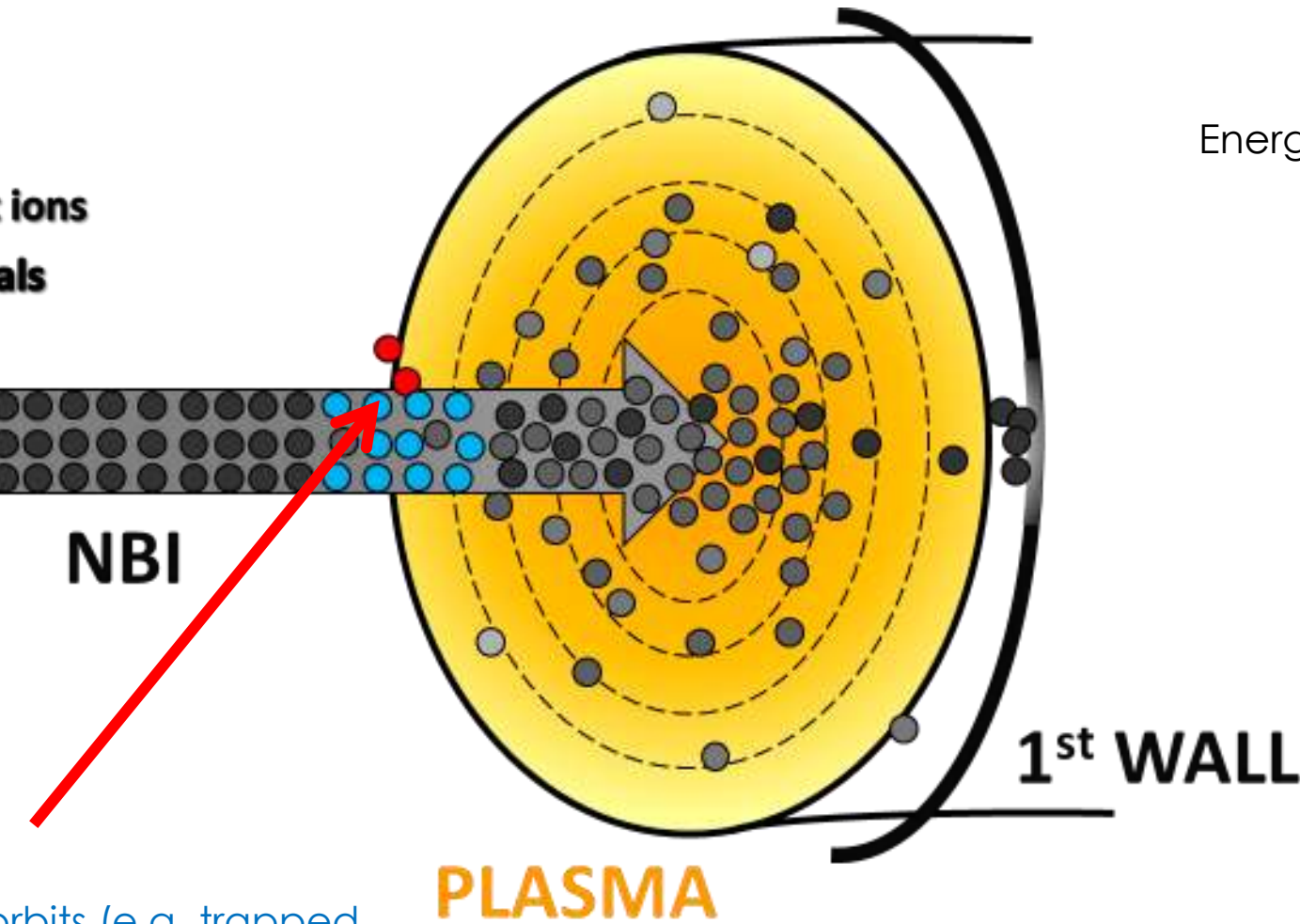
- neutral particles
- fast ions
- slowing down fast ions
- background neutrals



NBI

First orbit losses:

Fast ions born on non-confined orbits (e.g. trapped outward bananas)



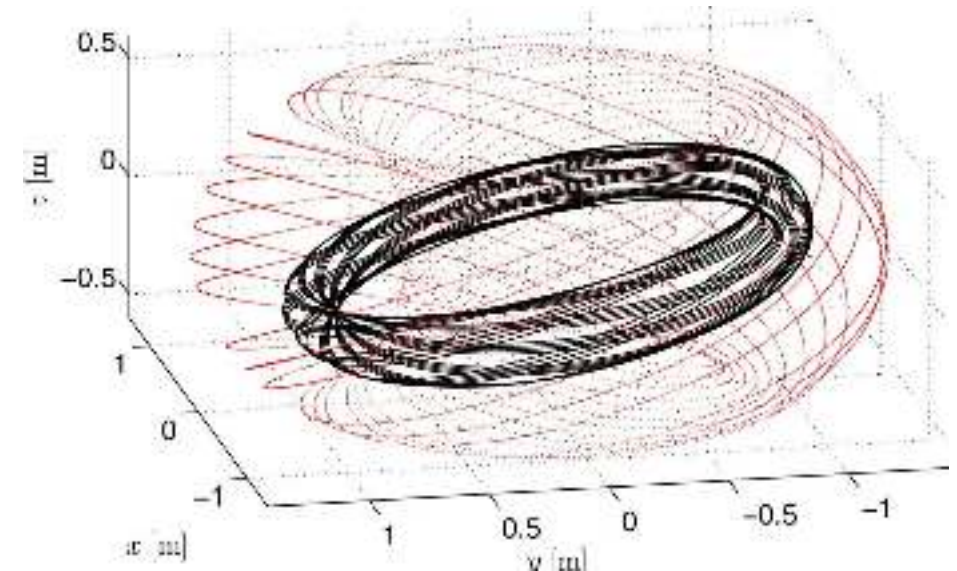
Energetic particle losses:  
Scrape-off layer  
**First orbit**  
Charge-exchange  
Orbit  
Shine-through



# First orbit losses

Fast ions born on non-confined orbits causes first orbit losses

- Most of fist orbit losses are **due to banana orbits**, when part of the banana orbit cross the separatrix (as we have seen before when describing beam fast ion banana orbits)
- A particular case with very high first orbit losses is represented by **NBI counter-current injection**, because banana orbits move fast ions outwards
- Depending on plasma parameters and injection direction, these losses can be relevant
- An analytical formulation is available to estimate first orbit losses



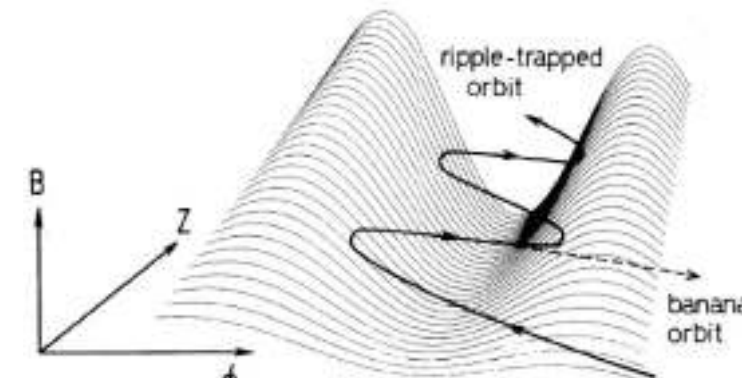
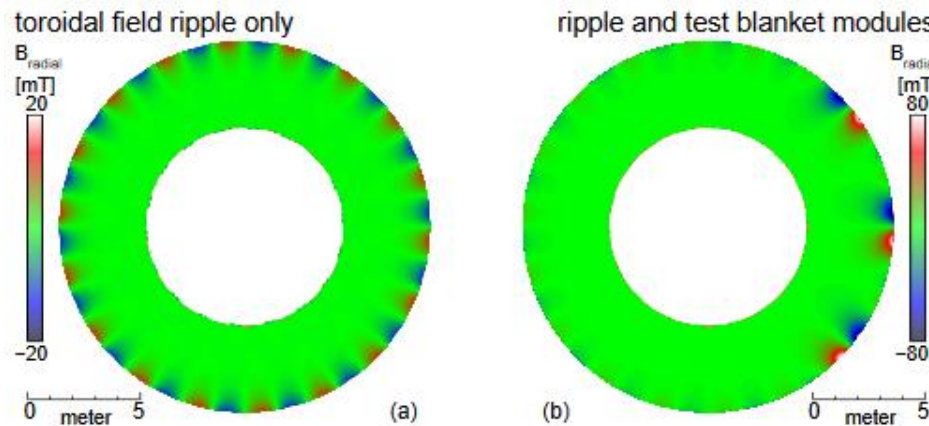
NBI particle trajectory in 3D for MAST  
[D. Pfefferlé et al., 2014 Nucl. Fusion **54** 064020]



# First orbit losses

Also magnetic field ripple can cause immediate orbit losses (collisionless process)

- Magnetic field perturbation due to the finite number of toroidal field coils.
- It can be mitigated with ferritic inserts.
- The ripple modifies the trajectories of fast ions causing localized losses (wall hot spots)
- Both NBI fast ions and alphas (for reactors) will suffer this issue
- Mitigated in ITER, negligible in DTT [Spizzo et al., NF 2021]



Ex. of collisionless trapping of a banana particle

Example for alphas in ITER

[G. J. Kramer, R. B. White, R. Nazikian, H. L. Berk, "Fusion-born alpha particle ripple loss studies in ITER", 22nd IAEA Fusion Energy Conf., 2008-Oct.]

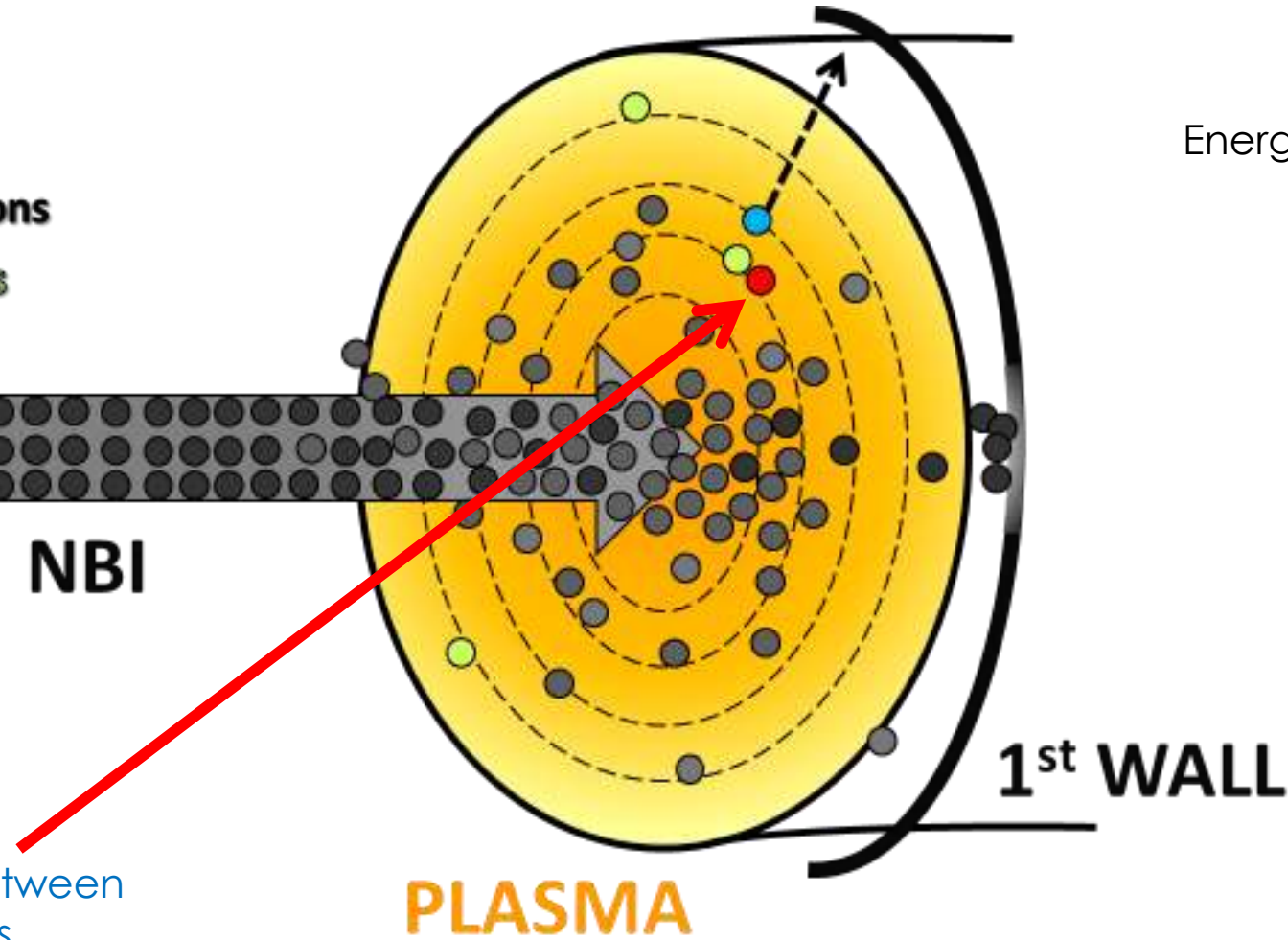


# Energetic particle losses

- neutral particles
- fast ions
- slowing down fast ions
- background neutrals



NBI



Charge-eXchange (CX) losses between  
fast ions and background neutrals



Energetic particle losses:  
Scrape-off layer  
First orbit  
**Charge-exchange**  
Orbit  
Shine-through



# Charge-eXchange (CX) losses

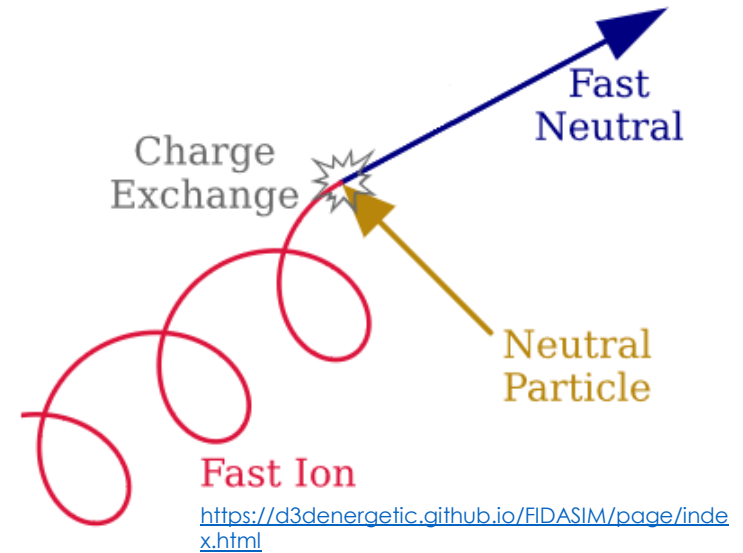
Losses due to Charge eXchange (CX) reaction between a fast ion and a neutral particle in the plasma (pay attention, it is a different reaction wrt to NBI fast particle ionization by CX, but beam halo can contribute to these losses)



Fast neutrals escape the plasma, with lower probability of being ionized

Where do the neutrals come from?

- Gas puff (cold neutrals)
- Pellet injection
- CX NBI ionization (thermal neutrals = beam halo)



- In small experiments CX losses can be up to 20-30% of the injected NBI power
- $H_{fast}^0$  can then be re-ionized before leaving the plasma, broadening the power deposition profile
- In future reactors we expect very high temperature and density, therefore small neutral density in the plasma and low CX fast ion losses



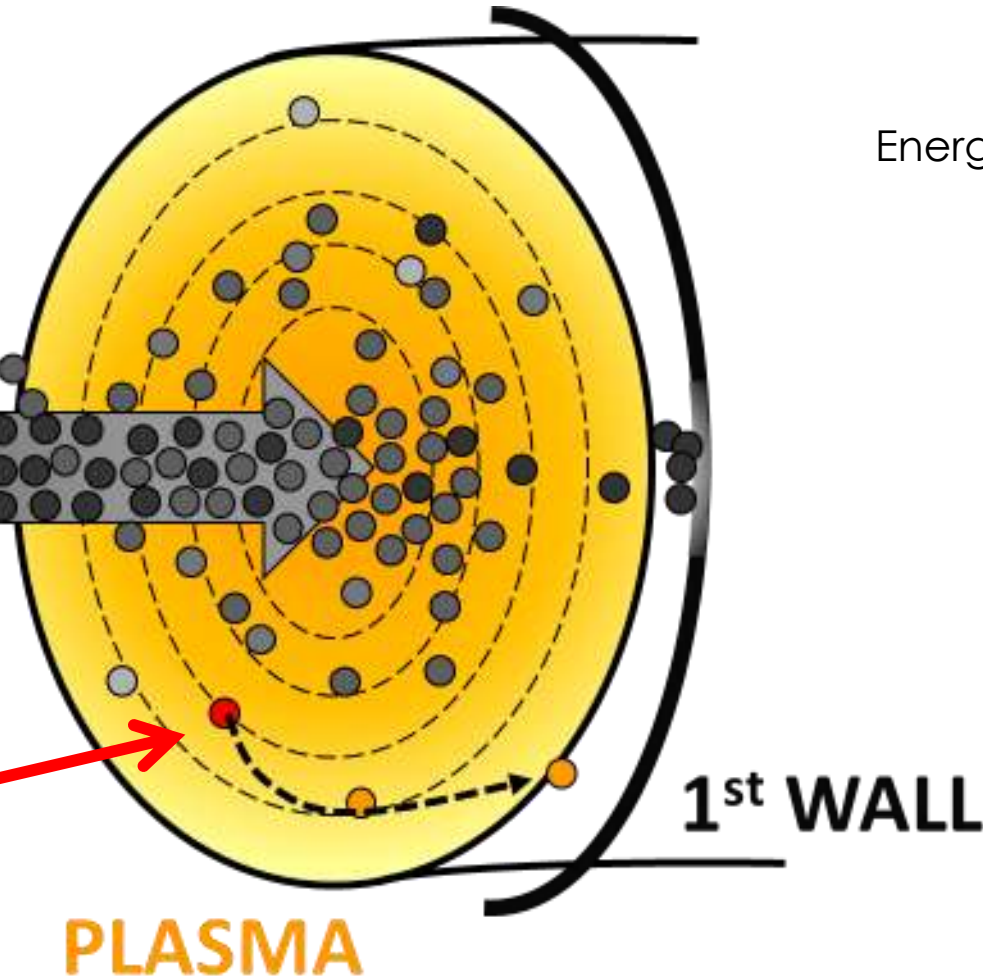
# Energetic particle losses

- neutral particles
- fast ions
- slowing down fast ions
- background neutrals



NBI

Orbit losses  
e.g. due to scattering processes



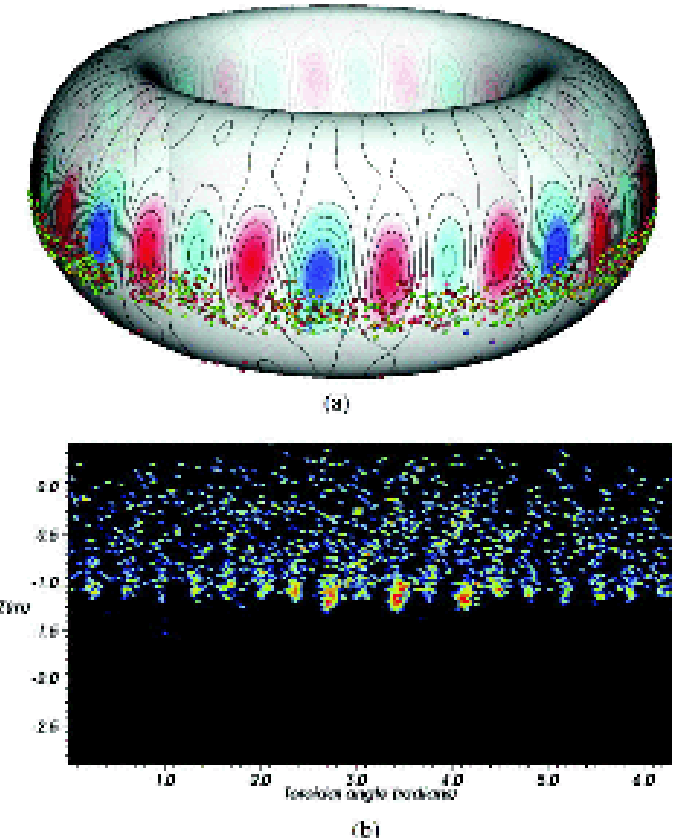
Energetic particle losses:  
Scrape-off layer  
First orbit  
Charge-exchange  
Orbit  
Shine-through



# Orbit losses

Similar to first orbit losses but happening for confined **fast ions that move into unconfined orbits**:

- Losses can be due to pitch-angle scattering: after a collision the fast ions move into a unconfined orbit
- Since the **pitch-angle scattering** is stronger with ion-ion collisions, these losses are more probable when  $E_{\text{fast ion}} \approx E_c$
- Orbit losses are more probable for edge fast ions
- Orbit losses can be a result also of fast ion redistribution due to **turbulence** and **instabilities**

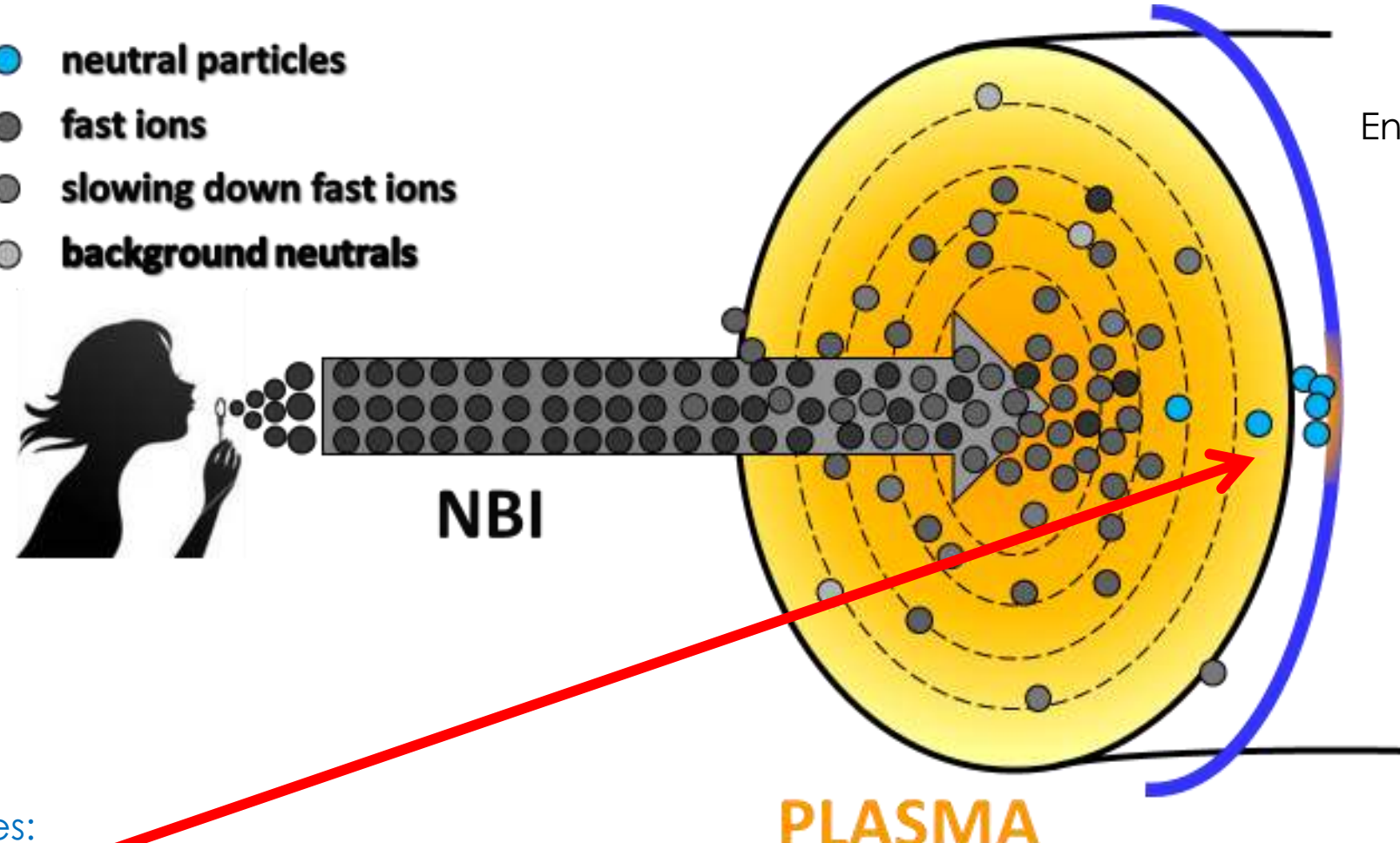


# Energetic particle losses

- **neutral particles**
- **fast ions**
- **slowing down fast ions**
- **background neutrals**



NBI



Shine through losses:

part of the beam not ionized passing through plasma

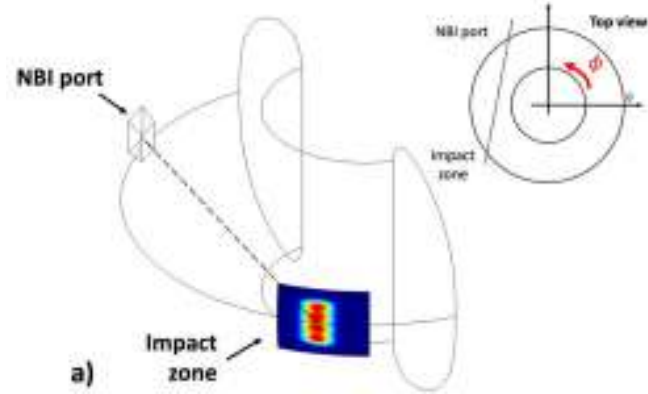
Energetic particle losses:  
Scrape-off layer  
First orbit  
Charge-exchange  
Orbit  
**Shine-through**



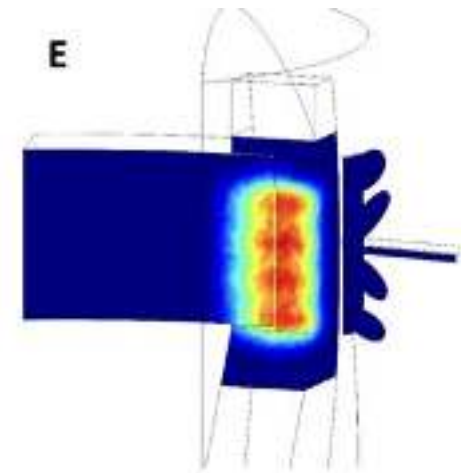
# Shine-through losses

The fraction of the **neutral beam, which is not ionised** in the plasma and passes through it colliding with the first wall causes the so-called **shine-through losses**.

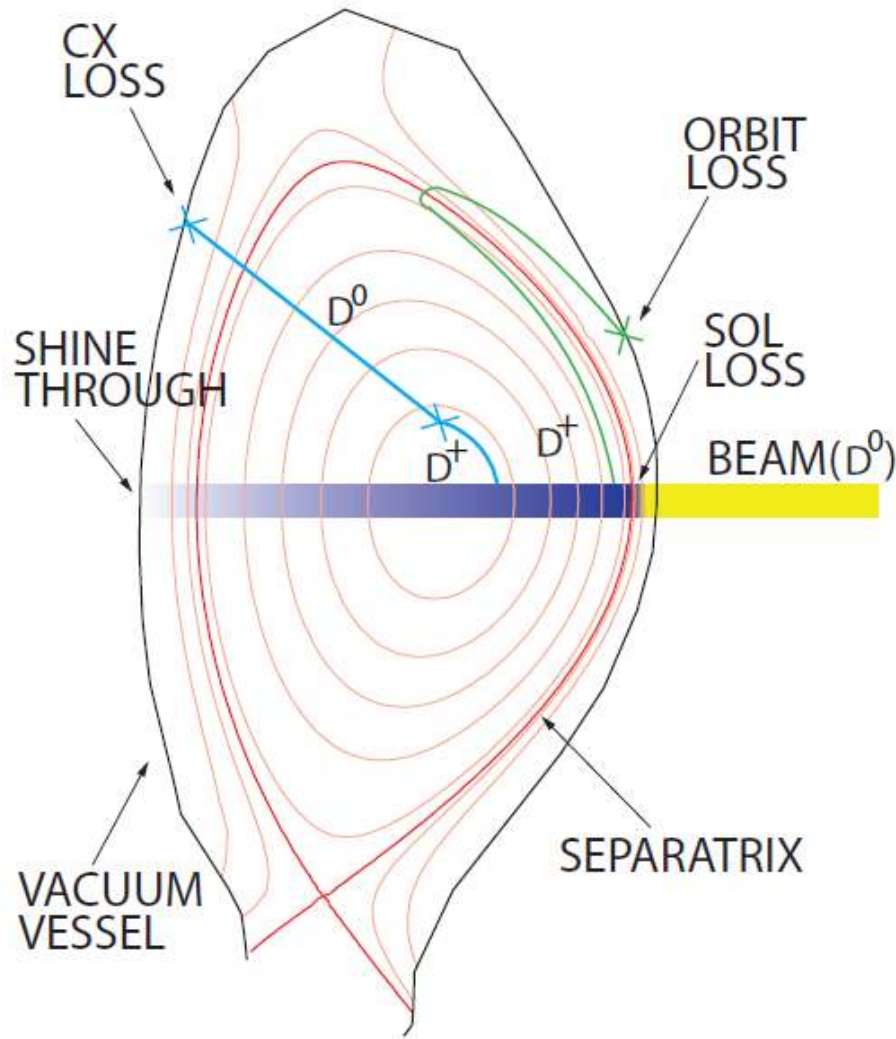
- shine-through losses can cause localized **wall hot spots** with the risk of exceeding the first wall thermal load limit (sometimes the wall is strengthened explicitly by armours)
- Shine-through increases exponentially with  $\sim E_{\text{NBI}}/n$
- Usually, a **lower limit on plasma density** is set for NBI operation due to shine-through
- In current experiments this is one of the highest loss channels for NBI (up to 5 - 10% or more); for ITER and future reactors it will be relevant only in low-density phases (e.g. ramp-up/down phase)



DTT case



# Energetic particle losses



# Contents

- Introduction
- H&CD systems
- Neutral Beam Injection (NBI)
- NBI: from generation to the plasma
  - Neutral beam generation
  - Neutral beam ionization
  - Fast ion orbits and slowing down
- Beam energetic particle losses
- **NBI modelling techniques**
- Conclusion



# Measuring NBI effectiveness is hard

Fast ion-related quantities are difficult to measure, e.g.:

## Heating:

- Indirect from estimation of NBI losses
- profile: indirectly from temperature measurements and modelling

## Total driven current:

- comparing the loop voltage between a current-drive discharge and reference discharge, matching the relevant plasma profiles (as much as possible)

## Driven current profile:

- using Motional Stark effect (MSE): local direction of  $B \rightarrow$  at best  $q(r)$  profile  $\rightarrow j(r)$  profile
- forward modelling on MSE measurements

## Fast ion distribution function:

- measuring the fast neutrals escaping the plasma generated by CX processes between fast ions and background neutrals (e.g. FIDA)

More information on diagnostics and NBI used as diagnostic in another lesson (?)



# NBI modelling

Estimating quantities related to NBI-plasma interaction requires **modelling**.

NBI modelling is used for data **interpretation** and for **predictions** (e.g. for design of future machines)

NBI modelling requires two steps:

1. Modelling the injection and ionization of energetic neutral particles



**Beam deposition codes**

Example of pure deposition codes: BBNBI, NEMO...

M. Schneider et al., 2015, 42<sup>nd</sup> EPS on Plasma Physics, P2.159

NEMO: M. Schneider et al 2011 Nucl. Fusion 51 063019

BBNBI: Asunta O et al 2015 Comput. Phys.Commun. 188 33–46



# NBI modelling

Estimating quantities related to NBI-plasma interaction requires modelling.

NBI modelling is used for data interpretation and for predictions (e.g. for design of future machines)

NBI modelling requires two steps:

1. Modelling the injection and ionization of energetic neutral particles



**Beam deposition codes**

2. Modelling the dynamics (slowing down) of NBI ions in the plasma



**Fokker-Planck solvers**

(↔ fast ion distribution function)

Example of pure Fokker-Planck solvers: ASCOT, SPOT, RISK...

M. Schneider et al., 2015, 42<sup>nd</sup> EPS on Plasma Physics, P2.159

ASCOT: E. Hirvijoki et al, Computer Physics Communications, pp. 1310-1321, 2014

SPOT: M. Schneider et al., Nucl. Fusion 49 (2009) 125005

RISK: M. Schneider et al., Nucl. Fusion 55 (2015) 013003

P. Vincenzi – Physics of NBI heating and current drive



# NBI modelling

NBI codes can have different approaches (impacting on precision and time consumption):

a. **(Semi-) Analytical** solutions / simplified modelling / scaling laws:

- Beam ionization solved numerically in small steps on straight line(s) representing the beam
- Simple beam geometry (pencil-like)
- Power deposition (total, to electrons, to ions), current-drive, momentum source calculated using analytical formulae
- Fast simulation time
- Stand-alone codes or modules of integrated codes (e.g. transport suites)

E.g.: PENCIL (JETTO suite), Rabbit (stand-alone),  
METIS (integrated), NEMO-RISK (CRONOS suite)

- 3D beam shape but analytical ionization calculation: BTR

PENCIL: M. Stubberfield and M.L. Watkins, Multiple Pencil Beam, JET-DPA(06)/87, 1987

Rabbit: M. Weiland et al 2018 Nucl. Fusion 58 082032

METIS: J.F. Artaud et al 2018 Nucl. Fusion 58 105001

NEMO: M. Schneider et al 2011 Nucl. Fusion 51 063019

BTR: E. Dlougach et al Appl. Sci. 2022, 12, 8404



# NBI modelling

A typical problem for fast ion modelling is the estimation of the fast ion distribution function.

In general, the time evolution of the distribution function can be described by the Fokker-Planck equation:

$$\frac{df}{dt} = C + S + L$$

- C is the collision term (fast ion – background plasma or fast ion – fast ion)
- S is the source term (beam ionization)
- L is a loss term (e.g. fast ion losses)

Many approximations can be done<sup>1,2</sup>, and usually we are interested of stationary solutions ( $df/dt=0$ ).

<sup>1</sup>Rome J A 1976 Nucl. Fusion 16 55

<sup>2</sup>R. Koch (2010) Fusion Science and Technology, 57:2T



# NBI modelling

A typical problem for fast ion modelling is the estimation of the fast ion distribution function.

In general, the time evolution of the distribution function can be described by the Fokker-Planck equation:

$$\frac{df}{dt} = C + S + L$$

In order to find an analytical solution for  $f$ , we assume<sup>1</sup>:

- Fast ion bounce frequency  $\gg$  collision frequency
  - In this approximation we have the following constant of motion:
    - Fast ion kinetic energy  $E = \frac{1}{2}mv^2$
    - Toroidal canonical angular canonical momentum  $P_\phi = mRv_{par} + q\psi$
    - Magnetic moment (adiabatic invariant)  $\mu = \frac{mv_{perp}^2}{2B_{tot}}$
  - $f(E, P_\phi, \mu)$
  - A point in the constant of motion phase space  $(E, P_\phi, \mu)$  represents an entire orbit
  - Collisions will move points in the phase space ("kicks")
- Still, the equation is too complex to be solved analytically

<sup>1</sup>Rome J A 1976 Nucl. Fusion 16 55



# NBI modelling

A typical problem for fast ion modelling is the estimation of the fast ion distribution function.

In general, the time evolution of the distribution function can be described by the Fokker-Planck equation:

$$\frac{df}{dt} = C + S + L$$

In order to find an analytical solution for  $f$ , we assume<sup>1</sup>:

- $f$  is independent of  $P_\phi$ , i.e. the fast ions remains close to a given flux surface during the slowing down (“small banana width approximation) – hardly true for trapped energetic particles
- neglecting trapped particles when performing the integral around an entire bounce orbit

<sup>1</sup>Rome J A 1976 Nucl. Fusion 16 55



# NBI modelling

The resulting analytic solution of the Fokker-Planck equation is:

$$f(v, \xi, t) = U\left[t - \frac{\tau_s}{3} \ln\left(\frac{v_0^3 + v_c^3}{v^3 + v_c^3}\right)\right] \frac{\tau_s}{2\pi(v^3 + v_c^3)} \left[\frac{v_0^3 + v_c^3}{v^3 + v_c^3}\right]^{-\frac{\tau_s}{3\tau_{cx}}} \times \sum_{n=0}^{\infty} \left(n + \frac{1}{2}\right) P_n(\xi) P_n(\xi_0) \left[\frac{v_0^3 + v_c^3}{v^3 + v_c^3} \frac{v^3}{v_0^3}\right]^{\frac{m_i n(n+1) \langle Z \rangle}{6m_{fast\ ion}[Z]}} U(v_0 - v)$$

- $U$  is the step function
- $P_n$  are Legendre polynomials
- $\xi$  is the pitch ( $\xi_0$  the initial pitch)
- $\tau_s$  the slowing down time
- $v_0$  the initial fast ion velocity,  $v_c$  the critical velocity  $v_c = \sqrt{\frac{2E_c}{m_{fast\ ion}}}$
- $\tau_{cx}$  the charge exchange time

$$[Z] \equiv \sum_j n_j z_j^2 \left(\frac{m_i}{m_j}\right) / \sum_j n_j z_j$$

$$\langle Z \rangle \equiv \sum_j n_j z_j^2 / \sum_j n_j z_j$$



# NBI modelling

The resulting analytic solution of the Fokker-Planck equation is:

$$f(v, \xi, t) = U \left[ t - \frac{\tau_s}{3} \ln \left( \frac{v_0^3 + v_c^3}{v^3 + v_c^3} \right) \right] \frac{\tau_s}{2\pi(v^3 + v_c^3)} \left[ \frac{v_0^3 + v_c^3}{v^3 + v_c^3} \right]^{-\frac{\tau_s}{3\tau_{cx}}} \times \sum_{n=0}^{\infty} \left( n + \frac{1}{2} \right) P_n(\xi) P_n(\xi_0) \left[ \frac{v_0^3 + v_c^3}{v^3 + v_c^3} \frac{v^3}{v_0^3} \right]^{\frac{m_i n(n+1)\langle Z \rangle}{6m_{fast ion}[Z]}} U(v_0 - v)$$

$= 1/2$

Approximations:

## 1. Neglect fast ion velocity distribution anisotropy

- $n=0 \rightarrow P_0(x) = 1$
- Legendre polynomials are even functions  $\rightarrow n=1$  term is zero  
 $\rightarrow$  No dependence from the pitch  $\xi$



# NBI modelling

The resulting analytic solution of the Fokker-Planck equation is:

$$f(v, \xi, t) = U \left[ t - \frac{\tau_s}{3} \ln \left( \frac{v_0^3 + v_c^3}{v^3 + v_c^3} \right) \right] \frac{\tau_s}{2\pi(v^3 + v_c^3)} \left[ \frac{v_0^3 + v_c^3}{v^3 + v_c^3} \right]^{-\frac{\tau_s}{3\tau_{cx}}} \times \sum_{n=0}^{\infty} \left( n + \frac{1}{2} \right) P_n(\xi) P_n(\xi_0) \left[ \frac{v_0^3 + v_c^3}{v^3 + v_c^3} \frac{v^3}{v_0^3} \right]^{\frac{m_i n(n+1)\langle Z \rangle}{6m_{fast ion}[Z]}} U(v_0 - v)$$

Approximations:

1. Neglect fast ion velocity distribution anisotropy
2. Stationary solution ( $t \gg \tau_s$ )  
→ No time dependence



# NBI modelling

The resulting analytic solution of the Fokker-Planck equation is:

$$f(v, \xi, t) = U \left[ t - \frac{\tau_s}{3} \ln \left( \frac{v_0^3 + v_c^3}{v^3 + v_c^3} \right) \right] \frac{\tau_s}{2\pi(v^3 + v_c^3)} \left[ \frac{v_0^3 + v_c^3}{v^3 + v_c^3} \right]^{-\frac{\tau_s}{3\tau_{cx}}} \times \sum_{n=0}^{\infty} \left( n + \frac{1}{2} \right) P_n(\xi) P_n(\xi_0) \left[ \frac{v_0^3 + v_c^3}{v^3 + v_c^3} \frac{v^3}{v_0^3} \right]^{\frac{m_i n(n+1)\langle Z \rangle}{6m_{fast ion}[Z]}} U(v_0 - v)$$

Approximations:

1. Neglect fast ion velocity distribution anisotropy
2. Stationary solution ( $t \gg \tau_s$ )
3. Neglect background neutrals  
→  $\tau_{cx} = \infty$

=1/2



# NBI modelling

The resulting analytic solution of the Fokker-Planck equation is:

$$f(v, \xi, t) = U \left[ t - \frac{\tau_s}{3} \ln \left( \frac{v_0^3 + v_c^3}{v^3 + v_c^3} \right) \right] \frac{\tau_s}{2\pi(v^3 + v_c^3)} \left[ \frac{v_0^3 + v_c^3}{v^3 + v_c^3} \right]^{-\frac{\tau_s}{3\tau_{cx}}} \times \sum_{n=0}^{\infty} \left( n + \frac{1}{2} \right) P_n(\xi) P_n(\xi_0) \left[ \frac{v_0^3 + v_c^3}{v^3 + v_c^3} \frac{v^3}{v_0^3} \right]^{\frac{m_i n(n+1)\langle Z \rangle}{6m_{fast ion}[Z]}} U(v_0 - v)$$

Approximations:

1. Neglect fast ion velocity distribution anisotropy
2. Stationary solution ( $t \gg \tau_s$ )
3. Neglect background neutrals  
→  $\tau_{cx} = \infty$

Resulting:

$$f(v) = \frac{\tau_s}{2\pi(v^3 + v_c^3)} \times \frac{1}{2} U(v_0 - v) = \frac{\tau_s}{4\pi(v^3 + v_c^3)} U(v_0 - v)$$

- Commonly used in fast NBI modelling tools (e.g. METIS)



# NBI modelling

The resulting analytic solution of the Fokker-Planck equation is:

$$f(v, \xi, t) = U \left[ t - \frac{\tau_s}{3} \ln \left( \frac{v_0^3 + v_c^3}{v^3 + v_c^3} \right) \right] \frac{\tau_s}{2\pi(v^3 + v_c^3)} \left[ \frac{v_0^3 + v_c^3}{v^3 + v_c^3} \right]^{-\frac{\tau_s}{3\tau_{cx}}} \times \sum_{n=0}^{\infty} \left( n + \frac{1}{2} \right) P_n(\xi) P_n(\xi_0) \left[ \frac{v_0^3 + v_c^3}{v^3 + v_c^3} \frac{v^3}{v_0^3} \right]^{\frac{m_i n(n+1)\langle Z \rangle}{6m_{fast ion}[Z]}} U(v_0 - v)$$

Approximations:

1. Neglect fast ion velocity distribution anisotropy
2. Stationary solution ( $t \gg \tau_s$ )
3. Neglect background neutrals  
→  $\tau_{cx} = \infty$

Resulting:

$$f(v) = \frac{\tau_s}{2\pi(v^3 + v_c^3)} \times \frac{1}{2} U(v_0 - v) = \frac{\tau_s}{4\pi(v^3 + v_c^3)} U(v_0 - v)$$

- Beam particle density:  $n_b f(v) = \frac{P}{eE_0} \frac{\tau_s}{4\pi(v^3 + v_c^3)} U(v_0 - v)$



# NBI modelling

NBI codes can have different approaches (impacting on precision and time consumption):

a. **(Semi-) Analytical** solutions / simplified modelling / scaling laws:

b. **Monte Carlo** solvers (e.g. orbit following in phase space):

- Initialization of a random test particle following a given distribution
- Each Monte Carlo test particle represents N real particles, through weights
- Random test particles are followed until particle thermalization (e.g.  $E > 3/2$  local  $T_i$ ) or loss
- Detailed beamline/tokamak geometries
- Detailed physics (e.g. collisions, impurities, orbit drifts, finite Larmor radius effects, 3D magnetic fields, ...)
- Long computational time
- Usually stand-alone codes, or used in detailed transport modelling

E.g.: BBNBI & ASCOT (stand-alone), NUBEAM (TRANSP suite), SPOT (CRONOS suite) etc...

BBNBI: Asunta O et al 2015 Comput. Phys.Commun. 188 33–46

ASCOT: E. Hirvijoki et al, Computer Physics Communications, pp. 1310-1321, 2014

NUBEAM: Pankin A. et al., 2004 Comput. Phys. Commun. 159 157–84

SPOT: M. Schneider et al., Nucl. Fusion 49 (2009) 125005



# NBI modelling

Fast codes using **analytical solutions** of fast ion Fokker-Planck equation, well suitable for sensitivity studies.

**Simplified approach**

Orbit-following **Monte Carlo codes** solving kinetic equation for fast ions, which can take into account fast ions orbit effects.

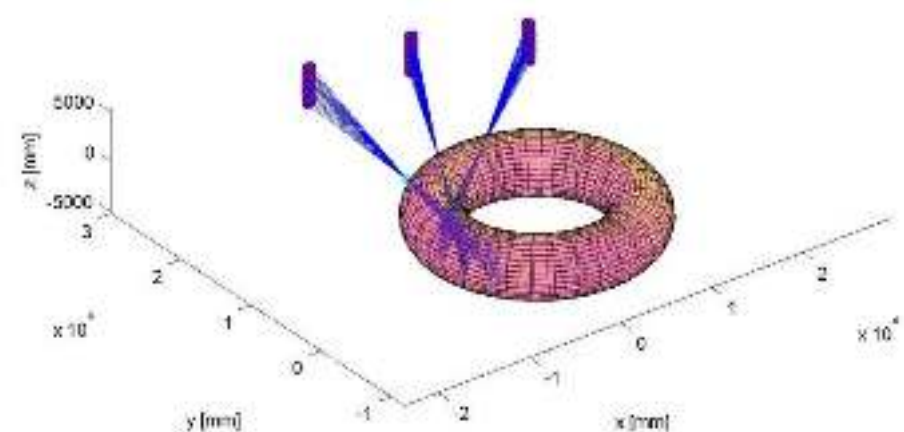
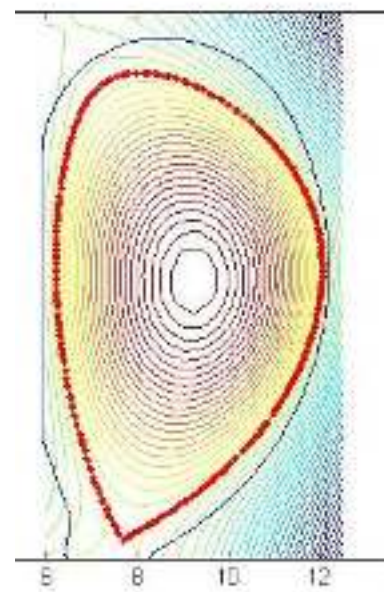
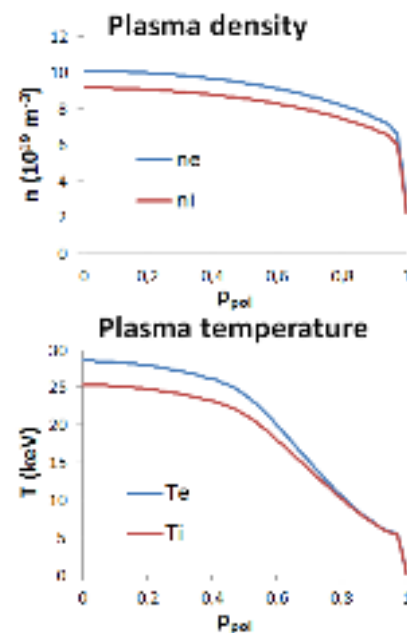
**Long simulation time, but detailed**



# NBI modelling

Typical **inputs** for NBI codes:

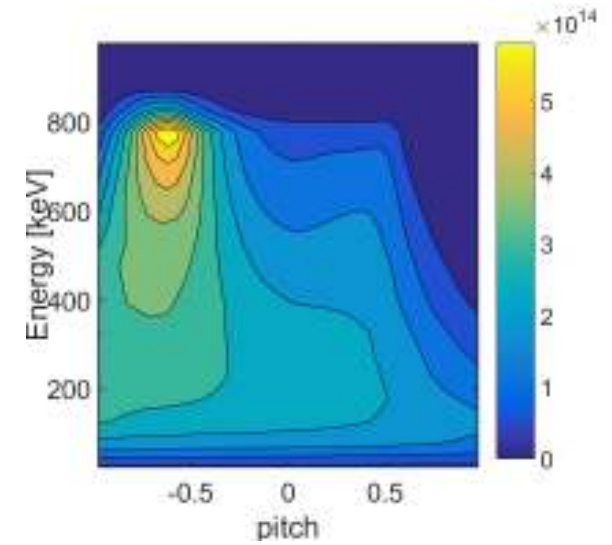
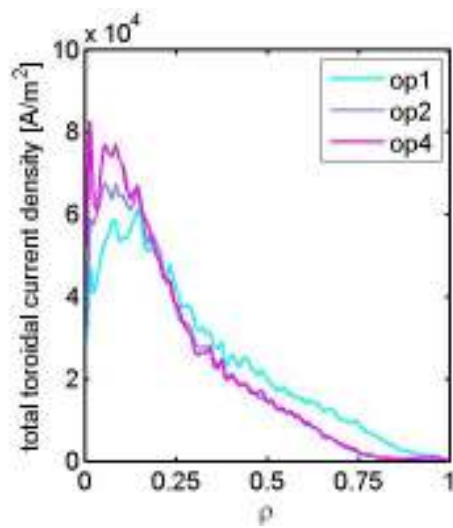
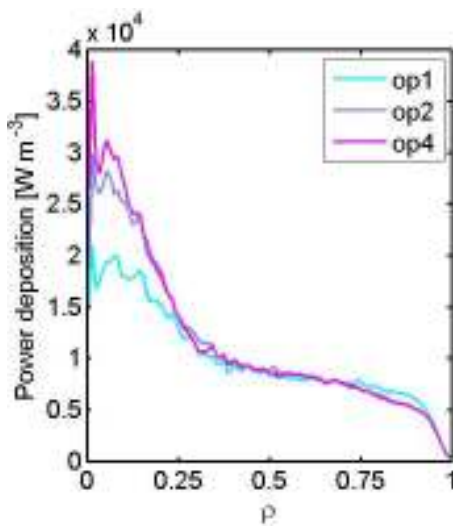
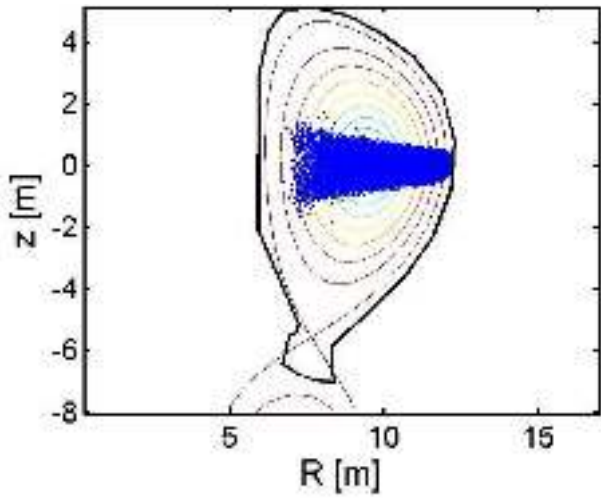
- Plasma profiles and characteristics (isotope, impurities, neutrals...)
- Plasma magnetic equilibrium (and MHD)
- Machine geometry (wall, size...)
- Injection and beam geometry (injection line, beamlets, divergence...)
- Beam parameters (energy, power, isotope)



# NBI modelling

Typical **outputs** of NBI codes:

- Beam ionization and shine-through losses
- Power deposition
- Orbit losses
- Current-drive
- Input torque
- Fast ion distribution function
- ...

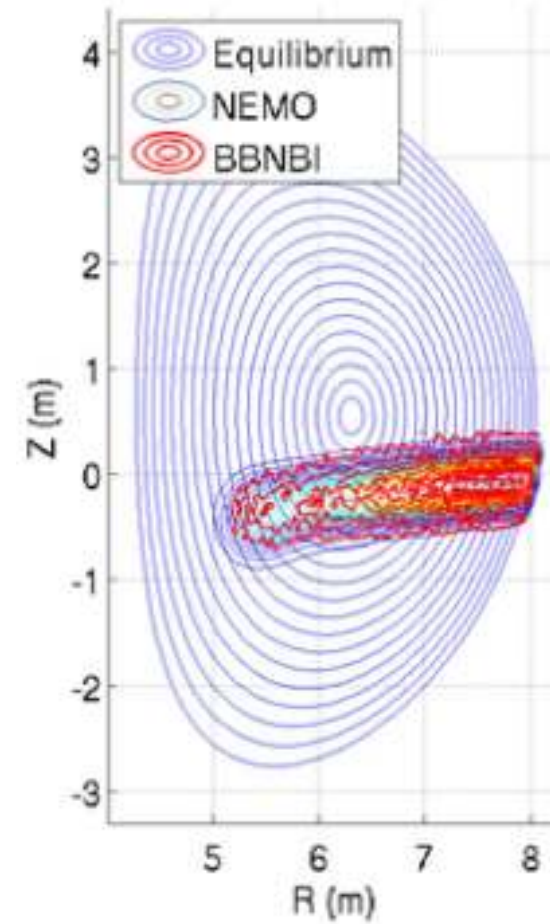
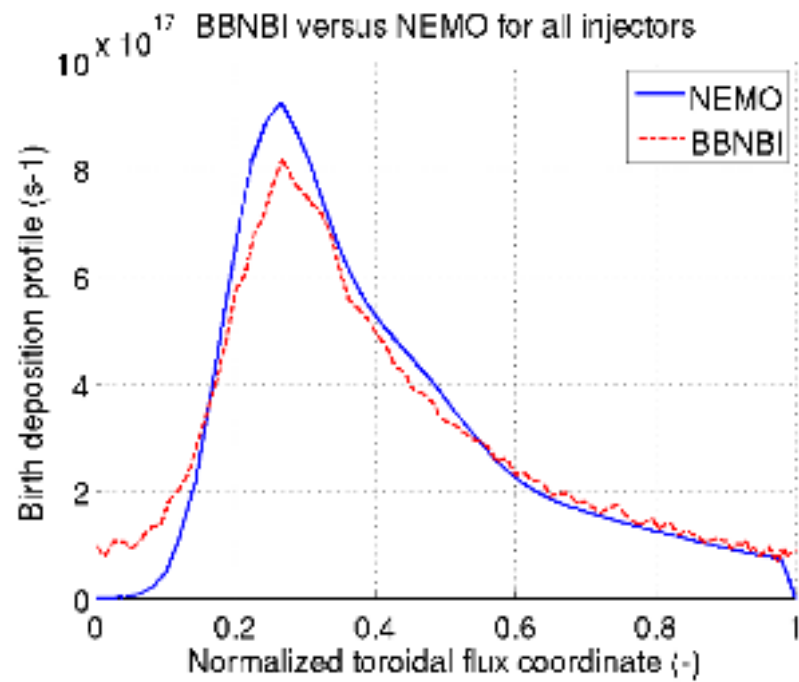


# NBI code benchmark

Different solutions (i.e. codes) of the same problem must agree if the inputs are the same.  
NBI models and numerical codes are benchmarked towards other codes to prove their reliability.  
Here an example for ITER studies:

Beam deposition codes:

BBNBI (Monte Carlo) vs NEMO (narrow-beam model)



# NBI code benchmark

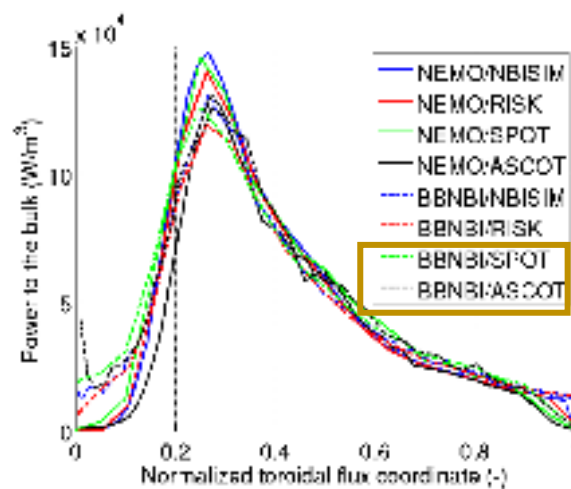
Different solutions (i.e. codes) of the same problem must agree if the inputs are the same.

NBI models and numerical codes are benchmarked towards other codes to prove their reliability.

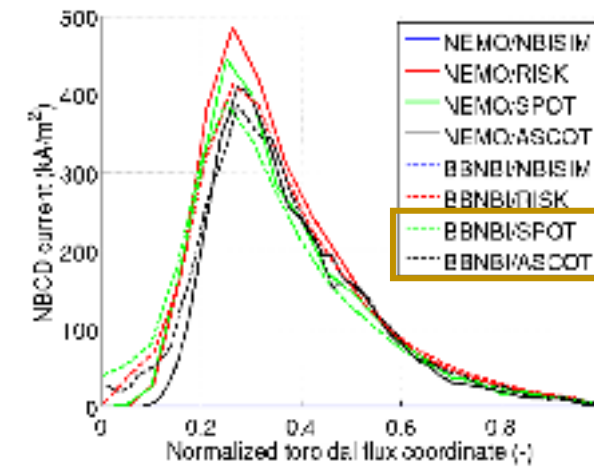
Here an example for ITER studies:

Some Fokker-Planck solvers (they can be combined with deposition codes):

- NBISIM\* is a simple 1D analytic model
- RISK\* is a 2D Fokker-Planck code that combines finite elements and an eigenfunction expansion
- ASCOT and SPOT are Monte Carlo codes with a high level of accuracy including orbit width effects



Highest accuracy



\*They use the so-called zero-banana-width limit



# Contents

- Introduction
- H&CD systems
- Neutral Beam Injection (NBI)
- NBI: from generation to the plasma
  - Neutral beam generation
  - Neutral beam ionization
  - Fast ion orbits and slowing down
- Beam energetic particle losses
- NBI modelling techniques
- **Conclusion**



# In the end

NBI works only because:

- ...the cross sections for CX and ionization between an ion beam and a neutral gas are just adequate for efficient neutralization
- ...the cross sections for ionization are just adequate for an efficient beam ionization in the plasma
- ...the collision frequency in the plasma is just adequate for slowing down of fast ions and energy transfer



# Bibliography

This presentation has been prepared with material from:

- ITER: [www.iter.org](http://www.iter.org)
- EUROfusion: [www.euro-fusion.org](http://www.euro-fusion.org)
- Consorzio RFX: [www.igi.cnr.it](http://www.igi.cnr.it)
- PPPL institute: [www.pppl.gov](http://www.pppl.gov)
- Max-Planck-Institut für Plasmaphysik: [www.ipp.mpg.de](http://www.ipp.mpg.de)
- Wesson John and Campbell David J., Tokamaks. Oxford University Press, 2004
- Kikuchi M., Lackner K. and Tran M. Q., Fusion Physics, IAEA, 2012
- Freidberg J., Plasma physics and fusion energy, Cambridge university press, 2007
- C. Hopf and A. Stäbler (IPP, DE) in "Neutral beam heating and current drive (physics)" for Fusion science and engineering course (European Doctorate)
- R. Koch (2010) Fast Particle Heating, *Fusion Science and Technology*, 57:2T, 185-195, DOI: 10.13182/FST10-A9409
- Egbert Westerhof (2010) Non-Inductive Current Drive, *Fusion Science and Technology*, 57:2T, 222-229, DOI: 10.13182/FST10-A9413
- M. Cavedon, IPP (Master thesis in Physics, "Power losses mechanisms for Neutral Beam injected particles in ASDEX Upgrade tokamak under different plasma configurations", 2012, Unipd)
- P. Vincenzi, "Interaction between neutral beam fast particles and plasma in fusion experiments", Ph.D thesis, Padova 2016 (<http://paduar esearch.cab.unipd.it/9280/>)

...and all the material cited in the slides!



*Joint European Doctorate in Fusion Science  
and Engineering*

***Physics of RF Heating and  
Current Drive***

**G.Granucci**

*DTT s.c.a r.l. - Frascati*

*Istituto per la Scienza e Tecnologia dei Plasmi – Milano*

International Joint Doctorate In Fusion Science  
And Engineering

## **FIRST PART**

- ❖ Introduction on RF wave in Plasmas
- ❖ Basic theory of wave-plasma interaction
  - ❖ Unmagnetized Plasma
  - ❖ Wave Damping

## **SECOND PART**

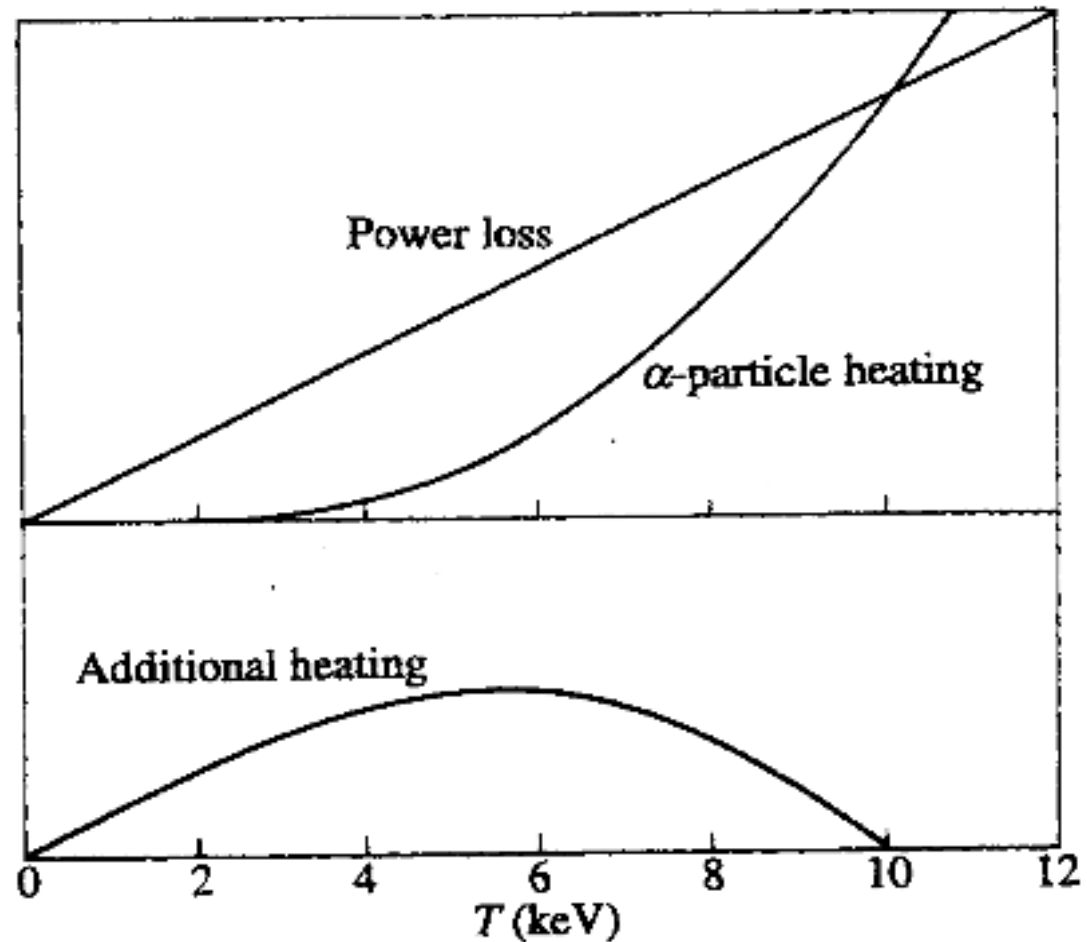
- ❖ Electron Cyclotron Heating in Fusion Plasmas
  - ❖ ECCD mechanism
  - ❖ Wave Polarization relevance
  - ❖ Propagation and absorption in tokamak
- ❖ Application of ECH waves:
  - ❖ EC assisted start-up
  - ❖ MHD Control

# Auxiliary Heating: why?

J.Wesson – Tokamaks –  
1<sup>st</sup> Edition – 1987

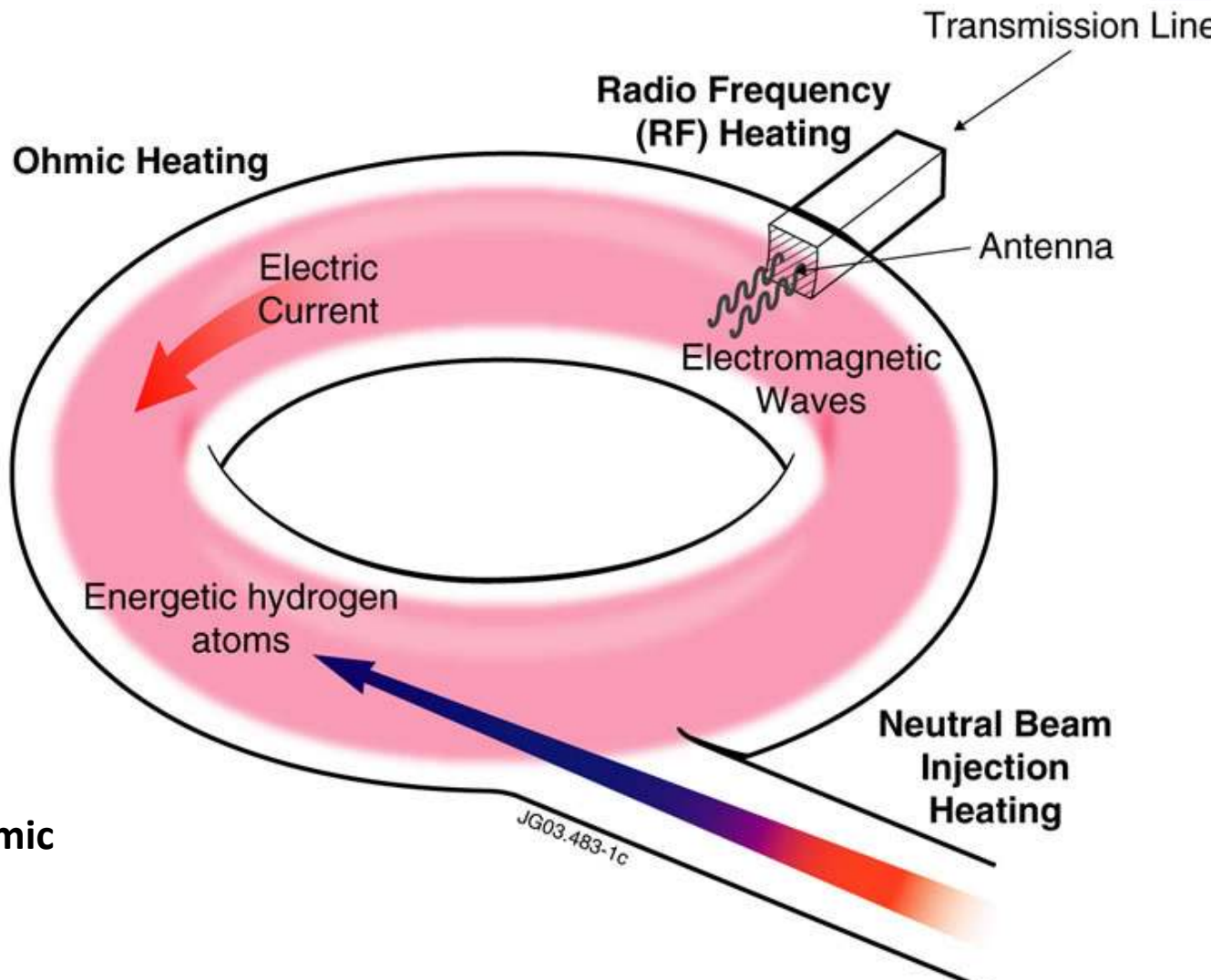
**Additional  
or  
Fundamental ?**

## 1.5 Ignition



*Without external plasma heating temperature for Nuclear Fusion cannot be reached in any magnetic confinement device.*

# How to heat Plasma



Internal heating : Ohmic

External heatings:

**NBI** by Kinetic Energy

**ICH, ECH, LH, IBW....** by E.M. wave

Main RF Heating waves exploited in Nuclear Fusion devices to heat plasma:

**ECW:** Electro Cyclotron Waves. Heat Electrons in millimetre wave range (2.45 GHz - 170 GHz)

LH: Lower Hybrid. Heat electrons in centimeter wave range

**ICW:** Ion Cyclotron Wave. Heat ions in RF wave range (MHz)

**IBW:** Ion Bernstein wave: Heat Ions in RF wave Range (MHz)

*E.M. waves transfers energy to charged particle in plasma in correspondence of resonances, a combination of local conditions between magnetic field, particles energy/temperature and wave frequency.*

# Heating System in main Experiments

Device	NBI	ECRH	ICRH	LH
JET	<i>32 MW</i>		<i>10 MW</i>	<i>7.2 MW</i>
AUG	20 MW	6 MW	6 MW	
FTU		<i>1.4 MW</i>	<i>0.5 MW of IBW</i>	<i>2.4 MW</i>
D-IIID	20 MW	4 MW	1 MW Helicon FW	
WEST		2 MW	9 MW	7MW
TCV	1MW	5 MW		
JT60-SA	34 MW	7MW		
W7-X	19 MW	10 MW	1.5 MW	
EAST	8 MW	4 MW	12 MW	10 MW
KSTAR	8 MW	0.5 MW	6 MW	

**ITER :**

**NNBI =32 MW**

**ECRH = 24 MW +24 MW + ?**

**ICRH= 10 MW**

**DTT :**

**NNBI = 10 MW**

**ECRH = 32 MW**

**ICRH= 8 MW**

**SPARC: ICRH for 48 MW**

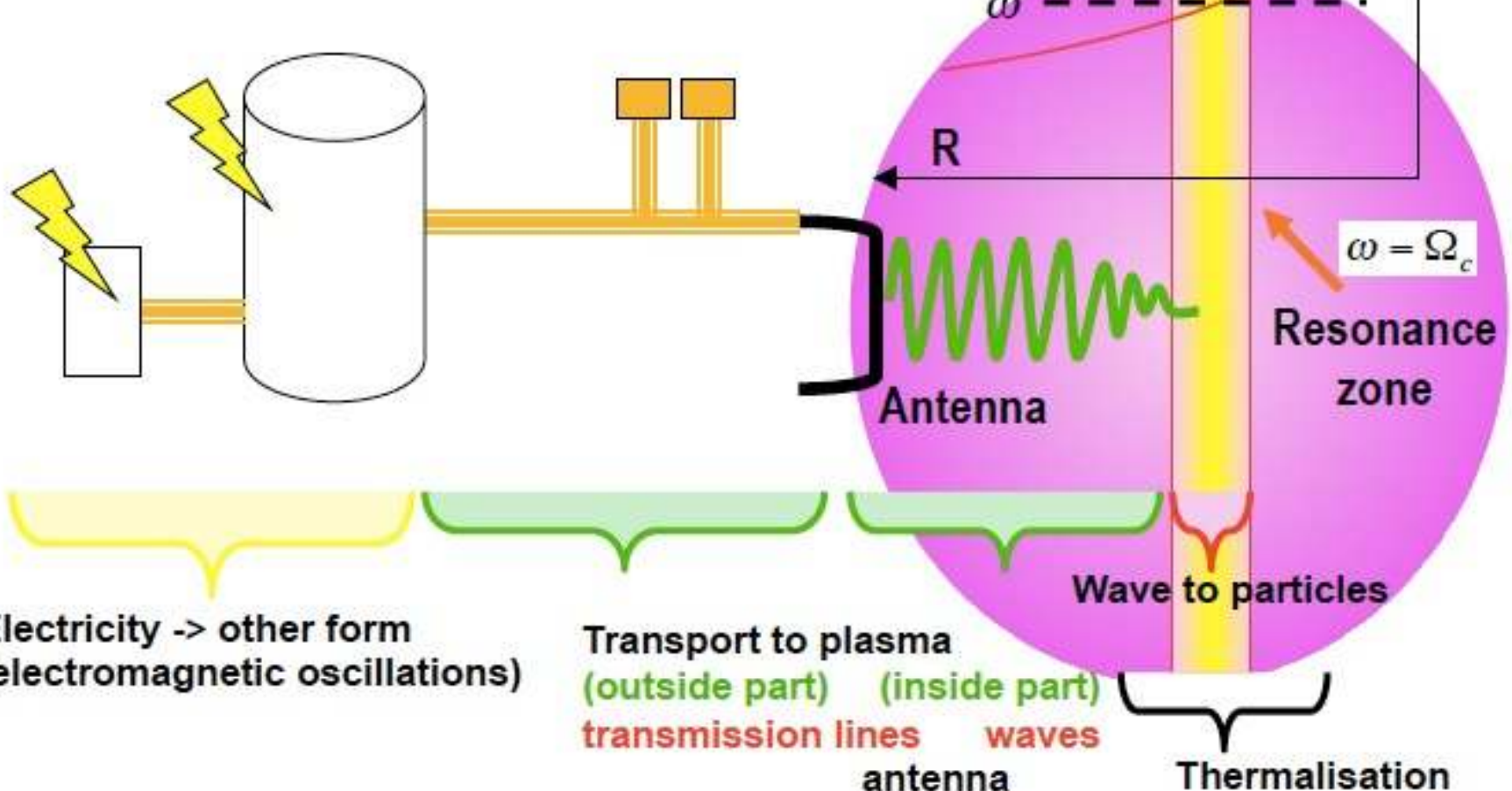
**DEMO project is studying an option fully relying on ECRH**

*RF heating system will play major role in future tokamaks and in perspective for the Reactor*

# Cyclotronic Wave Heating

$$\Omega_c = \frac{ZeB}{m}$$

IPP



# Typical Functions of RF Systems

Tasks	ECRH	ICRH	LH
Break down & Plasma start up	X	X	
Plasma Current Ramp up	X	X	X
H-mode access	X	X	X
Electron Heating	X	X	X
Direct Ion Heating		X	
Non Inductive Current drive	X		X
MHD Control	X	X	
Fast Particle Generation		X	
Profiles Control	X	X	X
Impurity Accumulation Avoidance	X	X	
Transport Studies	X		
Diagnostics (heat pulse)	X		
Wall Cleaning	X	X	

## Energy transfer from e.m. waves to plasma

When e.m. waves crosses plasma its **Electric field** accelerates charged particles that transfer this energy by collision to plasma

Collisional absorption scales with  $T_e^{-3/2}$  and is ineffective (as ohmic ones) to heat a hot plasma (as required to reach the fusion conditions)

Waves can transfer energy to plasma also trough **resonant mechanism** that are **collisionless** and can produce strong direct heating

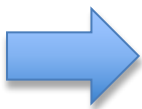
In a multispecies magnetized plasma there are several of resonances.

The variety of waves existing in a magnetized plasma allows different RF heating schemes, generally at different frequencies.

An RF Heating system based on e.m. waves is composed by 3 main elements:

- **Power generator**
- **Low loss transmission lines**
- **Antenna**

Antenna launches (couples) waves in the plasma

 waves propagate up to absorption layer and transfer energy (heat or momentum) to plasma

 The location of the absorption layer should be controlled

The study of the **waves propagation** is at the basis of the selection of the proper RF heating systems (i.e. of the frequency and of the antenna )

E.M. wave propagation in plasma is (can be) quite complex to be treated formally and is outside the scope of this lecture.

Some simplifications are considered to approach the problem of a realistic tokamak plasma.

The most common and valid approach is the:  
**cold magnetized plasma model**

*The model is enough accurate to describe wave propagation in plasma, **except in regions close to resonance and cut-off***

Close to these special regions the **thermal** corrections become important because the wave phase velocity is comparable to the thermal one and the perpendicular wave length (wrt the external magnetic field) is similar to the Larmor radius.

To study energy absorption it is necessary the ***warm model***

**Cold model** -> fluid equations, no temperature effect

**Warm Model** -> finite Larmor radius plays a role

- **Coupling** cold plasma
  - **Propagation** cold plasma (warm plasma)
  - **Absorption** warm plasma

The mathematical approach is the following:

**Maxwell equations + Generalize Ohm's law    applied to**

**Plane waves:**

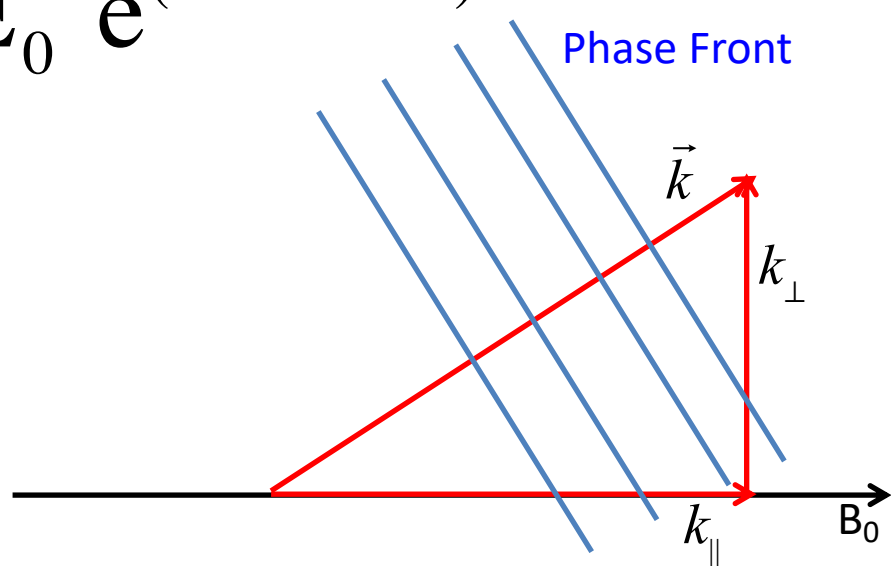
$$\tilde{E}(r,t) = \tilde{E}_0 e^{(-i\omega t + \vec{k} \cdot \vec{r})}$$

where

$\mathbf{k}$  = wave vector =  $2\pi/\lambda$

$\omega$  = angular frequency =  $2\pi f$

Other useful quantities:



$v_{ph}$  = phase velocity =  $\omega/k$

$v_g$  = group velocity =  $d\omega/dk$

$N = v_{ph}/c$  = refractive index =  $k/\omega c$

$\vec{k}$  Response of Plasma

$\omega$  Fixed by Generator

Maxwell equations



$$\left. \begin{array}{l} \vec{\nabla} \cdot \vec{B} = 0 \\ \vec{\nabla} \cdot \vec{E} = 4\pi\rho \\ \vec{\nabla} \times \vec{B} = \frac{4\pi}{c} \vec{j} + \frac{1}{c} \frac{\partial \vec{E}}{\partial t} \\ \vec{\nabla} \times \vec{E} = -\frac{1}{c} \frac{\partial \vec{B}}{\partial t} \end{array} \right\}$$

Generalized Ohm's Law



$$\vec{j} = j(\vec{E}, \vec{B}) \rightarrow \vec{j} = \underline{\underline{\sigma}}(\omega, k) \cdot \vec{E}_{\omega, k}$$

Dielectric Tensor

Plane waves:

$$\tilde{E} = E_0 \cos(\vec{k} \cdot \vec{r} - \omega t + \phi) = E_0 e^{i(\vec{k} \cdot \vec{r} - \omega t + \phi)}$$

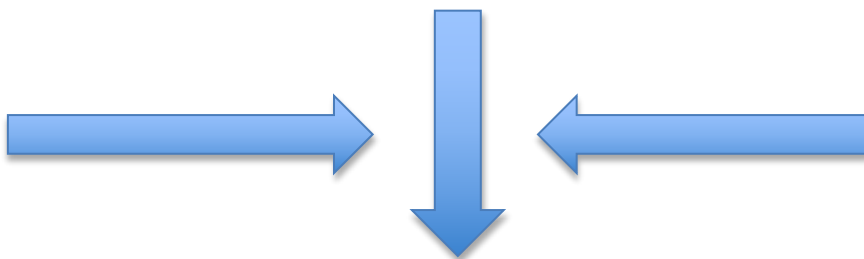


$$\frac{\partial}{\partial t} \rightarrow -i\omega$$

$$\vec{\nabla} \rightarrow i\vec{k}_{15}$$

$$\nabla \times (\vec{\nabla} \times \vec{E}) = -\frac{1}{c} \frac{\partial(\nabla \times \vec{B})}{\partial t}$$

$$\vec{\nabla} \cdot \vec{E} = 4\pi\rho$$



$$\vec{\nabla} \times \vec{B} = \frac{4\pi}{c} \vec{j} + \frac{1}{c} \frac{\partial \vec{E}}{\partial t}$$

$$4\pi\nabla\rho - \nabla^2\vec{E} = -\frac{1}{c} \frac{\partial}{\partial t} \left( \frac{4\pi}{c} \vec{j} + \frac{1}{c} \frac{\partial \vec{E}}{\partial t} \right) + \vec{j} = \underline{\underline{\sigma}}(\omega, k) \cdot \vec{E}_{\omega, k}$$

*Wave Equation*

$$\underline{k} \times (\underline{k} \times \underline{E}_{\omega, \underline{k}}) + \frac{\omega^2}{c^2} \underline{\underline{K}} \cdot \underline{\underline{\epsilon}}_{\omega, \underline{k}} = 0$$

$$\underline{\underline{K}} = \underline{\underline{1}} + \frac{\underline{\underline{\sigma}}}{i\omega \epsilon_0}$$

*Dielectric Tensor*

Wave Equation is **exact**, no approximations have been introduced



$$\underline{k} \times (\underline{k} \times \underline{E}_{\omega, \underline{k}}) + \frac{\omega^2}{c^2} \underline{\underline{K}} \cdot \underline{\underline{E}}_{\omega, \underline{k}} = 0$$

Admit solution only if



defining

$N$ = refractive index

$$\underline{N} = \frac{c}{v_{ph}} = \frac{ck}{\omega}$$

$$\det[\underline{N} \times (\underline{N} \times \underline{\underline{1}}) + \underline{\underline{K}}(\omega, \underline{N})] = 0$$

*Dispersion Relation*

$$\underline{\underline{K}} = \underline{\underline{1}} + \frac{\underline{\sigma}}{i\omega\varepsilon_0}$$

*Plasma*

Maxwell Equations

Motion Equation

$$n_\alpha m_\alpha \frac{\partial \bar{u}_\alpha}{\partial t} + n_\alpha m_\alpha (\bar{u}_\alpha \cdot \bar{\nabla}) \bar{u}_\alpha = n_\alpha q_\alpha (\bar{E} + \frac{\bar{u}_\alpha}{c} \times \bar{B})$$

Continuity  
Equation

$$\frac{\partial n_\alpha}{\partial t} + \bar{\nabla} \cdot (n_\alpha \bar{u}_\alpha) = 0$$

Perturbing Technique

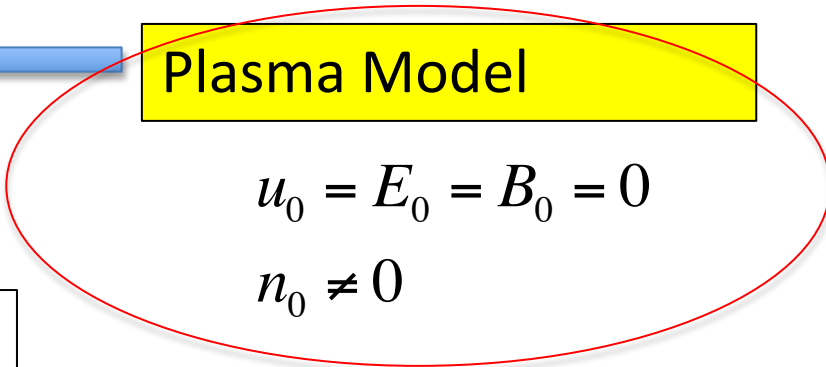
$$f = f_0 + f_1$$

Plasma Model

$$u_0 = E_0 = B_0 = 0$$

$$n_0 \neq 0$$

Dielectric Tensor



# Cold un-magnetized plasma

~~$$\eta_\alpha m_\alpha \frac{\partial \bar{u}_\alpha}{\partial t} + n_\alpha m_\alpha (\bar{u}_\alpha \cdot \bar{\nabla}) \bar{u}_\alpha = n_\alpha q_\alpha (\bar{E} + \frac{\bar{u}_\alpha}{c} \times \bar{B})$$~~

$$-i\omega m_\alpha \bar{u}_{\alpha 1} = q_\alpha \bar{E}_1$$

$$\bar{u}_{\alpha 1} = \frac{i}{\omega} \frac{q_\alpha}{m_\alpha} \bar{E}_1$$

$$u = u_0 + u_1 = u_1$$

$$E = E_0 + E_1 = E_1$$

$$B = B_0 + B_1 = B_1$$

$$\bar{j} = \sum q_\alpha n_\alpha \bar{u}_\alpha \quad \rightarrow \quad \bar{j} = \left( \frac{i}{\omega} \sum \frac{q_\alpha^2 n_\alpha}{m_\alpha} \right) \bar{E}_1 = \sigma \bar{E}_1$$

$$\bar{j} = \sum_{\alpha} q_{\alpha} n_{0\alpha} \bar{u}_{1\alpha} = \frac{i}{\omega} \left( \sum_{\alpha} \frac{n_{0\alpha} q_{\alpha}^2}{m_{\alpha}} \right) \bar{E}_1$$

  
 Electrical  
 conductivity

From motion equation:  
 Ohm's Law

- Scalar coefficient
- Independent from k

The dielectric tensor\*:

$$K = 1 - \frac{4\pi\sigma(\omega, k)}{i\omega} = 1 - \frac{1}{\omega^2} \sum_{\alpha} \frac{4\pi n_{0\alpha} q_{\alpha}^2}{m_{\alpha}} = 1 - \frac{\omega_p^2}{\omega^2}$$

\* Pay attention to different system (SI)

Where  $\omega_p^2 = \sum_{\alpha} \frac{4\pi n_{0\alpha} q_{\alpha}^2}{m_{\alpha}}$

Is the Plasma Frequency,  
summarized over all the  $\alpha$  species

And the Wave Equations is:

$$\left[ \frac{k^2 c^2}{\omega^2} \left( \frac{\underline{k}\underline{k}}{\underline{k}^2} - \underline{I} \right) + K \underline{I} \right] : \underline{E} = 0$$



Dielectric tensor

That written in matrix

$$\begin{pmatrix} K - \frac{k^2 c^2}{\omega^2} & 0 & 0 \\ 0 & K - \frac{k^2 c^2}{\omega^2} & 0 \\ 0 & 0 & K \end{pmatrix} \begin{pmatrix} E_x \\ E_y \\ E_z \end{pmatrix} = \begin{pmatrix} 0 \\ 0 \\ 0 \end{pmatrix}$$

Admits solution only if  $\text{Det}=0$  that leads to:

$$K \left( K - \frac{k^2 c^2}{\omega^2} \right) = 0$$

That has 2 solutions:

- $K=0$
- $K= k^2 c^2 / \omega^2$

$\kappa=0$

$$\omega^2 = \omega_p^2$$

Longitudinal

$$k \parallel E$$

From

$$\kappa = k^2 c^2 / \omega^2$$

$$\omega^2 = \omega_p^2 + k^2 c^2$$

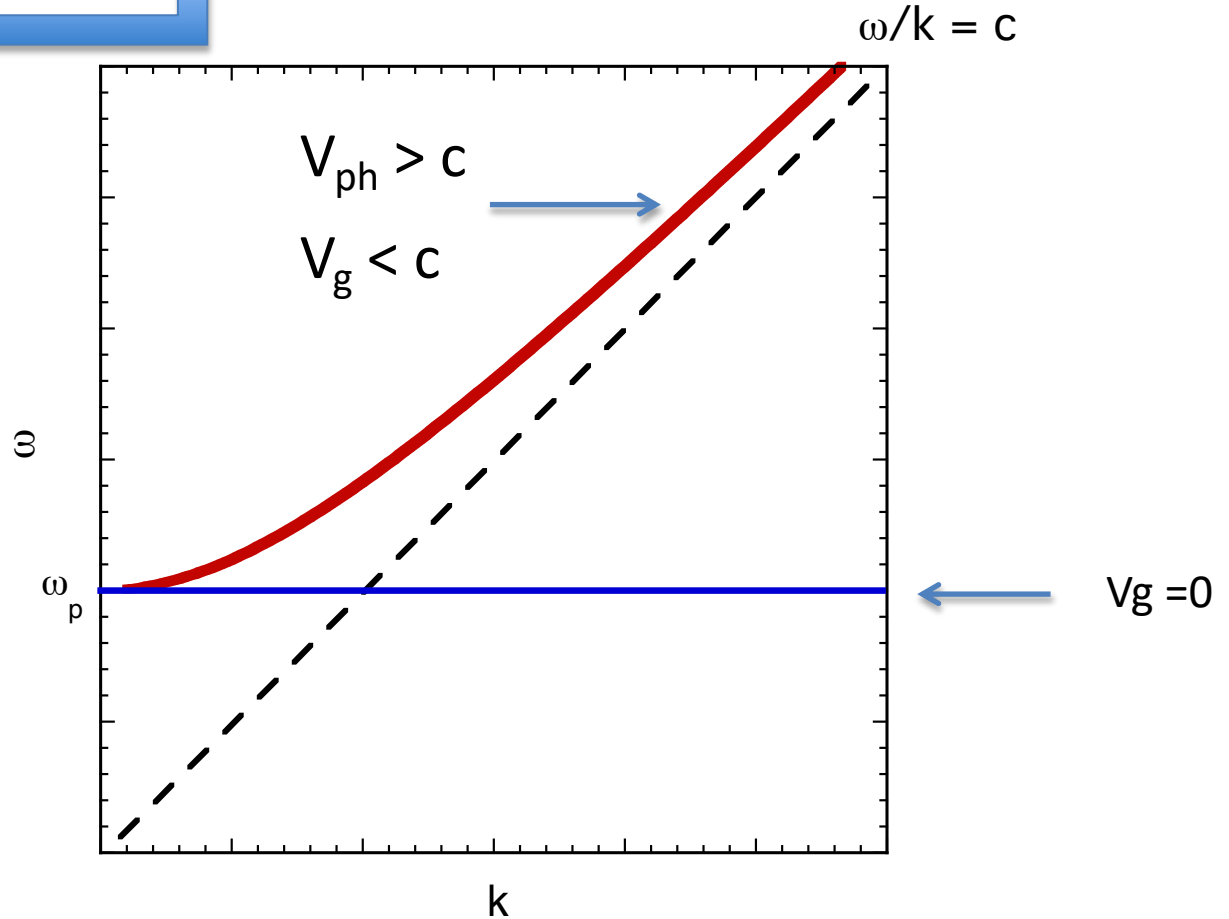
Transverse

$$k \perp E$$

$$K = 1 - \frac{\omega_p^2}{\omega^2}$$

$$v_{ph} = \frac{\omega}{k}$$

$$v_g = \frac{d\omega}{dk}$$

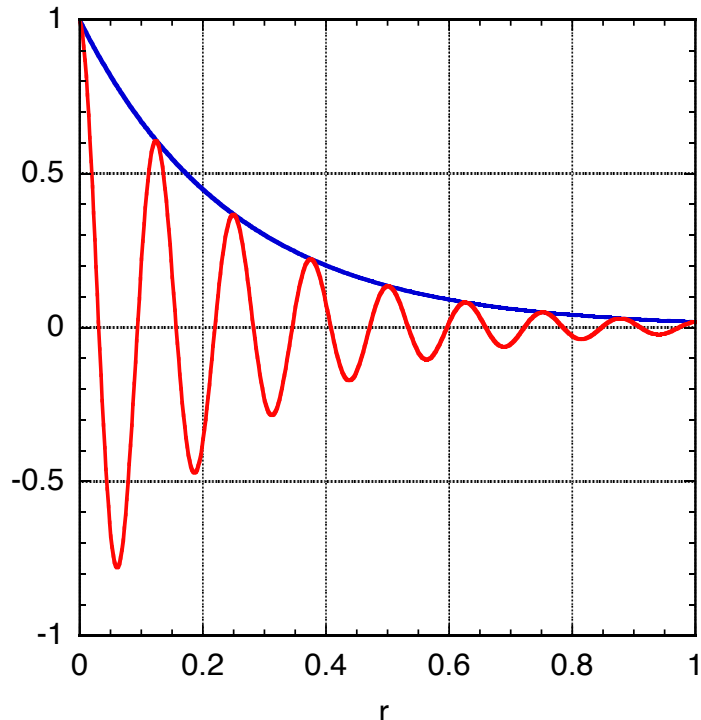


For a transverse wave, extracting  $k$ :

$$k = \sqrt{(\omega^2 - \omega_p^2) / c^2}$$

The wave can propagate only for

$$\omega > \omega_p$$



if

$$\omega < \omega_p$$



$$k = i |k|$$



$$\tilde{E} = E_0 e^{-kr} \cdot e^{-i(\omega t + \phi)}$$

# Wave Damping

Collisionless dissipation of an electromagnetic waves for

- Ion cyclotron
- Electron cyclotron
- Lower hybrid

is governed by the following relationship:

$$\omega - k_{\parallel} v_{\parallel j} - n |\omega_{cj}| = 0$$

# Landau Damping

$n=0$  correspond to **Landau damping**:

→  $E_{\parallel}$  accelerates particle in // direction

It is relevant for **Lower Hybrid** and for fast wave in **Ion cyclotron** range of frequency

Basically Landau damping occurs when electron velocity is equal to the phase velocity of the waves

As phase velocity ranges from thermal to light speed the wave can resonate with thermal and suprathermal electrons

# Absorption: Collisionless Damping

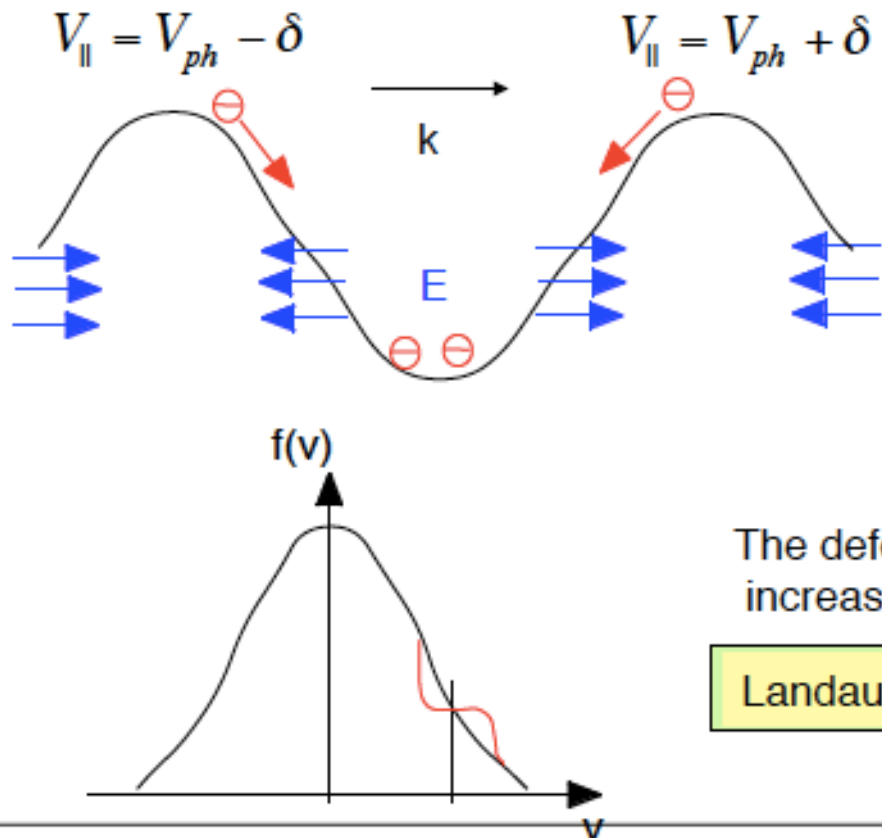
Energy transfer only if

$$\omega - n\omega_c = k_{\parallel}v_{\parallel}$$

$$n = 0$$

Resonance condition:

$$\omega - k_{\parallel}v_{\parallel} = 0$$



Condition for damping

$$\frac{\partial f(v)}{\partial v} < 0$$

The deformation of the distribution function increases the energy of the electron system.

Landau damping: Increase of parallel momentum

$n \neq 0$  correspond to **cyclotron resonance**

Particles gain energy in perpendicular direction

The condition of resonance can be written

$$v_{//j} = \frac{\omega}{k_{//}} - \frac{n|\omega_{cj}|}{k_{//}}$$

It is valid for particles with velocity smaller than the wave phase velocity ( $n > 0$ )

**$n=1$**  correspond to fundamental resonance:  
valid for

Electron cyclotron

Ion cyclotron minority heating

**$n=2$**  correspond to 2<sup>nd</sup> harmonic resonance:  
valid for

Electron cyclotron

Ion cyclotron

# Absorption: Cyclotron Damping

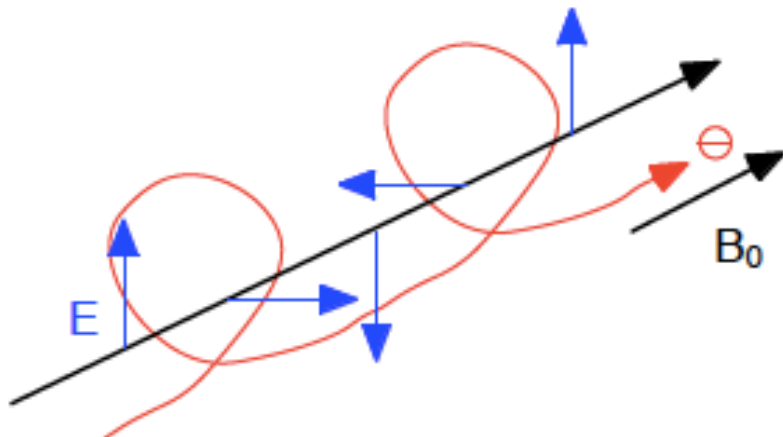
Energy transfer only if

$$\omega - n\omega_c = k_{\parallel}v_{\parallel}$$

$$n = 1$$

Resonance condition:

$$\omega - k_{\parallel}v_{\parallel} = \omega_c$$



Cyclotron Damping: increase of perpendicular momentum

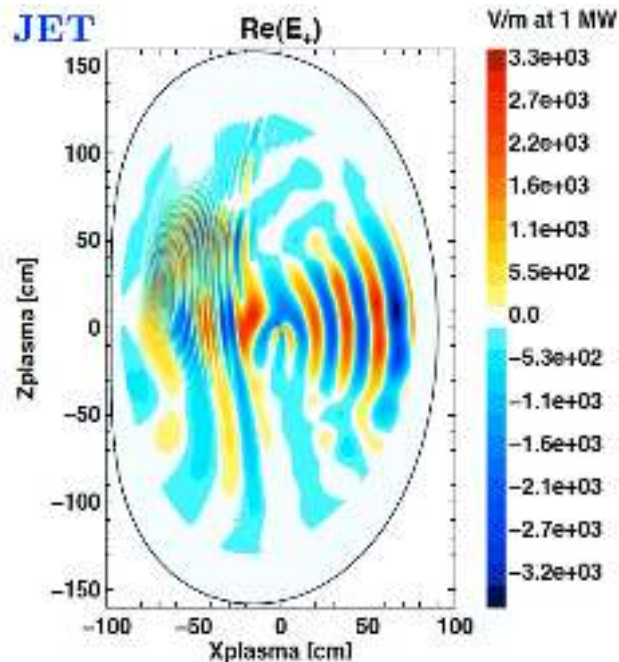
ICRH: can use both cyclotron or Landau damping, **used to heat ions and generate fast particle and current**

LHCD: only Landau damping, **to generate non inductive current**

ECRH: only cyclotron damping, **to heat electrons and generate non inductive current**

# RF simulations for JET

**f = 42 MHz**



**Ion Cyclotron Waves**

*courtesy R Bilato, MPI- IPP*

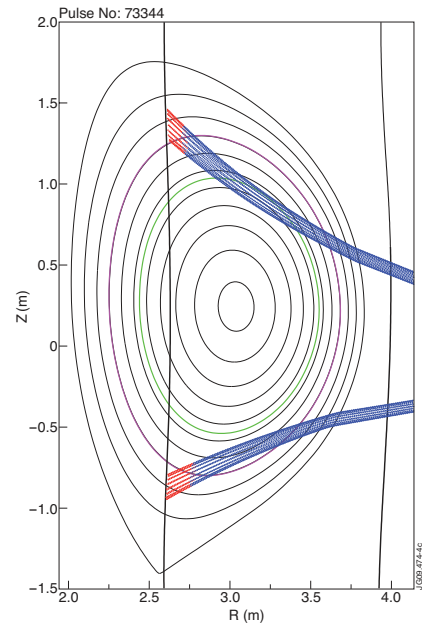
**f = 3.7GHz**



**Lower Hybrid Waves**

*courtesy R Bilato, MPI- IPP*

**f = 170 GHz**



**Electron Cyclotron Waves**

*D. Farina, IFP-CNR, 2010 proposal*

# *Physics of RF Heating and Current Drive*

## *Part II: Applications of EC waves*

## **SECOND PART**

- ❖ Electron Cyclotron Heating in Fusion Plasmas
  - ❖ ECCD mechanism
  - ❖ Wave Polarization relevance
  - ❖ Propagation and absorption in tokamak
- ❖ Application of ECH waves:
  - ❖ EC assisted start-up
  - ❖ MHD Control



**ECRH: Electron Cyclotron Resonant Heating**

**ECCD: Electron Cyclotron Current Drive**

*The only Heating System able to deposit power or current in  
highly localized and controllable way*

# Basic Physic Mechanism

The e.m. wave gives energy to particles rotating at the same frequency around the (toroidal) field  $B_T$ .

The simplest and quick formula for a specie  $x$  is:

$$\omega_0 = n\Omega_{cx} = n \frac{eB}{m_x c}$$

Harmonic



*For electrons:*

\* Maxwellian distribution & perpendicular injection

$$f_0(\text{GHz}) = 28(\text{GHz}) \cdot B_T(T) \cdot n$$

*For ions:*

$$f_0(\text{MHz}) = 15.2(\text{MHz}) \cdot B_T(T) \cdot \frac{Z}{A} \cdot n$$

# *Propagation, cut-off & resonances*

For ECRH/ECCD application we are considering transversal e.m. waves propagating in vacuum and in the plasma without evanescent region.

The waves met cut-off and/or resonances depending by: **wave polarization** & **harmonic**, **plasma density**, **magnetic field** and  $\theta$ .

*Propagation limits are defined by the two limits in the diffraction index*

$N=0 \rightarrow k=0 \rightarrow$  no wave propagation: **Cut-off**

$N=\infty \rightarrow k=\infty \rightarrow$  wave absorption: **Resonance**

**Cut-off**  $\rightarrow N=0 \quad \epsilon_R \epsilon_L \epsilon_3 = 0$

**Resonance**  $\rightarrow N=\infty$

$$N^2 = \frac{\epsilon_L \epsilon_R}{\epsilon_1}$$

$$\omega = \Omega_{ce}$$

*Electron Cyclotron*

$$\omega = \omega_p \quad \text{Density}$$

$$\omega = \omega_{R/L} \cong \frac{1}{2} (\pm |\Omega_e| + \sqrt{\Omega_e^2 + 4\omega_p^2})$$



$$\omega_{UH}^2 = \Omega_e^2 + \omega_{pe}^2$$

*Upper Hybrid*

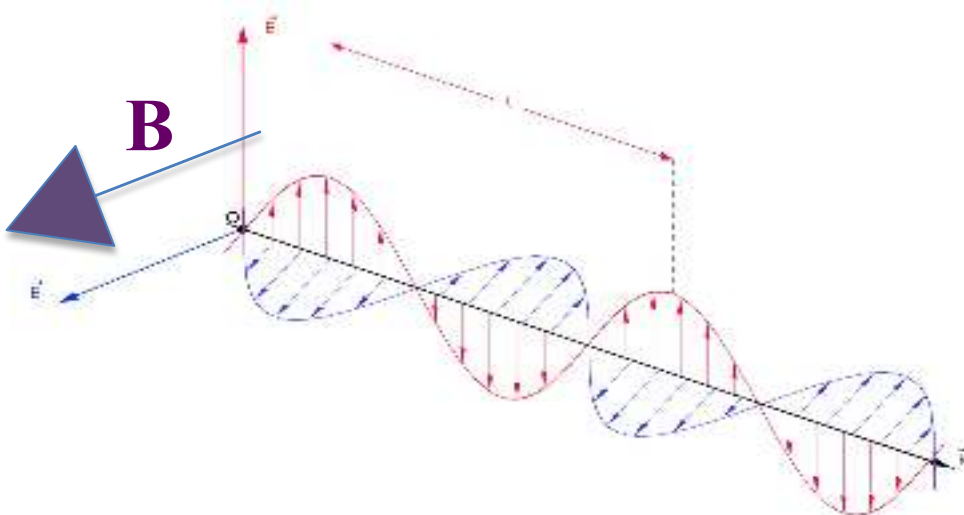
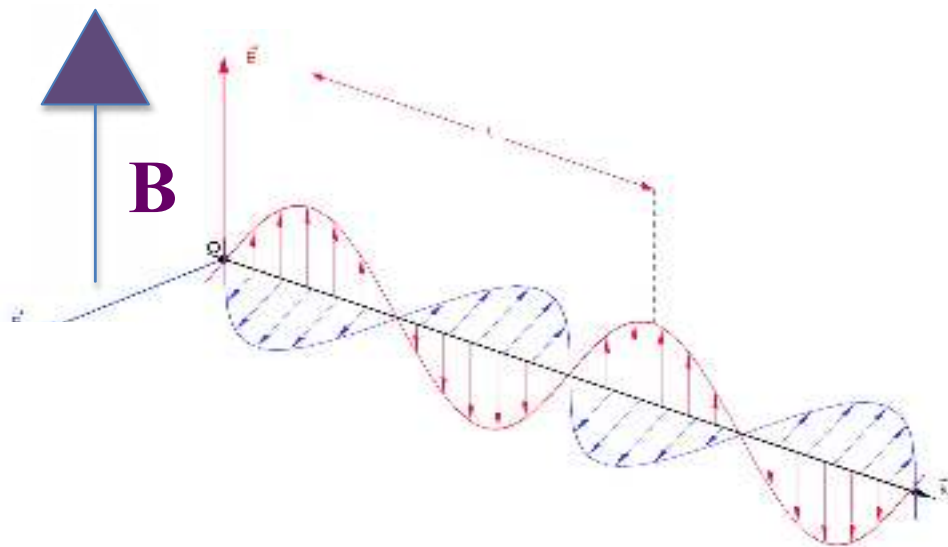
$$\omega_{LH}^2 \approx \Omega_e \Omega_i \frac{1 + \frac{\Omega_i^2}{\omega_{pi}^2}}{1 + \frac{\Omega_e^2}{\omega_{pe}^2}}$$

*Lower Hybrid*

# Wave polarization

The polarization of e.m. wave in magnetised plasma is defined as the direction of the Wave Electric Field respect to external Magnetic Field direction:

**O-Mode (ordinary)** when  
Electric field is parallel to  $B_0$



**X-Mode (extraordinary)**  
when Electric field is  
perpendicular to  $B_0$

- The modes exist only in plasma
- Propagation depends on plasma parameter and  $N_{\parallel}$
- The propagating wave is a mixture of the two (elliptic polarization)

# Cut-off & polarization

An e.m. wave propagating in plasma can meet **resonances** and **cut-off**:

At a cut-off surface the waves is reflected backward.

Cut-off (and some resonance) can depend on the polarization

Density Cut-off

$$\omega = \omega_p$$



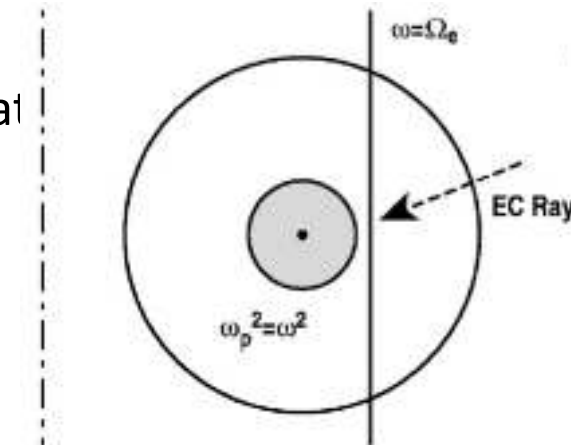
Ordinary Mode

$$n_e < n_c = \frac{m_e \omega_o^2}{4\pi e^2} = \frac{B_{\perp}^2(T)}{10.3} l^2 [10^{20} m^{-3}]$$



Extraordinary Mode

$$n_e < l(l-1)n_c \quad l > 1$$



$$f = 140 \text{ GHz}$$

$$\text{O1}_{\text{FTU}} \quad n_c = 2.4 \cdot 10^{20} \text{ m}^{-3}$$

$$\text{X2}_{\text{AUG}} \quad n_c = 1.21 \cdot 10^{20} \text{ m}^{-3}$$

$$\text{X3}_{\text{TCV}} \quad n_c = 1.61 \cdot 10^{20} \text{ m}^{-3}$$

## XM propagation & Cut-off

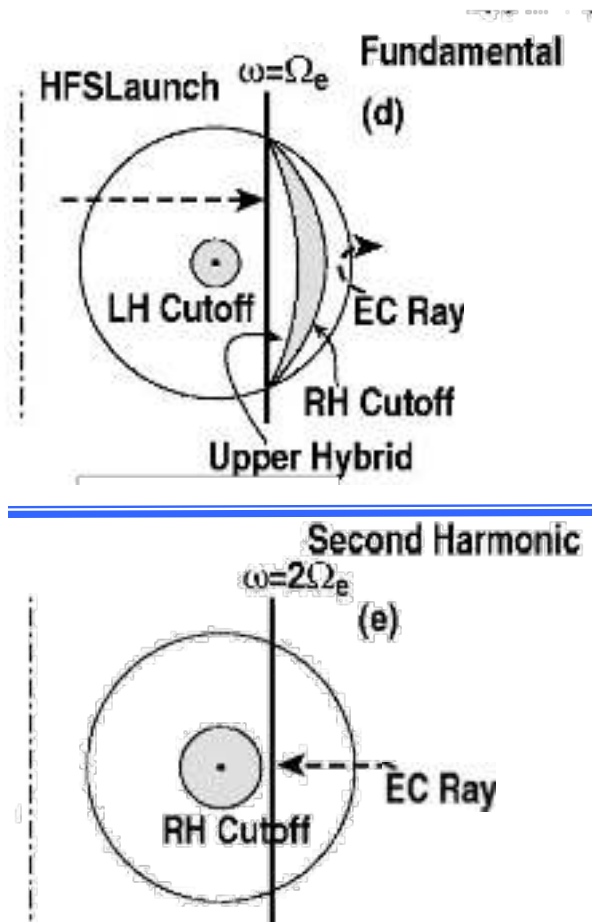
1<sup>st</sup> Harmonic XM has 2 additional cut-off, the right and left hand cut-off.

$$\omega = \omega_{R/L} \approx \frac{1}{2} (\pm |\Omega_e| + \sqrt{\Omega_e^2 + 4\omega_p^2})$$

The RH cut-off shield the Upper Hybrid and the cyclotron resonance for a wave coming from LFS.

For this reason the XM can be used only with second harmonic.

The LH cut-off is equivalent to a density cut-off.



$$P_{abs} = P_0(1 - e^{-\tau}) \quad \text{where} \quad \tau = \int \alpha \cdot dl$$

$\alpha$  = local absorption coefficient in m<sup>-1</sup>

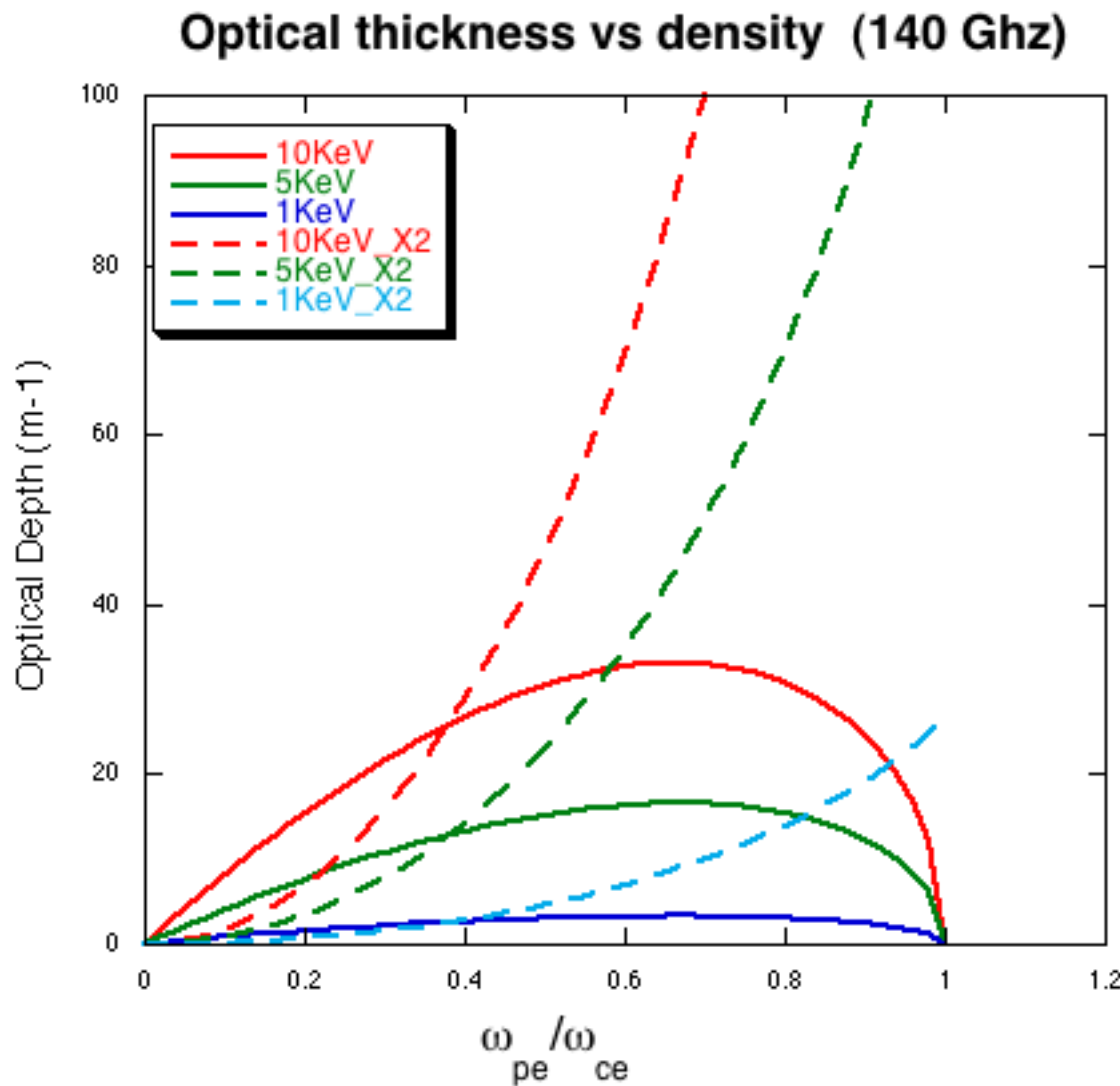
Optical thickness  $\tau$  changes with polarization,  $N_{//}$  and harmonic number. In case of fundamental OM with  $N_{//}=0$ :

$$\tau_{OM1} = \pi^2 \frac{\omega_{pe}^2}{\omega_{ce}^2} \left(1 - \frac{\omega_{pe}^2}{\omega_{ce}^2}\right)^{1/2} \frac{v_{Te}^2}{c^2} \frac{R}{\lambda}$$

Absorption depends  
on Te and n<sub>e</sub>

$$\tau_{OX2} = 2\pi^2 \frac{\omega_{pe}^2}{\omega_{ce}^2} \frac{\left(6 - \frac{\omega_{pe}^2}{\omega_{ce}^2}\right)^2}{\left(6 - 2\frac{\omega_{pe}^2}{\omega_{ce}^2}\right)^2} \frac{v_{Te}^2}{c^2} \frac{R}{\lambda}$$

# Optical thickness



$$f_o = 140 \text{ GHz}$$

$$N_{\parallel} = 0$$

with  $\tau > 3$ :  $P_{abs} \sim 95\%$

*Absorption depends on  $T_e$  and  $n_e$*   
*XM2 is stronger absorbed approaching cut-off*

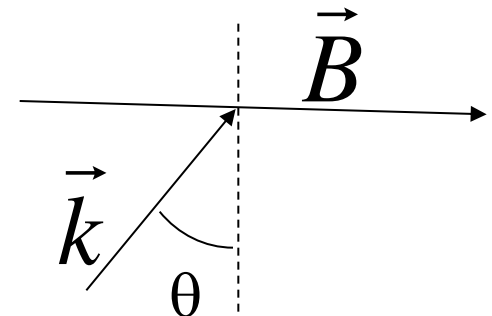
A more complete resonance condition is:

$$\frac{1}{\gamma} \cdot n\Omega_{ce} = \omega_o - \vec{k} \cdot \vec{v} = \omega_o - kv_{||} \cos \theta$$

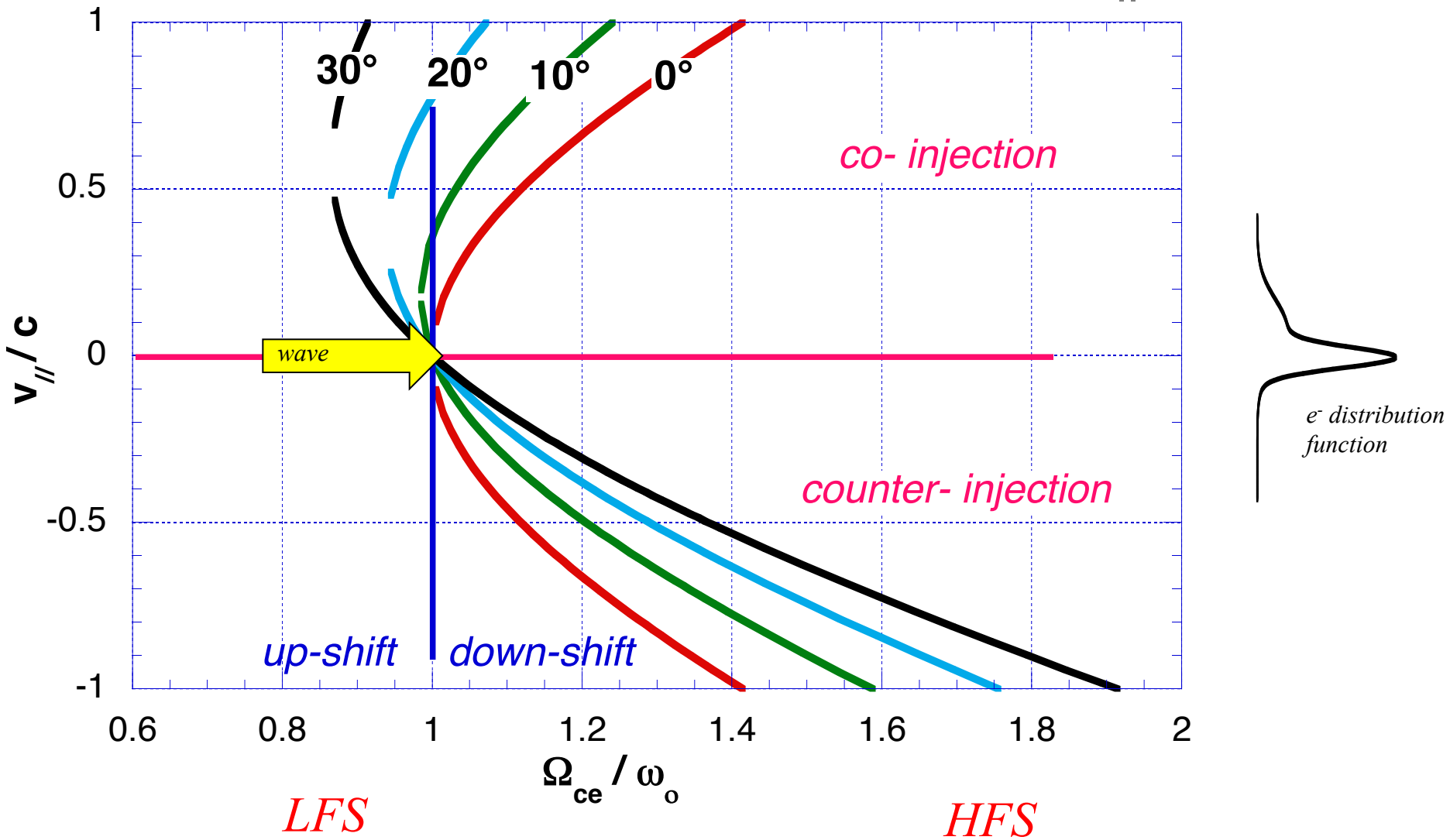
*Relativistic Gamma*                            *Electron velocity*                            *Angle between wave propagation and the perpendicular to the magnetic field*

$$\gamma = \frac{1}{\sqrt{1 - \frac{v_{||}^2}{c^2}}}$$

$$\frac{\Omega_{ec}}{\omega_o} = \frac{c/v_{||}}{\sqrt{c/v_{||}^2 - 1}} \left( 1 - \frac{N_{||}^{EC}}{c/v_{||}} \right)$$



# The Graphic Solution of Resonance Equation at different $N_{||}$



EC waves gives only **perpendicular energy** to electrons:  
no net longitudinal momentum transfer

The EC wave can produce non inductive current drive exploiting two different and opposite effects:

- **Fisch&Boozer effects** (effect on collisionality)
- **Ohkawa effects** (trapped particles balance)

ECCD **efficiency** is **low**, but the high **localization** can be exploited for **current profile control** aiming to **MHD stability** or  $q$  profile shaping.

Co-injection: power absorption on co-current electrons



⊥ Energy increase



Collisionality reduction



Not-symmetric losses (co electrons lost less than cnt electrons)



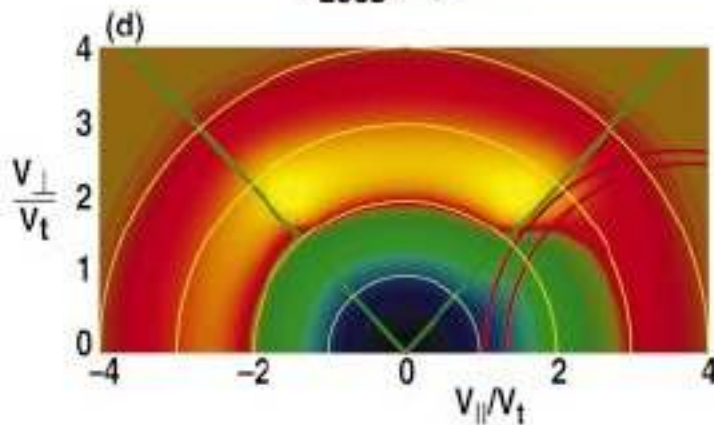
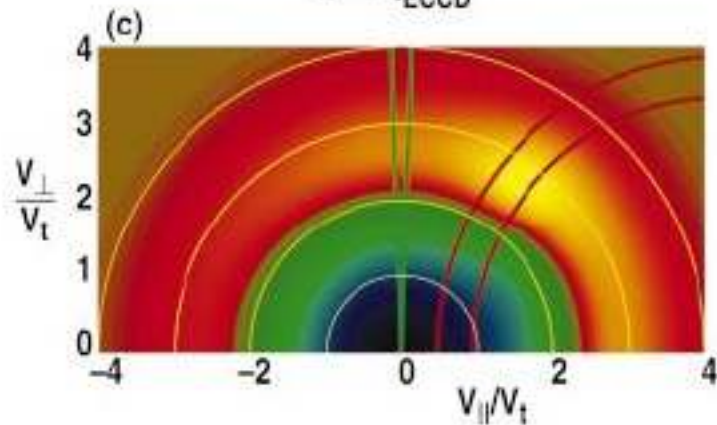
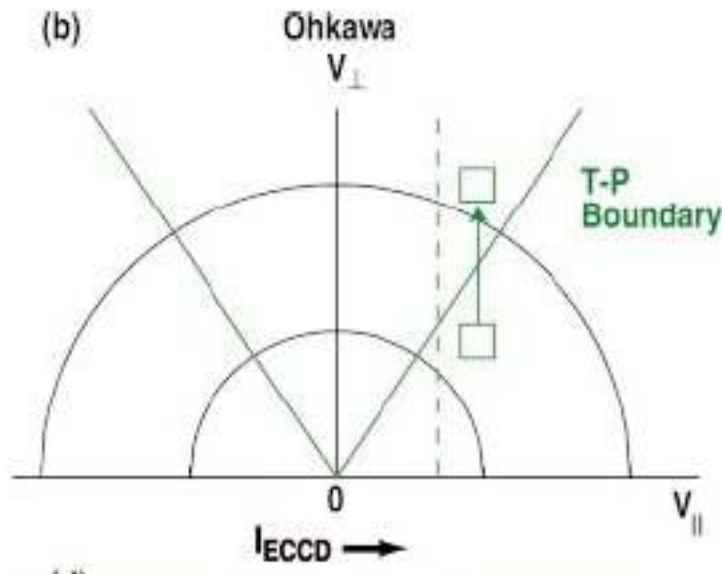
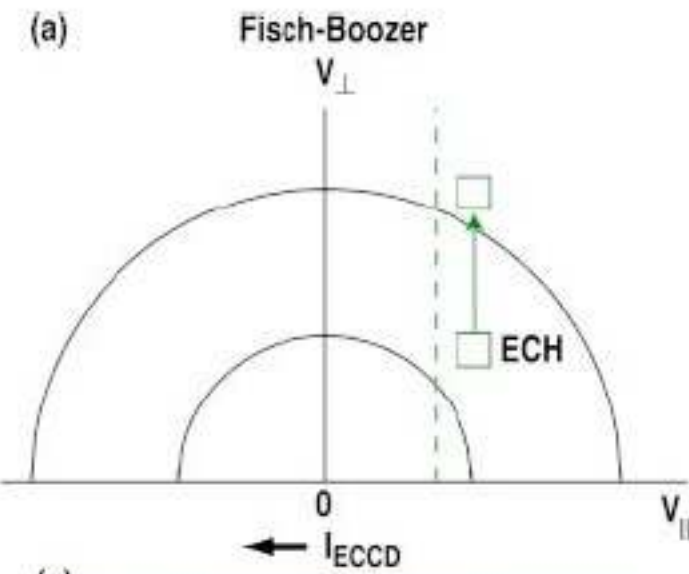
**Net co-current generation**

*In toroidal geometry the presence of trapped particle is at the basis of Okhawa ECCD effect.*

Electrons, gaining  $E_{\perp}$  from EC wave, can enter in the **trapped cone**, and stops to drive current (due to the bouncing of such particle in the trapped *banana*).

This create an **asymmetry** for the particles going in the opposite direction than does not absorb EC wave and continue to circulate.

This asymmetry produce a net current drive term in the **opposite** direction with respect to the resonant electrons absorbing the wave.



EC wave is usually fully absorbed at 1<sup>st</sup> pass (if  $T_e > 2$  KeV and  $n_e \sim 0.1 n_{\text{cutoff}}$ )

The deposited power is strongly localized, depending on the beam intersection with the resonant layer

The profile of power deposition is calculated (in all experiments) using Ray Tracing and/or Beam Tracing codes well consolidates and benchmarked. Result depends on accuracy of equilibrium,  $T_e$  and  $n_e$  profiles, being known the mirrors steering.

Main Codes used: **TORBEAM**, **ECGWB**, **GRAY**, **TORAY-GA**, **BANDIT-3D** (*beam tracing*, ray-tracing)

The amount of CD driven by EC wave is a function of :

Local Temperature

Local Zeff

Wave frequency

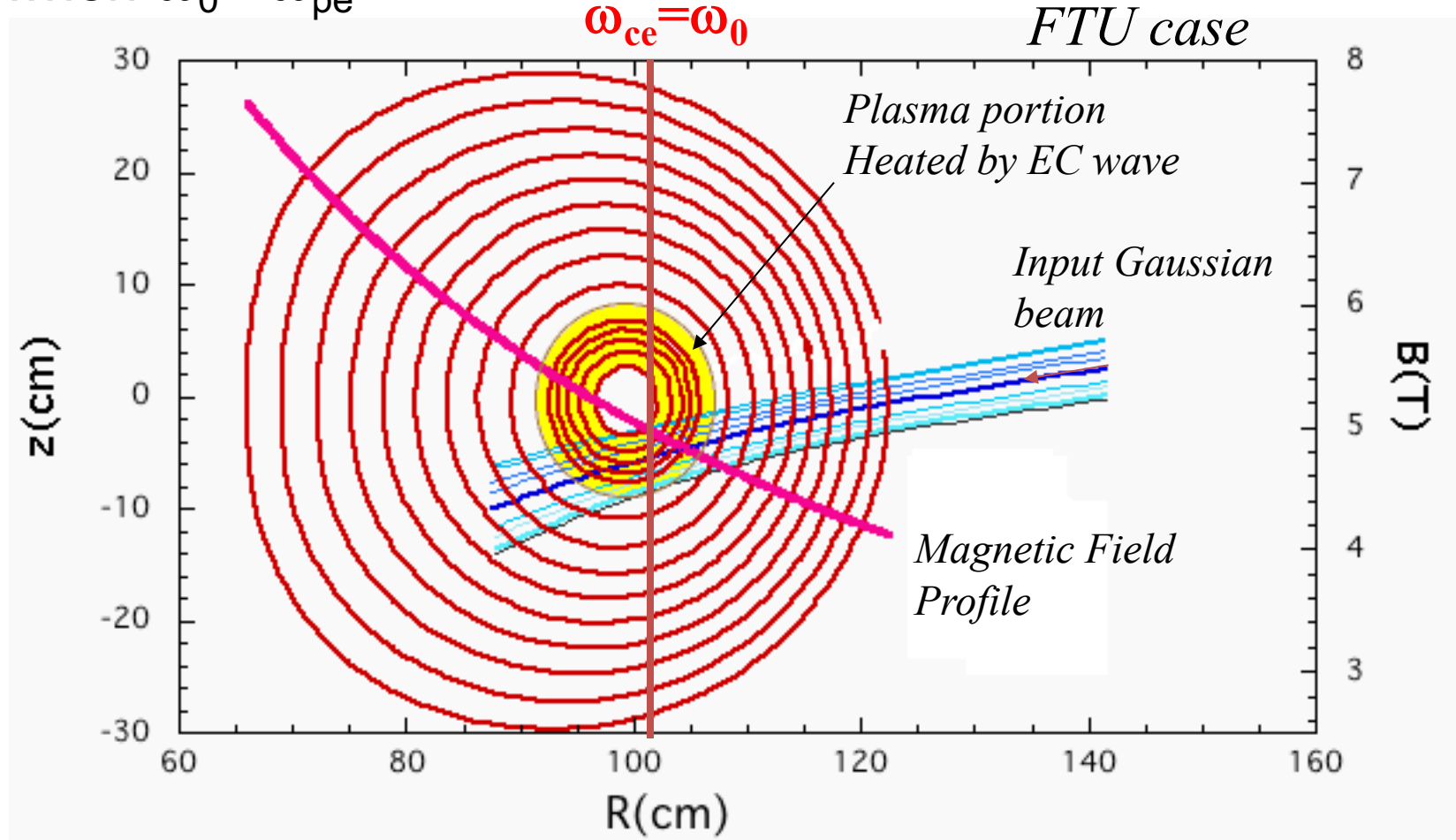
Local plasma density

Injection angle

Geometrical Effects

# Beam Propagation

The beam suffers of plasma refraction (when it crosses high density regions) up to a full bending (reflection) when  $\omega_0 = \omega_{pe}$



# Beam Propagation

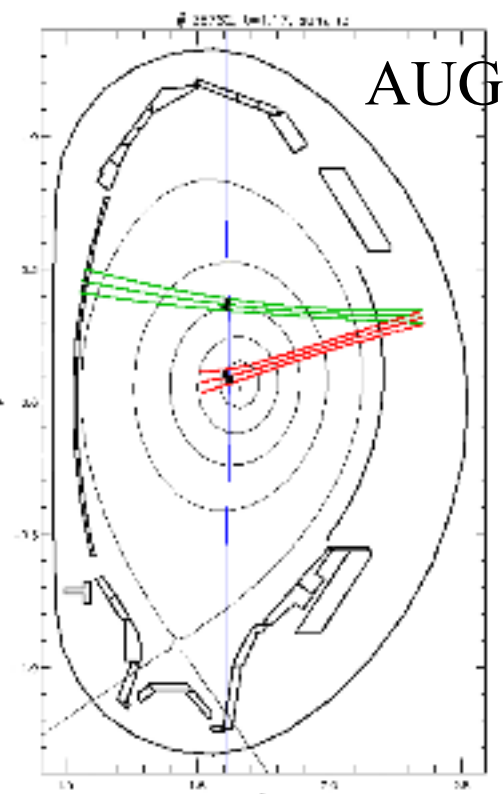
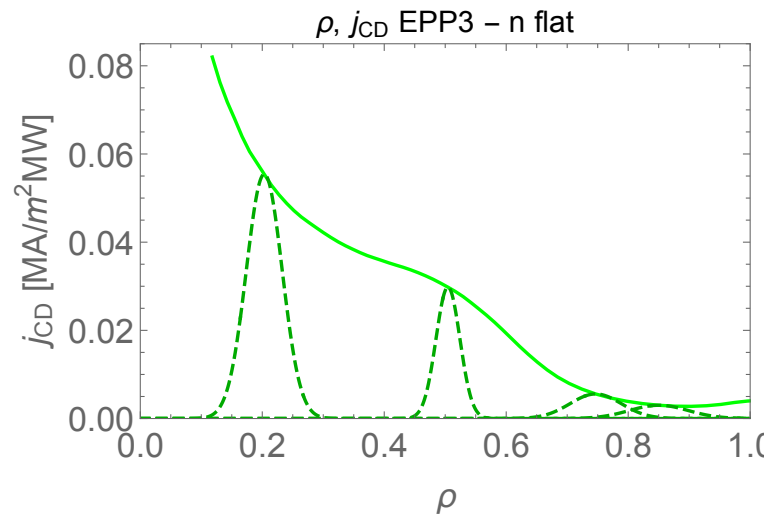
The profile of power deposition is calculated (in all experiments) using Ray Tracing and/or Beam Tracing codes well consolidated and benchmarked

Result depends on accuracy of equilibrium,  $T_e$  and  $n_e$  profiles, being known the mirrors steering.

Main Codes used:

**TORBEAM, GRAY**

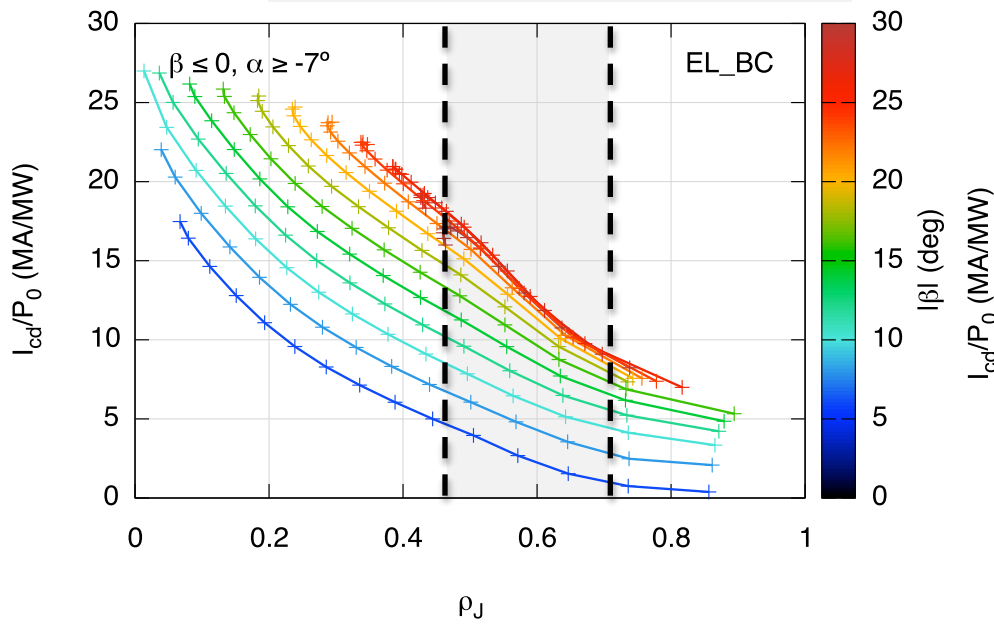
**TORAY-GA, BANDIT-3D**



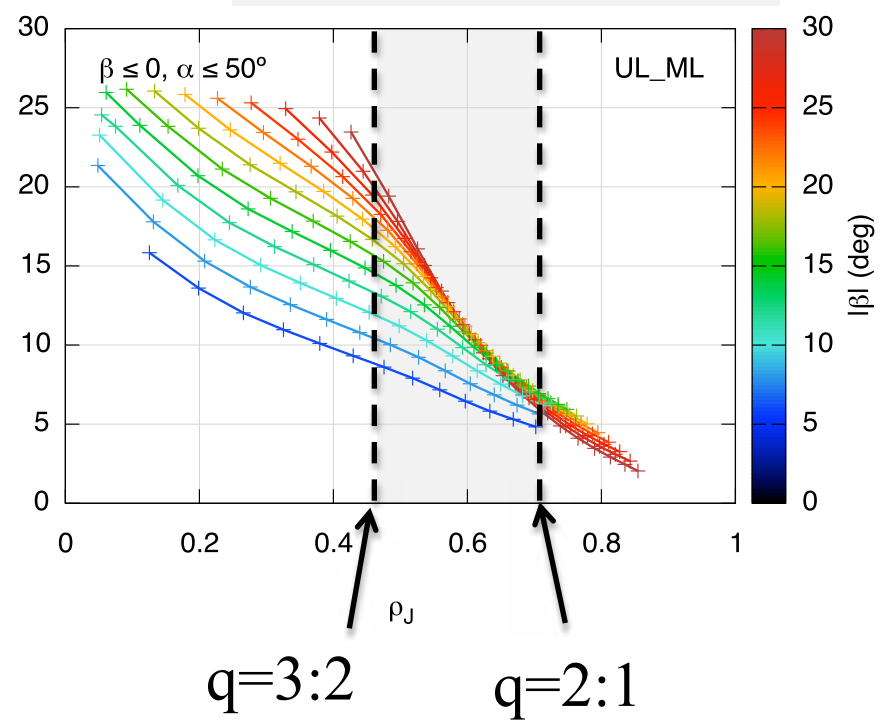
# Current drive $I_{CD}/P_0 (\rho)$

DTT case

Equatorial Launcher



Upper Launcher



Current drive efficiency depends on two parameters:  
 Local electron temperature  
 Toroidal angle (beta)

# *Application of EC power in experiments for Plasma operation and RT control*

# Introduction

Which are the characteristics of EC wave that make it a suitable tool for plasma control to be used in closed loops?

Easily predictable power deposition localization

→ geometrical ray tracing and beam tracing

Highly localized power deposition (strong local effect)

→ the EC wave can be launched as TEM00:

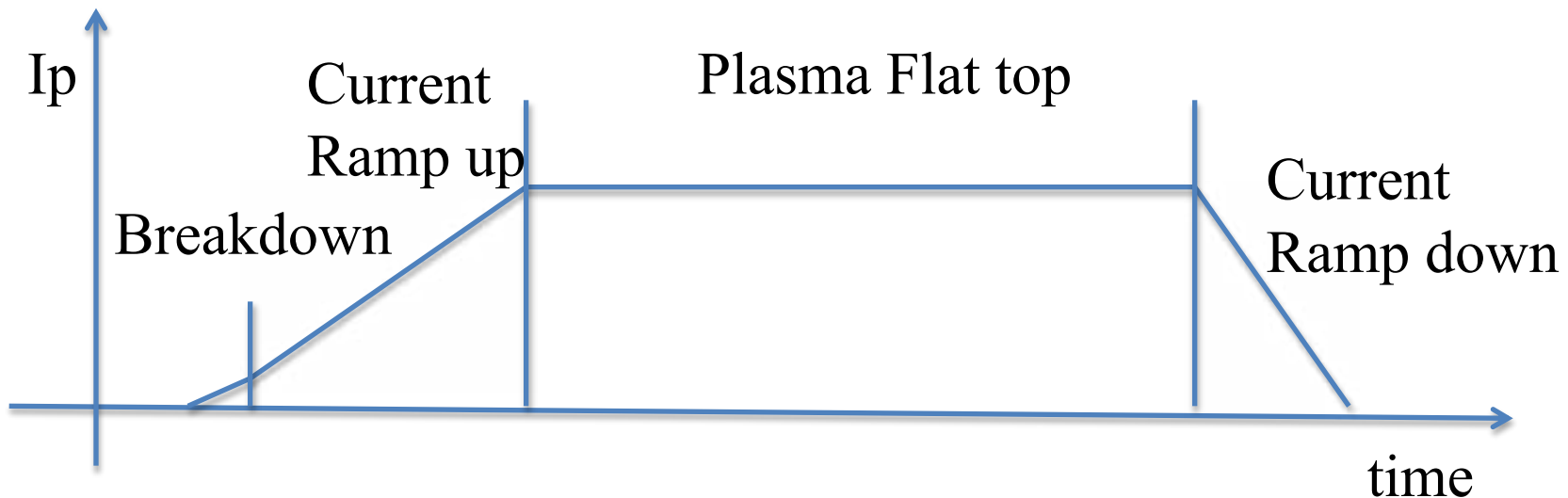
Gaussian beam with  $w_o \geq 2\lambda/\pi$  (100 GHz:  $w_o > 1.9$  mm!)

Easy control of deposition localization (radius)

→ use of steerable mirrors due to the possibility od Q.O. approach

Fast switch on/off time

power rise time limited by HVPS capability ( $\sim 100\mu s$ ). Modulation up to 10KHz demonstrated (5 KHz required for ITER)



**Breakdown:** pre-ionization, burn-through

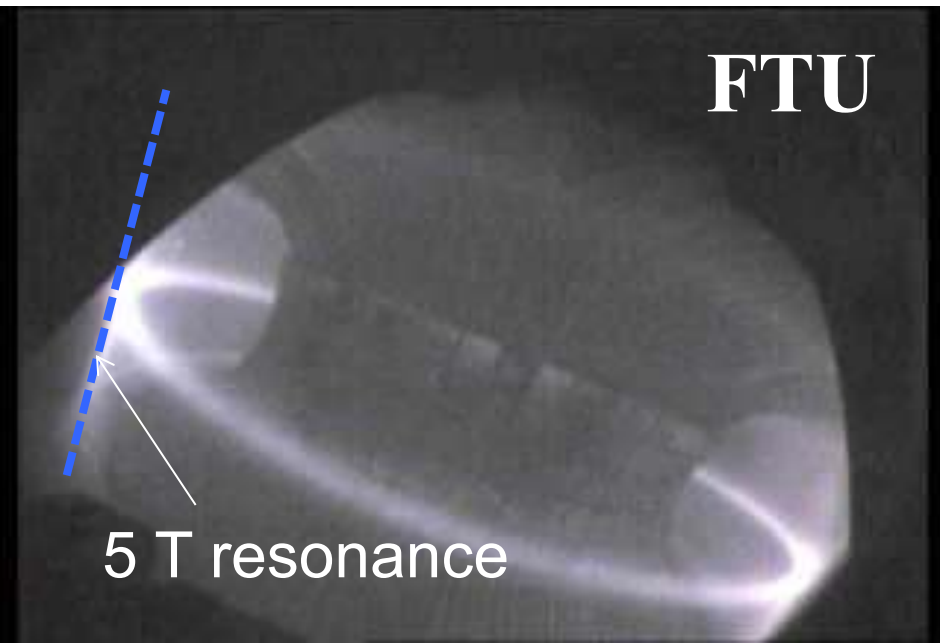
**Ramp up:** lower internal inductance, save transformer flux for longer pulses

**Flat top:** profiles control, **MHD Control** (NTM and ST), Impurity accumulation, localized CD

**Ramp-down:** avoid temperature collapse, **disruption avoidance/control**

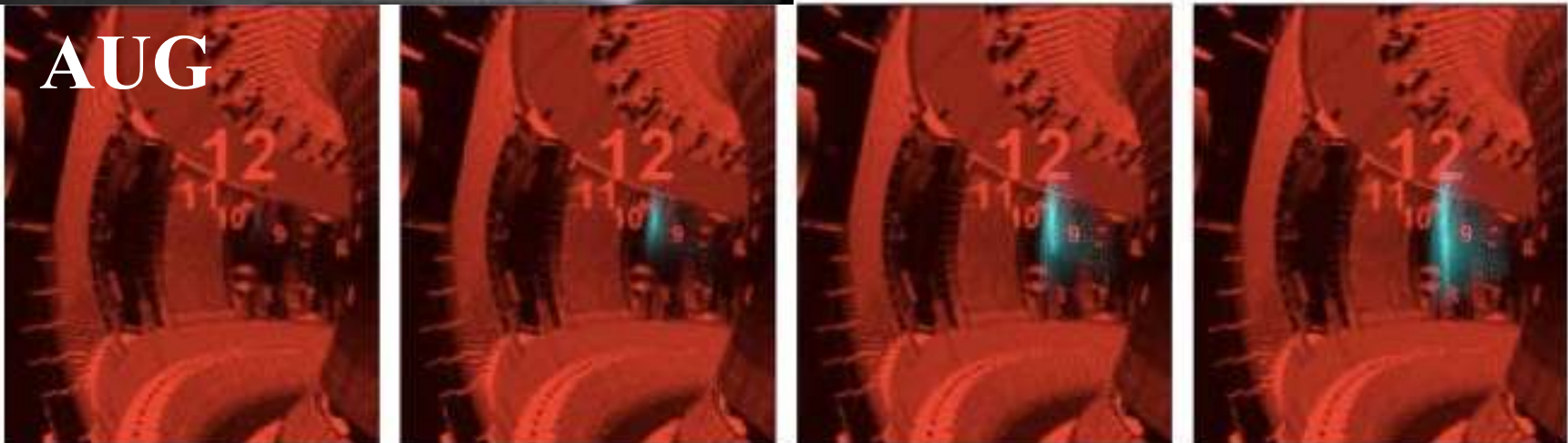
EC wave in presence of resonant magnetic field is able to accelerate electron up to ionization energy, starting the avalanche and sustaining a low temperature (20 eV) and low density ( $10^{18} \text{ m}^{-3}$ ) plasma.

This technique is used in stellarator to sustain plasma and in tokamak to initiate plasma and (applying electric field) ramp-up current.



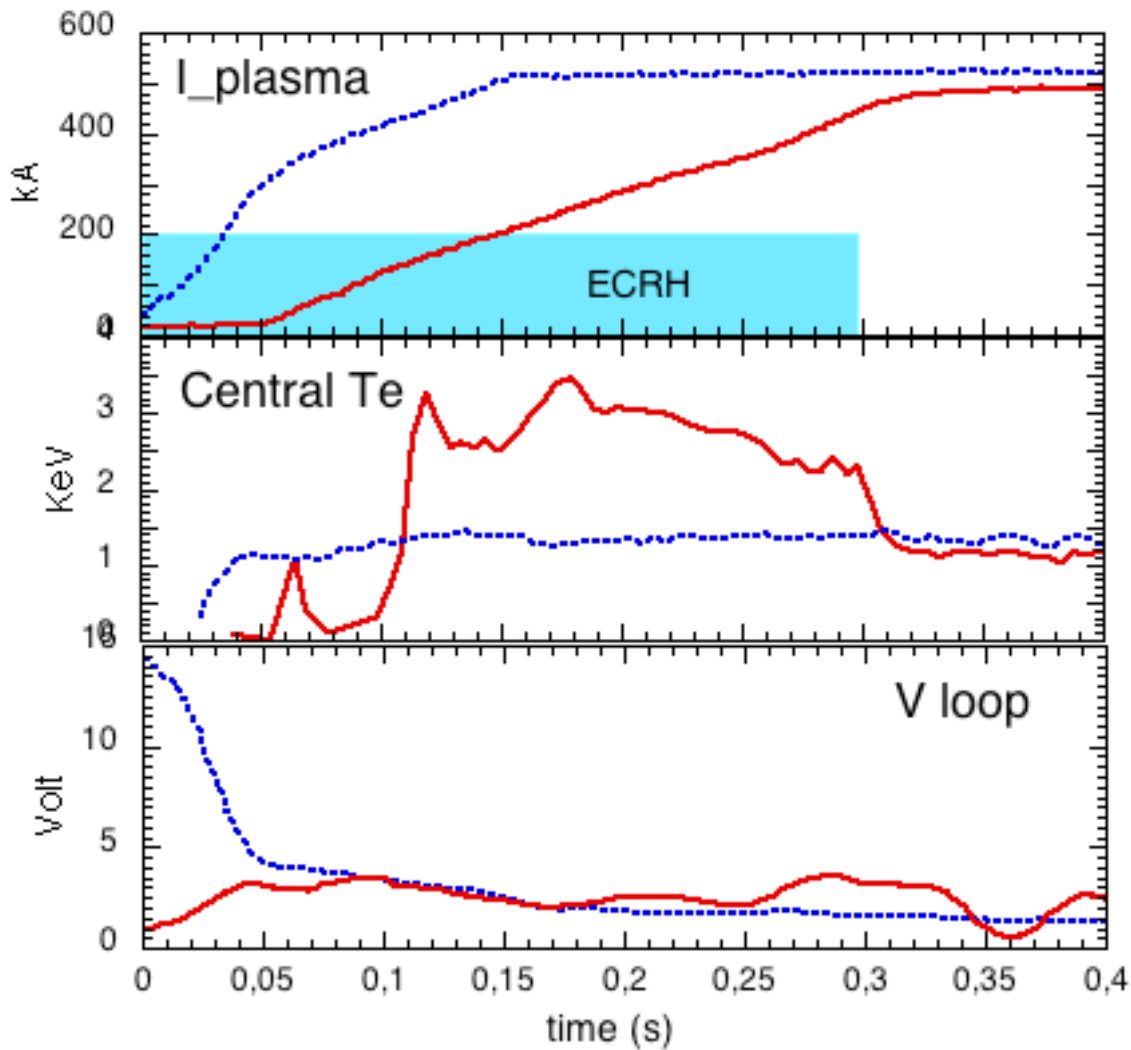
The plasma is ionized where the RF beam crosses the resonance cylinder.

The plasma drift in vertical and outer direction, until the current starts the confinement



# EC Assisted Break-down vs ohmic

FTU

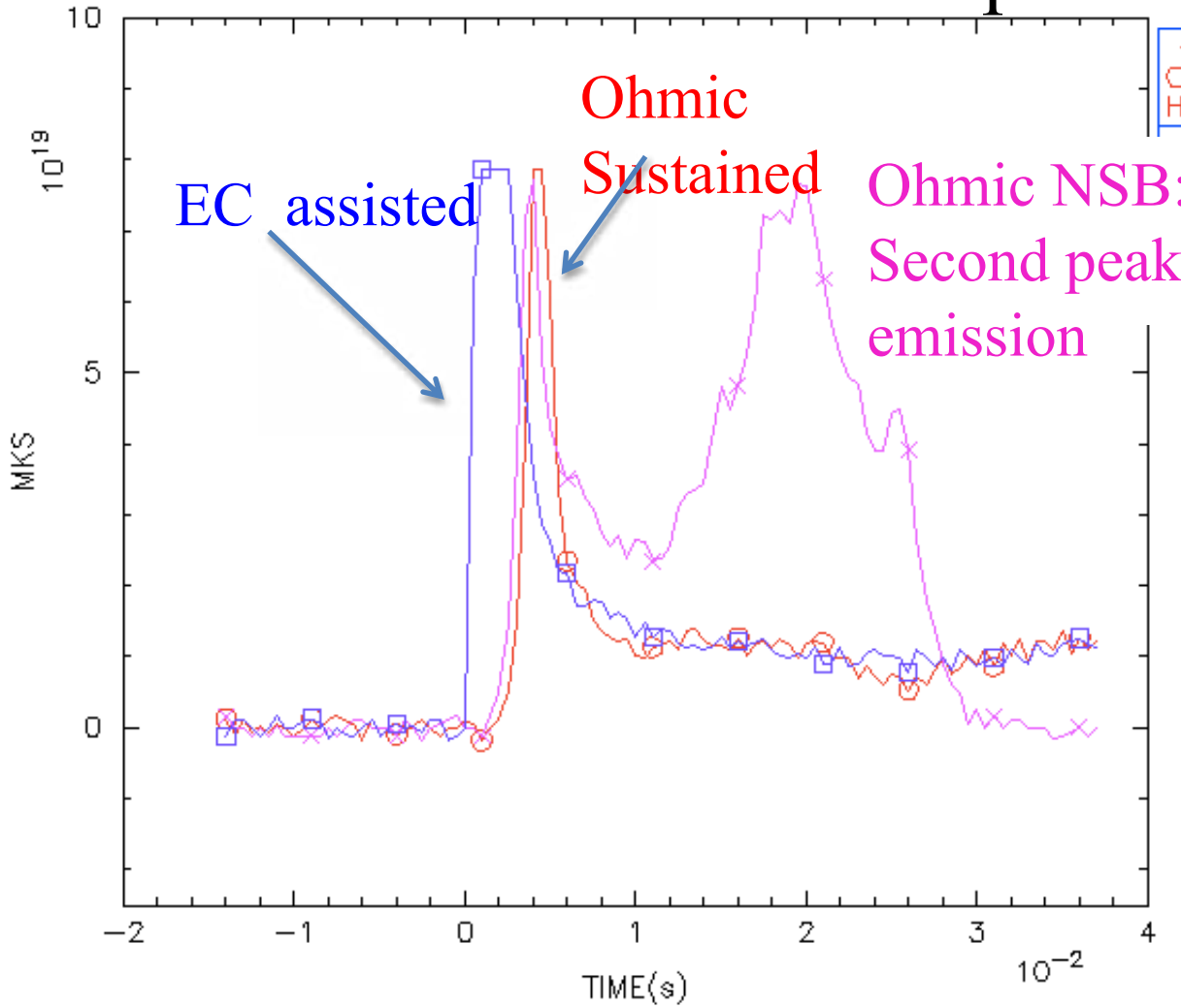


EC power is applied at  $t=0\text{s}$  and maintained for all the current ramp

With ECH assistance it is possible to start-up tokamak current at low  $V_{\text{loop}}$

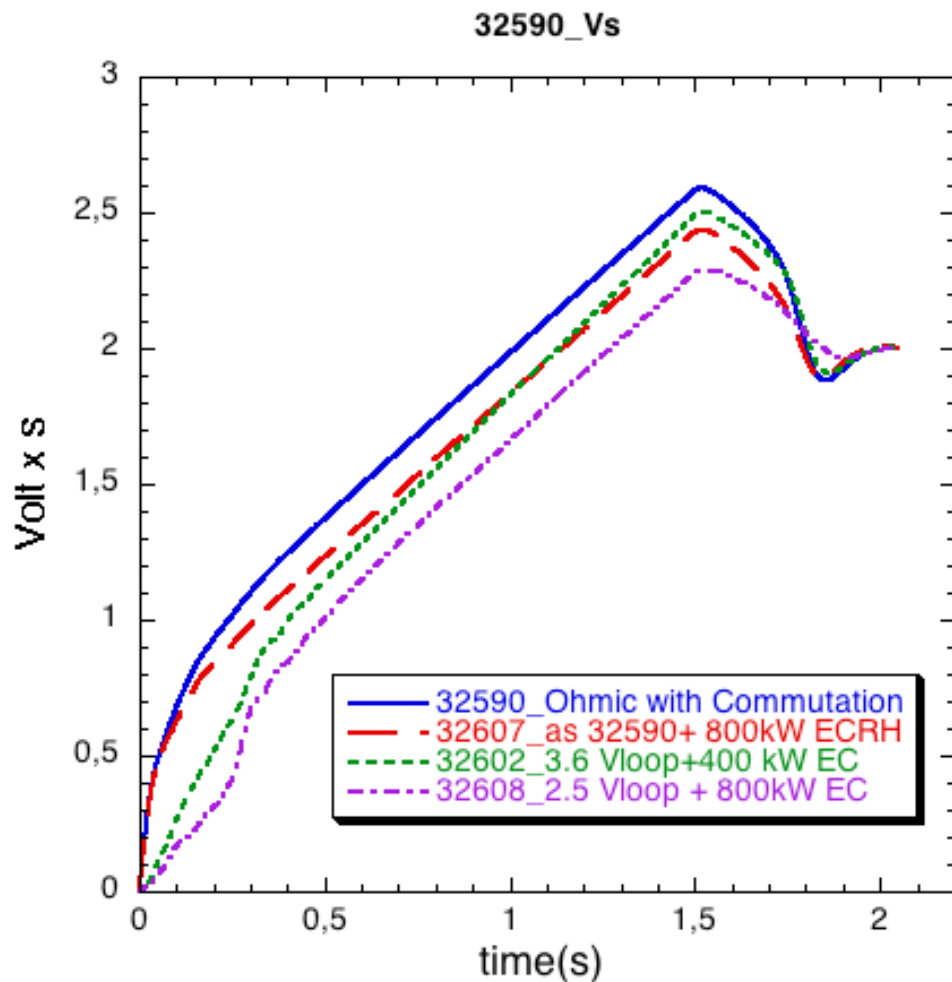
High Temperature after initial phase at low absorption

## D-alfa emission at start-up



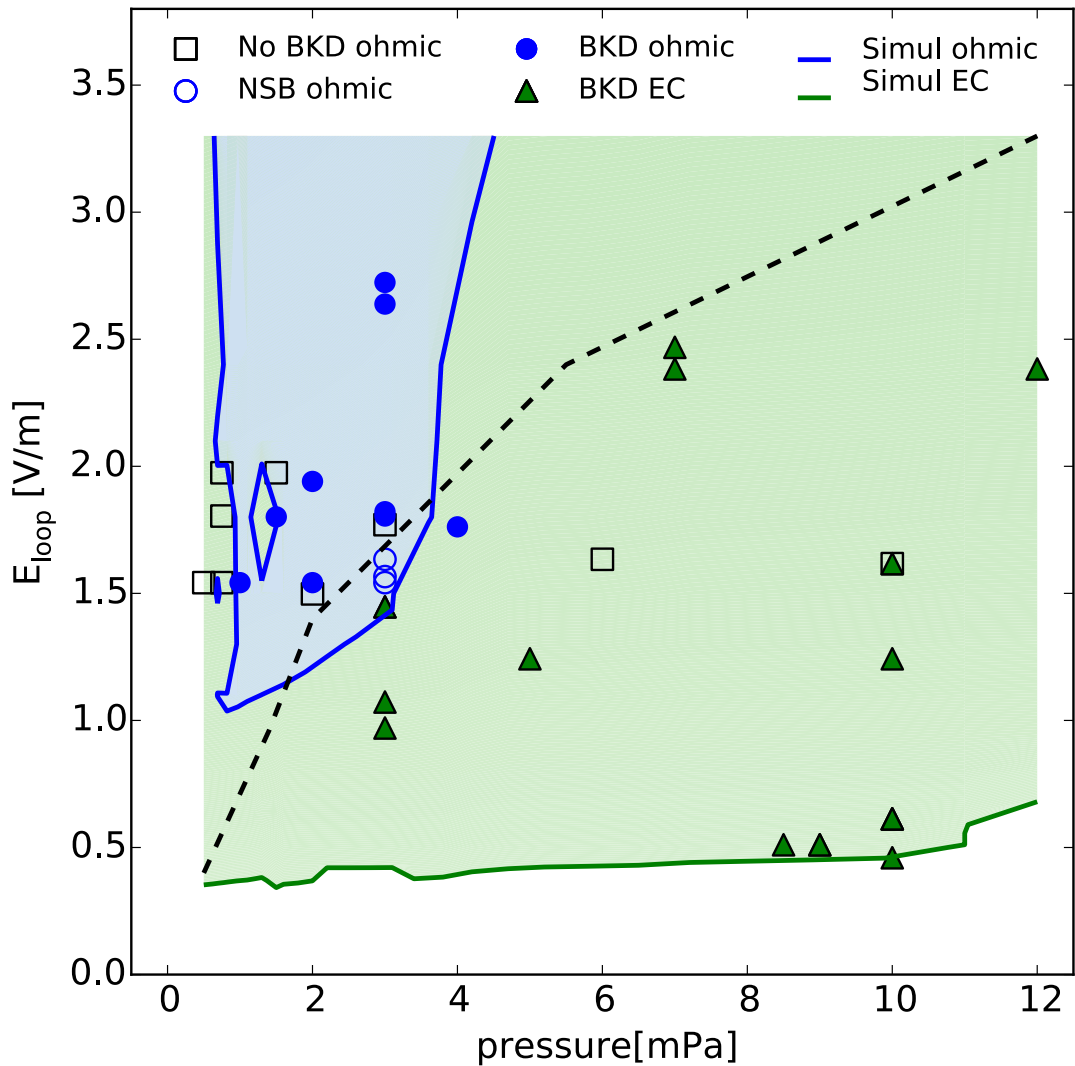
In case of low  $V_{\text{loop}}$  (or high impurity content) the hydrogen plasma cannot overcome the condition of H-alfa peak (at 20-100eV).

EC power gives energy to compensate radiation losses in the low temperature plasma, allowing to increase of temperature ( $>200\text{eV}$ ) necessary to ramp-up the plasma current



Application of EC power to start-up plasma current leads to flux saving for two main reasons:

- 1- Breakdown at low Vloop (a fast drop of  $I_{trafo}$  is not required)
- 2- Higher temperature during current ramp reduce plasma resistivity

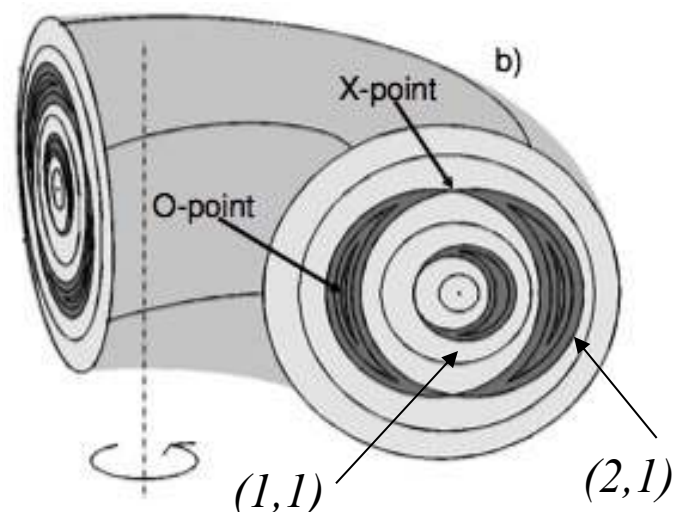


Use of EC power in the start up phase allows wider operational window in term of Electric field and Pressure

Here the FTU results together with simulation from BKD0 code.

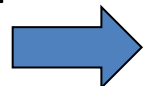
In a large scale machine (like reactor) the automatic **control** for plasma stability and **performance** is one of the main challenge.

Instabilities of Magnetic Hydrodynamic type (**MHD**) can produce a deformation in the magnetic configuration reducing **energy confinement** and increasing the risk of **plasma disruption**.



The control requires correct physic models and proper actuator. One of tool to perform plasma control is the Radio Frequency used as auxiliary heating as **Electron Cyclotron Resonance Heating** (ECRH).

Island width evolution



$$g_1 \frac{\tau_R}{r_s^2} \frac{dW}{dt} = \pm \Delta'_0 + a_1 \Delta'_{BS} - a_4 \Delta'_{cd}$$

$$\Delta'_0(W) = \Delta' - \alpha W = \lim_{\varepsilon \rightarrow 0} \frac{1}{\psi} \left[ \left( \frac{d\psi}{dr} \right)_{r_s+\varepsilon} - \left( \frac{d\psi}{dr} \right)_{r_s-\varepsilon} \right] - \alpha W$$

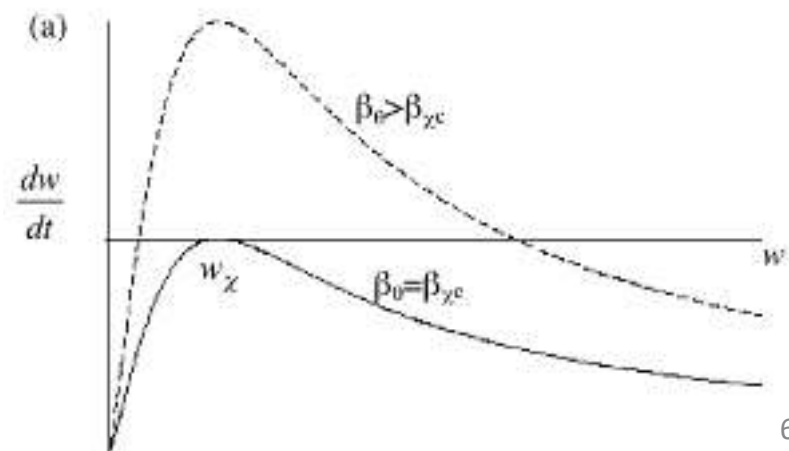
stabiliz./destab.  
depending on the  $\nabla_r J_{||}$

$$\Delta'_{bs} \propto \beta_p \frac{q'}{q} \frac{p'}{p} \frac{W}{W^2 + W_s^2}$$

significant for large plasma pressure

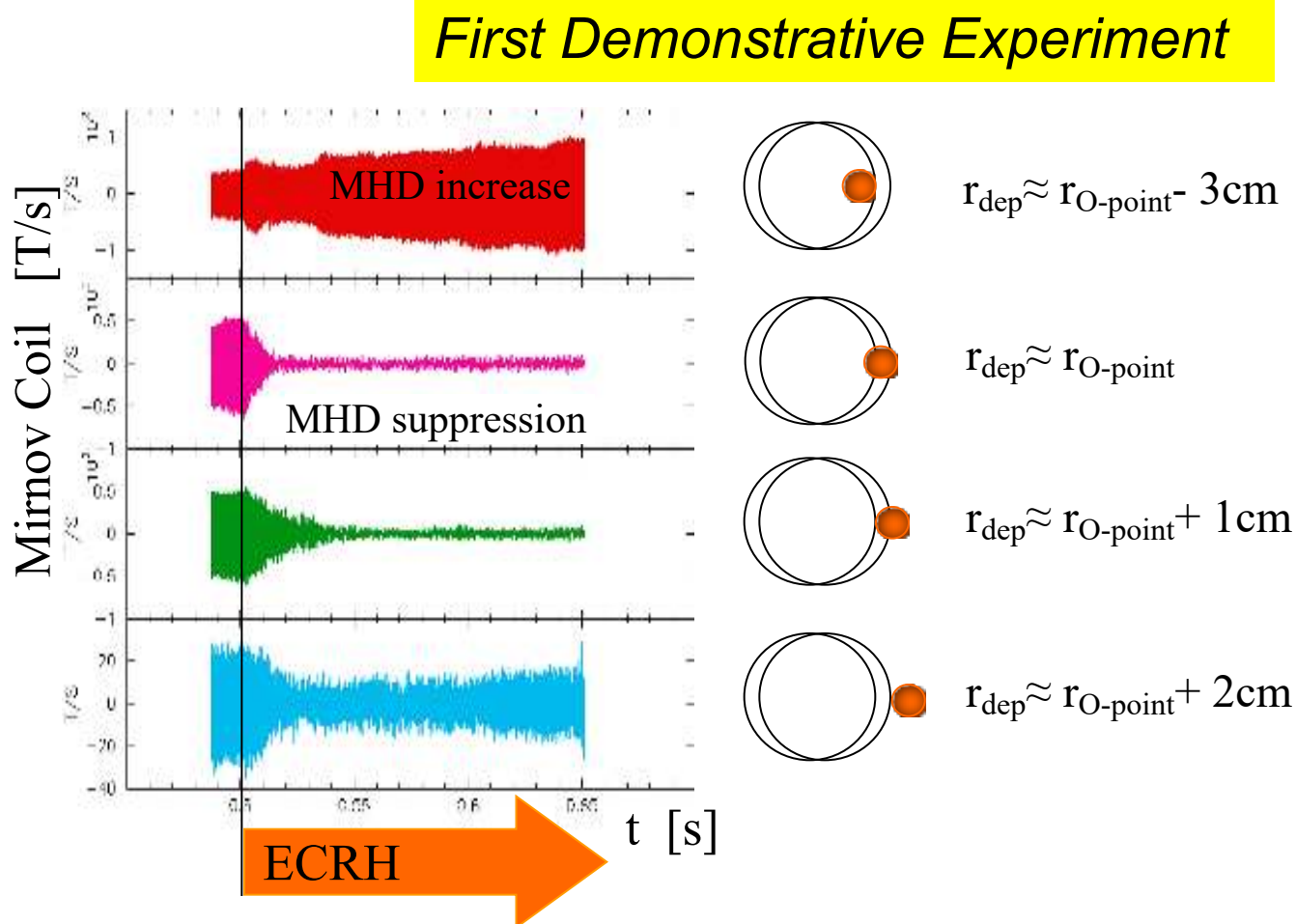
$$\Delta'_{cd} \propto \frac{I_{CD}}{I_p} \eta(W / \delta_{CD}) \frac{1}{W^2}$$

stabiliz./destab. depending on island radial centering



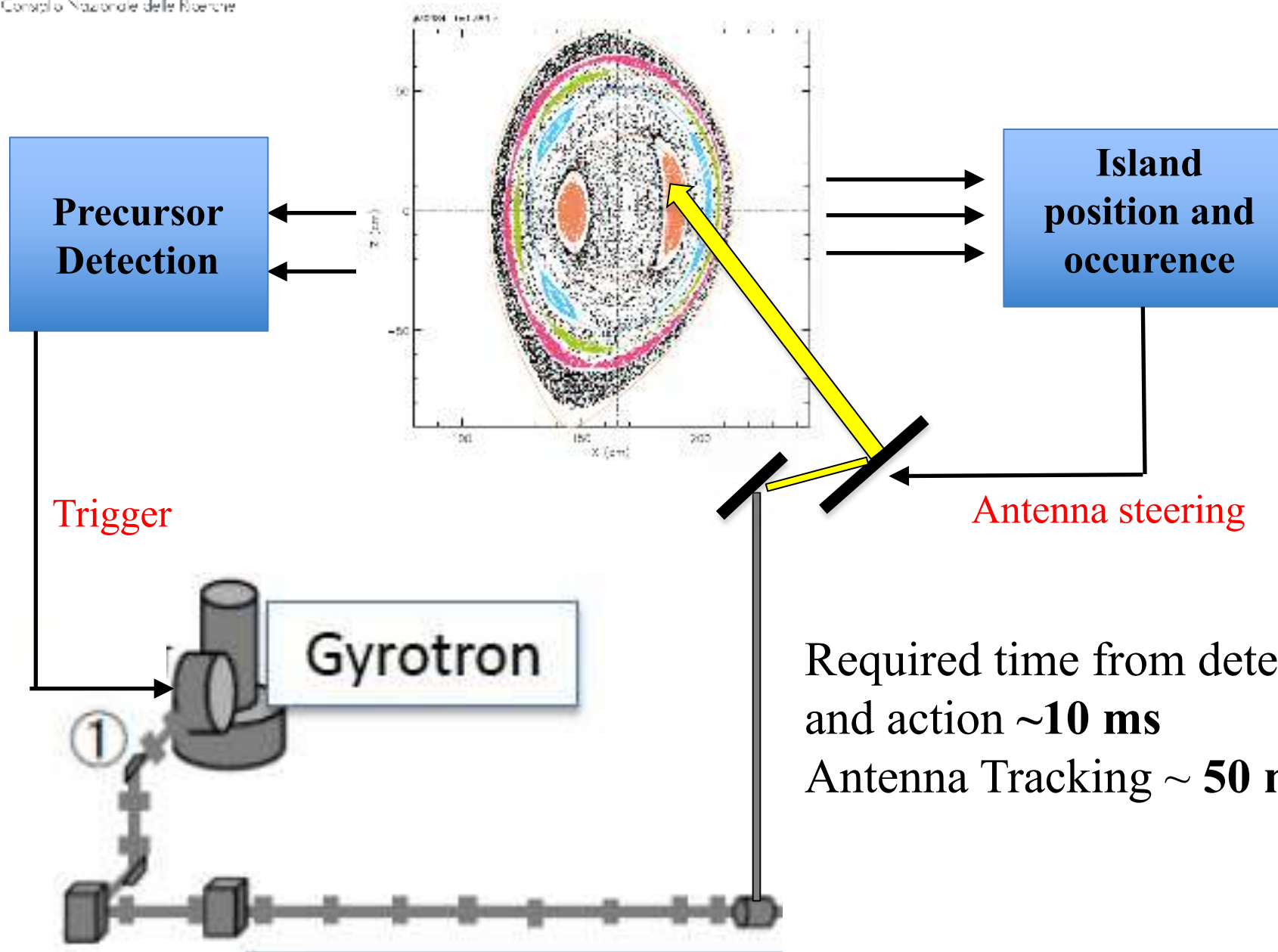
S.Cirant et al. IAEA  
Sorrento 2000

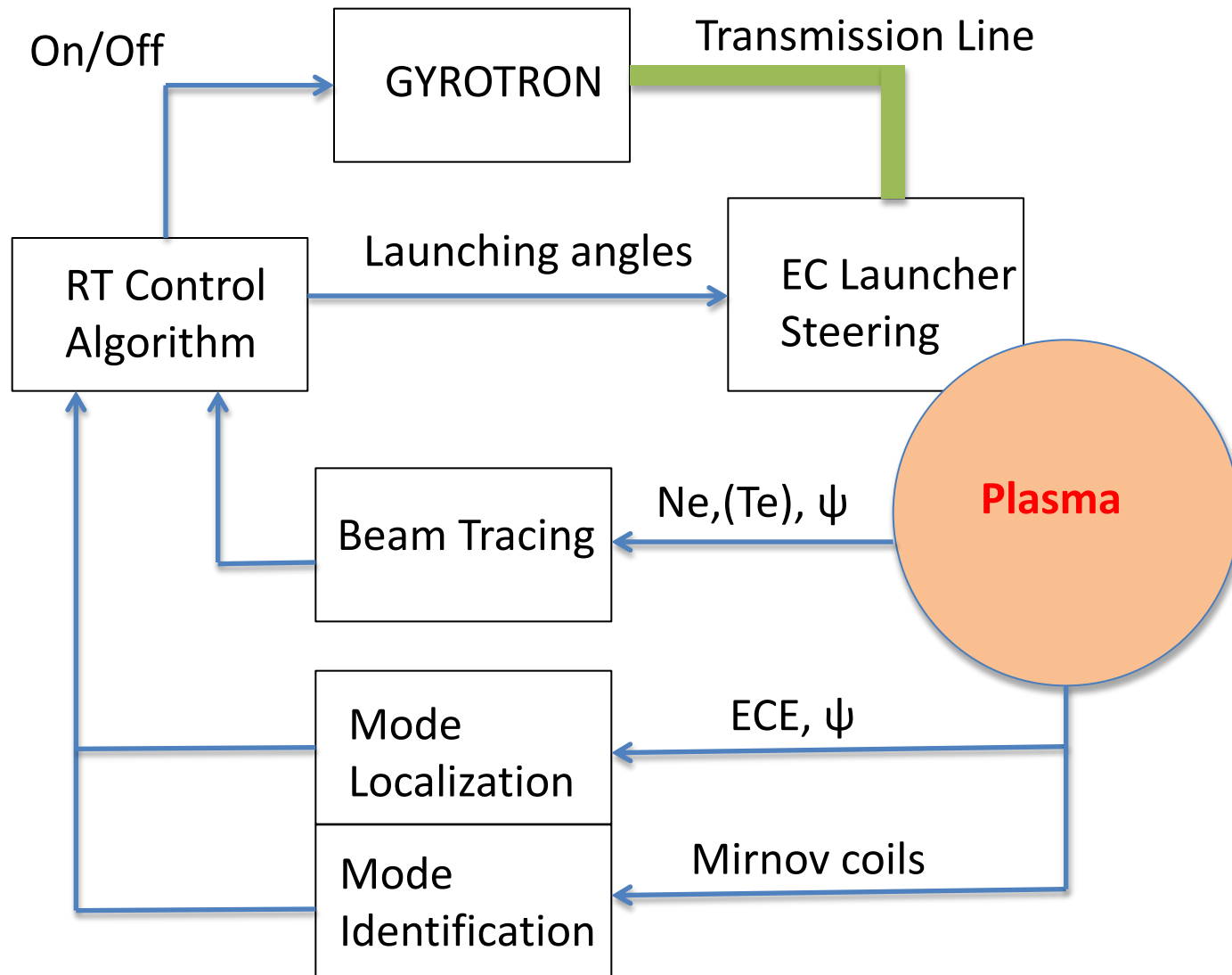
MHD instabilities are monitored by external magnetic signals with Mirnov coil



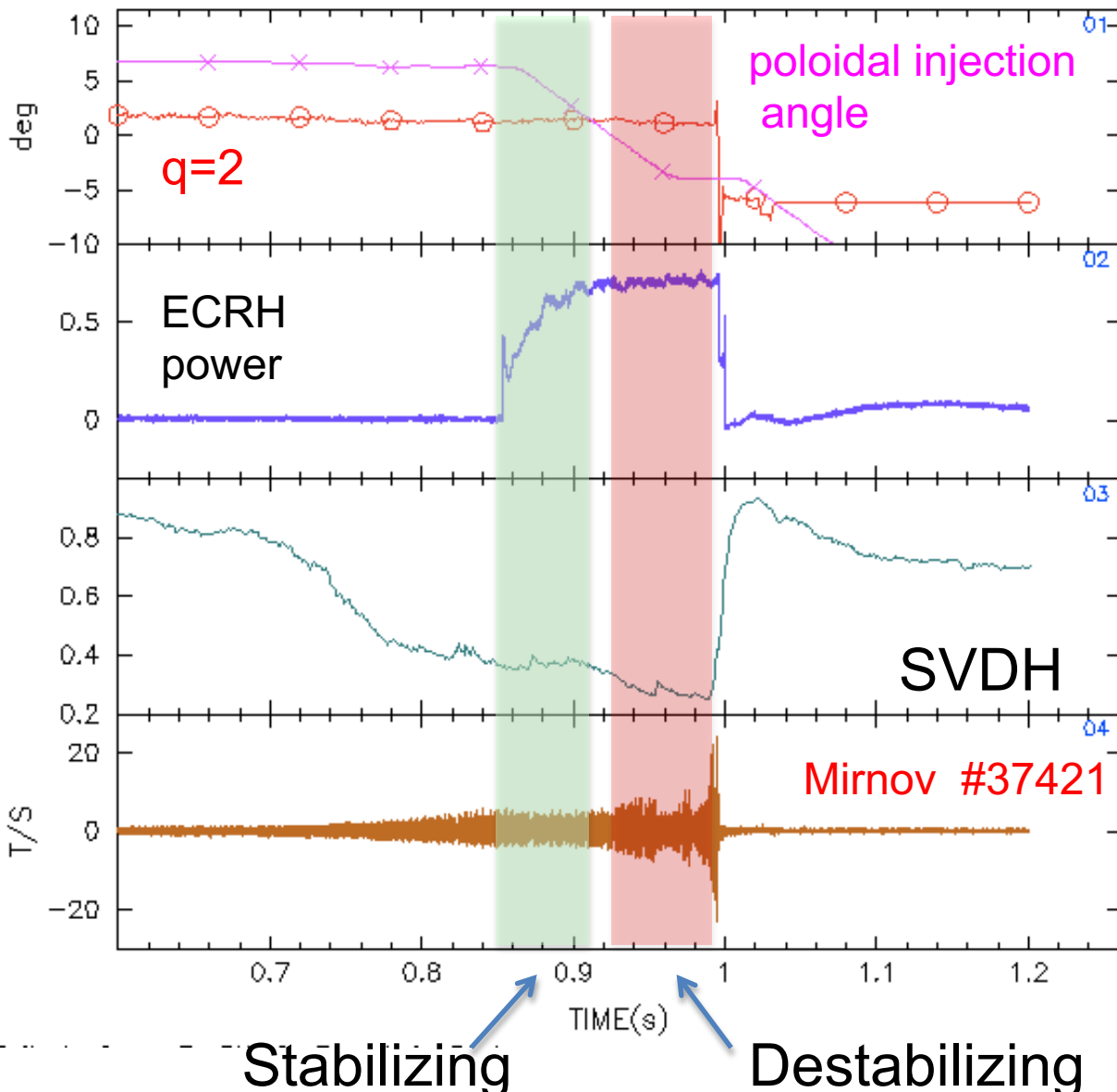
The islands can be reduced in width or completely suppressed by a current driven (also resistively) by absorption of electron cyclotron waves (EC) accurately located within the island.

# Loop di Control Loop for RT MHD stab.

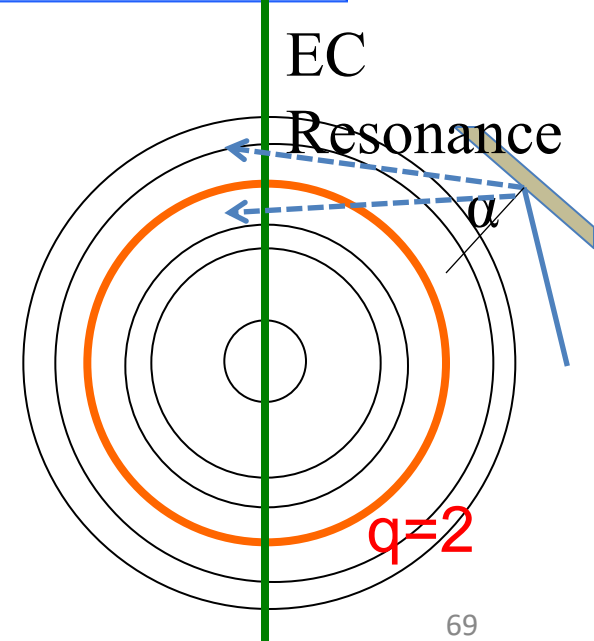




# Stabilization/destabilization depends on the ECRH absorption radius



37421	01/A
	MECRH.EQFQLOALPHA2
37421	01/B
	X ECRHL.ALFA2_Po
	ALFA L0 MIS.
37421	02/D
	MECRH.ADDGY4PWR
37421	03/E
	MECRH.svdh
37421	04/F
	%e.mhdfst(4)
	9D021PO

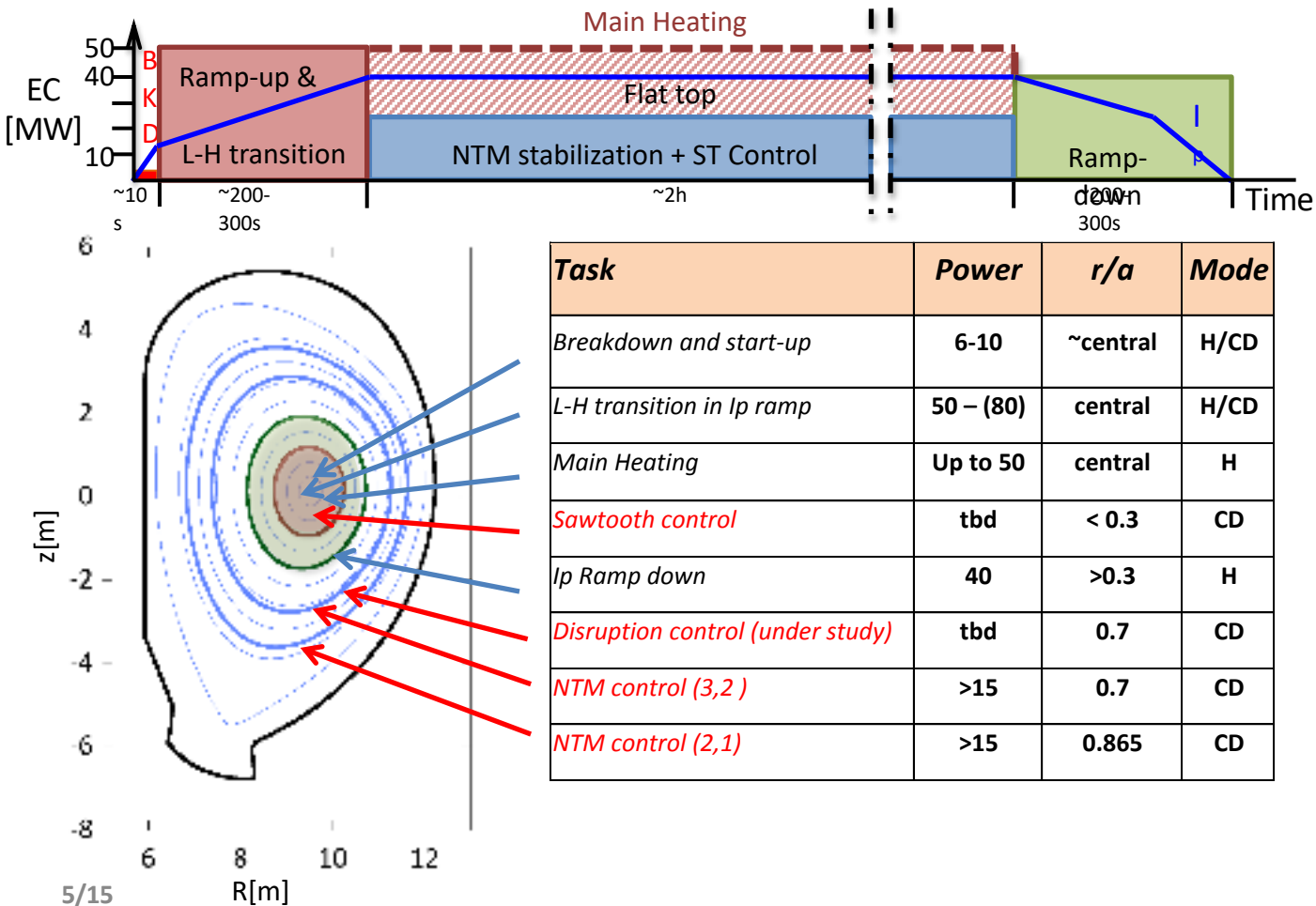


# Basic for a Design of an ECRH System

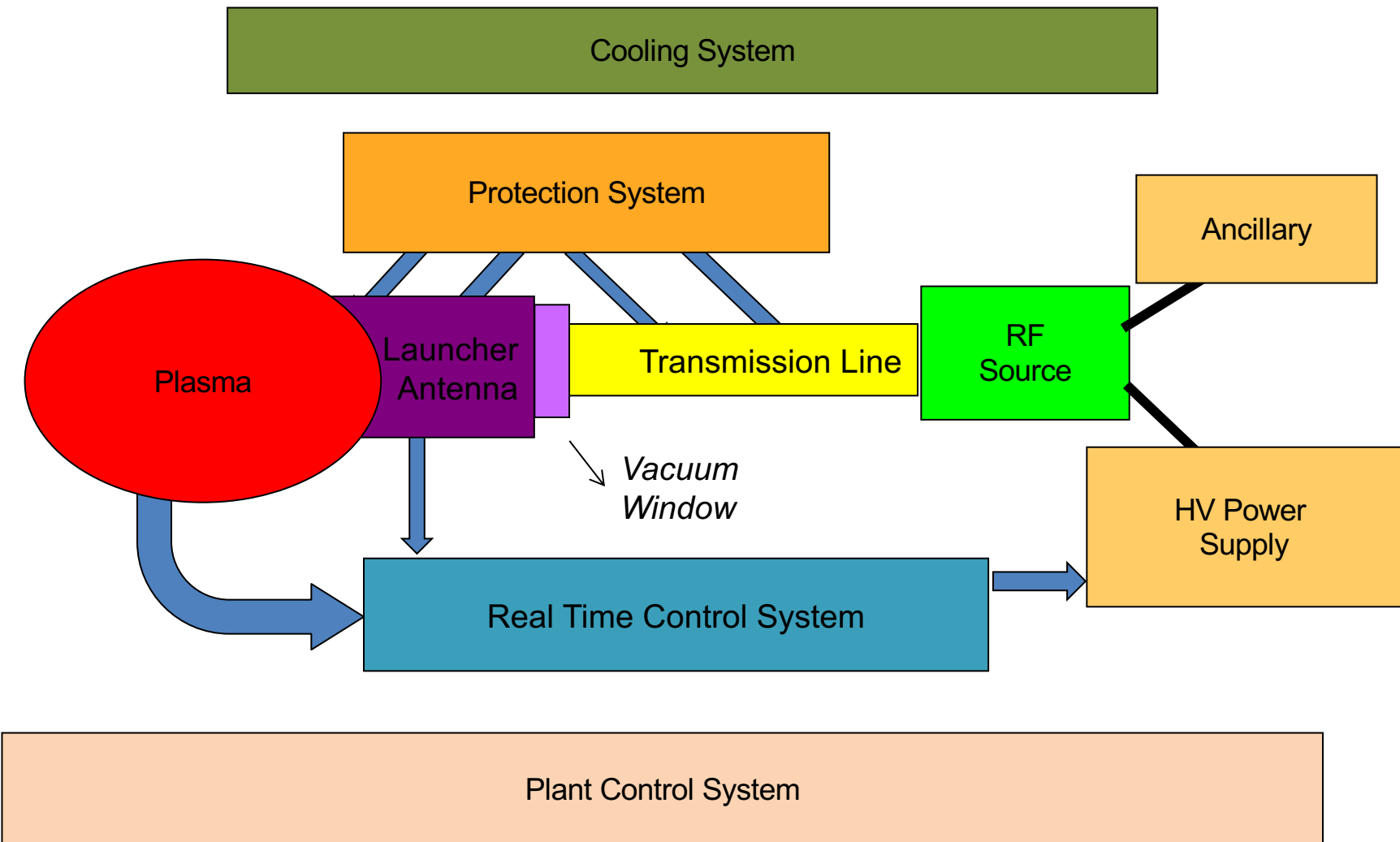
# Outline

- Main Physic requirement for ECRH system
- ECRH System General Overview
- RF Power Source
- Gyrotron Power Supply
- Transmission Line
- Polarizer
- Coupling EC power to plasma: Launcher
- Control System

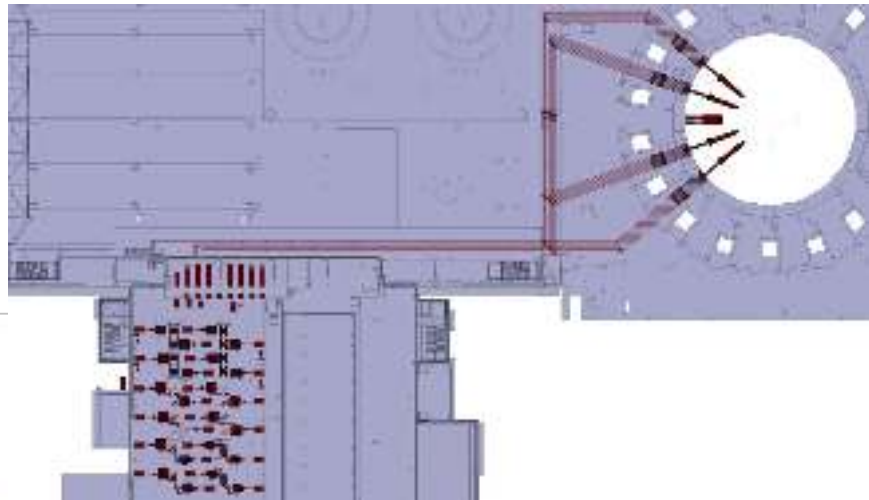
# EC System Physical Requirements



# ECRH system in blocks



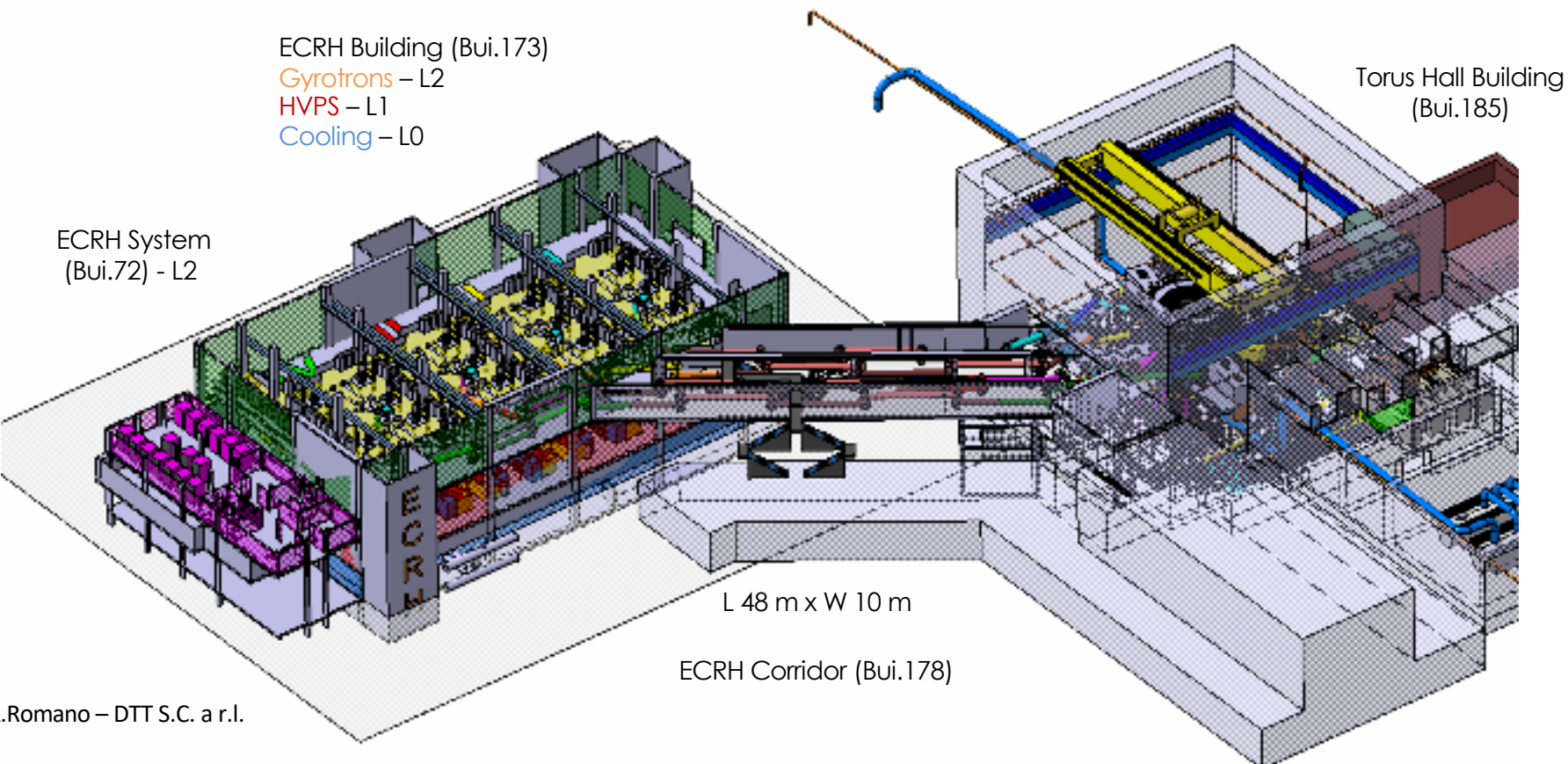
- ✓ EC system will inject 24 beams of 0.83 MW (20 MW total)
- ✓ Corresponding to **24 MW installed**



*Courtesy from F.Gandini – EC-20 - 2018*

**12 HVPS sets**  
**24 Auxiliaries set**  
**24 Gyrotrons**  
**24 Transmission Line**  
**4 Upper Launcher**  
**1 Equatorial Launcher**  
**1 Control system**

# ISTT - DTT- ECH System: General Layout



# RF Source

- *High Frequency (up to 170GHz)*
- *High Power (1 MW class)*
- *Pulse length: ~1000 s -> cw*
- *Gaussian output: 98%*
- *Reliability: > 94%*

- Klystron (for high frequency power decreases)
- Magnetron (i.e. 2.45 GHz : microwave oven)
- BWO (few watts, only for signal measurements)
- **Gyrotron : cw, up to 240GHz, 1-2 MW**
- FEM (Free Electron Maser): high frequency, only prototype study
- CARM: high frequency, high power: under consideration at Enea Lab

*In a Gyrotron an electron beam (emitted by a hot cathode) is accelerated in strong magnetic field crossing a cavity shaped for a specific mode. The electrons emit power at frequency:*

Effective frequency

$$\omega_c = n \frac{\Omega_{c0}}{\gamma} \quad \gamma = \left[ 1 - \left( \frac{v}{c} \right)^2 \right]^{1/2} = 1 + \frac{eV_0}{m_o c^2} = 1 + \frac{V(kV)}{511}$$

Relativistic term

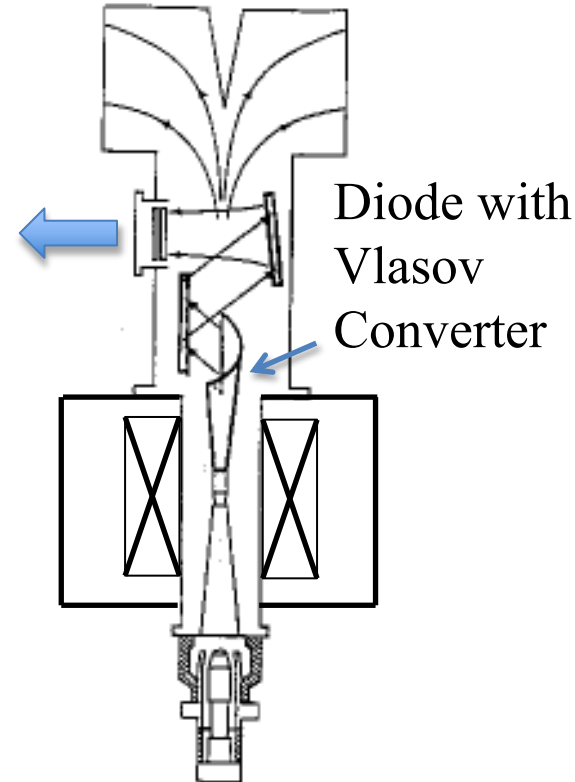
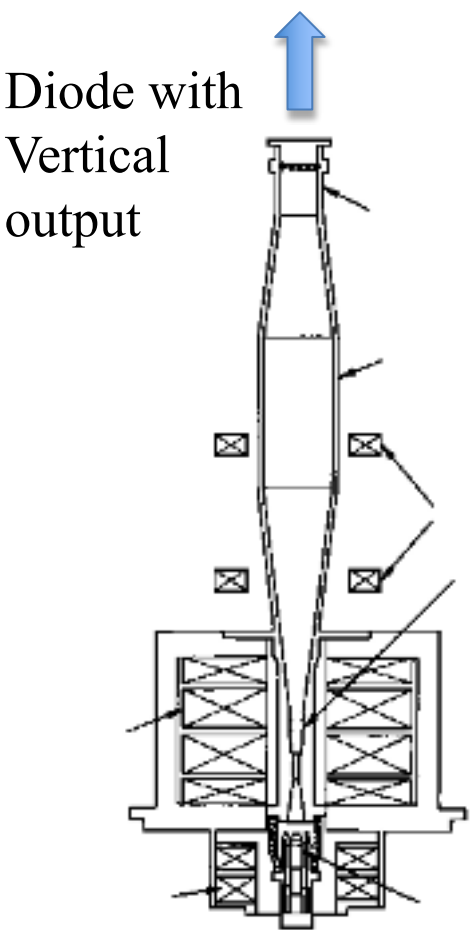
Gyrotron is an oscillating tube: not an amplifier

# Main Gyrotron Types

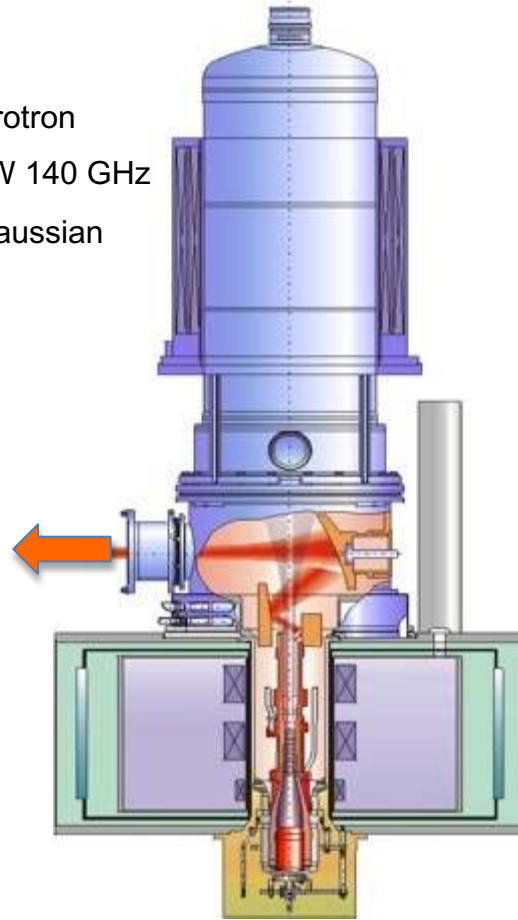


Diode, Triode or SPD (Depressed Collector efficiency ~50%)

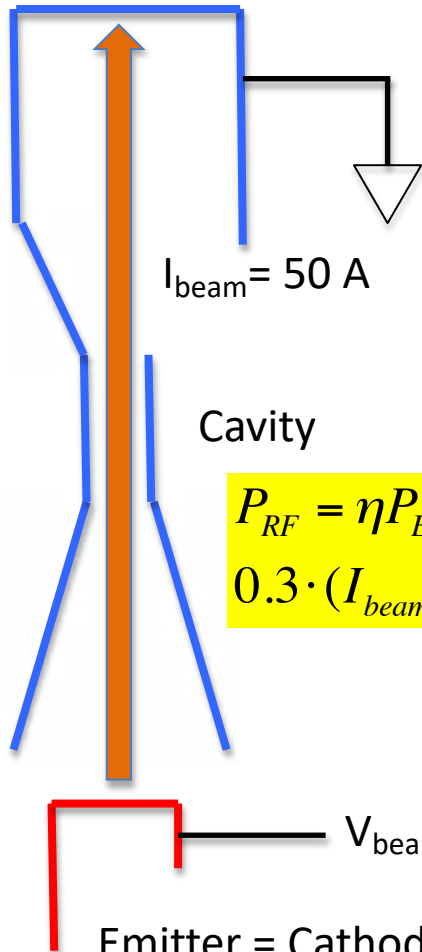
Vertical output or transversal gaussian output



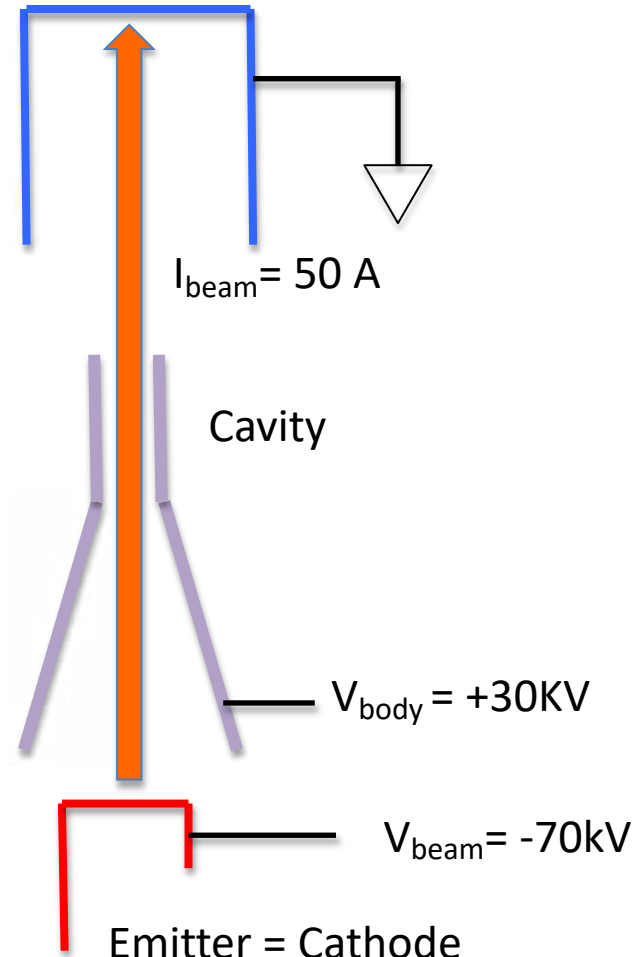
W7-X gyrotron  
1 MW CW 140 GHz  
Radial Gaussian Output



Collector = Anode



Collector = Anode



$$P_{RF} = \eta P_{EL} =$$

$$0.3 \cdot (I_{beam} \cdot V_{Cath-Body}) = 1.50MW$$



$$\eta = \frac{P_{RF}}{P_{EL}} = \frac{1.5MW}{3.5MW} \sim 42\%$$

# The Gyrotron RF output



The gyrotron RF output is not a pure gaussian beam. 10-15% of **spurious modes** are usually present. **Future goal < 2 - 5%**

The out put beam is modified by the use of two shaped mirrors (elliptic or phase corrected): Matching Optics Unit (**MOU**)

The output **polarization** is **linear and horizontal** (with respect to the tube vertical axis) in the last generation tube (with Vlasov Converter)

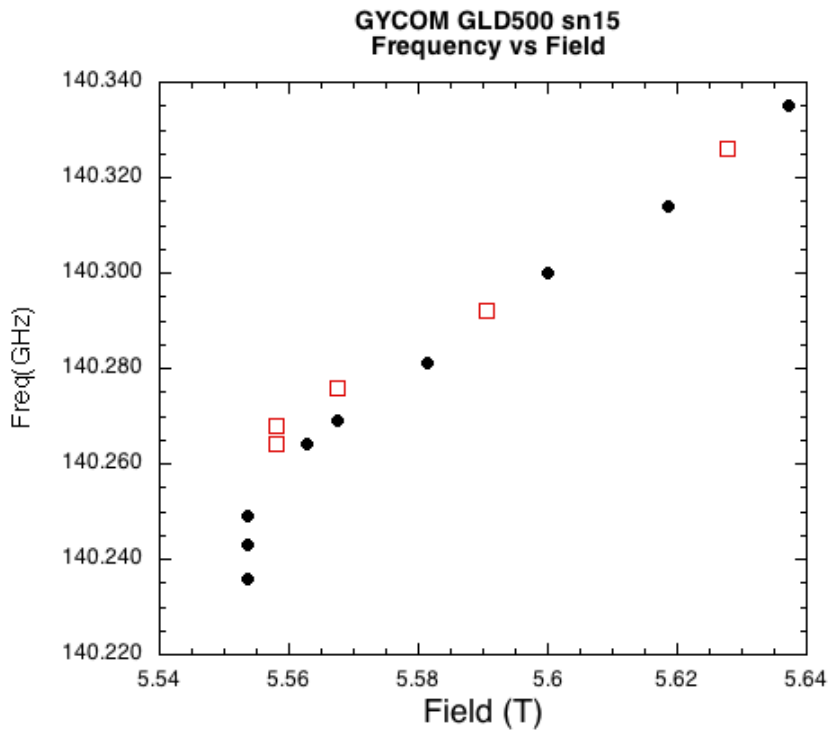
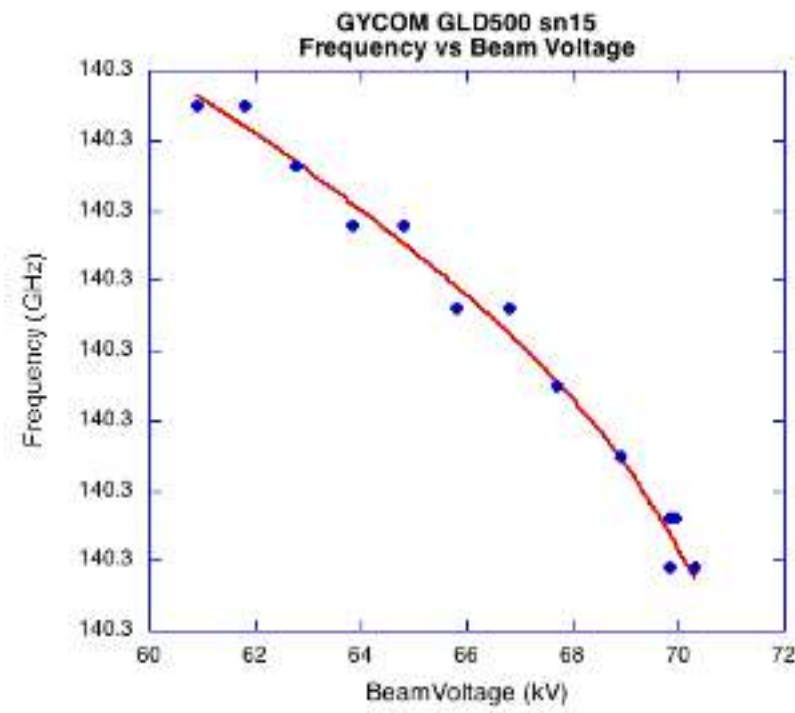
The beam must be matched with the Transmission Line minimizing the **conversion losses**.

***The lost power MUST be absorbed in some way therefore MUST be minimized***

$$\omega_c = n \frac{\Omega_{c0}}{\gamma}$$

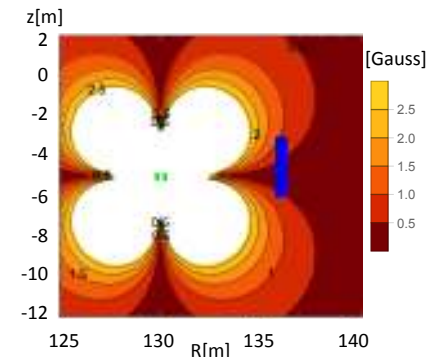
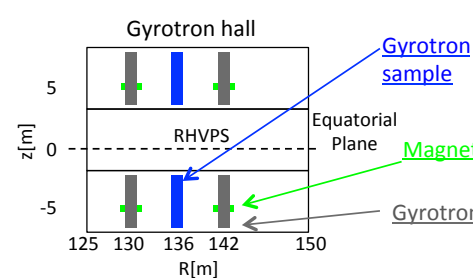
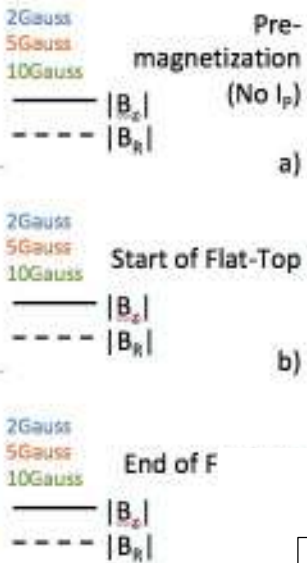
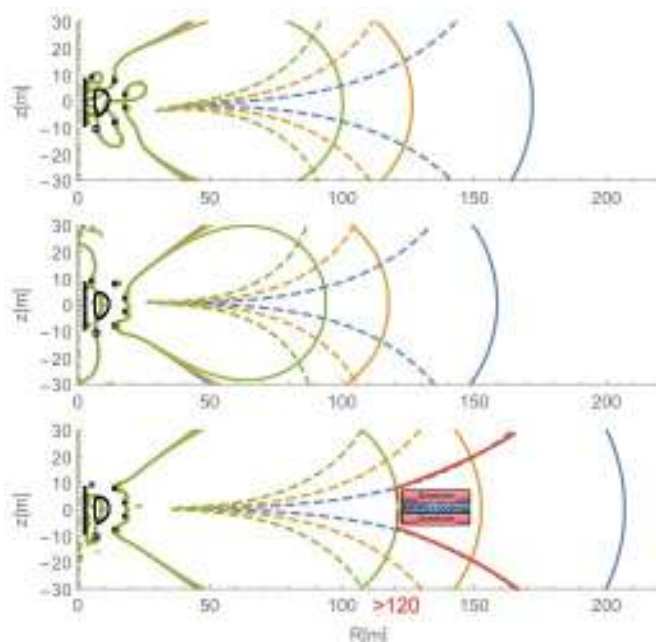
$$\gamma = \left[ 1 - \left( \frac{v}{c} \right)^2 \right]^{1/2} = 1 + \frac{eV_0}{m_o c^2} = 1 + \frac{V(kV)}{511}$$

Frequency depends on **magnetic field** and accelerating voltage (**beam voltage**)



Dependency on magnetic field is linear but too slow (high impedance) to be used

# Gyrotron and stray magnetic field



The stray field is generated by:

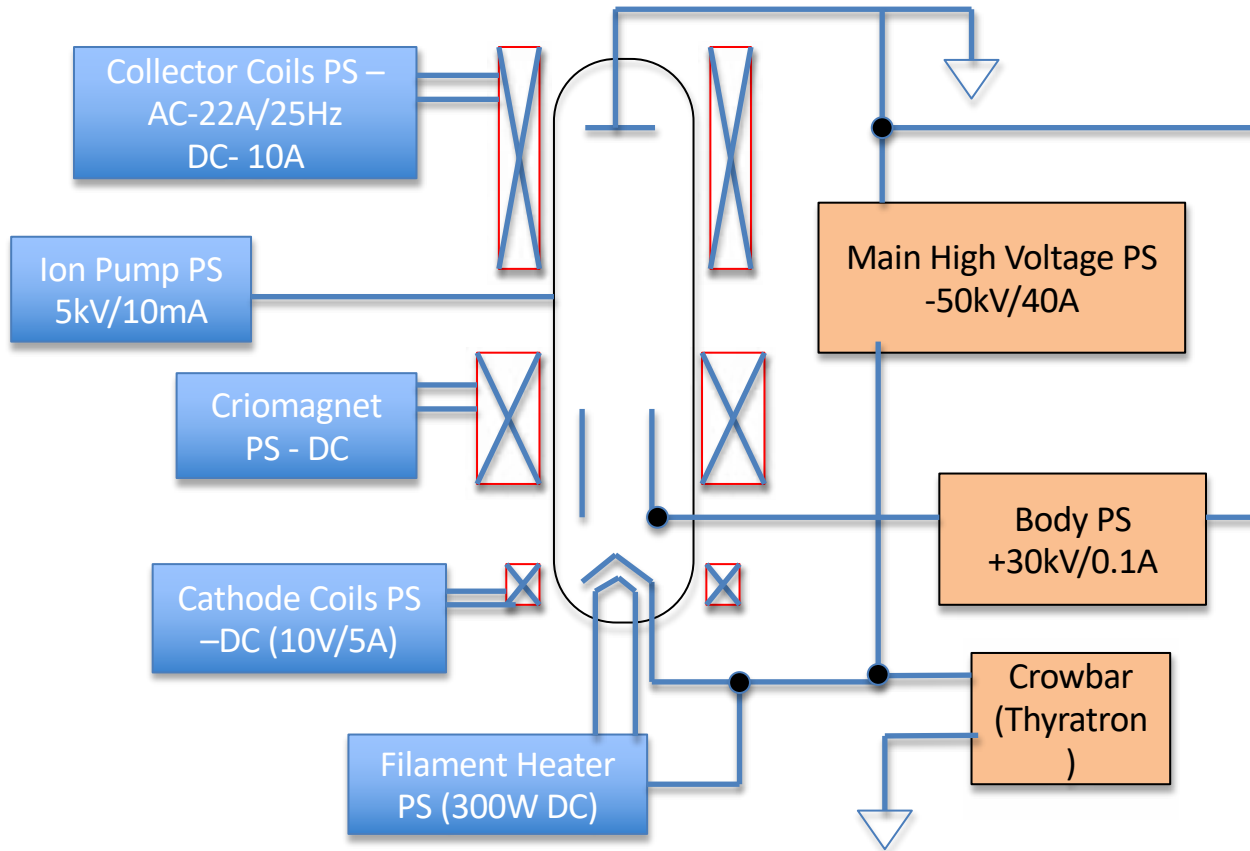
Plasma Current + Poloidal coils + Central Solenoid  
neighbour gyrotrons

Gyrotron can be damaged by a stray magnetic field at level of collector.

The MW level gyrotrons require:

2 G for radial component  
10 G for vertical component

# Gyrotron Auxiliaries



High stability:  $\pm 0.2\%$

Fast voltage ramp:  $\sim 1$  ms

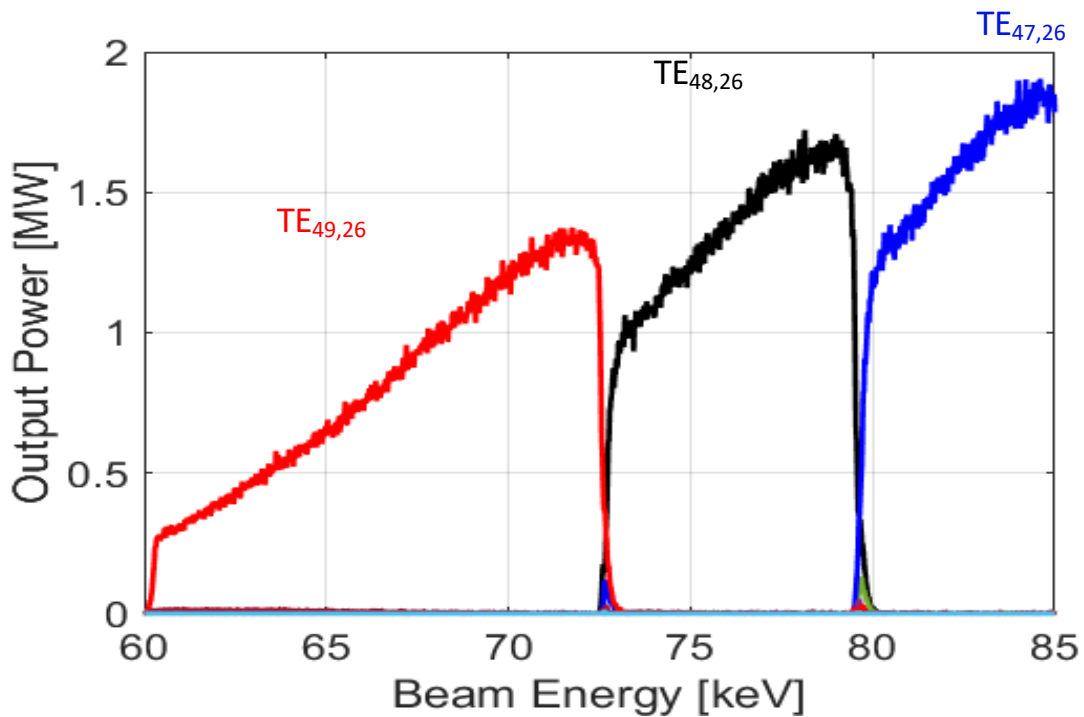
Fast protection time: 5-10  $\mu$ s (max energy in the fault = 10J)

Up to 5 KHz full modulation (for MHD control)

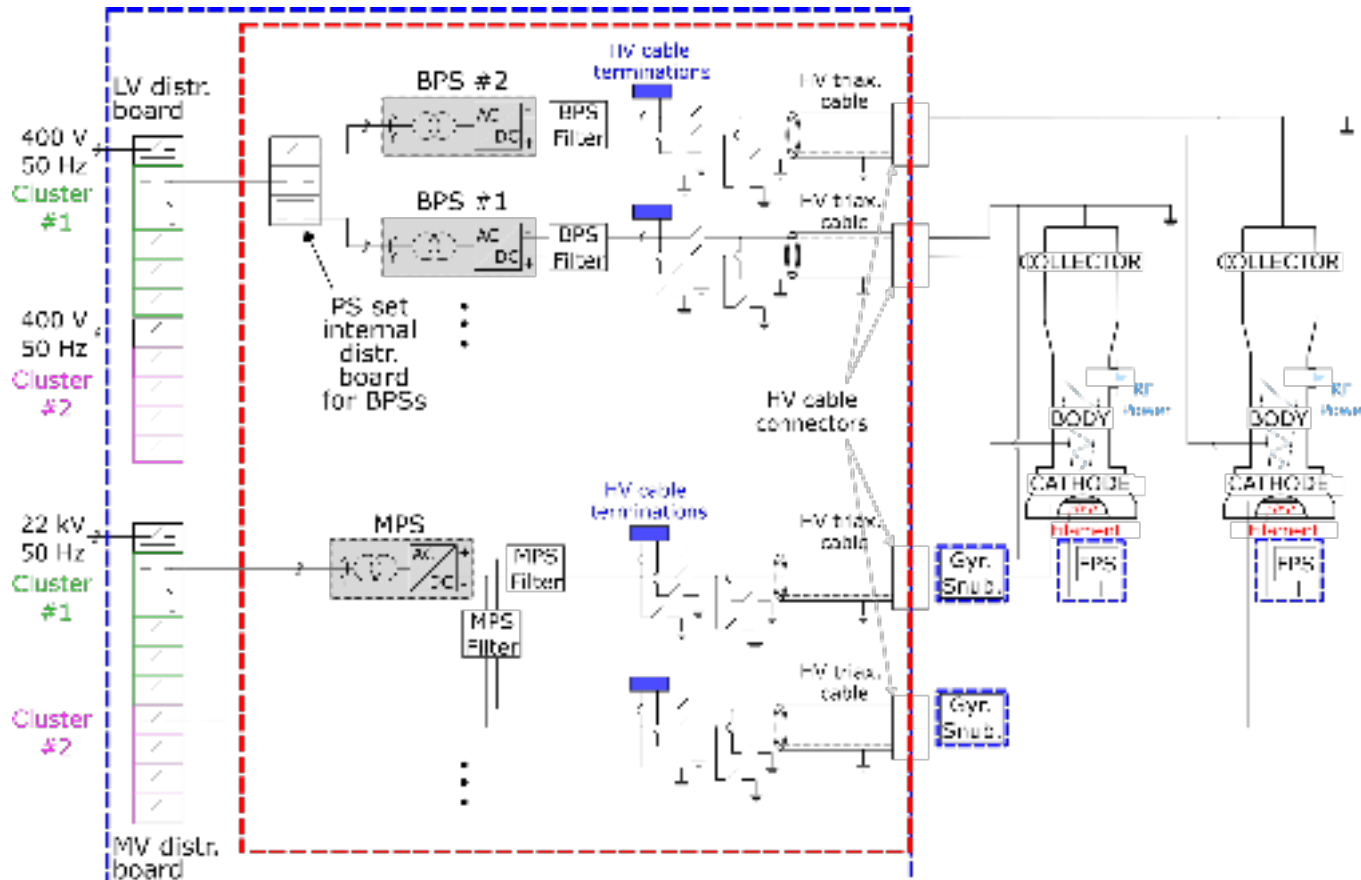
Short distance between PS and gyrotron (low parasitic capacity)

Stabilization using Body PS in feedback on the whole accelerating voltage ( $V_c + V_b$ ).

# Fast Rise time avoid competitive mode oscillation



# The HV Power Supplies for CPD Gyrotron



# *Objective of a Transmission System*

To transmit the power with the lower losses

To assure safe and stable operation for the source

To measure the delivered power

To control polarization

To match the delivered power with the plasma

To guarantee a friendly and effective control by operator

# Main Transmission Lines Type

**Wave guide:** metallic structure (cylindrical or rectangular) capable to transmit power at long distance with reduced attenuation

**Mirrors:** the microwave wavelengths allow a quasi-optical approach. The RF field can be treated as an electromagnetic wave. A set of focussing mirrors can be used to transmit power.

*Closed system:* over-moded waveguide

ITER (evacuated)

AUG (in air)

TCV (evacuated)

FTU (in air)

WEST (evacuated)

DIII-D (evacuated)

*Open system:* quasi-optical approach using reflecting mirror:

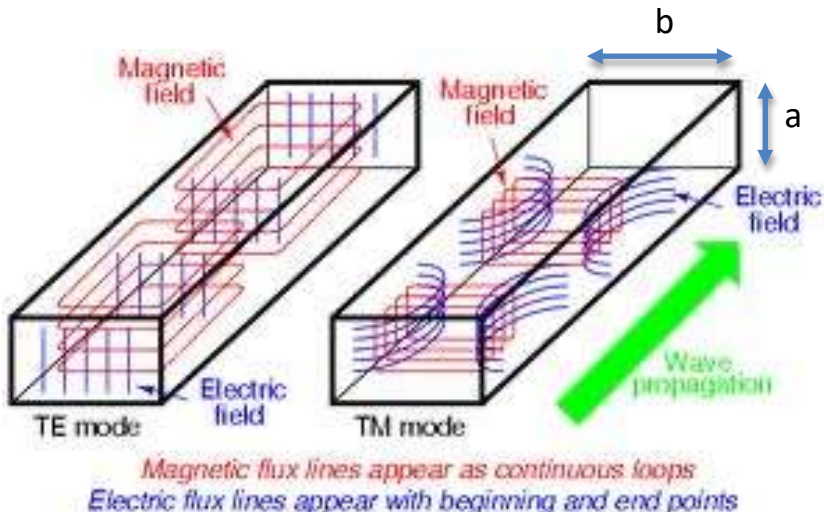
W7-X (in air)

DTT (evacuated)

DEMO (evacuated)

# Wave Guide concept

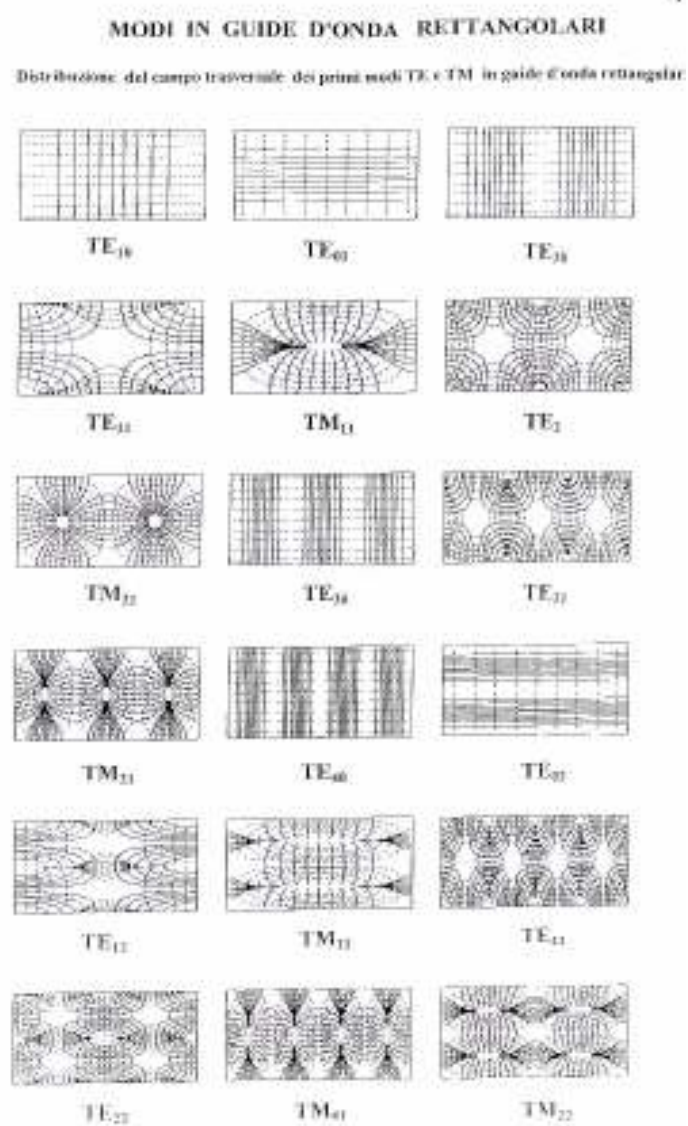
Propagation of e.m field is sustained by induced current in the metallic wall of the waveguide.



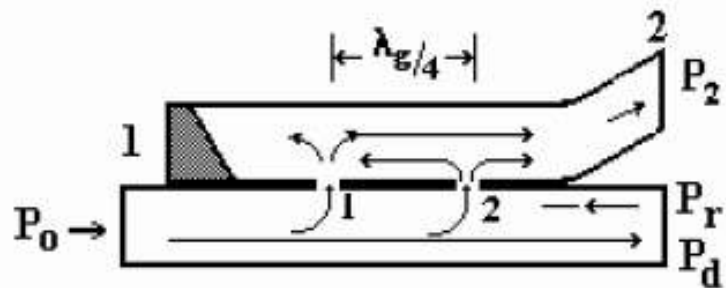
The propagating mode is based on the solution of the telegraphist equation, which is a combination of Bessel functions.

$$\lambda_c = \frac{2}{\sqrt{\left(\frac{m}{a}\right)^2 + \left(\frac{n}{b}\right)^2}}$$

For a given dimension (a,b) a cut-off lambda is defined: only waves with lower lambda can propagate or being excited



# Directional Coupler



This is used to pick-up part of the wave travelling in a wave guide.

It is used to measure forward (and reflected) power

The power is transmitted across a series of holes at a distance of  $\lambda_g/4$ .

The power depends on the holes dimension, the coupled wave maintain the propagation direction.

It can be used ONLY in a mono-modal waveguide.

# The circular over-mode WG

Transmission of high power requires enough power handling.

In dry air the break down electric field is **15 kV/cm**, from the mode choice and the power delivered is possible to fix the minimum i.d. of the waveguide:

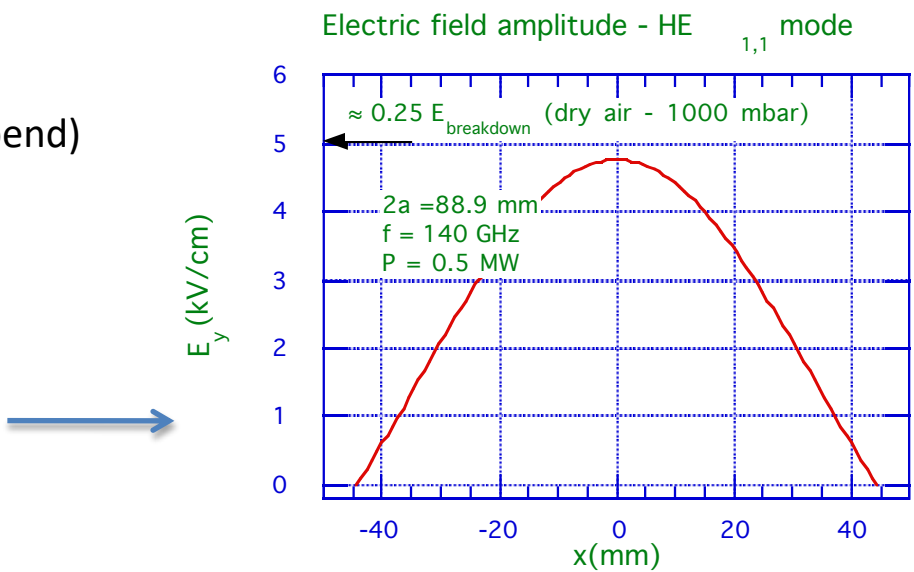
$$P = E_{\max}^2 1.99 \cdot 10^{-3} a^2 \frac{\lambda}{\lambda_g} \quad \text{TE1,1 in circular wg}$$

For  $P = 1\text{MW}$

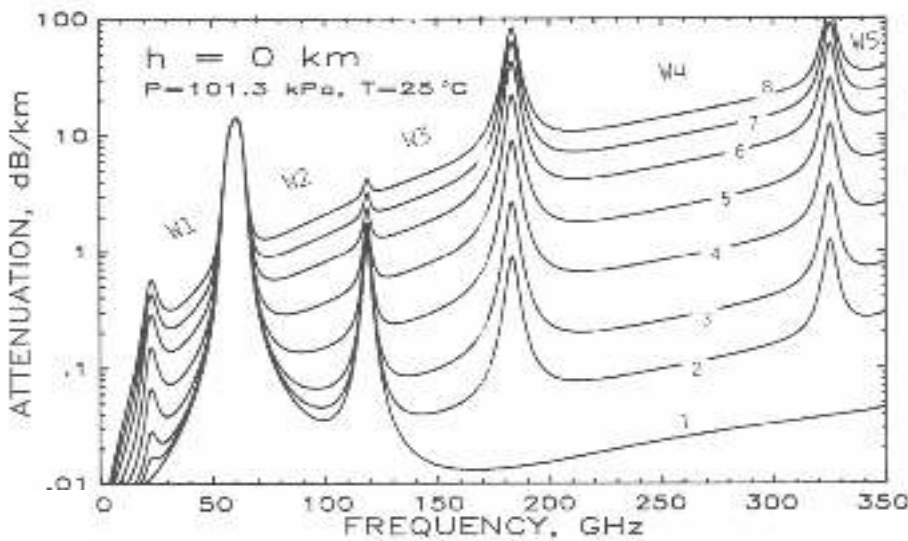
$E_{\max} = 7 \text{ kV/cm}$  (in case of reflection at mitre bend)

which requires a diameter of  $\sim 10 \text{ cm}$

HE1,1 in corrugated over-mode wg



- 1- Breakdown: transmission of high power wave is limited by air breakdown that gives a limit to the electric field
- 2- Losses: the air can absorb high frequencies (losses) depending on humidity, as a consequence it is necessary to cool down the heated.



Propagation in Vacuum reduces the risk of arc (only on metallic surfaces) and eliminates the air losses.

To keep under vacuum a transmission line required a specific design and additional cost.

Under vacuum lines exhibits less problem with the RF leakage

# Corrugated waveguide

A small corrugation on the wall of the wg produces a non zero impedance along wg axis (z), in this way a so called **hybrid modes** can propagate (combination of  $TE_{0N}$  and  $TM_{0N}$ ).

When the wg i.d.  $2a \gg \lambda > p$  (period of corrugation) the wg wall begin to look like a surface with an anisotropic reactance:



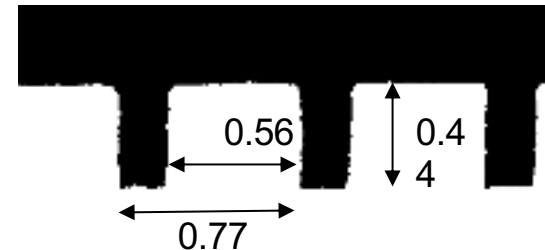
$$Z_\phi = \left. \frac{E_\phi}{H_z} \right|_a = 0$$

*Internal diameter 88.9 mm*

$$Z_z = -\left. \frac{E_z}{H_\phi} \right|_a \cong jZZ_0$$

$$Z = \frac{w}{p} \tan(kd)$$

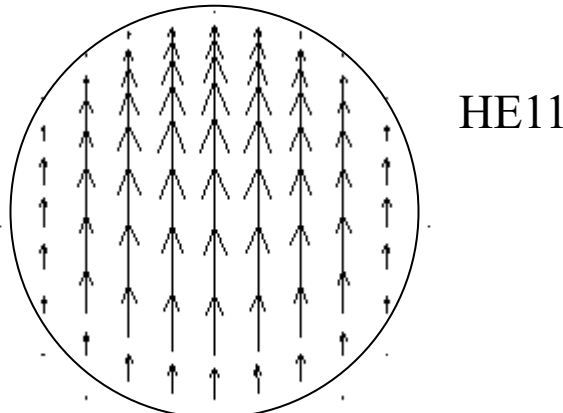
$$Z_0 = \sqrt{\mu_0 / \epsilon_0}$$



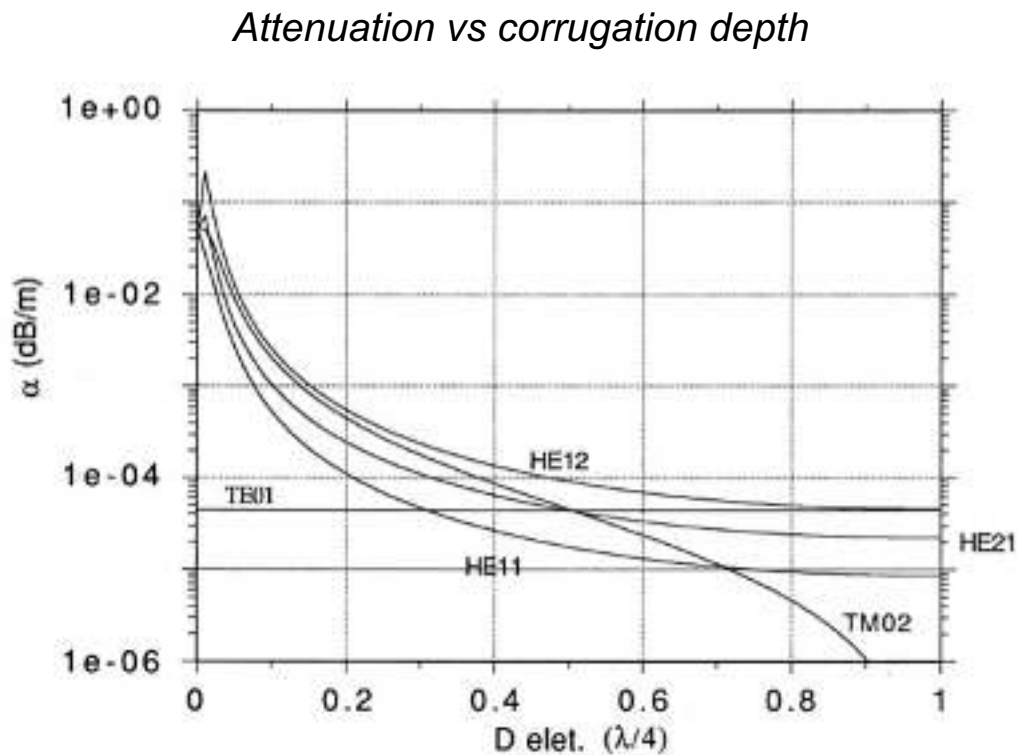
*Detail of the wg wall section for ECRH-FTU TL system at 140 GHz*

# Attenuation of Hybrid Mode

The different attenuation can be exploited as modal filtering



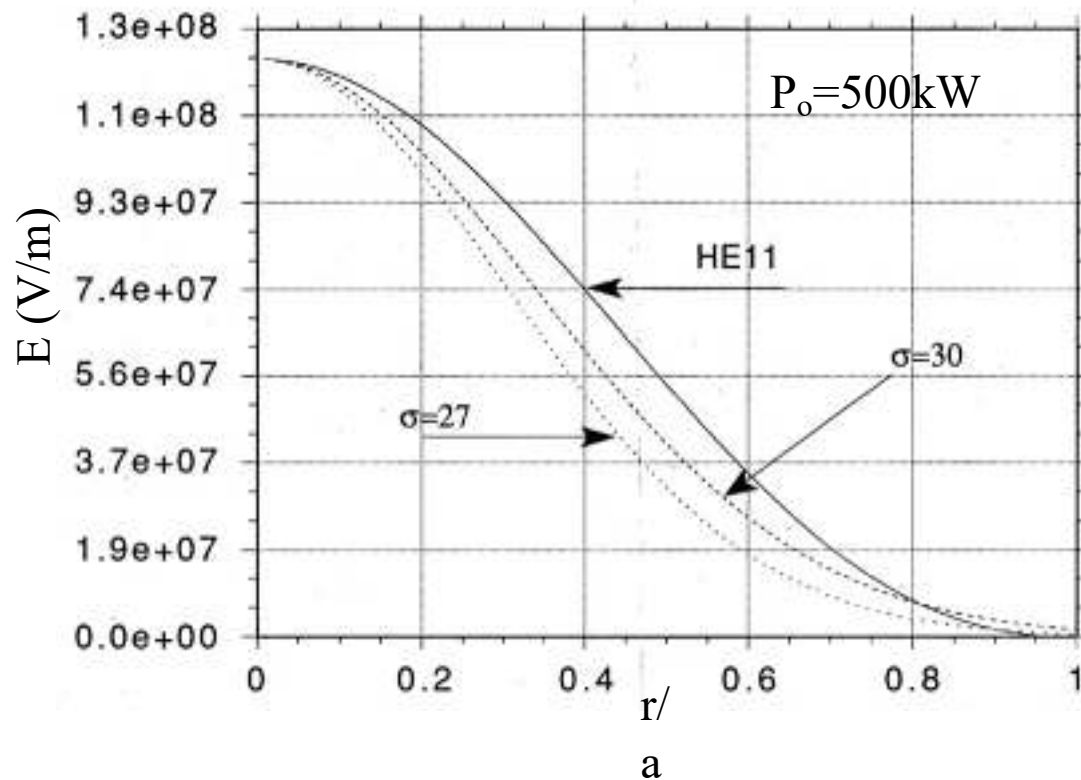
HE11 is the basic mode chosen in fusion application:  
 It has a **low attenuation**, it is **linearly polarized** and propagate in free space as a **gaussian mode** (TEM00)



The electric field is close to zero at the wall, with consequent low ohmic attenuation

## *Hybrid Mode Field Profile vs Gaussian mode*

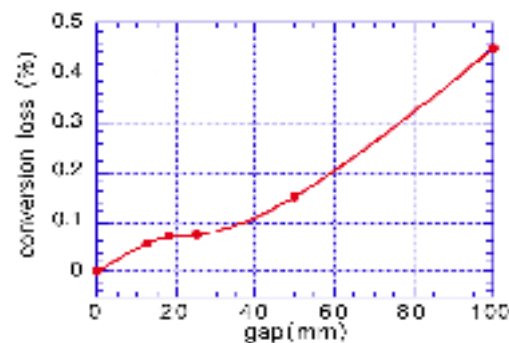
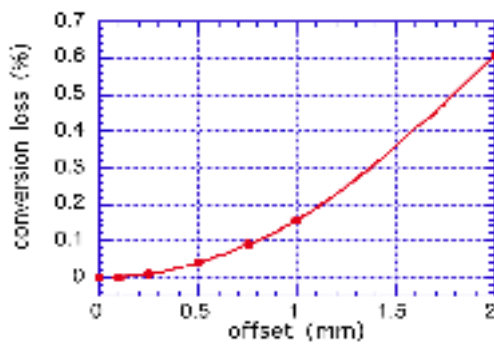
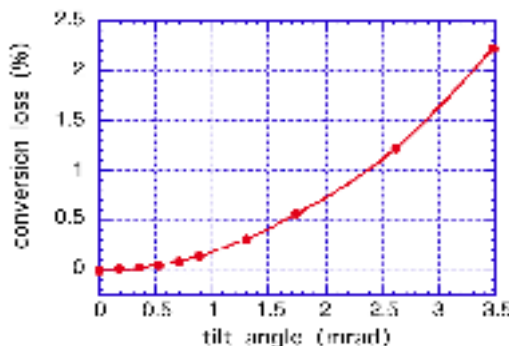
Comparison with Gaussian Distribution (TEM00) with different waist ( $\sigma$  in mm for  $a = 44.45$  mm)



In the conversion from TEM00 to HE11 and vice versa the 2.5% of power is lost

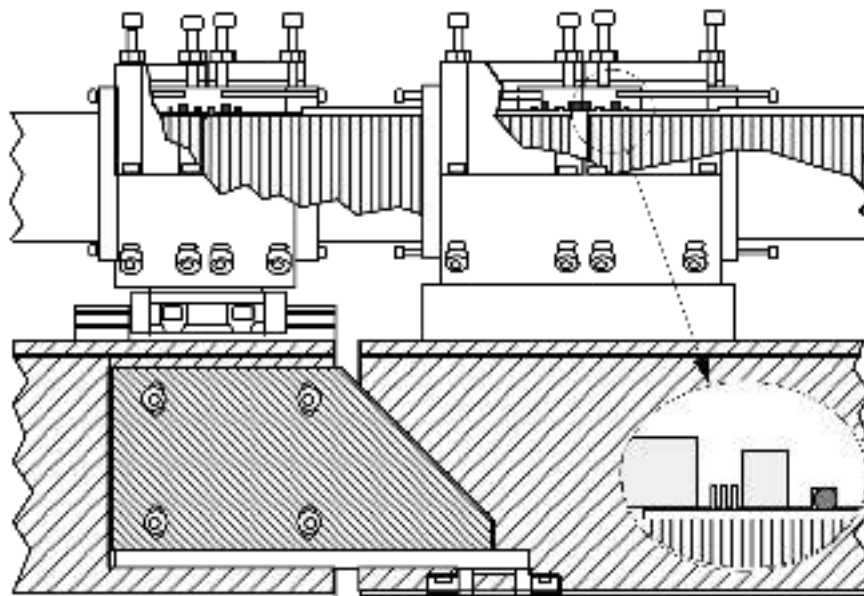
# Alignment Issues

## Conversion Losses due to alignment errors



Errors (tilt and/or offset) produce conversion to high order modes.

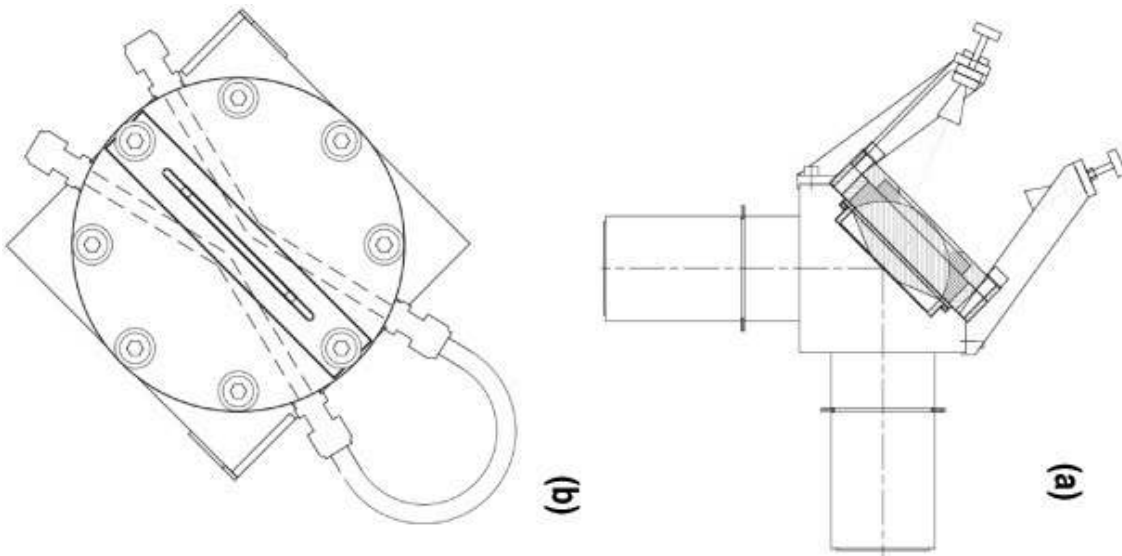
These modes are absorbed by wg requiring a larger cooling or a local increase of electric field (arc risk) .



Expansion Joint for FTU ECH system

In a over modal corrugated wg the change in direction can be done by reflection on flat mirror of the wave propagating after a open-ended wg.

The losses depends on the length of the gap and on the frequency (+ ohmic one on the mirror)



**GYCOM 170 GHz mitre bend and clamps for wg cooling**

All the component of a cw transmission line must be cooled

# WG evacuated components (GA)



# RF loads

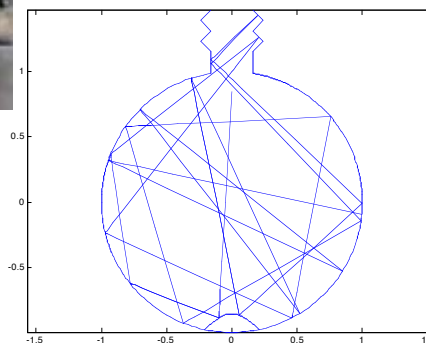
The Gyrotron power must be directed on a **dummy load** during commissioning test or **conditioning**.

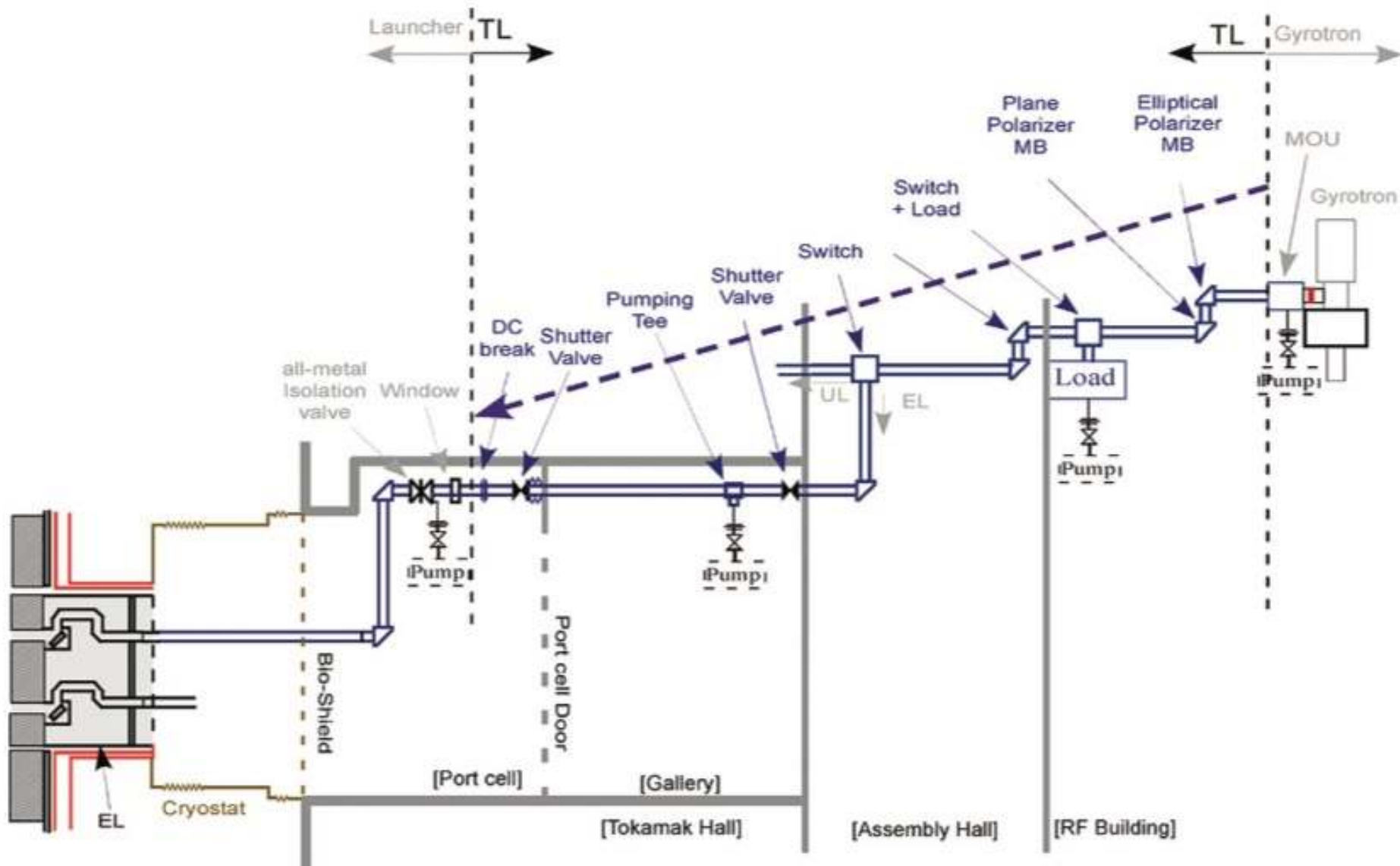
The load must have a low reflection (<4%) and the possibility to measure (bolometer) the absorbed power.



Gycom 2006 version  
load. 1MW cw in air

The sphere for FTU and 2MW EU project.





# The Quasi Optical Approach

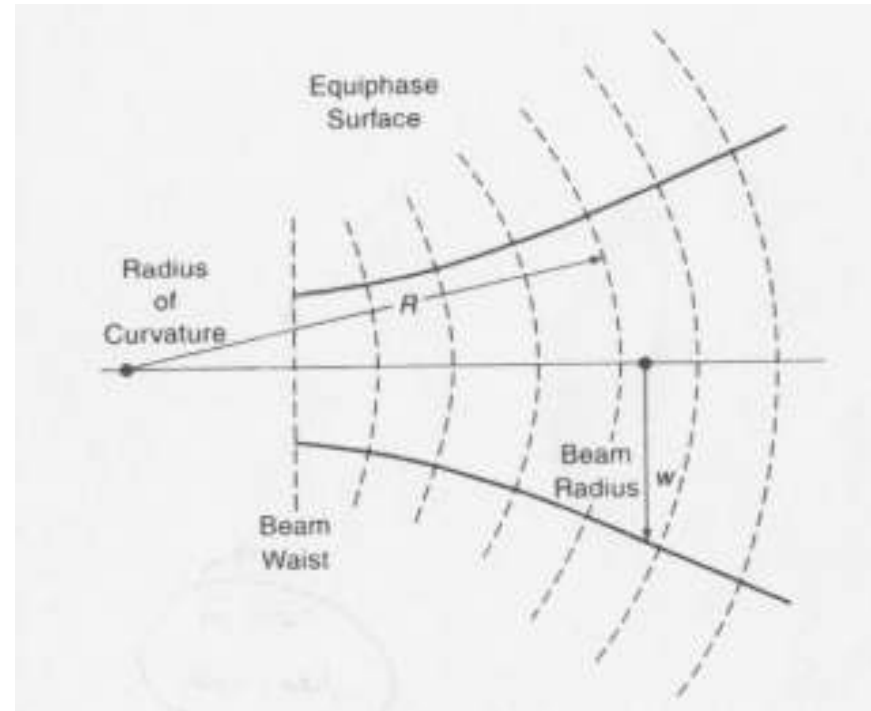
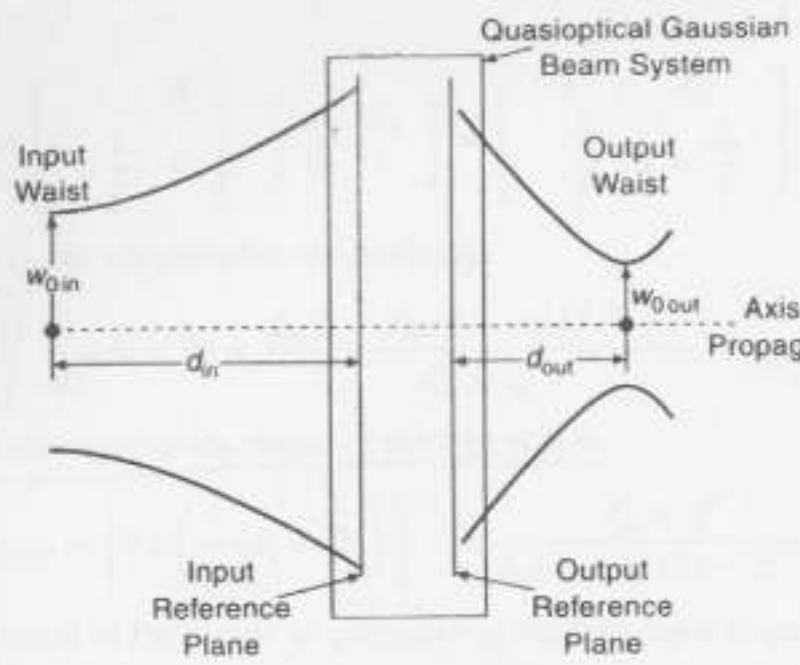
Considering wavelength (mm) the microwave beam can be approached using the optics propagation equations.

*Beam diameter*

$$w(z) = w_0 \left[ 1 + \left( \frac{\lambda z}{\pi w_0^2} \right) \right]^{1/2}$$

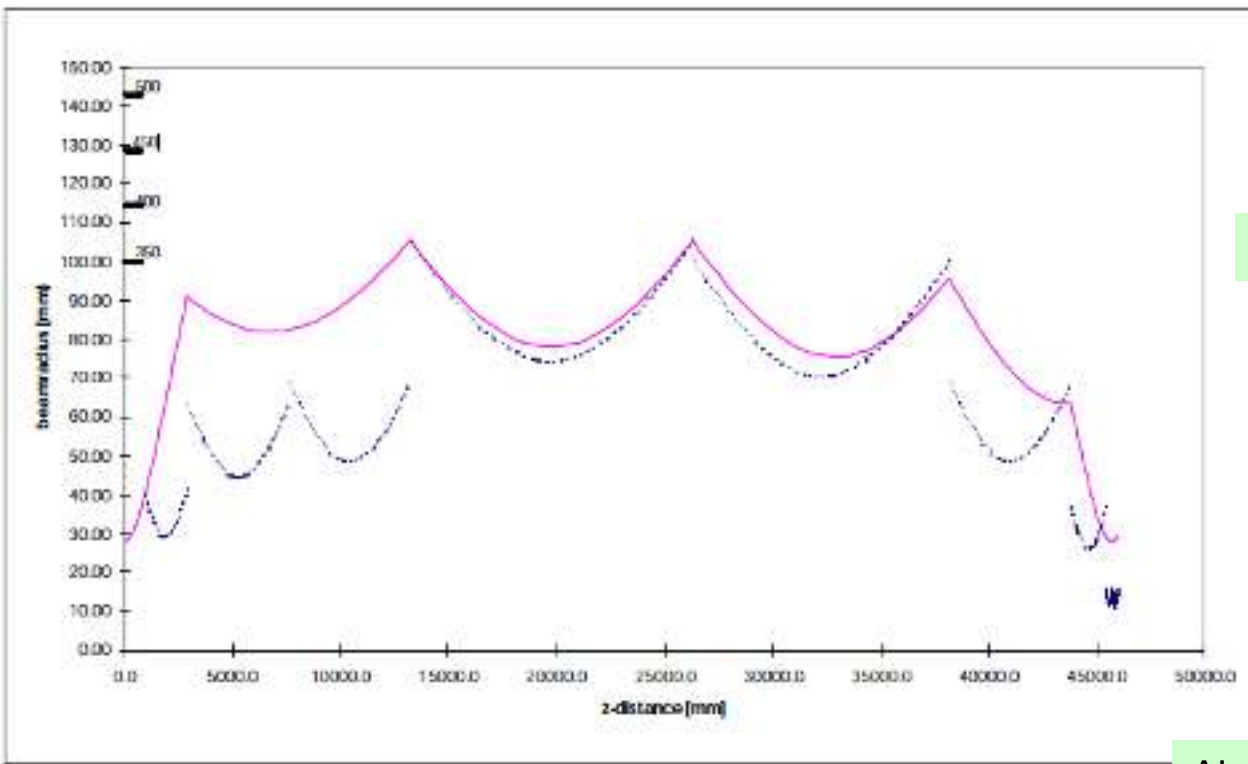
*Curvature of phase front*

$$R(z) = z \left[ 1 + \left( \frac{\pi w_0^2}{\lambda z} \right) \right]$$



# W7-X Q.O. Transmission Line

The power is reflected by large mirrors from the gyrotron output (MOU) to the vessel window.



Mirrors dimension  $\sim 4\text{ w}$

High frequency-> less divergence

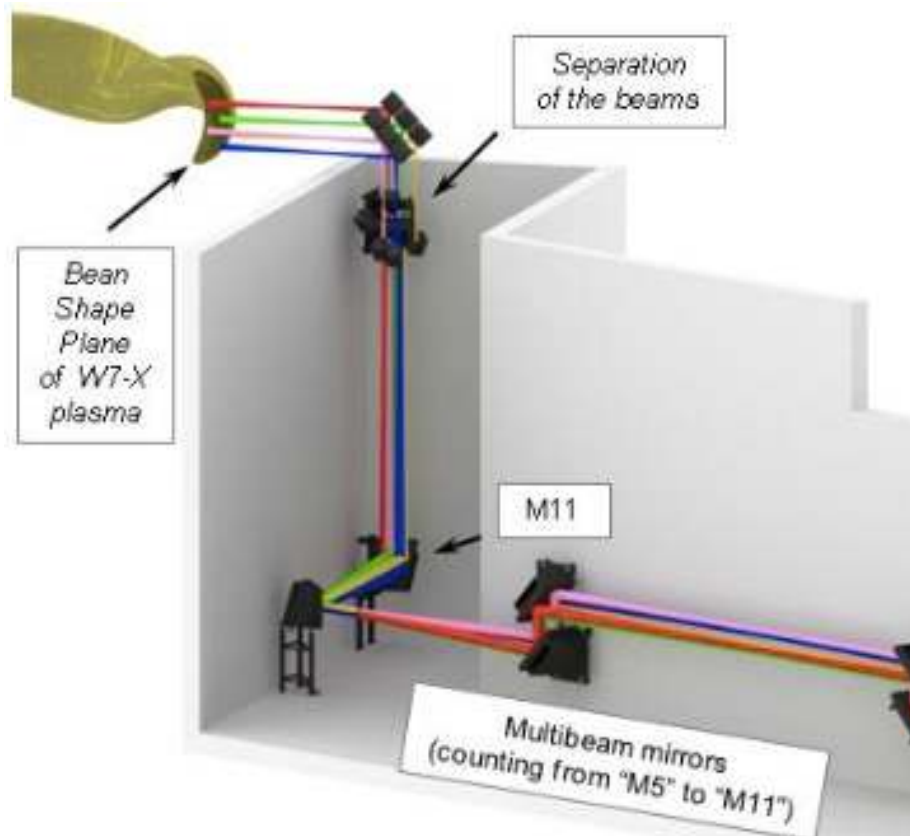
Only Ohmic losses ( $\sim 0.25\%$  per reflection)

Multi beam capability

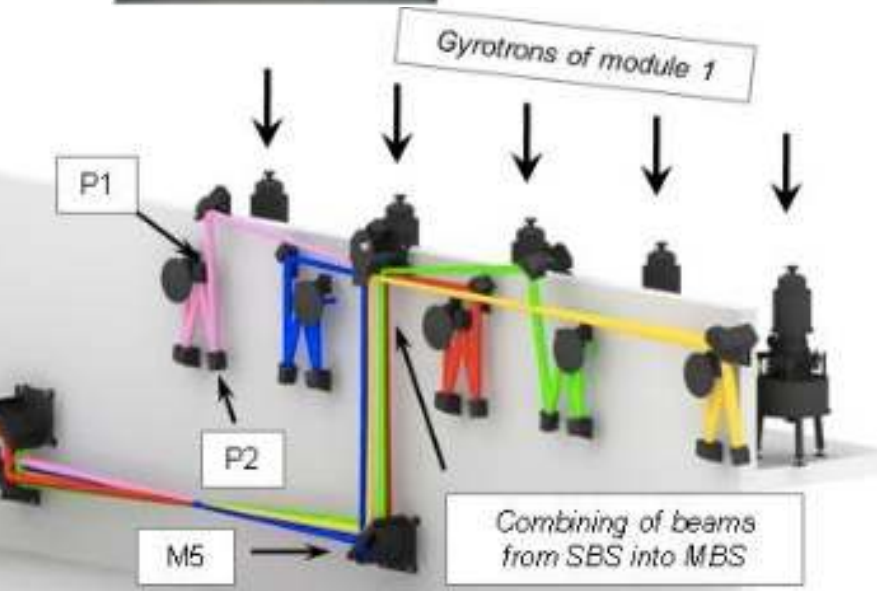
Low mode conversion

Air Conditioning ( to dry and to cool )

figure 5. Beam radius ( $1/e$  E-field radius) along the Q.O. section of the line



T. Stange et al, EPJ Web of Conferences **157**, 02008 (2017)

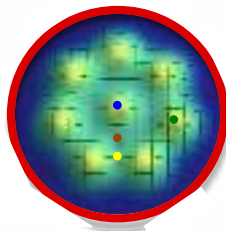
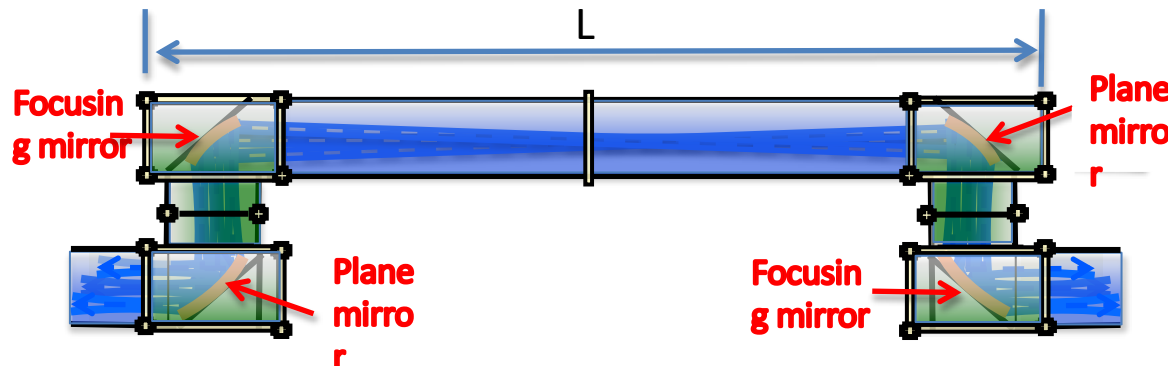


## Concept for Multibeam Evacuated QO Transmission Line

### Main DEMO TL requirements:

- Efficiency target: 90%
- Power handling: >1MW CW per line
- Multi-frequency (or broadband)
- Tritium compatible
- Large number of beams to be transmitted

The most promising and simple TL considered is a Quasi Optical Multi Beam Evacuated TL

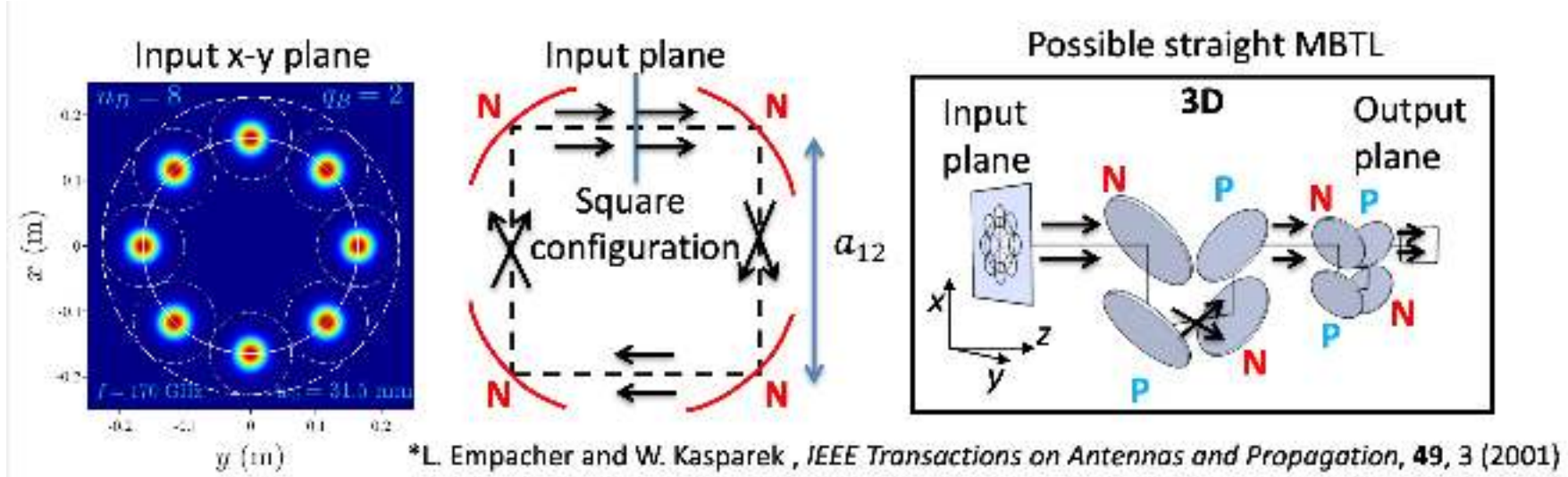


8 beams for each TL with a distance between Focussing units at  $L = 8-10$  m → mirror dimension: 0.6 – 0.8 m

# The confocal concept for QO TL



The arrangement with 4 non-plana mirrors allows to produce at the output the same image at the input, this is valid also in case of including 4 planar mirrors.



gyrotron

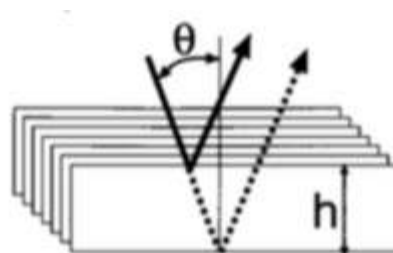
## The DTT ECH Evacuated Transmission Line



The linear polarization from the gyrotron must be rotated in order to launch the proper direction with respect the  $B_T$  pitch angle. **It is necessary for ECCD.**

Oblique injection requires further rotation in order to compensate the XM or OM components originated by inappropriate angle.

The polarizer are based on corrugated mirrors.



# Polarizer Concept

The component  $E_{//}$  (with respect to corrugation) is reflected at the bottom

The component  $E_{\perp}$  is reflected at the top

A phase shift of  $2h/\lambda$  of  $E_{//}$  respect to the  $E_{\perp}$  (reflected at the top).

This produces a rotation of the electric field.

Using a  $\lambda/4$  corrugation depth only linear rotation can be obtained, with  $\lambda/8$  one a circular component is introduced to obtain elliptical polarization to be used in case of oblique injection.

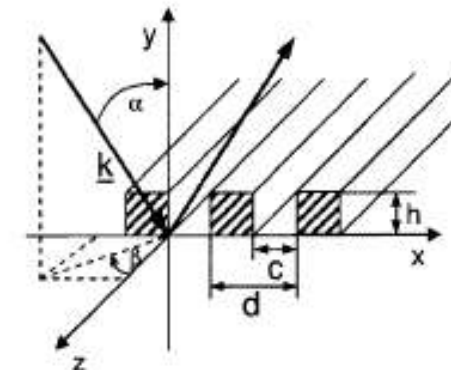
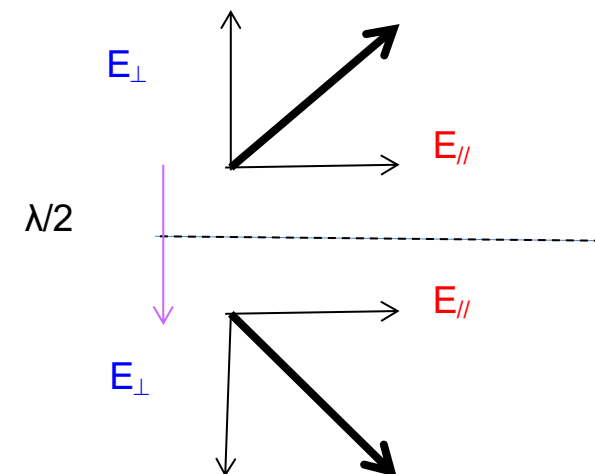
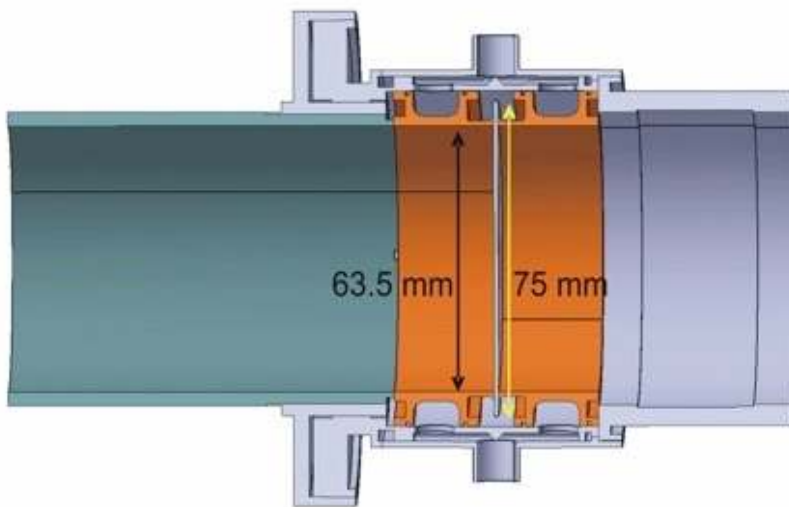


Fig.1 Polarizer corrugation.





Diamond disk Diameter: 75 mm  
Thickness: 1.11 mm

Loss measurements at 170 GHz:

$$\operatorname{tg} \delta_{\text{eff}} = 0.9 \times 10^{-5} \text{ (central area)}$$



T. A. Scherer et all 5th IAEA TM  
18-20/Feb. 2009 Gandhinagar, India

# Launcher

# The simpler launcher

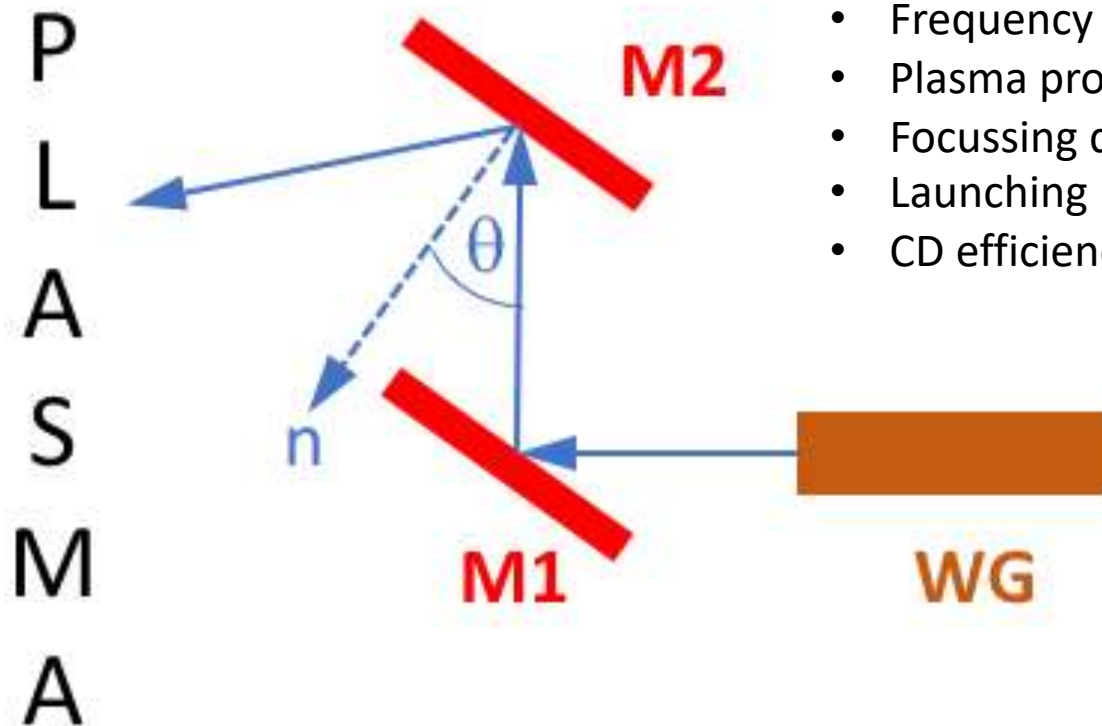
At the end of the transmission line the power must be coupled to the plasma. The TL must be connected to an **ANTENNA**. In the EC wave case the antenna becomes a **LAUNCHER**, being the frequency so high that the wave can be thought as propagating light beam.

A **truncated waveguide** propagating the delivered mode (TE0,1 or HE1,1) was the main launching antenna used in the pioneering experiments.

The **divergence of the beam** can be reduced increasing the wg diameter and the frequency.

This simple launcher is enough for **heating** experiments but not usable for **ECCD** and **MHD** control.

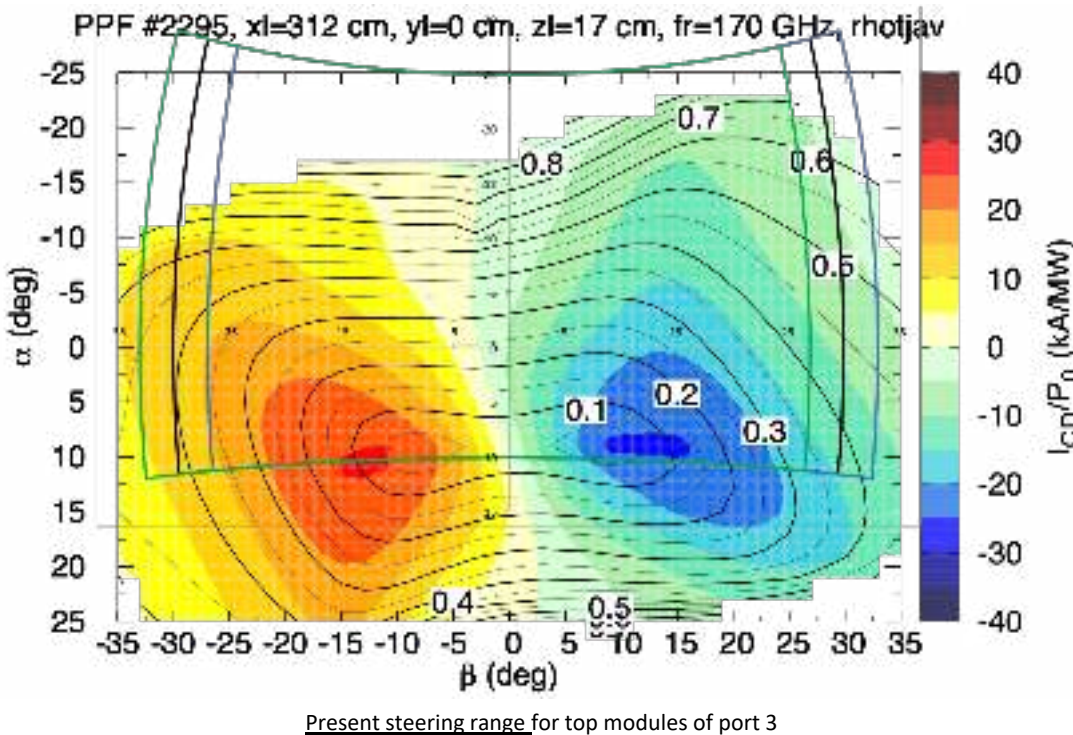
The most popular launcher is a Open Ended Wave Guide, at which is added a mirror to focus and steer the EC beam in plasma



The optics characteristics depend on:

- Frequency
- Plasma profiles
- Focussing distance (q surfaces position)
- Launching points
- CD efficiency required

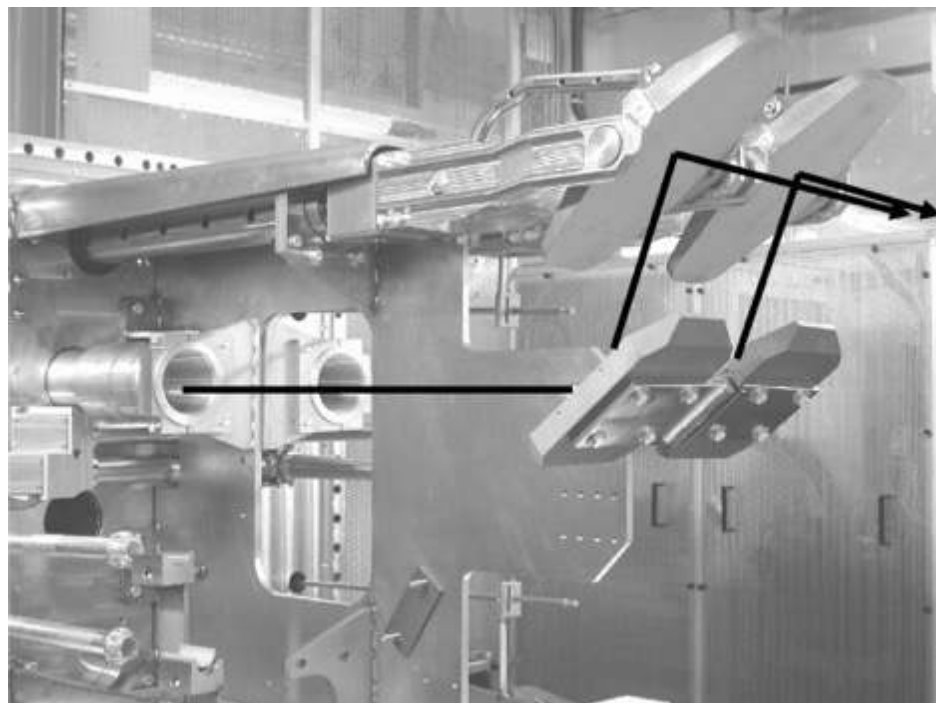
# Steering requirements



To fix the requirements for the steering ranges of the movable mirror a beam tracing map is usually generated.

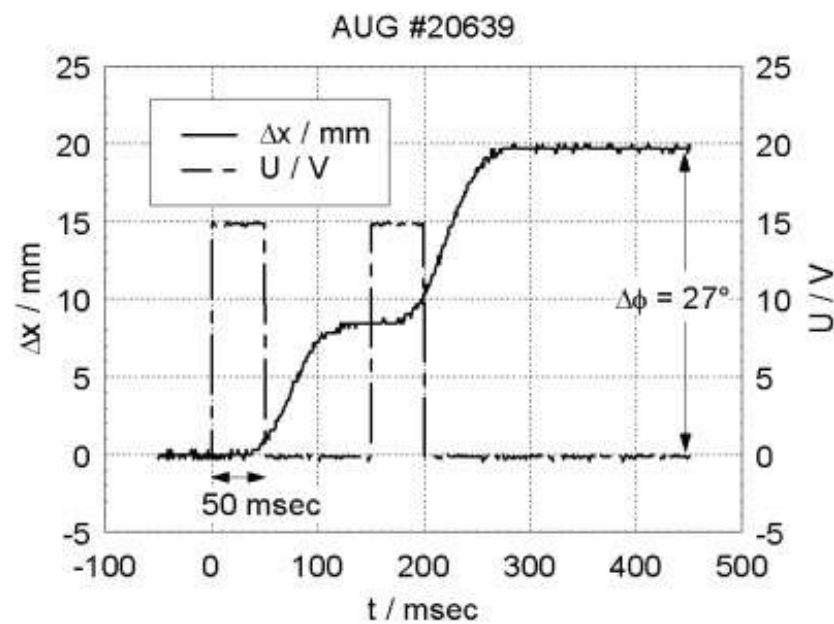
The CD efficiency is calculated as a function of launching angles, and the best range is defined starting from the requirements of the EC system.

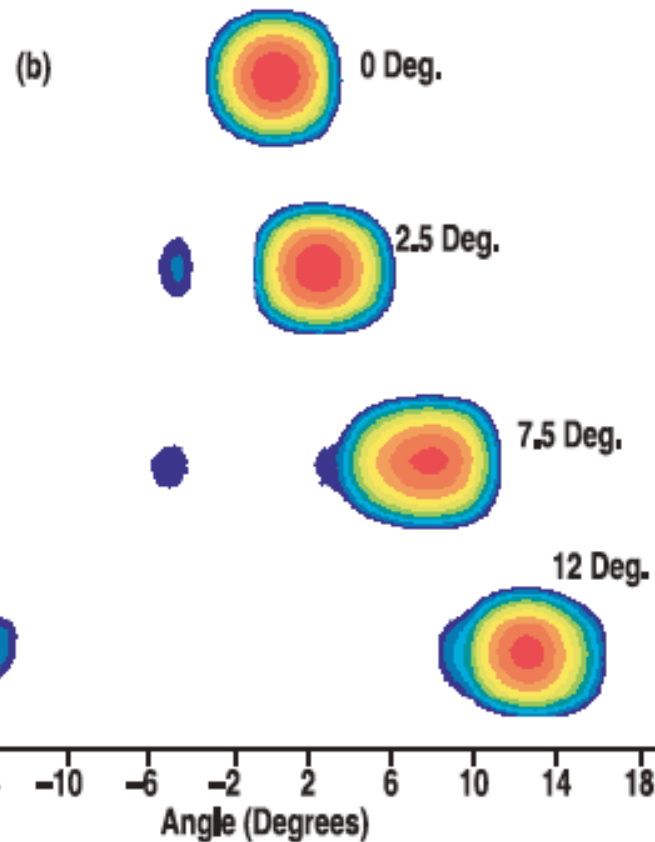
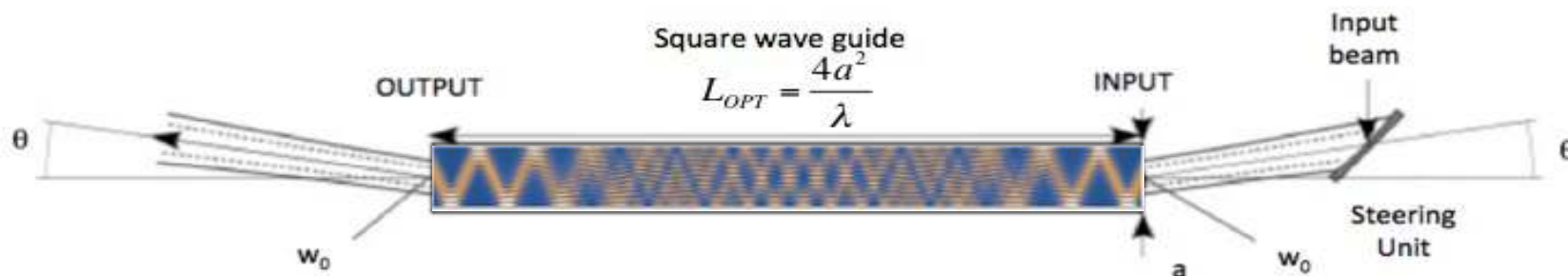
*GRAY code applied to DTT*



Real time mirrors steering  
(settling time  $\sim 100$  ms)

Movable mirrors in front of the plasma to steer the beam in the desired point



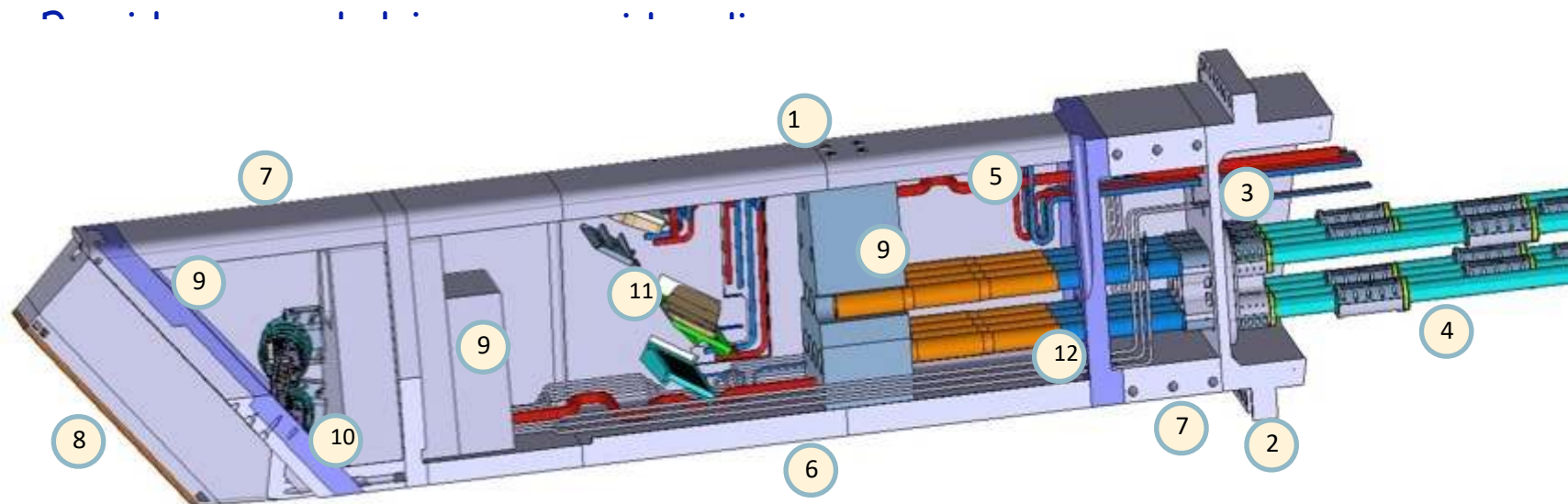


In a corrugated square waveguide the beam propagates decomposed in different modes that recombine after an integer number of coherent distances

Experimental Output pattern  
Good but not enough oblique angle

## Primary Role

- Stabilize MHD activity (Sawtooth and NTM), requiring narrow peaked deposition profile (Deposition width ~4cm)



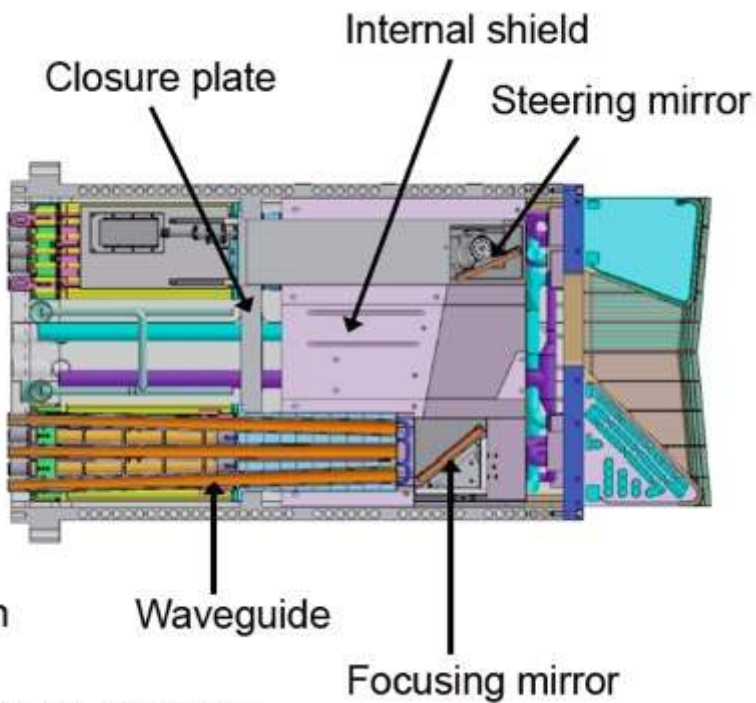
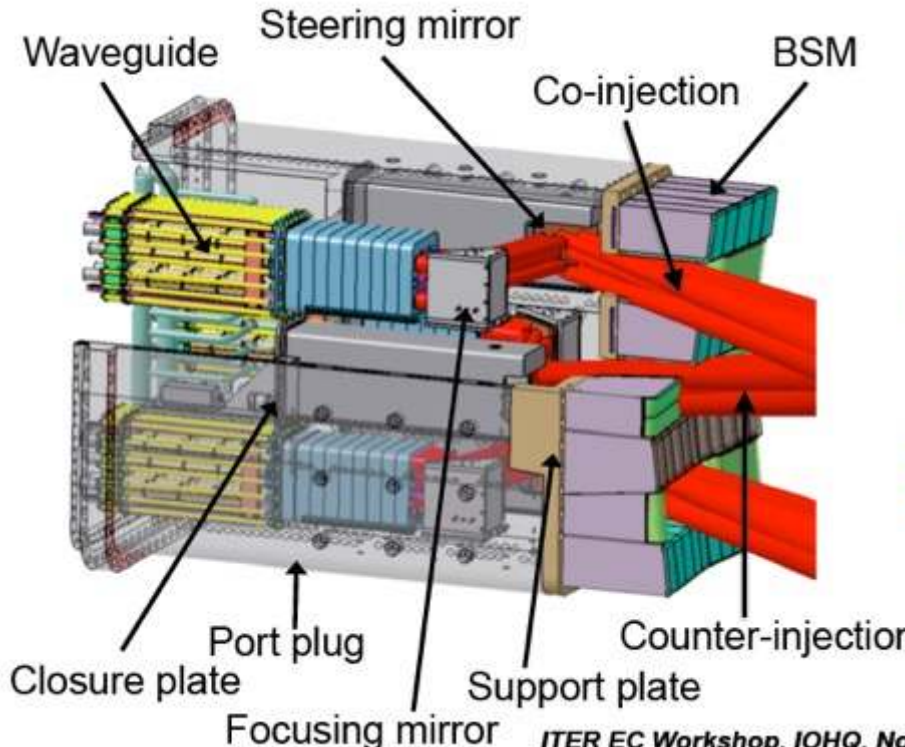
- Overall port plug length ≈ 6m
- Rear flange width ≈ 1.3m
- Wall thickness mid section = 90mm
- Total weight ≈ 18t (no water)
- Internal layout designed to allow guided and free propagation of 8 mm-wave beams

### **UL components:**

1. Port plug body
2. Rear flange
3. Closure plate and feedthroughs
4. Ex-vessel waveguide assembly
5. Services (cooling, gas, etc.)
6. Single wall structure
7. Double wall structure
8. BSM and first wall
9. Neutron shield
10. Steering mechanisms
11. Fixed mirrors
12. In-vessel waveguides

## Primary Role

- Central Heating and current drive
- Impurity control
- Breakdown and Burn through
- Current profile tailoring

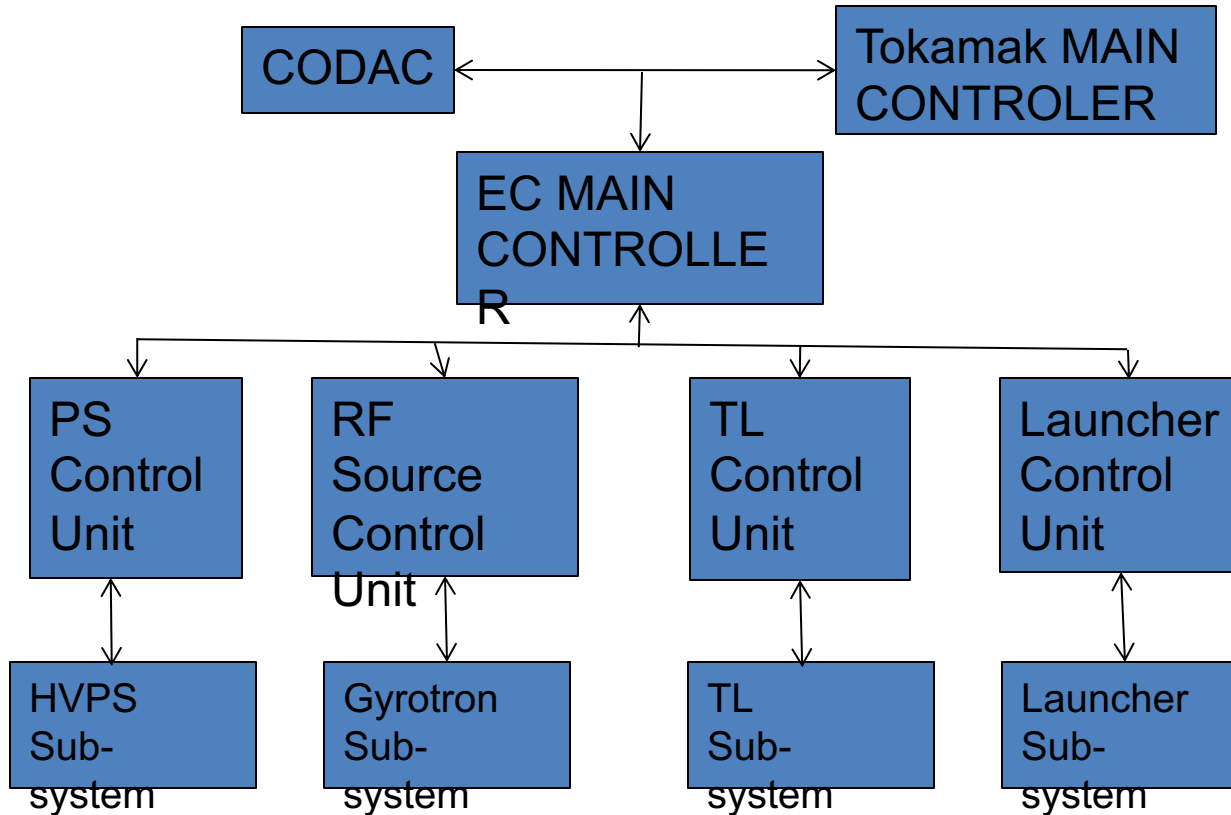


ITER EC Workshop, IOHQ, Nov. 18th – 22nd, 2013

Note that beams now steer in poloidal direction

# Control System

# The control system



# The EC control system

Four different levels of control system:

**Fast** control:  $t < 1\text{ms}$

Fast Sequence Control

Protection system

Real Time Control

**Local plant** control:  $t \sim 100\text{ms}$

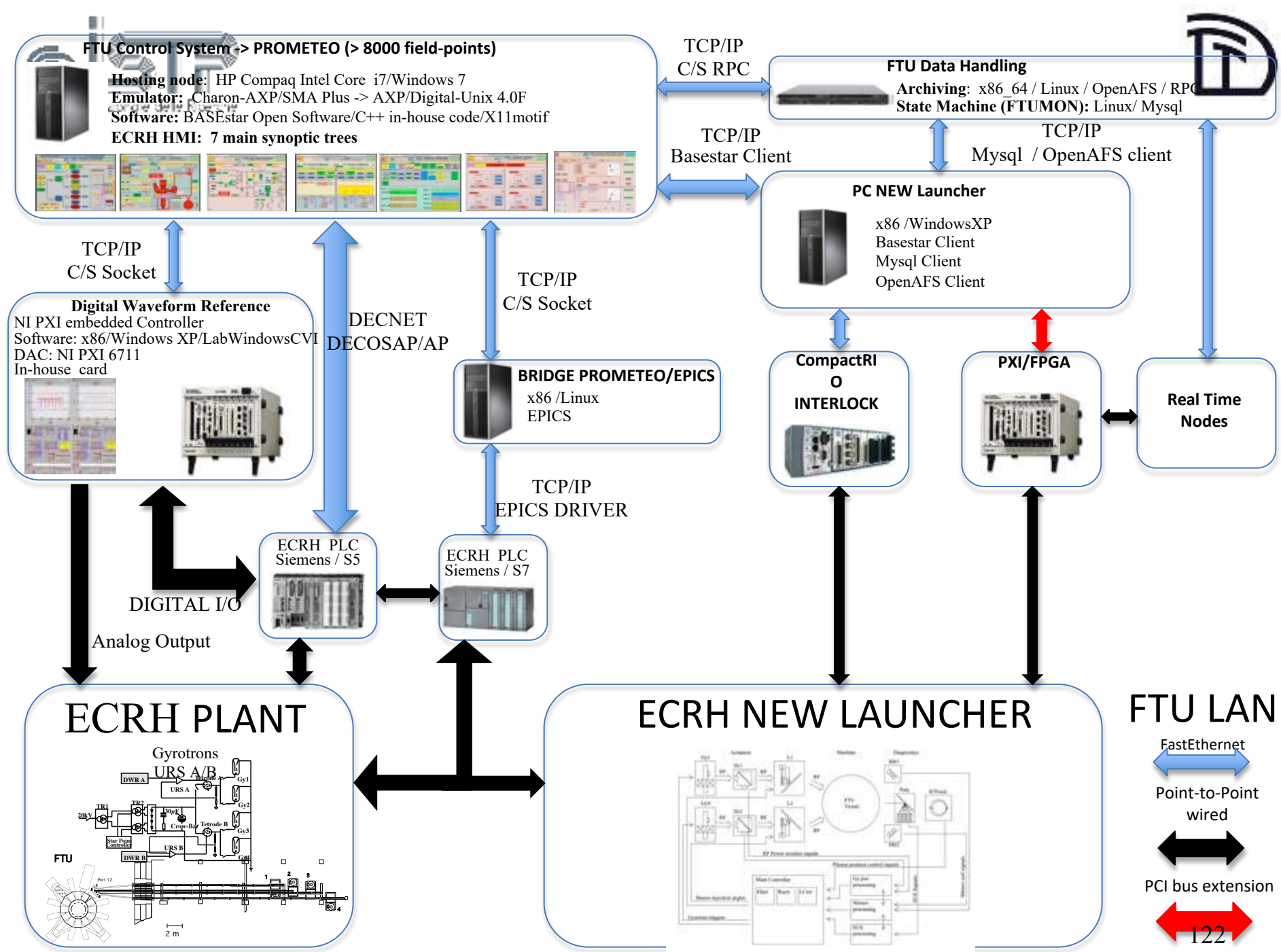
PLC

**Field to field** connections:

for higher level of safety:  $t \sim 10\text{ms}$

**Main controller** for human interface  $t \sim 1\text{s}$

mimic, sequence control:



EC Systems is nowadays the most promising Heating System for future reactor:

- No component close to plasma
- Remote power generation
- Simple transmission of the power
- Interaction plasma-wave well known
- Modular approach